

Global Mineral Resource Assessment

**Porphyry Copper Assessment of the Tethys Region of
Western and Southern Asia**



Prepared in cooperation with the Natural History Museum, London

Scientific Investigations Report 2010–5090–V

Global Mineral Resource Assessment

Michael L. Zientek, Jane M. Hammarstrom, and Kathleen M. Johnson, editors

Porphyry Copper Assessment of the Tethys Region of Western and Southern Asia

By Lukas Zürcher, Arthur A. Bookstrom, Jane M. Hammarstrom, John C. Mars, Steve Ludington, Michael L. Zientek, Pamela Dunlap, and John C. Wallis, with contributions from Lawrence J. Drew, David M. Sutphin, Byron R. Berger, Richard J. Herrington, Mario Billa, Ilkay Kuşcu, Charles J. Moon, and Jeremy P. Richards

Prepared in cooperation with the Natural History Museum, London

Scientific Investigations Report 2010–5090–V

U.S. Department of the Interior
U.S. Geological Survey

U.S. Department of the Interior
SALLY JEWELL, Secretary

U.S. Geological Survey
Suzette M. Kimball, Acting Director

U.S. Geological Survey, Reston, Virginia: 2015

For more information on the USGS—the Federal source for science about the Earth, its natural and living resources, natural hazards, and the environment, visit <http://www.usgs.gov> or call 1–888–ASK–USGS (1–888–275–8747).

For an overview of USGS information products, including maps, imagery, and publications, visit <http://www.usgs.gov/pubprod>.

To order this and other USGS information products, visit <http://store.usgs.gov>.

Any use of trade, firm, or product names is for descriptive purposes only and does not imply endorsement by the U.S. Government.

Although this report is in the public domain, permission must be secured from the individual copyright owners to reproduce any copyrighted material contained within this report.

Suggested citation:

Zürcher, L., Bookstrom A.A., Hammarstrom, J.M., Mars, J.C., Ludington, S., Zientek, M.L., Dunlap, P., and Wallis, J.C., with contributions from Drew, L.J., Sutphin, D.M., Berger, B.R., Herrington, R.J., Billa, M., Kuşcu, I., Moon, C.J., and Richards, J.P., 2015, Porphyry copper assessment of the Tethys region of western and southern Asia: U.S. Geological Survey Scientific Investigations Report 2010–5090–V, 232 p., and spatial data, <http://dx.doi.org/10.3133/sir20105090V>.

ISSN 2328-0328 (online)

Contents

Abstract.....	1
Introduction.....	2
Background	2
Report Format.....	6
Considerations for Users of this Assessment.....	6
Terminology	6
Porphyry Copper Deposit Models.....	8
Descriptive Models	8
Grade and Tonnage Models.....	9
Deposit Density Models	9
Permissive Porphyry Copper Tracts	9
Tectono-Magmatic Framework of the Tethys Region of Western and Southern Asia.....	9
Permian to Middle Jurassic.....	12
Paleotethys Ocean Realm.....	12
Neotethys Ocean Realm	12
Late Jurassic to Early Cretaceous.....	13
Late Cretaceous to Middle Miocene.....	13
Northern Neotethys Ocean Branch Realm.....	13
Southern Neotethys Ocean Branch Realm.....	24
Late Eocene to Middle Miocene	24
Late Miocene to Holocene.....	26
Neotectonic Setting of the Tethys Region of Western and Southern Asia	26
Western, Central, and Southern Turkey.....	26
Northern Turkey	27
Eastern Turkey, Lesser Caucasus, and Northwestern Iran	27
Greater Caucasus and Northern Iran	27
Eastern and Central-Eastern Iran	30
Central and Southeastern Iran.....	30
Southeastern Iran and Southwestern Pakistan	30
Assessment Data	30
Geologic Maps.....	31
Tectonic Maps.....	31
Mineral Occurrence Data	31
Known Porphyry Deposits and Prospects	31
Porphyry-Related Deposit Types	31
Spatial Rules for Grouping Deposits and Prospects	32
Exploration.....	32
Afghanistan	32
Armenia.....	32
Azerbaijan.....	33
Georgia.....	33
Iran.....	33
Pakistan	34

Turkey.....	34
Other Data.....	35
ASTER and HyMap Data	35
Geophysical Data	35
Preservation Level Data.....	35
Assessment Methods.....	36
Tract Delineation.....	36
Estimation of Numbers of Undiscovered Deposits	37
Porphyry Copper Assessment of the Tethys Region.....	37
Late Triassic to Early Cretaceous Tracts	38
Sanandaj-Sirjan Tract (142pCu9003)	38
Location	38
Tectonic Setting.....	50
Magmatism and Known Porphyry Deposits or Prospects	50
Qualitative Assessment	50
Cimmeride Greater Caucasus Tract (142pCu9002).....	52
Location	52
Tectonic Setting.....	52
Magmatism and Known Porphyry Deposits or Prospects	52
Qualitative Assessment	55
Lut Jurassic Tract (142pCu9000)	55
Location	55
Tectonic Setting.....	55
Magmatism and Known Porphyry Deposits or Prospects	55
Qualitative Assessment	58
Cimmeride Lesser Caucasus Tract (142pCu9001)	58
Location	58
Tectonic Setting.....	58
Magmatism	58
Known Porphyry Deposits and Prospects	58
Teghout Porphyry Deposit.....	61
Kedabek Porphyry Deposit.....	61
Kavarta (Kapan) Porphyry Deposit	61
Other Porphyry Prospects and Possible Porphyry-Related Mineral Occurrences.....	62
Preservation Level	62
Magnetic Anomalies	62
Probabilistic Assessment.....	62
Grade and Tonnage Model Selection.....	62
Estimates of Undiscovered Deposits and Rationale.....	62
Probabilistic Assessment Simulation Results.....	63
Late Cretaceous to Late Eocene Tracts	63
Pontide (Asia) Tract (142pCu9004)	63
Location	63
Tectonic Setting.....	63
Pontide (Asia)–NW Turkey Sub-tract (142pCu9004a).....	66

Magmatism	66
Known Porphyry Deposits and Prospects	66
Bakircay Porphyry Deposit	68
Dikmen Porphyry Prospect	68
Preservation Level	68
Magnetic Anomalies	68
Probabilistic Assessment	68
Grade and Tonnage Model Selection	68
Estimates of Undiscovered Deposits and Rationale	69
Probabilistic Assessment Simulation Results	69
Pontide (Asia)–NE Turkey Sub-tract (142pCu9004b)	69
Magmatism	69
Known Porphyry Deposits and Porphyry-Related Prospects	73
Balcili-Yüksekoba Porphyry Deposit	74
Güzelyayla Porphyry Deposit	74
Ulutaş Porphyry Deposit	74
Gümüşhane Porphyry Deposit	74
Sisorta Porphyry-Related Prospect	75
Preservation Level	75
Magnetic Anomalies	75
Probabilistic Assessment	75
Grade and Tonnage Model Selection	75
Estimates of Undiscovered Deposits and Rationale	76
Probabilistic Assessment Simulation Results	76
Pontide (Asia)–Caucasus-Iran Sub-tract (142pCu9004c)	76
Magmatism	76
Known Porphyry Prospects	77
Preservation Level	77
Magnetic Anomalies	77
ASTER Alteration Data	77
Probabilistic Assessment	78
Grade and Tonnage Model Selection	78
Estimates of Undiscovered Deposits and Rationale	78
Probabilistic Assessment Simulation Results	78
Anatolide-Tauride Tract (142pCu9005)	78
Location	78
Tectonic Setting	78
Anatolide-Tauride–Western Turkey Sub-tract (142pCu9005a)	80
Magmatism	80
Known Porphyry Deposits and Prospects	82
Muratdere Porphyry Deposit	82
Sarıçayiryayla Porphyry Deposit	82
Turkmen Porphyry Prospect	82
Preservation Level	82
Magnetic Anomalies	83
Probabilistic Assessment	83

Grade and Tonnage Model Selection.....	83
Estimates of Undiscovered Deposits and Rationale.....	83
Probabilistic Assessment Simulation Results.....	83
Anatolide-Tauride–Central Turkey Sub-tract (142pCu9005b).....	87
Magmatism	87
Known Porphyry Prospects.....	88
Balışeyh and Karacaali Porphyry Prospects	88
Başnayayla Porphyry Prospect.....	88
Preservation Level	89
Magnetic Anomalies	89
Probabilistic Assessment.....	89
Grade and Tonnage Model Selection.....	89
Estimates of Undiscovered Deposits and Rationale.....	89
Probabilistic Assessment Simulation Results.....	90
Anatolide-Tauride–Eastern Turkey-Caucasus Sub-tract (142pCu9005c).....	90
Magmatism	90
Known Porphyry Deposits and Prospects	90
Çöpler Porphyry Deposit.....	91
Karakartal Porphyry Deposit.....	91
Kabatas (South) Porphyry Prospect.....	91
Agarak and Dastakert Porphyry Deposits	91
Mamlis and Sin Porphyry Prospects	91
Preservation Level	92
Magnetic Anomalies	92
Probabilistic Assessment.....	92
Grade and Tonnage Model Selection.....	92
Estimates of Undiscovered Deposits and Rationale.....	92
Probabilistic Assessment Simulation Results.....	93
Lut Cretaceous Tract (142pCu9006).....	93
Location	93
Tectonic Setting.....	93
Magmatism and Known Porphyry Prospects.....	93
Qualitative Assessment	96
Border Folds Tract (142pCu9007)	96
Location	96
Tectonic Setting.....	96
Magmatism	96
Known Porphyry Deposits and Prospects	99
Ispendere Porphyry Prospect.....	99
Nazarusagi and Uslu Porphyry Prospects.....	99
Keban Porphyry-Skarn Deposit.....	100
Preservation Level	100
Magnetic Anomalies	100
Probabilistic Assessment.....	100
Grade and Tonnage Model Selection.....	100
Estimates of Undiscovered Deposits and Rationale.....	100

Probabilistic Assessment Simulation Results.....	101
Esfahan Tract (142pCu9008).....	101
Location.....	101
Tectonic Setting.....	101
Magmatism.....	104
East-Central Iran.....	104
Central Iran.....	105
Northwestern Iran.....	106
Western Iran.....	106
Southeastern Iran.....	106
Known Porphyry Deposits and Prospects.....	106
Kale Kafi Porphyry Deposit.....	107
Other Possible Porphyry-Related Prospects.....	107
Preservation Level.....	107
Magnetic Anomalies.....	107
ASTER Alteration Data.....	107
Probabilistic Assessment.....	108
Grade and Tonnage Model Selection.....	108
Estimates of Undiscovered Deposits and Rationale.....	108
Probabilistic Assessment Simulation Results.....	108
Khoreasan Tract (142pCu9009).....	110
Location.....	110
Tectonic Setting.....	110
Magmatism.....	110
Known Porphyry Prospects.....	113
Tannurjeh and Uchplang-Baharieh Porphyry Prospects.....	113
Kalateh Timour Porphyry Prospect.....	113
Halak Abad, Arghash, and Kalateh Now Porphyry Prospects.....	113
Chah Shirin Porphyry-Related Prospect.....	114
Other Possible Porphyry-Related Deposits and Prospects.....	114
Preservation Level.....	115
Magnetic Anomalies.....	115
ASTER Alteration Data.....	115
Probabilistic Assessment.....	115
Grade and Tonnage Model Selection.....	115
Estimates of Undiscovered Deposits and Rationale.....	115
Probabilistic Assessment Simulation Results.....	116
Makran Tract (142pCu9011).....	116
Location.....	116
Tectonic Setting and Magmatism.....	116
Porphyry-Related Prospects.....	120
Qualitative Assessment.....	120
Eocene to Miocene Tracts.....	120
Lut Tertiary Tract (142pCu9010).....	120
Location.....	120
Tectonic Setting.....	120

Magmatism	121
Known Porphyry Prospects.....	122
Shadan, Maher Abad, Sar Cha Shur, and Sheik Abad Porphyry Prospect District	123
Cha-Shaljami Porphyry Prospect.....	123
Deh-Salm Porphyry Prospect.....	123
Kajeh Porphyry Prospect.....	123
Other Porphyry-Related Mineral Occurrences	123
Preservation Level	123
Magnetic Anomalies	124
Probabilistic Assessment.....	124
Grade and Tonnage Model Selection.....	124
Estimates of Undiscovered Deposits and Rationale.....	124
Probabilistic Assessment Simulation Results.....	124
Sistan Tract (142pCu9012)	126
Location	126
Tectonic Setting.....	126
Magmatism	126
Known Porphyry Prospects.....	129
Shah-Kuh (Sistan) Porphyry Prospect	129
Kuh-e-Lar and Kuh-e-Assagi Porphyry Prospects.....	129
Kuh-e-Seyasteragi and Kuh-e-Janja Porphyry Prospects	129
Other Possible Porphyry-Related Deposits and Prospects.....	129
Preservation Level	130
Magnetic Anomalies	130
ASTER Alteration Data	130
Probabilistic Assessment.....	131
Grade and Tonnage Model Selection.....	131
Estimates of Undiscovered Deposits and Rationale.....	131
Probabilistic Assessment Simulation Results.....	131
Chagai Tract (142pCu9013).....	133
Location	133
Tectonic Setting.....	133
Magmatism	133
Known Porphyry Deposits and Prospects	136
Ziarate and Ganshero Porphyry Prospects.....	136
Dasht-e-Kain Porphyry Deposit.....	136
Tanjeel Porphyry Deposit	137
Saindak Porphyry Deposit.....	137
Ziarat Pir Sultan Porphyry Prospect.....	137
Kirtaka and Sor Baroot Porphyry Prospects.....	137
Reko Diq Porphyry Deposit	137
Koh-i-Dalil Porphyry Prospect.....	137
Preservation Level	138
Magnetic Anomalies	138
ASTER and Airborne Hyperspectral Alteration Data	138

Probabilistic Assessment	139
Grade and Tonnage Model Selection.....	139
Estimates of Undiscovered Deposits and Rationale.....	139
Probabilistic Assessment Simulation Results.....	139
Azerbaijan Tract (142pCu9014)	141
Location	141
Tectonic Setting.....	141
Azerbaijan–Western Turkey Sub-tract (142pCu9014a)	143
Magmatism	143
Known Porphyry Deposits and Prospects	143
Palamutoba Porphyry Prospect	143
Alankoy Porphyry Prospect	143
Halilaga Porphyry Deposit.....	145
Tepeoba Porphyry Deposit.....	145
Ayazmant Porphyry Deposit.....	145
Other Porphyry-Related Deposits and Prospects	145
Preservation Level	146
Magnetic Anomalies	146
Probabilistic Assessment	146
Grade and Tonnage Model Selection.....	146
Estimates of Undiscovered Deposits and Rationale.....	146
Probabilistic Assessment Simulation Results.....	147
Azerbaijan–Eastern Turkey Sub-tract (142pCu9014b)	147
Magmatism	147
Known Porphyry Deposits and Prospects	147
Cevizlidere Porphyry Deposit.....	147
Other Porphyry-Related Prospects.....	151
Preservation Level	152
Magnetic Anomalies	152
Probabilistic Assessment	152
Grade and Tonnage Model Selection.....	152
Estimates of Undiscovered Deposits and Rationale.....	152
Probabilistic Assessment Simulation Results.....	153
Azerbaijan–Caucasus-Iran Sub-tract (142pCu9014c)	153
Magmatism	153
Known Porphyry Deposits and Prospects	154
Kadjaran Porphyry Deposit	154
Ankavan Porphyry Deposit.....	154
Sungun Porphyry Deposit.....	154
Haft Cheshmeh Porphyry Deposit.....	155
Masjed Daghi Porphyry Deposit	155
Other Porphyry-Related Prospects and Possible Porphyry-Related Mineral Occurrences	155
Preservation Level	155
Magnetic Anomalies	156
ASTER Alteration Data	156

Probabilistic Assessment	156
Grade and Tonnage Model Selection.....	156
Estimates of Undiscovered Deposits and Rationale.....	156
Probabilistic Assessment Simulation Results.....	157
Yazd Tract (142pCu9015)	157
Location	157
Tectonic Setting.....	157
Magmatism	157
Known Porphyry Deposits and Prospects	160
Dalli Porphyry Deposit	160
Kahang (Gor Gor) Porphyry Deposit.....	160
Qahan Porphyry Prospect.....	161
Qamsar Porphyry Prospect.....	161
South of Ardestan and Sharif Abad Porphyry Prospects	161
Zafarghand Porphyry Prospect.....	161
Zefreh Porphyry Prospect.....	161
Other Porphyry-Related Prospects and Possible Porphyry-Related Mineral Occurrences.....	161
Preservation Level	162
Magnetic Anomalies	162
ASTER Alteration Data	162
Probabilistic Assessment	163
Grade and Tonnage Model Selection.....	163
Estimates of Undiscovered Deposits and Rationale.....	163
Probabilistic Assessment Simulation Results.....	163
Kerman Tract (142pCu9016)	165
Location	165
Tectonic Setting.....	165
Magmatism	165
Known Porphyry Deposits and Prospects	168
Sar Cheshmeh Porphyry Deposit	168
Now Chun and Sar Kuh Porphyry Deposits.....	168
Seridune Porphyry Prospect.....	169
Darrehzar Porphyry Deposit	169
Kuh Panj Porphyry Prospect.....	169
Dar Alu Porphyry Deposit.....	169
Meiduk Porphyry Deposit.....	170
Sara Porphyry Prospect	170
Cha Messi Porphyry-Related Deposit.....	170
Chah-Firuzeh Porphyry Deposit.....	170
God-e-Kolvari (Gowde Kolvary) Porphyry Prospect.....	170
Ali-Abad and Darreh-Zerreshk (Taft Project) Porphyry Deposits.....	171
Takht and Chahar Gonbad Porphyry Prospects	171
Dar Hamzeh Porphyry Prospect.....	171
Raigan (Rigan Bam) Porphyry Deposit.....	171
Bagh Khoshk Porphyry Deposit.....	172

Iju Porphyry Deposit and Abdar Porphyry Prospect.....	172
Preservation Level	172
Magnetic Anomalies	173
ASTER Alteration Data	173
Probabilistic Assessment.....	173
Grade and Tonnage Model Selection.....	173
Estimates of Undiscovered Deposits and Rationale.....	174
Probabilistic Assessment Simulation Results.....	174
Late Miocene to Holocene Tracts.....	174
Pliocene-Quaternary Tract (142pCu9017).....	174
Tectonic Setting.....	174
Pliocene-Quaternary–Konya Sub-tract (142pCu9017a)	177
Location	177
Tectonic Setting and Magmatism	177
Known Porphyry Prospects.....	177
Doğanbey Porphyry Prospect.....	180
Other Possible Porphyry-Related Prospects	180
Qualitative Assessment	180
Pliocene-Quaternary–Postcollisional Sub-tract (142pCu9017b)	180
Location	180
Tectonic Setting and Magmatism	180
Northern Turkey	180
Eastern Turkey, Lesser Caucasus, and Northwestern Iran	181
Greater Caucasus and Northern Iran.....	181
Eastern Iran	182
Central-Eastern Iran.....	182
Central and Southeastern Iran	182
Known Porphyry Deposits or Prospects, and other Possible Porphyry-Related Occurrences	182
Porphyry-Related Mineral Occurrences in Northern Turkey	183
Porphyry-Related Prospects and other Possible Porphyry-Related Mineral Occurrences in Eastern Turkey and Northwestern Iran	183
Porphyry-Related Prospects and Other Possible Porphyry-Related Mineral Occurrences in the Greater Caucasus and Northern Iran	183
Possible Porphyry-Related Mineral Occurrences in Eastern and Central- Eastern Iran	184
Porphyry-Related Prospects and Other Possible Porphyry-Related Mineral Occurrences in Central and Southeastern Iran	184
Qualitative Assessment	184
Pliocene-Quaternary–Bazman Sub-tract (142pCu9017c).....	184
Location	184
Tectonic Setting and Magmatism	184
Known Porphyry Prospects.....	185
Koh-i-Sultan Porphyry Prospect	185
Other Possible Porphyry-Related Prospects	185
Qualitative Assessment	185

Discussion	186
Tectonic Settings and Distribution of Porphyry Copper Deposits and Prospects	186
Postcollisional Magmatism and Porphyry Copper Mineralization	186
Preservation-Erosion Record and Porphyry Copper Deposits and Prospects	187
Changes in Tectonic Regime and Porphyry Copper Deposits.....	187
Concluding Remarks	187
Ore-Forming Environment, Level of Preservation and Exposure, Number of Porphyry Occurrences, Extent of Exploration, and Copper Endowment	187
Utility of Data.....	189
Utility of Available Models.....	189
Summary of Probabilistic Assessment Results	189
Acknowledgments	190
References Cited.....	195
Appendix A. Principal Sources of Information Used for the Porphyry Copper Assessment, Tethys Region of Western and Southern Asia	228
Appendix B. Geologic Map Units Used to Delineate Permissive Tracts (With References to Source Maps), Tethys Region of Western and Southern Asia.....	229
Appendix C. Significant Porphyry Copper Prospects and Occurrences, Tethys Region of Western and Southern Asia	229
Appendix D. Spatial Data.....	230
Appendix E. Assessment Team.....	230

Figures

1. Map showing the Tethyan Eurasian Metallogenic Belt and extent of the assessment area	3
2. Map showing major sutures, faults, and geologic and geographic features in the Tethys region of western and southern Asia (assessment area) and vicinity	4
3. Map showing tectono-stratigraphic terranes, accretionary prisms, and metamorphic belts of the Tethys region of western and southern Asia	14
4. Paleotectonic reconstructions of the Tethys region of western and southern Asia	16
5. Late Triassic to Early Cretaceous permissive tracts for porphyry copper deposits in the Tethys region of western and southern Asia	18
6. Late Cretaceous to late Eocene permissive tracts for porphyry copper deposits in the Tethys region of western and southern Asia	20
7. Eocene to Miocene permissive tracts for porphyry copper deposits in the Tethys region of western and southern Asia.....	22
8. Pliocene to Holocene permissive tract for porphyry copper deposits in the Tethys region of western and southern Asia.....	28
9. Time-space diagram of permissive tracts for porphyry copper deposits in the Tethys region of western and southern Asia.....	39
10. Map showing the location of possible porphyry-related copper occurrences for permissive tract 142pCu9003, Sanandaj-Sirjan—Iran, Iraq, and Turkey.....	49
11. Map showing the distribution of permissive intrusive and extrusive rocks used to define tract 142pCu9003, Sanandaj-Sirjan—Iran, Iraq, and Turkey.....	51

12. Map showing the location of permissive tract 142pCu9002, Cimmeride Greater Caucasus—Azerbaijan, Georgia, and Russian Federation	53
13. Map showing the distribution of permissive intrusive and extrusive rocks used to define tract 142pCu9002, Cimmeride Greater Caucasus—Azerbaijan, Georgia, and Russian Federation	54
14. Map showing the location of known porphyry copper deposits, prospects, and occurrences for permissive tract 142pCu9000, Lut Jurassic—Iran.....	56
15. Map showing the distribution of permissive intrusive and extrusive rocks used to define tract 142pCu9000, Lut Jurassic—Iran	57
16. Map showing the location of known porphyry copper deposits and prospects for permissive tract 142pCu9001, Cimmeride Lesser Caucasus—Armenia, Azerbaijan, Georgia, and Iran	59
17. Map showing the distribution of permissive intrusive and extrusive rocks used to define tract 142pCu9001, Cimmeride Lesser Caucasus—Armenia, Azerbaijan, Georgia, and Iran	60
18. Cumulative frequency plot showing the results of Monte Carlo simulation of undiscovered resources in porphyry copper deposits in tract 142pCu9001, Cimmeride Lesser Caucasus—Armenia, Azerbaijan, Georgia, and Iran	64
19. Map showing the location of known porphyry copper deposits and prospects for permissive tract 142pCu9004, Pontide (Asia)—Armenia, Azerbaijan, Georgia, Iran, and Turkey.....	65
20. Map showing the distribution of permissive intrusive and extrusive rocks used to define tract 142pCu9004, Pontide (Asia)—Armenia, Azerbaijan, Georgia, Iran, and Turkey	67
21. Cumulative frequency plots showing the results of Monte Carlo computer simulation of undiscovered resources in porphyry copper deposits in tract 142pCu9004, Pontide (Asia)—Armenia, Azerbaijan, Georgia, Iran, and Turkey.....	72
22. Map showing the location of known porphyry copper deposits and prospects for permissive tract 142pCu9005, Anatolide-Tauride—Armenia, Azerbaijan, Iran, and Turkey.....	79
23. Map showing the distribution of permissive intrusive and volcanic rocks used to define tract 142pCu9005, Anatolide-Tauride—Armenia, Azerbaijan, Iran, and Turkey..	81
24. Cumulative frequency plots showing the results of Monte Carlo computer simulation of undiscovered resources in porphyry copper deposits in tract 142pCu9005, Anatolide-Tauride—Armenia, Azerbaijan, Iran, and Turkey	86
25. Map showing the location of known porphyry copper prospects for permissive tract 142pCu9006, Lut Cretaceous—Iran	94
26. Map showing the distribution of permissive intrusive and extrusive rocks used to define tract 142pCu9006, Lut Cretaceous—Iran.....	95
27. Map showing the location of known porphyry copper prospects for permissive tract 142pCu9007, Border Folds—Iran, Iraq, and Turkey.....	97
28. Map showing the distribution of permissive intrusive and extrusive rocks used to define tract 142pCu9007, Border Folds—Iran, Iraq, and Turkey	98
29. Cumulative frequency plot showing the results of Monte Carlo computer simulation of undiscovered resources in porphyry copper deposits in tract 142pCu9007, Border Folds—Iran, Iraq, and Turkey	102
30. Map showing the location of known porphyry copper deposits and prospects for permissive tract 142pCu9008, Esfahan—Iran, Iraq, and Turkey	103
31. Map showing the distribution of permissive intrusive and extrusive rocks used to define tract 142pCu9008, Esfahan—Iran, Iraq, and Turkey	105

32.	Cumulative frequency plot showing the results of Monte Carlo simulation of undiscovered resources in porphyry copper deposits in tract 142pCu9008, Esfahan—Iran, Iraq, and Turkey.....	109
33.	Map showing the location of known porphyry copper prospects for permissive tract 142pCu9009, Khorasan—Afghanistan and Iran.....	111
34.	Map showing the distribution of permissive intrusive and extrusive rocks used to define tract 142pCu9009, Khorasan—Afghanistan and Iran.....	112
35.	Cumulative frequency plot showing the results of Monte Carlo simulation of undiscovered resources in porphyry copper deposits in tract 142pCu9009, Khorasan—Afghanistan and Iran.....	117
36.	Map showing the location of known porphyry copper prospects for permissive tract 142pCu9011, Makran—Iran.....	118
37.	Map showing the distribution of permissive intrusive and extrusive rocks used to define tract 142pCu9011, Makran—Iran.....	119
38.	Map showing the location of known porphyry copper prospects for permissive tract 142pCu9010, Lut Tertiary—Iran.....	121
39.	Map showing the distribution of permissive intrusive and extrusive rocks used to define tract 142pCu9010, Lut Tertiary—Iran.....	122
40.	Cumulative frequency plot showing the results of Monte Carlo simulation of undiscovered resources in porphyry copper deposits in tract 142pCu9010, Lut Tertiary—Iran.....	125
41.	Map showing the location of known porphyry copper prospects for permissive tract 142pCu9012, Sistan—Afghanistan, Iran, and Pakistan.....	127
42.	Map showing the distribution of permissive intrusive and extrusive rocks used to define tract 142pCu9012, Sistan—Afghanistan, Iran, and Pakistan.....	128
43.	Cumulative frequency plot showing the results of Monte Carlo simulation of undiscovered resources in porphyry copper deposits in 142pCu9012, Sistan—Afghanistan, Iran, and Pakistan.....	132
44.	Map showing the location of known porphyry copper deposits and prospects for permissive tract 142pCu9013, Chagai—Afghanistan, Iran, and Pakistan.....	134
45.	Map showing the distribution of permissive intrusive and extrusive rocks used to define tract 142pCu9013, Chagai—Afghanistan, Iran, and Pakistan.....	135
46.	Cumulative frequency plot showing the results of Monte Carlo simulation of undiscovered resources in porphyry copper deposits in tract 142pCu9013, Chagai—Afghanistan, Iran, and Pakistan.....	140
47.	Map showing the location of known porphyry copper deposits and prospects for permissive tract 142pCu9014, Azerbaijan—Armenia, Azerbaijan, Iran, and Turkey.....	142
48.	Map showing the distribution of permissive intrusive and extrusive rocks used to define tract 142pCu9014, Azerbaijan—Armenia, Azerbaijan, Iran, and Turkey.....	144
49.	Cumulative frequency plot showing the results of Monte Carlo computer simulation of undiscovered resources in porphyry copper deposits in tract 142pCu9014, Azerbaijan—Armenia, Azerbaijan, Iran, and Turkey.....	150
50.	Map showing the location of known porphyry copper deposits and prospects for permissive tract 142pCu9015, Yazd—Iran.....	158
51.	Map showing the distribution of permissive intrusive and extrusive rocks used to define tract 142pCu9015, Yazd—Iran.....	159
52.	Cumulative frequency plot showing the results of Monte Carlo simulation of undiscovered resources in porphyry copper deposits in tract 142pCu9015, Yazd—Iran.....	164

53. Map showing the location of known porphyry copper deposits and prospects for permissive tract 142pCu9016, Kerman—Iran.....	166
54. Map showing the distribution of permissive intrusive and extrusive rocks used to define tract 142pCu9016, Kerman—Iran.....	167
55. Cumulative frequency plot showing the results of Monte Carlo simulation of undiscovered resources in porphyry copper deposits in tract 142pCu9016, Kerman—Iran.....	175
56. Map showing the location of known porphyry copper prospects for permissive tract 142pCu9017, Plio-Quaternary—Afghanistan, Armenia, Azerbaijan, Georgia, Iran, Pakistan, Russian Federation, and Turkey.....	176
57. Map showing the distribution of permissive intrusive and extrusive rocks used to define tract 142pCu9017, Plio-Quaternary—Afghanistan, Armenia, Azerbaijan, Georgia, Iran, Pakistan, Russian Federation, and Turkey.....	178
58. Preservation and exposure levels of the 26 porphyry copper tracts and sub-tracts in the Tethys region of western and southern Asia.....	188
59. Summary of probabilistic assessment results by permissive tract for the Tethys region of western and southern Asia.....	194

Tables

1. Permissive tracts for porphyry copper deposits in the Tethys region of western and southern Asia.....	10
2. Porphyry copper deposits of the Tethys region of western and southern Asia.....	40
3. Statistical test results for grade and tonnage model selection for porphyry copper deposits in the Tethys region of western and southern Asia.....	48
4. Probabilistic assessment for tract 142pCu9001, Cimmeride Lesser Caucasus—Armenia, Azerbaijan, Georgia, and Iran.....	64
5. Probabilistic assessment for tract 142pCu9004, Pontide (Asia)—Armenia, Azerbaijan, Georgia, Iran, and Turkey.....	70
6. Probabilistic assessment for tract 142pCu9005, Anatolide-Tauride—Armenia, Azerbaijan, Iran, and Turkey.....	84
7. Probabilistic assessment for tract 142pCu9007, Border Folds—Iran, Iraq, and Turkey..	102
8. Probabilistic assessment for tract 142pCu9008, Esfahan—Iran, Iraq, and Turkey.....	109
9. Probabilistic assessment for tract 142pCu9009, Khorasan—Afghanistan and Iran.....	117
10. Probabilistic assessment for tract 142pCu9010, Lut Tertiary—Iran.....	125
11. Probabilistic assessment for tract 142pCu9012, Sistan—Afghanistan, Iran, and Pakistan.....	132
12. Probabilistic assessment for tract 142pCu9013, Chagai—Afghanistan, Iran, and Pakistan.....	140
13. Probabilistic assessment for tract 142pCu9014, Azerbaijan—Armenia, Azerbaijan, Iran and Turkey.....	148
14. Probabilistic assessment for tract 142pCu9015, Yazd—Iran.....	164
15. Probabilistic assessment for tract 142pCu9016, Kerman—Iran.....	175
16. Summary of estimates of numbers of undiscovered deposits, numbers of known deposits, tract areas, and deposit densities for the porphyry copper assessment of the Tethys region of western and southern Asia.....	191
17. Summary of simulations of undiscovered resources in porphyry copper deposits and comparison with identified copper and gold resources in porphyry copper deposits within each permissive tract, Tethys region of western and southern Asia.....	192

Conversion Factors

Inch/Pound to SI

Multiply	By	To obtain
Length		
inch (in)	25,400.0	micrometer (μm)
foot (ft)	0.3048	meter (m)
mile (mi)	1.609	kilometer (km)
yard (yd)	0.9144	meter (m)
Area		
acre	0.4047	hectare (ha)
acre	0.004047	square kilometer (km^2)
square mile (mi^2)	259.0	hectare (ha)
square mile (mi^2)	2.590	square kilometer (km^2)
Mass		
ounce, troy (troy oz)	31.103	gram (g)
ounce, troy (troy oz)	0.0000311	megagram (Mg)
ton, short (T) (2,000 lb)	0.9072	megagram (Mg)
Pressure		
kilobar (kb)	100,000	kilopascal (kPa)

SI to Inch/Pound

Multiply	By	To obtain
Length		
micrometer (μm)	0.00003937	inch (in)
meter (m)	3.281	foot (ft)
kilometer (km)	0.6214	mile (mi)
meter (m)	1.094	yard (yd)
Area		
hectare (ha)	2.471	acre
square kilometer (km^2)	247.1	acre
hectare (ha)	0.003861	square mile (mi^2)
square kilometer (km^2)	0.3861	square mile (mi^2)
Mass		
gram (g)	0.03215	ounce, troy (troy oz)
megagram (Mg)	1.102	ton, short (2,000 lb)
megagram (Mg)	0.9842	ton, long (2,240 lb)
Pressure		
kilopascal (kPa)	0.00001	megagram (Mg)
Other conversions used in this report		
centimeter per year (cm/yr)	2.54	inch per year (in/yr)
metric ton (t)	1	megagram (Mg)
troy ounce per short ton	34.2857	gram per metric ton (g/t)
percent (%)	10,000	part per million (ppm) or grams per metric ton (g/t)
percent metal	$0.01 \times$ metal grade, percent \times ore tonnage, metric tons	metric tons of metal

Acronyms and Abbreviations Used

ASTER	Advanced Spaceborne Thermal Emission and Reflection Radiometer
Bt	billion metric tons
GIS	geographic information system
g/t	grams per metric ton
IOCG	iron oxide-copper-gold
JORC	Australian Joint Ore Reserves Committee (or the Australian Code for Reporting of Exploration Results, Mineral Resources, and Ore Reserves)
kt	thousand metric tons
Ma	millions of years before present
MMAJ	Mining Metal Agency of Japan
MoS₂	molybdenum disulfide
MORB	mid-ocean ridge basalt
Mt	million metric tons
MTA	Republic of Turkey General Directorate of Mineral Research and Exploration
MVT	Mississippi Valley type
m.y.	million years
NA	not applicable
OIB	oceanic island basalt
REE	rare-earth elements
VMS	volcanogenic massive sulfide
SEDEX	sedimentary exhalative
SSIB	small-scale digital boundaries
t	metric ton (tonne) or megagram (Mg)
USGS	U.S. Geological Survey

Chemical Symbols Used

Ag	silver	Nd	neodymium
Al	aluminum	Ni	nickel
Ar	argon	Os	osmium
Au	gold	Pb	lead
Ba	barium	Re	rhenium
Bi	bismuth	Rb	rubidium
Co	cobalt	Sb	antimony
Cr	chromium	Sm	samarium
Cu	copper	Sn	tin
F	fluorine	Sr	strontium
Fe	iron	Th	thorium
K	potassium	W	tungsten
K₂O	potassium oxide	U	uranium
Mn	manganese	Zn	zinc
Mo	molybdenum		

This page left intentionally blank.

Porphyry Copper Assessment of the Tethys Region of Western and Southern Asia

By Lukas Zürcher¹, Arthur A. Bookstrom², Jane M. Hammarstrom³, John C. Mars³, Steve Ludington⁴, Michael L. Zientek², Pamela Dunlap¹, and John C. Wallis² with contributions from Lawrence J. Drew³, David M. Sutphin³, Byron R. Berger⁵, Richard J. Herrington⁶, Mario Billa⁷, Ilkay Kuşcu⁸, Charles J. Moon⁹, and Jeremy P. Richards¹⁰

Abstract

A probabilistic mineral resource assessment of undiscovered resources in porphyry copper deposits in the Tethys region of western and southern Asia was carried out as part of a global mineral resource assessment led by the U.S. Geological Survey (USGS). The purpose of the study was to delineate geographic areas as permissive tracts for the occurrence of porphyry copper deposits at a scale of 1:1,000,000 and to provide probabilistic estimates of amounts of copper likely to be contained in undiscovered porphyry copper deposits in those tracts. The team did the assessment using the USGS three-part form of mineral resource assessment, which is based on (1) mineral deposit and grade-tonnage models constructed from known deposits as analogs for undiscovered deposits, (2) delineation of permissive tracts based on geoscientific information, and (3) estimation of numbers of undiscovered deposits.

The assessment area includes the Asian part of Turkey and Georgia, Armenia, Azerbaijan, Iran, western Pakistan, and southwestern Afghanistan. Selected tracts also extend marginally into southwesternmost Russia and northeasternmost Iraq. This region is located in the central part of the larger Tethyan Eurasian Metallogenic Belt, which extends from western Europe to eastern Asia. Mining in this part of the Tethyan Eurasian Metallogenic Belt has occurred for thousands of years; in 2011 the region produced 420,000 metric tons (t) of copper (2.6 percent of

global production), 8,300 t of molybdenum (3 percent), and 29,600 kilograms of gold (1 percent).

The assessment team defined 26 tracts permissive for Late Triassic to Holocene porphyry copper-molybdenum and porphyry copper-gold deposits. Permissive tracts range in extent from 2,960 to 194,000 square kilometers (km²) and cover a total area of 924,000 km². Younger tracts overlap older tracts in several areas. Three permissive tracts include sub-tracts in order to separate tract segments on the basis of geography, data quality, or likelihood of occurrence of undiscovered deposits. About 65 percent of all known porphyry sites occur in only five tracts, which also host most of the identified copper resources. In terms of tectonic setting, 58 percent of the permissive tracts are related to continental arcs; 19 percent to island arcs or back arcs; and 24 percent to postcollisional settings. Of the known porphyry copper deposits, subequal fractions are spread among these three settings.

The spatial distribution of known porphyry deposits and prospects is also related to the level of erosion. Magmatic belts with numerous known porphyry sites exhibit subequal areas of coeval plutonic and volcanic units and lesser amounts of cover rocks. Belts with fewer known porphyry sites display either high or low volcanic-to-plutonic ratios and (or) greater cover, indicating crustal levels that are too shallow or too deep for exposure of porphyry deposits.

Probabilistic estimates of numbers of undiscovered porphyry copper deposits were made for 18 of the 26 tracts. The undiscovered porphyry copper endowment for 8 tracts is discussed qualitatively.

The assessment estimates that the Tethys region contains 47 undiscovered deposits within 1 kilometer of the surface. Probabilistic estimates of numbers of undiscovered deposits were combined with grade and tonnage models in a Monte Carlo simulation to estimate probable amounts of contained metal. The 47 undiscovered deposits are estimated to contain a mean of 180 million metric tons (Mt) of copper distributed among the 18 tracts for which probabilistic estimates were made, in addition to the 62 Mt of copper already identified in the 42 known porphyry deposits in the study area. Results of Monte Carlo simulations show that 80 percent of the estimated undiscovered porphyry copper resources in the Tethys region are located in four tracts or sub-tracts.

¹U.S. Geological Survey, Tucson, Arizona, United States.

²U.S. Geological Survey, Spokane, Washington, United States.

³U.S. Geological Survey, Reston, Virginia, United States.

⁴U.S. Geological Survey, Menlo Park, California, United States.

⁵U.S. Geological Survey, Denver, Colorado, United States.

⁶Natural History Museum, London, England.

⁷Bureau de Recherches Géologiques et Minières, Orléans, France.

⁸University of Muğla, Muğla, Turkey.

⁹Camborne School of Mines, Cornwall, England, United Kingdom.

¹⁰University of Alberta, Edmonton, Alberta, Canada.

Introduction

The Tethyan Eurasian Metallogenic Belt that extends from eastern Europe to western Asia marks the location of the former Neotethys Ocean that existed between the continents of Gondwana and Eurasia during the Mesozoic and Cenozoic eras (fig. 1; Janković, 1977; Janković and Petrascheck, 1987). The approximately 10,000-kilometer (km)-long Tethyan Eurasian Metallogenic Belt hosts porphyry, replacement, massive sulfide, and epithermal deposits. This study focuses on Late Triassic to Holocene porphyry copper mineralization in the central part of the belt; the Tethys region of western and southern Asia, extending from west to east across Turkey, Georgia, Armenia, Azerbaijan, Iran, western Pakistan, and southwestern Afghanistan (fig. 2).

The Tethys region of western and southern Asia hosts 4 giant¹¹ porphyry copper deposits—Reko Diq in Pakistan, Sar Cheshmeh and Sungun in Iran, and Kadjaran in Armenia—as well as 38 other porphyry deposits with reported grades and tonnages. Porphyry copper systems in the region span the spectrum of gold-copper (Au-Cu), copper-gold (Cu-Au), copper-molybdenum (Cu-Mo), molybdenum-copper (Mo-Cu), and molybdenum-copper-gold (Mo-Cu-Au) types. These porphyry systems formed as a result of the protracted history of tectono-magmatic events (subduction-related arc and back-arc events, as well as events not related to subduction) associated with convergence of several microcontinents of Gondwanan affinity with the Eurasian Plate during the closing of the Neotethys Ocean.

Background

The assessment of undiscovered resources in porphyry copper deposits in the Tethys region of western and southern Asia was done as part of a U.S. Geological Survey (USGS)-led global mineral resource assessment. This study complements porphyry copper assessments of the Tethys region of Europe (Sutphin and others, 2013) and the Tethys region of Afghanistan (Peters and others, 2011).

The assessment of undiscovered resources in porphyry copper deposits in the Tethys region of western and southern Asia began with a series of workshops led by a USGS team and international experts on the region from the Centre for Russian and Central EurAsian Mineral Studies (CERCAMS) of the Natural History Museum in London, Bureau de Recherches Géologiques et Minières (BRGM), the University of Muğla in Turkey, the Camborne School of Mines in England, and the University of Alberta in Canada. A preliminary assessment workshop was held in 2008 at the Natural History Museum in London to review the geology and evaluate available data. Preliminary results were presented at the 2009 Annual Meeting of the Geological Society of America (Drew and others, 2009; Sutphin, 2009). New data were acquired, and the results of the preliminary assessment were updated and revised by a USGS team in 2012, and they were further refined after internal USGS review in 2013.

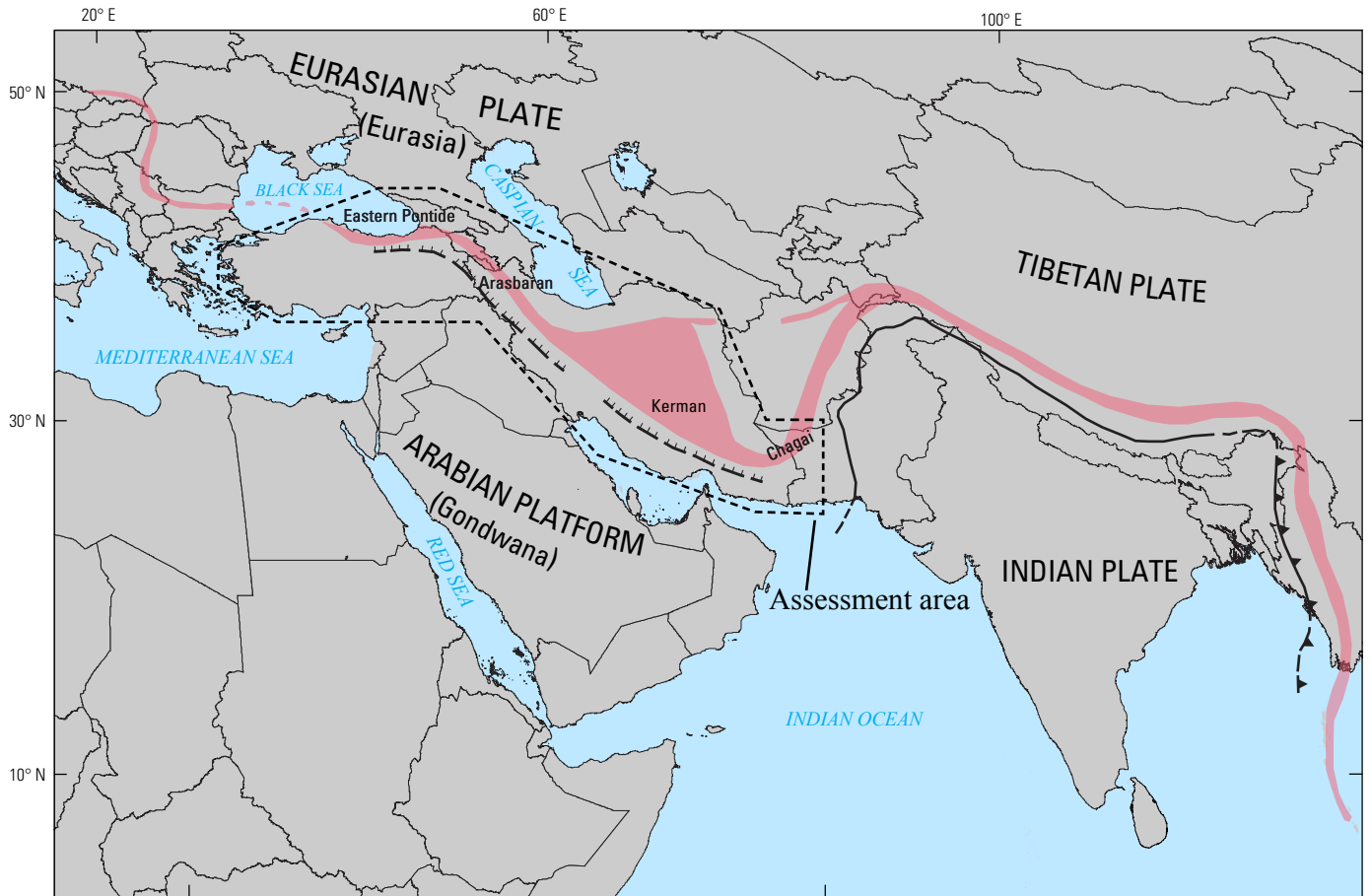
The assessment of undiscovered resources in porphyry copper deposits in the Tethys region was done using the three-part form of mineral-resource assessment, which consists of the following: (1) application of descriptive (Cox, 1986a, b; Berger and others, 2008; John and others, 2010) and grade-tonnage mineral deposit models (Singer and others, 2008), (2) delineation of permissive tracts, and (3) estimation of numbers of undiscovered deposits (Singer, 1993; Singer and Menzie, 2010). In this form of assessment, grade-tonnage mineral deposit models constructed from known deposits are used as analogs for undiscovered deposits. Researchers, guided by the descriptive deposit model, used geologic, geochemical, and geophysical features typically associated with porphyry copper deposits to delineate geographic areas as permissive tracts¹² for the occurrence of porphyry copper deposits. For selection of the best grade-tonnage model for assessment, we compared the grades and tonnages of known deposits within a permissive tract with grade and tonnage models using statistical tests. Metal associations reported for prospects that lack reliable resource data, along with other geologic information, contribute to selection of the appropriate model for assessment. Available data are evaluated and estimates of numbers of undiscovered deposits in each permissive tract are made at different confidence levels to express the probability that some fixed but unknown (that is, undiscovered) number of deposits exist within the tract (Singer, 2007a). Knowledge about the extent of exploration influences the estimation of numbers of undiscovered deposits in a permissive tract. Accordingly, these estimates reflect both the uncertainty of what may be present and a measure of the geologic favorability of the existence of the deposit type under consideration. Estimates can be based on, or compared to, estimates from deposit density models based on well-explored control tracts from around the world (Singer and others, 2005; Singer, 2008; Singer and Menzie, 2010). Results of estimates at the different confidence levels are combined with grade and tonnage models in a Monte Carlo simulation to produce a probabilistic estimate of undiscovered resources (Root and others, 1992).

In addition to providing probabilistic estimates of amounts of copper contained in undiscovered porphyry copper deposits for 18 permissive tracts and sub-tracts, this report includes tract by tract descriptions of the tectonic setting, associated magmatism and its geochemical affinity, the mineralization styles of representative porphyry deposits and prospects, and the preservation-erosion record for the 26 tracts and sub-tracts defined in the assessment area. The report includes a digital geographic information system (GIS) that includes the tract outlines, a database of porphyry deposits, porphyry and porphyry-related prospects, possible porphyry-related occurrences, and a table of references.

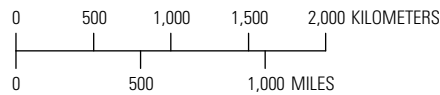
This study contributes to the understanding of the distribution and nature of magmatism and associated porphyry mineralization in the Tethys region of western and southern

¹¹Greater than 2 million metric tons (Mt) of contained copper.

¹²Tracts are assigned unique identifiers based on United Nations region designations (142 for Asia), deposit type (pCu for porphyry copper), and a four digit number (for example, 9000).



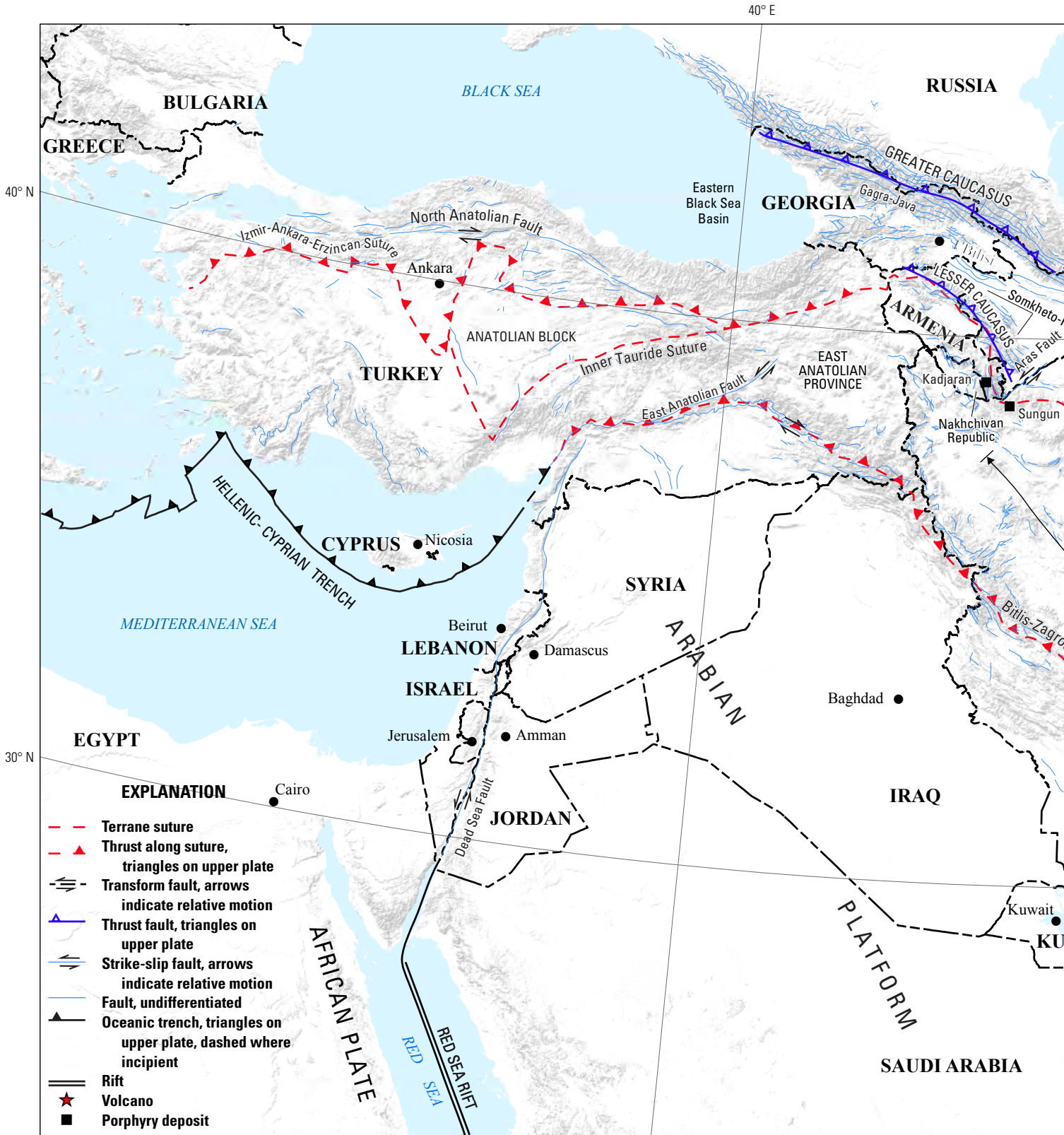
Political boundaries from U.S. Department of State (2009).
 Flat Polar Quartic Projection.
 Central meridian, 0°.



Modified from Janković, 1977

- EXPLANATION**
- Tethyan Eurasian Metallogenic Belt
 - Study area boundary
 - Chagai Named porphyry belt, generally located
 - Himalayan suture belt
 - Indoburman—Sunda subduction zone
 - Ophiolite belt in Iran and Anatolia

Figure 1. Map showing the Tethyan Eurasian Metallogenic Belt (modified from Janković, 1977) and extent of the assessment area in the Tethys region of western and southern Asia.



Base from SRTM Global Digital Elevation Model, U.S. Geological Survey EROS Data Center, 2006.
 Political boundaries from U.S. Department of State (2009).
 Asia North Albers Equal-Area Conic Projection.
 Central meridian, 50° E., latitude of origin, 35° N.

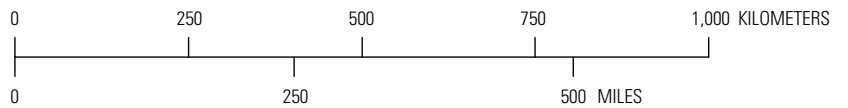
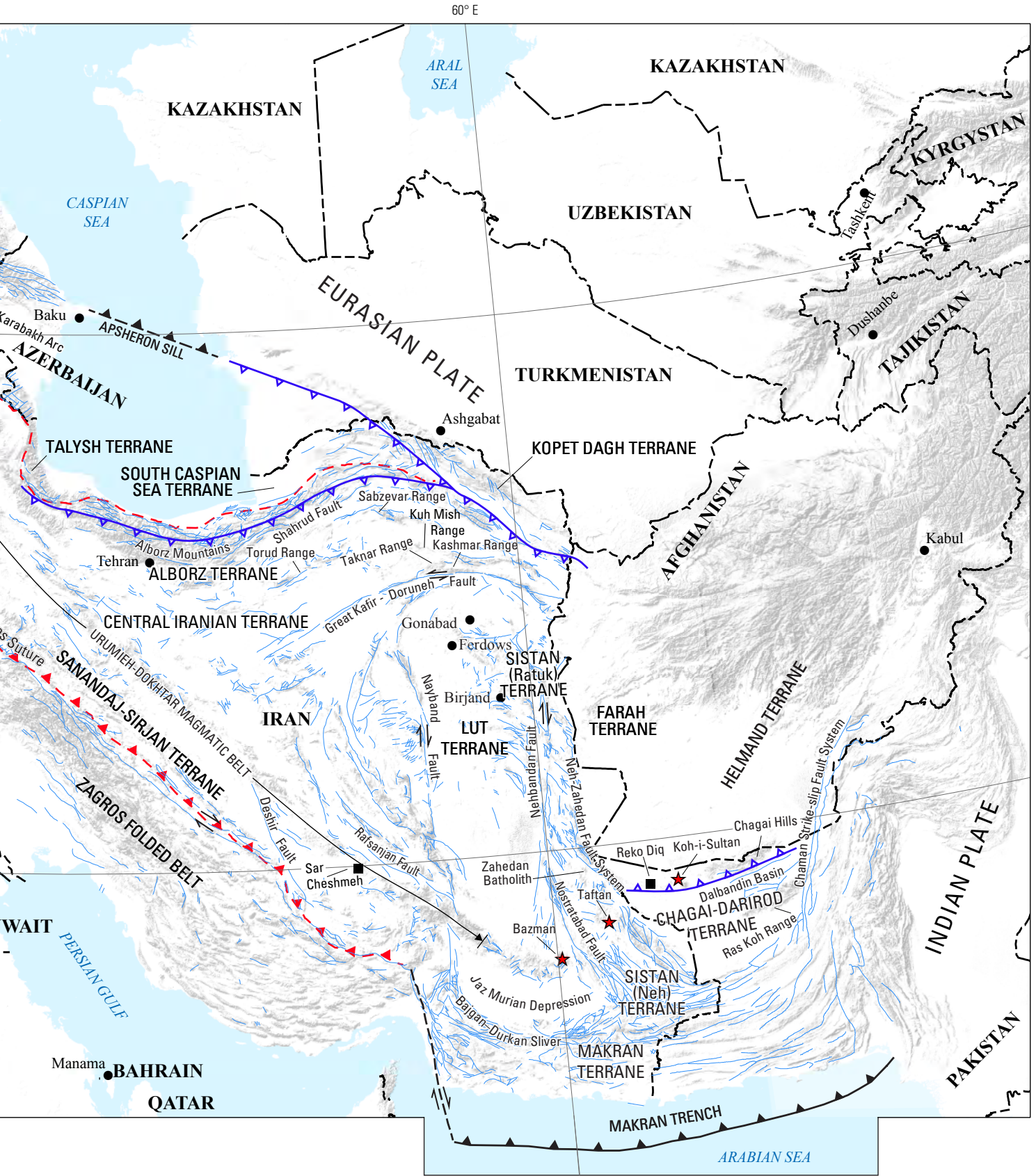


Figure 2. Map showing major sutures, faults, and geologic and geographic features in the Tethys region of western and southern Asia (assessment area) and vicinity on a digital elevation base.



Asia, an area that is receiving renewed attention from the minerals industry. It also provides an improved framework for establishing comparisons with other porphyry copper belts worldwide.

Report Format

This report begins with an introduction to models for porphyry copper deposits, a description of the permissive tract concept, and reviews of the tectono-magmatic evolution and the neotectonic setting of the assessment region. These introductory sections provide a framework for the diverse environments of porphyry copper formation and their present-day setting in the study area. The next sections describe the information used in this assessment, including the geologic maps, the porphyry deposit and prospect database, an account of the exploration history based on available information, the processed Advanced Spaceborne Thermal Emission and Reflection Radiometer (ASTER) alteration and regional magnetic anomaly maps, and level of preservation and exposure data. A section on assessment methodology describes the processes used for delineation of permissive tracts and estimation of numbers of undiscovered deposits, as well as application of statistical tests and use of Monte Carlo simulation to estimate total contained resources.

Subsequent sections of the report offer tract-by-tract descriptions of the tectonic setting, magmatism, characteristics of the porphyry deposits and prospects in the tract, exhumation and burial history, available geophysical and remote sensing data, and probabilistic assessment results. These tract descriptions are generally organized by geologic age, from oldest to youngest. The last section of the report includes a discussion and a summary of results.

The principal sources of information used in the assessment of each tract are listed in appendix A. The geologic map units that formed the basis for delineation of each permissive tract are listed in appendix B, along with references to the source maps. Known porphyry copper deposits and prospects identified in the Tethys region of western and southern Asia are tabulated in appendix C. Permissive tract boundaries, point locations, and descriptions of deposits and prospects are included in the spatial data described in appendix D. Brief biographical information about the participants in this assessment is provided in appendix E.

Considerations for Users of this Assessment

Assessment products represent a synthesis of information available at the time of the assessment. Ideally, assessments are done on a recurring basis and at a variety of scales because available data change over time. This assessment is based on the descriptive and grade and tonnage data contained in published mineral-deposit models (Cox, 1986a; Berger and others, 2008; John and others, 2010; Singer and others, 2008). Data in the grade and tonnage models represent grades of each

commodity of possible economic interest and tonnages based on the total of production, reserves, and resources at the lowest cutoff grade available at the time of model construction. The economic viability of the deposits used to construct the models varies widely, so care must be exercised when using the results of this assessment to answer questions that involve economics.

Estimates are of numbers of deposits that are likely to exist, not necessarily those likely to be discovered (Singer, 2007b). These probable deposits are referred to here by the term “undiscovered deposits.” Undiscovered deposits include unidentified deposits in new exploration areas and may also include known prospects that may become discovered deposits after further exploration.

This assessment considers the probability for concealed deposits within 1 km of the Earth’s surface. Very high grade deposits may be exploited at greater depths. However, if discovered, the costs and logistics related to mining a deeply buried porphyry deposit might prohibit the deposit’s development into a mine given current or near-term metal prices and technologies.

Permissive tracts are defined by geologic units, irrespective of political boundaries; therefore, tracts may cross country boundaries and (or) include lands that already have been developed for other uses or have been withdrawn from mineral development as protected areas. The tracts are constructed at a scale of 1:1,000,000 and are not intended for use at larger scales.

Terminology

The terminology used in this study follows the definitions used in the 1998 USGS assessment of undiscovered deposits of gold, silver, copper, lead, and zinc in the United States (U.S. Geological Survey National Mineral Resource Assessment Team, 2000 [Circular 1178]; U.S. Bureau of Mines and U.S. Geological Survey, 1980 [Circular 831]; Bates and Jackson, 1987 [Glossary of Geology (3rd ed.)]). This terminology is consistent with standard definitions and general usage by the resource assessment community. As such, it may not conform to more recently adopted definitions of terms for estimating mineral resources and mineral reserves, and for reporting exploration information to comply with legal mandates (Committee for Mineral Reserves International Reporting Standards, 2006). A list of definitions of selected terms is included below.

- **Calc-alkaline, calc-alkalic; alkaline, alkalic**—These terms are used in a general, nonrigorous manner to refer to igneous rocks of granitoid composition (calc-alkaline or calc-alkalic) and of syenitoid through dioritoid to gabbroid composition (alkaline or alkalic) and their volcanic equivalents (see Le Maitre and others, 2002, provisional field classifications, figs. 2.10 and 2.19). In the igneous literature, the terms “-alkaline” and “-alkalic” are defined and used in multiple and inconsistent ways (see Arculus, 2003). In this study, the term calc-alkalic is used synonymously for calc-alkaline,

and alkalic is used synonymously for alkaline, as well as for their associated deposits, which are classified as calc-alkaline (or calc-alkalic) or alkaline (or alkalic) porphyry copper deposit subtypes.

- **Cover**—Younger unconsolidated sediments, or consolidated rocks that overlie older rocks and associated mineral occurrences, or tectonically displaced rocks that may overlie deposits.
- **Deposit density model**—Frequency distribution of number of deposits from the grade and tonnage model per unit of permissive control area. These models are commonly applied in a regression of number of deposits versus permissive area. These models are used to make estimates of number of deposits or as a guide for making estimates (Singer, written commun., June 7, 2007).
- **Descriptive mineral deposit model**—A set of data available in a convenient, standardized form that describes a group of mineral deposits having similar characteristics. Descriptive models are the primary source of guidance for linking geoscience information to deposit types in the delineation of permissive tracts.
- **Geologic favorability**—A relative measure of the likelihood that an undiscovered mineral deposit could occur in a particular permissive setting.
- **Giant deposit (synonym, world-class deposit)**—A mineral deposit whose contained metal content ranks in the upper 10 percent of all known deposits. Accordingly, giant gold deposits contain at least 100 metric tons (t) of gold, giant silver deposits contain more than 2,400 t (77 million troy ounces, troy oz) of silver, and giant copper, zinc, and lead deposits contain at least 2, 1.7, and 1 million metric tons (Mt) of their respective metals (Singer, 1995).
- **Grade and tonnage model**—Frequency distributions of the grades and sizes of thoroughly explored, and (or) completely mined out, individual mineral deposits that are classified by a descriptive mineral deposit model. Grade-and-tonnage models occupy the position of being both a kind of deposit model and one of the three parts of an assessment. They are employed as analogs for grades and tonnages of undiscovered deposits of the same type in geologically similar settings.
- **Identified resources**—Resources whose location, quality, and quantity are known or can be estimated from specific geologic evidence. For this assessment, identified resources are the deposits that constitute the grade and tonnage models used (which can include measured, indicated, and inferred mineral resources at the lowest available cutoff grade). In addition, identified resources in deposits that are not included in the models used for the assessment may be considered if they are characterized well enough by deposit type, grade, and tonnage to meet U.S. Securities and Exchange Commission or CRIRSCO¹³ reporting guidelines.
- **Mineral deposit**—A mineral concentration of sufficient size and grade that it might, under the most favorable of circumstances, be considered to have potential for economic development.
- **Mineral occurrence**—(1) A concentration of a mineral that is considered valuable by someone somewhere, or that is of scientific or technical interest (Cox and Singer, 1986). (2) Any ore or economic mineral in any concentration found in bedrock or as float; especially a valuable mineral in concentration sufficient to suggest further exploration (Bates and Jackson, 1987).
- **Mineral prospect**—(1) An area that is a potential site of a mineral deposit, based on mineral exploration (Bates and Jackson, 1987). (2) An area that has been explored in a preliminary way but has not given evidence of economic value (Bates and Jackson, 1987). (3) An area to be searched by some investigative technique; for example, geophysical prospecting (Bates and Jackson, 1987). (4) A geologic or geophysical anomaly, especially one recommended for additional exploration (Bates and Jackson, 1987). (5) A mineral property whose value has not been proved by exploration (Bureau of Land Management, BLM, 2015).
- **Mineral resource assessment**—A study that estimates or evaluates the amount and (or) potential supply of mineral resources within a specific volume of the Earth's crust.
- **Mineralization**—(1) Any single mineral or combination of minerals occurring in a mass, or deposit, of economic interest. The term is intended to cover all forms in which mineralization might occur, whether by class of deposit, mode of occurrence, genesis, or composition (Committee for Mineral Reserves International Reporting Standards, 2006). (2) The process or processes by which a mineral or minerals are introduced into a rock, resulting in a valuable or potentially valuable deposit (Bates and Jackson, 1987).
- **Number of undiscovered mineral deposits estimates**—The probability, or degree of belief, that a fixed but unknown number of deposits like those in the grade and tonnage model exist in the delineated tracts (Singer and Menzie, 2005).
- **Permissive tract**—The surface projection of a volume of rock where the geology permits the existence of a mineral deposit of a specified type. The probability of deposits of the type being studied occurring outside the tract is negligible (that is, less than 1 in 100,000 or 1 in 1,000,000 [Singer and Menzie, 2010]).

¹³Committee for Mineral Reserves International Reporting Standards (2006); <http://www.criirco.com/welcome.asp>.

- **Permissive unit**—Geologic rock unit of a given age range and distinctive lithological character or compositional affinity emplaced in a particular geologic setting. The lithological character or compositional affinity and geologic setting are permissive for the occurrence of a mineral deposit of a specific type. The collection of units sharing these characteristics form the basis for defining a permissive tract.
- **Plutonic**—The term commonly applies to igneous bodies that have crystallized at relatively great depths of the Earth’s crust. For this assessment, the term plutonic is used in a more general way to designate any holocrystalline intrusive rock.
- **Quantitative assessment of undiscovered resources**—A study that presents a numerical estimate of the amount and quality of undiscovered mineral resources present within a specific volume of the Earth’s crust; because of the uncertainty inherent in assessment of an unknown resource, the results are presented probabilistically (Singer, written commun., 2008).
- **Reserve**—That part of a mineral deposit that could be economically and legally extracted or produced at the time of reserve determination.
- **Resource**—A concentration of naturally occurring solid, liquid, or gaseous material in or on the Earth’s crust in such a form that economic extraction of a commodity from the concentration is currently or potentially feasible (U.S. Bureau of Mines and U.S. Geological Survey, 1980).
- **Resource uncertainty**—Uncertainty means variability or being unknown; in mineral resource assessments it refers to possible locations of undiscovered resources and to the amounts and qualities of these resources. Location uncertainty is addressed by permissive tracts and uncertainty of amounts and qualities is addressed by estimates of undiscovered deposits and grade and tonnage models (Schulz, written commun., 2002).
- **Undiscovered mineral deposit**—(1) A mineral deposit that may exist within a specified volume of Earth’s crust. (2) An incompletely explored mineral occurrence or prospect that could have sufficient size and grade to be classed a deposit. (3) A mineral deposit whose location and (or) grade, quality, and quantity of mineralized material are unknown or incompletely characterized.
- **Undiscovered resources**—(1) Resources in undiscovered mineral deposits whose existence is postulated on the basis of indirect geologic evidence (U.S. Geological Survey National Mineral Resource Assessment Team, 2000). (2) Mineralized material whose location, grade, quality, and quantity are unknown or incompletely characterized. Undiscovered resources may include active mines if the resource is delineated incompletely. For example, a deposit that is explored only partially and reported as “open to the

west or open at depth” could be counted as an undiscovered deposit. Undiscovered resources in extensions to identified resources are not addressed explicitly in the assessment process.

- **Volcanic**—This term commonly applies to rocks that have vented onto the Earth’s surface, either extruded as lava, or ejected explosively as proximal pyroclastic or distal ash materials. For this assessment, the term volcanic refers to both hyalocrystalline extrusive (for example, lava flow) or subvolcanic intrusive rocks (for example, dacite porphyry dike).

Porphyry Copper Deposit Models

Porphyry copper deposits typically form in subduction-related compressional tectonic settings during active subduction of oceanic crust (Sillitoe, 2010; John and others, 2010). These deposits are commonly associated with shallowly emplaced calc-alkaline plutons. The Andes Mountains of South America are a classic continental arc-related porphyry deposit province (Kay and others, 1999). Magma associated with these deposits is typically hydrous, oxidized, rich in sulfur, and has likely undergone complex evolution (Richards and others, 2011; John and others, 2010). Island arcs in the southwest Pacific Ocean are the archetypes of island-arc-related porphyry mineralization (Garwin and others, 2005). Igneous rocks associated with island-arc porphyry deposits are similar to those associated with continental arcs, but diorite, quartz diorite, and other more mafic rocks are comparatively more abundant (Kesler and others, 1975).

In recent years, evidence has accumulated for the existence of a family of porphyry deposits that formed in a significantly different tectonic setting—extensional, transtensional, or transpressional regimes that have evolved within relatively cratonized regions after active subduction has ceased. Several porphyry deposits in Turkey, the Lesser Caucasus, and Iran may represent examples of this family (Hou and others, 2011). Their geology and mineralization style are broadly similar to subduction-related porphyry copper deposits; however, the magmas that are associated with them originated from as-yet only partially understood mantle-involved processes (Richards, 2009; Richards and Kerrich, 2007).

Descriptive Models

Descriptive models are the basis for linking geoscience information to deposit types and the delineation of permissive tracts. Descriptive deposit models identify the tectonic setting, geologic units, and metals associated with a mineral deposit type. Models used for this assessment include the descriptive porphyry copper models of Singer and others (2008), Cox (1986a, b), and John and others (2010). The recent reviews of salient features of porphyry deposits by Seedorff and others (2005) and Sillitoe (2010) were also considered.

Grade and Tonnage Models

Grade and tonnage models constructed from data for porphyry copper deposits from around the world are employed as analogs of grades and tonnages of undiscovered deposits of the same type in geologically similar settings. The grade and tonnage models of Singer and others (2008) were used in this assessment. In addition to the general porphyry Cu-Mo-Au model that is based on data from 422 deposits from around the world, the porphyry Cu-Au and Cu-Mo subtype models, which are based on subsets of the grade and tonnage data, were also used where classification criteria permit. The Cu-Mo subtype model includes 51 porphyry deposits that have Au/Mo ratios that are less than or equal to 3 or average molybdenum grades that are greater than 0.03 percent. The Cu-Au subtype model consists of 115 porphyry deposits that have Au/Mo ratios greater than 30 or average gold grades greater than 0.2 gram per metric ton (g/t) (Singer and others, 2008). For each tract, if sufficient grade and tonnage data were available, we tested the known deposits in the tract against the selected model using statistical tests (Student's *t*-test or analysis of variance) to determine the appropriate model to apply for quantitative assessment.

Deposit Density Models

Estimates of numbers of deposits made by the assessment team for each permissive tract were compared with numbers of undiscovered deposits predicted by mineral deposit density models. Density models provide an independent measure of expected numbers of deposits and serve as a guide in the estimation of expected numbers of deposits at different confidence levels (Singer and others, 2005; Singer, 2008; Singer and Menzie, 2010). The porphyry copper deposit density model of Singer and Menzie (2010) was used in this assessment.

Permissive Porphyry Copper Tracts

Subduction-related continental arc, island-arc, back-arc, or post-subduction magmatic events of a given age range are permissive settings for the occurrence of porphyry copper deposits. Descriptive deposit models characterize porphyry copper deposits as hydrothermal systems that are spatially and temporally associated with apical, generally porphyro-aphanitic, parts of felsic to intermediate stocks that were emplaced at depths that are typically between 1 and 5 km.

A permissive porphyry tract is the surface projection of a volume of rock where the geology permits the existence of a porphyry copper deposit. The probability of this deposit type occurring outside the tract is negligible. A magmatic setting is the fundamental geologic feature that delineates the geographic area occupied by permissive porphyry tract. Accordingly, volcanic and plutonic rocks of felsic to intermediate calc-alkaline to alkaline composition related to this magmatic setting are the geologic units that define the permissive tract. These geologic rock units

of particular compositional affinity that are emplaced in a specific geologic setting of a given age range are referred to as “permissive units.” To ensure inclusion of shallowly buried but otherwise potentially accessible porphyry copper deposits, the aerial extent of tracts not only encompasses geologic map units, but extensions of these geologic map units likely are present under less than 1 km of cover.

An effort was made to name permissive tracts and sub-tracts according to usage in the literature (for example, Border Folds, Chagai, Konya, Makran, Pontide, and Sistan). However, where names are not available or known, or do not appropriately outline the extent of the associated tectono-magmatic event, tracts and sub-tracts are named to identify their location within a major tectonic unit (for example, Sanandaj-Sirjan), and are followed by a general geographic descriptor where needed (for example, Anatolide-Tauride—Western Turkey). Where tracts of different ages are superimposed, names reflect their location within the major tectonic unit and are followed by a general age descriptor (for example, Lut Jurassic, Lut Cretaceous, Lut Tertiary). For large tracts that include tectonic units across the region, names were selected to convey the age, nature, and (or) location of the tectono-magmatic event (for example, Pliocene-Quaternary—Postcollisional, Cimmeride Lesser Caucasus, Cimmeride Greater Caucasus). Finally, where an unnamed tectono-magmatic setting lies generally within a province or the nature of a setting varies across the assessment region, the name of a province covered by the tract was used instead (for example, Khorasan) followed by a general geographic descriptor where needed (for example, Azerbaijan—Caucasus-Iran).

Tectono-Magmatic Framework of the Tethys Region of Western and Southern Asia

The following synopsis of the tectonic evolution and associated magmatism of the Tethys region of western and southern Asia provides the geologic framework and basis for delineation of the 26 permissive tracts and sub-tracts identified in the assessment area (table 1). These tracts delineate the Late Triassic to Holocene porphyry belts associated with magmatic events related to the opening and closing of the Neotethys Ocean. Middle Triassic and older magmatic events related to the opening and closing of the Paleotethys Ocean are not treated in this assessment.

The Eurasian active margin and the Arabian passive margin played major roles in the tectono-magmatic evolution of the Tethys region of western and southern Asia. Beginning in the Permian, continental fragments sequentially rifted off Gondwana in the south, drifted northward across the Tethys Ocean, and progressively converged with Eurasia in the north during the late Mesozoic and Cenozoic. Although substantial advances have been made in the understanding of the complex tectonic framework of the region (Stöcklin, 1968; Berberian and Berberian, 1981; Şengör,

Table 1. Permissive tracts for porphyry copper deposits in the Tethys region of western and southern Asia.[Coded_ID, a unique number assigned to each permissive tract in the geographic information system (appendix D); km², square kilometers; tract area reported to three significant figures; NA, not applicable]

Tract name	Coded_ID	Countries	Age	Geologic feature assessed	Tract area (km ²)	Deposits	Prospects and occurrences	Descriptive model	Grade and tonnage model
Anatolide-Tauride—Central Turkey sub-tract	142pCu9005b	Turkey	Late Cretaceous—middle Eocene	Late Cretaceous to middle Eocene syn- and postcollisional magmatism of the Tethyan Metallogenic Belt	36,200	None	5	Porphyry copper (John and others, 2010)	General porphyry copper (Singer and others, 2008)
Anatolide-Tauride—Eastern Turkey-Caucasus sub-tract	142pCu9005c	Armenia, Azerbaijan, Iran, Turkey	Late Cretaceous—late Eocene	Late Cretaceous to Late Eocene back-arc and island-arc magmatism of the Tethyan Metallogenic Belt	21,700	4	10	Porphyry copper (John and others, 2010)	General porphyry copper (Singer and others, 2008)
Anatolide-Tauride—Western Turkey sub-tract	142pCu9005a	Turkey	Late Cretaceous—middle Eocene	Late Cretaceous to middle Eocene arc-related magmatism of the Tethyan Metallogenic Belt	5,940	2	3	Porphyry copper (John and others, 2010)	General porphyry copper (Singer and others, 2008)
Azerbaijan—Caucasus-Iran sub-tract	142pCu9014c	Armenia, Azerbaijan, Iran	Late Eocene—early Miocene	Late Eocene to early Miocene postcollisional magmatism of the Tethyan Metallogenic Belt	58,300	5	52	Porphyry copper (John and others, 2010)	General porphyry copper (Singer and others, 2008)
Azerbaijan—Eastern Turkey sub-tract	142pCu9014b	Iran-Turkey	Late Eocene—early Miocene	Late Eocene to early Miocene back-arc magmatism of the Tethyan Metallogenic Belt	7,750	1	1	Porphyry copper (John and others, 2010)	General porphyry copper (Singer and others, 2008)
Azerbaijan—Western Turkey sub-tract	142pCu9014a	Turkey	Late Eocene—early Miocene	Late Eocene to early Miocene postcollisional and back-arc magmatism of the Tethyan Metallogenic Belt	65,200	3	16	Porphyry copper (John and others, 2010)	General porphyry copper (Singer and others, 2008)
Border Folds	142pCu9007	Iran, Iraq, Turkey	Late Cretaceous—early Paleocene	Late Cretaceous to early Paleocene continental arc of the Tethyan Metallogenic Belt	45,300	None	7	Porphyry copper (John and others, 2010)	General porphyry copper (Singer and others, 2008)
Chagai	142pCu9013	Afghanistan, Iran, Pakistan	Late Cretaceous—late Miocene	Late Cretaceous to late Miocene island to continental arc of the Tethyan Metallogenic Belt	19,100	4	22	Porphyry copper (John and others, 2010)	General porphyry copper (Singer and others, 2008)
Cimmeride Greater Caucasus ¹	142pCu9002	Azerbaijan, Georgia, Russian Federation	Middle Jurassic	Middle Jurassic back arc and island arc of the Tethyan Metallogenic Belt	16,700	None	None	Porphyry copper (John and others, 2010)	NA (qualitative)
Cimmeride Lesser Caucasus ¹	142pCu9001	Armenia, Azerbaijan, Georgia, Iran	Middle Jurassic—Lower Cretaceous	Middle Jurassic to Lower Cretaceous island to continental arc and back arc of the Tethyan Metallogenic Belt	17,400	3	9	Porphyry copper (John and others, 2010)	General porphyry copper (Singer and others, 2008)
Esfahan	142pCu9008	Iran, Iraq, Turkey	Late Cretaceous—late Eocene	Late Cretaceous to late Eocene back arc of the Tethyan Metallogenic Belt	56,900	1	13	Porphyry copper (John and others, 2010)	General porphyry copper (Singer and others, 2008)
Kerman	142pCu9016	Iran	Late Eocene—late Miocene	Late Eocene to late Miocene continental arc of the Tethyan Metallogenic Belt	32,800	12	65	Porphyry copper (John and others, 2010)	General porphyry copper (Singer and others, 2008)
Khorasan	142pCu9009	Afghanistan, Iran	Late Cretaceous—middle Miocene	Late Cretaceous to middle Miocene island arcs of the Tethyan Metallogenic Belt	38,300	None	13	Porphyry copper (John and others, 2010)	Porphyry copper, Cu-Au subtype (Singer and others, 2008)

Table 1.—Continued

Tract name	Coded_ID	Countries	Age	Geologic feature assessed	Tract area (km ²)	Deposits	Prospects and occurrences	Descriptive model	Grade and tonnage model
Lut Cretaceous	142pCu9006	Iran	Late Cretaceous–Paleocene	Cretaceous to Paleocene continental arc of the Tethyan Metallogenic Belt	12,000	None	2	Porphyry copper (John and others, 2010)	NA (qualitative)
Lut Jurassic	142pCu9000	Iran	Middle Jurassic	Middle Jurassic continental arc of the Tethyan Metallogenic Belt	2,960	None	1	Porphyry copper (John and others, 2010)	NA (qualitative)
Lut Tertiary	142pCu9010	Iran	Middle Eocene–early Miocene	Middle Eocene to early Miocene island to continental arc of the Tethyan Metallogenic Belt	56,300	None	11	Porphyry copper (John and others, 2010)	Porphyry copper, Cu–Au subtype (Singer and others, 2008)
Makran	142pCu9011	Iran	Late Cretaceous–late Eocene	Late Cretaceous to late Eocene island arcs of the Tethyan Metallogenic Belt	24,100	None	2	Porphyry copper (John and others, 2010)	NA (qualitative)
Pliocene–Quaternary—Bazman sub-tract	142pCu9017c	Afghanistan, Iran, Pakistan	Early Pliocene–Holocene	Early Pliocene to Holocene continental arc of the Tethyan Metallogenic Belt	21,300	None	2	Porphyry copper (John and others, 2010)	NA (qualitative)
Pliocene–Quaternary—Konya sub-tract	142pCu9017a	Turkey	Late Miocene–Holocene	Late Miocene to Holocene continental arc and back arc of the Tethyan Metallogenic Belt	11,800	None	1	Porphyry copper (John and others, 2010)	NA (qualitative)
Pliocene–Quaternary—Postcollisional sub-tract	142pCu9017b	Armenia, Azerbaijan, Georgia, Iran, Russian Federation, Turkey	Late Miocene–Holocene	Late Miocene to Holocene postcollisional magmatism of the Tethyan Metallogenic Belt	194,000	None	4	Porphyry copper (John and others, 2010)	NA (qualitative)
Pontide (Asia)—Caucasus-Iran sub-tract	142pCu9004c	Armenia, Azerbaijan, Georgia, Iran	Late Cretaceous–middle Eocene	Late Cretaceous to middle Eocene island to continental arc and back arc of the Tethyan Metallogenic Belt	24,300	None	2	Porphyry copper (John and others, 2010)	General porphyry copper (Singer and others, 2008)
Pontide (Asia)—NE Turkey sub-tract	142pCu9004b	Georgia, Turkey	Late Cretaceous–late Eocene	Late Cretaceous to late Eocene island to continental arc, back-arc, and postcollisional magmatism of the Tethyan Metallogenic Belt	45,500	4	39	Porphyry copper (John and others, 2010)	General porphyry copper (Singer and others, 2008)
Pontide (Asia)—NW Turkey sub-tract	142pCu9004a	Turkey	Late Cretaceous–late Eocene	Late Cretaceous to late Eocene fore-arc, back-arc, and postcollisional magmatism of the Tethyan Metallogenic Belt	32,700	1	4	Porphyry copper (John and others, 2010)	General porphyry copper (Singer and others, 2008)
Sanandaj–Sirjan	142pCu9003	Iran, Iraq, Turkey	Late Triassic–Early Cretaceous	Late Triassic to Early Cretaceous continental arc of the Tethyan Metallogenic Belt	20,200	None	1	Porphyry copper (John and others, 2010)	NA (qualitative)
Sistan	142pCu9012	Afghanistan, Iran, Pakistan	Late Cretaceous–early Miocene	Late Cretaceous to early Miocene island arcs of the Tethyan Metallogenic Belt	32,800	None	10	Porphyry copper (John and others, 2010)	General porphyry copper (Singer and others, 2008)
Yazd	142pCu9015	Iran	Middle Eocene–middle Miocene	Middle Eocene to middle Miocene back arc and continental arc of the Tethyan Metallogenic Belt	25,700	2	13	Porphyry copper (John and others, 2010)	General porphyry copper (Singer and others, 2008)

¹The Cimmeride Lesser Caucasus (142pCu9001) and Cimmeride Greater Caucasus (142pCu9002) tracts are segments of the larger Late Triassic–Early Cretaceous Cimmerian orogenic event of Turkey, the Caucasus, Iran, and Afghanistan.

1987; Shahabpour and Kramers, 1987; Alavi, 1994; and Golonka, 2004, among many others), many elements of the geodynamic evolution of the Tethys region of western and southern Asia remain the subject of debate. This overview attempts to integrate the salient aspects of the space-time distribution of magmatism and associated porphyry copper mineralization that formed during the compressional and extensional regimes that were active in the Neotethys realm beginning in the Late Triassic.

Permian to Middle Jurassic

The Tethys region preserves a record of the evolution of the margin of the Gondwana supercontinent in Permian to Middle Jurassic time. Between the late Carboniferous and the Middle Triassic, Eurasia was separated from Gondwana by the Paleotethys Ocean. By the Middle Jurassic, the Paleotethys Ocean was closing, and rifting of microcontinents from the Gondwana margin led to opening of the Neotethys Ocean.

Paleotethys Ocean Realm

In the assessment region, the Eurasian margin consisted of the Eurasian Scythian and Turan Terranes and the Istanbul (Western Pontides), Eastern Pontides, Transcaucasus, Talysh, South Caspian Sea, Alborz, and Kopet Dagh Terranes of Eurasian affinity. These terranes of Eurasian affinity had amalgamated with Eurasia for the first time during the Paleozoic (Golonka, 2004). However, they separated from Eurasia during the late Carboniferous to Middle Triassic, and collided again during the Late Triassic-Early Jurassic Cimmerian orogeny (Stampfli and Borel, 2002). In the western part of the assessment region, the Cimmerian orogeny ended with collision of the Sakarya Terrane, and in the eastern part of the assessment region, it terminated with collision of the Gondwana-derived Aghdarband, Lut, Farah, and Herat Terranes. This collisional event closed the Paleotethys Ocean by the Middle Jurassic (Golonka, 2004). The present-day distribution of these tectonic terranes is shown in orange (Eurasian) and light brown (Eurasian affinity) in figure 3.

Neotethys Ocean Realm

Between the Permian and Middle Jurassic, opening of the Neotethys Ocean in the south occurred concurrently with consumption of the Paleotethys Ocean in the north. In the late Permian, microcontinents began to rift from Gondwana, initiating the opening of the Neotethys Ocean (Golonka, 2004; Stampfli and Borel, 2002). These Gondwana-derived terranes are known as Cimmeria, and from west to east across the assessment region they include the (1) Anatolide-Tauride (composed of the Menderes, Central Anatolian Crystalline Complex, South Armenian Block, and Bitlis-Pötürge Terranes); (2) Sanandaj-Sirjan; (3) Central Iranian (composed of microcontinental fragments of the Alborz Terrane in the west and the Aghdarband Terrane in the east); (4) East-Central

Iranian (composed of the Yazd, Kashmar-Kerman, Tabas, and Lut Terranes); and (5) Helmand Terranes. While these terranes were in motion, the Neotethys Ocean consisted of a northern branch north of the Cimmerian terranes and a southern branch south of the Cimmerian terranes. The present-day disposition of these tectonic terranes of Gondwanan affinity is shown in light yellow in figure 3. The Izmir-Ankara-Erzincan, Sevan-Akera, and Rasht sutures mark the former location of the Northern Neotethys Ocean Branch. The former location of the Southern Neotethys Ocean Branch is marked by the Bitlis-Zagros Suture (fig. 3).

A Middle Jurassic (166 million years ago, Ma) tectonic plate reconstruction of the Tethys region of western and southern Asia is illustrated in figure 4A (Golonka, 2004). Not represented in figure 4A is the fact that the Sakarya Terrane had already formed part of Eurasia by this time. The Sakarya and Istanbul Terranes had already amalgamated along the Intra-Pontide Suture of northwestern Turkey (fig. 3), which marks the former location of the Paleotethys Ocean. The Paleotethys Ocean in this region closed in the Middle to Late Jurassic (Okay, 1989). The Jurassic disposition of the Lut Terrane, which experienced a 90-degree counterclockwise rotation between the Eocene and middle Miocene (Westphal and others, 1986), is also not represented in figure 4A.

Following the Late Triassic-Early Jurassic Cimmerian collisional event, northward-dipping subduction zones developed in the Northern Neotethys Ocean Branch along the new Eurasian margin formed by the largely amalgamated Pontides, Sakarya, Transcaucasus, Talysh, Alborz, and East-Central Iranian Terranes (Zanchi and others, 2009; Golonka, 2004). This compressional event produced a calc-alkaline continental arc and also a broad extensional calc-alkaline to alkaline back-arc rift basin north of these terranes (Stöcklin, 1968; Karimpour and others, 2011b). In the Caucasus and across northern Iran, this back-arc basin developed approximately at the location of the Paleotethys Ocean suture. Jurassic subduction-related igneous rocks are preserved in the eastern part of the Lut Terrane and in the Greater Caucasus part of the Transcaucasus Terrane (McCann and others, 2010; Hess and others, 1995; Lordkipanidze and others, 1989). In the Greater Caucasus region, back-arc and island-arc magmatism continued into the Early Cretaceous (fig. 4A,B; Golonka, 2004). These continental arc and intraoceanic volcano-plutonic events, respectively, are delimited in the Lut Jurassic and Cimmeride Greater Caucasus tracts in east-central Iran and the Greater Caucasus. The present-day location of these tracts is shown in red and light orange in figure 5. One porphyry copper prospect has been identified in the Lut Jurassic tract, and none are known in the Cimmeride Greater Caucasus tract.

In the Late Triassic, a north-dipping subduction zone was also initiated in the Southern Neotethys Ocean Branch (fig. 4A). This subduction-related event created a continental arc (fig. 4B) on the Sanandaj-Sirjan Terrane (Berberian and Berberian, 1981; Kazmin and others, 1986; Azizi and others, 2011). The Sanandaj-Sirjan Terrane had rifted off Gondwana in the late Permian (Ghasemi and Talbot, 2006) and during the Late Triassic to Early

Cretaceous was drifting northeastward across the Neotethys Ocean towards the Eurasian margin (Dewey and others, 1973; Berberian and King, 1981). This Late Triassic to Early Cretaceous continental arc is delimited by the Sanandaj-Sirjan tract, which is portrayed in blue in figure 5. Only one possible porphyry-related prospect has been identified in the highly exhumed Sanandaj-Sirjan tract.

Late Jurassic to Early Cretaceous

Island- to continental-arc and back-arc magmatism related to the northward-dipping subduction zone along the Eurasian margin in the Northern Neotethys Ocean Branch continued into the Early Cretaceous (Adamia and others, 1977; Lordkipanidze and others, 1989; Kazmin and others, 1986). Magmatism was particularly extensive and is well preserved in the Transcaucasus Terrane (Kekelia and others, 2001; Şengör and others, 1993; Şengör and others, 1991). This Middle Jurassic to Early Cretaceous island to calc-alkaline continental arc and calc-alkaline to alkaline back-arc setting is delimited by the Cimmeride Lesser Caucasus tract, which is depicted in lavender (light purple) in figure 5. Unlike the older Lut Jurassic, Cimmeride Greater Caucasus, and Sanandaj-Sirjan tracts, the Cimmeride Lesser Caucasus tract contains 3 known porphyry deposits, 8 porphyry prospects, and 1 possible porphyry-related occurrence.

Late Cretaceous to Middle Miocene

Increases in convergence rates between various terranes during the Late Cretaceous to Middle Miocene led to marked changes in the geodynamics of the region. As both the northern and southern branches of the Neotethys Ocean narrowed and closed, new subduction zones gave rise to island-arc, continental-arc, and postcollisional magmatism associated with generation of porphyry copper deposits.

Northern Neotethys Ocean Branch Realm

During the Late Cretaceous, increased convergence between the Cimmerian terranes and Eurasia began to narrow the Northern Neotethys Ocean Branch along north-dipping subduction zones located along the southern margin of Eurasia. These subduction zones produced island- to continental-arc magmatism on the amalgamated Pontide, Sakarya, Transcaucasus, and western Alborz Terranes. Figure 4C illustrates a Late Cretaceous-Paleocene (65 Ma) tectonic plate reconstruction of the Tethys region of western and southern Asia (Golonka, 2004).

Arc magmatism on these amalgamated terranes was accompanied by extensive back-arc magmatism (Adamia and others, 1981; Berberian and Berberian, 1981; Okay and Şahintürk, 1997). Rifting in the Black Sea, Transcaucasus, and Talysh Terranes of the Caucasus, which had been active since the Jurassic, continued until the middle Eocene and culminated with propagation of the back arc over the arc axis. Figure 4D illustrates

a middle Eocene (45 Ma) tectonic plate reconstruction of the Tethys region of western and southern Asia (Golonka, 2004).

Convergence in the western and central parts of the Northern Neotethys Ocean Branch resulted in collision of the Central Anatolian Crystalline Complex with the Sakarya Terrane in the Late Cretaceous, and collision of the South Armenian Block with the Transcaucasus Terrane in the middle Eocene (Golonka, 2004; Sosson and others, 2010b). These collisional events closed the Northern Neotethys Ocean along the Izmir-Ankara-Erzincan and Sevan-Akera suture zones (fig. 3). Widespread uplift, metamorphism, folding, and ophiolite obduction along south-vergent thrust sheets are associated with this collisional event.

Collision-arrested arc- and back-arc-related magmatism gave way to postcollisional magmatism. Late Cretaceous to middle-late Eocene postcollision-related igneous rocks are preserved on both sides of the Izmir-Ankara-Erzincan Suture, which separates the Sakarya Terrane from the Anatolide-Tauride Terrane. Figure 4E illustrates a late Eocene (36 Ma) tectonic plate reconstruction of the Tethys region of western and southern Asia (Golonka, 2004)

In the amalgamated Pontide, Sakarya, Transcaucasus, and Alborz Terranes, this Late Cretaceous to middle and late Eocene island- to continental-arc and back-arc and volcano-plutonic event is included in the Pontide permissive tract, which is shown in red in figure 6. The Pontide tract is further separated into the Pontide-NW Turkey, Pontide-NE Turkey, and Pontide-Caucasus-Iran sub-tracts, because different parts of its tectonic setting are exposed from west to east. The Pontide-NE Turkey sub-tract contains 4 known porphyry copper deposits and 39 porphyry prospects. In contrast, known porphyry deposits and prospects are few in the Pontide-NW Turkey (1 deposit and 4 prospects) and Pontide-Caucasus-Iran (0 deposits and 2 prospects) sub-tracts.

In the Late Cretaceous, increased convergence in the eastern part of the Northern Neotethys Ocean Branch also initiated closure of the Sabzevar-Sistan Ocean. The Sabzevar-Sistan Ocean (fig. 4C) was located between the East-Central Iranian Terrane and the Eurasian margin formed by the Kopet Dag, Farah, and Helmand Terranes (Dercourt and others, 1986; Şengör and others, 1993). Thus, this ocean connected the Northern Neotethys Ocean Branch with the Southern Neotethys Ocean Branch. In the north, the Sabzevar-Sistan Ocean closed along intraoceanic north-dipping subduction zones by the middle Miocene (Dercourt and others, 1986; Spies and others, 1984). Figure 4F illustrates an early Miocene (22 Ma) tectonic plate reconstruction of the Tethys region of western and southern Asia (Golonka, 2004). In the east, island-arc magmatism in the Sabzevar-Sistan Ocean ended between the Eocene and Miocene with collision of the East-Central Iranian terrane collage (Lut, Tabas, Kashmar-Kerman, and Yazd Terranes) with the Farah Terrane (Camp and Griffis, 1982; Tirrul and others, 1983). These Late Cretaceous to middle Miocene intraoceanic volcano-plutonic events are delimited by the Khorasan tract located in northeastern Iran (blue in fig. 6), and the Sistan tract located in easternmost Iran (orange in fig. 7). Thirteen porphyry copper, porphyry-related, and possible porphyry-related prospects have been identified in the Khorasan tract, and 10 porphyry copper and possible porphyry-related prospects are known in the Sistan tract.

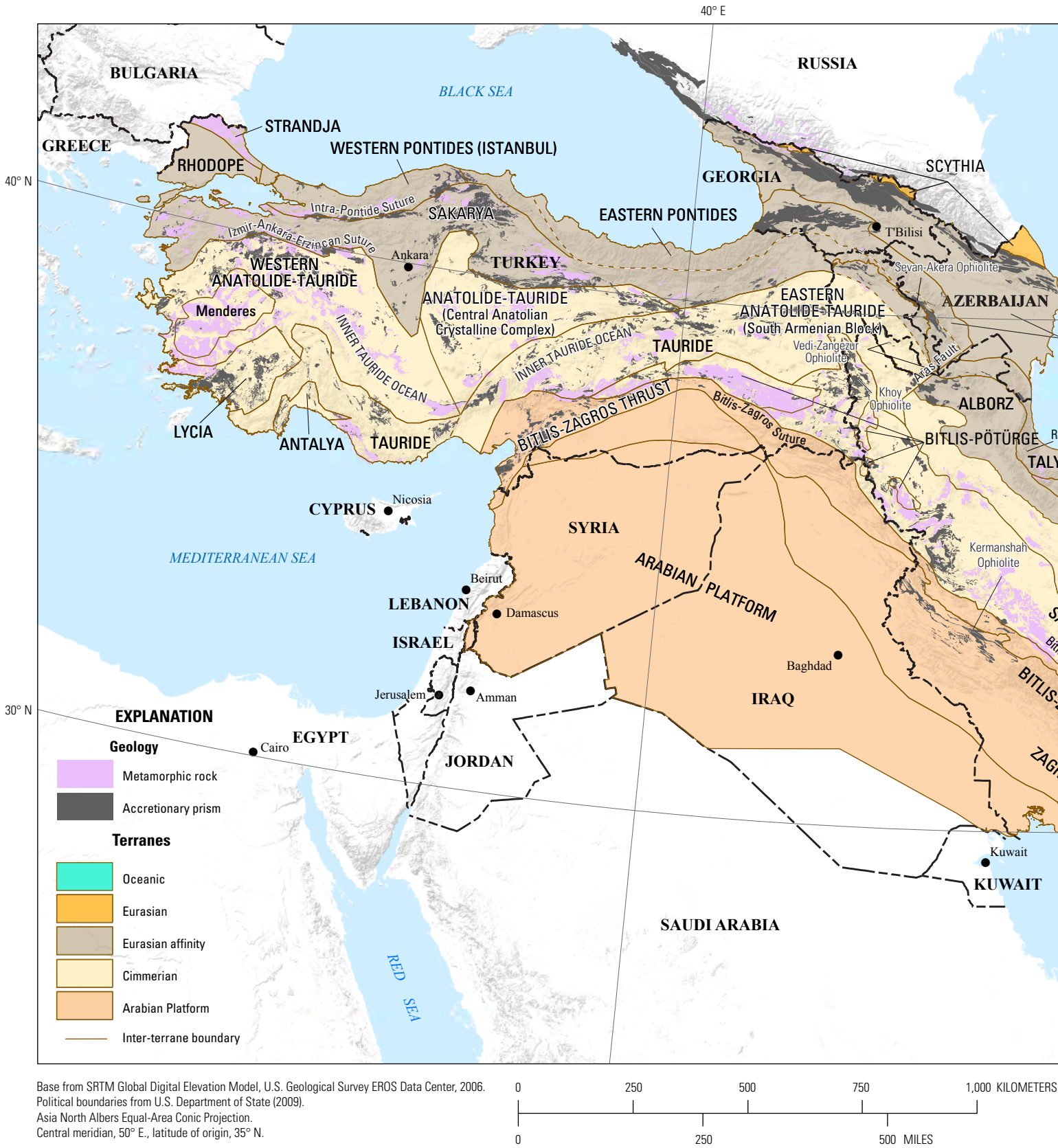
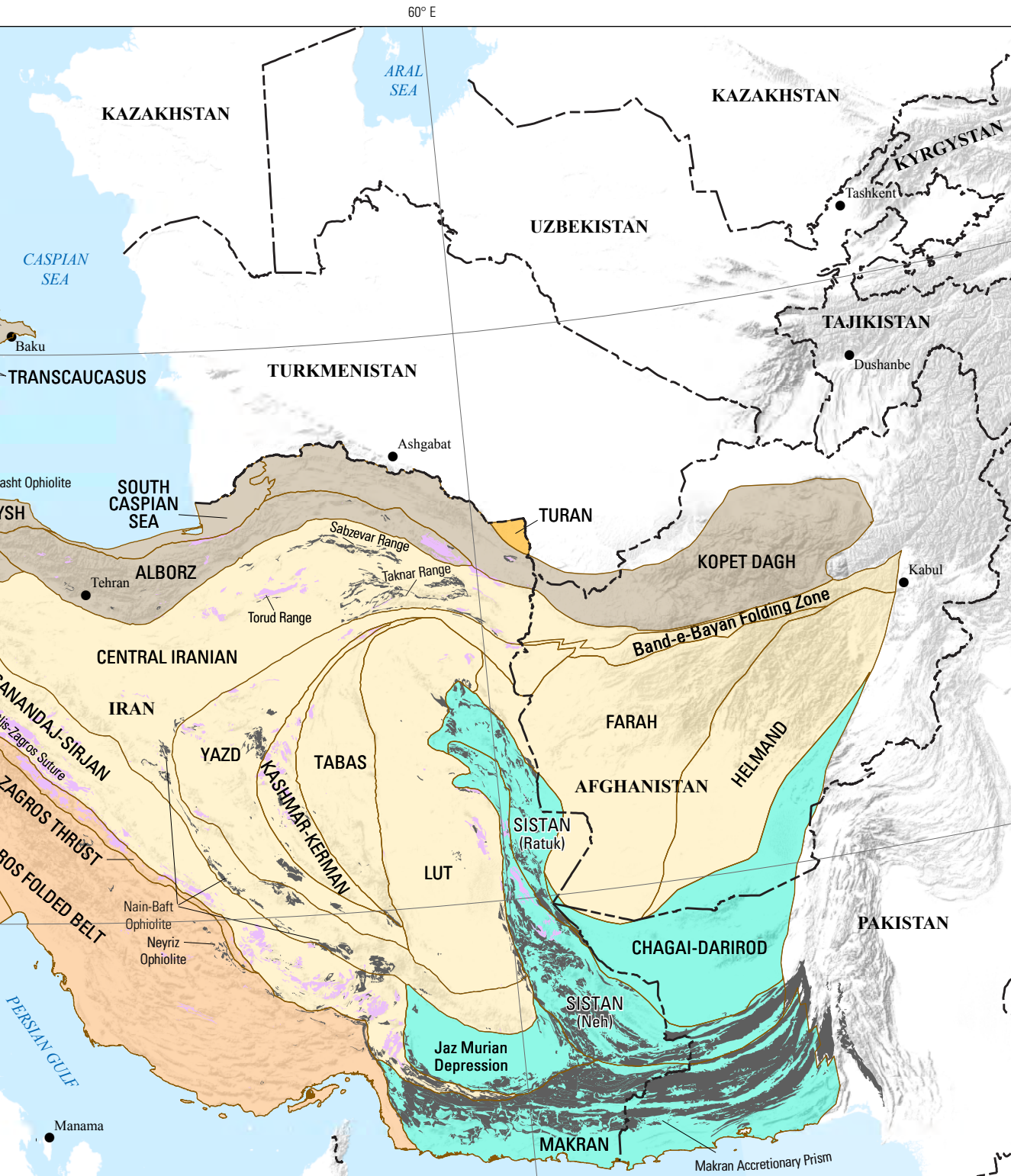
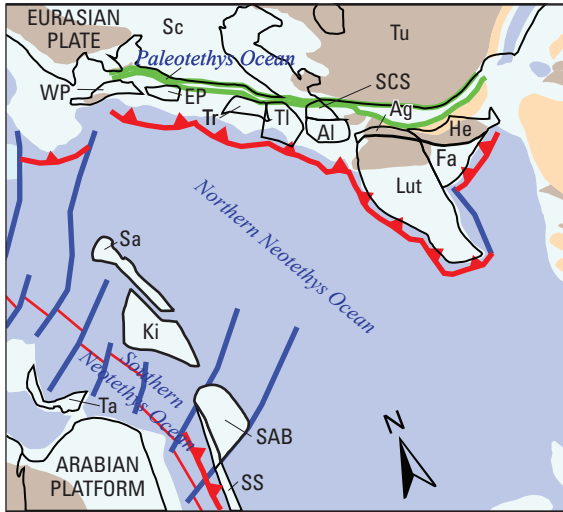


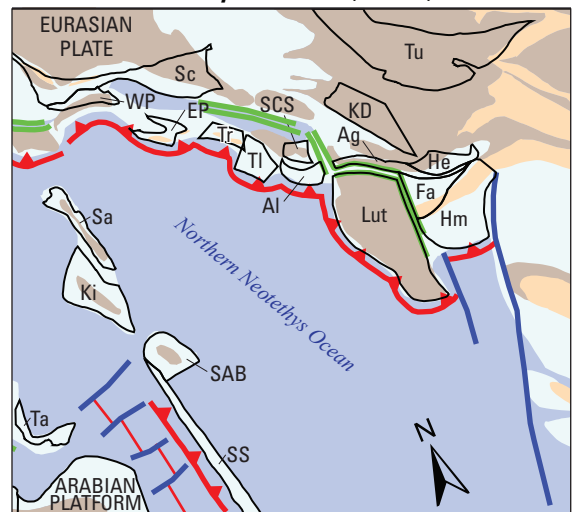
Figure 3. Map showing tectono-stratigraphic terranes, accretionary prisms, and metamorphic belts of the Tethys region of western and southern Asia. After Abdullah and Chmyriov (1977b) and Peters and others (2011) for Afghanistan, Kazmi and Rana (1982) for Pakistan, Stöcklin (1968) for Iran, Pollastro and others (1998) for Iraq, Kaymakci and others (2010) and Yigit (2009) for Turkey, and Kekelia and others (2001) for the Caucasus. Most terrane names conform to Golonka (2004).



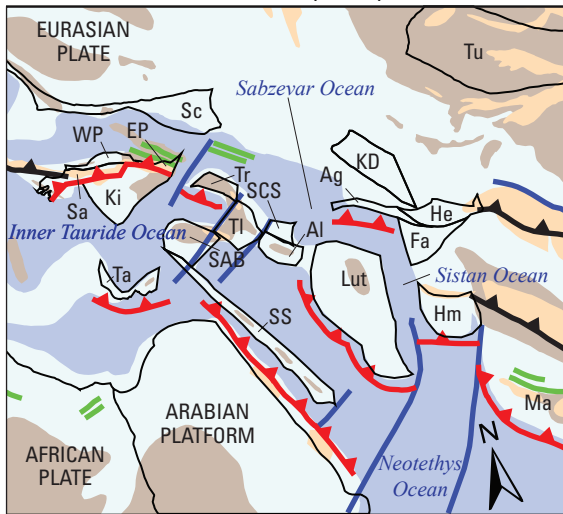
A. Middle Jurassic (166 Ma)



B. Late Jurassic-Early Cretaceous (140 Ma)



C. Late Cretaceous-Paleocene (65 Ma)



D. Middle Eocene (45 Ma)

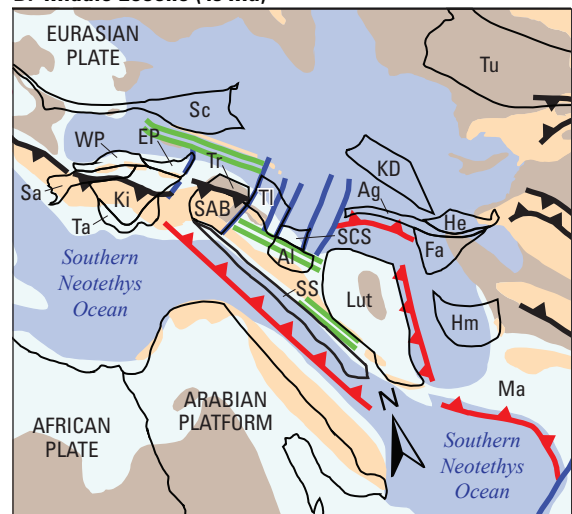
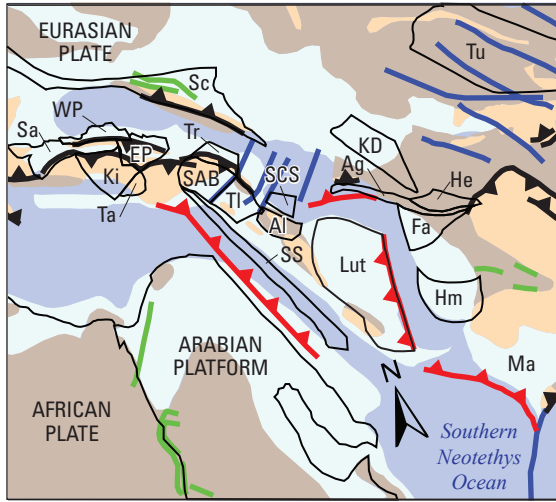
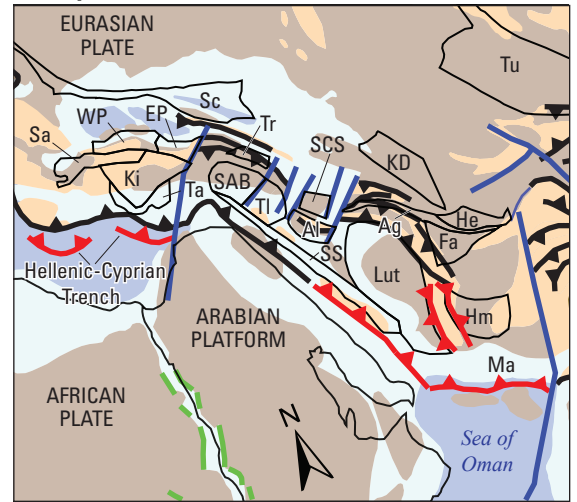


Figure 4. Paleotectonic reconstructions (A–G) of the Tethys region of western and southern Asia (modified from Golonka, 2004). Terranes: Ag—Southern Kopet Dagh (Aghdarband), Al—Alborz, EP—Eastern Pontides (eastern Sakarya), Fa—Farah, He—Herat, Hm—Helmand-Arghandab, KD—Kopet Dagh, Ki—Central Anatolian Crystalline Complex (Kirsehir), Lut—East-Central Iranian (Lut, Tabas, Kashmar-Kerman, Yazd), Ma—Makran, SAB—Eastern Anatolide-Tauride (South Armenian Block), Sa—Sakarya (western Sakarya), Sc—Scythia, SCS—South Caspian Sea, SS—Sanandaj-Sirjan, Ta—Taurus (includes Bitlis-Pötürge), TI—Talysh, Tr—Transcaucasus, Tu—Turan, and WP—Western Pontides (Istanbul, Strandja). Ma, million years before present.

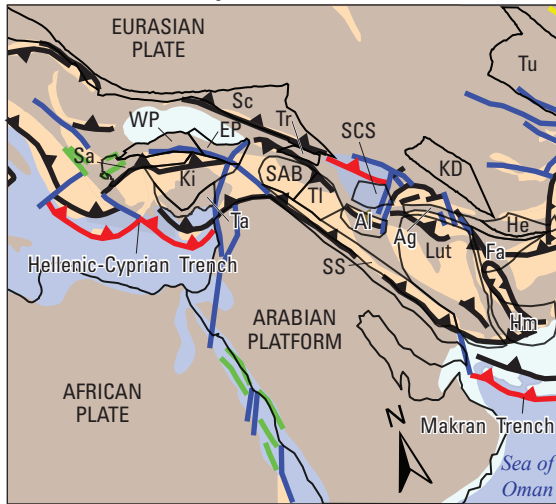
E. Late Eocene (36 Ma)



F. Early Miocene (22 Ma)



G. Late Miocene-Early Pliocene (6 Ma)



EXPLANATION

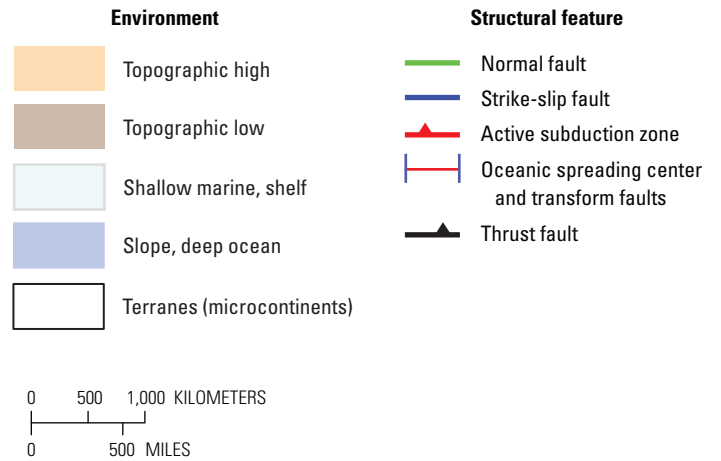


Figure 4.—Continued

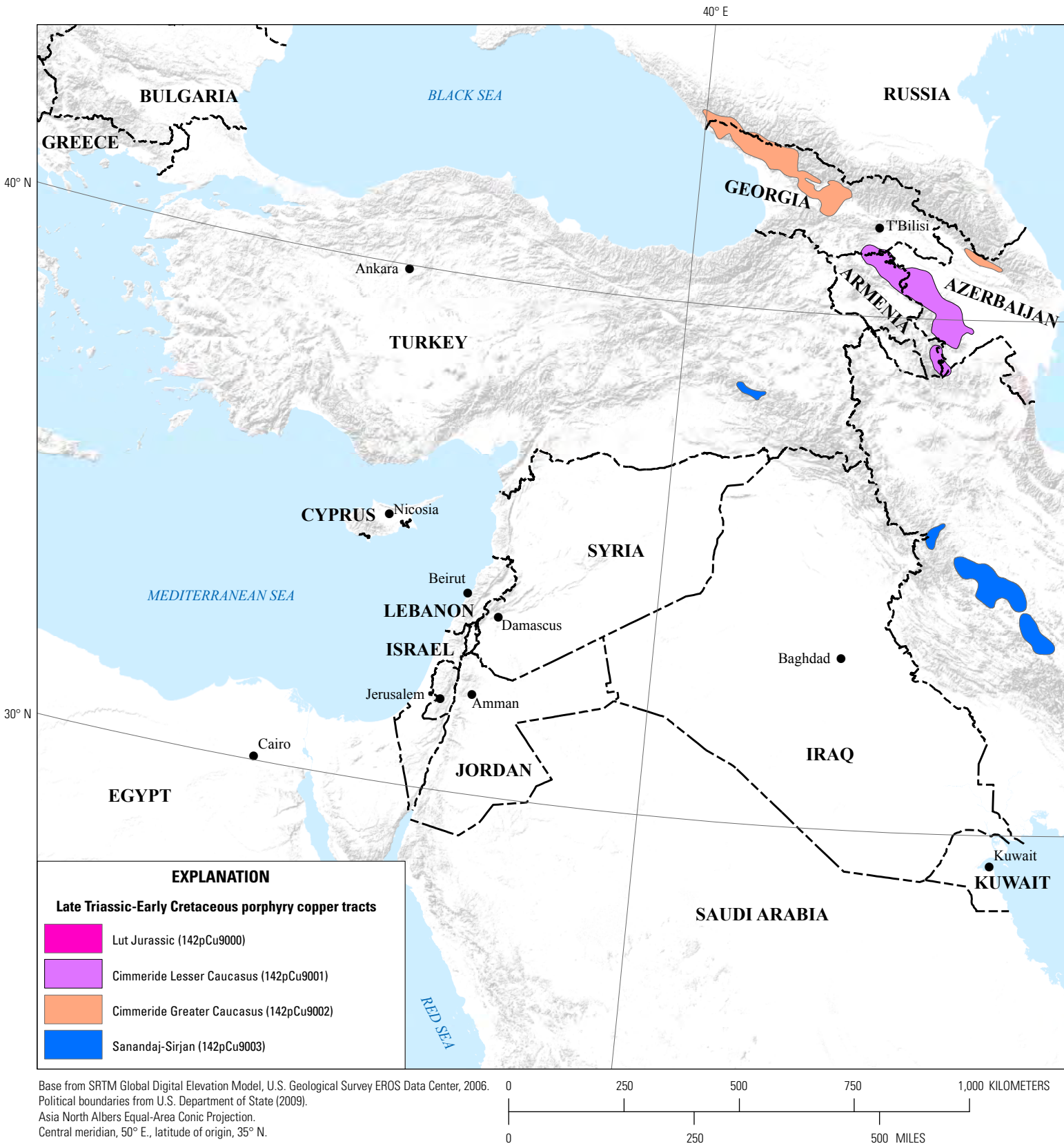
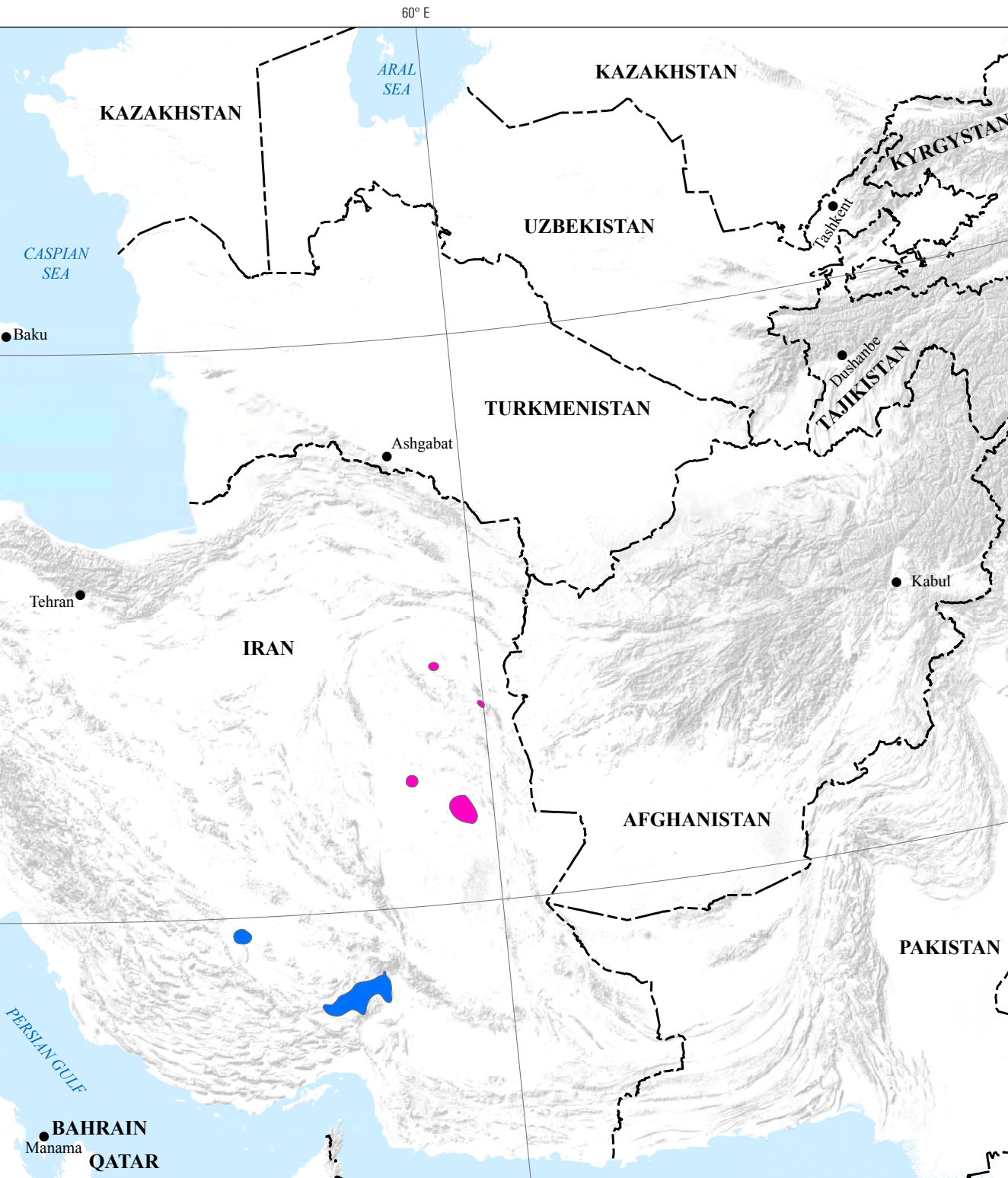


Figure 5. Late Triassic to Early Cretaceous permissive tracts for porphyry copper deposits in the Tethys region of western and southern Asia.



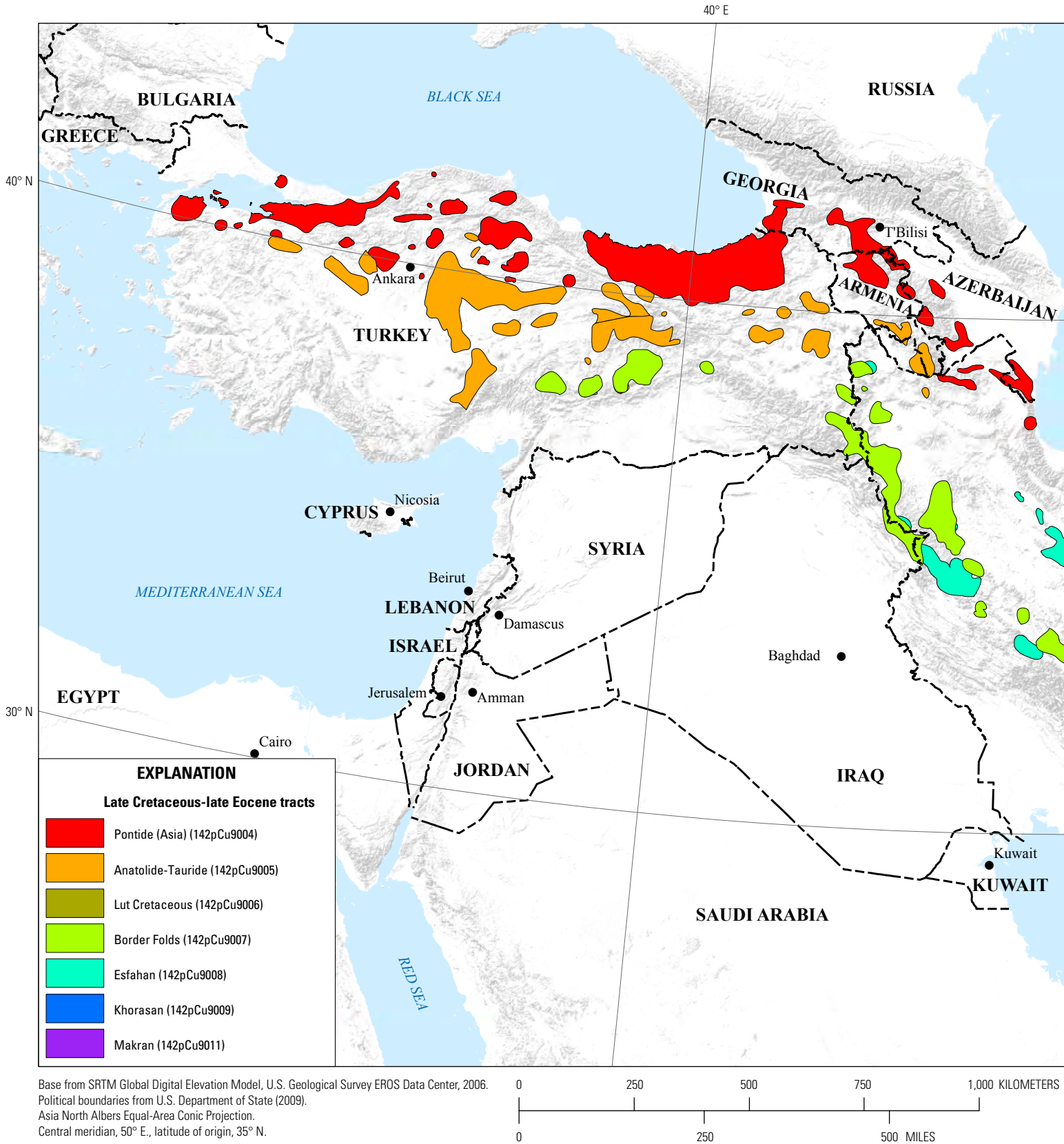
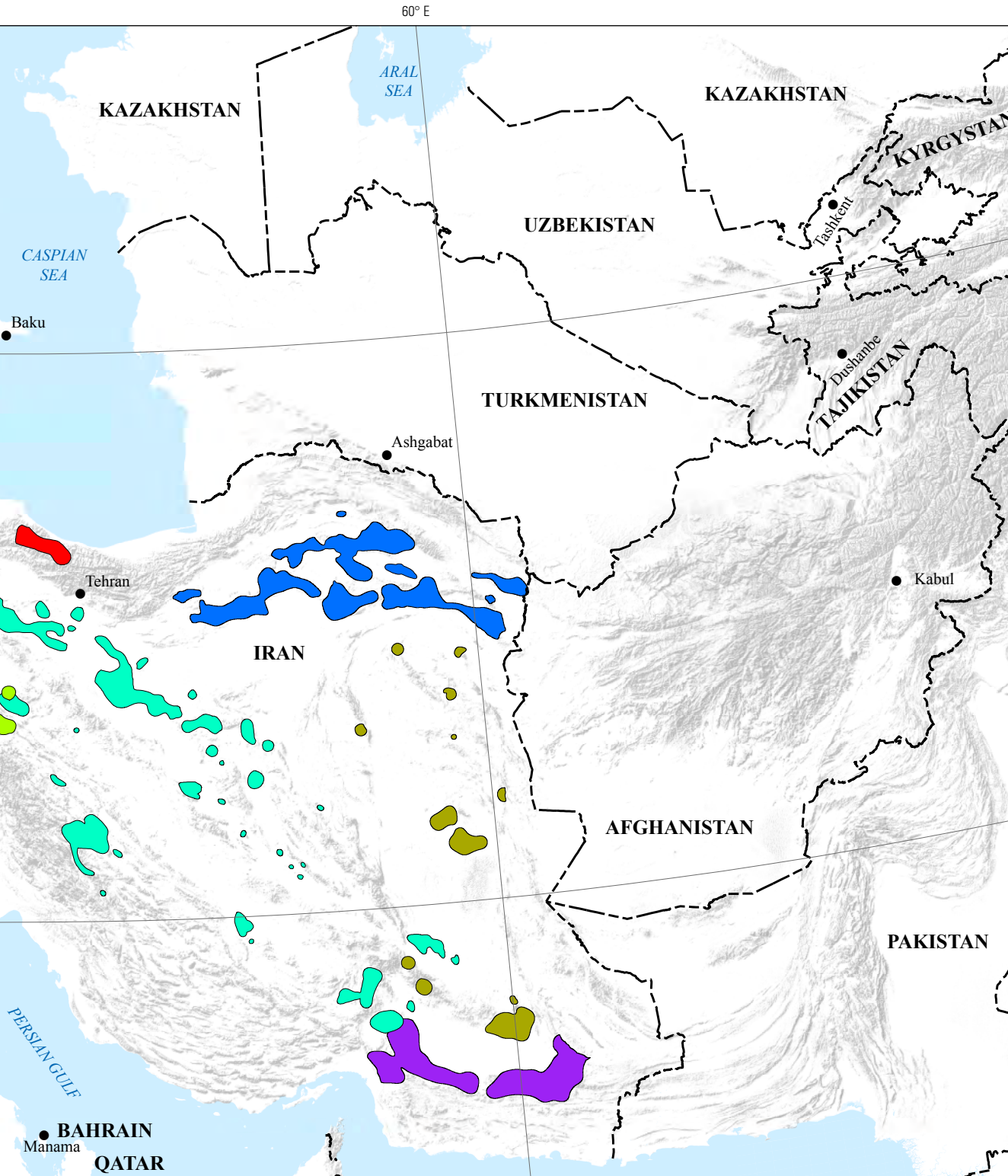


Figure 6. Late Cretaceous to late Eocene permissive tracts for porphyry copper deposits in the Tethys region of western and southern Asia.



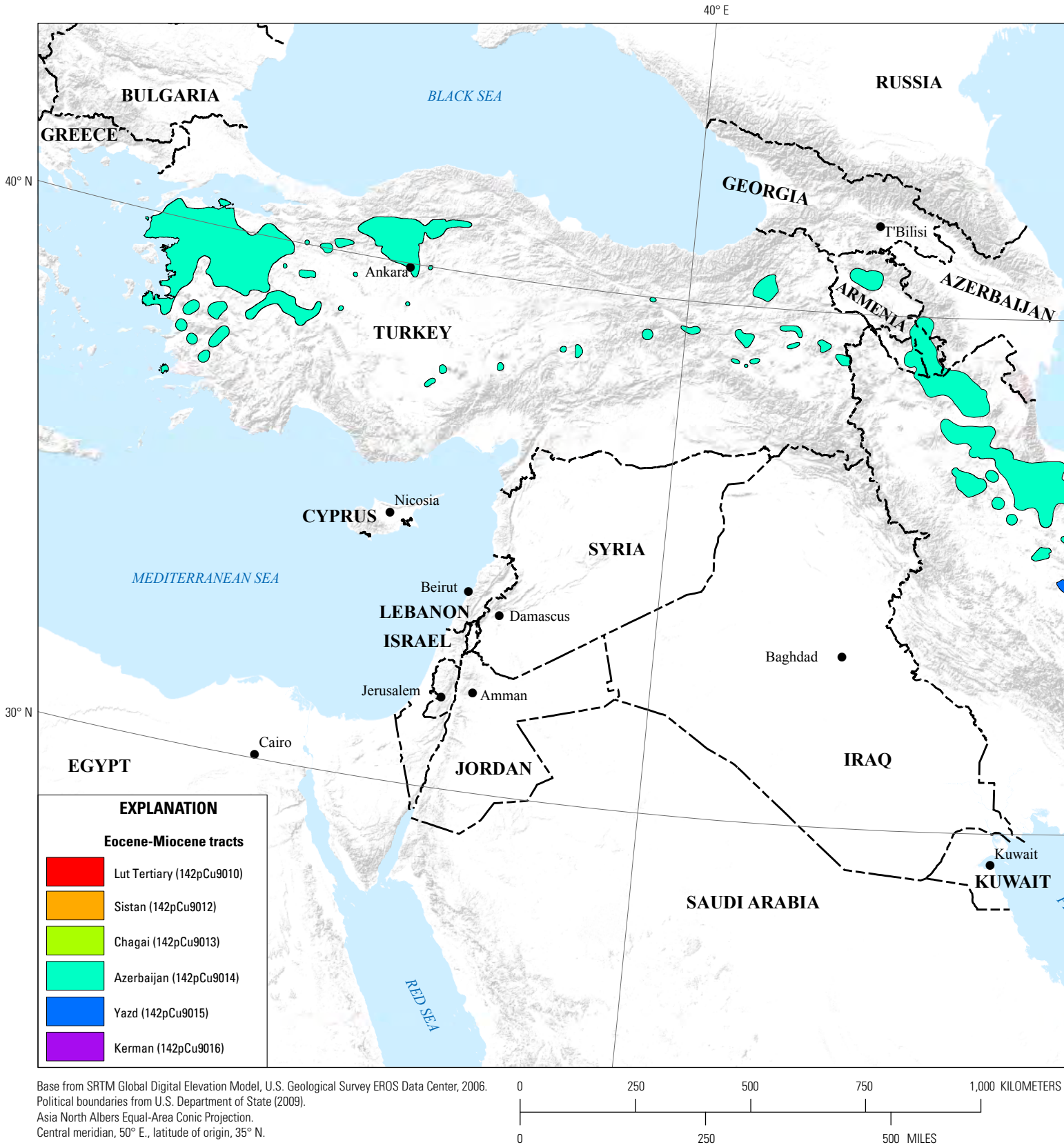
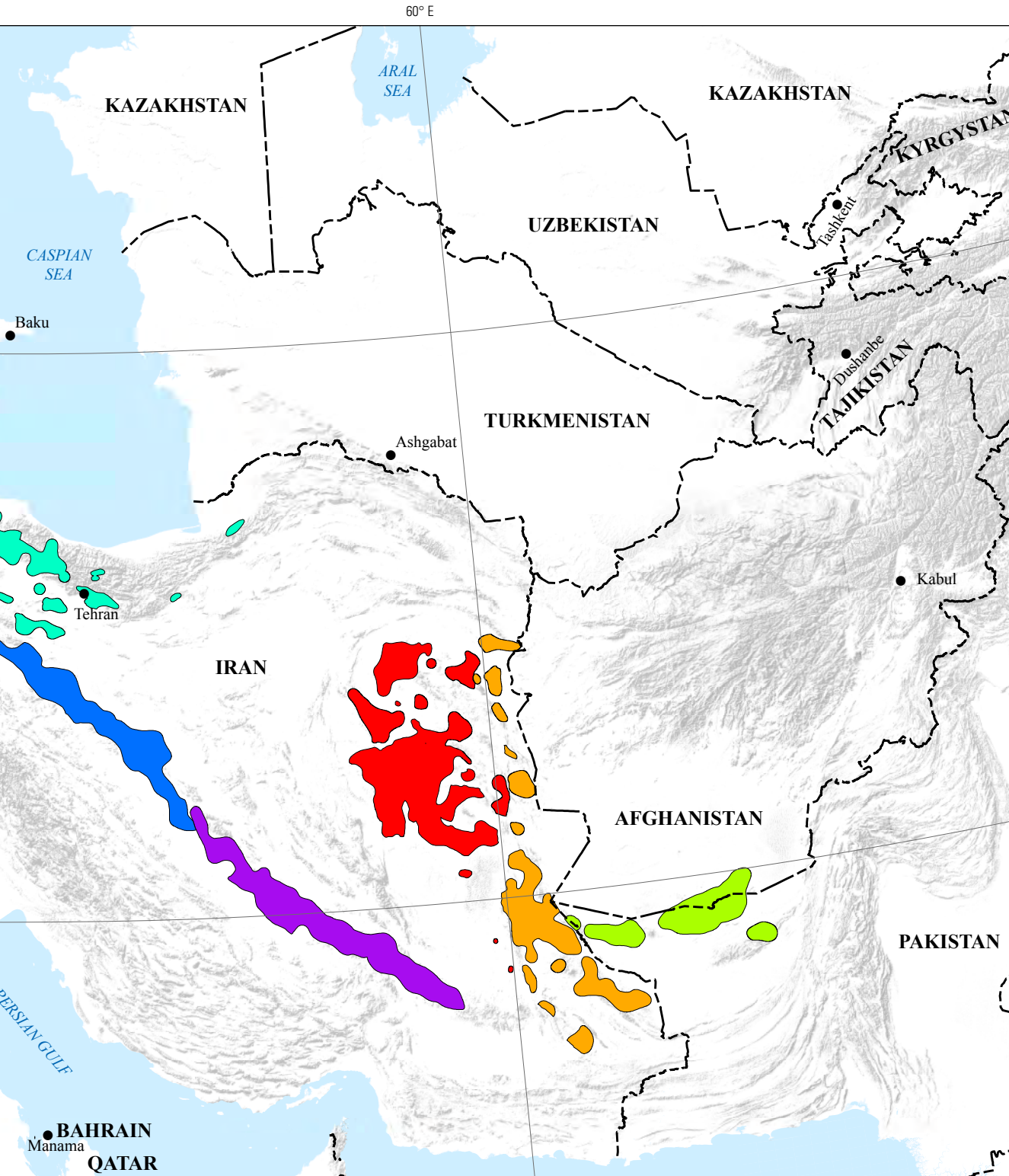


Figure 7. Eocene to Miocene permissive tracts for porphyry copper deposits in the Tethys region of western and southern Asia.



Between the middle Eocene and early Miocene, continued convergence in the Sistan Ocean (fig. 4E) also produced island to continental arc magmatism along the eastern margin of the Lut Terrane (Richards and others, 2012; Karimpour and Stern, 2011). Arc-related magmatism ended in the middle Miocene with final closure of the Sistan Ocean. This middle Eocene to early Miocene island- to continental-arc event is delimited by the Lut Tertiary permissive tract (displayed in red in fig. 7). Eleven porphyry copper and porphyry-related prospects are known in the Lut Tertiary tract.

Southern Neotethys Ocean Branch Realm

Between the Late Cretaceous and middle Eocene, increased convergence between the Arabian Platform (Afro-Arabian Plate) and the Cimmerian terranes (western Anatolide-Tauride, Central Anatolian Crystalline Complex, eastern Anatolide-Tauride or South Armenian Block, Bitlis-Pötürge, and Sanandaj-Sirjan) also began to narrow the Southern Neotethys Ocean Branch. At this time, the Cimmerian terranes were separated by intervening oceans (the Inner Tauride Ocean) that are preserved today as ophiolitic complexes that occur throughout Turkey, the Lesser Caucasus, and Iran (figs. 3, 4C). As a result, island- to continental-arc and intraoceanic back-arc magmatism was related to several subduction zones located offshore and along the southern margins of these terranes (Okay, 2008; Şengör and Yilmaz, 1981; Karimpour and others, 2011b; Alavi, 1994; Berberian and King, 1981). Non-subduction-related magmatism also occurred in the Central Anatolian Crystalline Complex during and after its Late Cretaceous collision with the Sakarya Terrane to the north (fig. 4C).

These Late Cretaceous to middle Eocene volcano-plutonic events are represented by a (possibly southward-transported) continental arc segment located in the northern part of the Western Anatolide-Tauride Terrane (fig. 3), syncollisional to postcollisional magmatism in the Central Anatolian Crystalline Complex, a Late Cretaceous-early Paleocene continental arc in the Bitlis-Pötürge and Sanandaj-Sirjan Terranes, and a vast Late Cretaceous to middle Eocene (fig. 4D) intraoceanic back arc to the north of the continental arc on the Eastern Anatolide-Tauride and Central Iranian Terranes (Kuşçu and others, 2010; Agard and others, 2011; Verdel and others, 2011). In central Iran, back-arc extension propagated over time to the north into the Alborz Terrane and to the south over the arc axis into the Sanandaj-Sirjan Terrane.

These Late Cretaceous to middle Eocene volcano-plutonic events are delimited, respectively, by the Border Folds tract (depicted in light green in fig. 6), the Anatolide-Tauride tract (shown in orange in fig. 6), and the Esfahan¹⁴ tract (depicted in turquoise in fig. 6). Given the contrasting tectonic settings, the Anatolide-Tauride tract is further separated into the Anatolide-Tauride–Western Turkey, the Anatolide-Tauride–Central Turkey, and the Anatolide-Tauride–Eastern Turkey-Caucasus sub-tracts.

The continental arc delimited by the Border Folds tract contains 7 known porphyry and porphyry-related prospects; the transported continental arc segment delimited by the Anatolide-Tauride–Western Turkey sub-tract contains 2 known porphyry copper deposits and 4 porphyry prospects; and the syncollisional to postcollisional magmatic belt delimited by the Anatolide-Tauride–Central Turkey sub-tract contains 5 known porphyry and porphyry-related prospects. In general, these volcano-plutonic belts are deeply exhumed. In comparison, the better preserved intra-arc and back arc delimited by the Anatolide-Tauride–Eastern Turkey-Caucasus sub-tract contains more porphyry copper occurrences (4 known porphyry deposits and 11 prospects), and the extension of this back arc delimited by the Esfahan tract in Iran contains 1 known deposit and 13 porphyry and possible porphyry-related prospects.

During the Late Cretaceous to Paleocene, a subduction-related continental arc was also built on the southern margin of the Lut Terrane (Karimpour and others, 2011b; Berberian and Berberian, 1981). At this time, the East-Central Iranian Terrane collage was separated from Eurasia by the Sabzevar-Sistan Ocean (fig. 4C) on the north and east, and from the Sanandaj-Sirjan Terrane by the extensional back-arc basin located in the Central Iranian Terrane on the west and south (Golonka, 2004; Dercourt and others, 1986). Note that the Late Cretaceous disposition of the Lut Terrane, which experienced a 90-degree counterclockwise rotation between the Eocene and middle Miocene, is not represented in figure 4C. Igneous rocks associated with this continental arc are delimited by the Lut Cretaceous tract, shown in dark green in figure 6. The poorly exposed Lut Cretaceous tract contains only 1 known porphyry prospect and 1 possible porphyry-related occurrence.

Late Cretaceous to middle-late Eocene island-arc magmatism in southern Iran and western Pakistan is represented by the Makran Terrane. This oceanic terrane includes offshore island arcs that during this time were converging northward toward the East-Central Iranian, Farah, and Helmand Terranes (McCall, 1997; Shahabpour, 2010; Berberian and Berberian, 1981). By the late Eocene, the Makran Terrane began to accrete with the Eurasian margin on the north, as well as with the converging Sanandaj-Sirjan Terrane on the west (fig. 4E). This Late Cretaceous-late Eocene intraoceanic volcano-plutonic event is delimited by the Makran tract (shown in purple in fig. 6). Only two possible porphyry-related occurrences are known in this tract.

Late Eocene to Middle Miocene

Late Eocene to middle Miocene tectono-magmatic events are related to the closure of the Southern Neotethys Ocean Branch. Magmatism associated with these events includes postcollisional-to-back-arc, back-arc, and postcollisional settings. Figures 4E and 4F illustrate late Eocene (36 Ma) and early Miocene (22 Ma) tectonic plate reconstructions of the Tethys region of western and southern Asia.

¹⁴Also spelled as Isfahan.

In western Turkey, the compressional regime associated with convergence and collision between the Anatolide-Tauride and Sakarya Terranes along the Izmir-Ankara-Erzincan Suture ended by the middle Eocene (Şengör and Yilmaz, 1981; Yilmaz, 2003b). This compressional event was followed by a late Eocene to middle Oligocene postcollisional magmatic episode (fig. 4F) that resulted from extension and tectonic collapse of the overthickened crust in the Anatolide-Tauride Terrane (Chakrabarti and others, 2012; Delaloye and Bingöl, 2000; Harris and others, 1994). This postcollisional event was superseded by the late Oligocene onset of subduction along the north-dipping Hellenic-Cyprian subduction zone in the Mediterranean Sea and associated magmatism (Şengör and Yilmaz, 1981; Meulenkamp and others, 1988; Delaloye and Bingöl, 2000; Bozkurt and others, 2000; Yilmaz, 2003b). Thus, late Eocene to middle Oligocene postcollisional magmatism in western Turkey is overprinted by late Oligocene to middle Miocene (and younger) subduction-related magmatism.

In eastern Turkey, the Late Cretaceous to middle Eocene continental arc and associated back-arc setting was followed by shallowing of the subduction slab angle between the late Eocene and early Miocene (fig. 4F) and by collision between the Arabian Platform and the now amalgamated Bitlis-Pötürge and Sanandaj-Sirjan Terranes in the middle Miocene (Yiğitbaş and Yilmaz, 1996; Şengör and Yilmaz, 1981; Kaymakci and others, 2010; Pearce and others, 1990). Shallowing of the subduction slab angle led to reduction in volume of associated late Eocene to early Miocene subduction-related arc and back-arc magmatism. The back-arc setting is preserved but poorly exposed across eastern Turkey.

In the Lesser Caucasus and northwestern Iran, Late Cretaceous to middle Eocene arc and associated back-arc magmatism were followed in the late Eocene-early Oligocene (fig. 4F) by the onset of oblique collision between the Arabian Platform and the Eurasian margin (Ghasemi and Talbot, 2006; Robertson and Mountrakis, 2006; Berberian and others, 1982; Agard and others, 2005). Collision and closure of the Southern Neotethys Ocean Branch in this region occurred earlier than in the west and east, because of the impinging geometry of the Arabian Platform. Collision was superseded by renewed late Oligocene to middle Miocene extension, subsidence, and formation of deep sedimentary basins across much of the preexisting extensional setting that had formed from eastern Turkey to central Iran (Morley and others, 2009; Reuter and others, 2009; Shahabpour, 2005, 2007). Mantle-involved tectono-magmatic processes, including slab break-off and asthenospheric upwelling, are believed to have played a major role in generating this extensional regime and related magmatism (Aghazadeh and others, 2010, 2011; Azizi and Moinevaziri, 2009; Dilek and others, 2010).

From Turkey to central Iran, the late Eocene to middle Miocene postcollisional-to-back-arc, back-arc, and postcollisional volcano-plutonic events are delimited by the Azerbaijan tract (depicted in blue-green in fig. 7). Given the differences in the tectonic settings from west to east,

this tract is separated into the Azerbaijan–Western Turkey, Azerbaijan–Eastern Turkey, and Azerbaijan–Caucasus–Iran sub-tracts, respectively. The postcollisional to back-arc volcano-plutonic event delimited by the Azerbaijan–Western Turkey sub-tract contains 3 known porphyry copper deposits and 16 porphyry-related prospects, the back-arc volcano-plutonic event delimited by the Azerbaijan–Eastern Turkey sub-tract has only 1 known porphyry deposit and 1 prospect, and the postcollisional volcano-plutonic event delimited by the Azerbaijan–Caucasus–Iran sub-tract contains numerous known porphyry occurrences, including 5 porphyry copper deposits and 52 porphyry and porphyry-related prospects.

Figures 4F and 4G illustrate early Miocene (22 Ma) and late Miocene-early Pliocene (6 Ma) tectonic plate reconstructions of the Tethys region of western and southern Asia. In central and southeastern Iran, the northwest to southeast oblique closure of the southern Neotethys Ocean and final collision between the Arabian Platform and Eurasia (Mohajjel and others, 2003; Berberian and others, 1982) along the Bitlis-Zagros Suture is marked by middle-late Miocene uplift that resulted in inversion of earlier basins across the Sanandaj-Sirjan, Central Iranian, and Alborz Terranes. Subduction along the Sanandaj-Sirjan Terrane was active until the middle Miocene along central segment of the Urumieh-Dokhtar Magmatic Belt and until the late Miocene along the southeastern segment of the Urumieh-Dokhtar Magmatic Belt (Mohajjel and others, 2003; Berberian and others, 1982; Shafiei and others, 2009). The Urumieh-Dokhtar Magmatic Belt is a prominent range that trends northwest-southeast along the southern margin of the Central Iranian Terrane from northwestern to southeastern Iran. It is a composite Late Cretaceous to recent igneous province that emerged above sea level during the north-to-south diachronous Oligocene-Miocene to late Miocene collision between the Arabian Platform and the Sanandaj-Sirjan Terrane. Subduction along the Makran Trench in southeastern Iran and western Pakistan continues today.

This middle Eocene to middle Miocene and late Eocene to late Miocene diachronous continental arc-building event is delimited by the Yazd and Kerman tracts, respectively (shown in blue and purple, respectively, in fig. 7). The Yazd tract contains 2 porphyry deposits and 13 porphyry and porphyry-related prospects. The Kerman tract, conversely, contains 12 porphyry deposits and 70 prospects.

In southwestern Pakistan, Late Cretaceous to late Miocene progressive accretion of the Makran island-arc system onto the southern margins of the Farah and Helmand Terranes on the Eurasian margin created island- to continental-arc magmatism (Perelló and others, 2008; Khan and others, 2010). By the late Oligocene, accretion and the transition from island- to continental-arc magmatism was established, with the arc axis largely positioned over the preexisting back-arc environment. This Late Cretaceous to late Miocene island to continental arc volcano-plutonic event is delimited by the Chagai tract (shown in light green in fig. 7), which contains 4 known porphyry copper deposits and 25 prospects.

Late Miocene to Holocene

The distribution of latest Miocene to Holocene magmatism is closely linked with the neotectonic evolution of the Tethys region of western and southern Asia. Pliocene-Holocene magmatism includes compressional subduction-related settings to extensional postcollisional settings. Two subduction-related and one postcollisional events are delimited by the Pliocene-Quaternary sub-tracts described below.

Latest Miocene to Holocene subduction-related arc magmatism prevails on the western (Boztağ and others, 2004; Yilmaz, 1990; Pasquarè and others, 1988) and eastern (Perelló and others, 2008; Siddiqui and others, 2007) extremities of the Tethys region of western and southern Asia. The last remnants of the Southern Neotethys Ocean Branch are still being consumed in these two areas. Compared to other subduction settings around the world, the Hellenic-Cyprian and the Makran subduction zones in the Mediterranean Sea and Arabian Sea, respectively, are associated with shallow-dipping slabs (Hatzfeld and others, 1989; Platt and others, 1985). These shallow subduction angles are generating voluminous accretionary fore-arc prisms and continental arcs that are being built several hundred kilometers inland from the associated trenches. These two latest Miocene to Holocene volcanic-dominated continental arcs are delimited by the Pliocene-Quaternary–Konya and Pliocene-Quaternary–Bazman porphyry copper sub-tracts (fig. 8). One known porphyry prospect is included in the Pliocene-Quaternary–Konya sub-tract of west-central Turkey, and one porphyry prospect and one possible porphyry-related occurrence were identified and are included in the Pliocene-Quaternary–Bazman sub-tract of southeastern Iran and western Pakistan.

Compared to subduction-related magmatism, which typically forms distinct arcuate belts, postcollisional magmatism in the assessment region occurs in widespread, but irregularly distributed and isolated outcrops. Pliocene-Holocene postcollisional magmatism is dominated by shallowly emplaced volcanic rocks. These exhibit diverse mafic to felsic compositions that cover the spectrum from tholeiitic to calc-alkaline and high-K calc-alkaline to alkaline, as well as ultra-alkaline (Keskin, 2003; Yilmaz, 1990; Dilek and others, 2010; Azizi and Moinevaziri, 2009; Jahangiri, 2007; Omrani and others, 2008; Jamali and others, 2012; Berberian and King, 1981). Pliocene-Holocene postcollisional igneous rocks are most extensive in the Lesser Caucasus region, where collision between the Arabian Platform and the Eurasian margin generated intense crustal shortening. Crustal shortening generated extensional grabens parallel to the compression direction, and pull-apart basins along strike-slip faults (Sossou and others, 2010b). This latest Miocene to Holocene non-subduction-related volcano-plutonic event is delimited by the Pliocene-Quaternary–Postcollisional porphyry copper sub-tract, which contains 4 porphyry and porphyry-related prospects (shown in pink in fig. 8). Figure 4G illustrates the late Miocene-early Pliocene (6 Ma) tectonic plate reconstruction of the Tethys region of western and southern Asia.

Neotectonic Setting of the Tethys Region of Western and Southern Asia

The neotectonic setting presented in this section is intended to familiarize the reader with the present-day physiography of the study region and to convey that several tracts are partially superimposed and variably preserved in complex fold-and-thrust belts, which are the result of more than one deformation, uplift, erosion, subsidence, and (or) burial event. Furthermore, latest Miocene to Holocene magmatism is intimately linked with the neotectonic evolution of the region and offers a snapshot of the processes that also operated to a larger or lesser extent in the past.

Western, Central, and Southern Turkey

The neotectonic framework of Turkey is outlined by four major structures that separate the region into distinct tectonic provinces. These are the dextral North Anatolian Fault, the sinistral East Anatolian Fault, the sinistral Dead Sea Fault, and the Hellenic-Cyprian Trench. The Dead Sea Fault, East Anatolian Fault, and Hellenic-Cyprian Trench meet in southeastern Turkey to form a continental triple junction that is bound by the Anatolian Block to the northwest, the East Anatolian Province to the east, and the African Plate to the south. The Anatolian Block is being extruded westward along the sinistral East Anatolian Fault and the dextral North Anatolian Fault in an extensional setting. The East Anatolian Province southeast of the East Anatolian Fault is being transported northward in a collision-related compressional setting. The African Plate in the Mediterranean Sea is being subducted northward along the Hellenic-Cyprian Trench (fig. 2), forming a compressional arc and extensional back-arc system across western and central Turkey. Igneous rocks associated with this event define the Pliocene-Quaternary–Konya sub-tract with only one known porphyry prospect (see above). However, a few acid-sulfate epithermal systems transition into porphyry-style mineralization at depth (Stratex International PLC, 2012a).

In the Mediterranean Sea south of western and central Turkey, the Hellenic-Cyprian subduction system forms the boundary between the African and Eurasian Plates. Northward subduction of the remnant Neotethys Ocean at least since about 26 Ma (Meulenkamp and others, 1988) has resulted in extension of about 3 centimeters per year (cm/yr) in the back-arc region, which is preserved in central and western Turkey. Southward migration of the Hellenic-Cyprian Arc by subduction rollback was initiated around 12 Ma (Le Pichon and Angelier, 1979; Delaloye and Bingöl, 2000) and continues today in response to the combined effects of the relative motion between the African and Eurasian Plates (less than or equal to, \leq , 4 cm/yr) and the westward escape of the Anatolian Block (\leq 3 cm/yr). Tectonic escape of the Anatolian Block was well established by about 6 Ma (Dilek, 2010; Bozkurt and others, 2000; Keskin, 2003). Thus, back-arc and tectonic escape extensional events are superimposed in this region. Igneous rocks associated with these events are dominated by mafic compositions.

Northern Turkey

In north-central and northeastern Turkey, folded and thrust-faulted Paleogene successions north of the North Anatolian Fault are unconformably overlain by Oligocene to middle Miocene evaporites and continental red beds that were deposited in semiclosed euxinic basins (Adamia and others, 2011). This extensional event was followed by transpression, which initiated the dextral North Anatolian Fault around 12 Ma. This transpressional regime continues to the present day and is expressed by an east-west trending regional-scale horst separated by normal fault-bounded grabens to the north and to the south (Yilmaz and others, 2001; Boztuğ and others, 2003). Structural studies show that multidirectional normal (20.5 Ma to 9.7 Ma) and later strike-slip faults (9.7 Ma to present) formed in part as a result of gravitational collapse following collision between the Arabian Platform and the Eurasian margin in the south (Bozkurt and others, 2000). Intrusions and fissure eruptions locally occur along these extensional structures. Where they exhibit permissive intermediate to felsic compositions, they define the Pliocene-Quaternary-Postcollisional sub-tract (see above). No porphyry copper prospects of latest Miocene to Holocene age are known in this area. However, several epithermal systems that are associated with intrusions of intermediate alkaline composition are reported to transition into porphyry-style mineralization at depth (Yigit, 2009).

Eastern Turkey, Lesser Caucasus, and Northwestern Iran

The 27–10 Ma collisional event between the Arabian Platform and Eurasia along the Bitlis-Zagros Suture (fig. 2) resulted in intense crustal shortening and thickening in this region, which formed the East Anatolian contractional province (Dercourt and others, 1986; McQuarrie and others, 2003). In eastern Turkey, the Lesser Caucasus, and northwestern Iran, north-northwest compression during the early Miocene shifted to north-northeast during the late Miocene (Sosson and others, 2010a; Dilek and others, 2010). This compressional regime prevails today and is expressed as an active northwest-trending and south-vergent fold-and-thrust belt. Associated west-northwest dextral and east-northeast sinistral transpressional faults parallel the North and East Anatolian Faults, and north-northeast-south-southwest-trending normal structures parallel the main compression direction (Gamkrelidze, 1986; Bozkurt and Mittweide, 2001). These structures control large volcanic edifices, which form a trail that extends into the Greater Caucasus (fig. 2). Latest Miocene to Holocene volcanism is widespread in this region, and where it exhibits permissive intermediate to felsic composition, it defines the Pliocene-Quaternary-Postcollisional sub-tract (see above). One known porphyry copper prospect has been identified in this part of the sub-tract. However, some geothermal systems transition into porphyry-style mineralization at depth (Bogie and others, 2005).

Greater Caucasus and Northern Iran

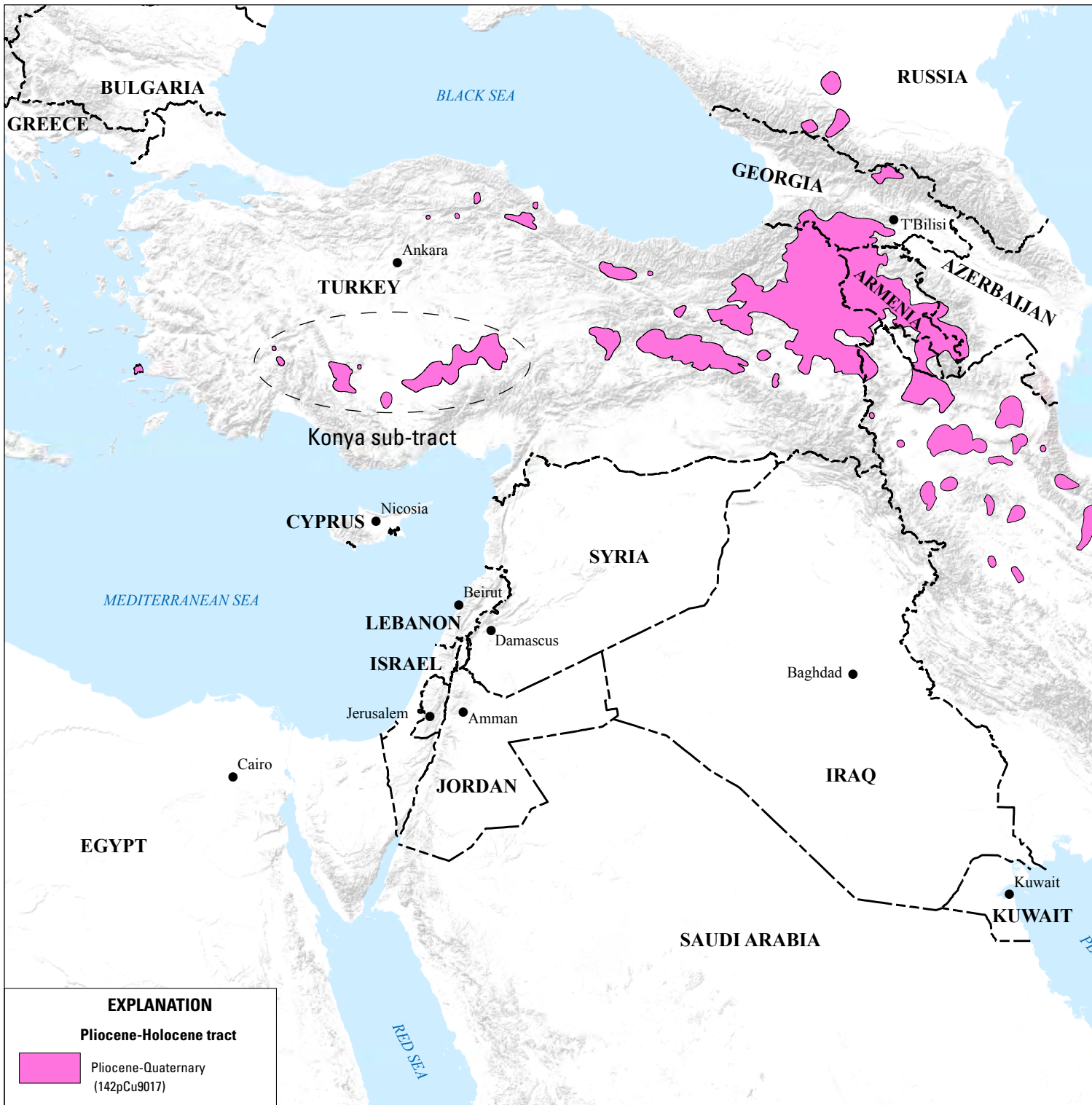
In the Greater Caucasus, paleogeographic reconstructions indicate that the region emerged above sea level only after the middle Miocene (13–14 Ma). Since then, the region has grown into a major mountain range formed by a doubly vergent fold-and-thrust belt (Saintot and others, 2006). Late Miocene (11–10 Ma) to middle-late Pliocene (3.4–1.8 Ma) compression and uplift were predominantly accommodated by west-northwest trending reverse faults (Mosar and others, 2010). A shift from a compressional to a transpressional regime over time resulted in northwest-southeast and thrust-parallel west-northwest oblique slip components, and associated north-northeast transtensional faults with left-lateral components along the main shortening direction (Saintot and others, 2006).

The compressional regime continues across northern Iran, where folding and thrusting in the Talysh and Alborz regions are a product of the far-field deformation associated with the middle Miocene collision between the Arabian Platform and Eurasia. Thrusting and folding dominate along the flanks of the Alborz mountain range (fig. 2). Thrusts dip north in the southern flanks, and south in the northern flanks of the range, creating a flower structure (Gansser and Huber, 1962). Deformation is accompanied by range-parallel steeply dipping sinistral strike-slip faults that are mainly located within the range interior (Mirnejad and others, 2010a), although the sense of strike-slip offset was just the opposite before 5 Ma (Zanchi and others, 2006; Axen and others, 2001). Faults with normal separation do occur and bound pull-apart basins along strike-slip faults (Ritz and others, 2006). Latest Miocene to Holocene volcanic edifices preferentially occupy these structural zones, and where they exhibit permissive intermediate to felsic composition, they define the Pliocene-Quaternary-Postcollisional sub-tract (see above). One deeply exhumed porphyry copper prospect is known in this part of the sub-tract.

In the Alborz range, as in the Greater Caucasus, thermochronological studies indicate rapid uplift and several kilometers of exhumation since 6 Ma (Axen and others, 2001). This age coincides with subsidence in the South Caspian Sea (fig. 3), where the larger fraction of the 10-km-thick sedimentary section there has been deposited since ~6 Ma (Guest and others, 2007).

The Kopet Dagh Terrane of northeastern Iran (fig. 2), like the Alborz Terrane, displays partitioning of the overall convergence into reverse and strike-slip components. In the western part of the Kopet Dagh Terrane, current shortening is accommodated by south-vergent west-southwest thrusts and thrust-parallel left-lateral strike-slip faults. In the eastern part of the Kopet Dagh Terrane, south-vergent east-southeast thrusts and right-lateral strike-slip faults parallel the Apsheron Sill that projects from the Caspian Sea into this region (Hollingsworth and others, 2010).

Structural elements in the Talysh, Alborz, and Kopet Dagh Terranes have not only been influenced by the far-field effects of the Arabian Platform-Eurasia collision to the south, but by their interaction with the adjacent South Caspian Sea Terrane to the north (fig. 3). Geophysical data suggest that South Caspian Sea Terrane is in the early stages of subducting north and possibly



Base from SRTM Global Digital Elevation Model, U.S. Geological Survey EROS Data Center, 2006.
 Political boundaries from U.S. Department of State (2009).
 Asia North Albers Equal-Area Conic Projection.
 Central meridian, 50° E., latitude of origin, 35° N.

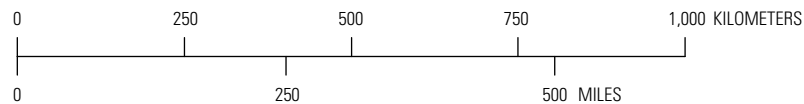
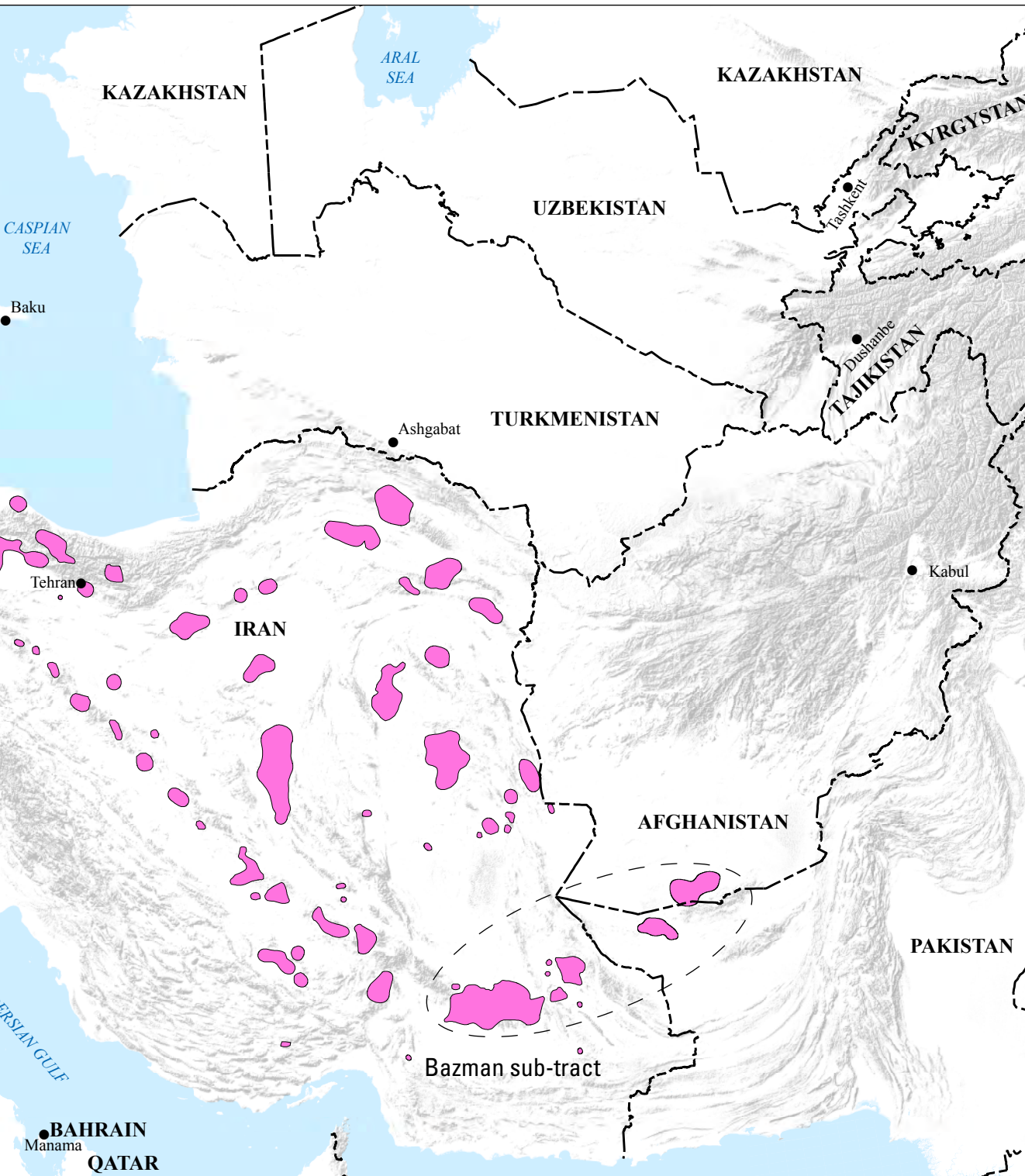


Figure 8. Pliocene to Holocene permissive tract for porphyry copper deposits in the Tethys region of western and southern Asia.



west under the Apsheron Sill and the Talysh regions, respectively (Golonka, 2004). Thus, the South Caspian Sea Terrane appears to be moving westward relative to the adjacent terranes of northern Iran, resulting in thrusting in the Talysh Terrane to the west, thrusting and left-lateral faulting in the Alborz and western Kopet Dagh Terranes to the south, and thrusting and right-lateral faulting along the on-land projection of the Apsheron Sill in the eastern Kopet Dagh Terrane to the east (Allen and others, 2006). Latest Miocene to Holocene volcanism preferentially occupies these structural zones, and where it shows permissive intermediate to felsic composition, it defines the Pliocene-Quaternary–Postcollisional sub-tract. No porphyry copper prospects have positively been identified in this part of the sub-tract.

Eastern and Central-Eastern Iran

In the Sistan suture zone of eastern Iran, east-northeast-directed convergence and final collision between the Lut Terrane of Iran on the west and the Farah Terrane of Afghanistan (fig. 3) on the east occurred between the middle Eocene and middle Miocene (Tirrul and others, 1983). Since then, continued compression is being accommodated by north-northwest- and northeast-trending en echelon dextral faults that are part of the greater Nehbandan Fault system (fig. 2). However, the major relative motions appear to be occurring along the Nehbandan fault proper (Allen and others, 2006).

In the Lut Terrane of central-eastern Iran, the neotectonic structure consists of a series of parallel north-northwest right lateral faults represented by the Nayband and Nehbandan transpressional systems (fig. 2) that bound the Lut Terrane to the east and west, respectively (Walker and Jackson, 2004). As in the Sistan suture zone, these structures are accommodating the ongoing east-northeast-directed horizontal shortening in the region, which is generally composed of dextral northeast and sinistral northwest faults (Wellman, 1966).

Latest Miocene to Holocene volcanic-dominated igneous rocks preferentially occupy structural zones in eastern and central Iran. Where they show permissive intermediate to felsic composition, they define the Pliocene-Quaternary–Postcollisional sub-tract. No porphyry copper prospects have positively been identified in this part of the sub-tract.

Central and Southeastern Iran

The diachronous northwest-to-southeast oblique collision between the Arabian Platform and the Eurasian margin occurred about the late Oligocene (~27 Ma) in the northwestern part, about the middle Miocene (~16 Ma) in the central part, and about the late Miocene (~7 Ma) in the southeastern part (Agard and others, 2011) of Iran. From northwestern to southeastern Iran, collision along the Bitlis-Zagros Suture triggered widespread crustal shortening and thickening, generating uplift and a fold-and-thrust belt in the Sanandaj-Sirjan and Central Iranian Terranes (fig. 3). Evidence of far-field deformation is also present to the north in the Talysh, Alborz, and Kopet Dagh Terranes. Since the early

Pliocene, folding associated with the south-vergent thrusting of the Sanandaj-Sirjan Terrane over the Arabian Platform has also propagated to the southwest across the Bitlis-Zagros Suture forming the present-day Zagros Folded Belt (Stöcklin, 1968; Alavi, 1994; Molinaro and others, 2005). To the northeast of the Bitlis-Zagros Suture, north-vergent thrusts and northwest-southeast en echelon strike-slip faults occur well into the Central Iranian Terrane (Alavi, 1994). Deformation is most intense along the Bitlis-Zagros Thrust, which consists of a combination of thrusting followed by Pliocene-Holocene right-lateral strike-slip movements (fig. 2). Strike-slip displacements are estimated at between 50 and 70 km over the past 3–5 million years (m.y.) (Talebian and Jackson, 2002; Jackson and McKenzie, 1984). This compressional to transpressional regime continues today.

Large volcanic edifices of latest Miocene to Holocene age occur along the Urumieh-Dokhtar Magmatic Belt in this region. Permissive intermediate to felsic igneous rocks associated with this event define the Pliocene-Quaternary–Postcollisional sub-tract. One known porphyry copper prospect of Latest Miocene to Holocene age is included in this part of the sub-tract. However, as many as five other porphyry and porphyry-related acid-sulfate systems are possibly also related to this postcollisional magmatic event (Biabangard and others, 2011; Shahabpour, 2007; Parsapoor and others, 2009).

Southeastern Iran and Southwestern Pakistan

The subduction-related Bazman-Taftan-Koh-i-Sultan continental arc of southeastern Iran, western Pakistan, and southern Afghanistan initiated in the Miocene-Pliocene as a result of southward migration and flattening of the subducted slab, now located along the Makran Trench. Large early Pliocene to Holocene volcanic edifices associated with this volcano-plutonic event define the Pliocene-Quaternary–Bazman sub-tract. The Bazman-Taftan-Koh-i-Sultan Arc hosts numerous epithermal systems, some of which are known to be porphyry-related. This sub-tract includes two positively identified porphyry prospects (Bhutta, 2004; Perelló and others, 2008; Samani, 1998).

Assessment Data

The assessment team used digital geologic, tectonic, geophysical, and remote sensing maps, topical data and maps at various scales, published literature, mineral occurrence databases, technical reports on prospects, and mining company Web sites to compile and analyze the complex interplay between the ore-forming environment, exposure level, and exploration extent supplied by the data. These data provided the foundation to select the appropriate grade-tonnage model, to delineate tracts, to evaluate favorability and associated uncertainty, and to make individual estimates of the numbers of undiscovered porphyry copper deposits in the assessment region. These estimates in turn were used in the probabilistic simulation of undiscovered resources in the assessment region.

Geologic Maps

Geologic maps were the primary source of information for delineating permissive tracts. Volcano-plutonic belts, the fundamental features used to delimit tracts permissive for the occurrence of porphyry copper deposits, were defined by creating derivative map layers that grouped geologic units of similar age and lithological character. For each tract, map units were categorized into (1) older basement rocks, (2) calc-alkaline and alkaline intrusive and extrusive units of felsic to intermediate composition and age range (that is, permissive units), (3) coeval sedimentary, volcano-sedimentary, and ultramafic and mafic igneous units (that is, nonpermissive units), and (4) younger cover rocks. This allowed for effective use of GIS tools in the evaluation and selection of those rock types likely or unlikely to be associated with a volcano-plutonic event and associated porphyry copper deposits.

The primary geologic base maps used for the identification of permissive igneous units used to define each porphyry copper tract included digital versions of the 1:1,000,000 geologic map of Iran (Huber, 1978), the 1:1,000,000 metallogenetic map of the Caucasus (Kekelia and others, 2001), the 1:500,000 geologic map of Turkey (General Directorate of Mineral Research and Exploration, 2000), the 1:1,000,000 geologic map of Pakistan (Qureshi and others, 1993), the 1:2,000,000 (Pollastro and others, 1998) and 1:1,000,000 (Sissakian, 2000) geologic maps of Iraq, and the 1:850,000 geologic map of Afghanistan (Peters and others, 2007). Numerous additional sources were used to further constrain ages, compositions, and other geologic features. Appendixes A and B list the principal sources of data and geologic map units used to define each permissive tract, respectively.

Tectonic Maps

Terrane boundaries were used to identify and delimit tectonic settings, and where applicable, the extent of tracts. Boundaries were digitized after Abdullah and Chmyriov (1977b) and Peters and others (2011) for Afghanistan, Kazmi and Rana (1982) for Pakistan, Stöcklin (1968) for Iran, Pollastro and others (1998) for Iraq, Kaymakci and others (2010) and Yigit (2009) for Turkey, and Kekelia and others (2001) for the Caucasus. Terrane names used throughout this report conform to these sources and also Golonka (2004). Additional sources used for tectonic features are listed in appendix A.

Mineral Occurrence Data

The database of porphyry copper deposits and prospects (appendix D) compiled for this assessment served two purposes—(1) porphyry deposits were used to compare reported geologic characteristics and resource data in the study area with descriptive and global grade and tonnage models for porphyry copper deposits, and (2) porphyry prospects were used to assist in the delimitation of tracts and the assessment of geologic favorability and uncertainty. Porphyry prospects may just be

small manifestations of the same processes that generate porphyry deposits. However, they are exceptional “geochemical samples,” because they may provide information on the location of permissive units that are not represented at the regional scale of the geologic map used, on the composition of the related intrusions, on the metal associations present, on the level of exhumation or burial, and on the extent of exploration (see below).

Known Porphyry Deposits and Prospects

The database of porphyry copper deposits and prospects resulted from a data compilation effort aimed at complementing and augmenting the Singer and others (2008) porphyry copper database with mineral occurrence databases from the Geological Survey of Iran (2012e), Kekelia and others (2001), Rundkvist (2001), Kirkham and Dunne (2000), and Engin and others (2000). Significant other sources of relevant information on porphyry deposits and prospects used for this study include Bazin and Hübner (1969a, b), Förster (1978), Karimpour and others (2011b), Boztağ and others (2003), Kuşçu and Erler (1998), Yigit (2006, 2009, 2012), Jamali and others (2010), Al-Bassam and Hak (2006), Richards and others (2012), Perelló and others (2008), and Orris and Bliss (2002). The reader is referred to appendix A for these and additional sources of information on porphyry and porphyry-related occurrences in the assessment region.

Forty-five porphyry copper deposits and 275 porphyry and porphyry-related prospects were identified (see appendix D). An additional 47 possible porphyry-related occurrences are also included in the database. These possible porphyry-related occurrences consist mainly of skarn and epithermal systems for which a relation to porphyry-style mineralization has not been established.

Porphyry-Related Deposit Types

Porphyry-related deposit types are mineral systems that may be related to undiscovered porphyry copper deposits (Arribas and others, 1995; Einaudi, 1982). These include intrusion-centered skarn, carbonate-replacement, and sediment-hosted deposits in increasingly peripheral locations, and superjacent high- and intermediate-sulfidation epithermal deposits. Porphyry $\text{Cu}\pm\text{Au}\pm\text{Mo}$ deposits are centered on the intrusions, whereas carbonate wall rocks host proximal Cu-Au skarns, distal $\text{Pb-Zn}\pm\text{Au}$ skarns, carbonate-replacement Cu and (or) $\text{Zn-Pb-Ag}\pm\text{Au}$ mantos and veins beyond the skarn front, and (or) sediment-hosted gold deposits (Sillitoe, 2010). Porphyry-related deposits also include porphyry systems that may share the same setting with porphyry copper deposits but exhibit more diverse igneous compositions and metal associations (Seedorff and others, 2005) that may not be well represented in available descriptive and grade-and-tonnage models. Recent literature, company Web sites, and technical reports for exploration projects were checked for descriptions of geology, mineralogy, deposit type, rock alteration, and sampling results to evaluate the likelihood that these prospects

were associated with a porphyry copper system similar to those in the descriptive model. In this assessment, 51 porphyry-related prospects are included in the database of 277 porphyry prospects (appendix C).

Spatial Rules for Grouping Deposits and Prospects

Spatial rules were used to define the sampling unit that represents a deposit to ensure consistency in defining deposits as geologic entities for mineral-resource assessment (Singer and Menzie, 2010). For porphyry copper deposits, two operational rules were applied in constructing the Singer and others (2008) grade and tonnage models—(1) all mineralized or altered rock within 4 km was combined as a single deposit, and (2) grade and tonnage data were compiled for these deposits based on total production, reserves, and resources at the lowest reported cutoff grade. In this assessment, these rules applied to the Reko Diq deposit.¹⁵

Exploration

The following sections offer a review of the history, environment, and extent of exploration for porphyry copper deposits that has occurred in the assessment region, by country, and based on available published literature. Knowledge about the extent and efficiency of exploration is relevant because it influences the uncertainty about where, how large, and how rich undiscovered mineral resources may be in a permissive tract (Singer and Menzie, 2010). Commonly, exploration is partial and its influence on the uncertainty associated with estimating numbers of undiscovered deposits requires evaluation in conjunction with other geological, geophysical, and mineral occurrence data. Where exploration efforts are known to have been extensive and thorough, uncertainty in estimating the numbers of undiscovered deposits is lowered. However, this may also have the effect of lowering estimates of the numbers of undiscovered deposits, given that most if not all deposits present in a specific tract may have already been identified. Conversely, where exploration extent is not known or has not occurred, estimates of undiscovered deposits rely on other available information to assess the uncertainty associated with favorability.

Afghanistan

Afghanistan is relatively underexplored geologically but believed to have large untapped energy and mineral resources

¹⁵The resource reported in the list of deposits for this report (table 2) is the weighted average of Reko Diq H8, Reko Diq H13, Reko Diq H14, and Reko Diq H35, whereas the spatial database (appendix D) reports each location individually. For this reason, table 2 contains 42 deposits, whereas the spatial database has 45 deposits. Similarly, a total of 318 porphyry prospects, porphyry-related prospects, and possible porphyry-related occurrences are reported in appendix C, but 322 occurrences of these types are included in the spatial database.

(British Geological Survey, 2006b). The mining industry is largely at an artisanal stage of development. The major mineral resources include chromium, copper, gold, iron, lead and zinc, lithium, marble, precious and semiprecious stones (lapis lazuli), sulfur, and talc (Kuo, 2011a).

Before 2001, exploration for mineral resources in Afghanistan was conducted by geologists from the Soviet Union who left geologic records that indicate significant mineral potential. Between 2005 and 2011, scientists with the USGS and the Afghanistan Geological Survey collaborated to collect and consolidate existing information about known mineral deposits. This countrywide geological integration effort culminated with the creation of mineral resource information packages that have been offered for bidding to international mining companies (Peters and others, 2011). The Government of Afghanistan has introduced new mineral and hydrocarbon laws to meet international standards of governance, including no local ownership requirements or exposure to possible nationalization, and a 20-percent corporate tax rate that is the lowest in the region.

Afghanistan has two known world-class mineral prospects in the development stage—the Aynak sediment-hosted stratiform copper (240 Mt at 2.3 percent copper; British Geological Survey, 2006a) and the Hajigak iron skarn (2 billion metric tons, Bt, at 63–69 percent iron; Orris and Bliss, 2002; Afghanistan Geological Survey, 2007). However, few porphyry systems have been identified (Ludington and others, 2007). They include the Okhankoshan Cu-Au-Mo porphyry and the possible porphyry-related Zarkashan and Ahonkashan copper-gold skarns (British Geological Survey, 2006b). In the southernmost part of the Afghanistan covered by this assessment, recent exploration for porphyry copper deposits has largely been limited to remote sensing studies (King and others, 2011; Kuo, 2011a).

Armenia

Armenia is a major producer of molybdenum. It was ranked seventh in the world in mine output in 2009 (Levine, 2011a). Besides molybdenum, Armenia produces other metals, which include iron, copper, lead, zinc, gold, and silver (Norwest Mineral Sector Investment Focus, 2003; Wikipedia, 2012a). Armenia's industrial-scale metal production began in the early 19th century with the opening of the Alaverdy and Kapan copper mines. In the early 1950s, the country's economy began to focus more on mining with the development of the Zangezur Copper Molybdenum Combine, which operates the world-class Kadjaran deposit. The Agarak Copper-Molybdenum Mine Complex was originally established in 1958.

Most known porphyry systems were identified through exploration efforts conducted during the Soviet Era. However, deposit-specific geologic information is sparse. Several decades of mine development were interrupted by the dissolution of the Soviet Union, coupled with the decline in commodity prices. Armenia's minerals sector also faced other challenges, such as the closure of both the Azerbaijani and Turkish borders, which hindered access to world markets and government efforts to attract foreign investment. Since 2000, however, revisions to the

regulatory framework have led to the liberalization of contractual mechanisms and privatization of mining companies. These reforms have lowered inflation and increased foreign investment in the country (Mining Journal, 2005).

Several international mining companies are now actively engaged in exploration and development efforts of porphyry copper deposits (Mining Journal, 2011a). Development was expected to start in the second half of 2013 at the Teghout porphyry deposit (Vallex Group, 2013), and the current capital investment program at Agarak includes installation of new flotation circuits and upgrades to existing equipment (GeoProMining, 2012). These renewed exploration efforts are producing more detailed deposit-specific and regional geologic information, augmenting the previously identified resources at several porphyry and porphyry-related deposits and prospects (Norwest Mineral Sector Investment Focus, 2003).

Azerbaijan

Azerbaijan's most economically significant natural resource is oil. The country has been a significant oil producer for more than a century and is currently developing its offshore resources in the Caspian Sea. However, Azerbaijan also has known iron, pyrite, molybdenum, bauxite, arsenic, industrial mineral, and polymetallic deposits (Levine, 2011b). Large resources of iron are located at the Dashkesan iron skarn, which contains an estimated 300 Mt at 45 and 60 percent iron assessed according to the Soviet reserve classification system. The deposit also contains as much as 0.04 percent cobalt and vanadium (Levine and Wallace, 2010).

Exploration for porphyry copper deposits since the Soviet Era includes recent efforts by Anglo Asian Mining PLC (2011). The company has been conducting exploration in several areas. To assist exploration, Anglo Asian Mining PLC has been analyzing older geological data under a production-sharing agreement with the Azerbaijan government (Anglo Asian Mining PLC, 2011). The company has developed and is mining the historic Kedabek gold-copper-silver porphyry deposit, which from 1864 to 1917 produced 56,000 t copper and 134 t of gold-silver doré from 1.72 Mt of ore (Anglo Asian Mining PLC, 2011). The company was expected to produce 25,000 troy ounces (troy oz) of gold in the year ending in July 2010 (Anglo Asian Mining PLC, 2011). Significant porphyry copper potential also exists in the Nakhchivan Autonomous Republic located southwest of Armenia. Anglo Asian Mining PLC holds exploration licenses at the Ordubad, Soyutlu, and Vezhnali prospects (Safirova, 2013a). In addition to gold, these prospects contain silver and copper, but their association to porphyry-style mineralization has not been confirmed (Azerbaijan Ministry of Ecology and Natural Resources, [2006?]).

Georgia

During the Soviet Era, many minerals were mined in Georgia. These included arsenic, barite, bentonite, coal, copper, diatomite, lead, manganese, zeolites, and zinc (Wikipedia, 2013b).

The country was a major producer of high-grade manganese ore from the Chiatura deposit and base metals from the Madneuli volcanogenic massive sulfide (VMS) Cu-Au-Zn-Ba deposit (Safirova, 2013b). Following the dissolution of the Soviet Union, the level of mineral production in Georgia declined sharply. Although production in the mineral industry was reviving in 2005, the government has lacked the financial resources to introduce modern mining and processing technologies. Therefore, growth in the mining and metallurgical sector has lagged (Levine, 2011c). Exploration of porphyry deposits in Georgia has been limited. Only a few porphyry-related prospects have been identified (Moon and others, 2001).

Iran

Iran's mineral wealth, in addition to oil and gas, includes chromite, lead, zinc, copper, coal, gold, tin, iron, manganese, ferrous oxide, and tungsten. Iran possesses large copper resources contained in porphyry deposits, including the world-class Sar Cheshmeh and Sungun mines.

Mining in Iran has taken place since about 5,000 B.C. Anarak, for example, was one of the earliest mining regions the world (Momenzadeh, 2005). Copper artifacts discovered during various studies and at sites of primitive smelting furnaces, still visible today, confirm that Iran has been mining and smelting copper for centuries. During the 1960s and 1970s, geologic surveys by the Iranian government led to the systematic recording of known deposits, as well as the search for new ones. As a result, about 250 copper occurrences and several potentially viable projects were recognized, including the Darreh-Zerreshk and Ali Abad porphyry systems (Zaravandi and others, 2005). At the same time, prospecting and drilling was underway at Sar Cheshmeh (Bazin and Hübner, 1969b). The Sungun deposit was discovered in the mid-1970s when fluid inclusion analysis suggested the presence of mineralization similar to that found at other world's large copper deposits (Etminan, 1977). In 1972, Sar Cheshmeh Copper Mines Joint Stock Co. of Kerman was established, which in 1976 was renamed as the National Iranian Copper Industries Company to encompass all copper mining operations throughout Iran. By 1977, about half the country had been surveyed from the air, but less than one-fifth had been explored on the ground (Metz, 1987).

Following the revolution in 1979 and the 1982 Iran-Iraq War, Australian, Canadian, French, and Yugoslavian mining companies joined the Geological Survey of Iran in the exploration effort. Since 1998, the Iranian government has allowed foreign investment in mineral exploration joint ventures. For its economic development plan 2000–2005, the government proposed to privatize 40 mineral industry companies affiliated with the Ministry of Industry and Mines, having already divested itself of more than 90 percent of its mineral enterprises. In 2009, Kazakhmys, Kazakhstan's largest mining and energy group and international natural resources company, announced that it would expand its activities in Iran and assist the country in projects to discover gold and copper deposits (PressTV, 2009).

Over the past 10 years, the National Iranian Copper Industries Company has led extensive exploration efforts for porphyry copper deposits, particularly in the northwestern Arasbaran and southeastern Kerman regions of the country. Sar Cheshmeh and Meiduk in Kerman Province and Sungun in eastern Azerbaijan Province are the three largest porphyry copper mines in the country (Etminan, 2003). Several other porphyry deposits are in development or have begun operations, including Haft Cheshmeh and Masjed Daghi in the northwestern part and Darrehzar, Chah-Firuzeh, Taft (Darreh-Zerreshk and Ali-Abad), and Dar Alu in the southeastern part of the country (National Iranian Copper Industries Company, 2012). More recent exploration efforts have also identified porphyry copper prospects in the Yazd (for example, Ayati and others, 2013), central-eastern Lut (for example, Richards and others, 2012) eastern Sistan (for example, Zarcán International Resources, 2000), and northeastern Khorasan (Karimpour and Malekzadeh, 2006; Alaminia and others, 2011) regions of the country. In contrast, limited porphyry-related exploration information available for the northern Alborz, western Sanandaj-Sirjan, central Iranian, and Makran regions of the country suggest that these regions may be comparatively underexplored for porphyry copper deposits.

Pakistan

Pakistan has copper, iron, limestone, and salt resources. Pakistan also has moderate oil and sizable gas resources, as well as high potential for coal (Kuo, 2011b). The Government of Pakistan encourages foreign investment in exploration and development of the mining sector. Under the government's investment incentives, foreign equity of as much as 100 percent is allowed. Remittance of capital and profits are permitted, and expatriate facilitation is offered. The government, through the Geological Survey of Pakistan, generates basic geologic data with the purpose of identifying exploration projects. However, in accordance with the Constitution of Pakistan and the National Mineral Policy (Pakistan Ministry of Petroleum and Natural Resources, 1995), the exploration for and development of minerals are under the authority of individual provinces. Each province develops its own mining code, which is based on the model set forth in the National Mineral Policy. The mineral policy is intended to provide the institutional and regulatory framework for ensuring an equitable and internationally competitive fiscal regime for the mineral sector (Kuo, 2011b).

The first systematic geological mapping of Pakistan at a scale of 1 inch to 4 miles (1:253,440) was undertaken in 1952–56 under the Canada-Pakistan Colombo Plan project. In 1956–70, mapping and appraisal of geological resources in Pakistan continued under a cooperative program between the Geological Survey of Pakistan and the USGS, which resulted in the discovery of the copper-mineralized quartz-diorite stocks at Saindak in the 1970s (Everest Gold, Inc., 2012; Wikipedia, 2013c). During this time, regional geologic and mineral deposits studies sponsored by the Development Corporation of Pakistan and the United Nations were also underway (Sillitoe, 1978). During 1991–93, Metallurgical Construction Corporation of

China (MCC) constructed a metallurgical plant and initiated the Saindak open pit mine. The project was transferred to Saindak Metals Limited in early 1996 after a successful trial operation that produced 1,550 t of blister copper. Due to a shortage of working capital, the mine was placed on a care-and-maintenance basis until 2003, when it was recommissioned by MCC (Everest Gold, Inc., 2012).

In the early 1990s, BHP (subsequently BHP Billiton) commenced an extensive exploration effort in the Chagai region, which resulted in the identification of several porphyry prospects and the discovery of the giant copper-gold porphyry deposit at Reko Diq (Mincor Resources NL, 2003). Tethyan Copper Company, Ltd., continued exploration under an agreement with BHP Billiton until early 2006, when Tethyan Copper Company, Ltd., was taken over by Antofagasta PLC. Between 2006 and 2011, the mineral interests of Tethyan Copper Company, Ltd., were managed and operated by a 50/50 joint venture between Antofagasta and Barrick Gold Corporation. In 2011, however, the Government of Balochistan rejected the application for a mining lease (Tethyan Copper Company, [n.d.]).

Turkey

Turkey is a country with a large and diverse mineral-resource base, and a history of mining dating back thousands of years (Yigit, 2012). During the past two decades, Turkey has become an exploration frontier. Roughly 40 percent of the total exploration projects and expenditures within the Tethyan Eurasian Metallogenic Belt have been in Turkey (Canby, 2007). Changes in the Turkish mining law in 1985 stimulated mineral exploration activities and resulted in several new discoveries. Furthermore, since amendment of the mining law in 2004, exploration licenses assigned by the Turkish Energy Ministry's General Directorate of Mining have almost tripled (Yigit, 2009). Today, foreign capital companies established in Turkey for mining purposes are entitled to hold mining rights (Önder, 2006).

Exploration for porphyry copper deposits in Turkey was started in the early 1970s by the United Nations Development Program and Turkey's General Directorate of Mineral Research and Exploration (MTA). Although the program identified several prospects, including the Bakırçay and Ulutaş systems (Akıncı, 2004), none of them appear economic at present. However, since enactment of the favorable changes to the mining and investment laws, exploration activity for base and precious metals in Turkey has grown considerably, generating several projects centered on porphyry mineralization. Two of these, the Kışladağ and Çöpler deposits, constitute at present the largest mining operations in Turkey.

Exploration efforts continue in the northeastern Pontides and more recently have also focused on the western and eastern Anatolian regions of Turkey (Mobbs, 2012). The northwestern Pontides, central Anatolian, and particularly the southeastern Border Folds regions of the country remain comparatively underexplored for porphyry copper deposits (Yigit, 2009; Global Business Reports, 2012).

Other Data

ASTER and HyMap Data

Processed Advanced Spaceborne Thermal Emission and Reflection Radiometer (ASTER) data were used to identify and characterize possible hydrothermal phyllic and argillic alteration zones associated with potential porphyry copper sites (Mars and Rowan, 2006; Mars, 2014). ASTER data coverage was available for parts of permissive tracts in Iran, western Pakistan, and southern Afghanistan. No ASTER data were available for tracts and extensions of tracts in Turkey and the Caucasus.

ASTER data consist of three bands in the 0.52–0.86 micrometer (μm) wavelength region (visible and near-infrared, VNIR); six bands in the 1.6–2.43 μm wavelength region (short-wavelength infrared, SWIR); and five bands of emitted radiation in the 8.125–11.65 μm wavelength region (Thermal infrared radiation, TIR) with 15-, 30-, and 90-meter (m) resolution, respectively. Logical operator algorithms developed to perform multiple band ratio and threshold value calculations were applied to each 30-m resolution scene to map spectral reflectance absorption features associated with likely argillic and phyllic hydrothermal alteration, as shown by the diagnostic absorption spectra of kaolinite and alunite, which are common in argillic-altered rocks, and muscovite, which is common in phyllic-altered rocks (Mars and Rowan, 2006).

Processed hyperspectral imaging spectrometer (HyMap) data were also available for the Chagai tract segment in Afghanistan. The HyMap imaging spectrometer measures the reflected visible to shortwave infrared wavelength range of 0.43 to 2.48 μm in 128 channels. The reflectance spectrum for each pixel in the image is compared against entries in a library of reference spectra, which can then be used to identify the occurrence of selected materials at the surface based on the presence and wavelength position of absorption features in the 0.45–2.48- μm -wavelength region. Two general categories of minerals are recognized—(1) iron-bearing minerals that have characteristic spectral absorption features that occur at wavelengths near the 1- μm region and (2) other minerals including carbonates, phyllosilicates, and sulfates that have diagnostic spectral absorptions near the 2- μm region. The identified minerals, mineral groups, and suites of minerals are used to define zones of hydrothermal alteration (King and others, 2011).

In combination with available age and deposit information, many ASTER-derived (and over Afghanistan also HyMap derived) alteration locations do coincide with known porphyry deposits and prospects, and where they are not associated with other types of known deposits, they mark not only the presence but the location of possible hydrothermal alteration potentially associated with unidentified porphyry-related systems.

Geophysical Data

The assessment team used the 2-arcminute resolution (1 arcminute=1/60 degree) Earth Magnetic Anomaly Grid (EMAG2) compilation of Maus and others (2009) to confirm

the location and character of regional geologic features (for example, arcs, basins, faults, terrane boundaries). EMAG2 is a compilation from satellite, ship, and airborne magnetic measurements reduced to 4 km above the geoid. In this version, interpolation between tracklines in the oceans was improved by directional gridding and extrapolation, based on the oceanic crustal age model. The longest wavelengths (larger than 330 km) were replaced with the latest CHAMP¹⁶ satellite magnetic field model (MF6). With the exception of northeastern Iraq, the EMAG2 covers all of the area in the assessment region. For Turkey, these data were complemented with the gravity and magnetic anomaly maps of Ates and others (1999).

At the regional scale, geologic features are well-imaged in several parts of the Tethys region of western and southern Asia. In general, magnetic highs were found to reflect mafic to intermediate rocks in accretionary- and arc-related environments, whereas magnetic lows were found to reflect sedimentary basins or sources that are either weakly magnetic or at considerable depth. Otherwise, 2-arc magnetic information was deemed to have insufficient resolution to allow interpretation of whether shallowly buried (for example, less than 1 km from the surface) extensions of permissive units of a given age range projected beyond tract boundaries. One of the main difficulties in attempting this is that tracts delimiting volcano-plutonic events of different ages in the assessment region are not only superimposed in many places but also variably “masked” by younger geologic formations with high magnetic susceptibilities (for example recent basalts).

Preservation Level Data

Tectono-magmatic processes played a key role in localizing porphyry deposits in the region. However, the level of erosion currently exposed by the interaction of exhumation and burial processes, not just the ore-forming environment, influenced the observed distribution of metallogenic patterns. For that reason, exploration for porphyry copper deposits and documentation of prospects typically occurs first and is longer lived where ideal levels of preservation of porphyry systems are exposed. Thus, the level of preservation in a given tract is reflected, at least in part, by the number of known porphyry occurrences (that is, the sum of deposits and prospects) within it. Analysis of exposure levels and numbers of porphyry occurrences provided information useful for assessing aspects of the geologic favorability and associated uncertainties, as well as the probable exploration extent in areas where this information was not available. Implications of these results are examined further in the discussion section at the end of this report.

Estimation of crustal levels of preservation in each tract made use of the derivative maps created to group geologic units of similar age and lithological character, as well as the finalized permissive tracts. To evaluate the level of crustal preservation, the relative aerial extent of older basement, permissive (intermediate to felsic plutonic and volcanic) and

¹⁶Challenging Minisatellite Payload.

nonpermissive (sedimentary, and mafic or ultramafic igneous) units of a given age range, and younger (plutonic, volcanic, volcano-sedimentary and sedimentary) cover units was calculated for each tract. We determined permissive volcanic-to-plutonic unit ratios expressed as percentages using the relation $\{\text{volcanic}/[\text{volcanic}+\text{plutonic}]\} \times 100$.

These procedures involved clipping the geologic base map to the tract extent, recalculating polygon areas, and querying the resulting data for lithological and age information. The results were then used to assess levels of crustal preservation across a delimited tract based on $\{\text{volcanic}/[\text{volcanic}+\text{plutonic}]\} \times 100$ as appropriate (about 33 to 66), too deep (less than 33), or too shallow (more than 66) for hypabyssally emplaced porphyry copper systems. These results also allowed estimation of the extent of younger cover rocks and the likelihood for porphyry systems to be buried or exposed.

Assessment Methods

Compilation and integration of data layers for the three-part form of mineral-resource assessment was followed by permissive porphyry tract delineation and estimation of numbers of undiscovered deposits. The following sections describe (1) the criteria and procedures used to define and delimit geographic areas permissive for porphyry copper deposits (tracts) and (2) the process of estimation of numbers of undiscovered deposits and probabilistic simulation of associated metal contents.

Tract Delineation

The geology-based strategy for permissive tract delineation used in this assessment was done in six stages. Digital geologic data were processed in a GIS using ArcMap software, as follows:

1. Regional-scale maps and geologic literature were used to identify the fundamental units for tract delineation—magmatic arcs or belts of igneous rocks of a given age range—as delimited by first-order tectonic features (for example, Eurasian, Cimmerian, and Afro-Arabian terranes and sutures marked by major ophiolite-bearing accretionary prisms marking the former location of the northern and southern Neotethys Oceans and other intraoceanic basins).
2. Digital geologic maps were then used to select map units to define preliminary tracts permissive for porphyry copper deposits. Map units were classified as permissive or nonpermissive based on lithology and further divided by age groups as bracketed by changes in first-order and second-order tectonic events. Permissive rocks include calc-alkaline to alkaline plutonic and volcanic rocks of intermediate to felsic composition. Nonpermissive rocks include ultramafic and mafic, volcano-sedimentary, and sedimentary rocks of that age group. Given their reduced extent, nonpermissive peraluminous intrusions could not be excluded effectively at the 1:1,000,000 scale used. Depending on their timing, most metamorphic rocks were also considered as nonpermissive.
3. Areas with postmineral intrusive, extrusive, sedimentary, and other forms of younger cover estimated to exceed 1 km in thickness for the tectono-magmatic event also delimited the extent of the tract boundary. At the resolution of the map scale used, and given that many of the tracts are preserved in synmineral and postmineral fold-and-thrust belts where structural relations are complex and thicknesses may vary widely across individual faults, it was not possible to estimate the thickness of cover with certainty. Thus, a 10-km buffer was applied to plutonic rock polygons and a 2-km buffer to volcanic rock polygons. These buffers were found to effectively encompass permissive units and most associated porphyry copper deposits and prospects and account for uncertainties in the cartographic position of mapped units and known permissive rocks not shown at the map scale used.
4. The boundaries of tracts were further refined by the team examining available data on mineral deposits and prospects, locations of dated igneous rock samples, and geophysical and geochemical information. This allowed identification of previously unrecognized or unmapped permissive units and associated porphyry systems. Scanned and rectified page-size illustrations from the literature were incorporated in the GIS to check locations and permissive rock boundaries. Where intrusive rocks were reported from the literature and depicted in deposit-scale maps, but not shown at the scale of the available digital map base, 10-km buffers were drawn around known porphyry copper deposits and prospects.
5. An aggregation and smoothing routine was then applied to the resulting polygons, and the tracts were further edited by hand to insure that all units were contained within the tract. In many cases, more detailed geologic maps were used to resolve tract boundary issues. Tract boundaries were edited to honor tectonic boundaries but not second-order structures such as individual thrust faults, given that these are not represented in enough detail at the available map scales.
6. The team clipped resulting tract boundaries to shorelines to eliminate undersea areas using boundary files from the U.S. Department of State (2009).¹⁷

¹⁷The political boundaries used in this report are, in accord with U.S. Government policy, the small-scale digital international boundaries (SSIB) provided by the U.S. Department of State (U.S. Department of State, 2009). In various parts of the world, some political boundaries are in dispute. The use of the boundaries certified by the U.S. Department of State does not imply that the U.S. Geological Survey advocates or has an interest in the outcome of any international boundary disputes.

Estimation of Numbers of Undiscovered Deposits

Once the tract delimitation process was completed, the assessment team evaluated the available data, selected the appropriate grade-tonnage model for the tract based on resource information from deposits in it, checked these for consistency with the grade-and tonnage model of Singer and others (2008) using statistical tests, and established the favorability and uncertainty rationale for estimation of the numbers of undiscovered deposits.

Assessors relied on their professional expertise and experience to appraise geologic variables such as arc size and longevity, tectonic environment (including evolution of stress and thermal regimes), dominant magmatic compositions and metal associations, relative magma emplacement levels, alteration and mineralization styles, structural controls, exposure levels of mineral systems, resources in known deposits, and metal associations in prospects. Assessors further relied on the extent of known exploration to arrive at an overall expected level of favorability and uncertainty for each tract.

On the basis of these rationales, assessors then made individual estimates of the numbers of undiscovered porphyry copper deposits at different levels of certainty for each tract. Individual estimates were made privately, recorded, and then discussed to arrive at a team consensus. The number of undiscovered deposits and associated levels of uncertainty were estimated by each assessor as the least number of porphyry deposits that in their judgment could be present at three specified levels of certainty (90, 50, and 10 percent). For example, on the basis of all the available data, a team member might have estimated that there was a 90-percent chance of at least 1, a 50-percent chance of at least 3, and a 10-percent chance of at least 5 undiscovered deposits in a permissive tract.

Individual estimates were then converted to a mean number of deposits and standard deviation based on the algorithm developed by Singer and Menzie (2005). The algorithm can be described by the following general equations to calculate a mean number of deposits (λ) and a standard deviation (s_x) based on estimates of numbers of undiscovered deposits predicted at different quantile levels¹⁸ (N_{90} =90-percent level, N_{50} =50-percent level, and so on):

$$\lambda = 0.233 N_{90} + 0.4 N_{50} + 0.225 N_{10} + 0.045 N_{05} + 0.03 N_{01}, \text{ and} \quad (1)$$

$$s_x = 0.121 - 0.237 N_{90} - 0.093 N_{50} + 0.183 N_{10} + 0.073 N_{05} + 0.123 N_{01} \quad (2)$$

These equations were programmed into a spreadsheet to allow the team to quickly evaluate estimates. The spread in the number of deposits associated with the 90th percentile to the 10th percentile or 1st percentile reflects uncertainty; large differences in the number suggest great uncertainty. The mean number of deposits for the permissive tract, or the numbers associated with

a given probability level, reflect favorability. A useful variable for reporting uncertainty associated with an estimate is the coefficient of variation (C_v), defined as:

$$C_v = s_x / \lambda. \quad (3)$$

The coefficient of variation is often reported as percent relative variation ($100 \times C_v$). Thus, the final team estimates reflected both the uncertainty in what may exist and the favorability of the tract (Singer, 1993).

The individual estimates were discussed as a group and compared to the independent measure of expected numbers of porphyry deposits provided by a porphyry deposit density model (Singer and Menzie, 2010). In this manner, the team agreed on a consensus estimate of the numbers of undiscovered porphyry copper deposits at different levels of certainty for each tract.

We then combined consensus estimates with the selected general Cu-Au-Mo or subtype Cu-Au grade and tonnage model in a Monte Carlo simulation using the EMINERS computer program (Bawiec and Spanski, 2012; Duval, 2012), based on the original Mark 3 computer program described by Root and others (1992), to provide a probabilistic estimate of amounts of resources that could be associated with the estimated undiscovered deposits at the different levels of certainty. Results for each permissive tract are reported at selected quantile levels, along with the mean expected amount of metal, the probability of the mean, and the probability of no metal. The amount of metal reported at each quantile indicates the least amount of metal expected from the ranked data of 4,999 Monte Carlo simulations. No economic filters were applied. Thus, results must be viewed with the realization that deposits, if discovered, might not be developed. The assessment team made estimates for undiscovered resources in the Tethys region in January 2012 and revised them in June 2013.

Porphyry Copper Assessment of the Tethys Region

Twenty-six permissive tracts and sub-tracts considered permissive for the occurrence of porphyry copper deposits were delimited within the Tethys region of western and southern Asia (table 1). For 18 of these, probabilistic estimates of numbers of undiscovered deposits were made. The team concluded that quantitative assessment of the other eight tracts was not warranted on the basis of available data and that these tracts would likely contribute insignificant amounts of copper to estimated endowment of the study area. These eight tracts are permissive but affected by geologic factors and deposit characteristics that considerably limit their favorability for the occurrence of porphyry copper deposits. Therefore, they are described in detail, but only assessed qualitatively.

Time-space relations between tracts, showing their distribution from Turkey in the west to Pakistan in the east, and

¹⁸To use the equation in cases where three nonzero quantiles (90-50-10) are estimated, use the N_{10} values for N_{05} and N_{01} ; where four quantiles (90-50-10-5) are estimated, use the N_{05} value for N_{01} .

from the Triassic to the Quaternary, are shown in figure 9. This schematic diagram encapsulates the relative location and age of the diverse magmatic settings of porphyry copper deposits underpinning the permissive tracts described in the following sections.

Porphyry copper deposits identified in the region are listed in table 2. The 42 records tabulate data by deposit name, tract identifier, geographic coordinates, age, tonnage, and copper grade, as well as by molybdenum, gold, and silver grades where data were available. Additional fields include porphyry deposit subtype where determined, comments, and references. Note that “deposit” is defined as a porphyry occurrence whose location and resource quality and quantity has been identified (for example, with drilling) and reported. If grade and tonnage have not been quantitatively estimated or are not available, the porphyry site is classified as a “prospect,” even if it has been subjected to detailed geologic study. The 275 known porphyry and porphyry-related prospects and the 47 possible porphyry-related occurrences are tabulated in appendix C, where they are identified by name, country, tract, geographic coordinates, age, comments, and references. The results of statistical tests for those tracts that contain known deposits and the basis for selecting the grade and tonnage model used for the probabilistic estimate of undiscovered resources are listed in table 3.

Individual tract descriptions are generally organized by geologic age, from oldest to youngest. Each permissive tract description begins with a reference to the descriptive and the grade and tonnage models used if the tract was assessed quantitatively and a brief statement describing the fundamental geologic feature that formed the basis for delineation of the tract. This is followed by descriptions of the (1) tract location, (2) tectonic setting, (3) character and composition of magmatism, (4) local geology and metal associations of selected porphyry deposits and prospects, (5) exhumation and burial history of tract and porphyry systems, (6) magnetic signatures, (7) remote sensing data where available, (8) criteria for grade-tonnage model selection, (9) rationale used to assess favorability and uncertainty factors to support the estimates of undiscovered porphyry copper deposits, and (10) probabilistic simulation results. Sections describing tracts assessed qualitatively generally include descriptions of numbers 1 through 5 and 9 above. For each tract, map figures show the permissive tract with known porphyry copper deposits and prospects within it and the distribution of permissive intrusive and extrusive rocks that formed the basis for tract delineation, along with labels for any features mentioned in the text.

For each tract that was assessed quantitatively, estimates of numbers of undiscovered deposits and results of the Monte Carlo simulation are presented in two tables and as cumulative frequency plots. The first table shows the consensus estimates at the different levels of certainty, the number of undiscovered deposits and associated statistical uncertainties, and the total (known plus undiscovered)

deposit density for the tract area. The second table shows the estimated amounts of undiscovered copper, molybdenum, gold, and silver resources in metric tons, and associated statistics obtained by Monte Carlo simulation. The amount of estimated mineralized rock (in million metric tons, Mt) is also included at the different probability levels. Cumulative frequency plots illustrate the estimated resources associated with the cumulative probabilities of occurrence, as well as the mean for each commodity and for the total tonnage of mineralized rock.

Appendix D is an accompanying geographic information system (GIS) with digital data files of permissive tracts, porphyry deposits and prospects, and tract and deposit reference lists. The GIS provides additional information on tracts, porphyry deposits and prospects.

Late Triassic to Early Cretaceous Tracts

The four Late Triassic to Early Cretaceous permissive tracts are shown on figure 5. A probabilistic assessment of undiscovered resources was carried out for the Cimmeride Lesser Caucasus tract; the other three tracts delineated for this age range (the Sanandaj-Sirjan, the Cimmeride Greater Caucasus, and the Lut Jurassic) are described because they are permissive for porphyry copper mineralization, but they were assessed only qualitatively.

Sanandaj-Sirjan Tract (142pCu9003)

Descriptive model: Porphyry copper (Cox, 1986a; Berger and others, 2008; John and others, 2010)

Geologic feature assessed: Late Triassic to Early Cretaceous continental arc of the Tethyan Eurasian Metallogenic Belt

Location

The Sanandaj-Sirjan tract covers an area of 19,400 km² (fig. 10). It delimits a partially preserved and irregularly exposed 1,850-km-long and as much as 70-km-wide northwest-southeast trending continental arc of Late Triassic to Early Cretaceous age. The tract is confined to the Sanandaj-Sirjan Terrane (fig. 3), which underlies southeastern Turkey and northwestern to southeastern Iran.

In Iran, the Sanandaj-Sirjan Terrane is bound by the Bitlis-Zagros Thrust to the southwest, and by the Central Iranian Terrane to the northeast (fig. 3). In southern Iran, a sliver of the Sanandaj-Sirjan is contained within the Makran Terrane. In southeastern Turkey, the Sanandaj-Sirjan Terrane is juxtaposed against the Bitlis-Pötürge Terrane to the north and against the Bitlis-Zagros Thrust to the south (fig. 3).

In southeastern Turkey and northwestern Iran, parts of the younger Border Folds tract, Anatolide-Tauride–Eastern Turkey–Caucasus sub-tract, and Esfahan tract (see below) are superimposed on the Sanandaj-Sirjan tract.

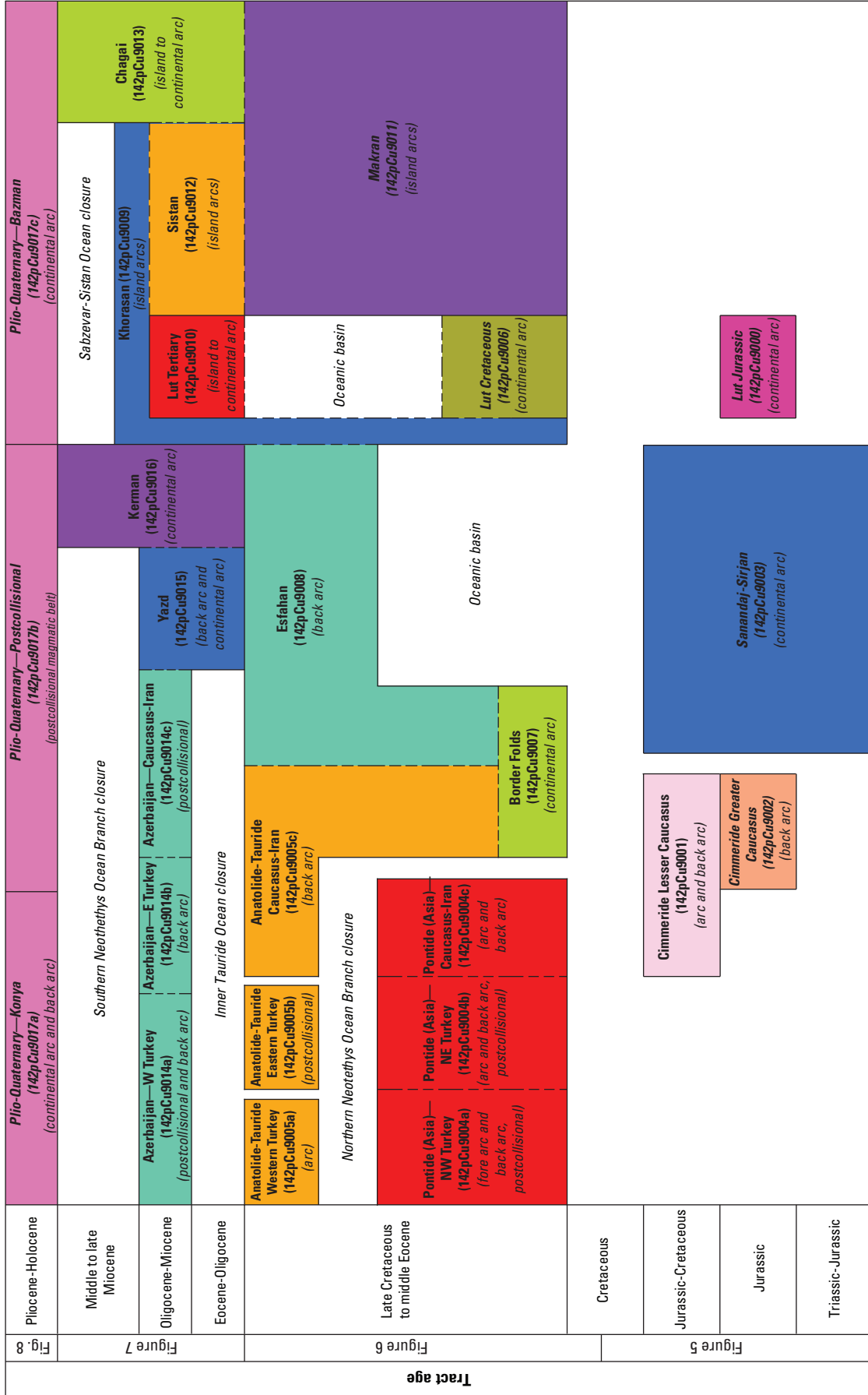


Figure 9. Time-space diagram of permissive tracts for porphyry copper deposits in the Tethys region of western and southern Asia. The diagram demonstrates the relative location and age of the magmatic settings of porphyry copper deposits included in the tracts and sub-tracts. Tract blocks are colored to conform to colors used in figures 5 through 8, as indicated. For each tract, the figure text shows tract (or sub-tract) name, tract (or sub-tract) ID, and the nature of the magmatic event(s) included in the tract. Tract names in italics indicate qualitative, rather than quantitative, assessment. In general, the areas in white depict intervening oceanic basins. Solid boundary lines between tracts represent magmatic events that developed in relative isolation from one another (for example, back-arc and postcollisional magmatism), whereas dashed boundary lines show magmatic events that crossed terrane boundaries (for example, back-arc and postcollisional magmatism).

Table 2. Porphyry copper deposits of the Tethys region of western and southern Asia.

[Coded_ID, a unique number assigned to each permissive tract in the geographic information system (appendix D); Ma, million years; Mt, million metric tons; t, metric ton; %, percent; g/t, grams per metric ton; n.d., no data; Cu, copper; Mo, molybdenum; Au, gold; Ag, silver. Deposits and prospects within ~4 kilometers (km) of each other are grouped. Cu-Mo subtype, deposits that have Au/Mo ratios less than 3 or average Mo grades greater than 0.03%; Cu-Au subtype, deposits that have Au/Mo ratios greater than 30 or average Au grades greater than 0.2 g/t; NA, formal subtype criteria not applicable. Contained copper and gold reported to two significant figures. Porphyry copper deposits in the European sector of Turkey (Derekoy, Ikitzepler, Karadere, and Sukrupasa) are not listed here but are included in the accompanying spatial data]

Name	Country	Tract name	Coded_ID	Latitude	Longitude	Sub-type	Comments	Age (Ma)	Tonnage (Mt)	Cu (%)	Mo (%)	Au (g/t)	Ag (g/t)	Contained copper (t)	Contained gold (t)	References
Agarak	Armenia	Anatolide-Tauride—Eastern Turkey-Caucasus sub-tract	142pCu9005c	38.9219	46.1882	NA	Cu-Mo-Au porphyry deposit; calc-alkaline to alkaline; open pit; in production.	44	125	0.56	0.0250	0.60	n.d.	700,000	80	GeoProMining (2012), Global Metals, Ltd. (2013), Gugushvili and others (2010), InfoMine, Inc. (2013a), Jamali and others (2010), Kekelia and Kekelia (2001), Kirkham and Dunne (2000), Mining Journal (2005), Moritz and others (2012), Norwest Mineral Sector Investment Focus (2003), Rundkvist (2001), Singer and others (2008), U.S. Geological Survey (2012), Zvezdov and others (1993)
Ali-Abad'	Iran	Kerman	142pCu9016	31.6490	53.8280	NA	Cu-Mo-(Ag) porphyry deposit; calc-alkaline; in production; open pit; Taft project expansion to be completed in 2015.	16.7	40	0.73	0.0059	n.d.	19.00	300,000	n.d.	Forster (1978), Hassanzadeh (1993), InfoMine, Inc. (2013b), Leaman and Staude (2002), National Iranian Copper Industries Co. (2012), Samani (1998), Singer and others (2008), Zarasvandi and others (2005), Zarasvandi and others (2007)
Ankavan	Armenia	Azerbaijan—Caucasus-Iran sub-tract	142pCu9014c	40.6307	44.4841	NA	Cu-Mo-Au porphyry-skarn deposit; calc-alkaline to alkaline; past producer; open pit/underground.	33.0	115	0.57	0.0540	1.42	n.d.	660,000	163	InfoMine, Inc. (2013c), Kekelia and Kekelia (2001), Kirkham and Dunne (2000), Mining Journal (2005), Rundkvist (2001), Singer and others (2008), U.S. Geological Survey (2012)
Ayazmant	Turkey	Azerbaijan—Western Turkey sub-tract	142pCu9014a	39.2616	27.1130	NA	Cu porphyry-related Fe-Cu-(Au) skarn deposit; calc-alkaline; in production.	20.1	5.8	0.60	n.d.	n.d.	n.d.	30,000	n.d.	Oyman (2010), Yigit (2006), Yigit (2009)
Bagh Khoshk	Iran	Kerman	142pCu9016	29.8270	55.9960	NA	Cu-Mo porphyry deposit; alkaline to calc-alkaline; exploration.	Early Oligocene	24	0.27	n.d.	n.d.	n.d.	65,000	n.d.	Arian and others (2011), Dargahi and others (2010), Emali and others (2011), Haschke and others (2010), National Iranian Copper Industries Co. (2012), Ranjbar and Honarmand (2004), Ranjbar and others (2005), Shafiei and others (2009), Shafiei and Shahabpour (2008)
Bakırçay	Turkey	Pontide (Asia)—NW Turkey sub-tract	142pCu9004a	40.9609	35.3959	NA	Cu-Au-Mo porphyry-skarn deposit; calc-alkaline; postcollisional(?); exploration.	38.6	200	0.20	n.d.	n.d.	n.d.	400,000	n.d.	Engin and others (2000), Kirkham and Dunne (2000), Singer and others (2008), Soyulu (1999), Taylor (1978), Taylor (1981), Taylor and Fryer (1980), Yigit (2009)
Balcılı-Yüksekoba	Turkey	Pontide (Asia)—NE Turkey sub-tract	142pCu9004b	41.0204	41.4450	NA	Cu-Mo porphyry deposit; calc-alkaline; exploration.	62.3	140	0.20	n.d.	n.d.	n.d.	300,000	n.d.	Akinci (2004), Engin and others (2000), Richard Herrington, written commun. (2005), Soyulu (1999), Yavuz and others (1999), Yigit (2009)

Table 2.—Continued

Name	Country	Tract name	Coded_ID	Latitude	Longitude	Sub-type	Comments	Age (Ma)	Tonnage (Mt)	Cu (%)	Mo (%)	Au (g/t)	Ag (g/t)	Contained copper (t)	Contained gold (t)	References
Cevizlidere	Turkey	Azerbaijan—Eastern Turkey	142pCu9014b	39.2726	39.0418	NA	Cu-Mo-Au porphyry deposit; calc-alkaline; advanced exploration.	26.0	445	0.38	n.d.	0.11	n.d.	1,700,000	49	Engin and others (2000), InfoMine, Inc. (2013e), Kocumbas and Page (2009), Letya Madencilik (2013g), Marinov and others (2011), Mining Journal (2010), Singer and others (2008), Yigit (2009)
Chah-Firuzeh	Iran	Kerman	142pCu9016	30.3984	55.0158	NA	Cu-Mo porphyry deposit; calc-alkaline to alkaline; in production; expansion to be completed in 2015; includes Kahtokartha porphyry prospect located less than 4 km from deposit.	Late Miocene	149.1	0.41	n.d.	n.d.	n.d.	610,000	n.d.	Afzal and others (2011), Alirezai and Mohammadzadeh (2009), Hezarkehani (2009), Honarmand and others (2011), Mirnejad and others (2010b), National Iranian Copper Industries Co. (2012)
Çöpler	Turkey	Anatolide-Tauride—Eastern Turkey-Caucasus sub-tract	142pCu9005c	39.4285	38.5024	Cu-Au	Au-(Cu) porphyry-skarn and epithermal deposit; calcic calc-alkaline to alkaline; in production; open pit; second-largest mine in Turkey; includes recently-discovered Zanga Dere porphyry prospect.	44.6	80.9	0.12	n.d.	1.43	4.24	97,000	116	Bascombe and others (2012), Engin and others (2000), Imer and others (2013), InfoMine, Inc. (2013g), Kirkham and Dume (2000), Kuşcu (2007), Kuscü and others (2010), Marek and others (2008), Marinov and others (2011), Mining Journal (2010), Northern Miner (2009), Yigit (2006), Yigit (2009)
Dalli	Iran	Yazd	142pCu9015	34.2719	50.3242	Cu-Au	Cu-Au porphyry deposit; calcic calc-alkaline; in development.	21	8	0.50	n.d.	0.75	n.d.	40,000	6	Ayati and others (2008), Ayati and others (2013), Dorsa PLC (2012a), Dorsa PLC (2013), Haroni (2005), Haroni (2008), InfoMine, Inc. (2013h), Leaman and Staude (2002), Samami (1998), Singer and others (2008)
Dar-Abu	Iran	Kerman	142pCu9016	29.4167	57.1000	NA	Cu-Mo-(Au) porphyry deposit; calc-alkaline; in production; expansion to be completed in 2015.	Late Miocene	186.1	0.36	n.d.	n.d.	n.d.	670,000	n.d.	Bazin and Hübner (1969a), Iran Geological Survey (2012a), Iran Geological Survey (2012e), National Iranian Copper Industries Co. (2012), Pour and others (2011), Salehian and Ghaderi (2010a), Salehian and Ghaderi (2010b), Samami (1998), Shafiei (2010), Shafiei and others (2008), Shafiei and others (2009), Shafiei and Shahabpour (2008), U.S. Geological Survey (2012)

Table 2.—Continued

Name	Country	Tract name	Coded_ID	Latitude	Longitude	Sub-type	Comments	Age (Ma)	Tonnage (Mt)	Cu (%)	Mo (%)	Au (g/t)	Ag (g/t)	Contained copper (t)	Contained gold (t)	References
Darreh Zar	Iran	Kerman	142pCu9016	29.8838	55.9090	NA	Cu-Mo-(Au) porphyry deposit; calc-alkaline; in production; open pit; expansion to be completed in 2015.	14.9	282.6	0.38	0.0040	n.d.	n.d.	1,100,000	n.d.	Aghazadeh and others (2012), Arian and others (2011), Derakhshani and Abdolzadeh (2009), Haschke and others (2010), InfoMine, Inc. (2013i), Iran Geological Survey (2012a), Iran Geological Survey (2012e), Kirkham and Dunne (2000), Mirnejad and others (2010b), National Iranian Copper Industries Co. (2012), Pour and others (2011), Ranjbar and Honarmand (2004), Ranjbar and others (2005), Shafiei (2010), Shafiei and others (2009), Shafiei and Shahabpour (2008), Shahabpour (1999), Singer and others (2008), U.S. Geological Survey (2012)
Darreh-Zerreshk ¹	Iran	Kerman	142pCu9016	31.5620	53.8280	NA	Cu-Mo-(Ag) porphyry-skarn deposit; calc-alkaline; in production; open pit; Taft project expansion to be completed in 2015.	16.1	23	0.90	0.0040	n.d.	1.00	200,000	n.d.	Aghazadeh and others (2012), Förster (1978), Hassanzadeh (1993), Hosseini and others (2010), InfoMine, Inc. (2013j), Leaman and Staudé (2002), National Iranian Copper Industries Co. (2012), Samani (1998), Shahabpour and Kramers (1987), Singer and others (2008), Somarin and others (2005), Zarasvandi and others (2007)
Dasht-e-Kain	Pakistan	Chagai	142pCu9013	29.5560	64.6040	NA	Cu-Mo-Au porphyry deposit; calcic calc-alkaline; exploration, drilling.	31.6	350	0.30	0.0010	n.d.	n.d.	1,000,000	n.d.	Ahmad (1986), Ahmad (1992), Ahmad and others (1986), Breitzman and others (1983), Everest Gold, Inc. (2012), Kazmi and Qasim Jan (1997), Kirkham and Dunne (2000), Perelló and others (2008), Singer and others (2008)
Dastakert	Armenia	Anatolide-Tauride—Eastern Turkey-Caucasus sub-tract	142pCu9005c	39.3914	46.0148	Cu-Mo	Cu-Mo-(Au) porphyry deposit; calc-alkaline to alkaline; past producer; drilling pads evident in satellite imagery.	44	33	0.62	0.0470	n.d.	n.d.	200,000	n.d.	Förster (1978), Global Metals, Ltd. (2013), Kekelia and Kekelia (2001), Kirkham and Dunne (2000), Mining Journal (2005), Moritz and others (2012), Rundkvist (2001), Singer and others (2008), U.S. Geological Survey (2012), Zvezdov and others (1993)
Gümtüşhane	Turkey	Pontide (Asia)—NE Turkey sub-tract	142pCu9004b	41.1315	41.9562	NA	Acid-sulfate Au-Ag and Cu-Mo porphyry deposit; calc-alkaline; 2013 combined Ardala-Salinbaş project resource estimate stands at 26.87 Mt at 1.26 g/t Au, 4.78 g/t Ag, including 4.66 Mt at 0.22% Cu and 18 Mt at 0.0136% Mo; advanced exploration.	52.5	80	0.50	n.d.	0.20	n.d.	400,000	20	Akay and Gündüz (2004), Ariana Resources PLC (2013), Arslan and Aliyazicioğlu (2001), Ergin and others (2000), Grima (2008), InfoMine, Inc. (2012a), InfoMine, Inc. (2013p), KEFI Minerals (2012), Kirkham and Dunne (2000), Leaman and Staudé (2002), Mining Journal (2010), Moon and others (2001), Singer and others (2008), Soyulu (1999), Yigit (2006), Yigit (2009)

Table 2.—Continued

Name	Country	Tract name	Coded_ID	Latitude	Longitude	Sub-type	Comments	Age (Ma)	Tonnage (Mt)	Cu (%)	Mo (%)	Au (g/t)	Ag (g/t)	Contained copper (t)	Contained gold (t)	References
Güzelçayla	Turkey	Pontide (Asia)—NE Turkey sub-tract	142pCu9004b	40.6616	39.5088	NA	Cu-Mo porphyry-skarn deposit; calc-alkaline; exploration.	59	186.2	0.30	n.d.	n.d.	n.d.	600,000	n.d.	Akinci (2004), Bozbug and others (2003), Engin and others (2000), Richard Herrington, written commun. (2005), Kirkham and Dunne (2000), Moon and others (2001), Singer and others (2008), Soylu (1999), U.S. Geological Survey (2012), Yigit (2009)
Haft Cheshmeh	Iran	Azerbaijan—Caucasus-Iran sub-tract	142pCu9014c	38.8167	46.6500	NA	Cu-Mo-Au porphyry-skarn deposit; alkaline to calc-alkaline postcollisional; in development; projected to start in 2015.	Miocene	184.0	0.26	n.d.	n.d.	n.d.	480,000	n.d.	Hassanpour and Afzal (2013), Hassanpour and others (2010), Iran Geological Survey (2012a), Iran Geological Survey (2012c), Jamali and others (2010), Jamali and others (2012), National Iranian Copper Industries Co. (2012), Samami (1998)
Hallaga	Turkey	Azerbaijan—Western Turkey sub-tract	142pCu9014a	39.9383	26.8537	Cu-Au	Cu-Au-(Mo) porphyry, Au acid-sulfate, and Cu-Mo-Zn-Pb skarn deposit; calc-alkaline; prefeasibility stage.	Oligocene or younger	371.7	0.26	0.0065	0.29	n.d.	970,000	110	Engin and others (2000), InfoMine, Inc. (2013q), Mining Journal (2010), Pilot Gold, Inc. (2011), Pilot Gold, Inc. (2012a), Pilot Gold, Inc. (2012b), Pilot Gold, Inc. (2012c), Scott and others (2012), Yigit (2009), Yigit (2012)
Iju	Iran	Kerman	142pCu9016	30.5333	54.9583	NA	Cu-Mo porphyry deposit; calc-alkaline; postcollisional; in production; expansion to be completed in 2015; deposit listed with older upper Eocene-upper Miocene tract 142pCu9016, but more likely belongs with upper Miocene-Holocene sub-tract 142pCu9017b.	9.2	73.9	0.31	n.d.	n.d.	n.d.	230,000	n.d.	Arian and others (2011), Förster (1978), Honarmand and others (2011), Iran Geological Survey (2012a), Iran Geological Survey (2012e), Mirmejad and others (2010b), Mirmejad and others (2013), National Iranian Copper Industries Co. (2012), Pour and others (2011), Shafiei (2010), Shafiei and others (2009), Shafiei and Shahabpour (2008), U.S. Geological Survey (2012)
Kadjaran	Armenia	Azerbaijan—Caucasus-Iran sub-tract	142pCu9014c	39.1403	46.1369	NA	Cu-Mo-Au porphyry deposit; alkaline to calc-alkaline postcollisional; open pit; in production.	27.0	1700	0.27	0.0550	0.65	2.00	4,600,000	1,100	Förster (1978), Gilmour and others (1995), Gugushvili and others (2010), Kekelia and Kekelia (2001), Kekelia and others (2004), Kirkham and Dunne (2000), Mining Journal (2005), Mining Journal (2011a), Moritz and others (2012), Murakami and others (2010), Norwest Mineral Sector Investment Focus (2003), Rundkvist (2001), Singer and others (2008), Tarkian and Siribny (1999), U.S. Geological Survey (2012), Zvezdov and others (1993)

Table 2.—Continued

Name	Country	Tract name	Coded_ID	Latitude	Longitude	Sub-type	Comments	Age (Ma)	Tonnage (Mt)	Cu (%)	Mo (%)	Au (g/t)	Ag (g/t)	Contained copper (t)	Contained gold (t)	References
Kahang	Iran	Yazd	142pCu9015	32.9257	52.4653	NA	Cu-Mo porphyry deposit; calc-alkaline; in production; expansion to be completed in 2015.	Oligocene-Miocene	38.7	0.59	n.d.	n.d.	n.d.	230,000	n.d.	Afzal and others (2010), Aghazadeh and others (2012), Dorsa PLC (2012b), National Iranian Copper Industries Co. (2012)
Kale Kafi	Iran	Esfahan	142pCu9008	33.3990	54.2380	NA	Cu-Mo-(Au-W) porphyry deposit; calc-alkaline; exploration.	53.0	245	0.26	0.0260	0.10	n.d.	640,000	20	Ahmadian and others (2009), Bazin and Hibner (1969a), Iran Geological Survey (2012a), Iran Geological Survey (2012e), Kirkham and Dumne (2000), Moghaddasi and Mohammadi (2010), Nezampour and Rassa (2005), Samani (1998), Singer and others (2008)
Karakartal	Turkey	Anatolide-Tauride—Eastern Turkey-Caucasus	142pCu9005c	39.3102	38.6963	Cu-Au	Cu-Au porphyry deposit; calcic calc-alkaline to alkaline; advanced exploration.	Early Eocene	70.8	0.25	n.d.	0.32	n.d.	180,000	23	Alacer Gold (2012), InfoMine, Inc. (2013), Kocumbas and Page (2009), Lydia Madencilik (2013f), Mining Journal (2010), Northern Miner (2009)
Kavarta	Armenia	Cimmeride Lesser Caucasus	142pCu9001	39.2331	46.3977	NA	Cu-Mo-Au porphyry deposit and polymetallic veins; calcic calc-alkaline; past producer; 2009 combined porphyry and polymetallic resource estimate of 466.3 Mt at 0.09% Cu, 0.37 g/t Au, 6.5 g/t Ag, and 0.32% zinc; in development.	144.7	50	1.20	n.d.	n.d.	n.d.	600,000	n.d.	Gugushvili and others (2010), Kirkham and Dumne (2000), Moritz and others (2012), Rundkvist (2001), U.S. Geological Survey (2012), Wolfe and Gossage (2009)
Kedabek	Azerbaijan	Cimmeride Lesser Caucasus	142pCu9001	40.5867	45.8603	Cu-Au	Cu-Au-(Mo) porphyry deposit; calcic calc-alkaline; new 2012 resource estimate of 48 Mt at 0.197% Cu, 0.825 g/t Au, and 6.65 g/t Ag; open pit; in production.	Jurassic-Cretaceous	16	0.24	n.d.	1.40	12.20	38,000	22	Anglo Asian Mining PLC (2009), Anglo Asian Mining PLC (2011), Baba-Zade and others (1990), Bortnikov and others (1993), CAE Mining (2012), Kekelia and Kekelia (2001), Levine (2011b), Singer and others (2008), U.N. Economic and Social Commission for Asia and the Pacific (2000), U.S. Geological Survey (2012)
Masjed Daghi	Iran	Azerbaijan—Caucasus-Iran-sub-tract	142pCu9014c	38.8772	45.9386	Cu-Au	Acid-sulfate Au and Cu-Au-(Mo) porphyry deposit; calc-alkaline; postcollisional; in production; expansion to be completed in 2015.	Oligocene-Miocene	204	0.34	n.d.	2.00	n.d.	690,000	400	Alirezai and others (2008), Ebrahimi (2011), Iran Geological Survey (2010), Jamali and others (2010), Jamali and others (2012), National Iranian Copper Industries Co. (2012)

Table 2.—Continued

Name	Country	Tract name	Coded_ID	Latitude	Longitude	Sub-type	Comments	Age (Ma)	Tonnage (Mt)	Cu (%)	Mo (%)	Au (g/t)	Ag (g/t)	Contained copper (t)	Contained gold (t)	References
Meidluk (Shahre Babak)	Iran	Kerman	142pCu9016	30.4256	55.1740	NA	Cu-Mo-(Au-Ag) porphyry deposit; calc-alkaline; in production; open pit; expansion to be completed in 2015; includes Lachah, Latela, NW-Meidluk, and S-Silicate vein porphyry prospects located less than 4 km from deposit.	12.5	176	0.61	0.0070	n.d.	1.80	1,100,000	n.d.	Aliani and others (2009), Arian and others (2011), Bazin and Hübner (1969a), Bazin and Hübner (1969b), Boomeri and others (2009), Derakhtshani and Mehrabi (2009), Espanhod (1992), Hassanzadeh (1993), Honarmand and others (2011), InfoMine, Inc. (2013z), Iran Geological Survey (2012a), Iran Geological Survey (2012b), Iran Geological Survey (2012e), Kirsham and Dunne (2000), Leaman and Staude (2002), McInnes and others (2005), National Iranian Copper Industries Co. (2012), Samani (1998), Shafiei and others (2009), Shafiei and Shahabpour (2008), Shahabpour (1992), Shahabpour (1999), Shahabpour (2005), Shahabpour (2007), Singer and others (2008), Taghipour and others (2008), Tangestani and Moore (2001), Tangestani and Moore (2002a), Tangestani and Moore (2002b), U.S. Geological Survey (2012)
Muratdere	Turkey	Anatolide-Tauride—Western Turkey	142pCu9005a	39.8922	29.8966	NA	Cu-Mo-Au porphyry deposit; calc-alkaline; advanced exploration.	50	51	0.36	0.0125	0.12	2.40	180,000	6	Cliff (2007), Engin and others (2000), HB Corporate (2005), InfoMine, Inc. (2012b), Mining Journal (2010), Stratex International PLC (2012b), Yigit (2009)
Now Chun	Iran	Kerman	142pCu9016	29.9333	55.8500	NA	Cu-Mo porphyry deposit; calc-alkaline; in production; expansion to be completed in 2015.	Oligocene-Miocene or late Miocene(?)	527	0.26	n.d.	n.d.	n.d.	1,400,000	n.d.	Abedi and Norouzi (2012), Arian and others (2011), Haschke and others (2010), Iran Geological Survey (2012a), Iran Geological Survey (2012b), Iran Geological Survey (2012e), National Iranian Copper Industries Co. (2012), Pour and others (2011), Ranjbar and Honarmand (2004), Ranjbar and others (2005), Saein and others (2012), Shafiei (2010), Shafiei and others (2009), Shafiei and Shahabpour (2008)
Raigan	Iran	Kerman	142pCu9016	29.3200	57.0500	NA	Cu porphyry deposit; alkaline to calc-alkaline; exploration.	29.7	10	0.63	n.d.	n.d.	n.d.	60,000	n.d.	Hassanzadeh (1993), Hezarkhani (2006a), Hezarkhani (2006b), Hezarkhani (2006d), Karimi and Valadan Zojj (2004), Samani (1998), Shafiei and others (2009), Singer and others (2008)
Reko Diq ²	Pakistan	Chagai	142pCu9013	29.1153	62.0730	Cu-Au	Cu-Au-(Mo) porphyry deposit; calcic calc-alkaline; feasibility stage; includes Reko Diq H7, Reko Diq H9, Reko Diq H10, Reko Diq H27, and Reko Diq H79 porphyry prospects	12.3	4692	0.49	n.d.	0.29	n.d.	22,300,000	1,370	Antofagasta PLC (2010), Perelli and others (2008), Schloderer (2003), Singer and others (2008)

Table 2.—Continued

Name	Country	Tract name	Coded_ID	Latitude	Longitude	Sub-type	Comments	Age (Ma)	Tonnage (Mt)	Cu (%)	Mo (%)	Au (g/t)	Ag (g/t)	Contained copper (t)	Contained gold (t)	References
Saundak ³	Pakistan	Chagai	142pCu9013	29.2506	61.6150	Cu-Au	Cu-Au-(Mo) porphyry deposit; calcic calc-alkaline; open pit; in production.	22.2	440	0.41	0.0020	0.50	n.d.	1,800,000	200	Ahmad (1992), Ahmed and others (1972), Breitzman and others (1983), Kazmi and Qasim Jan (1997), Kirkham and Dunne (2000), Leaman and Staude (2002), Perello and others (2008), Richards and Khan (2012), Sillitoe (1978), Sillitoe and Khan (1977), Singer and others (2008), U.S. Geological Survey (2012), Wikipedia (2013c)
Sar Cheshmeh	Iran	Kerman	142pCu9016	29.9503	55.8721	Cu-Mo	Cu-Mo-(Ag-Au) porphyry deposit; calc-alkaline; in production; open pit; expansion 2013–2015.	13.6	1538	0.58	0.0300	0.06	1.14	8,900,000	90	Aftabi and Atapour (2011), Aghazadeh and others (2012), Arian and others (2011), Atapour and Aftabi (2007), Bazzin and Hübner (1969a, b), Boomeri and others (2010b), Ellis (1991), Espanhod (1992), Ghorashi-Zadeh (1978), Hassanzadeh (1993), InfoMine, Inc. (2013ad), Iran Geological Survey (2012a, b, e), Kirkham and Dunne (2000), McInnes and others (2005), National Iranian Copper Industries Co. (2012), Ranjbar and others (2005), Samani (1998), Shafiei (2010), Shafiei and others (2009), Shafiei and Shahabpour (2008), Shahabpour (1991, 1992, 1999, 2005, 2007), Shahabpour and Kramers (1987), Singer and others (2008), Tarkian and Stribny (1999), U.S. Geological Survey (2012), Waterman and Hamilton (1975)
Sar Kuh	Iran	Kerman	142pCu9016	29.9350	55.8170	NA	Cu-Mo-(Au) porphyry deposit; calc-alkaline; exploration.	15.1	16	0.46	n.d.	n.d.	n.d.	74,000	n.d.	Arian and others (2011), Iran Geological Survey (2012a), Iran Geological Survey (2012b), Iran Geological Survey (2012e), Mimejad and others (2013), National Iranian Copper Industries Co. (2012), Pour and others (2011), Ranjbar and others (2005), Shafiei (2010), Shafiei and others (2008), Shafiei and others (2009), Shafiei and Shahabpour (2008)
Sarıçayrıyayla	Turkey	Anatolide-Tauride—Western Turkey sub-tract	142pCu9005a	39.9069	29.4613	NA	Cu-Mo-Au porphyry-skarn deposit; calc-alkaline; exploration; drilling; includes Topukdere Cu-Mo-Au porphyry-skarn prospect.	50	120.3	0.17	n.d.	n.d.	n.d.	200,000	n.d.	Engin and others (2000), Ludyva Madencilik (2013a), Yigit (2009)

Table 2.—Continued

Name	Country	Tract name	Coded_ID	Latitude	Longitude	Sub-type	Comments	Age (Ma)	Tonnage (Mt)	Cu (%)	Mo (%)	Au (g/t)	Ag (g/t)	Contained copper (t)	Contained gold (t)	References
Sungun	Iran	Azerbaijan—Caucasus-Iran sub-tract	142pCu9014c	38.6948	46.7028	NA	Cu-Mo-(Au-Ag) porphyry-skarn deposit; alkaline to calc-alkaline; postcollisional; in production; open pit; expansion 2013–2015.	Early Miocene	846	0.60	0.0240	n.d.	n.d.	5,000,000	n.d.	Afzal and others (2011), Aghazadeh and others (2012), Asghari and Hezarkhani (2010), Bazin and Hübner (1969a), Calagari (2003), Calagari (2004), Calagari and Hosseinzadeh (2006), Elmman (1977), Elmman (2003), Ghanbari (2000), Hezarkhani (1997), Hezarkhani (2006e), Hezarkhani and others (1999), Hezarkhani and Williams-Jones (1998), InfoMine, Inc. (2013ae), Iran Geological Survey (2012a), Iran Geological Survey (2012e), Jamali and others (2010), Jamali and others (2012), Kirkham and Dunne (2000), Leaman and Staude (2002), Mobin Co. (2012), National Iranian Copper Industries Co. (2012), Samani (1998), Singer and others (2008), Somarin (2004), Somarin and Moayyed (2002), Somarin and others (2005), Tah-masebi and others (2010), U.S. Geological Survey (2012)
Tanjeel (H4)	Pakistan	Chagai	142pCu9013	29.1122	62.1017	NA	Cu-Mo porphyry deposit; calc-alkaline; advanced exploration.	23.8	214	0.60	0.0100	n.d.	n.d.	1,000,000	n.d.	InfoMine, Inc. (2013af), Mincor Resources NL (2003), Perelló and others (2008), Schloderer (2003)
Teghout	Armenia	Cimmeride Lesser Caucasus	142pCu9001	41.1180	44.8457	NA	Cu-Mo-(Au) porphyry deposit; calc-alkaline; past producer; in development.	145.9	460	0.35	0.0200	n.d.	n.d.	1,600,000	n.d.	Gugushvili and others (2010), Kekelia and Kekelia (2001), Levine (2011a), Mining Journal (2005), Moritz and others (2012), Norwest Mineral Sector Investment Focus (2003), Rundkvist (2001), Singer and others (2008), Thalenhorst (2005), Thalenhorst (2007), Vallex Group (2013), Zvezdov and others (1993)
Tepeoba	Turkey	Azerbaijan—Western Turkey sub-tract	142pCu9014a	39.6300	27.1069	Cu-Mo	Cu-Mo-(Au) porphyry-skarn deposit (W-Mo area); metaluminous to per-aluminous; advanced exploration.	25.6	24.1	0.33	0.0420	n.d.	n.d.	80,000	n.d.	Engin and others (2000), Institute for Geo-Resources and Environment (2005), Murakami and others (2005), Singer and others (2008), Yigit (2009), Yigit (2012)
Ulutaş	Turkey	Pontide (Asia)—NE Turkey sub-tract	142pCu9004b	40.5777	40.9047	NA	Cu-Mo porphyry deposit; calcic calc-alkaline; exploration.	59	74	0.31	0.0220	n.d.	n.d.	230,000	n.d.	Engin and others (2000), Kirkham and Dunne (2000), Leaman and Staude (2002), Moon and others (2001), Singer and others (2008), Soyulu (1999), Taylor (1978), Taylor and Fryer (1980), Yigit (2009)

¹Combined proven and probable reserve base reported for Ali-Abad and Darreh-Zerreshk is 167 Mt of 0.43% copper at a 0.15% copper cutoff (Taft Project; National Iranian Copper Industries Co., 2012).

²Reko Diq resource reported here is weighted average of Reko Diq H8, Reko Diq H13, Reko Diq H14, and Reko Diq H35. Resource at Reko Diq H15 unknown at the time of writing. Data for individual sites are available in the accompanying spatial data (appendix D). The global resource at the Reko Diq district stands at 5.9 billion tons at 0.41% copper and 0.22 g/t gold. Movable reserves are 2.2 billion tons at 0.53% copper and 0.3 g/t gold (Antofagasta PLC, 2010).

³Saindak resource reported above is weighted average of North, East, and South ore bodies.

⁴Notes: (1) Kışladağ Au-Mo porphyry deposit (41.2 Mt at 0.78 g/t gold) not included in this assessment because copper resources are deemed improbable (see appendix C and accompanying spatial data for additional data). (2) Copper resources at Ağrı Dağı and Kirazlı are not reported but deemed probable (see appendix C and accompanying spatial data for resource data on these sites). (3) Tonnages and copper grades are reported for the Anjerd, Chah Messi, Chahar Gonbad, Gavdel, Keban, Lachah, Lalleh Zar F3, Mazraeh, Palangy, Sharif Abad, and Takht porphyry and porphyry-related systems; sites listed as prospects because contained copper in each is estimated to be less than 70,000 t (see appendix C). Copper reserve growth is deemed probable.

Table 3. Statistical test results for grade and tonnage model selection for porphyry copper deposits in the Tethys region of western and southern Asia.

[Pooled t -test results assuming equal variances; $p > 0.01$ indicates that the deposits in the tract are not significantly different from those in the model in terms of tonnage and commodity grades at the 1-percent level; $p < 0.01$ indicates that the deposits in the tract are significantly different from those in the model at the 1-percent level and, therefore, the tract fails the selected test (as indicated by the *) and the model is inappropriate for the assessment. See table 1 for data used in tests against models of Singer and others (2008). N_{known} , number of known deposits in the tract; Mt, million metric tons; n.d., no data. Cu, copper; Mo, molybdenum; Ag, silver; Au, gold; NA, not applicable]

Tract name	Coded_ID	N_{known}	Model for t -test	Global porphyry Cu-Au-Mo model (p values)					Model selected	Basis for selection	
				Tonnage	Cu	Mo	Ag	Au			Contained Cu
Anatolide-Tauride—Central Turkey sub-tract	142pCu9005b	0	NA	n.d.	n.d.	n.d.	n.d.	n.d.	n.d.	General	No known deposits; default to general model.
Anatolide-Tauride—Eastern Turkey-Caucasus sub-tract	142pCu9005c	4	General	0.1	0.2	0.14	0.37	0.06	0.06	General	Available data fit general model.
Anatolide-Tauride—Western Turkey sub-tract	142pCu9005a	2	General	0.3	0.09	0.98	0.001*	0.04	0.15	General	Test fails for silver, but only one of the two deposits has reported silver grade. General model is acceptable for tonnage, copper, molybdenum, and gold.
Azerbaijan—Caucasus-Iran sub-tract	142pCu9014c	5	General	0.95	0.57	0.04	0.99	0.01	0.83	General	Available data fit general model.
Azerbaijan—Eastern Turkey sub-tract	142pCu9014b	1	General	0.68	0.79	n.d.	n.d.	0.79	0.76	General	Available data fit general model.
Azerbaijan—Western Turkey sub-tract	142pCu9014a	3	General	0.03	0.58	0.22	n.d.	0.64	0.03	General	Available data fit general model.
Border Folds	142pCu9007	0	NA	n.d.	n.d.	n.d.	n.d.	n.d.	n.d.	General	No known deposits; default to general model.
Chagai	142pCu9013	4	General	0.97	0.88	0.009*	0.1	0.23	0.99	General	Test fails for molybdenum. However, available data fit general model for tonnage, copper, silver, and gold; default to general model.
Cimmeride Lesser Caucasus	142pCu9001	3	General	0.16	0.73	0.56	0.03	0.1	0.23	General	Both Cu-Mo and Cu-Au porphyry subtypes are present; available data fit the general model.
Esfahan	142pCu9008	1	General	0.99	0.27	0.45	n.d.	n.d.	0.77	General	Available data fit general model.
Kerman	142pCu9016	12	General	0.22	0.02	0.31	0.6	0.47	0.03	General	Available data fit general model.
Khorasan	142pCu9009	0	NA	n.d.	n.d.	n.d.	n.d.	n.d.	n.d.	Cu-Au subtype	No known deposits; Cu-Au model selected based on dominant Cu-Au metal association.
Lut Tertiary	142pCu9010	0	NA	n.d.	n.d.	n.d.	n.d.	n.d.	n.d.	Cu-Au subtype	No known deposits; Cu-Au model selected based on dominant Cu-Au metal association.
Pontide (Asia)—Caucasus-Iran sub-tract	142pCu9004c	0	NA	n.d.	n.d.	n.d.	n.d.	n.d.	n.d.	General	No known deposits; default to general model.
Pontide (Asia)—NE Turkey sub-tract	142pCu9004b	4	General	0.31	0.16	0.56	n.d.	n.d.	0.18	General	Available data fit general model.
Pontide (Asia)—NW Turkey sub-tract	142pCu9004a	1	General	0.76	0.23	n.d.	n.d.	n.d.	0.71	General	Available data fit general model.
Sistan	142pCu9012	0	NA	n.d.	n.d.	n.d.	n.d.	n.d.	n.d.	General	No known deposits; default to general model.
Yazd	142pCu9015	2	General	0.01	0.74	n.d.	n.d.	0.05	0.04	General	Available data fit general model.

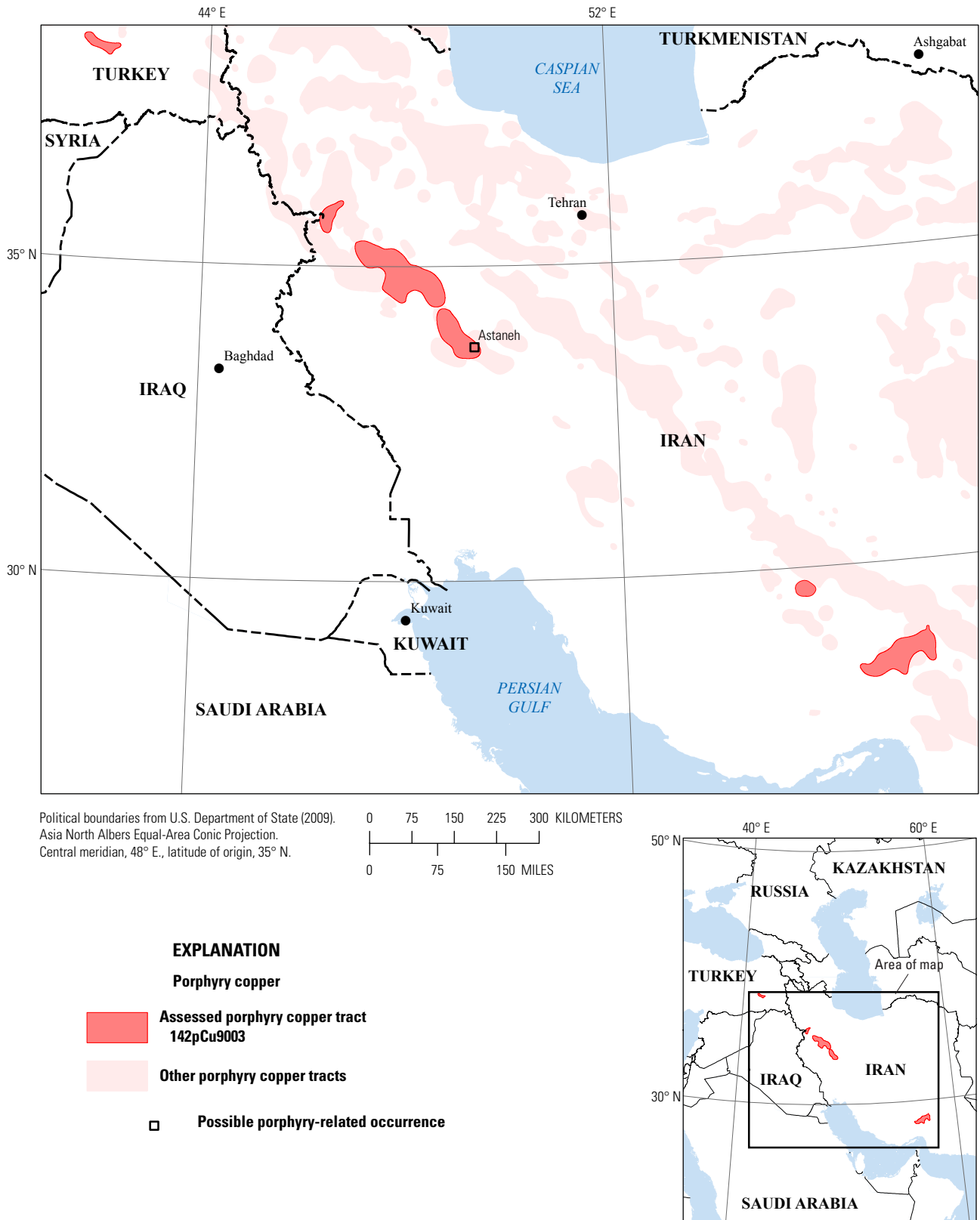


Figure 10. Map showing the location of possible porphyry-related copper occurrences for permissive tract 142pCu9003, Sanandaj-Sirjan—Iran, Iraq, and Turkey. See appendix C for additional information and appendix D for accompanying spatial data.

Tectonic Setting

The Sanandaj-Sirjan Terrane rifted from the Arabian Platform in the late Permian, opening the Southern Neotethys Ocean Branch (Golonka, 2004; Ghasemi and Talbot, 2006). A Middle to Late Triassic extensional setting is recorded by mafic alkaline to tholeiitic volcanism in northwestern Iran and southeastern Turkey. As early as the Late Triassic-Early Jurassic, this rift setting became large enough to develop a convergent margin, initiating an oblique north-dipping subduction zone under the Sanandaj-Sirjan Terrane (fig. 4.4) that propagated from the southeast to the northwest over time (Stöcklin, 1968; Omrani and others, 2008; Agard and others, 2011; Verdel and others, 2011). Remnants of associated Middle Jurassic to Early Cretaceous igneous rocks are only preserved in the southeastern and northwestern parts of the Sanandaj-Sirjan Terrane (Berberian and Berberian, 1981; Şengör and others, 1993; Şengör and others, 1991), suggesting that arc magmatism may not have been active in the central part.

Magmatism and Known Porphyry Deposits or Prospects

Permissive igneous units (appendix B) used to define the Sanandaj-Sirjan tract are shown in figure 11, along with locations of igneous complexes and other geologic features mentioned in this section.

Triassic-Early Jurassic plutonic rocks are exposed in the southeastern part of the Sanandaj-Sirjan Terrane. Their absence in the central and northwestern parts of the terrane suggests that subduction in the Southern Neotethys Ocean Branch started from the southeast and propagated northward (Berberian and Berberian, 1981; Kazmin and others, 1986). Triassic-Early Jurassic magmatism is represented by the (199±3 Ma Nd-Sm “errorchron”) Siah Kuh batholith (fig. 11), which is composed of subduction-related metaluminous to slightly peraluminous calc-alkaline, I-type leucogranodiorite, leucomonzogranite, and alkali granite with subordinate syenite. These units have been affected by argillic, sericitic, and chloritic alteration, but the age of these hydrothermal products remains uncertain (Arvin and others, 2007).

Middle-Late Jurassic intrusions in the Sanandaj-Sirjan Terrane consist of ~170–150 Ma tholeiitic gabbro, calc-alkaline I-type diorite, quartz-diorite, tonalite, granodiorite and granite suites, and partly peraluminous granitoids at Chah-Dozdan in the southern part of the Sanandaj-Sirjan Terrane (Fazlnia and others, 2007) and at Boroujerd (Khalaji and others, 2007; Ahmadi Khalaji and others, 2009), Astaneh and Alvand (Shahbazi and others, 2010; Baharifar and others, 2004; Esna-Ashari and others, 2012; Tahmasbi and others, 2009; Masoudi and others, 2002) in the Hamedan area of the Sanandaj-Sirjan Terrane (fig. 11).

Al-in-hornblende barometry on the Astaneh pluton points to emplacement depths between 5 and 8 km (Tahmasbi and others, 2009), consistent with relatively high exhumation levels and the presence of relatively deeply seated W-Cu-Sn-Au skarn mineralization (Geological Survey of Iran, 2012b). However, some intrusive phases at Astaneh exhibit porphyritic textures that suggest shallower levels of intrusion (Bazin and Hübner, 1969a; Shahabpour, 1999). However, the age of mineralization that is

spatially associated with these shallower intrusions is poorly constrained. It may be middle Eocene (Nezafati, 2006). Thus, the W-Cu-Sn-Au-bearing Astaneh skarn is only tentatively included in the Sanandaj-Sirjan tract as a possible porphyry-related occurrence (see fig. 10 and appendix C).

The Alvand plutonic suite consists of 167 Ma gabbros, 164–162 Ma intermediate granitoids, and 154–153 Ma leucocratic granites. Geochemical data indicate emplacement in a dominantly calc-alkaline continental-arc setting (Shahbazi and others, 2010). As at Astaneh, minor tungsten-tin mineralization is related to the Alvand batholith (Salehi and others, 2009).

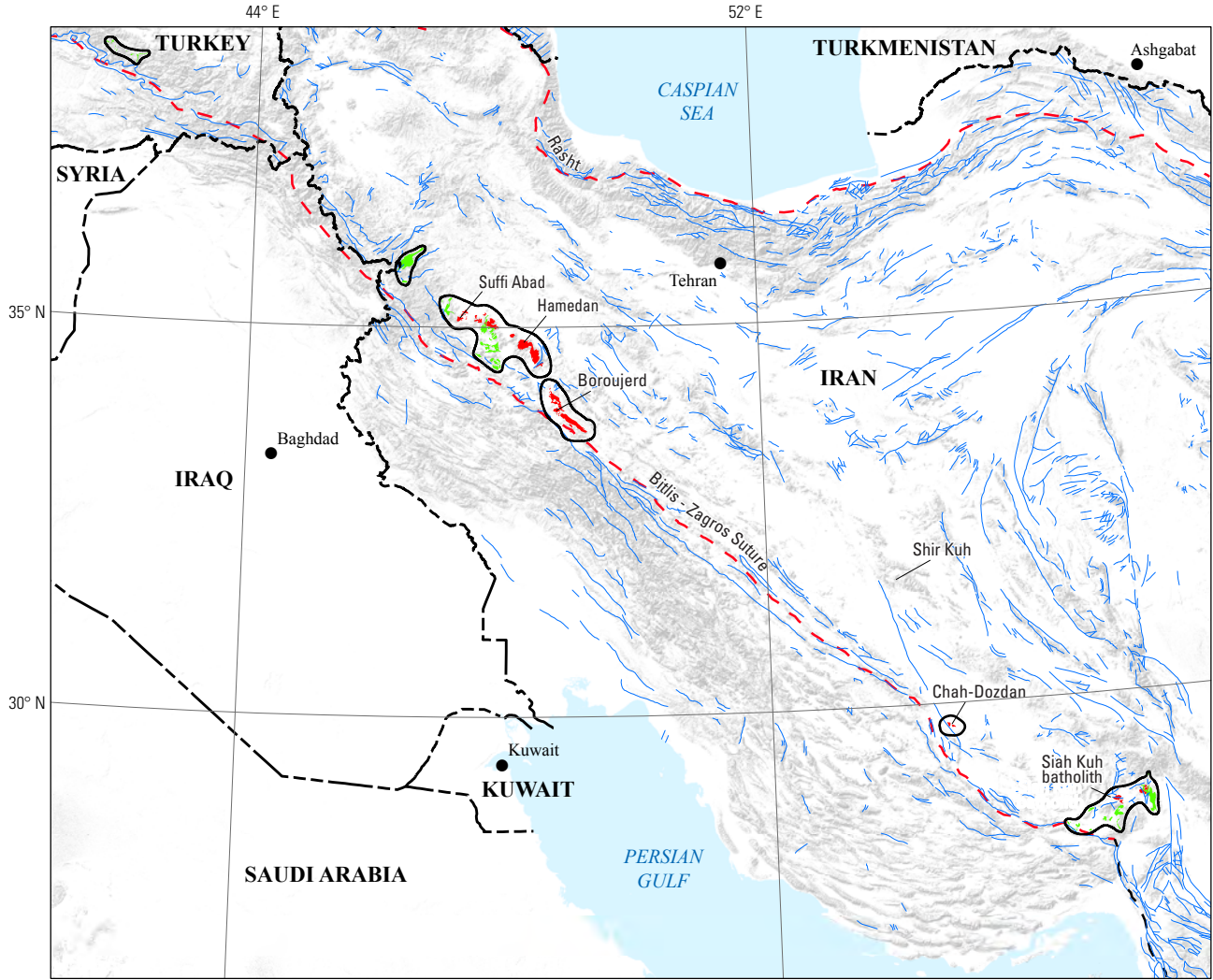
Late leucocratic intrusive phases at Alvand and Chah Dozdan exhibit comparable characteristics to the Middle Jurassic Shir Kuh metaluminous to peraluminous batholith (Sheibi and others, 2010) and associated Damak porphyry-related copper skarn (Mackizadeh and Taghipour, 2010) located in the Central Iranian Terrane north of the Nain-Baft ophiolitic complex (see fig. 3 and fig. 11). The Shir Kuh batholith is part of the larger Cimmerian orogenic event that occurred along the Eurasian margin. However, its relation to the Sanandaj-Sirjan continental arc event is uncertain.

Widespread Late Jurassic-Early Cretaceous calc-alkaline intrusive and extrusive rocks, uplift, and deformation indicate that subduction under the northern Sanandaj-Sirjan Terrane was well established by this time (Berberian and King, 1981; Boulin, 1991). The Suffi Abad plutonic complex in the northern part of the tract is representative of Late Jurassic-Early Cretaceous magmatism in the Sanandaj-Sirjan Terrane (Azizi and others, 2011). At Suffi Abad (fig. 11), 149–144 Ma calc-alkaline quartz syenite, syenite, monzosyenite, syenogranite, and leucogranite intrude Triassic-Jurassic sedimentary and trachytic to rhyolitic volcanic rocks. Geochemical data indicate subduction-related affinities for the early igneous phases, and assimilation of preexisting I-type granitoids in the upper continental crust for the late leucocratic granites. Rocks in the area have been affected by abundant iron-rich quartz veins. However, the age and nature of these hydrothermal products are not well constrained.

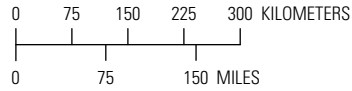
Thus, no known porphyry copper systems are known to be preserved in the Late Jurassic to Early Cretaceous part of the continental arc in the Sanandaj-Sirjan Terrane (Jamali and others, 2012). Moreover, Late Triassic to Early Cretaceous arc magmatism is absent in middle part of the Sanandaj-Sirjan Terrane. During this time period, the central part of the Sanandaj-Sirjan Terrane appears to have been part of a back-arc or rift basin where Pb-Zn-Ba Mississippi Valley type (MVT), sedimentary exhalative (SEDEX), and VMS occurrences developed instead of porphyry-related mineralization (Ghazban and others, 1994; Mirnejad and others, 2011; Rajabi and others, 2012; Förster, 1978; Meshkani and others, 2011).

Qualitative Assessment

This long-lived and mature continental-arc setting is permissive for the occurrence of porphyry copper deposits. However, factors that considerably diminish the favorability in this tract include synmineralization and postmineralization



Base from SRTM Global Digital Elevation Model, U.S. Geological Survey EROS Data Center, 2006. Political boundaries from U.S. Department of State (2009). Asia North Albers Equal-Area Conic Projection. Central meridian, 48° E., latitude of origin, 35° N.



- EXPLANATION**
- Porphyry copper**
 - Assessed porphyry copper tract 142pCu9003
 - Permissive intrusive rock
 - Permissive extrusive rock
 - Fault
 - Suture
 - Transform fault
 - Shir Kuh **Geologic features discussed in the text**



Figure 11. Map showing the distribution of permissive intrusive and extrusive rocks used to define tract 142pCu9003, Sanandaj-Sirjan—Iran, Iraq, and Turkey. See appendix A for principal sources of information, and appendix B for source map units.

deformation events that have highly exhumed this region, largely exposing metamorphosed rocks and the deeper more evolved peraluminous plutons and associated tungsten and tin mineralization. No information is available on the possible copper resources contained in these deposits.

Permissive Late Triassic to Early Cretaceous volcanic and plutonic units that define the tract amount to 8 and 7 percent, respectively, of the tract area (fig. 11). Older basement underlies about 13 percent, broadly coeval nonpermissive rocks (sedimentary, volcano-sedimentary, and mafic units) account for 25 percent, and widespread younger rocks cover about 50 percent of the tract area. The low percentage of permissive units and high percentage of younger cover imply that levels of preservation are too deep and that the extent of younger cover is too extensive for porphyry systems to be exposed. However, the otherwise appropriate permissive volcanic-to-plutonic ratio ($\{\text{volcanic}/[\text{volcanic}+\text{plutonic}]\} \times 100=52$) suggests that appropriate preservation of porphyry copper mineralization cannot be precluded, given that both permissive volcanic and plutonic units occur in fold limbs in this terrane.

The assessment team determined that undiscovered copper resources associated with these deeply exhumed metaluminous to slightly peraluminous tungsten-bearing granitoids are likely negligible. Furthermore, the low number of known porphyry occurrences (deposits, prospects, and possible porphyry-related sites), which are not only an indication of the geologic endowment and level of exposure but also a probable reflection of the limited extent of exploration, add considerable uncertainty. Despite the permissive continental-arc setting, the geologic favorability was considered too low to add significant copper resources to the overall assessment (less than a 10-percent chance of one undiscovered deposit). Therefore, quantitative assessment of undiscovered deposits in the Sanandaj-Sirjan tract was not done.

Cimmeride Greater Caucasus Tract (142pCu9002)

Descriptive model: Porphyry copper (Cox, 1986a; Berger and others, 2008; John and others, 2010)

Geologic Feature Assessed: Middle Jurassic back arc and island arc of the Tethyan Eurasian Metallogenic Belt

Location

The Cimmeride Greater Caucasus tract covers an area of 16,700 km² across northern Georgia, southernmost Russia, and northern Azerbaijan (fig. 12). It delimits a 375 km-long and as much as 70-km-wide northwest-southeast trending intraoceanic volcano-plutonic belt of Middle Jurassic age that is continuously exposed in the Greater Caucasus fold-and-thrust belt along the Georgia-Russia border. An additional isolated approximately 95 km-long by 20 km-wide segment of this volcano-plutonic belt is also exposed along the Azerbaijan-Russia border.

The Cimmeride Greater Caucasus tract is located in the northern part of the Transcaucasus Terrane, which represents the suture zone that separates the Transcaucasus from the Scythian Terrane to the north (fig. 3).

Tectonic Setting

The back-arc and intraoceanic arc environment that formed in the Middle Jurassic between the Scythian and Transcaucasus Terranes (figs. 3, 4A)—the Cimmeride Greater Caucasus tract described here—is part of the larger Late Triassic to Late Jurassic Cimmerian Orogeny (Golonka, 2004). This orogeny produced the final closure of the Paleotethys Ocean, generating a new northward-dipping subduction zone south of the accreted continents along the Northern Neotethys Ocean Branch (McCann and others, 2010). In the Greater Caucasus, this event is represented by the back-arc rift setting that developed behind the subduction zone. This back-arc setting is also known as the Gagra-Java Zone (Saintot and others, 2006).

This event was followed by renewed arc magmatism along the southern margin of the Transcaucasus Terrane in the Late Jurassic-Early Cretaceous (see Cimmeride Lesser Caucasus tract below)—and in the Late Cretaceous-Eocene (see Pontide (Asia) tract below)—which resulted in continued back-arc extension throughout the Greater Caucasus region (Adamia and others, 2011; Kazmin and others, 1986). Structural inversion of this protracted extensional basin and creation of the present-day fold-and-thrust belt of the Greater Caucasus was initiated in the late Eocene-early Oligocene as a result of the onset of collision between the Arabian Platform in the south and the Eurasian margin in the north (Saintot and others, 2006).

Magmatism and Known Porphyry Deposits or Prospects

Permissive igneous units used to define the Cimmeride Greater Caucasus tract (appendix B) are shown in figure 13, along with locations of igneous complexes and other geologic features mentioned in this section.

Middle Jurassic back-arc and intraoceanic island-arc magmatism between the Transcaucasus and the Scythian Terranes developed on thin crust and is characterized by predominantly mafic tholeiitic in the east, tholeiitic to calc-alkaline in the center, and bimodal mafic-felsic calc-alkaline to alkaline volcanic successions in the west (Kazmin and others, 1986; Lordkipanidze and others, 1989; Hess and others, 1995). Volcanic rocks are locally intruded by calc-alkaline granitoids. No porphyry copper mineralization is known to be related to these granitoids. Instead, Cu-Pb-Zn VMS systems and iron and Cu-Pb-Zn skarn and vein occurrences of economic consequence developed in and about these Middle Jurassic volcanic rocks and intrusions, respectively (Gugushvili and others, 2010; Kekelia and others, 2001; Kekelia and others, 2004; Rundkvist, 2001). It is possible that some of the Jurassic iron and base-metal skarns could be related to coeval porphyry mineralization. However, this relation has not been established in the region.

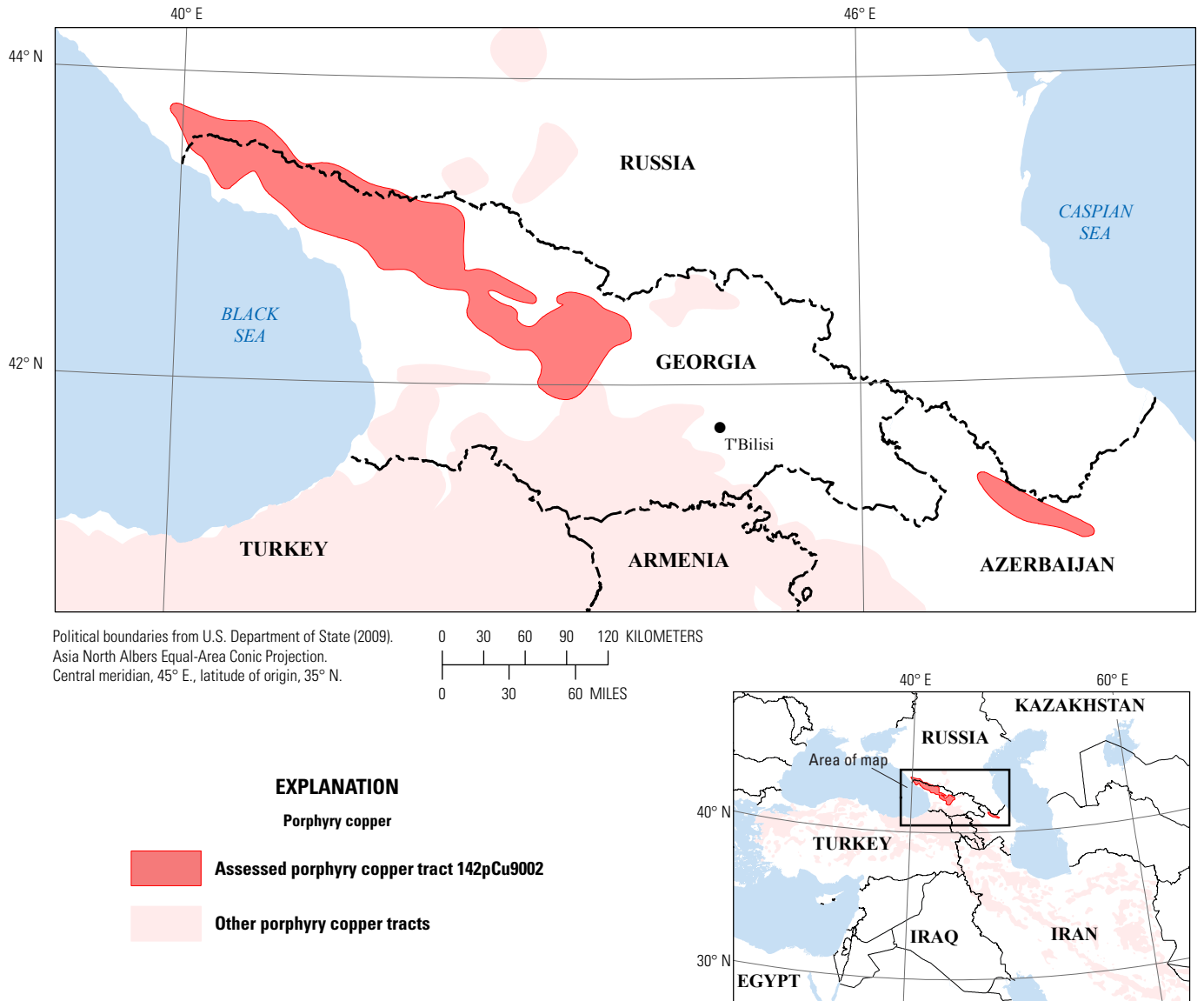


Figure 12. Map showing the location of permissive tract 142pCu9002, Cimmeride Greater Caucasus—Azerbaijan, Georgia, and Russian Federation. See appendix D for accompanying spatial data.

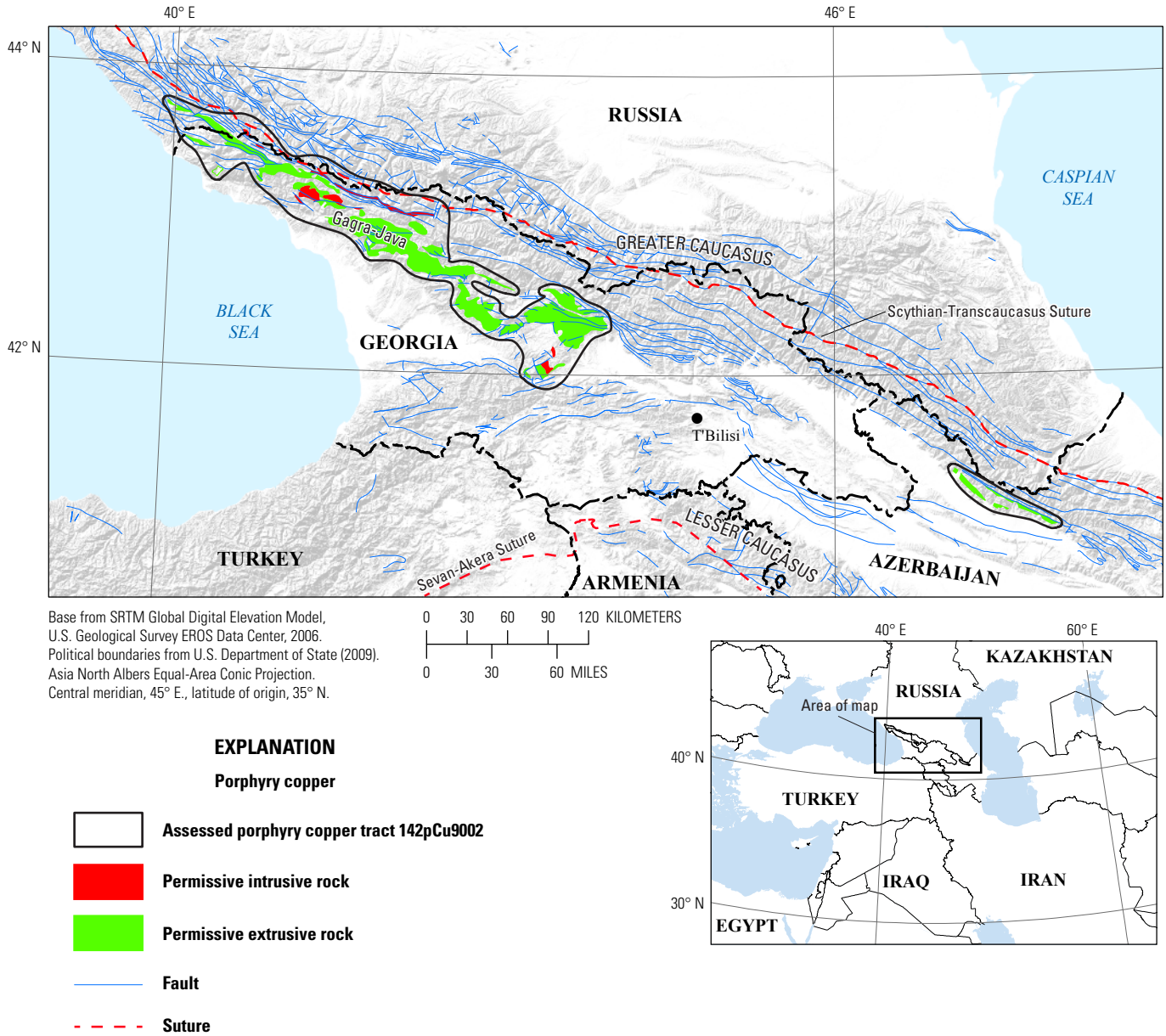


Figure 13. Map showing the distribution of permissive intrusive and extrusive rocks used to define tract 142pCu9002, Cimmeride Greater Caucasus—Azerbaijan, Georgia, and Russian Federation. See appendix A for principal sources of information and appendix B for source map units.

Qualitative Assessment

The back-arc and island-arc setting delimited by the Cimmeride Greater Caucasus tract is permissive for the occurrence of porphyry copper deposits, despite the fact that no porphyry-related systems are known. The very high ratio of permissive Middle Jurassic units ($\{\text{volcanic}/[\text{volcanic}+\text{plutonic}]\}=91$) in this complex fold-and-thrust belt implies that any porphyry copper systems may largely be lithologically or tectonically concealed (fig. 13). The absence of known porphyry-related occurrences further suggests that the region may have experienced limited exploration for this type of deposit, adding considerable uncertainty. Thus, despite the permissive geology, the assessment team felt that favorability was too low to add significant undiscovered copper resources to the overall assessment (less than a 10-percent chance of 1 undiscovered deposit). Therefore, the team concluded that a quantitative assessment for the Cimmeride Greater Caucasus tract was not warranted.

Lut Jurassic Tract (142pCu9000)

Descriptive model: Porphyry copper (Cox, 1986a; Berger and others, 2008; John and others, 2010)

Geologic feature assessed: Middle Jurassic continental arc of the Tethyan Eurasian Metallogenic Belt

Location

The Lut Jurassic tract located in eastern Iran covers an area of 2,960 km² (fig. 14). It delimits a poorly preserved and irregularly exposed 300-km-long, subduction-related magmatic arc of Middle Jurassic age that is preserved in the Lut Terrane (fig. 3).

The Lut Terrane is bounded by the right-lateral Nayband Fault on the west and by the right-lateral Nehbandan Fault on the east. The northern and southern limits of the Lut Terrane are further marked by the left-lateral Great Kafir-Doruneh Fault system on the north, and the Makran Terrane's Jaz Murian Depression on the south (fig. 3). Parts of the younger Lut Cretaceous and Lut Tertiary tracts (see below) are superimposed on the Lut Jurassic tract.

Tectonic Setting

The Lut Terrane (fig. 3), which formed part of the larger Cimmerian continental collage between the closing Paleotethys and opening Neotethys Oceans, collided for the first time with the southern margin of Eurasia in the Late Triassic-Early Jurassic (Golonka, 2004; Kazmin, 1991; Horton and others, 2008). The collision resulted in closure of the Paleotethys Ocean, and is recorded on both sides of the suture in the Kopet Dagh and Lut Terranes (fig. 3) by major deformation and uplift of Triassic and older rocks (Stöcklin, 1968; Şengör, 1979). By the Early Jurassic, the Lut, Tabas, Kashmar-Kerman, and Yazd Terranes (fig. 3) had amalgamated to form the east-central Iranian microcontinental collage. During that time, the present-day eastern margin of the Lut Terrane is believed to have been facing south (Westphal and others, 1986). Much of the 90-degree counterclockwise rotation

of Lut Terrane occurred between the Eocene and middle Miocene. This fact is not represented in the simplified paleotectonic reconstructions of fig. 4. Following collision in the north, a new northward-dipping subduction zone developed along this southern margin (fig. 4A). Middle Jurassic magmatism in the Lut block developed as a consequence of this subduction-related event.

Magmatism and Known Porphyry Deposits or Prospects

Permissive igneous units used to define the Lut Jurassic tract (appendix B) are shown in figure 15, along with locations of igneous complexes and other geologic features mentioned in this section. Middle Jurassic magmatism in the Lut Terrane is represented by the Shah-Kuh (Lut), Klatah Ahani, and Sorkh-Kuh plutons (Karimpour and others, 2011b; Bazin and Hübner, 1969a).

The Sorkh-Kuh pluton (figs. 14, 15 and appendix C) consists of 170 Ma granodiorite and 165 Ma granite phases intruded into slate and quartzite of the Lower Jurassic Shemshak Formation, which were affected by coeval synkinematic metamorphism. Geochemical and isotopic data from the Sorkh-Kuh pluton indicate peraluminous-dominated compositions derived from significant assimilation of relatively thick upper cratonic crust (Karimpour and others, 2011b) in a subduction-related setting (Arjmandzadeh and others, 2011b). The Sorkh Kuh porphyry Cu-Mo prospect is associated with this pluton (Ziaii and others, 2007; Karimpour and Stern, 2011).

The 162.9 Ma Shah-Kuh (Lut) batholith (fig. 15) is a northwest-southeast trending body about 50 km long and 12 km wide (Karimpour and others, 2011b). It was emplaced between 168–158 Ma into metamorphic basement and the overlying Lower Jurassic Shemshak Formation. Contact metamorphic effects are most noticeable along the northern side of the batholith. The batholith consists of a granodioritic unit to the northwest and a younger syenogranitic unit to the southeast. The granodioritic unit displays seriate textures and contains locally abundant mafic enclaves, whereas the syenogranitic unit is medium to coarse grained but exhibits porphyritic textures towards its margins. Fine-grained aplitic bodies cut both units. The rocks are metaluminous to slightly peraluminous (I-type) and peraluminous (S-type). Fractional crystallization appears to have been the principal differentiation process in the formation of both units. Trace-element and isotopic compositions are indicative of assimilation of felsic upper crustal materials in an active margin setting. No copper mineralization is present but tin mineralization in sheeted quartz-tourmaline-(cassiterite) veins is spatially associated with the granodioritic unit (Esmaeily and others, 2005; Karimpour and Stern, 2011; Karimpour and others, 2011b).

The Klatah Ahani batholith (fig. 15) consists of a 162.4 Ma biotite granodiorite, hornblende biotite granite, and biotite granite that intrude the Lower Jurassic Shemshak Formation. Geochemical and isotopic data indicate similar reduced ilmenite-series S-type affinities derived from significant assimilation of upper cratonic crust. Tin mineralization is also hosted by this pluton (Karimpour and others, 2011b; Karimpour and Stern, 2011).

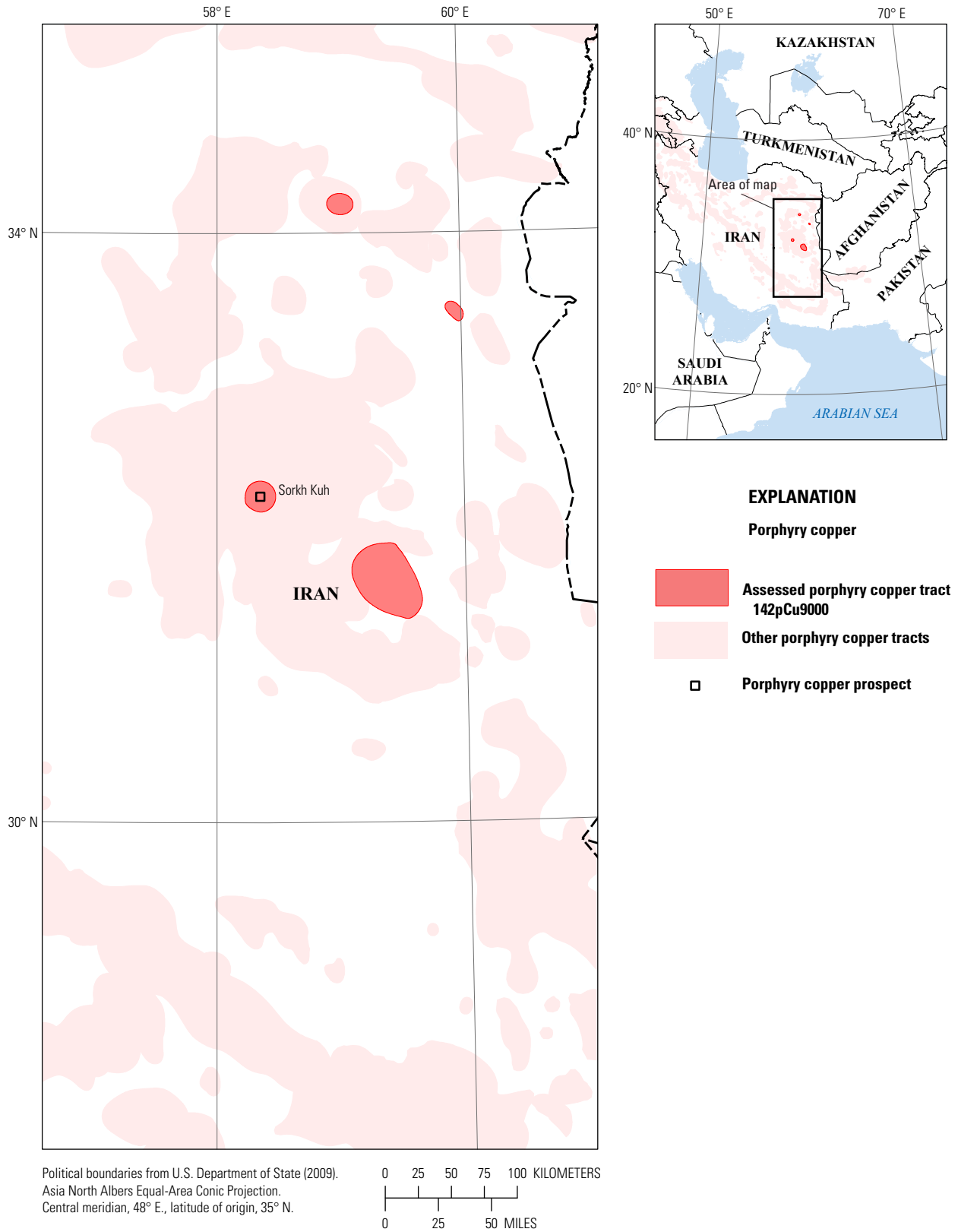


Figure 14. Map showing the location of known porphyry copper deposits, prospects, and occurrences for permissive tract 142pCu9000, Lut Jurassic—Iran. See appendix C for prospect information and appendix D for accompanying spatial data.

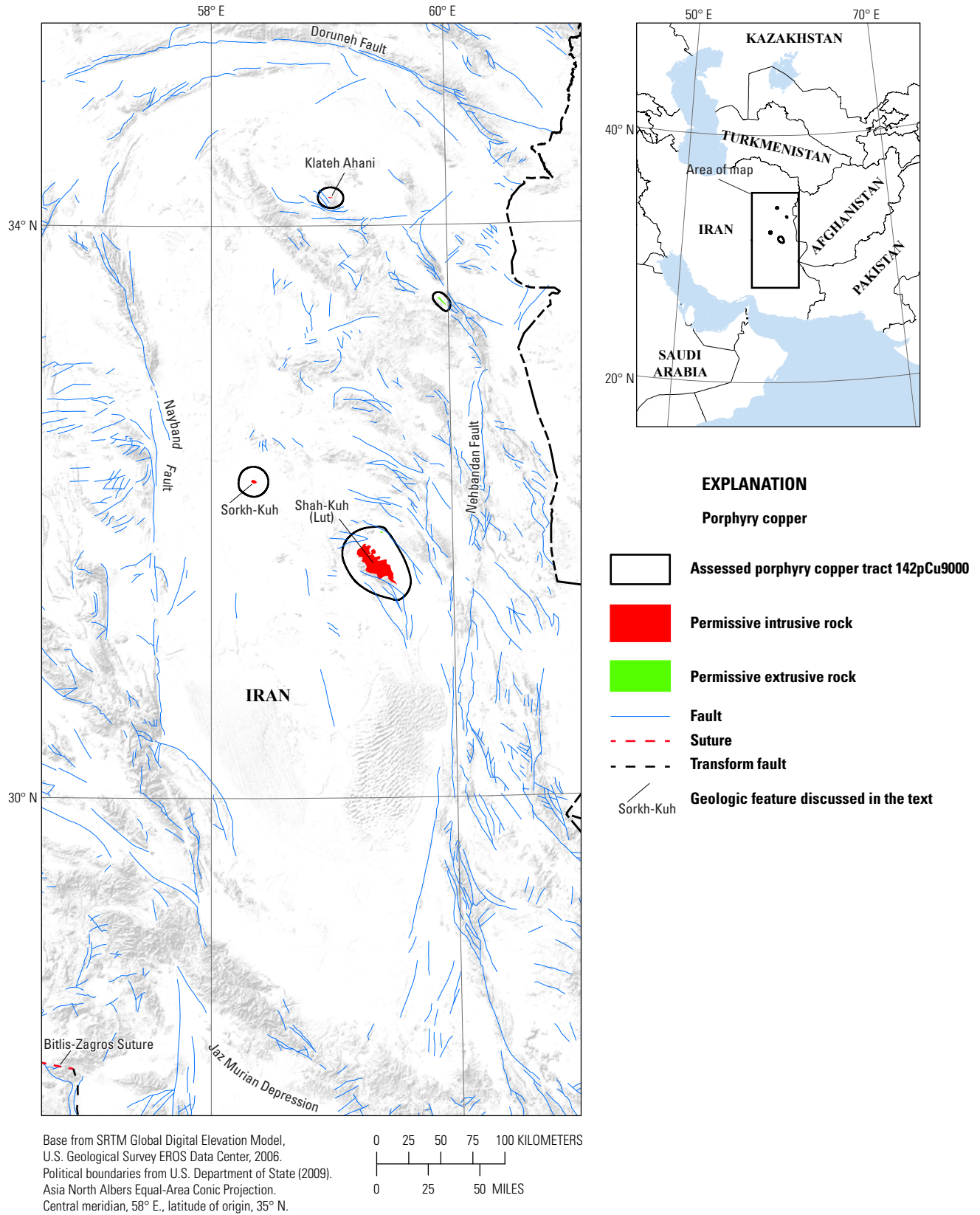


Figure 15. Map showing the distribution of permissive intrusive and extrusive rocks used to define tract142pCu9000, Lut Jurassic—Iran. See appendix A for principal sources of information and appendix B for source map units.

Qualitative Assessment

The Middle Jurassic continental-arc setting is permissive for porphyry copper deposits. However, insufficient information is available to satisfactorily characterize the geology and copper resources of the only porphyry copper prospect (Sorkh Kuh) positively identified to date in the poorly preserved, deeply exhumed, and extensively covered Lut Jurassic tract. This is supported by a permissive ($\{\text{volcanic}/[\text{volcanic}+\text{plutonic}]\} \times 100$) ratio of 3, the dominance of felsic calc-alkaline to peraluminous igneous compositions, deep-seated tin-bearing metal associations in related hydrothermal systems, and younger rocks that cover about 67 percent of the tract area (fig. 15). The near absence of porphyry prospects of this age range further adds considerable uncertainty. Given these factors, the assessment team felt that contained copper resources in the tract were likely negligible (less than a 10-percent chance of 1 undiscovered deposit). Thus, despite the permissive geology and the presence of one positively identified porphyry copper prospect, the geologic favorability was deemed too low to add significant undiscovered copper resources to the overall assessment. Therefore, quantitative assessment of the Lut Jurassic tract was not warranted.

Cimmeride Lesser Caucasus Tract (142pCu9001)

Descriptive model: Porphyry copper (Cox, 1986a; Berger and others, 2008; John and others, 2010)

Grade and tonnage model: General Cu-Au-Mo porphyry copper model (Singer and others, 2008)

Geologic feature assessed: Middle Jurassic to Early Cretaceous island to continental arc and back arc of the Tethyan Eurasian Metallogenic Belt

Location

The Cimmeride Lesser Caucasus tract covers an area of 17,400 km² across the Lesser Caucasus fold-and-thrust belt of southernmost Georgia, eastern Armenia, and western Azerbaijan (fig. 16). It delimits a 350-km-long by 70-km-wide northwest-trending island- to continental-arc and back-arc volcano-plutonic belt of Middle Jurassic-Early Cretaceous age that was built on the Transcaucasus Terrane. To the southwest, the tract is bounded by the Sevan-Akera and Vedi-Zangezur ophiolitic sutures (fig. 3), which mark the boundary between the Transcaucasus and the eastern Anatolide-Tauride Terrane (South Armenian Block) to the south. To the northeast, the tract is delimited by a thick section of younger cover rocks. Parts of the younger Pontide (Asia)–Caucasus-Iran sub-tract and Azerbaijan–Caucasus-Iran tract (see below) are superimposed on the Cimmeride Lesser Caucasus tract.

Tectonic Setting

During Late Triassic-Early Jurassic times, several microplates were sutured to the Eurasian margin, closing the Paleotethys Ocean (Şengör, 1979). Following collision in the north, an extensive northward-dipping subduction zone developed

to the south of these microplates (Golonka, 2004), extending from the Lut Terrane of Iran in the east to the Istanbul Terrane of Turkey in the west (fig. 4B). In the Lesser Caucasus, Jurassic-Cretaceous subduction along the new Eurasian margin created an island- to continental-arc and back-arc setting in the Transcaucasus Terrane (Kekelia and others, 2001; Şengör and others, 1993; Şengör and others, 1991). Intense magmatism occurred along this arc, which is also known as the Somkheto-Karabakh Arc delimited here by the Cimmeride Lesser Caucasus tract (Gamkrelidze, 1986; Sosson and others, 2010b).

Magmatism

Permissive igneous units used to define the Cimmeride Lesser Caucasus tract (appendix B) are shown in figure 17, along with locations of igneous complexes and other geologic features mentioned in this section.

In the Lesser Caucasus, deformation, uplift, and magmatism associated with this arc-building event were most intense in the Middle Jurassic-Early Cretaceous, but continued into the Late Cretaceous in the back-arc region, when an as much as 3.5-km-thick calc-alkaline island-arc sequence of mafic-to-felsic but dominantly andesitic flows were erupted in a shallow-sea environment (Adamia and others, 1977). These volcanic rocks were, in turn, overlain by an as much as 2.5-km-thick volcano-sedimentary succession with interlayered shoshonitic mafic volcanic rocks (Adamia and others, 1981). The composition of volcanic rocks changes from low-K calc-alkaline about the arc axis in the south to shoshonitic in the back-arc region in the north, consistent with northward subduction polarity (Kazmin and others, 1986; Adamia and others, 1981; Khain, 1975). Volcanic rocks are intruded by gabbro and plagiogranite, calc-alkaline diorite-tonalite-granodiorite-granite-monzonite, and lesser monzonite-syenite plutons (Kekelia and others, 2001; Lordkipanidze and others, 1989). To the rear of the arc, in the northern part of the Transcaucasus Terrane (fig. 3), the back-arc sequence is formed by a 3- to 3.5-km-thick section of dominantly tholeiitic back-arc alkali basalts and trachytes that were deposited alongside salt- and gypsum-bearing lagoonal and continental deposits (Adamia and others, 2011).

Volcanic and plutonic units associated with this event were deformed by Paleocene-early Eocene folding and thrusting and late Miocene to present folding, thrusting, and strike-slip events (Sosson and others, 2010b).

Known Porphyry Deposits and Prospects

Middle Jurassic-Early Cretaceous porphyry copper and associated iron and base-metal skarn systems in the Cimmeride Lesser Caucasus tract are exposed in erosional windows into overlying and tectonically juxtaposed volcanic and volcano-sedimentary successions, which also host several Jurassic-Cretaceous copper-(gold-lead-zinc) volcanogenic massive sulfide occurrences of economic consequence (Gugushvili and others, 2010; Moon and others, 2001; Kekelia and others, 2001; Kekelia and others, 2004; Rundkvist, 2001).

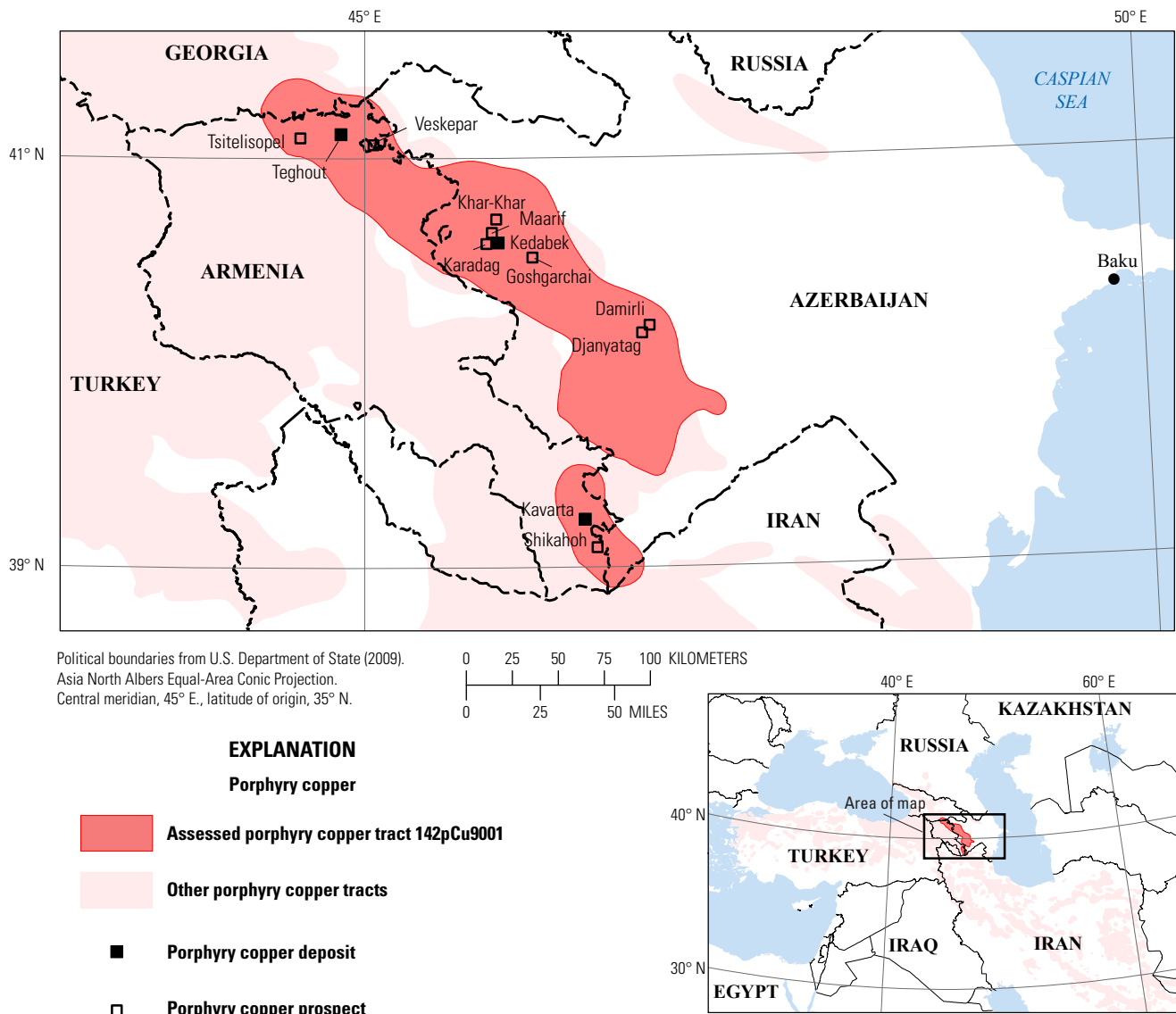
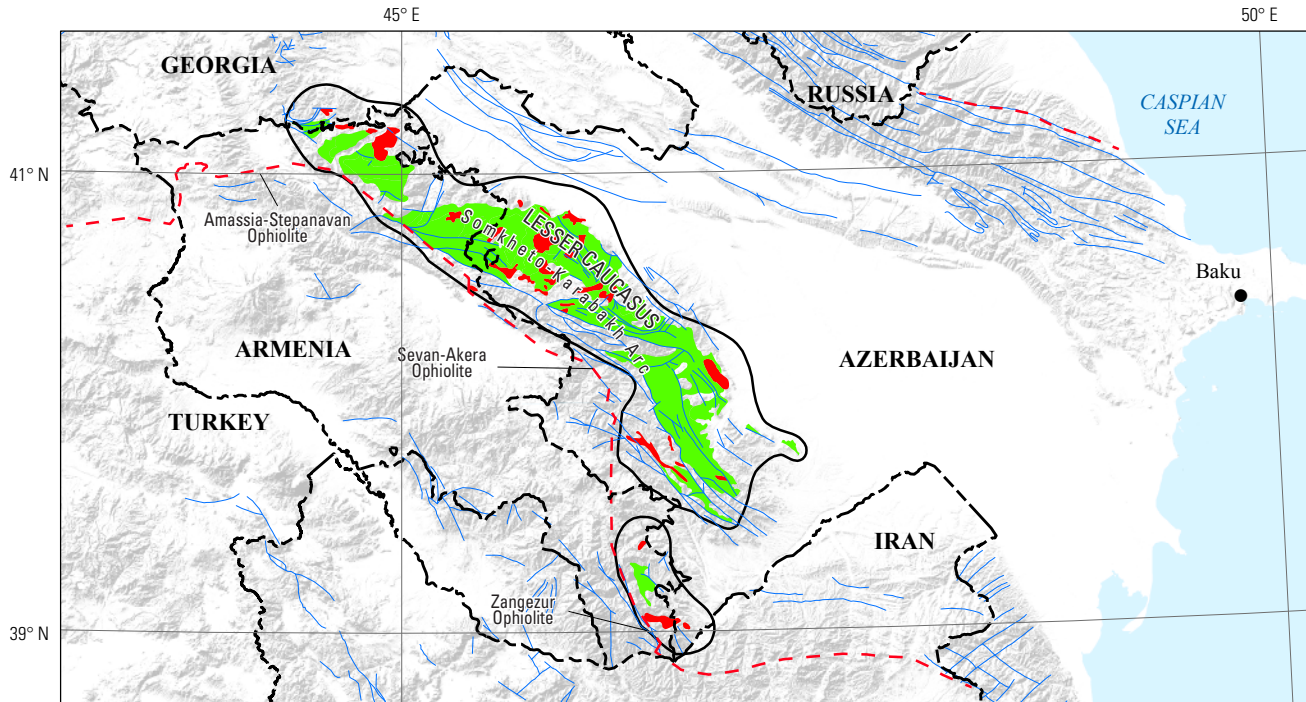
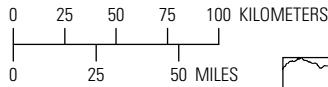


Figure 16. Map showing the location of known porphyry copper deposits and prospects for permissive tract 142pCu9001, Cimmeride Lesser Caucasus—Armenia, Azerbaijan, Georgia, and Iran. See table 2 for deposits, appendix C for prospects, and appendix D for accompanying spatial data.



Base from SRTM Global Digital Elevation Model, U.S. Geological Survey EROS Data Center, 2006. Political boundaries from U.S. Department of State (2009). Asia North Albers Equal-Area Conic Projection. Central meridian, 45° E., latitude of origin, 35° N.



- EXPLANATION**
- Porphyry copper**
- Assessed porphyry copper tract 142pCu9001
 - Permissive intrusive rock
 - Permissive extrusive rock
 - Fault
 - Suture
 - Sevan-Akera Ophiolite
 - Geologic feature discussed in the text

Figure 17. Map showing the distribution of permissive intrusive and extrusive rocks used to define tract 142pCu9001, Cimmeride Lesser Caucasus—Armenia, Azerbaijan, Georgia, and Iran. See appendix A for principal sources of information and appendix B for source map units.

In the Cimmeride Lesser Caucasus tract, VMS and porphyry deposits occur in a back-arc tectonic environment that is permissive for both. A genetic relation between these two deposit types is not implied here, but it has been proposed in several mineral districts (Kekelia and others, 2004). Depending on the level of preservation, however, only the more eroded windows expose the more deeply emplaced porphyry systems. Furthermore, the postmineral deformational history tectonically juxtaposed these two shallow and deeper hypabyssal ore-forming environments. This is evident not only in the Lesser Caucasus but elsewhere in the Tethys region of western and southern Asia.

The Cimmeride Lesser Caucasus tract contains 3 (Teghout, Kavarta (Kapan), and Kedabek) known porphyry copper deposits (table 2) and 9 porphyry prospects (fig. 16 and appendix C). Other Middle Jurassic-Early Cretaceous mineral occurrences with more debatable genetic association to porphyry-style mineralization include Kizilbulag and Gosha. Gugushvili and others (2010) interpret them as porphyry related, whereas Kekelia and others (2001) classify them as VMS systems. These two prospects are not included in the database (appendix D)

Teghout Porphyry Deposit

The Teghout Cu-Mo-(Au) porphyry deposit is located in the northern part of the tract. It is Armenia's second largest Cu-Mo deposit after Kadjaran (Mining Journal, 2005). The Teghout deposit has reported resources of 460 Mt at 0.35 percent copper and 0.02 percent molybdenum (Singer and others, 2008), or 450 Mt at 0.36 percent copper and 0.022 percent molybdenum (Mining Journal, 2005). Exploratory work has been ongoing since the Soviet Era. In 2008, a renewed exploration program was put in place to develop the deposit (Thalenhorst, 2005, 2007). The 145.9 Ma (Moritz and others, 2012) Teghout diorite to granite and rhyodacite porphyry deposit consists of a large stockwork with hypogene chalcocite and molybdenite, and chalcocite in a supergene enrichment zone. Mineralization is also hosted by skarn. Gold, silver, and rhenium are reported byproducts (Levine, 2011a). Available information suggests emplacement of the Teghout Cu-Mo-(Au) porphyry deposit in an arc setting.

Kedabek Porphyry Deposit

The Kedabek Cu-Au-(Mo) porphyry deposit is located in the back-arc part of the tract, about 100 km southeast of the Teghout deposit (fig. 16; Singer and others, 2008). Mineralization occurs in quartz diorite and diorite porphyry, as well as diabase dikes, which are overlain by a series of altered volcano-sedimentary rocks. Three stages have been established in the mineral paragenesis (Bortnikov and others, 1993). The products of the earliest stage consist of pyrite, pyrrhotite, and arsenopyrite. The principal minerals of the second stage are pyrite, arsenopyrite, chalcocopyrite, sphalerite, and tetrahedrite. Gold, molybdenite, and pyrite were deposited during the third stage. The mineralized bodies also include

massive covellite-bornite-chalcocite-chalcocopyrite in skarn at the contact zone of the Jurassic to Early Cretaceous intrusive complex (United Nations Economic and Social Commission for Asia and the Pacific, 2000). Mining may have occurred at Kedabek as early as 2,000 years ago.

The combined JORC¹⁹-compliant indicated-and-inferred resource base is 15.6 Mt at 0.24 percent copper, 1.4 grams per metric ton (g/t) gold, and 12.2 g/t silver (Anglo Asian Mining PLC, 2009). The updated measured and indicated reserve and inferred resource has grown to 48 Mt at 0.197 percent copper, 0.825 g/t gold, and 6.65g/t silver; CAE Mining, 2012). The first gold from the open-pit, heap-leach-operation mine was poured in May 2009. Plans are to produce in excess of 310,000 oz gold over the initial 6-year mine life (Anglo Asian Mining PLC, 2011). Given the grades in the current reserve base, the mine is contemplated as a gold operation. However, additional copper resources are likely present at depth.

Kavarta (Kapan) Porphyry Deposit

The Kavarta Cu-Mo-Au porphyry deposit is located about 150 km south of Kedabek in the southern part of the tract (fig. 16). In 1978, the resource was estimated at 50 Mt at 1.2 percent copper (Singer and others, 2008), or 50 Mt at 0.6 percent copper and 0.025 percent molybdenum (Kirkham and Dunne, 2000). However, the Kapan-Shahumyan porphyry and polymetallic vein district has seen renewed exploration that has resulted in a significant update of the resource base. In 2009, inferred resources at the Kapan porphyry-polymetallic vein deposit were estimated at 466.3 Mt and 0.09 percent copper, 0.37 g/t gold, 6.5 g/t silver, and 0.32 percent zinc (Wolfe and Gossage, 2009).

In the Kapan-Shahumyan district, highly deformed Middle to Upper Jurassic volcanogenic and sedimentary formations host the copper-molybdenum and polymetallic stockwork and vein deposits, respectively. The 1,000-m-thick volcanogenic sequence is composed of two cycles of basaltic andesite to rhyodacite extrusive and porphyry stocks and north-west to east-west dikes of andesitic, tonalitic, and dacitic composition that were emplaced in an extensional back-arc setting. Both the disseminated copper and polymetallic vein mineralization are centered about the porphyry intrusions (Wolfe and Gossage, 2009).

Upper Jurassic volcanogenic and sedimentary rocks are overlain by a 2,500-m-thick Jurassic-Cretaceous postmineral volcanic and sedimentary sequence. Both rock successions are preserved in a doubly plunging northwest-southeast anticline, with the younger Jurassic-Cretaceous strata localized on the northeastern and northern limbs of the structure. These successions are furthermore crosscut by 125-Ma north-west gabbroic dikes, as well as Paleogene extrusive and subvolcanic diabase, andesite, and dacite dikes (Wolfe and Gossage, 2009).

¹⁹Australian Joint Ore Reserves Committee (or the Australian Code for Reporting of Exploration Results, Mineral Resources, and Ore Reserves).

Other Porphyry Prospects and Possible Porphyry-Related Mineral Occurrences

Most of the known Jurassic-Cretaceous porphyry copper prospects (Kekelia and others, 2001; Rundkvist, 2001) occur about the plutons that also host the known deposits. The Tsitelisopel and Vekepar prospects are in the vicinity of the Teghout deposit; the Goshgarchai, Khar Khar (133.3 Ma; Moritz and others, 2012), Karadag, and the possible porphyry-related Maarif prospects occur around the Kedabek deposit, and the Shikahoh prospect is located near the Kapan deposit. The Djanyatag and Damirli prospects, on the other hand, are about 100 km north of the Kapan and southeast of the Kedabek porphyry deposits, respectively. On the basis of the Cu-Mo metal associations reported (Mining Journal, 2011a; Wikipedia, 2013a), other possible porphyry-related mineral occurrences are located at Aramazd (Cu-Mo-Au-Ag-Pb-Zn), Bartsravan-Brnakot (Cu-Mo-Au-Pb), Balishen (Cu-Au-Ag-Mo-Pb), and Hankasar (Cu-Mo-Au-Ag). However, the deposit type and age of these occurrences is uncertain. Therefore, they are not included in the database.

Preservation Level

The Cimmeride Lesser Caucasus tract delineates the extent of this arc to back-arc setting, which is well preserved along the southern margin of the Transcaucasus Terrane. However, it does not include much of the back-arc environment to the rear, because these rocks are buried under thick Neogene molassic deposits.

The four more eroded windows that contain most of the plutonic outcrops and known porphyry deposits and prospects in the tract appear to exhibit appropriate levels of preservation for porphyry copper mineralization of this age. Conversely, Jurassic-Cretaceous VMS systems are distributed outside these erosional windows in more volcanic-dominated areas of the tract, indicating preservation of shallower paleodepositional environments.

As derived from the 1:1,000,000-scale geologic map of the Caucasus (Kekelia and others, 2001), permissive Jurassic-Cretaceous volcanic and plutonic units are relatively well exposed throughout much of Cimmeride Lesser Caucasus tract area (34 and 5 percent, respectively), but the overall permissive unit $\{\text{volcanic}/[\text{volcanic}+\text{plutonic}]\} \times 100$ ratio across the tract is high at 87 (fig. 17). Nonpermissive mafic, sedimentary, and volcano-sedimentary units occupy an additional 27 percent, and younger rocks cover the remaining 33 percent of the tract area. Older basement rocks within the tract account for less than 1 percent. Overall, these data suggest that undiscovered porphyry copper deposits may largely be concealed under permissive volcanic units, nonpermissive volcano-sedimentary and sedimentary units, and younger cover.

Magnetic Anomalies

The global aeromagnetic map Maus and others (2009) was used to confirm the location and character of regional geologic features (for example, arcs, basins, faults, terrane

boundaries). On the basis of magnetic responses that are likely related to mafic accretionary prisms and other units associated with younger events, the Cimmeride Lesser Caucasus tract occupies a region that does not appear to exhibit significant magnetic relief. However, magnetic gradients do occur about the Kavarta-Shikahoh, Goshgarchai, and Teghout-Tsitelisopel-Vekespar districts (fig. 16). Magnetic contrasts are also evident north of the Khar-Khar and south of the Goshgarchai porphyry prospects, where they may image the location of regional structures that separate the arc from the back-arc environment. Beyond the tract boundary to the northeast, a broad positive magnetic anomaly likely reflects the long-lived Middle Jurassic-Paleogene mafic rock-dominated extensional back-arc rift environment that is buried under thick Neogene deposits.

Probabilistic Assessment

Grade and Tonnage Model Selection

In the Cimmeride Lesser Caucasus tract, resource data allow classification of Kedabek as Cu-Au and Teghout as a Cu-Mo porphyry deposit subtypes, based on the Au/Mo ratio and criteria for gold and molybdenum content used in this assessment. Available descriptions of the Kavarta deposit indicate contents of both molybdenum and gold. With the exception of the Goshgarchai prospect in the Kedabek district, for which relatively high gold grades are reported, available information on the other eight known porphyry prospects suggests that these may conform more to the Cu-Mo subcategory.

Pooled *t*-test results assuming equal variances show that the three known deposits in the tract are not significantly different at the 1-percent level from tonnages and grades in the general porphyry Cu-Au-Mo model of Singer and others (2008). Therefore, the general model was selected to estimate undiscovered copper, gold, molybdenum, and silver resources in this tract. Compared to the median tonnage and grade in the general porphyry Cu-Au-Mo model, Teghout exhibits larger tonnage and higher molybdenum grade and Kavarta shows smaller tonnage but higher copper grade (when the smaller more copper-rich older resource base reported in Wolfe and Gossage (2009) is considered). Kedabek is also smaller than the median deposit in the model but has higher gold grades.

Estimates of Undiscovered Deposits and Rationale

Favorable geologic factors for the occurrence of undiscovered porphyry copper deposits likely present in the island-to-continental and back-arc setting delineated by the Cimmeride Lesser Caucasus tract include (1) a well-exposed segment of a long-lived arc to back-arc system, (2) permissive calc-alkaline and alkaline magmatic compositions, (3) three known Cu-Au-Mo and Cu-Mo-Au porphyry deposits with one containing tonnages and molybdenum grades that exceed those of the median deposit around the world, (4) favorable conditions for supergene enrichment, and (5) appropriate

preservation levels for porphyry copper systems in erosional windows. Unfavorable geologic factors include (1) levels of preservation in 70 percent of the tract area that are too shallow for porphyry systems or otherwise covered by younger rocks and (2) superimposed postmineral fold-and-thrust events that likely have concealed or exhumed porphyry systems.

The density of known porphyry deposits across the entire tract is lower compared to densities in well-explored tracts of this size around the world, suggesting that undiscovered deposits are likely present. In addition, a relatively low level of uncertainty to which the number of undiscovered deposits can be estimated is in part supported by the comparatively large number (albeit unevenly distributed) of known porphyry occurrences (the sum of deposits and prospects), and the fact that the area is experiencing renewed exploration efforts that are being successful in incrementing the resource base (such as at the Kedabek and Kavarta deposits).

The assessment team concluded that the Cimmeride Lesser Caucasus porphyry tract was geologically favorable and that estimates of numbers of undiscovered porphyry copper deposits could be carried out with a moderate level of uncertainty. The tract would contribute significant copper resources from undiscovered deposits to the overall assessment. Therefore, quantitative assessment of undiscovered deposits in this tract was completed. Table 4A shows the consensus estimates for undiscovered porphyry copper deposits in the Cimmeride Lesser Caucasus tract at the 90-, 50-, and 10-probability levels and the associated summary statistics. The 90-percent probability estimates were equally divided among assessors at 0 and 1 undiscovered deposits. At the 50-percent probability the numbers ranged from 1 to 3 undiscovered deposits, and at the 10-percent probability level, the numbers increased to between 2 and 6. On the basis of these numbers, the team reached a consensus estimate of 0, 2, and 3 undiscovered deposits for the 90-, 50-, and 10-percent probability levels, respectively, which resulted in a mean of 1.85 undiscovered deposits with a standard deviation of 1.46 (C_v percent (%)=79). This result reflects the level of favorability and moderate uncertainty assessed for this tract. The estimated total (that is, known + undiscovered) deposit density per 100,000 km² obtained is comparable to median porphyry deposit densities in well-explored tracts of equivalent size elsewhere around the world (Singer and Menzie, 2010).

Probabilistic Assessment Simulation Results

Simulation results for estimates of copper, molybdenum, gold, silver, and the total volume of mineralized rock are summarized in table 4B. The mean estimate of undiscovered copper resources in the Cimmeride Lesser Caucasus porphyry tract is 7.1 Mt. Results of the Monte Carlo simulation are also presented as cumulative frequency plots (fig. 18). The cumulative frequency plots show the cumulative probabilities of occurrence-estimated resources and total mineralized rock, as well as the mean for each commodity and for total mineralized rock.

Late Cretaceous to Late Eocene Tracts

The seven Late Cretaceous to late Eocene permissive tracts are shown in figure 6. A probabilistic assessment of undiscovered resources was conducted for the Pontide, Anatolide-Tauride, Border Folds, Esfahan, and Khorasan tracts; the other two tracts delineated for this age range (the Lut Cretaceous and the Makran) were assessed qualitatively.

Pontide (Asia) Tract (142pCu9004)

Location

The Pontide (Asia) tract covers an area of 102,500 km² (fig. 19). It delimits a 2,300-km-long and 100–200-km-wide subduction- to postsubduction-related volcano-plutonic belt of Late Cretaceous to late Eocene age that extends across northern Turkey, southern Georgia, eastern Armenia, western Azerbaijan, and northern Iran. The Pontide (Asia) tract occurs in the Istanbul, eastern Pontide, Sakarya, Transcaucasus, Talysh, and Alborz Terranes (fig. 3). These terranes and the Pontide (Asia) tract are bounded to the south by the Izmir-Ankara-Erzincan, Sevan-Akera, and Rasht suture zones. To the north and northeast the Pontide (Asia) tract is delimited by the Black Sea and younger cover rocks in the Caucasus, respectively (fig. 6). The Pontide (Asia) tract is partially superimposed on the older Cimmeride Lesser Caucasus tract (see fig. 16).

Tectonic Setting

The Late Cretaceous to middle-late Eocene island- to continental-arc event that occurred in the Northern Neotethys Ocean Branch associated with a north-vergent subduction zone on the Eurasian margin is known as the Pontide Arc (Janković, 1977; Yılmaz and others, 1997b; Kaymakci and others, 2010). The Pontide (Asia) tract delimits the extent of the Pontide Arc in the assessment region. Across northern Turkey, the Lesser Caucasus, and northern Iran, it consists of a fore-arc, arc, and back-arc-to-postcollisional environment that developed in front of and on the Pontides (the amalgamated Strandja, Istanbul, and Sakarya Terrane collage; Okay, 1989; Richard Herrington, written commun., 2005), the Transcaucasus, and the Talysh and Alborz Terranes (figs. 3, 4C). From west to east, Pontide Arc magmatism is located about and north of the ophiolite-bearing Izmir-Ankara-Erzincan Suture (fig. 3) in Turkey (Dilek and others, 2010), about and northeast of the Sevan-Akera and Vedi-Zangezur Sutures in the Lesser Caucasus (Rolland and others, 2009, 2010; Sosson and others, 2010b), and about the Rasht Suture in northwest Iran (Adamia and others, 2011; Salavati, 2008).

Closure of the Northern Neotethys Ocean Branch and accretion-collision of the Anatolide-Tauride and South Armenian Block (eastern Anatolide-Tauride) Terranes onto the Eurasian margin progressed in time and space from the Late Cretaceous (Central Anatolian Crystalline Complex Terrane) in central Turkey, to the late Paleocene-early Eocene (western Anatolide-Tauride

Table 4. Probabilistic assessment for tract 142pCu9001, Cimmeride Lesser Caucasus—Armenia, Azerbaijan, Georgia, and Iran.

A. Undiscovered deposit estimates, deposit numbers, tract area, and deposit density.

[N_{xx} , estimated number of deposits associated with the xxth percentile; N_{und} , expected number of undiscovered deposits; s , standard deviation; $C_v\%$, coefficient of variance; N_{known} , number of known deposits in the tract that are included in the grade and tonnage model; N_{total} , total of expected number of deposits plus known deposits; tract area, area of permissive tract in square kilometers (km^2); deposit density reported as the total number of deposits per 100,000 km^2 . N_{und} , s , and $C_v\%$ are calculated using a regression equation (Singer and Menzie, 2005)]

Consensus undiscovered deposit estimates					Summary statistics					Tract area (km^2)	Deposit density ($N_{total}/100,000 km^2$)
N_{90}	N_{50}	N_{10}	N_{05}	N_{01}	N_{und}	s	$C_v\%$	N_{known}	N_{total}		
0	2	3	5	5	1.8	1.5	79	3	4.8	17,400	28

B. Results of Monte Carlo simulations of undiscovered resources.

[Cu, copper; Mo, molybdenum; Au, gold; and Ag, silver; in metric tons; Rock, in million metric tons]

Material	Probability of at least the indicated amount						Probability of	
	0.95	0.9	0.5	0.1	0.05	Mean	Mean or greater	None
Cu	0	0	2,500,000	16,000,000	27,000,000	7,100,000	0.25	0.19
Mo	0	0	22,000	430,000	830,000	200,000	0.19	0.37
Au	0	0	36	450	790	180	0.24	0.33
Ag	0	0	130	5,400	10,000	2,400	0.19	0.46
Rock	0	0	540	3,300	5,600	1,400	0.26	0.19

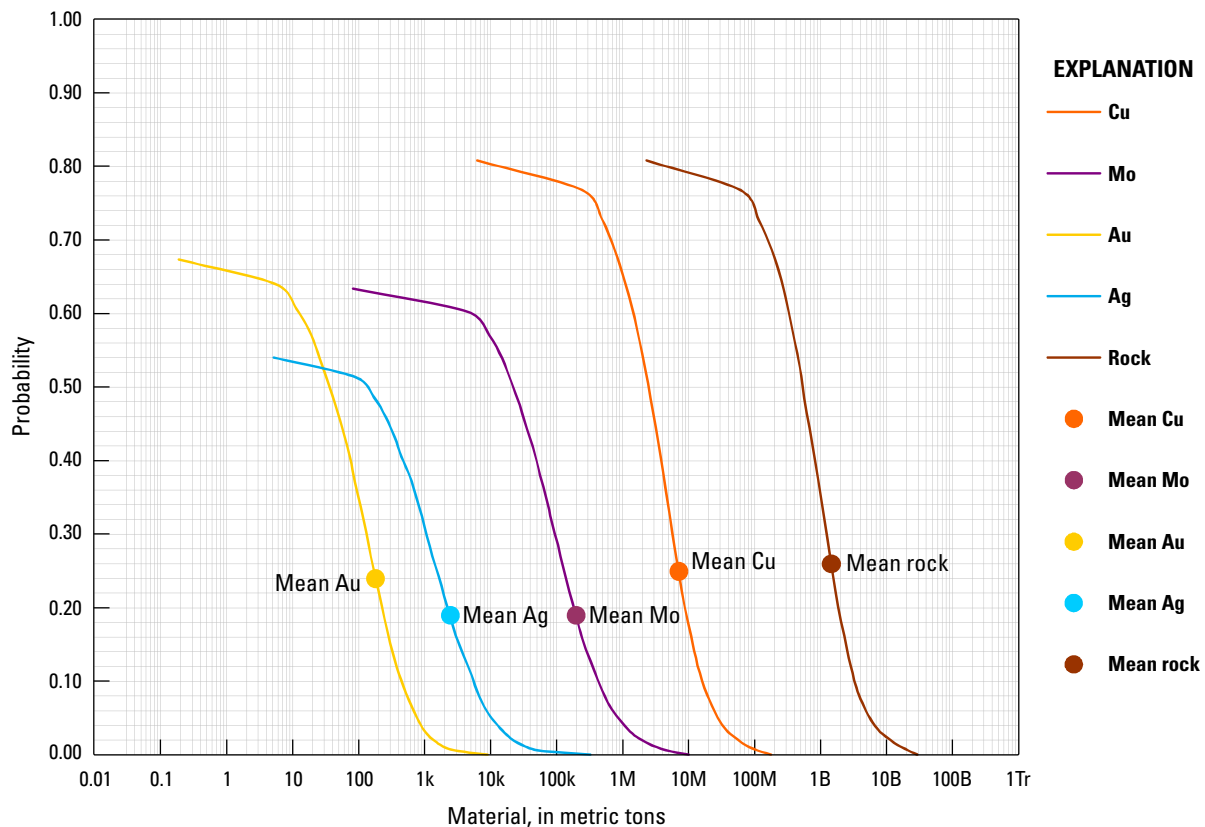


Figure 18. Cumulative frequency plot showing the results of Monte Carlo simulation of undiscovered resources in porphyry copper deposits in tract 142pCu9001, Cimmeride Lesser Caucasus— Armenia, Azerbaijan, Georgia, and Iran. k, thousand; M, million; B, billion; Tr, trillion.

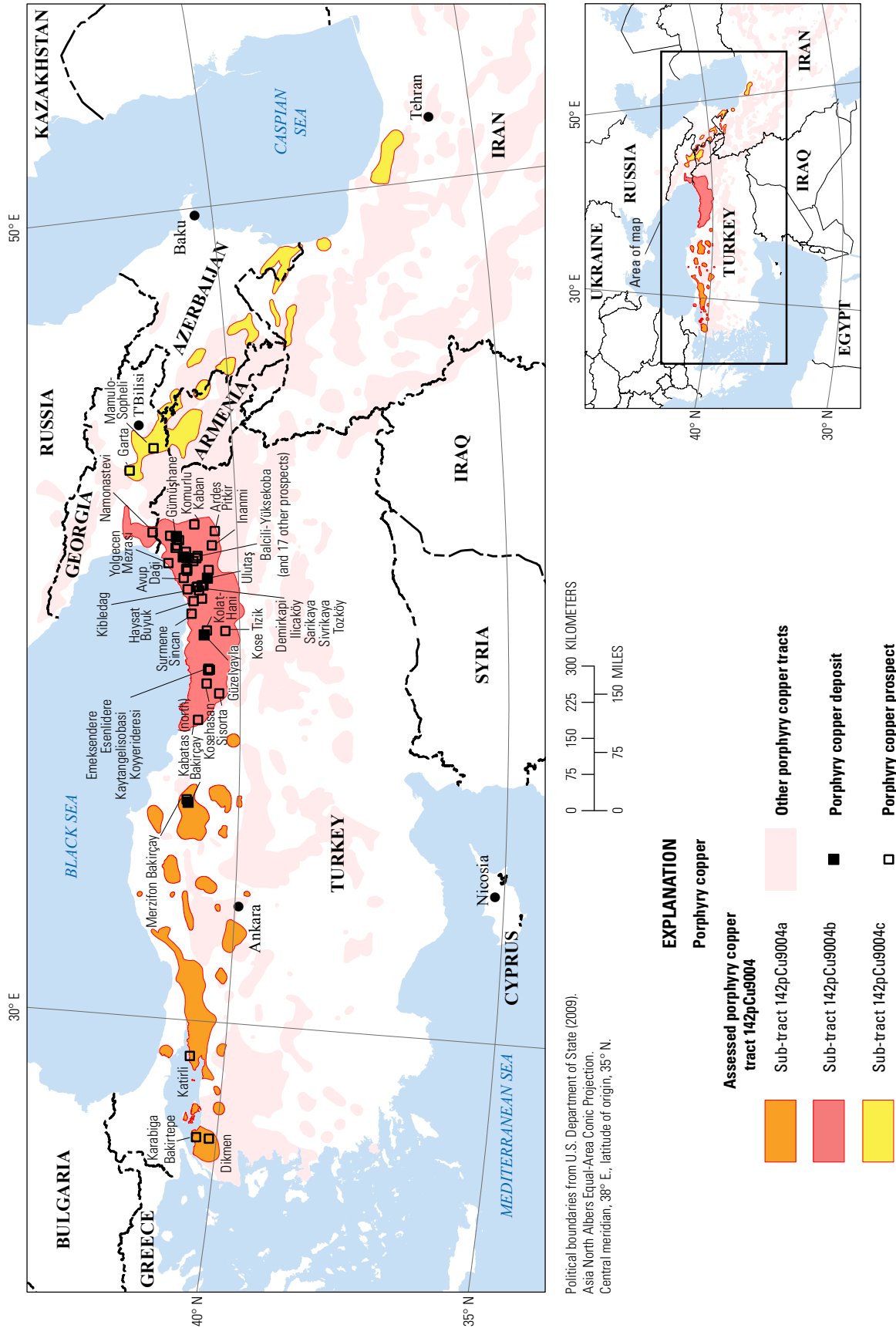


Figure 19. Map showing the location of known porphyry copper deposits and prospects for permissive tract 142pCu9004, Pontide (Asia)—Armenia, Azerbaijan, Georgia, Iran, and Turkey. Sub-tracts: 142pCu9004a, Pontide (Asia)—NW Turkey, Turkey; 142pCu9004b, Pontide (Asia)—NE Turkey, Georgia and Turkey; 142pCu9004c, Pontide (Asia)—Caucasus-Iran, Armenia, Azerbaijan, Georgia, and Iran. See table 2 for deposits, appendix C for prospects, and appendix D for accompanying spatial data.

Terrane) in western Turkey (Moix and others, 2008; Şengör and Yılmaz, 1981; Okay, 2008), and to the early to middle Eocene (eastern Anatolide-Tauride Terrane) in eastern Turkey, the Lesser Caucasus, and northern Iran (Sosson and others, 2010; Dilek and others, 2010; Golonka, 2004).

Oblique closure of the Southern Neotethys Ocean Branch along Late Cretaceous and middle Eocene to middle-late Miocene continental-arc subduction zones (Neotethys I and Neotethys II of Ghasemi and Talbot, 2006) also occurred diachronously with island-arc accretion in the Late Cretaceous, followed by continental collision in the (1) early Miocene in northwestern Iran, (2) middle Miocene in central Iran (Ghasemi and Talbot, 2006; Kazmin and others, 1986; Saintot and others, 2006), and (3) middle Miocene in southeastern Turkey (Yılmaz, 1993) and southeastern Iran (Berberian and Berberian, 1981). The remaining segments of the Southern Neotethys Ocean Branch are presently being subducted under western Turkey in the west and southeastern Iran and Pakistan in the east (Şengör, 1987). As a consequence, Eocene and Miocene to recent south-vergent folding and thrusting that deformed the Pontide Arc (Popovic, 1975) were not only a result of the closing of Northern Neotethys Ocean Branch but also of the closing of both the Northern and Southern Neotethys Ocean Branches across Turkey, the Lesser Caucasus, and northern Iran (Mosar and others, 2010).

From west to east, variations in the tectonic setting occur across the Pontide (Asia) porphyry tract. The segment of the Pontide Arc in northwestern Turkey is dominated by fore-arc and superimposed back-arc rock associations; the segment of the Pontide Arc in northeastern Turkey and southern Georgia includes mainly arc and back-arc rock associations, whereas the segment of the Pontide Arc in the Lesser Caucasus is dominated by back-arc rock associations. In the Alborz of northern Iran, the Pontide Arc is deeply exhumed. Accordingly, the nature of Late Cretaceous to middle-late Eocene magmatism and associated porphyry mineralization also varies across these distinct tectonic environments. Therefore, the tract is separated here into distinct sub-tracts (Pontide (Asia)–NW Turkey, Pontide (Asia)–NE Turkey, and Pontide (Asia)–Caucasus-Iran). These sub-tracts are described below and are assessed individually.

Pontide (Asia)–NW Turkey Sub-tract (142pCu9004a)

Descriptive model: General porphyry copper (Cox, 1986a; Berger and others, 2008; John and others, 2010)

Grade and tonnage model: General Cu-Au-Mo porphyry copper model (Singer and others, 2008)

Geologic feature assessed: Late Cretaceous to late Eocene fore-arc, back-arc, and postcollisional magmatism of the Tethyan Eurasian Metallogenic Belt

Magmatism

Across northwestern and north-central Turkey, the Pontide (Asia)–NW Turkey sub-tract delimits a fore-arc and superimposed back-arc segment of the Pontide Arc. The sub-tract covers an area of 32,700 km² (fig. 19). In this region, the Pontide Arc is largely

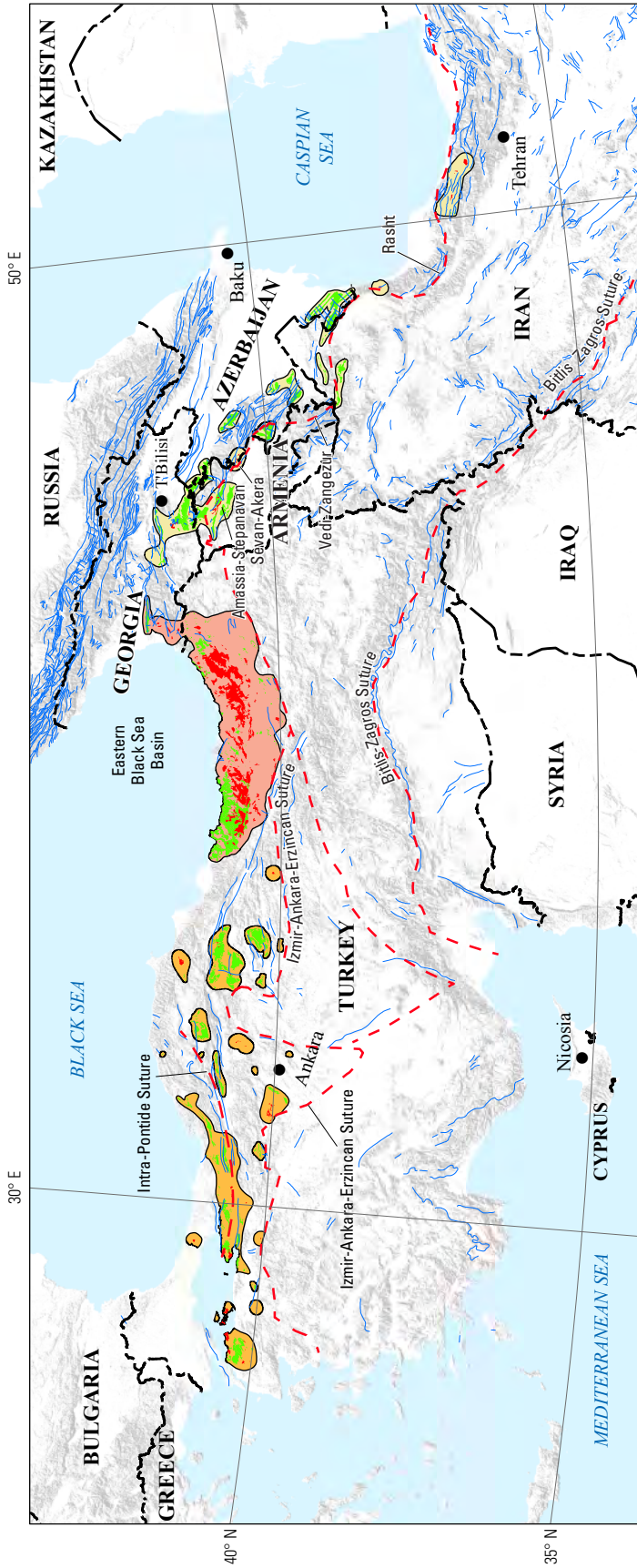
contained within a stack of thrust sheets of Late Cretaceous-early Eocene age preserved along and north of the Izmir-Ankara-Erzincan Suture (Rice and others, 2006). Permissive igneous units (appendix B) used to define Pontide (Asia)–NW Turkey sub-tract are shown in figure 20, along with locations of igneous complexes and other geologic features mentioned in this section.

In the Istanbul and Sakarya Terranes of northwestern Turkey (fig. 3), late Lower Cretaceous (Aptian-Cenomanian) shallow marine clastic rocks of a broad marginal back-arc rift basin that separated terranes of Gondwanan affinity from Eurasia are superseded by a thick sequence of Late Cretaceous (Robinson and others, 1995; Okay and Şahintürk, 1997) volcanic and volcano-sedimentary rocks that mark the onset of Pontide Arc magmatism. These rocks are represented by Upper Cretaceous (Santonian-Campanian) interlayered sedimentary and calc-alkaline andesitic to rhyolitic volcanic rocks that were deposited in a fore-arc environment (Şengör and Yılmaz, 1981). The axis of the arc lies to the north and is presently submerged under the Black Sea. Associated Late Cretaceous intrusive rocks cut the volcanic and sedimentary rock succession, show geochemical signatures that are consistent with a subduction-related origin, and commonly exhibit high-temperature metamorphic aureoles (Delaloye and Bingöl, 2000; Tüysüz and others, 1995). Late Cretaceous units are overlain by late Upper Cretaceous (Campanian) to Paleocene pelagic limestones and early Eocene turbidites, which are in turn unconformably capped by a middle Eocene volcano-sedimentary succession that is preserved along narrow belts about the Intra-Pontides and the Izmir-Ankara-Erzincan Sutures (Keskin and others, 2008). The middle Eocene sequence that consists of shallow marine to subaerial sedimentary rocks at the base and subaerial volcanic units towards the top is intruded by late Eocene plutons. Associated lavas span the whole compositional range from basalts to rhyolites and display subduction-related calc-alkaline character except at the top of the section, where extension-related mildly alkaline to alkaline compositions do occur.

The Paleocene to middle Eocene depositional environment coupled with progressive calc-alkaline to alkaline compositional evolution of igneous rocks indicate southward propagation of an evolving back arc over the arc axis (Manetti and others, 1983, 1988). Early Eocene uplift related to collision with the Anatolide-Tauride Terrane to the south resulted in termination of subduction-related arc magmatism. Thus, the occurrence of younger late Eocene granitoids indicates that magmatism continued into the postcollisional extensional setting that followed.

Known Porphyry Deposits and Prospects

With exception of the Late Cretaceous Derekoy and İkiztepeliler porphyry Cu-Mo deposits in the European part of Turkey (Sutphin and others, 2013) and the middle Eocene Bakırçay porphyry deposit in north-central Turkey, few porphyry copper occurrences related to the Pontide volcano-plutonic event have been identified across northwestern Turkey. The only economically significant copper mineralization identified in the region is associated with VMS deposits hosted by older Early Jurassic ophiolite complexes (Yigit, 2006, 2009).



Base from SRTM Global Digital Elevation Model, U.S. Geological Survey EROS Data Center, 2006. Political boundaries from U.S. Department of State (2009). Asia North Albers Equal-Area Conic Projection. Central meridian, 36° E, latitude of origin, 35° N.

0 100 200 300 400 KILOMETERS
0 100 200 MILES

EXPLANATION

Porphyry copper

Assessed porphyry copper tract 142pCu9004

- Sub-tract 142pCu9004a
- Sub-tract 142pCu9004b
- Sub-tract 142pCu9004c

- Permissive intrusive rock
- Permissive extrusive rock

- Fault
- Suture

Rasht **Geologic feature discussed in the text**

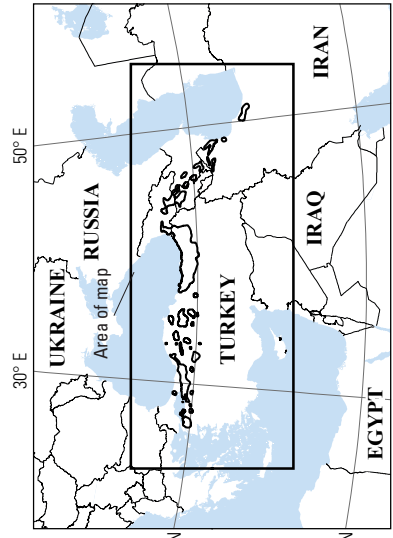


Figure 20. Map showing the distribution of permissive intrusive and extrusive rocks used to define tract 142pCu9004, Pontide (Asia)—Armenia, Azerbaijan, Georgia, Iran, and Turkey. Sub-tracts: 142pCu9004a, Pontide (Asia)—NW Turkey, Turkey; 142pCu9004b, Pontide (Asia)—NE Turkey, Georgia and Turkey; 142pCu9004c, Pontide (Asia)—Caucasus-Iran, Armenia, Azerbaijan, and Iran. See appendix A for principal sources of information and appendix B for source map units.

The Pontide (Asia)–NW Turkey sub-tract (fig. 19) includes one known porphyry copper deposit (Bakırçay; table 2) and four porphyry prospects (appendix C). One porphyry prospect is associated with Bakırçay in north-central Turkey, and the other three are located in the western part of the sub-tract (Dikmen, Karabiga Bakırtepe, and Katirli). Like the Bakırçay deposit, the Dikmen and Katirli porphyry prospects exhibit gold-bearing Cu–Mo metal associations, whereas the Karabiga Bakırtepe prospect is better characterized as a Cu–Au porphyry system. Another possible Cu–Mo quartz diorite porphyry prospect of probable early Eocene age occurs at Camyurt in the northern Biga Peninsula (Yigit, 2012).

Bakırçay Porphyry Deposit

The Bakırçay Cu–Au–Mo porphyry–skarn deposit was one of the first porphyry copper systems described in Turkey (Taylor, 1978, 1981). The deposit has reported resources of 200 Mt at 0.2 percent copper+molybdenum equivalent (Singer and others, 2008; Yigit, 2009). Northeast-trending copper–molybdenum mineralization is associated with middle Eocene granodiorite and dacite porphyry intrusions and associated Cu–Pb–Zn–Mo–W skarn emplaced into Paleozoic and Mesozoic marble and metaquartzite hosts (Yigit, 2009; Taylor, 1981). The granodiorite porphyry intrusion covers an area of 4.5 km by 0.6 km. A central zone of biotite, quartz, magnetite, K-feldspar, chalcocopyrite-(bornite), and molybdenite is overprinted by peripheral propylitic alteration associations including chlorite-epidote-calcite, and lesser structurally controlled quartz-sericite-pyrite, suggesting that the deep root zone of a porphyry system is exposed there (Taylor and Fryer, 1980; Soyulu, 1999). The age constraints available for porphyry emplacement and mineralization at Bakırçay (44.3–40.3 Ma and 38.6–37.4 Ma K–Ar dates on primary and secondary biotite, respectively; Taylor, 1981) suggest that this deposit was emplaced during or shortly after the early Eocene collision between the eastern Anatolide–Tauride and Pontide–Sakarya Terranes (and certainly after the Late Cretaceous collision of the Central Anatolian Crystalline Complex adjacent to the south).

Dikmen Porphyry Prospect

The Dikmen Mo–Cu–Au-bearing porphyry–skarn prospect was discovered by a joint venture between MTA and Mining Metal Agency of Japan (MMAJ) in 1988–91 (Yigit, 2012). It is associated with quartz–feldspar porphyry, granodiorite and aplitic dikes of early Eocene age that intruded metasedimentary and metavolcanic rocks of Triassic age. At Dikmen, a 3-km long and as much as 0.5-km wide alteration zone occurs along a northeast structural trend. Quartz-sericite-pyrite and kaolinite-dickite alteration host stockworks and sheeted veins with molybdenite, chalcocopyrite, and supergene copper minerals including brochantite (Yigit, 2009). Preliminary geochemical sampling indicates highly anomalous gold, molybdenum, zinc, lead, and copper contents (Yigit, 2012).

Preservation Level

As derived from the 1:500,000-scale geologic map of Turkey (General Directorate of Mineral Research and Exploration, 2000), 24 percent of the sub-tract area is underlain by older basement, of which about half consists of deeply exhumed metamorphic rocks. The proportions of Late Cretaceous to middle-late Eocene permissive (plutonic and volcanic) and nonpermissive (mafic, sedimentary, and volcano-sedimentary) units are 17 and 23 percent of the sub-tract area, respectively, whereas younger rocks and inland water bodies cover the remaining 35 percent of the sub-tract area (fig. 20). A high permissive volcanic-to-plutonic ratio ($\{\text{volcanic}/[\text{volcanic}+\text{plutonic}]\} \times 100=92$) across the sub-tract further suggests that the level of preservation of porphyry systems is in general too shallow for exposure, and (or) that they may also be buried under younger cover across large sections of the sub-tract.

Magnetic Anomalies

Regional aeromagnetic maps (Ates and others, 1999; Maus and others, 2009) were used to confirm the location and character of regional geologic features (for example, arcs, basins, faults, terrane boundaries). A prominent positive magnetic anomaly forms a ribbon-shaped area along northern Turkey. The magnetic anomaly occurs on land in the Eastern Pontide Arc segment, but it lies almost entirely offshore across northwestern Turkey. The latter likely images the Pontide Arc axis that is now largely submerged under the Black Sea. In the European part of the Pontide Arc, the magnetic anomaly continues in the area of the Strandja Terrane (fig. 3), which hosts several porphyry copper deposits—for example, Derekoç and İkiztepe (Sutphin and others, 2013). Isolated but prominent magnetic highs that may be partially associated with the Pontide fore arc occur in the westernmost part of the Sakarya Terrane (Biga Peninsula) and in the central parts of the Istanbul and Sakarya Terranes. However, these highs may be an indication of older metamorphic basement, ultramafic units, or younger volcano-plutonic rocks. The Bakırçay porphyry deposit occurs on the northern margin of an isolated east-west trending magnetic anomaly.

Probabilistic Assessment

Grade and Tonnage Model Selection

Available resource data for the only known deposit in the Pontide (Asia)–NW Turkey sub-tract were insufficient to allow classification into Cu–Mo or Cu–Au porphyry subtype category based on the criteria for gold and molybdenum contents that were used in this assessment. Notwithstanding that gold is reported to occur in 4 of the 5 porphyry occurrences in this sub-tract, the dominance of a copper–molybdenum metal association is apparent. Pooled *t*-test results assuming equal variances show that the tonnage and copper grade of the only known deposit in the sub-tract are not significantly different at the 1-percent level from tonnages and grades in the general porphyry Cu–Au–Mo model of Singer and others (2008). Therefore, the general model was used to estimate undiscovered copper, gold, molybdenum, and silver

resources in this sub-tract. In comparison to the median tonnage and grade in the general porphyry Cu-Au-Mo model, Bakırçay exhibits comparable size but lower copper grade.

Estimates of Undiscovered Deposits and Rationale

Favorable geologic factors for the occurrence of undiscovered porphyry copper deposits in the Pontide (Asia)–NW Turkey sub-tract include (1) a fore-arc and prominent superimposed back-arc environment related to a large and long-lived island to mature continental arc segment partially built on thick cratonic crust, (2) permissive calc-alkaline arc and alkaline back-arc and postcollisional magmatic rocks, (3) known Cu porphyry deposits (for example, Bakırçay), and (4) favorable environment for development of supergene enrichment. Unfavorable geologic factors include (1) overall high volcanic-to-plutonic ratios that suggest that levels of preservation for porphyry systems may not be appropriate and (2) complex fold-and-thrust events, where deposits can be exhumed, tectonically concealed, or buried under younger cover.

The density of known porphyry deposits in the Pontide (Asia)–NW Turkey sub-tract is low compared to densities in well-explored tracts of this size around the world. This suggests that undiscovered deposits are likely present. However, the low number of known porphyry occurrences may not only reflect the limited extent of exploration that the region has experienced (Yigit, 2009) but also the degree of efficiency of ore-forming processes and (or) the level of preservation of porphyry systems.

In combination, these factors (for example, tectonic setting, level of exposure, extent of cover, exploration) led the assessment team to establish that the Pontide (Asia)–NW Turkey sub-tract exhibited relatively low geologic favorability and that high levels of uncertainty in the estimation of undiscovered porphyry deposits were expected. Nevertheless, the tract would contribute significant copper resources from undiscovered deposits to the overall assessment. Therefore, quantitative assessment of undiscovered deposits in this tract was warranted. Estimates for undiscovered porphyry copper deposits in the Pontide (Asia)–NW Turkey sub-tract at the 90-, 50-, and 10-percent probability levels and the associated summary statistics are listed in table 5a–A.²⁰ The team reached a consensus estimate of 0, 1, and 2 undiscovered deposits for the 90-, 50-, and 10-percent probability levels, respectively, which resulted in a mean of 1.15 undiscovered deposits with a standard deviation of 1.18 ($C_v\%=102$). This result reflects the limited favorability and high uncertainty assessed for this porphyry copper sub-tract.

Probabilistic Assessment Simulation Results

Simulation results for estimated copper, molybdenum, gold, silver, and the total volume of mineralized rock are summarized in table 5a–B. The mean estimate of undiscovered copper resources

in the Pontide (Asia)–NW Turkey porphyry sub-tract is 4.1 Mt. Results of the Monte Carlo simulation are also presented as cumulative frequency plots (fig. 21). The cumulative frequency plots show the cumulative probabilities of occurrence-estimated resources and total mineralized rock, as well as the mean for each commodity and for total mineralized rock.

Pontide (Asia)–NE Turkey Sub-tract (142pCu9004b)

Descriptive model: General porphyry copper (Cox, 1986a; Berger and others, 2008; John and others, 2010)

Grade and tonnage model: General Cu-Au-Mo porphyry copper model (Singer and others, 2008)

Geologic feature assessed: Late Cretaceous to late Eocene island to continental arc, back-arc, and postcollisional magmatism of the Tethyan Eurasian Metallogenic Belt

Magmatism

Across northeastern Turkey and southwestern Georgia, the Pontide (Asia)–NE Turkey sub-tract delimits an arc- and back-arc-dominated segment of the Pontide Arc. The sub-tract covers an area of 45,500 km² (fig. 19). Permissive igneous units (appendix B) used to define the Pontide (Asia)–NE Turkey sub-tract are shown in figure 20, along with locations of igneous complexes and other geologic features mentioned in this section. This segment of the Pontide Arc is preserved in thrust sheets containing units of Late Cretaceous to early Eocene age that can be restored as (1) a subduction-accretion complex and fore arc, (2) an arc, and (3) a back arc about and north of the Izmir-Ankara-Erzincan Suture (Rice and others, 2006).

In the amalgamated Eastern Pontides and Sakarya terranes of northeastern Turkey (fig. 3), older and Late Jurassic to Early Cretaceous variably metamorphosed subduction-related plutonic, volcanic, and volcanoclastic units (Ustaömer and Robertson, 2010; Yılmaz and Boztuğ, 1986) form the basement on which the early Late Cretaceous (Turonian) to Paleocene eastern segment of the Pontide Arc was built. In this region, the Pontide Arc is represented by a tholeiitic to alkaline island-arc environment preserved along the structurally imbricated Izmir-Ankara-Erzincan Suture (Koçyiğit and others, 1988) and an associated calc-alkaline continental arc (Tüysüz and others, 1995) on the Eastern Pontides-Sakarya Terrane to the north (Yılmaz, 1993; Yılmaz and others, 2001). The southern margin of the arc along the Izmir-Ankara-Erzincan Suture (figs. 3, 20) is composed of Late Cretaceous flysch and limestone intercalations representing the fore-arc setting, whereas the central and northern margins of the Pontide Arc consist of a greater than 2-km-thick submarine succession of Late Cretaceous to Paleocene high-K calc-alkaline mafic to felsic intrusive, volcanic, and volcano-sedimentary rocks deposited mostly in a back-arc setting (Bektaş and others, 1995; Yılmaz and Korkmaz, 1999; Çamur and others, 1996).

A large composite batholithic mass occupies the arc axis (Yılmaz-Şahin and others, 2004). It consists of Paleozoic intrusions cut by Late Cretaceous and Paleocene plutons that exhibit typical calc-alkaline to high-K calc-alkaline granodioritic

²⁰Note that for tables in this report where numbers are followed by lowercase letters (for example, table 5a), numbers group tracts (for example, Pontide (Asia)) and letters correspond to the letter at the end of sub-tract designations (for example, 142pCu9004b).

Table 5. Probabilistic assessment for tract 142pCu9004, Pontide (Asia)—Armenia, Azerbaijan, Georgia, Iran, and Turkey.

[Coded_ID, a unique number assigned to each permissive tract in the spatial data (appendix D)]

Sub-tract name	Coded_ID	Countries
Pontide (Asia)—NW Turkey	142pCu9004a	Turkey
Pontide (Asia)—NE Turkey	142pCu9004b	Georgia and Turkey
Pontide (Asia)—Caucasus-Iran	142pCu9004c	Armenia, Azerbaijan, Georgia, and Iran

Table 5a. Probabilistic assessment for sub-tract 142pCu9004a, Pontide (Asia)—NW Turkey sub-tract, Turkey.

A. Undiscovered deposit estimates, deposit numbers, tract area, and deposit density.

[N_{xx} , estimated number of deposits associated with the xxth percentile; N_{und} , expected number of undiscovered deposits; s , standard deviation; $C_v\%$, coefficient of variance; N_{known} , number of known deposits in the tract that are included in the grade and tonnage model; N_{total} , total of expected number of deposits plus known deposits; tract area, area of permissive tract in square kilometers (km²); deposit density reported as the total number of deposits per 100,000 km². N_{und} , s , and $C_v\%$ are calculated using a regression equation (Singer and Menzie, 2005)]

Consensus undiscovered deposit estimates					Summary statistics					Tract area (km ²)	Deposit density ($N_{total}/100,000$ km ²)
N_{90}	N_{50}	N_{10}	N_{05}	N_{01}	N_{und}	s	$C_v\%$	N_{known}	N_{total}		
0	1	2	4	4	1.2	1.2	100	1	2.2	32,700	7

B. Results of Monte Carlo simulations of undiscovered resources.

[Cu, copper; Mo, molybdenum; Au, gold; and Ag, silver; in metric tons; Rock, in million metric tons]

Material	Probability of at least the indicated amount						Probability of	
	0.95	0.9	0.5	0.1	0.05	Mean	Mean or greater	None
Cu	0	0	840,000	8,900,000	17,000,000	4,100,000	0.23	0.29
Mo	0	0	0	230,000	460,000	110,000	0.17	0.53
Au	0	0	4	260	510	100	0.22	0.48
Ag	0	0	0	2,600	5,200	1,400	0.16	0.62
Rock	0	0	200	1,900	3,500	830	0.24	0.29

Table 5b. Probabilistic assessment for sub-tract 142pCu9004b, Pontide (Asia)—NE Turkey sub-tract, Georgia and Turkey.

A. Undiscovered deposit estimates, deposit numbers, tract area, and deposit density.

[N_{xx} , estimated number of deposits associated with the xxth percentile; N_{und} , expected number of undiscovered deposits; s , standard deviation; $C_v\%$, coefficient of variance; N_{known} , number of known deposits in the tract that are included in the grade and tonnage model; N_{total} , total of expected number of deposits plus known deposits; tract area, area of permissive tract in square kilometers (km²); deposit density reported as the total number of deposits per 100,000 km². N_{und} , s , and $C_v\%$ are calculated using a regression equation (Singer and Menzie, 2005)]

Consensus undiscovered deposit estimates					Summary statistics					Tract area (km ²)	Deposit density ($N_{total}/100,000$ km ²)
N_{90}	N_{50}	N_{10}	N_{05}	N_{01}	N_{und}	s	$C_v\%$	N_{known}	N_{total}		
1	3	9	9	9	4.1	3.0	73	4	8.1	45,500	18

B. Results of Monte Carlo simulations of undiscovered resources.

[Cu, copper; Mo, molybdenum; Au, gold; and Ag, silver; in metric tons; Rock, in million metric tons]

Material	Probability of at least the indicated amount						Probability of	
	0.95	0.9	0.5	0.1	0.05	Mean	Mean or greater	None
Cu	0	260,000	7,100,000	37,000,000	57,000,000	15,000,000	0.30	0.07
Mo	0	0	120,000	1,100,000	1,800,000	420,000	0.25	0.19
Au	0	0	160	990	1,500	390	0.29	0.16
Ag	0	0	1,200	12,000	22,000	5,100	0.24	0.26
Rock	0	64	1,600	7,400	12,000	3,100	0.32	0.07

Table 5c. Probabilistic assessment for sub-tract 142pCu9004c, Pontide (Asia)—Caucasus-Iran sub-tract, Armenia, Azerbaijan, Georgia, and Iran.

A. Undiscovered deposit estimates, deposit numbers, tract area, and deposit density.

[N_{xx} , estimated number of deposits associated with the xxth percentile; N_{und} , expected number of undiscovered deposits; s , standard deviation; $C_v\%$, coefficient of variance; N_{known} , number of known deposits in the tract that are included in the grade and tonnage model; N_{total} , total of expected number of deposits plus known deposits; tract area, area of permissive tract in square kilometers (km²); deposit density reported as the total number of deposits per 100,000 km². N_{und} , s , and $C_v\%$ are calculated using a regression equation (Singer and Menzie, 2005)]

Consensus undiscovered deposit estimates					Summary statistics					Tract area (km ²)	Deposit density ($N_{total}/100,000$ km ²)
N_{90}	N_{50}	N_{10}	N_{05}	N_{01}	N_{und}	s	$C_v\%$	N_{known}	N_{total}		
0	1	1	3	3	0.85	0.80	94	0	0.85	24,300	3

B. Results of Monte Carlo simulations of undiscovered resources.

[Cu, copper; Mo, molybdenum; Au, gold; and Ag, silver; in metric tons; Rock, in million metric tons]

Material	Probability of at least the indicated amount						Probability of	
	0.95	0.9	0.5	0.1	0.05	Mean	Mean or greater	None
Cu	0	0	470,000	7,000,000	13,000,000	3,300,000	0.20	0.31
Mo	0	0	0	170,000	390,000	91,000	0.15	0.59
Au	0	0	0	190	380	86	0.18	0.55
Ag	0	0	0	1,800	4,200	1,200	0.14	0.69
Rock	0	0	120	1,500	2,700	670	0.21	0.31

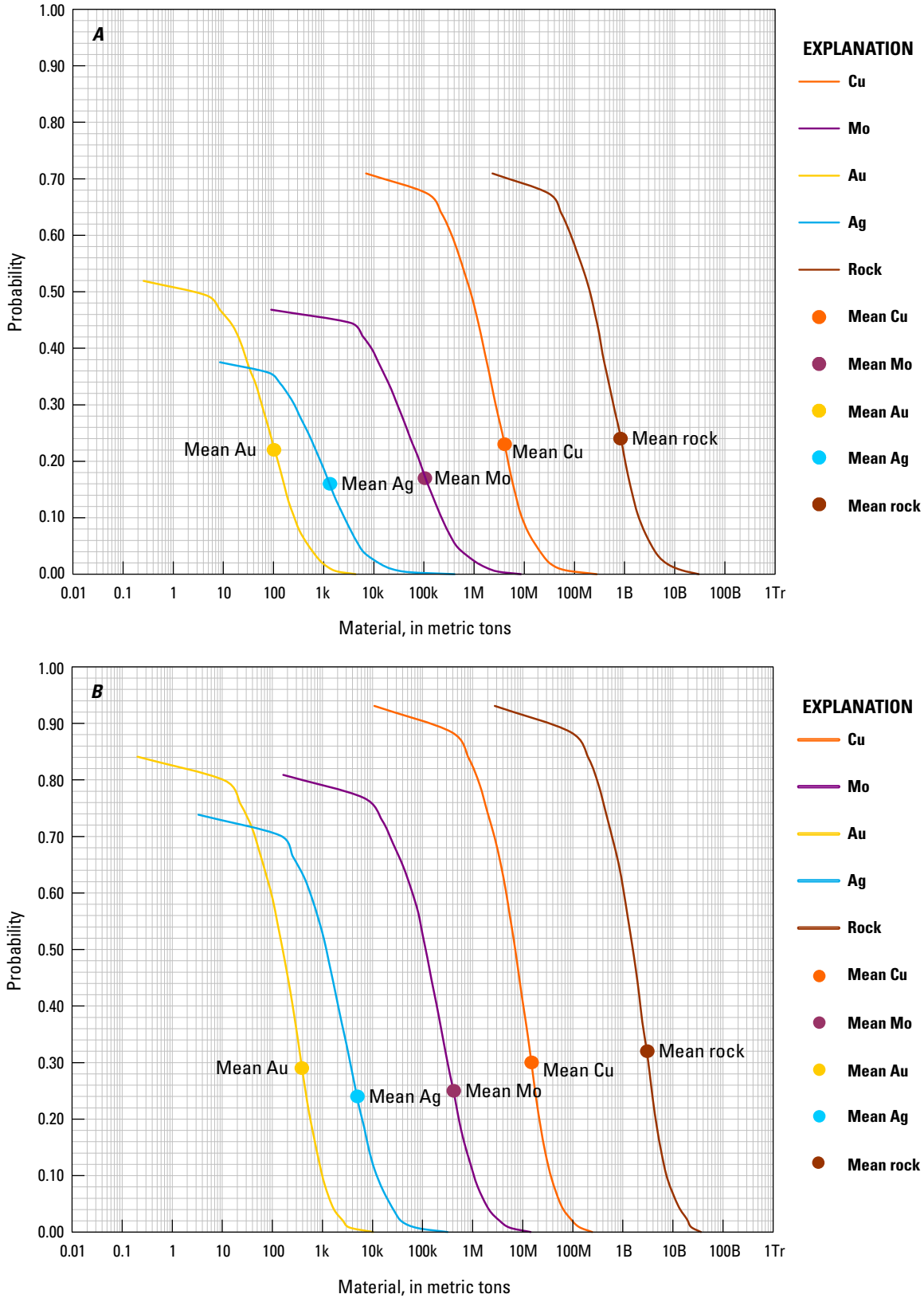


Figure 21. Cumulative frequency plots showing the results of Monte Carlo computer simulation of undiscovered resources in porphyry copper deposits in tract 142pCu9004, Pontide (Asia)—Armenia, Azerbaijan, Georgia, Iran, and Turkey. *A*, Sub-tract 142pCu9004a, Pontide (Asia)—NW Turkey, Turkey. *B*, Sub-tract 142pCu9004b, Pontide (Asia)—NE Turkey, Georgia and Turkey. *C*, Sub-tract 142pCu9004c, Pontide (Asia)—Caucasus-Iran, Armenia, Azerbaijan, Georgia, and Iran. k, thousand; M, million; B, billion; Tr, trillion.

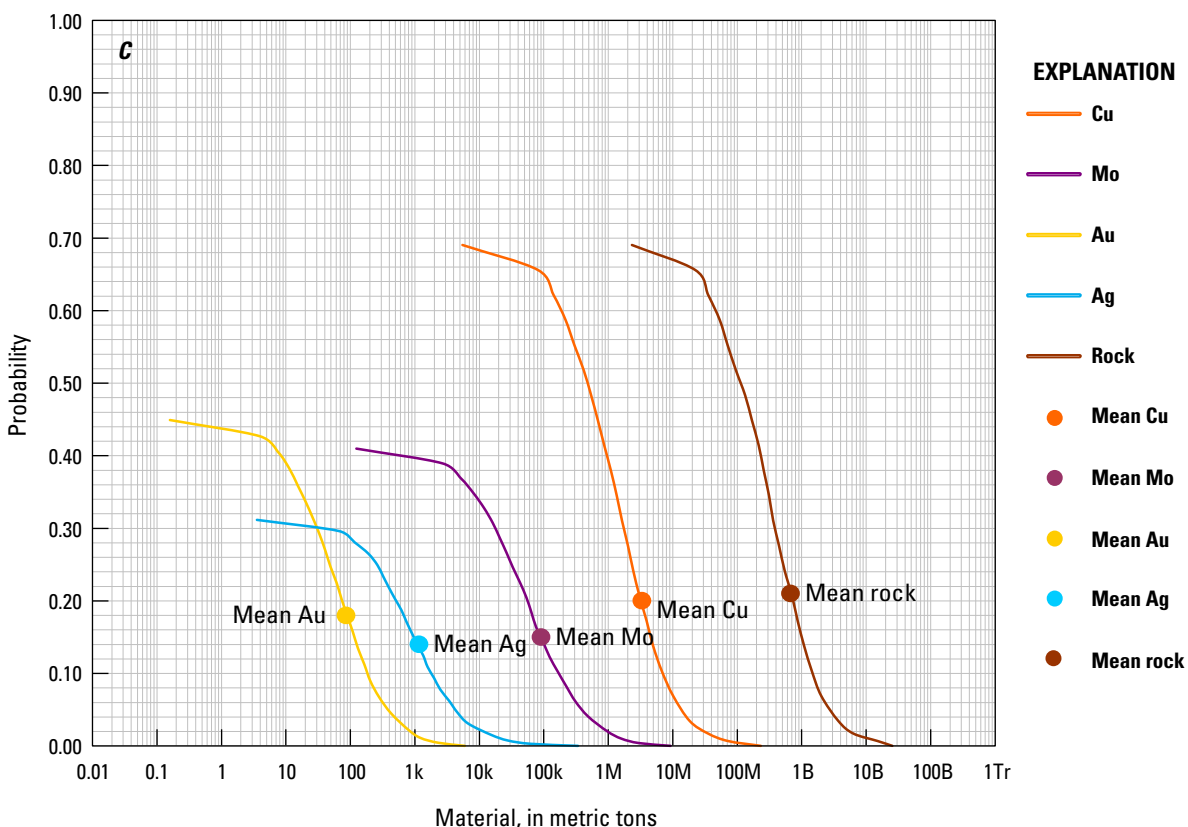


Figure 21.—Continued

to granitic compositions. These plutons include shallow-seated porphyritic stocks, and locally are also intruded by Paleocene highly fractionated peraluminous leucogranites (Boztuğ and others, 2006; Yılmaz-Şahin, 2005).

After deformation and uplift related to the late Paleocene-early Eocene island-arc accretion and collisional event between the eastern Anatolide-Tauride and the Eastern Pontides-Sakarya terranes, middle Eocene volcanic rocks were deposited unconformably on older folded and thrust-faulted volcanic units. In the northern part of the belt, middle Eocene volcanic rocks are dominated by alkaline compositions, and associated plutons exhibit A-type monzonite, quartz monzonite, monzodiorite, and quartz monzodiorite compositions consistent with emplacement in a postcollisional extensional regime. In the southern part of the belt, however, middle Eocene volcanic rocks are calc-alkaline, and coeval stocks retain I-type monzogranite and granodiorite compositions (Şen and others, 1998; Arslan and Aslan, 2006).

In contrast to Late Cretaceous-Paleocene calc-alkaline to high-K calc-alkaline granitoids, middle Eocene dioritic, and monzodioritic to syenitic stocks (including porphyry intrusions) exhibit high-K calc-alkaline to alkaline compositions and trace-element contents that are consistent with emplacement in an extensional setting (Boztuğ and others, 2004, 2006) in thickened crust (Arslan and Aliyazicioglu, 2001). This postcollisional extensional regime is believed to have been associated with the ongoing opening of the Eastern Black Sea Basin to the north (Görür, 1988; Okay and others, 1994), but it was also likely influenced by the intraoceanic extensional environment that had

been active since the Late Cretaceous in the Anatolide-Tauride Terrane to the south (Yılmaz and others, 1997a).

In contrast with northwestern Turkey, the Pontide arc axis in northeastern Turkey is located on land. However, as in northwestern Turkey, back-arc volcanism is believed to have propagated southwards across the arc axis over time (Yılmaz and others, 1997a; Okay and Şahintürk, 1997). Compared with the narrow late Eocene postcollisional volcanic belt preserved in the Western Pontide Arc segment, the middle Eocene postcollisional (Yılmaz Şahin and others, 2004) volcanic belt in the Eastern Pontide Arc segment is much wider (Keskin and others, 2008).

Known Porphyry Deposits and Porphyry-Related Prospects

Mineralization in the Pontide (Asia) tract includes Late Cretaceous Pb-Zn-Cu and copper VMS deposits (Akin, 1978; Moon and others, 2001; Akıncı, 1984; Karakaya and others, 2012; Kekelia and others, 2004) and Late Cretaceous-Paleocene and middle Eocene Cu-Mo porphyry, Cu-Pb-Zn skarn (Kuşçu, 2005), and Au-Ag epithermal systems (Akçay and Moon, 2004; Moon and others, 2001; Yigit, 2009; Kekelia and others, 2001; Boztuğ and others, 2003; Engin and others, 2000; Kirkham and Dunne, 2000).

In the Pontide (Asia)-NE Turkey sub-tract, VMS and porphyry deposits occur in a back-arc tectonic environment that is permissive for both (Yigit, 2009). A genetic relation between these two deposit types is not implied here, but it has been proposed

(Kekelia and others, 2004). However, depending on the level of preservation, only the more eroded windows expose the more deeply emplaced porphyry systems. Furthermore, the postmineral deformational history tectonically juxtaposed these two shallow and deeper hypabyssal ore-forming environments. This is evident not only in northeastern Turkey but in the Lesser Caucasus (see Cimmeride–Lesser Caucasus tract above and Pontide (Asia)–Caucasus-Iran sub-tract below).

The Pontide (Asia)–NE Turkey sub-tract contains four known porphyry copper deposits (table 2). These are the Balcili-Yüksekoba, Gümüşhane, Güzelyayla, and Ulutaş deposits. Available age constraints at Balcili-Yüksekoba, Güzelyayla, Ulutaş, and Gümüşhane suggest that all four porphyry deposits formed in the arc (or the superimposed back-arc) setting that prevailed before the early Eocene collision between the Pontide-Sakarya and Anatolide-Tauride terranes in this region. These deposits are small and low in copper grade, but Balcili-Yüksekoba, Gümüşhane, and Ulutaş are reported to contain gold (Yigit, 2006, 2009).

Thirty-nine porphyry prospects were identified and are included in the Pontide (Asia)–NE Turkey sub-tract (appendix C, fig. 19). With the exception of the Namonastevi porphyry prospect that occurs in Georgia, the remaining 38 prospects are located in northeastern Turkey. Overall, a Cu-Mo±(Au) metal association is apparent in 18, and a Cu-Au association characterizes another 5. Four of these 5 porphyry prospects are typified by the presence of acid-sulfate alteration and mineralization. Despite relatively extensive exploration in northeastern Turkey, no sizeable porphyry systems have been identified to date. However, current exploration efforts at the acid sulfate Berta and Sisorta prospects, may result in the identification of economically significant porphyry copper mineralization (Nuinsco Resources, Ltd., 2013; Vigar and others, 2009).

Balcili-Yüksekoba Porphyry Deposit

The early Paleocene (62.3 Ma; Soyly, 1999) Balcili-Yüksekoba Cu-Mo porphyry deposit has reported resources of 140 Mt at 0.2 percent copper, or 145 Mt at 0.25 percent Cu+Mo equivalent (Yigit, 2009). The deposit consists of two nearby porphyry intrusions at Balcili and Yüksekoba, respectively (Yavuz and others, 1999; Akinci, 2004; Dumanlilar and others, 1999; Engin and others, 2000; Soyly, 1999). At the Yüksekoba Cu-Mo-(Au) porphyry system, three synmineral granodiorite porphyry and a postmineral feldspar porphyry and pebble dike intrude a granodiorite pluton emplaced in felsic pyroclastic units. A central K-silicate alteration zone is surrounded by intense quartz sericite and weak argillic alteration mineral associations. Chalcopyrite and molybdenite are mostly associated with the quartz-sericite zone. A jarositic leached cap developed over this pyrite-rich alteration zone (Soyly, 1999).

At the Balcili porphyry system, a northeast-trending granodiorite pluton that can be correlated with the one at Yüksekoba is intruded by porphyritic (tonalite)-granodiorite and by unmineralized pebble dikes (Yigit, 2009). Mineralization is controlled by stockworks and breccias and K-silicate alteration.

Balcili is believed to represent the roots of a porphyry system (Yigit, 2009; Soyly, 1999).

Güzelyayla Porphyry Deposit

The 59-Ma (Singer and others, 2008) or 72-Ma (Richard Herrington, written commun., 2005) Güzelyayla Cu-Mo porphyry-skarn deposit has a resource of 186 Mt at 0.3 percent Cu+Mo equivalent (Yigit, 2009). The deposit is centered on late Paleocene premineral granodiorite and synmineral dacite porphyry intrusions emplaced in Jurassic volcanic and Jurassic-Cretaceous carbonate rocks. Jurassic-Cretaceous country rocks are unconformably overlain by Late Cretaceous volcanic and volcano-sedimentary units (Soyly, 1999). Copper-molybdenum mineralization is related to K-silicate and quartz-sericite, weakly developed argillic alteration, and calc-silicate alteration (Akinci, 2004; Moon and others, 2001). The oxidation zone is shallow, reaching only a 10–30-m depth (Yigit, 2009). However, the oxidation zone is followed at depth by an enriched zone (Akinci, 2004) with copper grades as high as 0.8 percent (Soyly, 1999).

Ulutaş Porphyry Deposit

The Ulutaş Cu-Mo porphyry deposit has reported resources of 74 Mt at 0.31 percent copper and 0.022 percent molybdenum (Yigit, 2009), or 140 Mt at 0.27 percent copper and 0.018 percent molybdenum (Singer and others, 2008). The deposit is related to late Paleocene (59 Ma; Singer and others, 2008) tonalitic and quartz-monzonitic porphyry intrusions and intrusive breccias emplaced into pre-Jurassic amphibolite-grade basement and Early Cretaceous plutonic and volcano-sedimentary rocks (Taylor, 1978; Soyly, 1999). Hydrothermal alteration occupies a north-northeast-trending zone approximately 3 km long by 1.5 km wide. Potassic and propylitic alteration assemblages are masked by an extensive phyllic overprint (Taylor and Fryer, 1980; Akinci, 2004). Unlike other porphyry deposits in the region, Ulutaş contains a fairly well-developed leached cap (Yigit, 2009).

Gümüşhane Porphyry Deposit

At the Gümüşhane (also known as Ardala; InfoMine, Inc., 2012a) Cu-Mo porphyry deposit and associated Sanlinbaş acid-sulfate gold-silver prospect, historic reported resources were 80 Mt at 0.5 percent Cu+Mo equivalent and 0.2 g/t gold (Soyly, 1999; Singer and others, 2008). The current JORC-compliant indicated and inferred resource estimate at the combined Ardala-Salinbaş project is 26.87 Mt at 1.26 g/t gold and 4.78 g/t silver, including 4.66 Mt at 0.22 percent copper and 18 Mt at 0.0136 percent molybdenum (Ariana Resources PLC, 2013).

At Gümüşhane, a series of nested quartz-diorite to granodiorite intrusions of early Eocene age (52.5 Ma; Singer and others, 2008) are emplaced in an Upper Cretaceous volcano-sedimentary sequence. Exposed parts of the porphyry deposit have dimensions of 600 by 700 m, and ground magnetic data suggest further lateral continuity beneath limestone units. The porphyry intrusion is multistage, consisting of premineralization feldspar and quartz-feldspar porphyry, synmineralization

feldspar-amphibole porphyry, and postmineralization feldspar porphyry intrusions. Porphyry-style mineralization is controlled by a north-northwest-trending fault (Yigit, 2006). Sericitic alteration is dominant, but K-silicate alteration characterized by K-feldspar, biotite, quartz, anhydrite, magnetite and pyrite is also observed (Akçay and Gündüz, 2004). Proximal manganese, lead, zinc, copper, gold, and barium carbonate replacement mineralization developed in places within its periphery. Sulfides in these carbonate replacement zones are dominated by galena, and lesser sphalerite, chalcopyrite, tetrahedrite, and bismuth minerals (Yigit, 2009).

Sisorta Porphyry-Related Prospect

The Sisorta prospect consists of an acid-sulfate system that developed in a porphyry stock and dikes of Late Cretaceous to early Eocene age (Eurasian Minerals, Inc., 2012). The porphyry intrusions cut Late Cretaceous intermediate to basic volcanic and pyroclastic units intruded by a diorite to granodiorite pluton. Advanced argillic and vuggy silica alteration zones are primarily controlled by northeast and northwest structures, which are in turn cut by postmineral graben-bounding normal faults (Chesser Resources, Ltd., 2011b; Vigar and others, 2009).

Drilling results show that gold generally occurs from the surface to depths from 23 to more than 100 m, with intervals ranging from 0.47 g/t to more than 5 g/t gold. In addition, drill holes targeting the deeper parts of the system have intersected porphyry-style alteration and anomalous copper mineralization. Peripheral zinc-lead-silver veins are also present. Current exploration efforts are focused on the gold resource in the lithocap. At a 0.4 g/t gold cutoff, NI 43-101-compliant indicated reserves are estimated to be 3.17 Mt at 0.89 g/t gold. Inferred resources amount to an additional 11.38 Mt at 0.58 g/t gold (Vigar and others, 2009).

Preservation Level

Northeastern Turkey hosts the majority of the known porphyry occurrences in the Pontide (Asia) tract. As derived from the 1:500,000-scale geologic map of Turkey (General Directorate of Mineral Research and Exploration, 2000) and the 1:1,000,000-scale map of Kekelia and others (2001), the area of the Pontide (Asia)-NE Turkey sub-tract (fig. 21) is divided into older basement rocks (23 percent), permissive Late Cretaceous to late Eocene plutonic (14 percent) and volcanic units (10 percent), broadly coeval nonpermissive mafic, sedimentary, and volcano-sedimentary rocks (44 percent), and younger cover (9 percent). This sub-tract exhibits not only the largest exposures of permissive rocks and an appropriate subequal volcanic-to-plutonic proportion ($\{\text{volcanic}/[\text{volcanic}+\text{plutonic}]\} \times 100 = 40$) but also the least amount of cover compared to sub-tracts of the Pontide (Asia) tract to the west and east.

Overall, the Pontide Arc segment delimited by the Pontide (Asia)-NE Turkey sub-tract exhibits levels of crustal preservation that are appropriate for porphyry systems. It also shows an extent of cover that is limited. However, lithologic and (or) tectonic concealment of porphyry systems in this fold-and-thrust belt

cannot be precluded. Furthermore, volcanic-to-plutonic ratios in northeastern Turkey increase from south to north between the arc axis and the back-arc environment. VMS occurrences appear more abundant in the volcanic-dominated and tectonically juxtaposed back-arc environment, indicating exposure of shallow paleodepositional environments that are more appropriate for exposure of this type of mineralization, and less so for more deeply emplaced porphyry copper systems.

Magnetic Anomalies

Regional aeromagnetic maps (Ates and others, 1999; Maus and others, 2009) were used to confirm the location and character of regional geologic features (for example, arcs, basins, faults, terrane boundaries). A prominent positive magnetic anomaly forms a ribbon-shaped area along northeastern Turkey, mainly along the southern margin of the Eastern Pontide Terrane, which hosts most of the known porphyry copper occurrences in the Pontide (Asia)-NE Turkey sub-tract. A number of these porphyry copper occurrences are located along high gradients along the boundaries of magnetic anomalies. Furthermore, the four known porphyry deposits are located within 15 km of the Eastern Pontide-Sakarya Terrane boundary. Unlike the Eastern Pontide Terrane to the north, the Sakarya Terrane is characterized by both magnetic highs and lows. Few porphyry occurrences have been identified in this southern half of the Pontide (Asia)-NE Turkey sub-tract. A parallel positive magnetic ribbon-shaped area also occurs about the ophiolite-bearing Izmir-Ankara-Erzincan Suture.

Probabilistic Assessment

Grade and Tonnage Model Selection

Available resource data for the four known deposits in the Pontide (Asia)-NE Turkey sub-tract were insufficient to allow classification into Cu-Mo or Cu-Au subtype categories based on the criteria for gold and molybdenum content that were used in this assessment. Notwithstanding that gold occurs in a number of deposits and prospects in the sub-tract, the prevalence of a copper-molybdenum metal association is, however, apparent at these deposits, as well as at most porphyry prospects in the tract. In addition, it is difficult to assess how much of the gold occurs with associated skarn or acid-sulfate systems. Out of the 39 prospects of this sub-tract included in the porphyry copper occurrence database (see references therein), gold-bearing acid sulfate systems are described from 4 (Berta, Celtik, Namonastevi, and Sisorta), and a Mo-Cu metal association is reported from another 4 (the Emeksendere, Esenlidere, Kaytangelisobasi, and Koyyerideresi cluster in central-northeastern Turkey). Pooled *t*-test results assuming equal variances show that tonnages and copper and molybdenum grades in the four known deposits in the tract are not significantly different at the 1-percent level from tonnages and grades in the general porphyry Cu-Au-Mo model of Singer and others (2008). Therefore, the general model was used to estimate undiscovered copper, gold, molybdenum, and silver resources in this sub-tract. In comparison to the median tonnage and grade in

the general porphyry Cu-Au-Mo model, deposits in this sub-tract are smaller and generally of lower copper grade. However, Gümüşhane shows higher gold grades and Ulutaş contains higher molybdenum grades than the median deposit in the model.

Estimates of Undiscovered Deposits and Rationale

Favorable geologic factors for the occurrence of undiscovered porphyry copper deposits in Pontide (Asia)–NE Turkey sub-tract include (1) a large and long-lived island-arc to mature continental-arc and prominent back-arc segment partially built on thick cratonic basement, (2) permissive calc-alkaline and alkaline magmatic rocks, (3) known Cu porphyry deposits (for example, Balcili-Yüksekoba, Gümüşhane, Güzelyayla, and Ulutaş), (4) favorable environment for development of supergene enrichment, and (5) synmineral and postmineral uplift, erosion, subsidence, and burial events that resulted in appropriate exposure of porphyry systems in several areas. However, unfavorable factors include (1) below-median contained metal in known porphyry deposits and (2) an otherwise permissive postcollisional environment that does not appear to host many porphyry systems. A possible geologic explanation could be that this otherwise prominent magmatic arc may have overall developed under a fairly neutral stress regime, where subduction-related compressional stresses were compensated by back-arc- and postcollisional-related extensional stresses.

The density of known porphyry deposits in the Pontide (Asia)–NE Turkey sub-tract is low when compared to densities in well-explored tracts of this size around the world. This suggests that undiscovered deposits are likely present. However, deposit density contrasts markedly with the very high number of identified porphyry occurrences, which is in part a reflection of the relatively high levels of exploration that the region has experienced. Given that the levels of exposure for porphyry systems are favorable, other factors (for example, a lack of efficiency in the ore-forming process?) could be responsible for the apparent absence of larger porphyry deposits.

The assessment team determined that the Pontide (Asia)–NE Turkey sub-tract was geologically favorable and that estimates of numbers of undiscovered porphyry copper deposits could be carried out with a low level of uncertainty. The tract would contribute significant copper resources from undiscovered deposits to the overall assessment. Therefore, quantitative assessment of undiscovered deposits in this tract was completed. Estimates for undiscovered porphyry copper deposits in the Pontide (Asia)–NE Turkey sub-tract at the 90-, 50-, and 10-percent probability levels and the associated summary statistics are listed in table 5b–A. The team reached a consensus estimate of 1, 3, and 9 undiscovered deposits for the 90-, 50-, and 10-percent probability levels, respectively, which resulted in a mean of 4.13 undiscovered deposits with a standard deviation of 3.02 ($C_v\%=73$). These estimates reflect the team's opinion that the favorable geologic factors outweighed the negative ones and that ongoing exploration will eventually result in the identification of additional copper resources in undiscovered but also incompletely outlined porphyry deposits and (or) prospects in this region.

At least a couple of projects in the advanced exploration stages (for example, Ardala, Sisorta) will likely result in development. The estimated total deposit density per 100,000 km² obtained is comparable to median porphyry deposit densities expected in well-explored tracts of equivalent size elsewhere around the world (Singer and Menzie, 2010).

Probabilistic Assessment Simulation Results

Simulation results for estimated copper, molybdenum, gold, silver, and the total volume of mineralized rock are summarized in table 5b–B. The mean estimate of undiscovered copper resources in the Pontide (Asia)–NE Turkey porphyry sub-tract is 15 Mt. Results of the Monte Carlo simulation are also presented as cumulative frequency plots (fig. 21). The cumulative frequency plots show the cumulative probabilities of occurrence-estimated resources and total mineralized rock, as well as the mean for each commodity and for total mineralized rock.

Pontide (Asia)–Caucasus-Iran Sub-tract (142pCu9004c)

Descriptive model: General porphyry copper (Cox, 1986a; Berger and others, 2008; John and others, 2010)

Grade and tonnage model: General Cu-Au-Mo porphyry copper model (Singer and others, 2008)

Geologic feature assessed: Late Cretaceous to middle Eocene island to continental arc and back arc of the Tethyan Eurasian Metallogenic Belt

Magmatism

The Pontide (Asia)–Caucasus-Iran sub-tract extends across the Transcaucasus, Talysh, and Alborz Terranes of the Lesser Caucasus and northern Iran, where the sub-tract delimits a back-arc-dominated segment of the Pontide Arc. The sub-tract covers an area of 24,300 km² (fig. 19). In this region, late Early to Late Cretaceous (Aptian-Campanian) shallow marine, rift-related volcano-sedimentary units are overlain by Late Cretaceous to middle Eocene Pontide Arc and back-arc rock successions (Adamia and others, 1977; Kazmin and others, 1986; Khain, 1975; Lordkipanidze and others, 1989) near and to the northeast of the Sevan-Akera and Rasht Sutures (fig. 3; Sosson and others, 2010b). Permissive igneous units (appendix B) used to define the Pontide (Asia)–Caucasus-Iran sub-tract are shown in figure 20, along with locations of igneous complexes and other geologic features mentioned in this section.

The Pontide Arc is well preserved in the fold-and-thrust belt of the Lesser Caucasus. It is represented by a voluminous 3–4-km-thick shallow marine to subaerial arc and back-arc succession of Late Cretaceous calc-alkaline basalts, andesites, dacites, rhyolites, and associated pyroclastics and ignimbrites north of the Sevan-Akera Suture (Adamia and others, 2011) and calc-alkaline to alkaline island-arc volcanic rocks about the Sevan-Akera suture zone. Late Cretaceous arc magmatism was followed by a 2–2.5-km-thick early and middle Eocene back-arc

shallow-marine sedimentary and calc-alkaline to shoshonitic basalt, andesite, dacite, and rhyolite section on both sides of the Sevan-Akera suture zone (Adamia and others, 1977, 2011). Overall, K_2O contents in volcanic rocks increase from south to north toward the Sevan-Akera suture zone. North of the suture, low K_2O contents increase to the northeast into the back-arc rift setting, where volcanic rocks are characterized by thick successions of mildly alkaline to tholeiitic basalts deposited in a moderately deep sea (Adamia and others, 1981; Kazmin and others, 1986).

In the folded and thrust-faulted Talysh and Alborz Terranes (fig. 3) of northern Iran, a Late Cretaceous to middle Eocene back-arc sequence of lavas and volcanoclastic units of basic composition alternate with shallow-water carbonates and sandstones (Kazmin and others, 1986). Late Cretaceous granodioritic to monzonitic-syenitic intrusions (Berberian and Berberian, 1981; Stöcklin, 1974; Axen and others, 2001) are sparsely exposed along strike-slip faults, where they are deeply eroded as a result of Paleogene and Miocene-Pliocene uplift and exhumation events (Rezaeian, 2008; Axen and others, 2001). Representative intrusions include the 98-Ma Nusha diorite to granite and the 58-Ma Akapol granite. Both intrusions are foliated and exhibit rapakivi texture that suggests emplacement in an extensional setting (Guest and others, 2006; Axen and others, 2001).

Late Cretaceous to middle Eocene Pontide Arc magmatism in the Lesser Caucasus and northern Iran is dominantly represented by voluminous back-arc successions (Shahidi and others, 2007) that developed on the Transcaucasus, Talysh, northern flanks of the Alborz, and South Caspian Sea Terranes (Vincent and others, 2005). This extensional regime prevailed during the shift in magmatism from the northern Neotethys waning subduction zone to the southern Neotethys active subduction zone (Stöcklin, 1968; Dercourt and others, 1986), which produced Late Cretaceous arc magmatism in the Sanandaj-Sirjan Terrane (see Border Folds tract below) and Late Cretaceous to middle Eocene back-arc magmatism in the Central Iranian Terrane, shown on figure 3 (see Esfahan tract below).

Late Cretaceous to middle Eocene magmatism along the northern Neotethys Ocean is unexposed or absent to the east across the central Alborz Terrane, which is instead represented by shallow marine to coastal sedimentary successions. However, Late Cretaceous-Paleogene magmatism reappears again further east in the island-arc setting of the Sabzevar Ocean of northeastern Iran (see Khorasan tract below).

Known Porphyry Prospects

Mineralization in the back-arc-dominated Pontide (Asia)–Caucasus-Iran sub-tract is represented by Late Cretaceous base-metal VMS deposits and prospects (some of which are gold bearing) and Late Cretaceous to middle Eocene iron skarn, as well as intrusion-related gold occurrences (Kekelia and others, 2004; Geological Survey of Iran, 2012e). However, only two porphyry prospects have been positively identified in the northern part of the sub-tract (fig. 19). These are the Mamulo-Sopheli Mo-Cu-(Au)- and Garta Cu-Mo-bearing systems in southern Georgia

(Rundkvist, 2001; Kekelia and others, 2001; Zvezdov and others, 1993; Moon and others, 2001).

Preservation Level

As derived from the 1:1,000,000-scale geologic maps of the Caucasus (Kekelia and others, 2001) and Iran (Huber, 1978), permissive units in the Pontide (Asia)–Caucasus-Iran sub-tract exhibit a very high volcanic-to-plutonic ratio ($\{ \text{volcanic} / [\text{volcanic} + \text{plutonic}] \} \times 100 = 95$). Across the sub-tract, older basement rocks underlie 23 percent and permissive volcanic and plutonic units amount, respectively, to 23 and 1 percent of the area (fig. 20). Late Cretaceous to middle Eocene nonpermissive and younger late Eocene to Holocene rocks overlie the remaining 30 and 22 percent of the sub-tract area.

However, when examined in more detail, the relative proportions of permissive plutonic and volcanic rocks in the sub-tract vary significantly from the Caucasus to northern Iran. Shallowly emplaced permissive volcanic units dominate in the Caucasus, whereas deeply exhumed permissive plutonic units dominate in the Alborz Terrane of northern Iran. Thus, data indicate overall levels of preservation for porphyry systems of this age range that are too shallow in the Caucasus and too deep in northern Iran.

Magnetic Anomalies

The regional aeromagnetic map (Maus and others, 2009) was used to confirm the location and character of regional geologic features (for example, arcs, basins, faults, terrane boundaries). In the Lesser Caucasus, a broad northwest-southeast magnetic anomaly occurs to the north and east of the Pontides (Asia)–Caucasus-Iran sub-tract boundary. This magnetic anomaly likely reflects the long-lived Middle Jurassic-Paleogene mafic rock-dominated extensional back-arc rift environment that is buried under thick Neogene deposits. The Mamulo-Sopheli and Garta porphyry prospects are located on the margin of two isolated positive magnetic anomalies. Across the Talysh and western Alborz Terranes of northern Iran, a broad magnetic low (back-arc basin?) contains isolated magnetic highs that may be reflecting permissive Late Cretaceous to middle Eocene igneous units.

ASTER Alteration Data

Processed ASTER data (Mars, 2014) were used to evaluate potential hydrothermal alteration that could be associated with unidentified porphyry systems in the Pontides (Asia)–Caucasus-Iran sub-tract. However, ASTER coverage was available only for a small part of the tract (12 percent) in northern Iran. In this area, five ASTER-derived alteration zones are associated with permissive Late Cretaceous volcanic units, but none are spatially associated with known metallic or industrial mineral occurrences. Moderately developed northeast-striking 2-km-long and 0.5-km-wide ASTER-derived phyllic alteration zones with a very subdued argillic component occur at another two locations. The nature of these seven alteration zones is unknown. If hydrothermal in origin, they could also be related to younger mineralization.

Another broad ASTER-derived alteration zone consists of an argillic-dominated area that is associated with volcano-sedimentary units adjacent to a granodiorite pluton. This alteration zone could be related to the historic copper district at Medjar, where the existence of younger Oligocene-Miocene porphyry-related mineralization has been proposed (Vasigh and Zamani, 2010). Overall, ASTER data suggest the existence of several sites of potential hydrothermal alteration that could be associated with unidentified porphyry occurrences. However, these porphyry systems are probably younger than Late Cretaceous to middle Eocene in age.

Probabilistic Assessment

Grade and Tonnage Model Selection

No known deposits occur in this sub-tract. Thus, resource data in the Pontide (Asia)–Caucasus-Iran sub-tract were not available to classify porphyry systems into Cu-Mo or Cu-Au subtype categories or to run pooled *t*-tests. Cu-Mo and Mo-Cu-(Au) metal associations are, however, apparent at the Garta and Mamulo-Sopheli prospects, respectively. Therefore, the general porphyry Cu-Au-Mo model of Singer and others (2008) was used to estimate undiscovered copper, gold, molybdenum, and silver resources in this sub-tract.

Estimates of Undiscovered Deposits and Rationale

Favorable geologic factors for the occurrence of undiscovered porphyry copper deposits in Pontide (Asia)–Caucasus-Iran sub-tract include (1) a large and long-lived island to mature continental arc and prominent back-arc segment partially built on thick cratonic crust, (2) permissive calc-alkaline and alkaline magmatic rocks, and (3) a few possibly porphyry-related ASTER-derived alteration zones in the Iranian part of the sub-tract. Unfavorable factors include (1) 0 deposits and only 2 known porphyry prospects and (2) overall volcanic-to-plutonic ratios that suggest levels of preservation for porphyry systems are too shallow in the Caucasus, and too deep in the Alborz Terrane of northern Iran. The near absence of known porphyry prospects associated to this Late Cretaceous to middle Eocene magmatic event in the region suggests that only limited exploration for porphyry systems of this age range may have occurred and that the level of preservation of porphyry systems, in general, is not appropriate.

Overall, these factors led the assessment team to conclude that the Pontide (Asia)–Caucasus-Iran sub-tract exhibited limited favorability and that moderate to high levels of uncertainty in the estimation of undiscovered deposits were expected. Table 5c–A shows the estimates for undiscovered porphyry copper deposits in the Pontide (Asia) sub-tract of the Caucasus and northern Iran at the 90-, 50-, and 10-percent probability levels and the associated summary statistics. The team reached a consensus estimate of 0, 1, and 1 undiscovered deposits for the 90-, 50-, and 10-percent probability levels, respectively, which resulted in a mean of 0.85 undiscovered deposits with a standard deviation of 0.80 ($C_v\%=94$).

This result reflects the limited favorability and moderate to high uncertainty assessed for this porphyry copper sub-tract.

Probabilistic Assessment Simulation Results

Simulation results for estimated for copper, molybdenum, gold, silver, and the total volume of mineralized rock are summarized in table 5c–B. The mean estimate of undiscovered copper resources in the Pontide (Asia)–Caucasus-Iran porphyry sub-tract is 3.3 Mt. Results of the Monte Carlo simulation are also presented as cumulative frequency plots (fig. 21). The cumulative frequency plots show the cumulative probabilities of occurrence-estimated resources and total mineralized rock, as well as the mean for each commodity and for total mineralized rock.

Anatolide-Tauride Tract (142pCu9005)

Location

The Anatolide-Tauride tract covers an area of 63,800 km². It delimits a broad but irregularly exposed 1,500-km-long and 30–250-km-wide diverse volcano-plutonic belt of Late Cretaceous to late Eocene age that extends across the composite Anatolide-Tauride Terrane of western, central (Central Anatolian Crystalline Complex), and eastern Turkey, southwestern Armenia, Azerbaijan (Nakhchivan), and northernmost Iran (fig. 22). To the north, the Anatolide-Tauride tract is delimited by the Sakarya and Transcaucasus Terranes along the İzmir-Ankara-Erzincan, Sevan-Akera and Vedi-Zangezur Sutures. To the south, it is limited by the Arabian Platform along the Bitlis-Zagros Thrust. Parts of the Anatolide-Tauride tract are superimposed by the younger Azerbaijan tract (see below).

Tectonic Setting

The composite Anatolide-Tauride Terrane of Turkey (Ketin, 1966) consists of several subterrains that rifted from Gondwana during the Triassic (Şengör and others, 1993; Bortolotti and Principi, 2005). These terranes gradually reassembled during the Late Cretaceous-Paleogene and Oligocene-Miocene during collision with the Sakarya and Transcaucasus Terranes to the north and during collision with the Arabian Platform to the south, respectively (Dercourt and others, 1986; Kaymakci and others, 2010; Moix and others, 2008).

The composite Anatolide-Tauride Terrane can be subdivided into two tectono-stratigraphic units (fig. 3). The first tectono-stratigraphic unit, the Anatolide, represents the metamorphic northern part of the Anatolide-Tauride Terrane, which is underlain by two main Precambrian-Paleozoic metamorphic microcontinents—the Menderes Massif in western Turkey and the Central Anatolian Crystalline Complex in central Turkey. The Menderes Massif underwent greenschist- to amphibolite-grade metamorphism during the Paleocene-Eocene and the Miocene. The first metamorphic episode is related to collision-related burial associated with

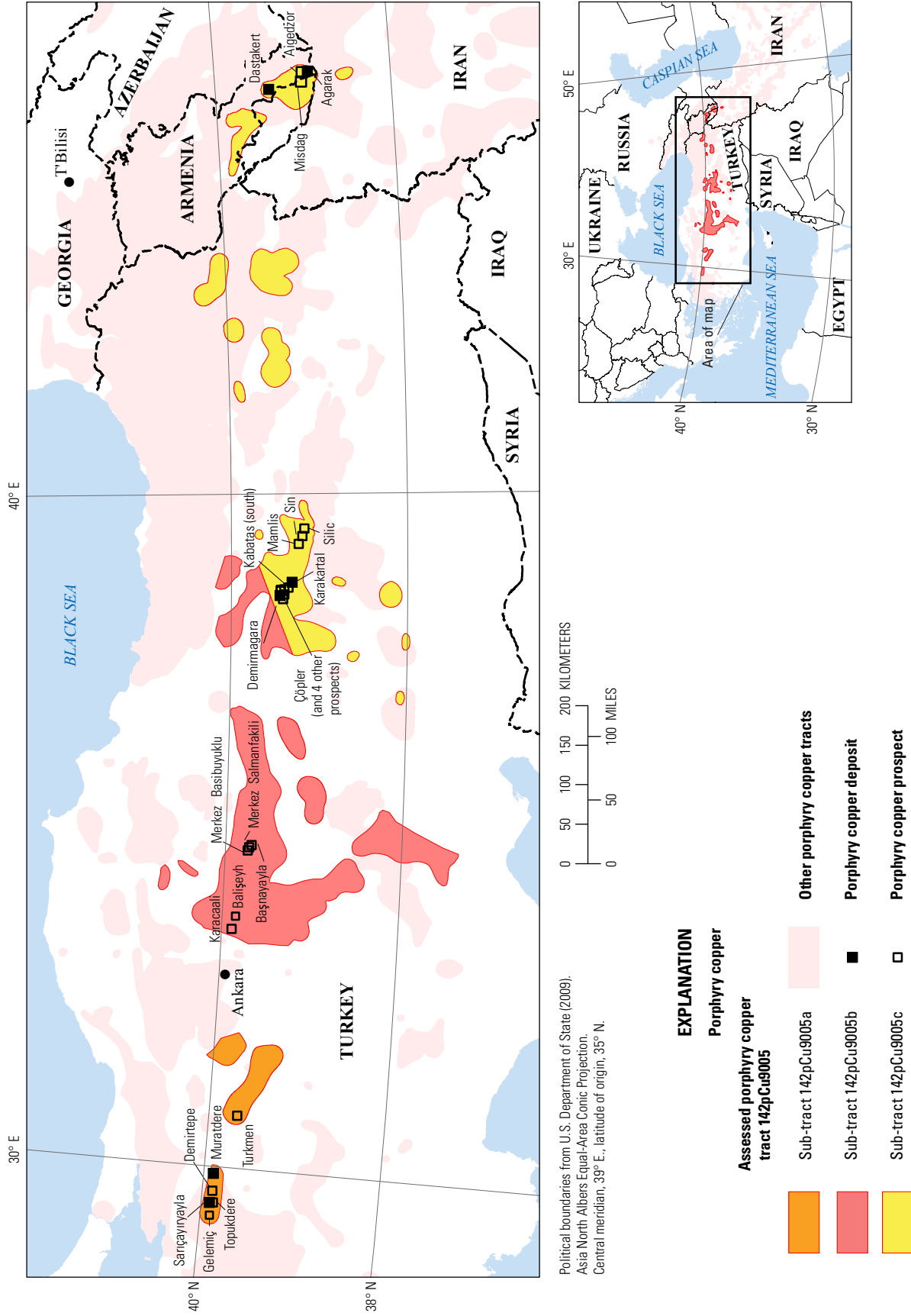


Figure 22. Map showing the location of known porphyry copper deposits and prospects for permissive tract 142pCu9005, Anatolide-Tauride—Armenia, Azerbaijan, Iran, and Turkey. Sub-tracts: 142pCu9005a Anatolide-Tauride—Western Turkey, Turkey; 142pCu9005b, Anatolide-Tauride—Central Turkey, Turkey; 142pCu9005c, Anatolide-Tauride—Eastern Turkey-Caucasus, Armenia, Azerbaijan, Iran, and Turkey. See table 2 for deposits, appendix C for prospects, and appendix D for accompanying spatial data.

thrust-sheet load, and the second one is related to extension-derived exhumation (Bozkurt and Mittweide, 2001). The Central Anatolian Crystalline Complex underwent Late Cretaceous greenschist- to granulite-facies metamorphism during collision between the Anatolide-Tauride and Sakarya Terranes along the Izmir-Ankara-Erzincan Suture (Golonka, 2004), which was followed by orogenic collapse and extension.

The second tectono-stratigraphic unit to the south, the Tauride, is the relatively unmetamorphosed equivalent of the Anatolide unit. It consists of a stack of south-vergent thrust and fold sheets, each generally formed by Paleozoic to Eocene low-grade metamorphic, sedimentary, and ophiolitic rocks. Along its southern margin, the basement of the Tauride tectono-stratigraphic terrane is formed by the Bitlis-Pötürge Massif, a microcontinent consisting of Precambrian high-grade metamorphic rocks and Paleozoic-Mesozoic polydeformed sedimentary and volcanic units affected by greenschist- and amphibolite-facies metamorphism (Kuşcu and others, 2010; Okay, 2008; Richard Herrington, written commun., 2005). In the northern part of the Tauride Terrane, the lower parts of thrust sheets exhibit high pressure/low temperature metamorphism, whereas in the southern part the upper parts of these form large unmetamorphosed nappes. Thrusting events occurred in the late Paleocene-early Eocene following the collision with the Sakarya Terrane to the north, and in the middle Miocene as a result of the collision of the Anatolide-Tauride Terrane with the Arabian Platform to the south. The intervening middle Eocene to early Miocene time period was dominated by subsidence and associated extensional tectonics and associated back-arc magmatism (Şengör and Yılmaz, 1981; Dilek, 2010).

Several possibly interconnected oceans existed around the Menderes, Central Anatolian Crystalline Complex, and Bitlis-Pötürge continental fragments (fig. 4D) between the late Campanian and Eocene (Richard Herrington, written commun., 2005). Closure of these oceans occurred during collision of the Arabian Platform along the Bitlis-Zagros Thrust (Gürer and Aldanmaz, 2002). These ocean basins are represented by shallow-marine sediments underlain by accretionary prisms and ophiolite mélanges associated with subduction zones. Their relative position is preserved along suture zones distributed within the Anatolide-Tauride Terrane (fig. 3). These marine basins are regarded as the Inner Tauride Ocean (Şengör and Yılmaz, 1981), which gradually closed along subduction zones producing Late Cretaceous to middle-late Eocene intraoceanic arc and back-arc magmatism (Gençaloğlu-Kuşcu and others, 2001).

In the late Eocene-Oligocene, propagation of folding, thrusting, and the onset of a transpressional regime occurred all along the Anatolide-Tauride Terrane during the initial oblique collisional process between the Arabian Platform along the Bitlis-Zagros Suture. Paleogene and older formations were uplifted and eroded giving way to deposition of evaporitic and red clastic successions. This stage was followed by a north-south extensional regime, which led to the formation of shallow marine deposits during

Oligocene and middle Miocene times (Adamia and others, 2011). This extensional event was superseded by the final collision between the Arabian Platform and the Bitlis-Pötürge microcontinent (Şengör and Kidd, 1979), causing renewed transpression and deposition of evaporitic, lagoonal, and continental clastics in synorogenic pull-apart basins during the late Miocene and Pleistocene.

In the composite Anatolide-Tauride Terrane, the origin of Late Cretaceous to middle-late Eocene volcano-plutonic activity is related to closure of both the northern and southern branches of the Neotethys Ocean, as well as closure of the intracontinental Inner Tauride Ocean (Gökten, 1993; Görür and others, 1984; Dilek and others, 1999). As a consequence, variations in the overall tectonic setting do occur along this volcano-plutonic belt. In general, Late Cretaceous to middle Eocene (possibly transported southward) arc rocks are preserved in western Turkey, Late Cretaceous island-arc and Late Cretaceous to middle Eocene syncollisional to postcollisional rocks are exposed in the Central Anatolian Crystalline Complex, and Late Cretaceous to middle-late Eocene intraoceanic arc to back-arc rock associations occur in eastern Turkey and the southwestern Lesser Caucasus and northernmost Iran. Accordingly, the nature of Late Cretaceous to middle-late Eocene magmatism associated with these distinct tectonic environments is separated here into the Anatolide-Tauride–Western Turkey (142pCu9005a), the Anatolide-Tauride–Central Turkey (142pCu9005b), and the Anatolide-Tauride–Eastern Turkey-Caucasus (142pCu9005c). These individually assessed sub-tracts are described below.

Anatolide-Tauride–Western Turkey Sub-tract (142pCu9005a)

Descriptive model: General porphyry copper (Cox, 1986a; Berger and others, 2008; John and others, 2010)

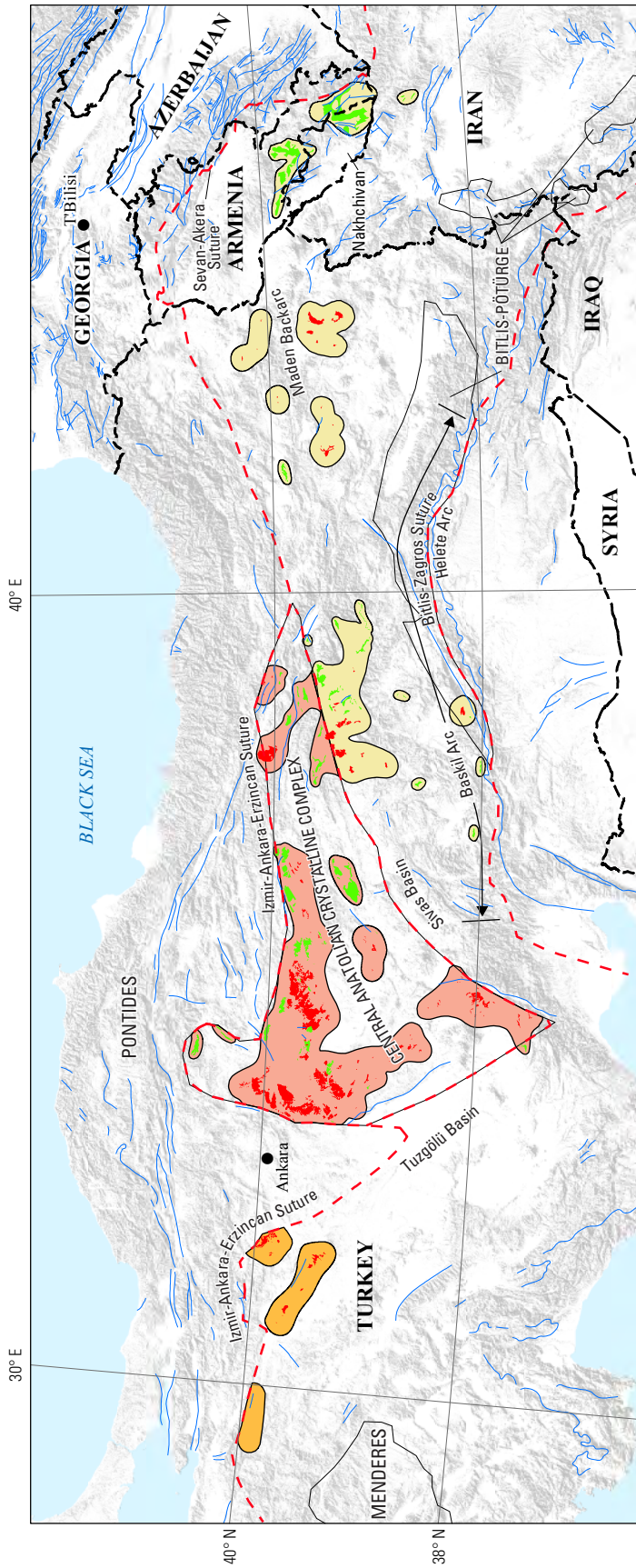
Grade and tonnage model: General Cu-Au-Mo porphyry copper model (Singer and others, 2008)

Geologic feature assessed: Late Cretaceous to middle Eocene arc-related magmatism of the Tethyan Eurasian Metallogenic Belt

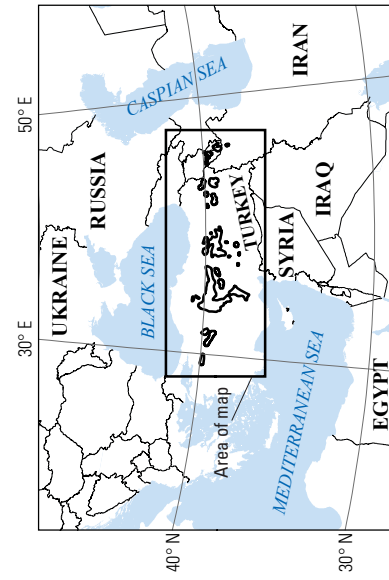
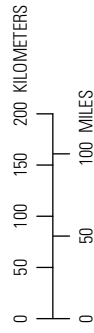
Magmatism

The Anatolide-Tauride–Western Turkey sub-tract covers an area of 5,900 km² (fig. 22). The sub-tract delimits a 250-km-long by 40-km-wide subduction-related to syncollisional magmatic belt on the northern margin of the Anatolide-Tauride Terrane south and along the Izmir-Ankara Suture. Permissive igneous units (appendix B) used to define this sub-tract are shown in figure 23, along with locations of igneous complexes and other geologic features mentioned in this section.

This magmatic belt of western Turkey consists of locally foliated Late Cretaceous to middle Eocene metaluminous calc-alkaline granodioritic intrusions with metamorphic aureoles (Okay and others, 2001; Okay and others, 1996). Plutons intrude ophiolitic complexes that tectonically overlie blueschist-facies rocks with Late Cretaceous metamorphic



Base from SRTM Global Digital Elevation Model, U.S. Geological Survey EROS Data Center, 2006. Political boundaries from U.S. Department of State (2009). Asia North Albers Equal-Area Conic Projection. Central meridian, 39° E., latitude of origin, 35° N.



EXPLANATION

- Assessed porphyry copper tract 142pCu9005**
 - Sub-tract 142pCu9005a
 - Sub-tract 142pCu9005b
 - Sub-tract 142pCu9005c
- Porphyry copper**
 - Permissive extrusive rock
 - Permissive intrusive rock
- Geologic feature discussed in the text**
 - Fault
 - Suture
 - Terrane

Helilete Arc

Figure 23. Map showing the distribution of permissive intrusive and volcanic rocks used to define tract 142pCu9005, Anatolide-Tauride—Armenia, Azerbaijan, Iran, and Turkey. Sub-tracts: 142pCu9005a Anatolide-Tauride—Western Turkey, Turkey; 142pCu9005b, Anatolide-Tauride—Central Turkey, Turkey; 142pCu9005c, Anatolide-Tauride—Eastern Turkey-Caucasus, Armenia, Azerbaijan, Iran, and Turkey. See appendix A for principal sources of information and appendix B for source map units.

ages (Okay, 2008). They exhibit typical subduction-related igneous compositions (Delaloye and Bingöl, 2000). However, emplacement of the middle Eocene intrusive suite occurred after the Paleocene-early Eocene collision between the Anatolide-Tauride and Sakarya Terranes (Okay and Satir, 2006; Harris and others, 1994). Available Al-in-hornblende barometer data indicate deep emplacement pressures of approximately 3 kilobars (kb) during uplift associated with collision (Harris and others, 1994). However, geobarometric studies on metamorphic rocks and the presence of hypabyssal porphyry intrusions also support shallower emplacement depths (based on emplacement pressures around 2 ± 1 kb; Okay and Satir, 2006). Consequently, this Late Cretaceous to middle Eocene event includes both precollisional and postcollisional magmatism.

The origin of Late Cretaceous to middle Eocene granitoids in western Turkey remains controversial (Yigit, 2006). It has been explained by postcollisional rapture (slab break-off) of the oceanic lithosphere in the south from the Sakarya continental lithosphere in the north (Altunkaynak, 2007), by derivation from an intraoceanic arc within the Inner Tauride Ocean to the southeast (Şengör and Yilmaz, 1981), or by relation to the Hellenic-Cyprian subduction zone further south in the Mediterranean Sea (Delaloye and Bingöl, 2000). Alternatively, given that Late Cretaceous to middle Eocene granitoids north of the Izmir-Ankara-Erzincan Suture in the western Sakarya Terrane exhibit comparable petrogenetic characteristics (Okay and Satir, 2006), this magmatic belt may be an overthrust part of the Pontide Arc (fig. 19) located to the north (Yilmaz, 2003b).

Late Eocene to early Miocene granitoids that intrude unconformable middle Eocene neritic limestones also occur in the area. These granitoids were emplaced in an extensional setting and form part of a younger tectono-magmatic event (see Azerbaijan tract below).

Known Porphyry Deposits and Prospects

In western Turkey, Late Cretaceous to early Eocene Cu-Mo-(Au-W) porphyry and base-metal skarn systems (Kuşcu, 2005) are related to variably exhumed I-type granitoids. The Anatolide-Tauride-Western Turkey sub-tract contains two known porphyry copper deposits (table 2). These are the Muratdere porphyry and Sariçayiryayla porphyry-skarn Cu-Mo-Au deposits. In addition to these deposits, four Cu-Mo-(Au-W) porphyry and porphyry-skarn prospects (Gelemic, Demirtepe, Topukdere, and Turkmen) are known (appendix C; fig. 22). The first three occur in the Muratdere-Sariçayiryayla district, where several younger porphyry systems are also present (see Azerbaijan-Western Turkey sub-tract below). The fourth one (Turkmen) is a porphyry-related skarn prospect that occurs in a batholith located about 80 km east-southeast of the Muratdere-Sariçayiryayla district.

Muratdere Porphyry Deposit

The early Eocene (50 Ma; Yigit, 2009; InfoMine, Inc., 2012b) Muratdere Cu-Mo-Au porphyry deposit was originally

identified by the MTA following a regional geochemical survey program in 1998–99 (Cliff, 2007). The deposit has a JORC-compliant inferred resource of 51 Mt at 0.36 percent copper, 0.0125 percent molybdenum, 0.12 g/t gold, and 2.4 g/t silver (Stratex International PLC, 2012b). The porphyry deposit is associated with a granodiorite that intruded schist, metabasite, marble, and an ophiolitic mélange. It extends east-west along the south side of an east-southeast-trending fault that is parallel to the Izmir-Ankara-Erzincan Suture for a distance of about 4 km, and it has a width of between 500 and 1,700 m. Mineralization consists of narrow magnetite- and pyrite-chalcopyrite quartz veins associated with K-silicate alteration. The phyllic alteration association comprises quartz-sericite veinlets. The deposit has a jarositic leached cap with a supergene enrichment overprint, where relict pyrite and chalcopyrite are partially replaced by chalcocite and covellite. The higher grade copper data (greater than 0.4 percent copper) mostly correlate with intercepts of enriched supergene material (Stratex International PLC, 2012b).

Sariçayiryayla Porphyry Deposit

The early Eocene (50 Ma; Yigit, 2009) Sariçayiryayla Cu-Mo-Au porphyry-skarn deposit and adjacent (47.8 Ma) Topukdere skarn prospect exhibit similar characteristics to the Muratdere porphyry deposit located about 35 km to the east. However, reported resources at Sariçayiryayla are larger at 120.3 Mt at 0.168 percent copper (Yigit, 2009). Mineralization is related to a granitoid that intruded schist and carbonate rocks, which is in turn cut by quartz porphyry and late-stage aplite dikes (Okay and Satir, 2006; Yigit, 2009).

Turkmen Porphyry Prospect

Numerous small ancient workings occur at the Late Cretaceous (67 Ma; Yilmaz, 2003b) Turkmen porphyry-related skarn prospect located about 80 km east-southeast of Muratdere (Yigit, 2009). Proximal Pb-Zn-Ag-Cu-(Au-Mo-W) skarn is surrounded by Au-Zn-Pb-As skarn and distal Pb-Zn-Ag-Au replacement mineralization. Quartz-base-metal stockworks occupy a 2-km² zone about a Late Cretaceous to Paleocene granodiorite-tonalite porphyry stock that intrudes a granodioritic-granitic-monzonitic batholith. The batholith is emplaced into highly deformed and variably metamorphosed late Paleozoic to Triassic schists and serpentinites capped by only locally metamorphosed Triassic sedimentary units (Yilmaz, 2003b).

Preservation Level

As derived from the 1:500,000-scale geologic map of Turkey (General Directorate of Mineral Research and Exploration, 2000), 21 percent of the Anatolide-Tauride-Western Turkey sub-tract area is underlain by older basement dominated by exhumed metamorphic units and ophiolitic complexes. Late Cretaceous to middle Eocene permissive units are only represented by plutons (fig. 23). No coeval volcanic rocks are preserved. This suggests that levels of preservation are

deep and only the deeper parts of porphyry systems are exposed if they are not buried under younger cover. Younger cover rocks are extensive. They overlie 67 percent of the sub-tract area.

Magnetic Anomalies

Regional aeromagnetic maps (Ates and others, 1999; Maus and others, 2009) were used to confirm the location and character of regional geologic features (for example, arcs, basins, faults, terrane boundaries). Porphyry copper occurrences in the western part of the Anatolide-Tauride–Western Turkey sub-tract occur around local magnetic highs that image the Late Cretaceous-Eocene and Oligocene-Miocene composite batholiths in the area. However, a more striking feature of the magnetic map of western Turkey is the prominent positive anomaly trending northwest-southeast along the Upper Cretaceous to Oligocene Tuzgölü Basin (Arikan, 1975; Görür and others, 1984). The Tuzgölü Basin is part of the former Inner Tauride Ocean, which in the region separated the western Anatolide-Tauride Terrane from the Central Anatolian Crystalline Complex. The lower part of the stratigraphic section in the Tuzgölü Basin consists of Late Cretaceous-Paleocene ophiolites and island-arc-related volcanoclastic rocks that appear to project to the northwest into the eastern part of the Anatolide-Tauride–Western Turkey sub-tract that hosts the Turkmen porphyry-related skarn prospect (figs. 22, 23). Thus, the volcano-plutonic event delimited by the Anatolide-Tauride–Western Turkey sub-tract could potentially extend into the intraoceanic-arc setting that underlies the Tuzgölü Basin, albeit under thick late Eocene and younger cover. Furthermore, negative and residual gravity anomalies in western Turkey image the attenuated cratonic crust that formed during the post-Eocene extensional tectonic events that followed (Ates and others, 1999).

Probabilistic Assessment

Grade and Tonnage Model Selection

Insufficient resource information on the Sariçayiryayla and Muratdere porphyry deposits precluded classification according to the molybdenum and gold contents and ratios criteria used here. However, the Cu-Mo-(Au-W) metal association suggests that these deposits belong to the Cu-Mo porphyry subtype. Pooled *t*-test results assuming equal variances show that the two known deposits in the tract are not significantly different at the 1-percent level from tonnages and copper, molybdenum, and gold grades in the general porphyry Cu-Au-Mo model of Singer and others (2008). Therefore, the general model was selected to estimate undiscovered copper, gold, molybdenum, and silver resources in the Anatolide-Tauride–Western Turkey sub-tract. Compared to the median tonnage and grade in the general porphyry Cu-Au-Mo model, Sariçayiryayla and Muratdere exhibit smaller tonnages and lower copper grades, but Muratdere contains higher molybdenum grades.

Estimates of Undiscovered Deposits and Rationale

In the Anatolide-Tauride–Western Turkey sub-tract, geologic factors favorable for the occurrence of undiscovered porphyry deposits include (1) tectonically transported(?) continental-arc segment; (2) permissive calc-alkaline compositions; (3) known Cu-Mo porphyry deposits; and (4) favorable conditions for supergene enrichment (likely enhanced by postmineral extensional tectonics). Unfavorable factors for the occurrence of undiscovered porphyry deposits include (1) small arc segment (as exposed), (2) known porphyry deposits that exhibit smaller tonnages and copper grades than the median porphyry deposit around the world, (3) deeper levels of exposure for porphyry systems, and (4) extensive cover.

The somewhat lower density of known porphyry deposits relative to worldwide densities for tracts of this size suggest that undiscovered deposits are likely present. Furthermore, the relatively high number of known porphyry occurrences within this small sub-tract, which is in part a reflection of the high levels of exploration that the region is experiencing, support moderate levels of uncertainty expected in the estimation of numbers of undiscovered deposits.

Overall, these factors led the assessment team to conclude that the Anatolide-Tauride–Western Turkey Caucasus sub-tract exhibited limited geological favorability and that moderate levels of uncertainty in the estimation of undiscovered deposits were expected. Nevertheless, the tract would contribute significant copper resources from undiscovered deposits to the overall assessment. Therefore, quantitative assessment of undiscovered deposits in this tract was warranted. Table 6a–A shows the estimates of undiscovered porphyry copper deposits in the Anatolide-Tauride–Western Turkey sub-tract at the 90-, 50-, and 10-percent probability levels and the associated summary statistics. The team reached a consensus estimate of 0, 1, and 1 undiscovered deposits for the 90-, 50-, and 10-percent probability levels, respectively, which resulted in a mean of 0.78 undiscovered deposits with a standard deviation of 0.60 ($C_v\%=78$). This result reflects the level of favorability and moderate uncertainty assessed for this tract. The estimated total deposit density per 100,000 km² obtained is comparable to median porphyry deposit densities expected in well-explored tracts of equivalent size elsewhere around the world (Singer and Menzie, 2010).

Probabilistic Assessment Simulation Results

Simulation results for estimated for copper, molybdenum, gold, silver, and the total volume of mineralized rock are summarized in table 6a–B. The mean estimate of undiscovered copper resources in the Anatolide-Tauride–NW Turkey porphyry sub-tract is 3 Mt. Results of the Monte Carlo simulation are also presented as cumulative frequency plots (fig. 24A). The cumulative frequency plots show the cumulative probabilities of occurrence-estimated resources and total mineralized rock, as well as the mean for each commodity and for total mineralized rock.

Table 6. Probabilistic assessment for tract 142pCu9005, Anatolide-Tauride—Armenia, Azerbaijan, Iran, and Turkey.

[Coded_ID, a unique number assigned to each permissive tract in the spatial data (appendix D)]

Sub-tract name	Coded_ID	Countries
Anatolide-Tauride—Western Turkey	142pCu9005a	Turkey
Anatolide-Tauride—Central Turkey	142pCu9005b	Turkey
Anatolide-Tauride—Eastern Turkey-Caucasus	142pCu9005c	Armenia, Azerbaijan, Iran, and Turkey

Table 6a. Probabilistic assessment for sub-tract 142pCu9005a, Anatolide-Tauride—Western Turkey sub-tract, Turkey.**A.** Undiscovered deposit estimates, deposit numbers, tract area, and deposit density.

[N_{xx} , estimated number of deposits associated with the xxth percentile; N_{und} , expected number of undiscovered deposits; s , standard deviation; $C_v\%$, coefficient of variance; N_{known} , number of known deposits in the tract that are included in the grade and tonnage model; N_{total} , total of expected number of deposits plus known deposits; tract area, area of permissive tract in square kilometers (km^2); deposit density reported as the total number of deposits per 100,000 km^2 . N_{und} , s , and $C_v\%$ are calculated using a regression equation (Singer and Menzie, 2005)]

Consensus undiscovered deposit estimates					Summary statistics					Tract area (km^2)	Deposit density ($N_{total}/100,000 \text{ km}^2$)
N_{90}	N_{50}	N_{10}	N_{05}	N_{01}	N_{und}	s	$C_v\%$	N_{known}	N_{total}		
0	1	1	2	2	0.78	0.60	78	2	2.8	5,940	47

B. Results of Monte Carlo simulations of undiscovered resources.

[Cu, copper; Mo, molybdenum; Au, gold; and Ag, silver; in metric tons; Rock, in million metric tons]

Material	Probability of at least the indicated amount						Probability of	
	0.95	0.9	0.5	0.1	0.05	Mean	Mean or greater	None
Cu	0	0	460,000	6,100,000	11,000,000	3,000,000	0.20	0.31
Mo	0	0	0	140,000	330,000	79,000	0.14	0.62
Au	0	0	0	170	320	65	0.20	0.56
Ag	0	0	0	1,600	3,700	900	0.14	0.70
Rock	0	0	110	1,300	2,400	610	0.21	0.31

Table 6b. Probabilistic assessment for sub-tract 142pCu9005b, Anatolide-Tauride—Central Turkey sub-tract, Turkey.

A. Undiscovered deposit estimates, deposit numbers, tract area, and deposit density.

[N_{xx} , estimated number of deposits associated with the xxth percentile; N_{und} , expected number of undiscovered deposits; s , standard deviation; $C_v\%$, coefficient of variance; N_{known} , number of known deposits in the tract that are included in the grade and tonnage model; N_{total} , total of expected number of deposits plus known deposits; tract area (km²), area of permissive tract in square kilometers; deposit density reported as the total number of deposits per 100,000 km². N_{und} , s , and $C_v\%$ are calculated using a regression equation (Singer and Menzie, 2005)]

Consensus undiscovered deposit estimates					Summary statistics					Tract area (km ²)	Deposit density ($N_{total}/100,000$ km ²)
N_{90}	N_{50}	N_{10}	N_{05}	N_{01}	N_{und}	s	$C_v\%$	N_{known}	N_{total}		
0	0	1	1	2	0.33	0.62	190	0	0.33	36,200	1

B. Results of Monte Carlo simulations of undiscovered resources.

[Cu, copper; Mo, molybdenum; Au, gold; and Ag, silver; in metric tons; Rock, in million metric tons]

Material	Probability of at least the indicated amount						Probability of	
	0.95	0.9	0.5	0.1	0.05	Mean	Mean or greater	None
Cu	0	0	0	2,200,000	5,100,000	1,300,000	0.15	0.70
Mo	0	0	0	30,000	110,000	41,000	0.09	0.84
Au	0	0	0	50	140	35	0.12	0.82
Ag	0	0	0	270	1,400	460	0.08	0.87
Rock	0	0	0	520	1,100	270	0.15	0.70

Table 6c. Probabilistic assessment for sub-tract 142pCu9005c, Anatolide-Tauride—Eastern Turkey-Caucasus sub-tract, Armenia, Azerbaijan, Iran, and Turkey.

A. Undiscovered deposit estimates, deposit numbers, tract area, and deposit density.

[N_{xx} , estimated number of deposits associated with the xxth percentile; N_{und} , expected number of undiscovered deposits; s , standard deviation; $C_v\%$, coefficient of variance; N_{known} , number of known deposits in the tract that are included in the grade and tonnage model; N_{total} , total of expected number of deposits plus known deposits; tract area, area of permissive tract in square kilometers (km²); deposit density reported as the total number of deposits per 100,000 km². N_{und} , s , and $C_v\%$ are calculated using a regression equation (Singer and Menzie, 2005)]

Consensus undiscovered deposit estimates					Summary statistics					Tract area (km ²)	Deposit density ($N_{total}/100,000$ km ²)
N_{90}	N_{50}	N_{10}	N_{05}	N_{01}	N_{und}	s	$C_v\%$	N_{known}	N_{total}		
0	2	4	7	7	2.2	2.0	92	4	6.2	21,700	29

B. Results of Monte Carlo simulations of undiscovered resources.

[Cu, copper; Mo, molybdenum; Au, gold; and Ag, silver; in metric tons; Rock, in million metric tons]

Material	Probability of at least the indicated amount						Probability of	
	0.95	0.9	0.5	0.1	0.05	Mean	Mean or greater	None
Cu	0	0	2,700,000	19,000,000	32,000,000	8,200,000	0.25	0.21
Mo	0	0	26,000	530,000	1,000,000	230,000	0.20	0.36
Au	0	0	48	550	910	220	0.25	0.33
Ag	0	0	170	5,900	12,000	2,700	0.20	0.45
Rock	0	0	590	3,900	6,800	1,700	0.27	0.21

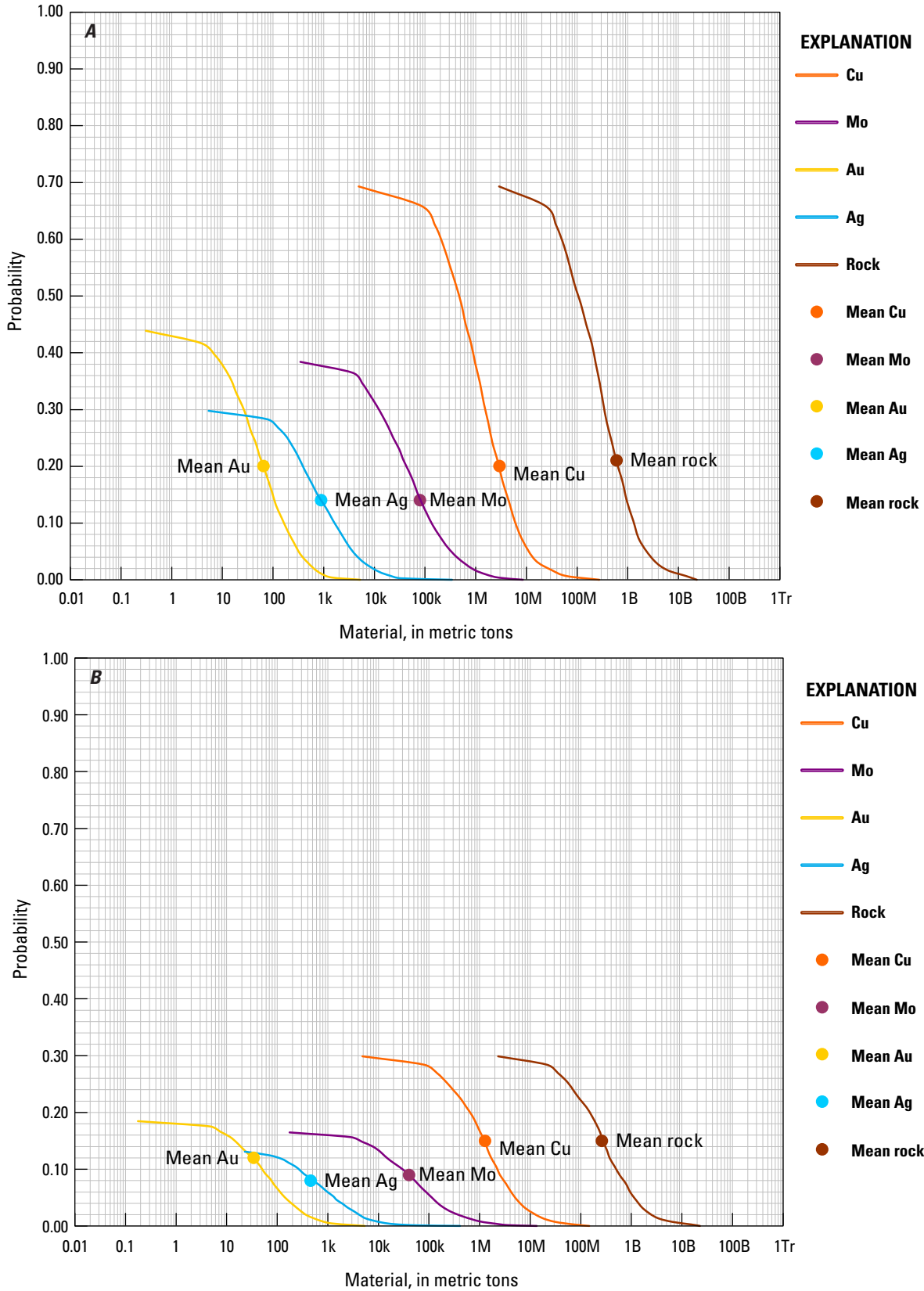


Figure 24. Cumulative frequency plots showing the results of Monte Carlo computer simulation of undiscovered resources in porphyry copper deposits in tract 142pCu9005, Anatolide-Tauride—Armenia, Azerbaijan, Iran, and Turkey. *A*, Sub-tract 142pCu9005a Anatolide-Tauride—Western Turkey, Turkey. *B*, Sub-tract 142pCu9005b, Anatolide-Tauride—Central Turkey, Turkey. *C*, Sub-Tract 142pCu9005c, Anatolide-Tauride—Eastern Turkey-Caucasus, Armenia, Azerbaijan, Iran, and Turkey. k, thousand; M, million; B, billion; Tr, trillion.

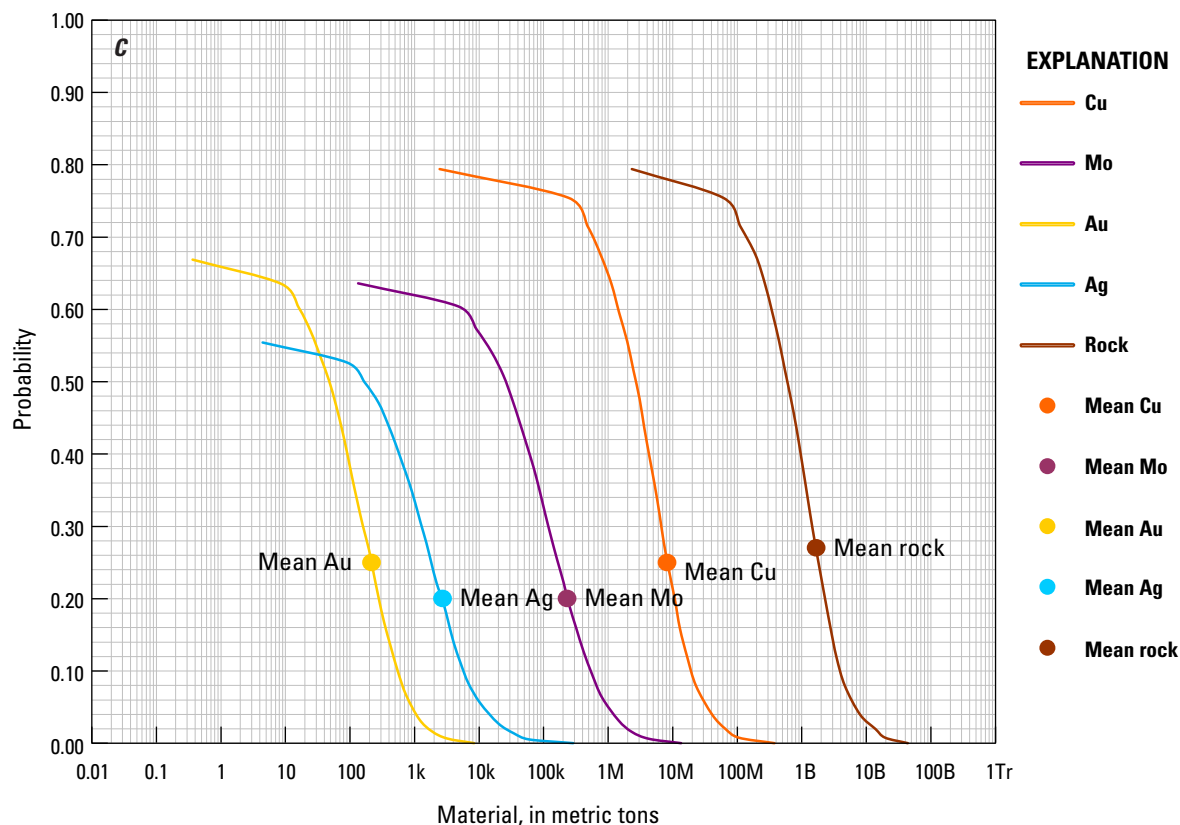


Figure 24.—Continued

Anatolide-Tauride–Central Turkey Sub-tract (142pCu9005b)

Descriptive model: General porphyry copper (Cox, 1986a; Berger and others, 2008; John and others, 2010)

Grade and tonnage model: General Cu-Au-Mo porphyry copper model (Singer and others, 2008)

Geologic feature assessed: Late Cretaceous to middle Eocene syncollisional and postcollisional magmatism of the Tethyan Eurasian Metallogenic Belt

Magmatism

The Anatolide-Tauride–Central Turkey sub-tract covers an area of 36,200 km² (fig. 22). It delimits the Late Cretaceous to middle Eocene syncollisional to postcollisional magmatic belt in the Central Anatolian Crystalline Complex. The Central Anatolian Crystalline Complex is bounded on the north by the Izmir-Ankara-Erzincan suture zone, and on the west and east by fault-bounded sedimentary basins (Aktimur and others, 1990; Görür and others, 1984) that mark the previous location of the Inner Tauride Ocean (fig. 3). Permissive igneous units (appendix B) used to define this sub-tract are shown in figure 23, along with locations of igneous complexes and other geologic features mentioned in this section.

Constraints on the ages, conditions of formation, and tectonic affinities of magmatism in the Central Anatolian Crystalline Complex are the subject of continuing studies. However, it is

generally accepted that precollisional island-arc gabbros and plagiogranites obducted onto the Central Anatolian Crystalline Complex were followed by local 110–95-Ma syncollisional S-type granites, more extensive 85–75-Ma postcollisional I-type (or H-type) quartz monzogranites, tonalites, and granodiorites, and widespread latest Cretaceous extension-related A-type monzonites and syenites (İlbeyli, 2005; Boztuğ and others, 2009; Delibaş and Genç, 2012; Lefebre and others, 2013). A-type alkaline magmatism evolved in time from silica-saturated to silica-undersaturated nepheline-normative compositions (Aydin and others, 1998).

Older variably deformed S-type and I-type granitoids preferentially occur along the northern and western margins of the Central Anatolian Crystalline Complex, and they were largely emplaced during metamorphism (Whitney and others, 2003). The present-day disposition of these magmatic belts is believed to have resulted, at least in part, from deformation related to dextral transpression and rotation of the Central Anatolian Crystalline Complex during Late Cretaceous oblique collision with the Sakarya Terrane (Lefebre and others, 2013; Norman, 1984). Relatively undeformed latest Cretaceous A-type alkaline plutons are located toward the inner parts of Central Anatolian Crystalline Complex, where they intrude both metamorphic basement and overthrust ophiolitic complexes (Akiman and others, 1993; Boztuğ and Arehart, 2007; Düzgören-Aydin and others, 2001; Boztuğ and others, 2003; İlbeyli and others, 2009).

Geochemical data from Late Cretaceous plutonic suites indicate evolved radiogenic signatures for the S- and I-type suites and variable but generally less evolved radiogenic signatures for the latest Cretaceous A-type suite (Köksal and Göncüoğlu, 2008). These magmatic units exhibit volcanic arc to syncollisional affinities and volcanic arc to within-plate affinities, respectively (Lefebvre and others, 2013). $^{40}\text{Ar}/^{39}\text{Ar}$ and K–Ar hornblende and biotite cooling ages reflect rapid exhumation of a mid-crustal section during the Late Cretaceous (Campanian–Maastrichtian). Apatite fission-track ages further support continuing uplift during the early to middle Paleocene (57–62 Ma; Boztuğ and others, 2009). Emplacement pressures estimated from available Al-in-hornblende geobarometry for S-, I-, and A-type plutonic suites range from 2.6 to 5.3 kb, suggesting deep emplacement depths (İlbelyli, 2005). However, in contrast to older plutonic suites, latest Cretaceous alkaline magmatism in the Central Anatolian Complex includes both intrusive and extrusive units that overall indicate preservation of shallower emplacement levels (Köksal and others, 2001; Kuşçu and Erler, 1998).

As represented in the 1:500,000-scale geologic map of Turkey (General Directorate of Mineral Research and Exploration, 2000), younger calc-alkaline and alkaline volcanic and plutonic units of Paleocene and Eocene age are also present, and they are distributed preferentially along the eastern and northern parts of the Central Anatolian Crystalline Complex. These include middle Paleocene alkaline intrusions with volcanic-arc geochemical signatures (Richard Herrington, written commun., 2005). Emplacement of these middle Paleocene igneous units would predate the Late Paleocene to middle Eocene terrestrial to shallow marine extensional environment that followed (Boztuğ and others, 2009).

Known Porphyry Prospects

In the Central Anatolian Crystalline Complex, mineralization associated with early Late Cretaceous S-type granites includes greisen-type tin and tungsten, whereas mineralization related to Late Cretaceous dominantly felsic I-type plutons consists of proximal iron-tungsten and distal lead-zinc skarn, as well as porphyry Mo-Cu systems. Iron skarn or iron oxide copper gold (IOCG) and quartz-fluorite-gold veins appear to be preferentially associated with younger latest Cretaceous and younger(?) A-type alkalic intrusions (Kuşçu and Erler, 1998; Boztuğ and others, 2003; Delibaş and Genç, 2012).

Five Mo-Cu porphyry and porphyry-related prospects (Balişeyh, Karacaali, Başnayayla, Merkez Basibuyuklu, and Merkez Salmanfakili) were identified and are included in the porphyry occurrence database (fig. 22). All five prospects occur in a magmatic belt that is located in the northern part of the Central Anatolian Crystalline Complex. The Balişeyh and Karacaali porphyry prospects are located in the western part of this belt. This area also hosts other possible porphyry-related Mo-(W) vein occurrences (Karamustafa, Dagevi, and Karaahmetli). The Başnayayla porphyry prospect lies in the

central part of the belt and includes the Merkez Basibuyuklu and Merkez Salmanfakili porphyry-related Mo-(Cu) prospects. An additional third area occurs in the eastern part of the belt, where lead-zinc skarns are reported to be spatially associated with granite porphyry intrusions (Engin and others, 2000).

Molybdenum resources have been mined at Balişeyh and Başnayayla. However, no copper is known to have been produced. Therefore, these small porphyry deposits are listed as prospects in this study.

Balişeyh and Karacaali Porphyry Prospects

At the Balişeyh Mo-(Cu) porphyry prospect (Kuşçu and Erler, 1998; Yigit, 2009; Delibaş and Genç, 2012), a 74-Ma calc-alkaline metaluminous to peraluminous granodiorite, quartz monzonite and hornblende-biotite granite pluton is encircled by propylitic, sericitic, and K-silicate alteration, which host quartz stockworks and east-west trending pegmatitic veins that contain molybdenite, magnetite, pyrite, covellite, wolframite, and scheelite. Mineral exploration and mining were conducted at the Balişeyh prospect between 1936 and 1940 by the MTA and the Eti Mine Company. The total estimated reserves in 1937 were 6,600 t at a grade of 2.2 percent MoS_2 (molybdenum disulfide). Since then, the Balişeyh mine has been operated by several companies. About 11,977 t of ore with 1–1.5 percent molybdenum was extracted by the TurkMaadin Company in 1984 (Delibaş and Genç, 2012).

At the Karacaali historical mining district, the Mo-Cu-bearing porphyry prospect (Kuşçu and Erler, 1998; Delibaş and Genç, 2012) is centered on a 76–74-Ma calc-alkaline I-type porphyritic quartz monzonite, quartz monzonite, and fine-grained granite intrusions. Actinolite, epidote, and chlorite alteration host north-south trending quartz, quartz-carbonate, and quartz-tourmaline veins containing chalcopyrite, molybdenite, galena, sphalerite, pyrite, and magnetite, as well as minor covellite and bornite. Between 1999 and 2001, the MTA conducted 1,825 m of diamond drilling. Sampling indicates 1.4 percent copper, 0.4 percent molybdenum, 0.1 percent lead, 0.2 percent zinc, and 15–60 percent iron. (Delibaş and Genç, 2012).

Başnayayla Porphyry Prospect

The Başnayayla Mo-Cu prospect (Kuşçu and Erler, 1998; Delibaş and Genç, 2012) was discovered by the MTA in 1993 as part of an exploration program that included five diamond-drill holes. Measured and indicated reserves are 9,375 t at 0.02 percent molybdenum. Porphyry-related mineralization at Başnayayla is centered on a 78- to 77-Ma calc-alkaline metaluminous to peraluminous biotite granite with andalusite and sillimanite, which is cut by quartz-feldspar-biotite and quartz-sericite-pyrite stockworks. Northwest-southeast quartz veins and stockworks contain chalcopyrite, molybdenite, pyrite, and magnetite, as well as lesser pyrrhotite, sphalerite and galena (Delibaş and Genç, 2012).

Preservation Level

As derived from the 1:500,000-scale geologic map of Turkey (General Directorate of Mineral Research and Exploration, 2000), 14 percent of the Anatolide-Tauride–Central Turkey sub-tract area is underlain by older basement dominated by deeply exhumed metamorphic units and ophiolitic complexes. Permissive volcanic and plutonic unit proportions are small (4 and 7 percent of the sub-tract area, respectively) and exhibit a relatively low ($\{\text{volcanic}/[\text{volcanic}+\text{plutonic}]\} \times 100$) ratio of 35 (fig. 23). Broadly coeval nonpermissive (ultramafic, mafic, and sedimentary) units are more abundant (24 percent), and younger cover rocks are fairly widespread (49 percent of the sub-tract area).

However, proportions of permissive units in the Anatolide-Tauride–Central Turkey sub-tract vary. Late Cretaceous permissive units are represented by plutons only, suggesting that levels of preservation are too deep for porphyry copper systems. This is supported by the known Late Cretaceous porphyry systems, which exhibit tungsten and Mo-Cu metal associations that are consistent with deep preservation levels. In contrast, younger latest Cretaceous to middle Eocene permissive units consist of both volcanic and plutonic rocks. This implies that more appropriate levels of preservation for porphyry systems may exist in the sub-tract. No porphyry copper prospects are known to be related to these younger alkalic igneous suites. If present, however, these porphyry systems are likely buried under younger cover, which is widespread in this sub-tract.

Magnetic Anomalies

Regional aeromagnetic maps (Ates and others, 1999; Maus and others, 2009) were used to confirm the location and character of regional geologic features (for example, arcs, basins, faults, terrane boundaries). The location of the plutonic belts across the northern and western margins of the Central Anatolian Crystalline Complex are well imaged by magnetic highs. The five Mo-Cu prospects in the northern part of this sub-tract appear to lie along the margins of magnetic anomalies. An additional magnetic high straddles the eastern margin of the Central Anatolian Crystalline Complex. This magnetic high is generally associated with Mesozoic ophiolitic and younger Neogene basaltic units.

Overall, positive residual gravity anomalies (Ates and others, 1999) in the Central Anatolian Crystalline Complex reflect the cratonic nature of the crust, which was attenuated by extensional processes during the latter part of the volcano-plutonic event delimited by the Anatolide-Tauride–Central Turkey sub-tract.

Probabilistic Assessment

Grade and Tonnage Model Selection

Insufficient resource information on the porphyry occurrences in the Central Anatolian Crystalline Complex precluded classification according to the molybdenum and gold contents and ratio criteria used here. However, available information indicates a Mo-(Cu) metal association in known Late

Cretaceous porphyry prospects, consistent with their relation to relatively exhumed felsic I-type metaluminous to peraluminous intrusions. Porphyry-style mineralization related to younger latest Cretaceous (to middle Eocene?) extensional A-type alkaline magmatism has not been confirmed. However, some of the numerous quartz-fluorite-gold veins associated with syenitic intrusions in this cratonic setting could potentially represent the upper parts of underlying alkalic porphyry systems (Jensen and Barton, 2000).

Given that there was no sufficient resource data, a pooled *t*-test assuming equal variances could not be run. Thus, the general porphyry Cu-Au-Mo model of Singer and others (2008) was selected to estimate undiscovered copper, gold, molybdenum, and silver resources in this sub-tract, realizing that the Mo-(Cu) metal association in these small porphyry deposits is not well represented in the grade-and-tonnage model.

Estimates of Undiscovered Deposits and Rationale

In the Anatolide-Tauride–Central Turkey sub-tract, geologic factors favorable for the occurrence of undiscovered porphyry deposits include (1) permissive Late Cretaceous calc-alkaline magmatism and (2) permissive latest Cretaceous (to middle Eocene?) extension-related alkaline magmatism developed in thick and warm cratonic crust. Unfavorable factors for the occurrence of undiscovered porphyry copper deposits include (1) Late Cretaceous collisional setting with magma compositions that appear, in general, too felsic, (2) negligible sizes and copper grades in known Mo-(Cu) porphyry deposits (for example, Balışeyh), (3) metal associations in porphyry systems that are probably not well represented in the grade-and-tonnage model, (4) high exhumation and deeper levels of preservation, (5) lack of known younger latest Cretaceous to middle Eocene porphyry-related prospects, and (6) extensive post-middle Eocene cover.

The density of known porphyry deposits in the Pontide (Asia)–Central Turkey sub-tract is low compared to densities in well-explored tracts of this size around the world, which suggests that undiscovered deposits are likely present. However, the low numbers of known porphyry occurrences observed in the Central Anatolian Crystalline Complex also suggest that the geologic conditions for generation and exposure of Late Cretaceous porphyry copper systems are unfavorable and (or) that undiscovered deposits (particularly those that may be related to the younger alkalic suite) may be present but remain unidentified.

Overall, these factors led the assessment team to establish that the Anatolide-Tauride–Central Turkey sub-tract exhibited low geological favorability and that high levels of uncertainty in the estimation of undiscovered deposits were expected. Nevertheless, it was decided that quantitative assessment of undiscovered deposits in this tract was warranted. Table 6b–A shows the consensus estimates for undiscovered porphyry copper deposits in the Anatolide-Tauride–Central Turkey sub-tract at the 90-, 50-, and 10-percent probability levels and the associated summary statistics. At the 90- and 50-percent probability levels, the likelihood of undiscovered deposits was estimated at zero. At the 10-percent probability level, assessors thought that there were

grounds for the presence of one undiscovered porphyry copper deposit. This resulted in a mean of 0.33 undiscovered deposits with a standard deviation of 0.62 ($C_v\%=189$), reflecting the limited favorability and high uncertainty assessed for this porphyry copper sub-tract.

Probabilistic Assessment Simulation Results

Simulation results for estimates for copper, molybdenum, gold, silver, and the total volume of mineralized rock are summarized in table 6b–B. The mean estimate of undiscovered copper resources in the Anatolide–Tauride–Central Turkey porphyry sub-tract is 1.3 Mt. Results of the Monte Carlo simulation are also presented as cumulative frequency plots (fig. 24B). The cumulative frequency plots show the cumulative probabilities of occurrence–estimated resources and total mineralized rock, as well as the mean for each commodity and for total mineralized rock.

Anatolide–Tauride–Eastern Turkey–Caucasus Sub-tract (142pCu9005c)

Descriptive model: General porphyry copper (Cox, 1986a; Berger and others, 2008; John and others, 2010)

Grade and tonnage model: General Cu–Au–Mo porphyry copper model (Singer and others, 2008)

Geologic feature assessed: Late Cretaceous to late Eocene back-arc and island-arc magmatism of the Tethyan Eurasian Metallogenic Belt

Magmatism

The Anatolide–Tauride–Eastern Turkey–Caucasus sub-tract covers an area of 21,700 km² (fig. 22). It delimits a Late Cretaceous to late Eocene intraoceanic volcano–plutonic belt in the eastern Anatolide Tauride Terrane. Permissive igneous units (appendix B) used to define this sub-tract are shown in figure 23, along with locations of igneous complexes and other geologic features mentioned in this section.

Across eastern Turkey, the southern Lesser Caucasus, and northernmost Iran, Late Cretaceous to middle late Eocene magmatism consists of Late Cretaceous–Paleocene continental–arc magmatism in the Bitlis–Pötürge Terrane and latest Cretaceous to middle–late Eocene back-arc and intraoceanic–arc magmatism in the eastern Anatolide–Tauride Terrane (South Armenian Block). Late Cretaceous–Paleocene continental arc magmatism is separated here into another tract, given that it is believed to have developed offshore on the Bitlis–Pötürge microcontinent before it amalgamated with the Anatolide–Tauride Terrane (see Border Folds tract below). Thus, this section focuses only on the magmatism associated with the latest Cretaceous to middle–late Eocene extensional back-arc and island-arc environment of the Inner Tauride Ocean in the region. Back-arc and intraoceanic–arc rocks extend into central Iran and form part of the Esfahan tract, which, given differences in the tectonic evolution, is also treated separately in this report (see Esfahan tract below).

In eastern Turkey, Late Cretaceous to middle Eocene back-arc magmatism is represented by early calc-alkaline to late alkaline felsic to intermediate plutons that intruded ophiolite-bearing thrust sheets derived from the Northern Neotethys Ocean Branch, as well as coeval Paleocene–Eocene marine successions deposited in an extensional back-arc setting related to the north-dipping subduction zone and associated Baskil or Border Folds Arc along the Southern Neotethys Ocean Branch. Geochronologic and geochemical data from major plutons in this region indicate a general younging of magmatism from about 83 Ma in the south to 69 Ma in the north and a south-to-north progression from arc-related I-type calc-alkaline to back-arc-related alkaline compositional signatures (Kuşçu and others, 2010).

Back-arc and intraoceanic magmatism is represented by ± 44 -Ma volcano–plutonic units that are spatially associated with the northeast-striking accretionary belt that trends along the boundaries between the Anatolide–Tauride Terrane and the Central Anatolian Crystalline Complex in the west and the Transcaucasus Terrane in the east. These igneous rocks were emplaced during convergence of the Inner Tauride Ocean. They host well-known Au–(Cu) and Cu–Mo–Au porphyry systems. Geochemical data on these igneous units indicate a transitional calc-alkaline to alkaline setting (Kadioglu and Dilek, 2010; Gençlioğlu–Kuşçu and others, 2001; Boztuğ and others, 2007; Kuşçu and others, 2010).

Late Cretaceous to middle Eocene rocks are superseded by younger middle to late Eocene andesitic rocks and associated shallow-water sediments, which are overthrust by nappes containing ophiolite and Paleocene to middle Eocene volcanic and flysch, as well as metamorphic basement (Yığıtbaş and Yılmaz, 1996). These middle–late Eocene rocks are part of the calc-alkaline intermediate to felsic Helete intraoceanic island arc (fig. 23) that was active between the Arabian Platform and the Bitlis–Pötürge microcontinent and associated alkaline to tholeiitic mafic Maden back-arc rift that developed to the rear in eastern Turkey (Aktaş and Robertson, 1984; Yılmaz, 1993; Şengör and Yılmaz, 1981; Dercourt and others, 1986; Kazmin and others, 1986). This intraoceanic arc and back arc projects into northwestern Iran where it is juxtaposed against the Late Cretaceous Kermanshah and Late Cretaceous to Eocene Khoy (fig. 3) ophiolite-bearing accretionary complexes (Azizi and Moinevaziri, 2009; Agard and others, 2011; Hassanipak and Ghazi, 2000; Azizi and Jahangiri, 2008). The Maden Basin closed during collision between the Arabian Platform and Eurasia (Gençlioğlu–Kuşçu and others, 2001; Yılmaz, 1993).

Known Porphyry Deposits and Prospects

In the back-arc environment of the eastern Anatolide–Tauride Terrane, mineralization includes porphyry systems associated with calc-alkaline to alkaline intrusions that are preserved in accretionary complexes (Kuşçu, 2007). Intrusion-related mineralization is represented by Late Cretaceous Fe–(Cu–Au) skarns or iron oxide copper gold (IOCG) deposits, such as at Divriği, and middle Eocene porphyry deposits, such as at Çöpler and Agarak. Ophiolite-bearing accretionary complexes also host

volcanogenic massive sulfide and podiform chromite deposits of mainly Late Cretaceous age (Yigit, 2009; Engin and others, 2000).

The Anatolide-Tauride–Eastern Turkey-Caucasus sub-tract (fig. 22) includes 4 known porphyry copper deposits (table 2) and 11 porphyry prospects (appendix C). Deposits are represented by the 44-Ma Çöpler and Karakartal Au-(Cu) porphyry systems in eastern Turkey (İmer and others, 2013) and the 40–44-Ma Agarak and Dastakert Cu-Mo-Au porphyry systems in southern Armenia (Moritz and others, 2012). Six Cu-Au prospects (Bahce, Bayramdere, Demirmagara, Kabatas, Sabirli, and Zangadere) are located in the Çöpler-Karakartal porphyry district, and three Cu-Mo prospects (Mamlis, Silic, and Sin) occur some 60–80 km further south and east of the Çöpler-Karakartal district (Yigit, 2009). A Late Cretaceous to middle Eocene age for the likely younger Mamlis, Silic, and Sin Cu-Mo porphyry prospects has not been confirmed. The remaining two Cu-Mo prospects (Aigedzor and Misdag) occur in the Agarak-Dastakert porphyry district in southern Armenia.

Çöpler Porphyry Deposit

In eastern Turkey, the 44-Ma (Marinov and others, 2011; İmer and others, 2013) Çöpler Au-(Cu) porphyry-skarn deposit is the site of the second largest mine in the country (Yigit, 2009). In 2007, reported measured and indicated resources were 32.159 Mt at 1.090 g/t gold and 3.46 g/t silver, and inferred resources were estimated at 43.603 Mt at 1.715 g/t gold and 3.13 g/t silver (Yigit, 2009). Copper grade was not reported. However, current proven and probable reserves at Çöpler include 86.4 Mt at 0.117 percent copper, 1.53 g/t gold, and 4.47 g/t silver. Measured and indicated resources are 139.9 Mt at 0.15 percent copper, 1.6 g/t gold, and 4.74 g/t silver (Bascombe and others, 2012).

The deposit is centered on a composite diorite to monzonite porphyry stock emplaced into metasediments and limestone-marbles producing both stockwork- and skarn-type mineralization. The two dominant alteration styles are (1) quartz-manganese-carbonate-barite veinlets hosted by K-silicate alteration and (2) quartz-pyrite replacements in limestone (Yigit, 2006). The bulk of the mineralization is associated with the former alteration style. Mineralization related to main-stage K-silicate and quartz-pyrite replacement is overprinted by late-stage base-metal intermediate-sulfidation epithermal mineralization (Marek and others, 2008).

Karakartal Porphyry Deposit

The Karakartal (formerly known as Kabatas) Cu-Au deposit is located about 10 km southeast of Çöpler. It is described as a porphyry copper-gold deposit with a surface projection that is about 350 m in diameter (Alacer Gold, 2012; Lıdy Madencilik, 2013f). Drilling has identified copper and gold mineralization to a depth of 235 m (Kociumbas and Page, 2009). Reported resources are 70.8 Mt at 0.25 percent copper and 0.32 g/t gold (Mining Journal, 2010). The deposit is centered on a diorite to monzonite porphyry stock that intrudes hornfelsed metasediments and limestones. A strong K-silicate core with chalcocopyrite, pyrite, and magnetite stockworks is bordered by quartz-sericite-pyrite alteration (Alacer Gold, 2012).

Kabatas (South) Porphyry Prospect

The 51-Ma (Marinov and others, 2011) Kabatas (South) Cu-Au-(Mo)-bearing porphyry and associated skarn prospect is located about 15 km southeast of Çöpler. Here, diorite, monzonite, and monzodiorite porphyry sills, dikes, and stocks intrude Late Cretaceous metacarbonates (Yigit, 2009). Biotite alteration hosts chalcocopyrite and bornite mineralization and is overprinted by sericite and clay alteration (Kuşcu and others, 2013).

Agarak and Dastakert Porphyry Deposits

The Agarak and Dastakert porphyry deposits are located in southern Armenia. These deposits are characterized by high molybdenum and gold grades associated with partly alkaline intrusive complexes (Zvezdov and others, 1993; Gugushvili and others, 2010; Kirkham and Dunne, 2000).

The 44–40-Ma (Moritz and others, 2012) Agarak Cu-Mo-Au porphyry deposit (Kekelia and others, 2001; GeoProMining, 2012) has a reported resource of 125 Mt at 0.56 percent copper, 0.025 percent molybdenum, and 0.6 g/t gold (Singer and others, 2008). The deposit is centered on calc-alkaline to alkaline porphyry intrusions of syenite-granite and granodiorite composition. Cu-Mo-Au-(Ag-Zn-Pb-Bi) mineralization occurs as bornite, chalcocopyrite, molybdenite, sphalerite, galena, enargite, tetrahedrite/tennantite, and bismuthinite (Singer and others, 2008). The occurrence of enargite suggests the presence of a high-sulfidation environment.

The nearby 44–40-Ma (Moritz and others, 2012) Dastakert Cu-Mo-(Au) porphyry deposit has a reported resource of 33 Mt at 0.62 percent copper and 0.047 percent molybdenum (Global Metals, Ltd., 2013). Here, andesite, gabbro-diorite, granodiorite, quartz diorite, and hornfels are cut by calc-alkaline to alkaline synmineral diorite porphyry and late lamprophyre dikes (Singer and others, 2008). Cu-Mo-Au-(Ag-Zn-Pb-Bi) mineralization occurs as bornite, chalcocopyrite, molybdenite, sphalerite, galena, enargite, tetrahedrite/tennantite, and bismuthinite (Singer and others, 2008). The occurrence of enargite and chalcocite and covellite, respectively, suggests the presence of high-sulfidation and supergene environments.

Mamlis and Sin Porphyry Prospects

At the Mamlis Cu-Mo-Au-bearing porphyry prospect, highly altered Eocene (and Miocene?) dacitic pyroclastics and andesitic lavas subjected to greenschist metamorphism are intruded by quartz diorite and quartz monzonite porphyry intrusions (Yigit, 2009). The mineralization consists of quartz-chalcocopyrite veins accompanied by molybdenum and stockworks with galena and sphalerite. Around 1 g/t of gold is associated with mineralization. Numerous limonite-quartz veins, breccia zones, and gossans cover an area of 1 by 2 km. At the nearby Sin Cu-Mo-Au-bearing porphyry prospect, disseminated and stockwork copper and gold mineralization at the periphery of a dacite unit occupies an area of 300 by 1,000 m (Akinci, 2004). Mineralization could be middle Eocene but is more likely Oligocene-Miocene in age (see Azerbaijan tract below).

Preservation Level

As derived from the geologic maps of Turkey (General Directorate of Mineral Research and Exploration, 2000), the Lesser Caucasus (Kekelia and others, 2001), and Iran (Huber, 1978), overall volcanic-to-plutonic ratios of permissive Late Cretaceous to middle Eocene units in the Anatolide-Tauride–Eastern Turkey-Caucasus sub-tract are relatively high ($\{\text{volcanic}/[\text{volcanic}+\text{plutonic}]\} \times 100 = 74$). However, Late Cretaceous to middle Eocene plutons are well exposed around the Çöpler deposit, to the east in easternmost Turkey (where coeval volcanic rocks are entirely absent), and around the Agarak deposit in Armenia (where the batholith is composed of older Eocene, as well as younger Oligocene-Miocene, plutons).

Across the entire sub-tract, proportions of basement (20 percent), permissive plutonic and volcanic (2 and 7 percent, respectively; see fig. 23), nonpermissive mafic, volcano-sedimentary and sedimentary (16 percent), and cover units (50 percent) suggest that permissive unit exposures are reduced, levels of preservation for porphyry systems are shallow, and the extent of younger cover is relatively extensive. In general, these factors limit appropriate exposure of porphyry systems in much of the sub-tract.

Magnetic Anomalies

Regional aeromagnetic maps (Ates and others, 1999; Maus and others, 2009) were used to confirm the location and character of regional geologic features (for example, arcs, basins, faults, terrane boundaries). Across eastern Turkey and the Lesser Caucasus, magnetic anomalies are difficult to interpret, because signatures are not systematic. They appear to reflect igneous rocks of different compositions and ages, which are in part preserved in ophiolite-bearing accretionary belts. Both the Çöpler and Agarak porphyry districts in eastern Turkey and Armenia are surrounded by horseshoe-shaped magnetic highs. The gravity anomaly map of Turkey (Ates and others, 1999), in general, shows a more systematic negative anomaly across much of the eastern Anatolide-Tauride Terrane, which indicates increasingly thicker crust towards the east. Much of the crustal thickening occurred during the late Miocene to Holocene following collision between the Arabian Platform and Eurasia.

Probabilistic Assessment

Grade and Tonnage Model Selection

In the Anatolide-Tauride–Eastern Turkey-Caucasus sub-tract both Au-(Cu) and Cu-Mo metal associations of porphyry systems are found. The Au-(Cu) association such as that exhibited by the Çöpler deposit is related to intermediate alkaline to calc-alkaline intrusions characteristic of intraoceanic island-arc or back-arc settings. The more felsic alkaline to calc-alkaline Cu-Mo-Au metal association at the Agarak deposit indicates a similar setting but also indicates increased assimilation of continental crust or craton-derived materials. Criteria based on molybdenum and gold allow classification of the Çöpler and Karakartal porphyry deposits in

the eastern segment of the tract into the Cu-Au subtype. Resource data are not sufficient to classify the Agarak Cu-Mo-Au deposit. However, pooled *t*-test results assuming equal variances show that the known deposits in this sub-tract are not significantly different at the 1-percent level from tonnages and copper, molybdenum, silver, and gold grades in the general porphyry Cu-Au-Mo model of Singer and others (2008). Therefore, the general model was selected to estimate undiscovered copper, gold, molybdenum, and silver resources in this sub-tract. In comparison to the median tonnage and grade in the general porphyry Cu-Au-Mo model, deposits in this tract exhibit smaller tonnages. However, Çöpler and Karakartal show higher gold grades and Agarak shows higher copper, molybdenum, and gold grades than the median deposit in the model.

Estimates of Undiscovered Deposits and Rationale

In the Anatolide-Tauride–Eastern Turkey-Caucasus sub-tract, geologic factors favorable for the occurrence of undiscovered porphyry deposits include (1) island arc(s) emplaced in a large extensional intraoceanic basin, (2) permissive alkaline to calc-alkaline magmas, (3) known Au-(Cu) porphyry-skarn (for example Çöpler) and Cu-Mo-Au porphyry (for example, Agarak) deposits, and (4) appropriate levels of exposure along uplifted accretionary prisms. Unfavorable factors for the occurrence of undiscovered porphyry deposits include (1) relatively extensive cover and (2) tonnages in known deposits that are lower than the median in the global porphyry copper tonnage model.

The density of known porphyry copper deposits is lower than that of well-explored tracts of equivalent aerial extent elsewhere. This suggests that undiscovered deposits are likely present. The assessment team felt that the relatively small copper resources presently identified at the Çöpler and Karakartal Au-Cu deposits will likely grow as deeper parts of these porphyry systems are mined. A moderate level of exploration is also suggested by the relatively low number of known porphyry occurrences in this favorable geologic setting. These factors led the assessment team to establish that the Anatolide-Tauride–Eastern Turkey-Caucasus sub-tract was favorable but that moderate to high levels of uncertainty in the estimation of undiscovered deposits were expected. The tract would contribute significant copper resources from undiscovered deposits to the overall assessment. Therefore, quantitative assessment of undiscovered deposits in this tract was warranted.

Table 6c–A shows the consensus estimates for undiscovered porphyry copper deposits in the Anatolide-Tauride–Eastern Turkey-Caucasus sub-tract at the 90-, 50-, and 10-percent probability levels and the associated summary statistics. At the 90-percent probability level, the likelihood of undiscovered deposits was estimated at zero. The estimates increased to 2 and 4 at the 50- and 10-percent probability levels, respectively. This resulted in a mean of 2.23 undiscovered deposits with a standard deviation of 2.04 ($C_v\% = 92$). This result reflects the level of favorability

and moderate to high uncertainty assessed for this tract. The estimated total deposit density per 100,000 km² obtained is comparable to median porphyry deposit densities expected in well-explored tracts of equivalent size elsewhere around the world (Singer and Menzie, 2010).

Probabilistic Assessment Simulation Results

Simulation results for estimated for copper, molybdenum, gold, silver, and the total volume of mineralized rock are summarized in table 6c–B. The mean estimate of undiscovered copper resources in the Anatolide–Tauride–Eastern Turkey–Caucasus porphyry sub-tract is 8.2 Mt. Results of the Monte Carlo simulation are also presented as cumulative frequency plots (fig. 24C). The cumulative frequency plots show the cumulative probabilities of occurrence–estimated resources and total mineralized rock, as well as the mean for each commodity and for total mineralized rock.

Lut Cretaceous Tract (142pCu9006)

Descriptive model: Porphyry copper (Cox, 1986a; Berger, 2008; John and others, 2010)

Geologic feature assessed: Late Cretaceous to Paleocene continental arc of the Tethyan Eurasian Metallogenic Belt

Location

The Lut Cretaceous tract covers an area of 12,000 km² within the Lut Terrane of eastern Iran (fig. 25). It delimits a poorly preserved and erratically exposed north-northwest–south-southeast 800-km-long subduction-related magmatic arc of Late Cretaceous–Paleocene age. The Lut Terrane is bounded by the right-lateral Nayband Fault on the west and by the right-lateral Nehbandan Fault on the east. The northern and southern limits of the Lut Terrane are further marked by the left-lateral Doruneh Fault on the north and the Jaz Murian Depression of the Makran Terrane on the south, respectively (fig. 3). The Lut Cretaceous tract is superimposed in part by the younger Lut Tertiary tract (see below).

Tectonic Setting

By the Early Jurassic, the Yazd, Kashmar–Kerman, and Tabas Terranes had amalgamated with the Lut Terrane to form the east-central Iranian microcontinental collage. During Early Jurassic–Early Cretaceous times, rifting along the northern and eastern margins of this microcontinent opened the Sabzevar and Sistan Oceans, respectively (Dercourt and others, 1986). This event was followed by Late Cretaceous resumption of northward convergence (fig. 4C), as well as subduction and arc magmatism along the southern margin of the Lut Terrane (Golonka, 2004). At that time, the present-day eastern margin of the Lut Terrane was facing south. Magmatism associated with this event defines the Lut Cretaceous tract described in this section.

This event was followed by middle Eocene to early Oligocene convergence between India, Afghanistan, and the East-Central Iranian Terranes with Eurasia (fig. 4E), initiating

closure of the Sistan Ocean (Golonka, 2004) and concurrent ±90-degree counterclockwise rotation of the east-central Iranian microcontinental collage (Westphal and others, 1986; Dercourt and others, 1986).

Magmatism and Known Porphyry Prospects

Permissive igneous units (appendix B) used to define the Lut Cretaceous tract are shown in figure 26, along with locations of igneous complexes and other geologic features mentioned in this section. Late Cretaceous plutonism in the Lut Terrane (fig. 25) is represented by the Gazu, Bajestan, and Bazman volcano-plutonic complexes and associated porphyry and possible porphyry-related occurrences (Karimpour and Stern, 2011; Berberian and others, 1982; Geological Survey of Iran, 2012e).

The Gazu (75.2 Ma) and Bazman (74.2 Ma) granodiorites are I-type calc-alkaline plutons with evolved geochemical signatures that indicate formation in a continental-arc setting in felsic cratonic crust (Karimpour and others, 2011b). Geochemical results on the Bajestan (76.6 Ma) granite indicate a more peraluminous S-type affinity, suggesting emplacement in a collisional setting. However, this signature is also consistent with assimilation of large fractions of felsic crustal materials in a subduction-related environment. Related Late Cretaceous–Paleocene volcanism is represented by the Vaghi (61.6 Ma) and Junchi (56.7 Ma) felsic ignimbrites, which exhibit evolved geochemical signatures similar to those at Gazu and Bajestan (Karimpour and Stern, 2011).

The Gazu Cu–Mo–(Au) porphyry-skarn prospect (appendix C) is located near the Lut–Tabas Terrane boundary (fig. 25). It consists of a stockwork and minor hydrothermal breccia related to Late Cretaceous diorite, monzodiorite, and monzonite porphyry intrusion emplaced into Triassic and Jurassic sedimentary rocks. Reported grades are 0.4–2 percent copper, 5–12 part per million (ppm) molybdenum, and 2.4 ppm gold (Samani, 1998). Alteration includes strong quartz-sericite-pyrite, calc-silicate, and propylitic mineral associations. High concentrations of copper and zinc occur along the contact zone between intrusive and country rocks. Extensive gossan developed over the deposit (Darbani and others, 2005).

The Bajestan batholith is a 26- by 4-km east-west trending pluton that intrudes Jurassic slates and quartzites (appendix C). The pluton consists of pyroxene quartz microdiorite in the east and hornblende-biotite granodiorite-granite in the west. The granitic phase displays porphyritic textures about its margins. Hydrothermal alteration is characterized by tourmaline, but no significant tin, molybdenum, or copper mineralization is reported (Karimpour and others, 2011b). This possible porphyry-related occurrence is included in appendix C.

Possible porphyry-related mineralization may also occur in the Bazman Complex (fig. 26). This Late Cretaceous complex is composed of minor hornblende-biotite diorite-granodiorite and augite-hornblende gabbro that are cut by porphyritic hornblende-biotite granite (74.2 Ma; Karimpour and others, 2011b). Aplitic dikes intrude these units and are themselves cut by younger diabasic dikes (Berberian and Berberian, 1981; Berberian and others, 1982). These rocks

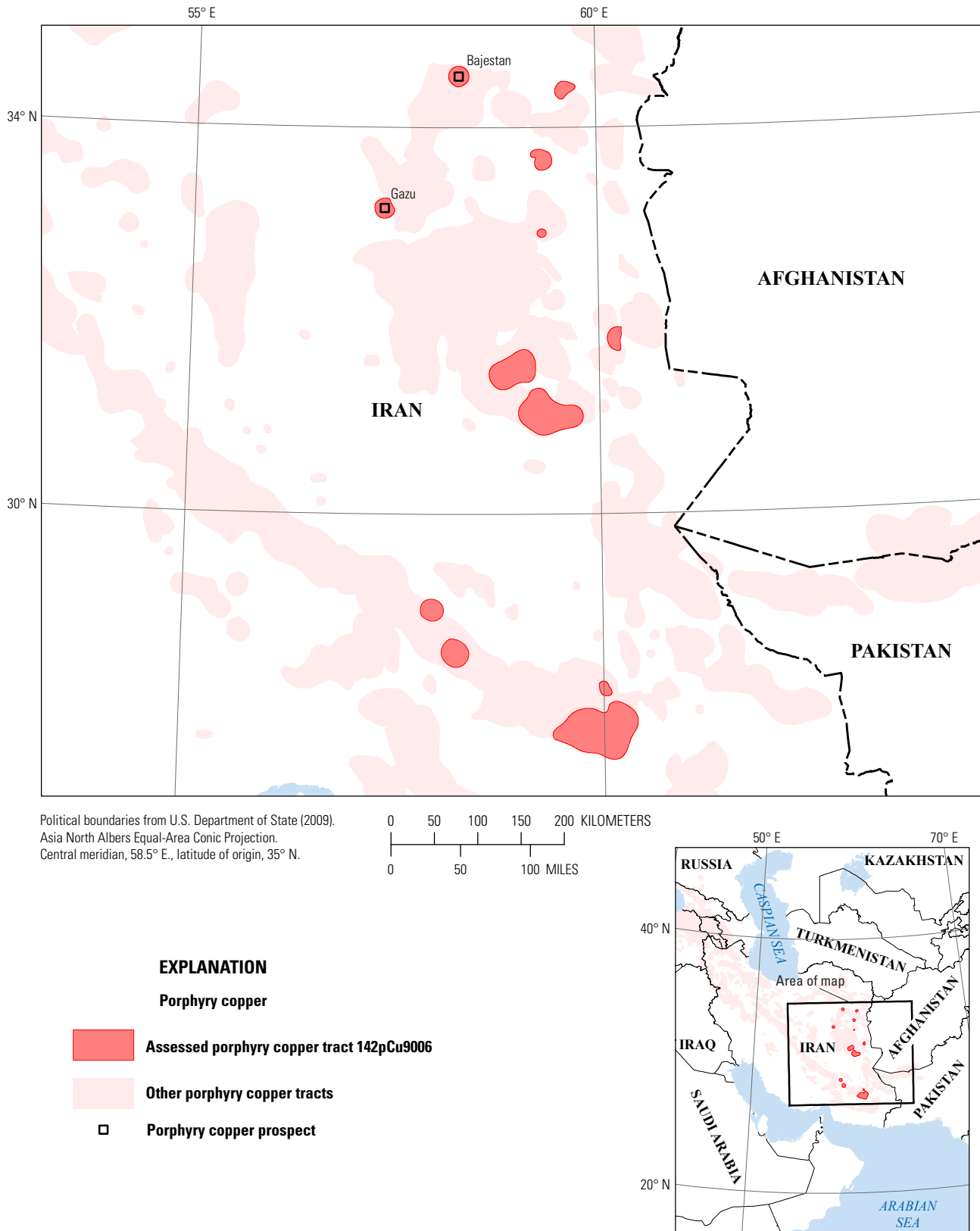
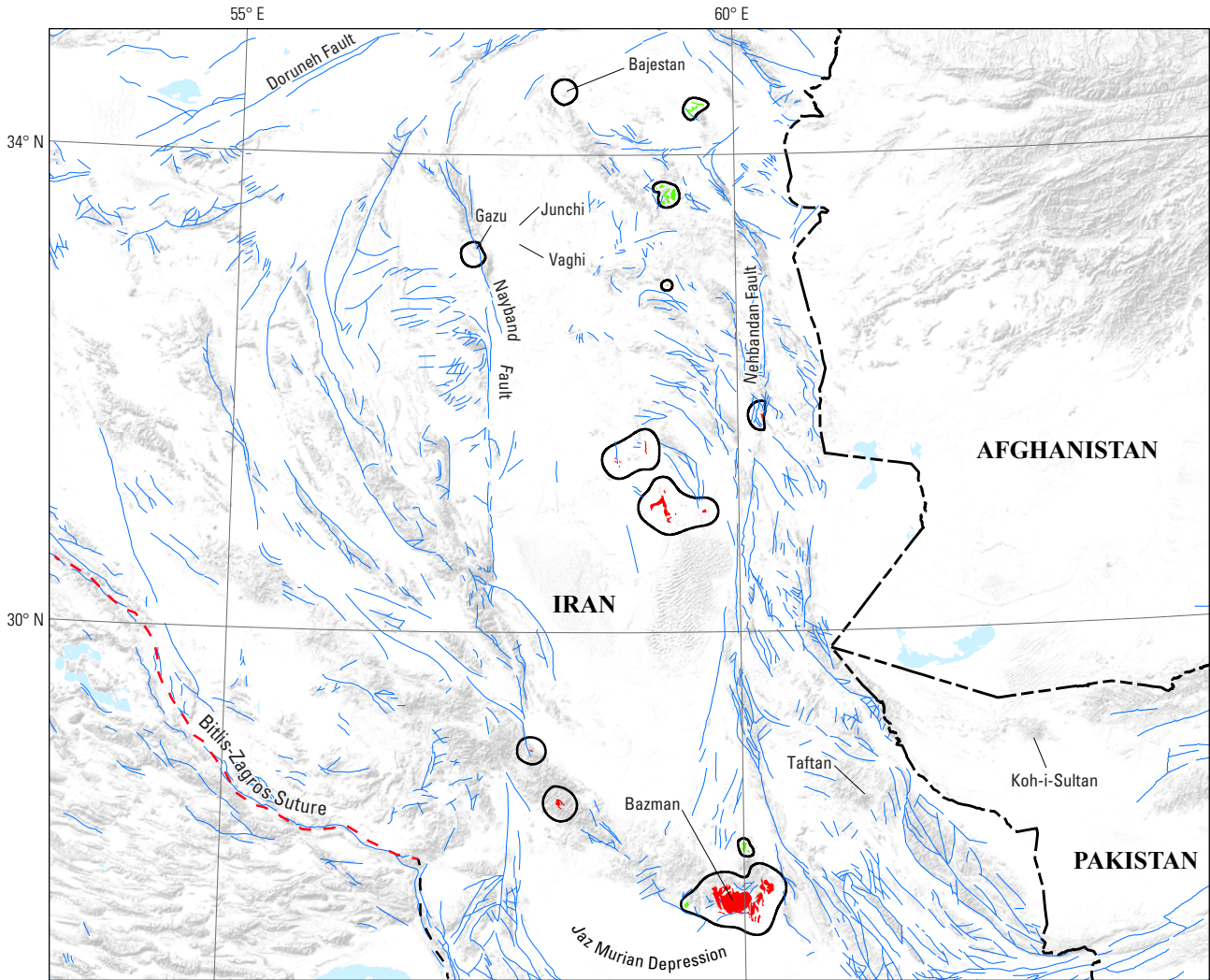
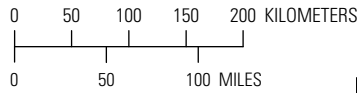


Figure 25. Map showing the location of known porphyry copper prospects for permissive tract 142pCu9006, Lut Cretaceous—Iran. See appendix C for prospects and appendix D for accompanying spatial data.



Base from SRTM Global Digital Elevation Model, U.S. Geological Survey EROS Data Center, 2006. Political boundaries from U.S. Department of State (2009). Asia North Albers Equal-Area Conic Projection. Central meridian, 58.5° E., latitude of origin, 35° N.



- EXPLANATION**
- Porphyry copper**
 - Assessed porphyry copper tract 142pCu9006
 - Permissive intrusive rock
 - Permissive extrusive rock
 - Fault
 - Suture
 - Transform fault
 - Junchi **Geologic feature discussed in the text**



Figure 26. Map showing the distribution of permissive intrusive and extrusive rocks used to define tract 142pCu9006, Lut Cretaceous—Iran. See appendix A for principal sources of information and appendix B for source map units.

are hydrothermally altered in parts. However, the Bazman Complex is largely covered by Pliocene-Holocene volcanic rocks of the Bazman-Taftan-Koh-i-Sultan Arc, which are also hydrothermally altered. Therefore, the age of this hydrothermal alteration has not been established. A 5-km-wide ASTER-derived phyllic alteration zone occurs in this area (Mars, 2014).

Qualitative Assessment

The occurrence of porphyry copper deposits is permissive in this relatively long-lived and mature continental-arc setting. However, factors that considerably diminish the likelihood for the occurrence of undiscovered deposits in this tract include poor preservation, extensive cover (74 percent of the tract area), and deeper levels of preservation of porphyry systems as suggested by a low {volcanic/[volcanic+plutonic]} \times 100 ratio of 16 and by the existence of peraluminous compositions (fig. 26). No resource estimate is available for the only positively identified porphyry copper prospect (Gazu). In addition, the low number of known porphyry-related occurrences, which are not only an indication of limited geologic endowment and (or) inadequate level of exposure but also a likely reflection of the lack of exploration, further add considerable uncertainty. Despite the permissive geology and the presence of one positively identified porphyry prospect, the assessment team felt that the favorability was too low to add significant undiscovered copper resources to the overall assessment (less than a 10-percent chance of 1 undiscovered deposit). Therefore, quantitative assessment of the Lut Cretaceous tract was not warranted.

Border Folds Tract (142pCu9007)

Descriptive model: Porphyry copper (Cox, 1986a; Berger and others, 2008; John and others, 2010)

Grade and tonnage model: General Cu-Au-Mo porphyry copper model (Singer and others, 2008)

Geologic feature assessed: Late Cretaceous to early Paleocene continental arc of the Tethyan Eurasian Metallogenic Belt

Location

The Border Folds tract covers an area of 45,300 km² across southeastern Turkey, northeasternmost Iraq, and northwestern Iran (fig. 27). It delimits a variably exhumed and irregularly preserved 1,500-km-long and 70–150-km-wide continental arc of Late Cretaceous-early Paleocene age. The Border Folds tract trends parallel to the Bitlis-Zagros Suture, which represents the former site of the associated subduction zone. The tract is generally confined to the Bitlis-Pötürge and Sanandaj-Sirjan Terranes. However, small segments of it also project into the Bitlis-Zagros Thrust Zone. The Border Folds tract is partially superimposed by the associated back-arc settings of the Late Cretaceous to late Eocene volcano-plutonic events delimited by the Anatolide-Tauride–Eastern Turkey-Caucasus sub-tract (see above) and Esfahan tract (see below).

Tectonic Setting

The ophiolite-bearing Bitlis-Zagros Suture marks the location of not only 1 but 2 north-dipping subduction zones that developed in the Southern Neotethys Ocean Branch (Robertson and others, 2006). The first subduction event (Neotethys I of Ghasemi and Talbot, 2006; Yilmaz, 1993) is preserved in ophiolite complexes and island-arc rock associations that were obducted over the northeastern margin of the Arabian Platform in the Late Cretaceous (Moghadam and others, 2009; Dewey and others, 1973). This accretional event is represented by the Kermanshah and Neyriz intraoceanic arc systems (fig. 3). The second subduction event (Neotethys II of Ghasemi and Talbot, 2006) occurred along the southern margin of the Sanandaj-Sirjan Terrane (fig. 4C) and had been active since the Jurassic (see Sanandaj-Sirjan Tract above). It generated Late Cretaceous-early Paleocene Andean-type continental arc magmatism that propagated over time from the southeast to the northwest across northwestern Iran and southeastern Turkey (Azizi and Jahangiri, 2008; Shahabpour, 2005, 2007; Şengör and Yilmaz, 1981; Şengör and others, 1993). This volcano-plutonic event is known as the Baskil Arc (Kuşçu and others, 2010) or Border Folds Arc (Yigit, 2009). Associated deformation produced southwest-vergent folds, an overprint of greenschist facies metamorphism (Azizi and Jahangiri, 2008; Mohajjel and others, 2003; Kaymakci and others, 2010), and mafic to felsic calc-alkaline and alkaline magmatism (Berberian and Berberian, 1981; Berberian and King, 1981; Şengör and others, 1991).

Late Cretaceous-early Paleocene compression was followed by pronounced back-arc extension and magmatism (Alavi, 1994; Shahabpour, 2007; Omrani and others, 2008; Agard and others, 2011; Verdel and others, 2011). This event deposited voluminous largely subaqueous late Paleocene to middle Eocene calc-alkaline to shoshonitic rocks (see Anatolide-Tauride–Eastern Turkey-Caucasus sub-tract above and Esfahan tract below) and widespread subaqueous to subaerial late Oligocene-early Miocene calc-alkaline to alkaline rocks (see Azerbaijan–Eastern Turkey sub-tract below). These Paleocene-Eocene and Oligocene-Miocene events preceded the collision and related deformation between the Arabian Platform and the Eurasian margin.

Magmatism

In the Bitlis-Pötürge and Sanandaj-Sirjan Terranes (fig. 3), middle to Late Cretaceous andesite, andesitic basalt, and basalts interbedded with shale, sandstone, and calcareous rocks indicate a period of subsidence (Azizi and Moinevaziri, 2009). This event was followed by the compressional Late Cretaceous-early Paleocene Baskil or Border Folds juvenile to mature continental arc (the Border Folds tract described in this section). This volcano-plutonic event was associated with a north-dipping subduction zone located in the Southern Neotethys Ocean Branch between the converging Arabian Platform and the Eurasian margin (Golonka, 2004; Kazmin and others, 1986). Permissive igneous units used to define the Border Folds tract (appendix B) are shown in figure 28, along with locations of igneous complexes and other geologic features mentioned in this section.

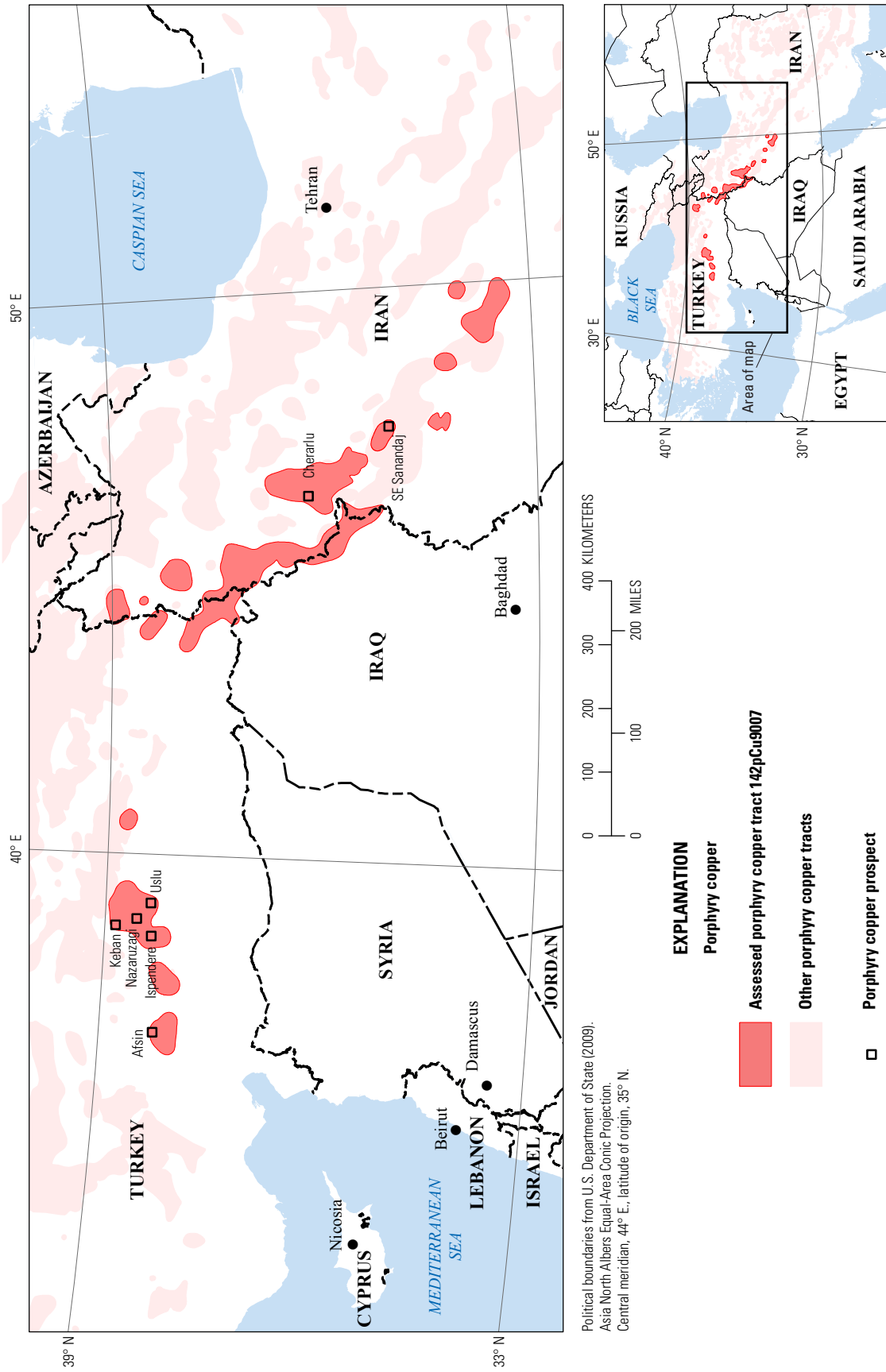


Figure 27. Map showing the location of known porphyry copper prospects for permissive tract 142pCu9007, Border Folds—Iran, Iraq, and Turkey. See appendix C for prospects and appendix D for accompanying spatial data.

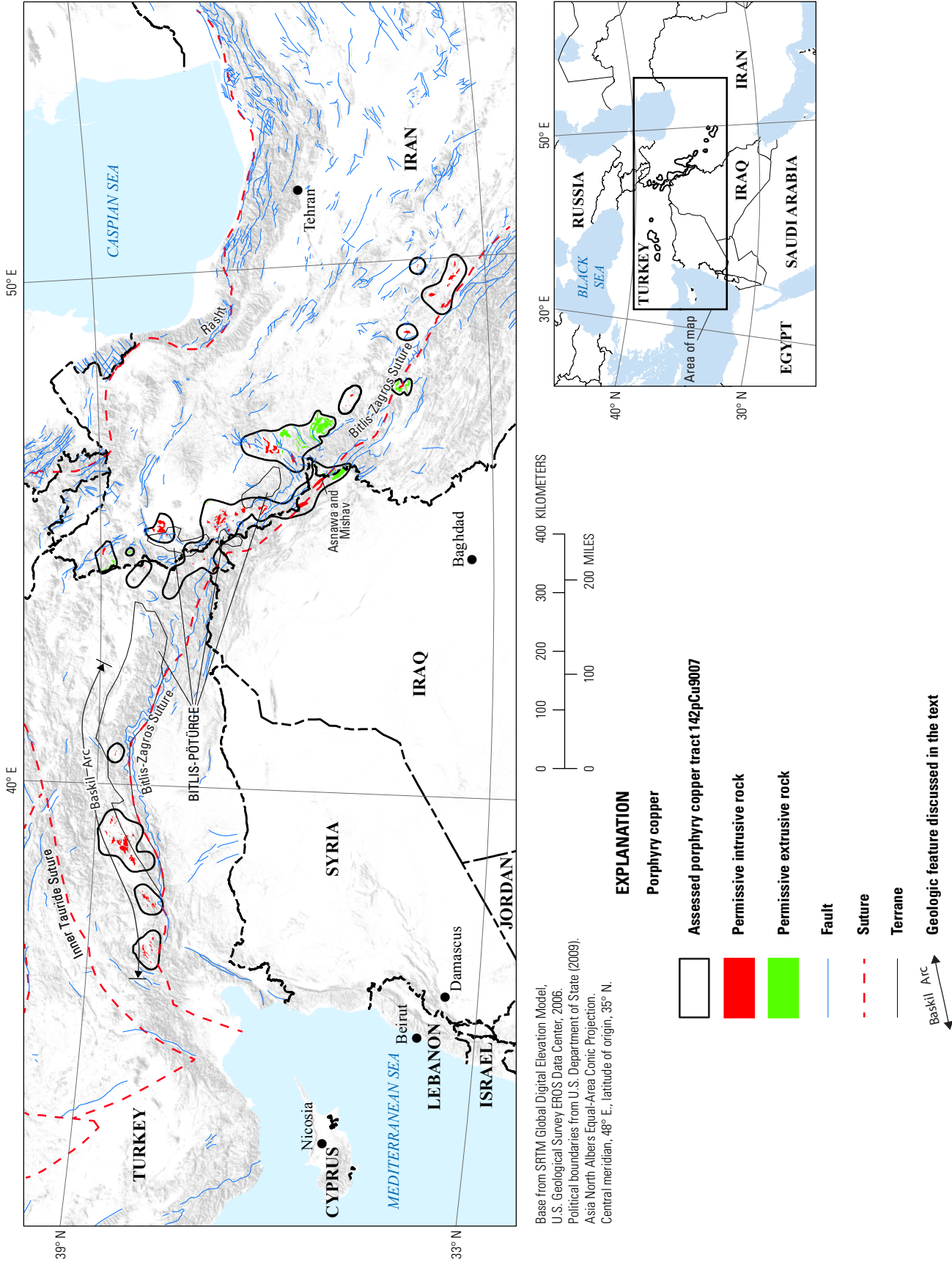


Figure 2B. Map showing the distribution of permissive intrusive and extrusive rocks used to define tract 142pCu9007, Border Folds—Iran, Iraq, and Turkey. See appendix A for principal sources of information and appendix B for source map units.

In southeastern Turkey, Campanian calc-alkaline to Maastrichtian alkaline volcanic and intrusive rocks postdate ophiolite obduction and unconformably overlie and intrude low-grade metamorphic Paleozoic and Mesozoic basement rocks (Oberhänsli and others, 2010). In general, Campanian calc-alkaline suites crop out toward the south about the Bitlis-Pötürge Terrane, whereas younger Maastrichtian alkaline suites occur toward the north in the back-arc setting of the eastern Anatolide-Tauride Terrane (see Anatolide-Tauride–Eastern Turkey-Caucasus sub-tract). Geochemical data on these plutons indicate a transition from island-arc-related juvenile calc-alkaline (83–80 Ma), to mature continental arc-related calc-alkaline and alkaline (75–73 Ma), and to alkaline (71–70 Ma) arc and back arc-related compositions over time (Kuşçu and others, 2010). Intrusive phases include tonalite, granodiorite, diorite, gabbro, and quartz monzonite, which are intruded by younger microdiorite, porphyritic quartz microdiorite, aplite, syenite, and lamprophyre dikes. Late Cretaceous porphyry-skarns, as well as VMS systems, are preserved in this arc back-arc setting (Kuşçu, 2007).

In the northwestern part of the Sanandaj-Sirjan Terrane of Iran, Late Cretaceous volcanic and intrusive rocks also exhibit arc-related calc-alkaline geochemical affinities (Azizi and Jahangiri, 2008). Plutons are commonly surrounded by hornfels halos, exhibit foliation, and intrude greenschist-facies host rocks that are strongly folded along northwest-southeast trending axes. Intrusive complexes are exemplified by 100–93-Ma I-type diorites and granites, 80-Ma alkalic syenites, and S-type muscovite-biotite-garnet granites (Ghahamghash, Nédélec, and others, 2009; Ghahamghash, Bouchez, and others, 2009). Selected Al-in-hornblende data indicate deep exhumation with emplacement depths of 10–14 km in several parts, but coeval volcanic rocks are preserved in fold limbs. Despite permissive igneous compositions, porphyry-related copper mineralization has not been positively identified in this region (Jamali and others, 2012).

Known Porphyry Deposits and Prospects

The Border Folds tract, with only a few known porphyry prospects, is the least explored porphyry belt in Turkey (Yigit, 2009; Global Business Reports, 2012). Porphyry copper prospects are only known in the western part of the tract segment in southeastern Turkey. These include the small Keban Cu-Mo-W-F-Au porphyry and associated skarn deposit and the Ispendere, Uslu, and Nazarusagi Cu-Au porphyry prospects (fig. 27; appendix C). A recent report also adds a Cu-Au porphyry-related prospect at Afsin (Tilavsun), which is located in the westernmost part of the tract (Kuşçu and others, 2013).

With exception of few potential porphyry occurrences of unknown age (Shahabpour, 1999; Azizi and others, 2007; Bazin and Hübner, 1969a; Geological Survey of Iran, 2012e), porphyry copper systems have not been positively identified in the Sanandaj-Sirjan Terrane in Iran. Two possibly porphyry-related occurrences of Late Cretaceous age are tentatively included in appendix C (SE Sanandaj and Cherarlu). The Sanandaj-Sirjan Terrane, instead, is known for its middle to late Mesozoic Pb-Zn-Ba MVT, SEDEX, and VMS (Ghazban and others, 1994; Mirnejad and others, 2011; Rajabi and others, 2012; Förster, 1978;

Meshkani and others, 2011) and for its mostly Eocene orogenic and intrusion-related gold deposits (Niroomand and others, 2011; Nezafati and others, 2005; Nezafati, 2006; Moritz and others, 2006; Richards and others, 2006).

Based on permissive igneous units derived from the geologic map bases of Pollastro and others (1998) and Sissakian (2000), as well as descriptions of the geology (Karim and others, 2008), the Border Folds tract projects into the Bitlis-Zagros thrust zone of northeastern Iraq. This area hosts Triassic-Jurassic stratabound Zn-Pb, Late Cretaceous ophiolite-related Mn-Fe and Cr-Ni-Cu-Fe, and Late Cretaceous-Paleogene iron skarn occurrences (Al-Bassam and Hak, 2006). Of the latter, notable iron skarns occur at Asnawa and Mishav. At Asnawa, two northeast-southwest magnetite replacement bodies with subordinate pyrite, pyrrhotite, chalcopyrite, and arsenopyrite are spatially associated with a diorite that intrudes Late Cretaceous-Paleogene schist and recrystallized limestone units (Al-Bassam, 2008). At Mishav, magnetite-hematite garnet-actinolite skarn replaces limestone and andesitic flows and tuffs. Mineralization appears to be related to small granodioritic intrusions (Al-Bassam and Hak, 2006). The origin of these iron skarns is not well constrained, and an association with porphyry-style mineralization is highly uncertain (G. Fernet, written commun., 2013).

Ispendere Porphyry Prospect

The Ispendere porphyry Cu-Au-bearing prospect is associated with 81-Ma I-type calc-alkaline granodiorite, diorite, and dacite porphyry intrusions. These juvenile arc-related intrusions are part of a 86–75-Ma tonalitic pluton that intruded a Jurassic-Cretaceous ophiolitic complex (Kuşçu, 2007). The east-trending hydrothermal zone consists of weak potassic, phyllic, argillic, and propylitic alteration. Vein and disseminated magnetite-pyrite-chalcopyrite-(bornite) mineralization is generally surrounded by phyllic alteration. Limited chalcocite and covellite are found as supergene minerals (Dumanlilar and others, 1999; Yigit, 2006, 2009; Kuşçu and others, 2013).

Nazarusagi and Uslu Porphyry Prospects

The Nazarusagi (Baskil) Au-Cu-bearing porphyry prospect is related to a 78-Ma arc-related calc-alkaline to alkaline pluton (Kuşçu and others, 2010; Yigit, 2009). Granodiorite, granodiorite porphyry, dacite porphyry, and diorite stocks are cut by granitic and post-ore diabase dikes. These igneous units intrude metamorphic and ophiolitic country rocks. The deposit exhibits biotite, actinolite, epidote-chlorite±(carbonate-magnetite) and quartz-sericite alteration. Mineralization occurs in the form of quartz stockworks and sheeted veins with chalcopyrite, bornite, molybdenite, gold, and bismuth (Kuşçu and others, 2013).

The newly discovered Uslu porphyry copper prospect is located about 30 km southeast of Nazarusagi (Yigit, 2009). Little about this prospect is mentioned in the available literature (Engin and others, 2000). However, the age and dominant copper mineralization suggest that the Nazarusagi and Uslu prospects may be more similar to the Ispendere Cu-Au than to the Keban Cu-Mo-W-F-Au porphyry systems.

Keban Porphyry-Skarn Deposit

The small Keban Cu-Mo-W-F-Au-Pb-Zn porphyry-skarn and vein deposit has a reported resource of 4.5 Mt at 0.092 percent copper and 0.14 percent molybdenum (Engin and others, 2000). The deposit is related to a 69.9-Ma syenite porphyry stock that intrudes a 74-Ma calc-alkaline-alkaline pluton, Late Cretaceous low-grade metamorphic volcanic rocks, and Paleozoic-Lower Triassic phyllites and marbles (Kuşcu and others, 2013). Sericitic, K-silicate, and calc-silicate alteration host pyrite, arsenopyrite, galena, sphalerite, chalcopyrite, and enargite mineralization (Kines, 1969; Kuşcu and others, 2010; Yigit, 2009; Kalender, 2011; Kuşcu and others, 2013). The younger age, geochemical affinity, and metal association of the Keban porphyry system suggest that it was emplaced in an extensional back-arc setting, as proposed by Imer and others (2013).

Preservation Level

In the highly deformed and variably exhumed region delimited by the Border Folds tract, adequacy of exposure levels of porphyry-related mineralization is difficult to assess based on preservation-level data alone. Other geologic factors (such as folding and faulting) likely played a substantial role in either eroding, exposing, or concealing porphyry mineralization.

As derived from the geologic maps of Turkey (General Directorate of Mineral Research and Exploration, 2000), Iran (Huber, 1978), and Iraq (Pollastro and others, 1998), limited preservation of permissive volcanic and plutonic units is evident, with proportions that amount only to 3 and 5 percent, respectively, of the tract area (fig. 28). Older basement (37 percent), broadly coeval nonpermissive units (20 percent), younger cover (30 percent), and inland water bodies (4 percent) occupy the remainder of the tract. Permissive volcanic-to-plutonic ratios across the tract appear appropriate ($\{\text{volcanic}/[\text{volcanic}+\text{plutonic}]\} \times 100 = 42$) for preservation of porphyry systems. However, volcanic-to-plutonic ratios vary from Turkey to Iran across the northwestern, central, and southeastern parts of the Border Folds tract. Very low volcanic-to-plutonic ratios occur in the northwestern and southeastern parts of the tract, whereas higher volcanic-to-plutonic ratios exist in the intervening central part of the tract in northwestern Iran and northeastern Iraq. This central part is also characterized by the occurrence of fewer metamorphic rocks.

Overall, preservation level data suggest that any undiscovered porphyry copper deposits in this otherwise permissive continental-arc setting are (1) completely exhumed in the western part of southeastern Turkey (where there is no tract delimited), (2) variably preserved in the northwestern and southeastern parts of the tract in Turkey and Iran, and (3) largely concealed by coeval volcanic and sedimentary and (or) younger cover units in the intervening central part of the tract in northwestern Iran and northeastern Iraq. Porphyry copper systems (that is, Ispendere, Nazarusagi, Uslu, Afsin, Keban) have only been positively identified in the better preserved northwestern part of the Border Folds tract in

southeastern Turkey. The two possible porphyry occurrences in Iran tentatively included with the Border Folds tract (that is, Chararlu and SE Sanandaj) are also located in a better preserved southeastern part of the tract.

Magnetic Anomalies

Regional aeromagnetic maps (Ates and others, 1999; Maus and others, 2009) were used to confirm the location and character of regional geologic features (for example, arcs, basins, faults, terrane boundaries). The reduced area of the Border Folds tract in northeastern Iraq could not be evaluated because regional aeromagnetic data are not available. Across southeastern Turkey, regional magnetic anomalies that occupy the Bitlis-Pötürge Terrane appear to image its northern boundary. However, these anomalies reflect mostly late Miocene and younger mafic volcanic rocks and thus largely mask the signature of the underlying Late Cretaceous units that define the Border Folds tract. In northwestern Iran, in contrast, smaller and isolated magnetic anomalies do appear to image, at least in part, permissive Late Cretaceous plutonic units. The porphyry prospects in this tract lie along the margins of positive magnetic anomalies.

A relatively subdued but continuous magnetic anomaly projects beyond the boundary of the Border Folds tract to the south about 550 km into the central part of the Sanandaj-Sirjan Terrane. This anomaly reflects magnetic sources under early to Late Cretaceous carbonate rocks. However, these sources may be associated with younger Eocene plutons (see Esfahan tract below).

Probabilistic Assessment

Grade and Tonnage Model Selection

Positively identified porphyry prospects in the Border Folds tract occur only in southeastern Turkey and exhibit contrasting characteristics. The calc-alkaline Ispendere and Nazarusagi Cu-Au porphyry prospects and the small alkaline Keban Cu-Mo-W-F-Au porphyry deposit are 85–75-Ma and 70-Ma old, respectively. These contrasting igneous compositions, metal associations, and ages are consistent with the progressive arc to back-arc evolution of this volcano-plutonic event. There are no published copper resource data on the arc-related Cu-Au porphyry prospects, and the small back-arc-related Keban deposit exhibits a metal association and a copper resource that are not well-represented in the porphyry grade and tonnage models of Singer and others (2008). Consequently, the general porphyry Cu-Au-Mo model was selected to estimate undiscovered copper, gold, molybdenum, and silver resources in this tract.

Estimates of Undiscovered Deposits and Rationale

Favorable geologic factors for the occurrence of undiscovered porphyry copper deposits in the Border Folds tract include (1) a juvenile to mature Andean-type continental-arc setting, (2) permissive calc-alkaline to alkaline magmatic compositions, (3) known Cu-Au porphyry and Cu-Mo

porphyry-skarn occurrences in the western part of the tract, and (4) appropriate levels of exposure that are, however, only locally preserved. Unfavorable geologic factors for the occurrence of undiscovered porphyry copper deposits in the Border Folds tract include (1) superimposed Late Cretaceous and Miocene fold-and-thrust and metamorphic events, where deposits can be exhumed, tectonically concealed, or buried; and (2) the small size of the only known Cu-Mo-W porphyry-skarn deposit with available resource data (Keban) in the tract.

A density of known porphyry deposits that is negligible contrasts with that in other porphyry belts of equivalent size around the world. This suggests that undiscovered deposits are likely present. With exception of the Keban and Nazarusagi districts that are experiencing renewed exploration efforts that may result in the identification of larger copper resources, this region—which is otherwise geologically not only permissive but in parts deemed favorable for the occurrence of undiscovered porphyry deposits—remains underexplored (Yigit, 2009). Furthermore, undiscovered deposits may be concealed in large segments of this complexly deformed and variably preserved tract. Lack of exposure and exploration are reflected by the very low number of known porphyry occurrences.

Overall, these factors led the assessment team to establish that the Border Folds tract exhibited relatively low geological favorability and that high levels of uncertainty in the estimation of undiscovered deposits were expected. Nevertheless, the tract would contribute significant copper resources from undiscovered deposits to the overall assessment. Therefore, quantitative assessment of undiscovered deposits in this tract was warranted. Table 7A shows the consensus estimates for undiscovered porphyry copper deposits in the Border Folds tract at the 90-, 50-, and 10-percent probability levels and the associated summary statistics. At the 90-percent probability level, all assessors estimated that the likelihood of undiscovered deposits was 0. At the 50-percent probability level, several assessors thought that there were grounds for the presence of 1 undiscovered deposit. At the 10-percent probability level, the numbers increased to 2. On the basis of these numbers, the team reached a consensus estimate of 0, 1, and 2 undiscovered deposits at the 90-, 50-, and 10-percent probability levels, respectively. This resulted in a mean of 1.15 undiscovered deposits with a standard deviation of 1.18 ($C_v\%=102$), reflecting the limited favorability and high uncertainty assessed for this tract.

Probabilistic Assessment Simulation Results

Simulation results for estimates for copper, molybdenum, gold, silver, and the total volume of mineralized rock are summarized in table 7B. The mean estimate of undiscovered copper resources in the Border Folds porphyry tract is 4.6 Mt. Results of the Monte Carlo simulation are also presented as cumulative frequency plots (fig. 29). The cumulative frequency plots show the cumulative probabilities of occurrence-estimated resources and total mineralized rock, as well as the mean for each commodity and for total mineralized rock.

Esfahan Tract (142pCu9008)

Descriptive model: Porphyry copper (Cox, 1986a; Berger and others, 2008; John and others, 2010)

Grade and tonnage model: General Cu-Au-Mo porphyry copper model (Singer and others, 2008)

Geologic feature assessed: Late Cretaceous to late Eocene back arc of the Tethyan Eurasian Metallogenic Belt

Location

The Esfahan tract covers an area of 56,900 km². It delimits a large Late Cretaceous to middle and late Eocene back arc-rift volcano-plutonic belt. The tract mainly overlies the Central Iranian Terrane but partially extends to the north into the Alborz Terrane, to the east into the East-Central Iranian Terrane, and to the southwest into the Sanandaj-Sirjan Terrane (fig. 30). This back-arc setting continues to the northwest into the Lesser Caucasus and eastern Turkey, where it overlies the eastern Anatolide-Tauride Terrane (South Armenian Block). Here, it is delimited by the eastern Anatolide-Tauride–Eastern Turkey–Caucasus sub-tract (fig. 22). The Esfahan tract is partially superimposed on the older Sanandaj-Sirjan and Border Folds tracts (figs. 5, 6), and it is in part overlain by the younger Azerbaijan–Caucasus–Iran porphyry sub-tract (see below).

Tectonic Setting

Several scenarios have been proposed for the origin and subsequent evolution of the Late Cretaceous to late Eocene igneous rocks that occupy much of central Iran. However, it is generally accepted that they are associated with the extensive back-arc environment that developed to the rear of the Late Cretaceous–Paleocene Andean-type continental arc (Berberian and King, 1981) that occurred along the evolving Eurasian active margin to the southwest (see Border Folds tract above).

Berberian and Berberian (1981) and Omrani and others (2008) propose that the Late Cretaceous–Paleocene Border Folds Arc that developed across the Bitlis-Pötürge and Sanandaj-Sirjan Terranes migrated onto the southern margin of the Central Iranian Terrane. Igneous rocks associated with this arc-building event are best-preserved along the Urumieh-Dokhtar Magmatic Belt (fig. 2). This eastward arc migration is interpreted to have resulted from a shallowing of the subduction slab dip associated with a fast-to-slow change in convergence rate between the Arabian Platform and the Sanandaj-Sirjan Terrane (McQuarrie and others, 2003; Azizi and Jahangiri, 2008; Agard and others, 2011).

Ghasemi and Talbot (2006) and Azizi and Moinevaziri (2009), on the other hand, propose the existence of two subduction zones operating in the Southern Neotethys Ocean southwest of the Sanandaj-Sirjan Terrane. These two subduction zones were independently responsible for the generation of Late Cretaceous island-arc magmatism between the Arabian Platform and the Sanandaj-Sirjan Terrane (Kermanshah and Neyriz complexes of Azizi and Moinevaziri, 2009; and Babaie and others, 2001) and Late Cretaceous and younger continental arc magmatism on

Table 7. Probabilistic assessment for tract 142pCu9007, Border Folds—Iran, Iraq, and Turkey.

A. Undiscovered deposit estimates, deposit numbers, tract area, and deposit density.

[N_{xx} , estimated number of deposits associated with the xxth percentile; N_{und} , expected number of undiscovered deposits; s , standard deviation; $C_v\%$, coefficient of variance; N_{known} , number of known deposits in the tract that are included in the grade and tonnage model; N_{total} , total of expected number of deposits plus known deposits; tract area, area of permissive tract in square kilometers (km^2); deposit density reported as the total number of deposits per 100,000 km^2 . N_{und} , s , and $C_v\%$ are calculated using a regression equation (Singer and Menzie, 2005)]

Consensus undiscovered deposit estimates					Summary statistics					Tract area (km^2)	Deposit density ($N_{total}/100,000 km^2$)
N_{90}	N_{50}	N_{10}	N_{05}	N_{01}	N_{und}	s	$C_v\%$	N_{known}	N_{total}		
0	1	2	4	4	1.2	1.2	100	0	1.2	45,300	3

B. Results of Monte Carlo simulations of undiscovered resources.

[Cu, copper; Mo, molybdenum; Au, gold; and Ag, silver; in metric tons; Rock, in million metric tons]

Material	Probability of at least the indicated amount						Probability of	
	0.95	0.9	0.5	0.1	0.05	Mean	Mean or greater	None
Cu	0	0	760,000	10,000,000	20,000,000	4,600,000	0.22	0.31
Mo	0	0	0	250,000	570,000	120,000	0.16	0.54
Au	0	0	0	270	530	120	0.20	0.51
Ag	0	0	0	2,900	6,400	1,400	0.17	0.63
Rock	0	0	190	2,100	3,900	930	0.23	0.31

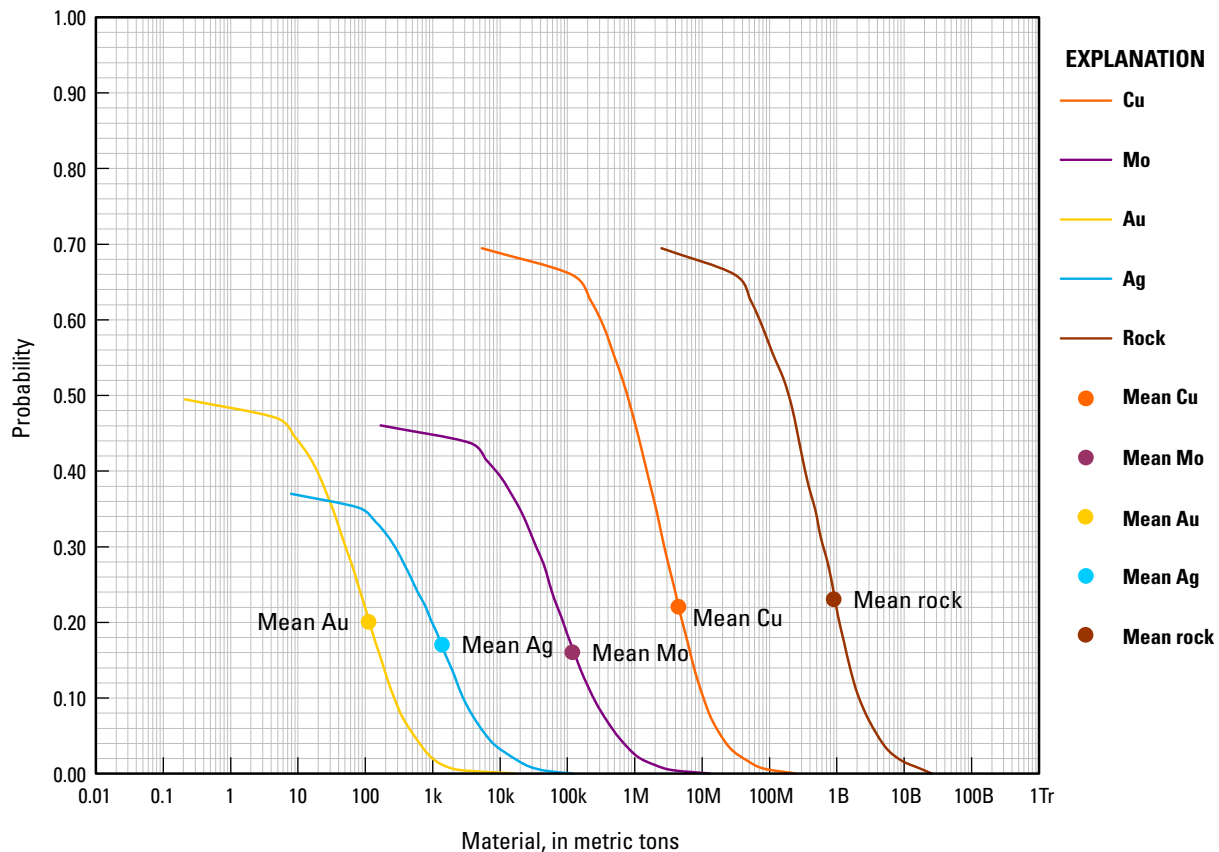


Figure 29. Cumulative frequency plot showing the results of Monte Carlo computer simulation of undiscovered resources in porphyry copper deposits in tract 142pCu9007, Border Folds—Iran, Iraq, and Turkey. k, thousand; M, million; B, billion; Tr, trillion.

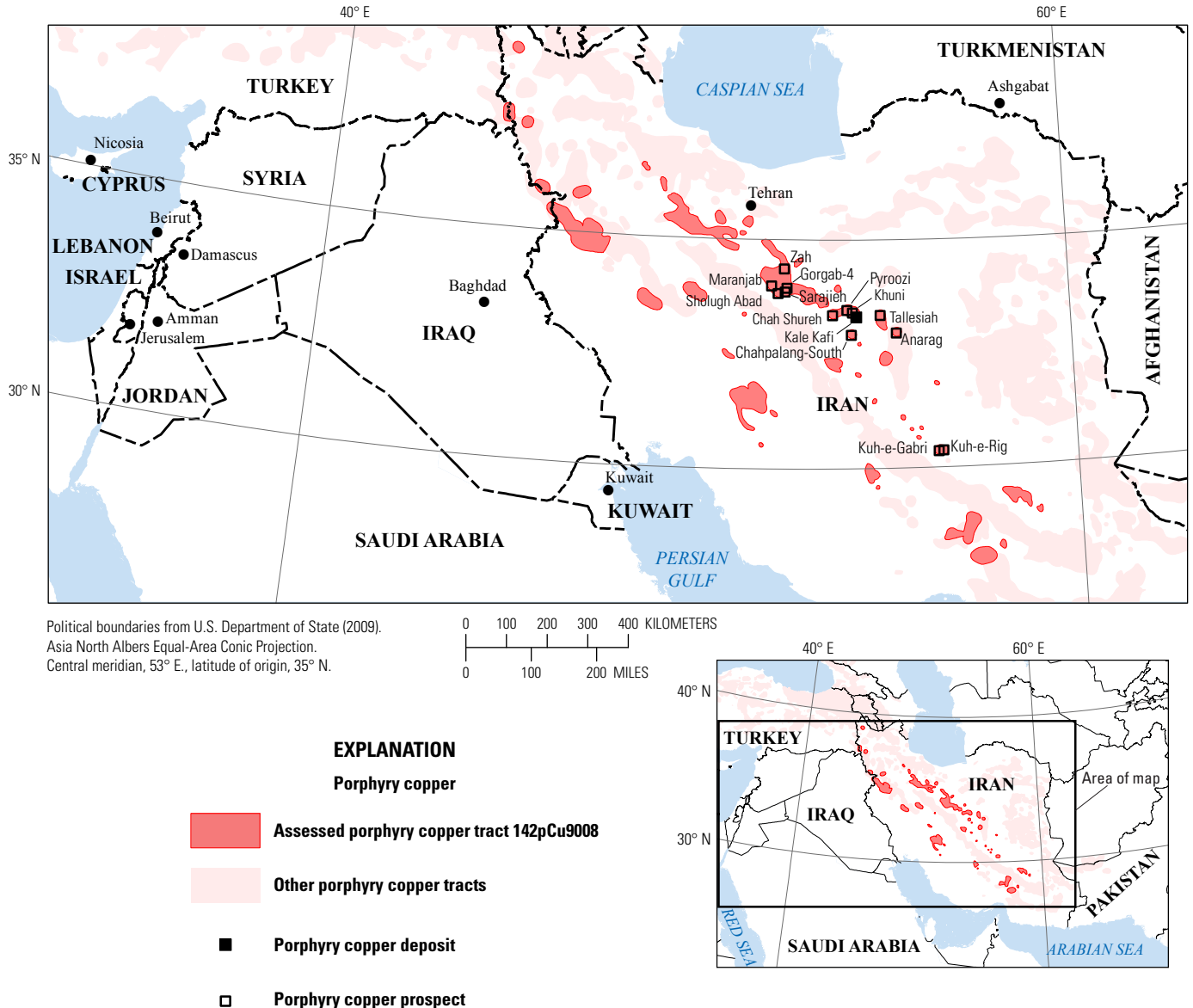


Figure 30. Map showing the location of known porphyry copper deposits and prospects for permissive tract 142pCu9008, Esfahan—Iran, Iraq, and Turkey. See table 2 for deposits, appendix C for prospects, and appendix D for accompanying spatial data.

the Sanandaj-Sirjan (that is, Border Folds) and Central Iranian Terranes (that is, Urumieh-Dokhtar Magmatic Belt).

Ghazi and Hassanipak (2000) and Arfania and Shahriari (2009) also propose two individual subduction-related arcs. However, to explain the Late Cretaceous Border Folds and younger Urumieh-Dokhtar arc settings, one subduction zone along the southern margin of the Sanandaj-Sirjan and the other one between the Sanandaj-Sirjan and Central Iranian Terranes, respectively, are proposed. Evidence given is that island-arc rocks are preserved in the ophiolitic mélanges, such as the Khoy and the Nain-Baft complexes (fig. 3), that mark the boundary between the Sanandaj-Sirjan and Central Iranian Terranes in northwestern and southeastern Iran.

In either of the scenarios proposed, geologic and geochemical data from Late Cretaceous to late Eocene

volcanogenic products support a widespread extensional back-arc rift setting that developed on the Central Iranian Terrane (fig. 4D) to the rear of the continental arc built on the Bitlis-Pötürge and Sanandaj-Sirjan Terranes (Alavi, 1994; Shahabpour, 2007; Verdel, 2009; Ghorbani, 2006).

In the middle Eocene, the rate of convergence between the Arabian Platform and the Eurasian margin increased again along a shallow-dipping subduction zone (McQuarrie and others, 2003) that produced slab-rollback (Verdel and others, 2011). The combined effect generated subsidence and subaqueous deposition of great volumes of calc-alkaline to shoshonitic and alkaline (Shahrbabaky, 1997) volcano-sedimentary, ignimbritic, and volcanic deposits in the back-arc region in the Central Iranian Terrane. During the middle and late Eocene, the back arc propagated rapidly to the north into

the Alborz Terrane (Stalder, 1971) and to the south across the arc axis into the Sanandaj-Sirjan Terrane (fig. 3). This extensional process culminated with formation of cordilleran metamorphic core complexes in the East-Central Iranian and Sanandaj-Sirjan Terranes (Verdel, 2009).

Back-arc extension across much of Iran was followed in the late Eocene-early Oligocene by the initiation of oblique collision between the Arabian Platform and the Eurasian margin in northwestern Iran (Ghasemi and Talbot, 2006; Robertson and Mountrakis, 2006; Berberian and others, 1982; Agard and others, 2005; Horton and others, 2008). Associated uplift was superseded in turn by renewed early Oligocene to middle Miocene subsidence and formation of a deep sedimentary basin across much of the preexisting Late Cretaceous to late Eocene back arc, further attenuating the continental crust in the region (Morley and others, 2009; Reuter and others, 2009; Shahabpour, 2005, 2007). Renewed uplift in the middle and late Miocene occurred during final collision between the Arabian Platform and the Eurasian margin in southeastern Iran (Mohajjel and others, 2003; Berberian and others, 1982). This changed the extensional regime to a compressional setting that resulted in inversion of earlier basins producing shortening distributed mostly across the Sanandaj-Sirjan and Alborz Terranes (fig. 3). Pliocene-Holocene right-lateral strike-slip displacements, principally along the Bitlis-Zagros suture zone where offset over the past 3–5 m.y. is estimated between 50 and 70 km, further document the oblique nature of the continuing collisional process (Talebian and Jackson, 2002).

Magmatism

The Esfahan tract (fig. 30) delimits calc-alkaline to shoshonitic and alkaline magmatism emplaced as part of a widespread and largely subaqueous Late Cretaceous to late Eocene volcano-sedimentary dominated back-arc rift event. However, it appears to be not only represented by intraoceanic arcs but also by arcs that partially developed on the margins of intervening microcontinental fragments rifted from the Alborz and Kopet Dagh Terranes to the north. The back-arc rock association consists mainly of subordinate volcanic flows that are interlayered with successions of volcano-sedimentary rocks as much as several kilometers thick (Alavi, 1996). Exposures of coeval plutonic rocks are rare, and they are only present along uplifted structural zones. Permissive igneous units (appendix B) used to define the Esfahan tract are shown in figure 31, along with locations of igneous complexes and other geologic features mentioned in this section.

East-Central Iran

The Lut, Tabas, Kashmar-Kerman, and Yazd Terranes (fig. 3) form the east-central Iranian microcontinental collage. These terranes are separated from each other along right-lateral fault systems and from the Central Iranian Terrane along the left-lateral Great Kafir-Doruneh Fault system.

In the Tabas and Lut Terranes, Late Cretaceous-Paleocene uplift and erosion associated with arc magmatism was followed by late Paleocene to middle Eocene normal faulting, subsidence, and unconformable deposition of

subaqueous and lesser subaerial calc-alkaline-dominated volcano-sedimentary and volcanic successions (Verdel and others, 2011). This extensional regime generally occurred in the back-arc region of the Late Cretaceous-Paleocene Border Folds Arc on the Sanandaj-Sirjan Terrane (see Border Folds tract above). However, association of this volcanism with the Late Cretaceous-Paleocene arc magmatism on the Lut Terrane cannot be precluded (see Lut Cretaceous above). If the Lut Terrane is restored to its more east-west disposition before its ± 90 -degree counterclockwise rotation, the Border Folds and Lut Cretaceous arcs may have formed part of a continuous subduction system.

In the Kashmar-Kerman Terrane to the west, a 52-Ma high-grade metamorphic gneissic and migmatitic complex is intruded by large late- to post-kinematic calc-alkaline diorite-granite plutons and aplitic dikes of early Eocene age (47–44 Ma; Ramezani and Tucker, 2003). The metamorphic complex is largely the product of anatexis followed by exhumation associated with extensional cordilleran metamorphic core complex formation (Verdel and others, 2007). A partially preserved and structurally juxtaposed Eocene succession of shallowly emplaced andesite, sandstone, and gypsiferous marl attest to the fact that extensional processes were active in the area during this time period. Furthermore, these rocks occur along a complex tectonic zone that includes post-Eocene collision-related deformation along right-lateral and reverse faults with horizontal block rotation and localized uplift (Verdel, Wernicke, Hassanzadeh, and others, 2011; Verdel, Wernicke, Ramezani, and others, 2007).

In the Yazd Terrane, middle and late Eocene submarine and subaerial basic to felsic volcano-sedimentary rocks, pyroclastics, and lesser lava flows were deposited under similar conditions to those in the Tabas and Lut Terranes. Early Eocene units are overlain by late Eocene volcanogenic successions that include greater volumes of trachybasalt to trachydacite, rhyolite, andesite, and dacite flows (Amidi and Michel, 1985). Exposed coeval plutonic rocks are scarce. However, in the structurally disrupted Kale-Kafi area near the tectonic boundary between the Yazd and Central Iranian Terranes, Proterozoic to Lower Cambrian metamorphic units and Paleocene latite, dacite, and andesite tuffs and lavas are intruded by monzogabbro, quartz syenite, muscovite pegmatite (56 Ma) and biotite-hornblende granite porphyry (53 Ma) stocks and dikes with associated porphyry-style mineralization (Nezampour and Rasa, 2005). Middle Eocene volcano-sedimentary and volcanic units with shoshonitic compositions that postdate the Kale-Kafi complex are widespread in the region (Ahmadian and others, 2009).

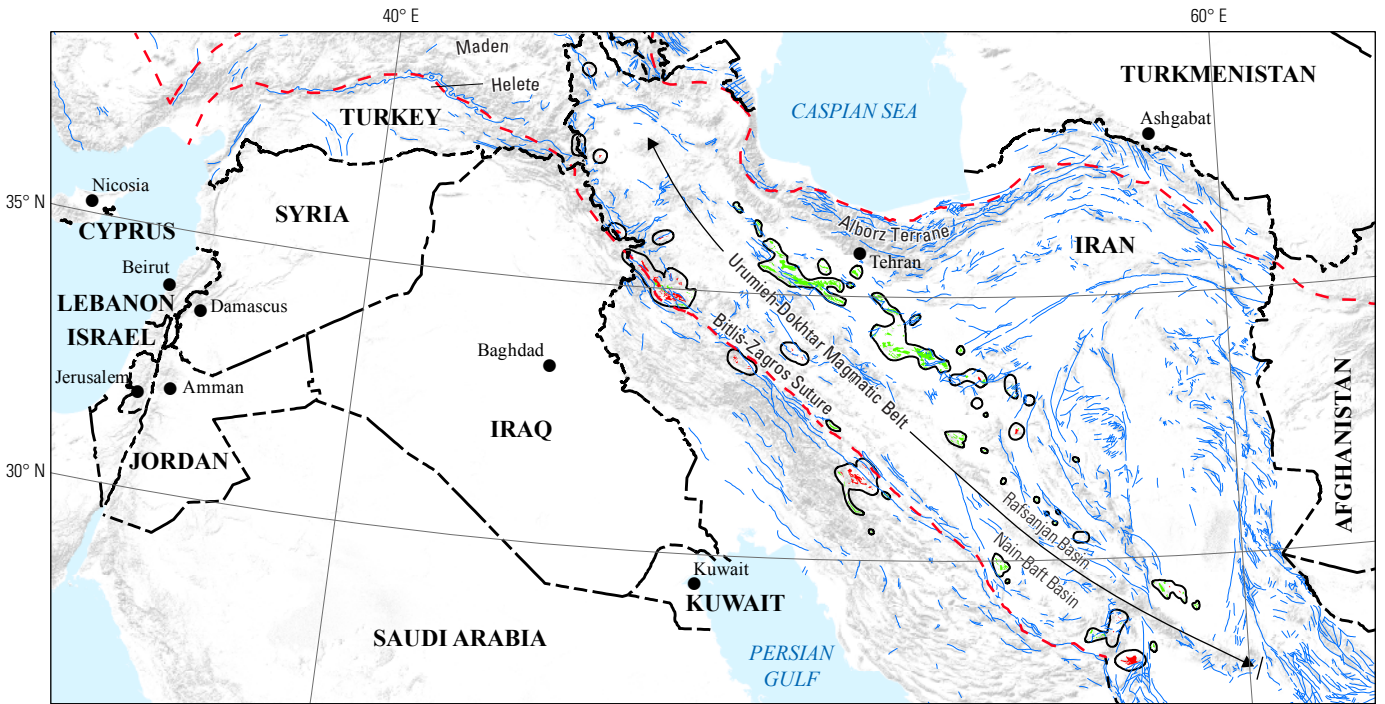
Further south along the boundary between the Yazd and Central Iranian Terranes, the Eocene section is exemplified by four volcano-sedimentary sequences that culminate with lava flows (Amidi and Michel, 1985). Flows in the first subaqueous sequence consist of alkaline mafic-intermediate lavas, the second subaerial and third subaqueous sequences include calc-alkaline dacites and rhyolite lavas, and the fourth sequence is capped by alkaline lavas. Coeval intrusive rocks are not exposed.

Central Iran

In the late Paleocene to late Eocene, central Iran experienced marked normal faulting, subsidence, and deposition of as much as 4-km-thick calc-alkaline, shoshonitic, and alkaline successions of mafic to felsic tuffs and lavas (Alavi, 1996; Azizi and Moinevaziri, 2009). These rocks have major- and trace-element contents that indicate continental-arc to back-arc affinity (Chatroodi and others, 2010; Verdel and others, 2011). The lavas are intercalated with shallow-water marine volcano-sedimentary rocks of the Karaj Formation, which unconformably overlie Paleocene and older

units (Ghasemi and Talbot, 2006). On the southern flanks of the central Alborz Mountains, the Karaj Formation alternates with thick evaporitic deposits, indicating less subsidence and deposition in a coastal environment (Stöcklin, 1968).

As many as six different early to late Eocene phases of volcanic activity have been recognized in central Iran (Torabi, 2009). Units consist of calc-alkaline rhyolite, tuff, and ignimbrite followed by mafic to felsic andesite, high-K andesite, dacite, rhyodacite, and rhyolite. An example of an Eocene section (Amidi and others, 1984; Omrani and others, 2008) includes, from bottom to top, (1) early Eocene alkaline trachybasaltic, trachyandesitic,



Base from SRTM Global Digital Elevation Model, U.S. Geological Survey EROS Data Center, 2006. Political boundaries from U.S. Department of State (2009). Asia North Albers Equal-Area Conic Projection. Central meridian, 53.5° E., latitude of origin, 35° N.

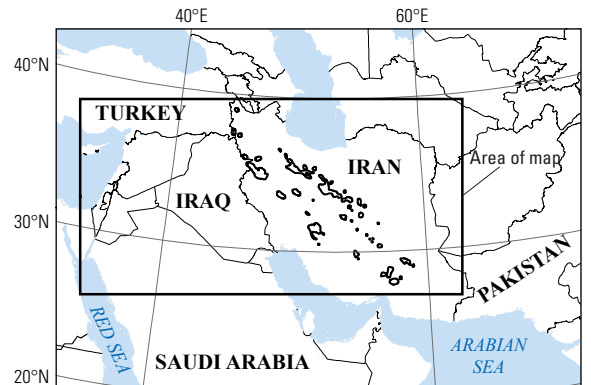
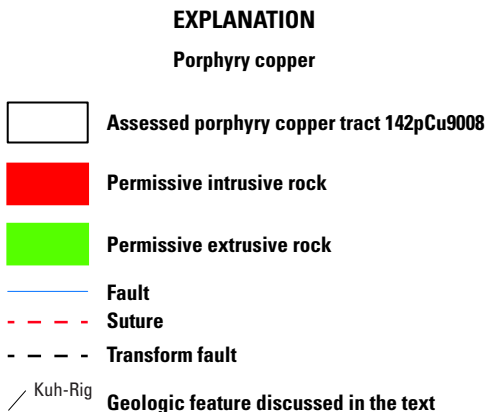
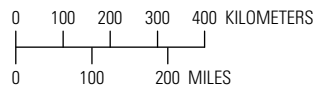


Figure 31. Map showing the distribution of permissive intrusive and extrusive rocks used to define tract 142pCu9008, Esfahan—Iran, Iraq, and Turkey. See appendix A for principal sources of information and appendix B for source map units.

shoshonitic, and trachytic lava flows interlayered with tufts and agglomerates capped by calc-alkaline rhyolitic lava flows; (2) middle Eocene gypsiferous marls, limestones, conglomerates and felsic tufts; and (3) late Eocene calc-alkaline rhyodacitic ignimbrites overlain by alkaline intermediate lava flows, subaerial rhyolitic to rhyodacitic tufts, and subaqueous calc-alkaline rhyolite and shoshonitic mafic to intermediate flows.

Northwestern Iran

The middle-late Eocene Helete island-arc and Maden back-arc environments of eastern Turkey (see Anatolide-Tauride–Eastern Turkey-Caucasus above) project into northwestern Iran (Azizi and Moinevaziri, 2009; Agard and others, 2011), where they form part of the Khoy ophiolite-bearing accretionary complex (fig. 3). The Khoy complex includes Late Cretaceous oceanic crust with tholeiitic MORB (mid-ocean-ridge basalt; Pessagno and others, 2005) and back-arc (Azizi and Jahangiri, 2008) signatures, and the complex is unconformably overlain by calc-alkaline island-arc pyroclastic units. This intraoceanic-arc and back-arc setting that projects from eastern Turkey into northwestern Iran closed by the early Oligocene, and thus it contrasts with the extensional regime that prevailed into the Miocene further south in central Iran.

Western Iran

In western Iran, late Paleocene to middle Eocene extension-related back-arc magmatism propagated westwards onto the Sanandaj-Sirjan Terrane, partially overprinting the Late Cretaceous Border Folds Arc and associated Kermanshah ophiolite-bearing island-arc complex. Plutonic rocks include calc-alkaline granodiorites and granites (Niroomand and others, 2011), syenogabbros, syenodiorites, and syenites (Agard and others, 2011; Leterrier, 1985) to more evolved high-K calc-alkaline, slightly peraluminous monzogranites (Mazahri and others, 2011). No porphyry mineralization has been identified in this region. Reported mineralization of Eocene age consists instead of orogenic and (or) intrusion-related gold deposits (Aliyari and others, 2012; Moritz and others, 2006; Nezafati and others, 2005; Nezafati, 2006; Niroomand and others, 2011). These deposits were emplaced along ductile-brittle normal faults in an extensional regime that included cordilleran metamorphic core complex formation (Verdel and others, 2007).

Southeastern Iran

Similar to eastern Turkey and northwestern Iran, but in contrast to central Iran, southeastern Iran hosts two parallel belts of ophiolite complexes: the Neyriz belt along the Zagros Thrust that marks the suture between the Arabian Platform and Sanandaj-Sirjan Terranes; and the Nain-Baft belt that marks the suture between the Sanandaj-Sirjan and Central Iranian Terranes (fig. 3). The Late Cretaceous Neyriz ophiolitic complex (which correlates in time and character with the Kermanshah ophiolite complex in northwestern Iran) includes Late Cretaceous ultramafic rocks intruded by Paleocene-Eocene early gabbros and late

calc-alkaline diorites and plagiogranites and associated volcanic and volcanoclastic rocks. Geochemical data show that these rocks have juvenile island-arc affinity (Babaie and others, 2001).

The Nain-Baft ophiolitic mélange (which correlates in time and character with the Khoy ophiolite complex in northwestern Iran) and associated basin to the rear consist of Late Cretaceous sedimentary rocks and Late Cretaceous to Paleocene ultramafic units, diabases, pillow lavas, andesites, dacites, and plagiogranites with diverse island-arc, tholeiite, oceanic island basalt (OIB), calc-alkaline, and within-plate geochemical signatures. These data are consistent with a back-arc setting (Arfania and Shahriari, 2009). These Late Cretaceous and Paleocene sedimentary and igneous rocks are unconformably overlain by Eocene shallow marine volcano-sedimentary successions, which are in turn unconformably covered by a younger Oligocene-Miocene sedimentary formation (Morley and others, 2009). Plutonic rocks emplaced in this Oligocene-Miocene basin, which has been under compression since the late Miocene, are represented by the high-K calc-alkaline, partially porphyritic Kuh-e-Gabri and Kuh-e-Rig intrusions (fig. 30) (Shahabpour, 2005, 2007).

Known Porphyry Deposits and Prospects

Porphyry copper systems have not been identified in the part of the Esfahan tract that lies in the highly exhumed Sanandaj-Sirjan Terrane. Late Cretaceous-Eocene mineralization is instead represented by relatively deep-seated orogenic and (or) intrusion-related gold deposits that have been exposed to the surface by extensional structures (Moritz and others, 2006). In contrast, porphyry copper systems may have not been identified in the part of the Esfahan tract that lies in the Central Iranian Terrane, likely because they are concealed under shallowly emplaced volcano-sedimentary and volcanic rocks. In this area, Late Cretaceous-Eocene mineralization is represented by abundant more shallowly emplaced VMS and epithermal deposits (Förster, 1978; Geological Survey of Iran, 2012e) and also several subvolcanic possible Climax-type porphyry molybdenum occurrences (Geomatics Management, [n.d.]).

Late Cretaceous-Eocene plutonic rocks and associated porphyry prospects are more widely exposed in the part of the Esfahan tract in the Yazd Terrane, where post-Eocene tectonic events have variably uplifted and exhumed rocks along structural zones (fig. 30). Accordingly, Cu-Mo-W porphyry and skarn systems are preserved in this region (Samani, 1998; Nezampour and Razza, 2005).

The Esfahan tract includes 1 porphyry deposit (Kale-Kafi; table 2), 4 known porphyry and porphyry-related prospects (Chah Shureh, Khuni, Maranjab, and Sholugh Abad), 9 other possible porphyry-related occurrences located around the boundary between the Yazd and Central Iranian Terranes (the Anarag historic mining district, Chapalang-South, Gorgab-4, Pyroozi, Sarajieh, Tallesiah, and Zah), and another 2 younger porphyry-related occurrences (Kuh-e-Gabri and Kuh-e-Rig) near the Kashmar-Kerman and Yazd Terrane boundary (appendix C, figs. 3, 30).

Kale Kafi Porphyry Deposit

The Kale Kafi Cu-Mo-(Au-W) deposit has a reported resource of 245 Mt at 0.26 percent copper, 0.026 percent molybdenum, and 0.1 g/t gold (Singer and others, 2008). The deposit is centered on premineral monzogabbro, quartz syenite, and muscovite pegmatite (56 Ma) and synmineral biotite-hornblende granite porphyry (53 Ma) stocks and dikes. These intrude highly exhumed Proterozoic schist and marble and tectonically juxtaposed Cretaceous sedimentary units and Paleocene tuffs and lavas (Moghaddasi and Mohammadi, 2010; Nezampour and Razza, 2005; Ahmadian and others, 2009; Kirkham and Dunne, 2000). Mineralization occurs within a 1,400- by 700-m zone of quartz stockwork with K-feldspar and weak biotite alteration. Early chalcopyrite and molybdenite in the central parts of the deposit give way to peripheral polymetallic fault-veins with a dominant north-south trend at the adjacent Khuni historic mine. In the central part of the deposit, the 10–15-m-thick oxidation zone is underlain by a supergene chalcocite enrichment zone that exhibits as much as 2–2.5 times the hypogene copper grade (Samani, 1998). At Kale Kafi, exposure of Precambrian basement, pegmatites, K-silicate alteration, and relatively molybdenum- and tungsten-rich mineralization suggest preservation of deeper levels of a porphyry system that may have been emplaced on the margins of a microcontinent within the back-arc environment.

Other Possible Porphyry-Related Prospects

The Yazd and Kashmar-Kerman Terranes host other relatively exhumed possible porphyry-related copper, molybdenum, and (or) tungsten-bearing vein and skarn prospects (Anarag, Chah Shureh, Chahpalang-South, Pyroozi). A porphyry-related origin for the Andakhan Mo-bearing district (U.S. Geological Survey, 2012) located about 130 km south of Kale Kafi is less certain. To the west in the Central Iranian Terrane, Eocene volcanic and volcano-sedimentary back-arc rift rocks host shallower level Pb-Zn-Mo-(Cu-Ag-Au) vein prospects (Gorgab-4, Sarajieh, Sholugh Abad) with possible porphyry association (Geological Survey of Iran, 2012c, d). Other possible porphyry-related systems occur at Kuh-e-Gabri and Kuh-e-Rig in southeastern Iran. Here, plutons of reported post-Eocene age consist of high-K calc-alkaline to alkaline partially porphyritic granitoids and associated W-Mo skarns (Shahabpour, 2005, 2007). At Kuh-e-Gabri, a granite and alkali granite intruded Late Cretaceous limestone and early Paleocene polygenetic conglomerates, producing contact metamorphism and formation of calcic skarn. The skarn consists of andradite- and hedenbergite-dominated grandite and pyroxene, wollastonite, epidote, and vesuvianite (Abedpour and Tarrah, 2010).

Preservation Level

As derived from the geologic map of Iran (Huber, 1978), older basement and Late Cretaceous to late Eocene permissive units used to define the Esfahan tract (fig. 31) exhibit volcanic-to-plutonic ratios that vary markedly between terranes. Tract areas

occupied by older basement rocks contrast across the Sanandaj-Sirjan (about half of the tract), the East-Central (about one quarter of the tract), and the Central (about 5 percent of the tract) Iranian terranes. Late Cretaceous to late Eocene permissive volcanic and plutonic rocks exposures are small at about 10 percent of the tract area in the Sanandaj-Sirjan and East-Central Iranian Terranes, but they increase to about 20 percent in the volcanic-dominated Central Iranian Terrane. Conversely, nonpermissive coeval rocks exhibit subequal proportions of about 10–15 percent across the Sanandaj-Sirjan, East-Central Iranian, and Central Iranian Terranes. Younger cover rocks are relatively widespread, forming 40–60 percent of the tract area across the entire Esfahan tract.

Overall, volcanic-to-plutonic ratios of permissive units imply that appropriate preservation levels for porphyry copper mineralization may only be locally present in the part of the tract in the highly exhumed Sanandaj-Sirjan Terrane. In contrast, crustal preservation levels in the volcanic-dominated part of the tract in the Central Iranian Terrane are for the most part too shallow for porphyry copper mineralization. Exposure of porphyry systems in the part of the tract in the Central Iranian Terrane is further limited by the extent of younger cover. On the other hand, the variably tectonized part of the tract in the East-Central Iranian Terrane generally exposes deeper levels of preservation for porphyry systems that are, accordingly, richer in tungsten and molybdenum.

Magnetic Anomalies

The regional aeromagnetic map (Maus and others, 2009) was used to confirm the location and character of regional geologic features (for example, arcs, basins, faults, terrane boundaries). Positive magnetic anomalies that likely are associated with Paleocene-Eocene extension-related magmatism are not readily obvious throughout the Sanandaj-Sirjan and Central Iranian Terranes. On the contrary, the Esfahan tract appears instead to generally straddle negative magnetic lows that likely reflect Paleocene-Eocene and younger basins. In the Yazd Terrane, however, a discontinuous east-west positive anomaly bounds the northern side of the Cha Shureh-Kale Kafi-Talesiah porphyry system trend (fig. 30). Its origin is uncertain, but ultramafic and mafic rocks associated with partially preserved ophiolitic complexes do occur in the area.

A relatively subdued but linear magnetic anomaly projects across the central part of the Sanandaj-Sirjan Terrane. This anomaly reflects magnetic sources under Early to Late Cretaceous carbonate rocks. These sources may be associated with the Eocene alkalic plutons that occur in the area.

ASTER Alteration Data

Processed ASTER data (Mars, 2014) available for 45 percent of the part of the Esfahan tract in the Central Iranian Terrane were used to evaluate potential hydrothermal alteration that could be associated with unidentified porphyry systems in that part of the tract. ASTER data were not available for the parts of the Esfahan tract in the Yazd, Kashmar-Kerman, Tabas, and Sanandaj-Sirjan Terranes.

Fifty-one ASTER-derived alteration zones were identified in the tract in the Central Iranian Terrane. Twelve are associated with Neogene and younger rocks, and two are spatially related to the possible porphyry-related prospects at Sholugh Abad and Sarajieh. Another seven coincide with volcanogenic massive sulfide prospects in the same part of the tract. Other ASTER-derived alteration zones coincide in space with 3 gold, 3 iron, and 6 lead-zinc occurrences of possible Eocene age. The remaining 18 ASTER-derived alteration zones are not associated with any known mineral occurrences. Two occur in south-central Iran, but the rest are located in the volcanic-dominated part of the tract in the Central Iranian Terrane.

Probabilistic Assessment

Grade and Tonnage Model Selection

Kale Kafi, the only porphyry deposit known in the Esfahan tract, does not meet the classification criteria for a Cu-Mo subtype based on reported gold and molybdenum grades. The Cu-Mo-Au-W metal association at Kale Kafi and other porphyry-related prospects in this part of the tract suggests that these systems adhere more to the Cu-Mo descriptive and grade-tonnage porphyry models (Cox and others, 1986; Singer and others, 2008). However, Cu-Au prospects are also known. Pooled *t*-test results assuming equal variances further show that the only known deposit in the tract is not significantly different at the 1-percent level from tonnages and copper and molybdenum grades in the general porphyry Cu-Au-Mo model of Singer and others (2008). Therefore, the general model was selected to estimate undiscovered copper, gold, molybdenum, and silver resources in this tract. Compared to the median deposit in the model, the Kale Kafi deposit exhibits comparable tonnage, higher molybdenum grade, and lower copper and gold grades.

Estimates of Undiscovered Deposits and Rationale

In the Esfahan tract, geologic factors favorable for the occurrence of undiscovered porphyry deposits include (1) intraoceanic island arc(s), (2) permissive calc-alkaline to alkaline magmatism emplaced in large and rapidly evolving back-arc-rift basin, (3) likely accretion of island arcs onto microcontinental fragments and related more mature calc-alkaline magmatism, (4) associated Cu-Mo-(Au-W) porphyry deposits (for example, Kale-Kafi), (5) favorable environment for development of supergene enrichment, (6) appropriate levels of exposure preserved, however, only locally along structurally disrupted zones (for example, strike-slip faults), and (7) ASTER-derived potential hydrothermal alteration zones that could be associated with unidentified porphyry systems. Unfavorable factors for the occurrence of undiscovered porphyry deposits include (1) similar size but copper and gold (not molybdenum) grades in the only known deposit that are lower relative to the median porphyry deposit around the world and (2) high volcanic-to-plutonic ratios and extensive cover in the central Iranian segment and low volcanic-to-plutonic ratios in the Sanandaj-Sirjan segment of the tract, which indicate levels of preservation for porphyry copper mineralization that are not appropriate.

Overall, the low density of known porphyry deposits compared to that in other tracts of equivalent aerial extent elsewhere suggests that undiscovered deposits likely are present. However, limited exploration levels suggested by the low numbers of known porphyry occurrences in this variably preserved but otherwise favorable tract indicate high uncertainty expected in the estimation process.

It is worth noting that parts of the central Iranian segment of the tract may host shallowly buried undiscovered porphyry deposits. In some areas, the Eocene rock section is dominated by volcanic (as opposed to volcano-sedimentary) units that appear to be relatively thin as a result of crustal attenuation along normal faults. As suggested by ASTER-derived data, some of the numerous alteration zones (which appear otherwise centered mostly on high- and low-sulfidation epithermal vein and VMS occurrences) in this region could conceivably be associated with underlying porphyry mineralization. Assuming comparable ratios of ASTER-derived alteration zones that coincide with known porphyry and other deposit-type occurrences of Eocene age, ASTER data suggest that perhaps two porphyry systems may remain to be identified in this part of the Esfahan tract. Furthermore, the tectonic environment represented by the Esfahan tract exhibits characteristics that are comparable to those of the adjacent Anatolide-Tauride–Eastern Turkey-Caucasus sub-tract, which contains the Çöpler Au-(Cu) and Agarak Cu-Mo-Au deposits.

The assessment team determined that the Esfahan tract was geologically favorable, but that estimates of numbers of undiscovered porphyry copper deposits could be only carried out with high uncertainty. The tract would contribute significant copper resources from undiscovered deposits to the overall assessment. Therefore, quantitative assessment of undiscovered deposits in this tract was completed. The consensus estimates for undiscovered porphyry copper deposits in the Esfahan tract at the 90-, 50-, and 10-percent probability levels and associated summary statistics are presented in table 8A. At the 90-percent probability level, all assessors felt that the likelihood of undiscovered deposits was 0. At the 50-percent probability level, the numbers ranged between 0 and 3 undiscovered deposits, and at the 10-percent probability level the numbers increased to 8. On the basis of these numbers, the team reached a consensus estimate of 0, 2, and 8 undiscovered deposits for the 90-, 50-, and 10-percent probability levels, respectively. This resulted in a mean of 3.95 undiscovered deposits with a standard deviation of 4.93 ($C_v\%=125$), reflecting the level of favorability and high uncertainty assessed for this tract. The estimated total deposit density per 100,000 km² obtained is comparable to the porphyry deposit density model of Singer and Menzie (2010).

Probabilistic Assessment Simulation Results

Simulation results for estimates for copper, molybdenum, gold, silver, and the total volume of mineralized rock are summarized in table 8B. The mean estimate of undiscovered copper resources in the Esfahan porphyry tract is 14 Mt. Results of the Monte Carlo simulation are also presented as cumulative frequency plots (fig. 32). The cumulative frequency plots show the cumulative probabilities of occurrence-estimated resources and total mineralized rock, as well as the mean for each commodity and for total mineralized rock.

Table 8. Probabilistic assessment for tract 142pCu9008, Esfahan—Iran, Iraq, and Turkey.

A. Undiscovered deposit estimates, deposit numbers, tract area, and deposit density.

[N_{xx} , estimated number of deposits associated with the xxth percentile; N_{und} , expected number of undiscovered deposits; s , standard deviation; $C_v\%$, coefficient of variance; N_{known} , number of known deposits in the tract that are included in the grade and tonnage model; N_{total} , total of expected number of deposits plus known deposits; tract area, area of permissive tract in square kilometers (km²); deposit density reported as the total number of deposits per 100,000 km². N_{und} , s , and $C_v\%$ are calculated using a regression equation (Singer and Menzie, 2005)]

Consensus undiscovered deposit estimates					Summary statistics					Tract area (km ²)	Deposit density (N_{total} /100,000 km ²)
N_{90}	N_{50}	N_{10}	N_{05}	N_{01}	N_{und}	s	$C_v\%$	N_{known}	N_{total}		
0	2	8	18	18	4.0	4.9	120	1	5.0	56,900	9

B. Results of Monte Carlo simulations of undiscovered resources.

[Cu, copper; Mo, molybdenum; Au, gold; and Ag, silver; in metric tons; Rock, in million metric tons]

Material	Probability of at least the indicated amount						Probability of	
	0.95	0.9	0.5	0.1	0.05	Mean	Mean or greater	None
Cu	0	0	4,100,000	39,000,000	64,000,000	14,000,000	0.27	0.21
Mo	0	0	53,000	980,000	390,000	390,000	0.23	0.34
Au	0	0	78	1,100	380	380	0.25	0.32
Ag	0	0	470	12,000	21,000	4,800	0.21	0.4
Rock	0	0	910	8,000	14,000	2,900	0.28	0.21

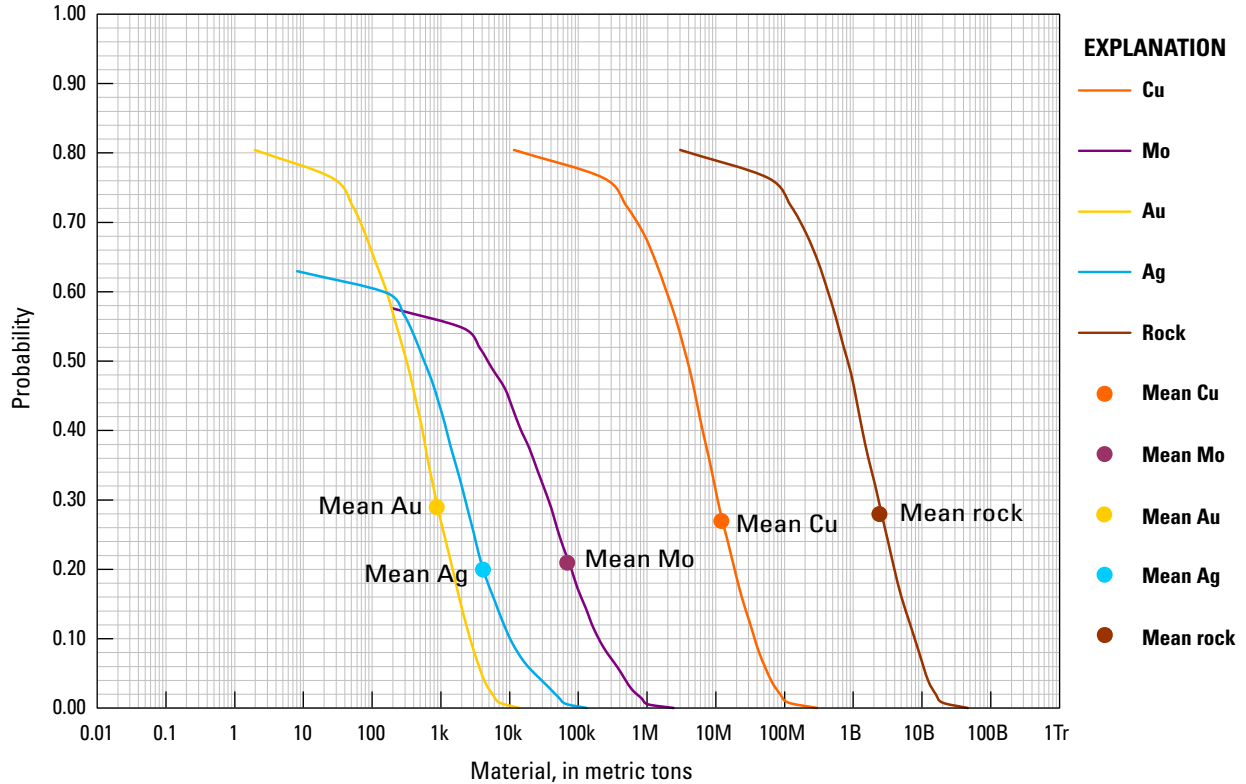


Figure 32. Cumulative frequency plot showing the results of Monte Carlo simulation of undiscovered resources in porphyry copper deposits in tract 142pCu9008, Esfahan—Iran, Iraq, and Turkey. k, thousand; M, million; B, billion; Tr, trillion.

Khorasan Tract (142pCu9009)

Descriptive model: Porphyry copper-gold (Cox, 1986b; Berger and others, 2008; John and others, 2010)

Grade and tonnage model: Porphyry copper, copper-gold subtype (Singer and others, 2008)

Geologic feature assessed: Late Cretaceous to middle Miocene island arcs of the Tethyan Eurasian Metallogenic Belt

Location

The Khorasan tract located in northeastern Iran (fig. 33) delimits a 600-km-long and 150-km-wide island-arc volcano-plutonic belt of Late Cretaceous to middle Miocene age. It covers an area of 38,300 km². The tract overlies the northeast extension of the Central Iranian Terrane that in the region separates the Lut Terrane along the left-lateral Great Kafir-Doruneh fault to the south and the Alborz and Kopet Dagh Terranes along the Shahrud south-vergent thrust fault system to the north, respectively (fig. 3).

Tectonic Setting

During the Late Cretaceous-early Paleocene, the Lut and Kopet Dagh Terranes were separated by the Sabzevar Ocean (fig. 4C), which at that time was likely connected to the southeast with the Sistan Ocean (Golonka, 2004; Stöcklin, 1968). The Sabzevar Ocean contained several small cratonic fragments that had rifted from the margins of the Kopet Dagh and Alborz Terranes during opening of this sea.

Between the Late Cretaceous and early Eocene, convergence was initiated along several north-dipping intraoceanic subduction zones (Desmons and Beccaluva, 1983; Delaloye and Desmons, 1980) creating island-arc magmatism, which by late Eocene-early Oligocene time was well established (figs. 4D, E). Evolution of island-arc magmatism continued in the Oligocene and middle Miocene, and it was followed by accretion and initiation of uplift in the eastern Alborz and Kopet Dagh Terranes to the north, which until then had remained largely submerged (Dercourt and others, 1986). In the middle Miocene, ongoing convergence closed the Sabzevar Ocean, terminating island-arc magmatism and intensifying uplift and deformation in the Alborz and Kopet Dagh Terranes (fig. 4F). This far-field compressional event likely was linked to the final Arabia-Eurasia continental collision that occurred along the Bitlis-Zagros Suture to the south (McQuarrie and others, 2003).

From the late Miocene to the present, dominantly south-vergent thrusts and folds, followed by strike-slip faults developed in the Kopet Dagh, Alborz, and Central Iranian Terranes as a result of continued suturing and collision (Hollingsworth and others, 2010). These terranes were then unconformably overlain by late Miocene and younger synorogenic sedimentary formations, as well as intruded and covered by alkaline plutonic and volcanic units.

Magmatism

The Khorasan tract of northeastern Iran delineates the Late Cretaceous to middle Miocene island-arc segments exposed along folded and thrust fault-bounded accretionary prisms that are separated by broad valleys. Precambrian to pre-Late Cretaceous

metamorphic basement is preserved along several of these ranges, suggesting that microcontinental fragments occupied parts of this intraoceanic basin. Ophiolite-bearing accretionary complexes exhibit both MORB and island-arc geochemical signatures (Delaloye and Desmons, 1980; Shojaat and others, 2003) and host chromium and manganese, as well as younger porphyry, skarn, and epithermal, mineralization (Förster, 1978; Geological Survey of Iran, 2012e). From south to north, they occur along three main ranges (Taknar-Kashmar, Sabzevar, and Torud), which suggests the presence of as many associated island arcs (Samani, 1998; Berberian and Berberian, 1981). Permissive igneous units used to define the Khorasan tract (appendix B) are shown in figure 34, along with locations of igneous complexes and other geologic features mentioned in this section.

Precambrian to pre-Late Cretaceous metamorphic basement and ophiolitic complexes in the tract are overlain by Late Cretaceous-Eocene sedimentary, volcanic and volcano-sedimentary successions, which consist of andesite to rhyolite lavas and tuffs intercalated with shallow-marine sedimentary units that are in turn intruded by shallowly emplaced mafic to felsic calc-alkaline and lesser alkaline plutons with juvenile and mixed isotopic signatures (Kazmin and others, 1986).

In the Taknar and Kashmar Ranges (fig. 2) along the southern part of the Khorasan tract, magmatism is exemplified by the east-west 50-km-long and 7-km-wide Eocene (~43 Ma) Kashmar batholith, which intrudes late Paleocene to broadly coeval middle Eocene andesite-dominated lavas and pyroclastic rocks (Soltani, 2000). Younger Oligocene-Miocene tonalite, granodiorite, granite, and alkali granite intrusions are locally porphyritic, and they are cut by aplitic and dacitic dikes. These shallow-level oxidized I-type calc-alkaline phases exhibit initial Sr and Nd isotopic compositions that are consistent with derivation from a relatively juvenile source. Along fault contacts, the southern margin of this batholith is affected by sericite-pyrite, sphene, epidote, chlorite, and minor carbonate alteration (Soltani, 2000).

In the central part of the Khorasan tract between the Taknar and Kashmar Ranges to the south and the Sabzevar Range to the north (fig. 2), the middle-late Eocene Kuh Mish pluton (fig. 34) includes progressively younger granodiorite stocks and quartz monzodiorite and gabbro dikes, which intrude Late Cretaceous andesite and early Eocene volcano-sedimentary rocks. These oxidized I-type calc-alkaline intrusions were emplaced at shallow levels. Compared to the Kashmar batholith, the Kuh Mish intrusions exhibit lower K₂O contents and more primitive isotopic signatures. Chlorite and actinolite are the main hydrothermal alteration products (Soltani, 2000). Eocene magmatism in this area was followed by Oligocene-Miocene calc-alkaline magmatism that included porphyritic intrusions (Spies and others, 1984).

In the Sabzevar Range along the northern part of the Khorasan tract, basaltic andesite to dacite and rhyolite plutons intrude ophiolitic complexes. These plutons were emplaced syntectonically during compressional shearing. U-Pb zircon and ⁴⁰Ar/³⁹Ar geochronology constrains the age of these granitoids to the late Paleocene (~58 Ma). Geochemical data further indicate a subduction-related medium-K calc-alkaline compositional range

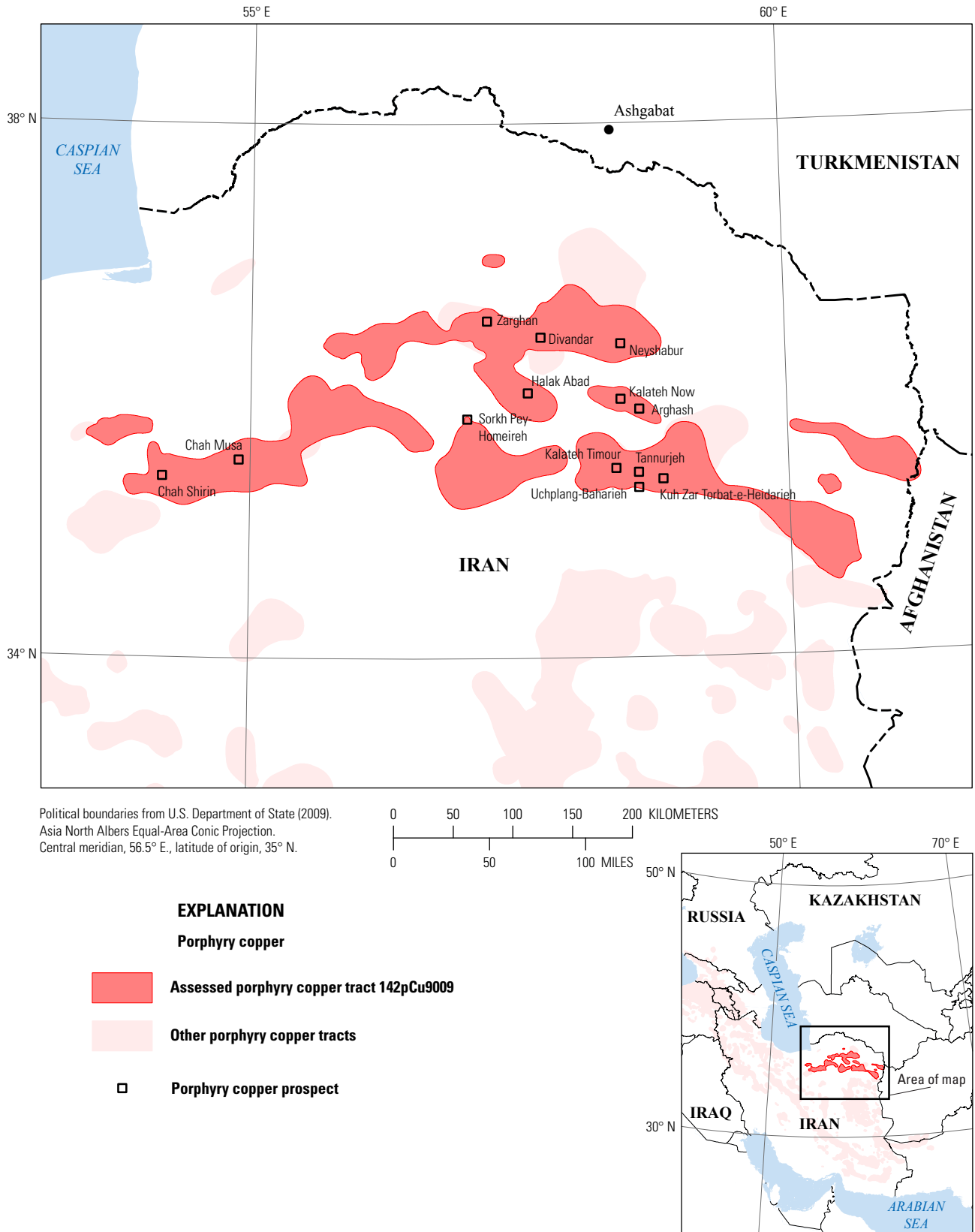
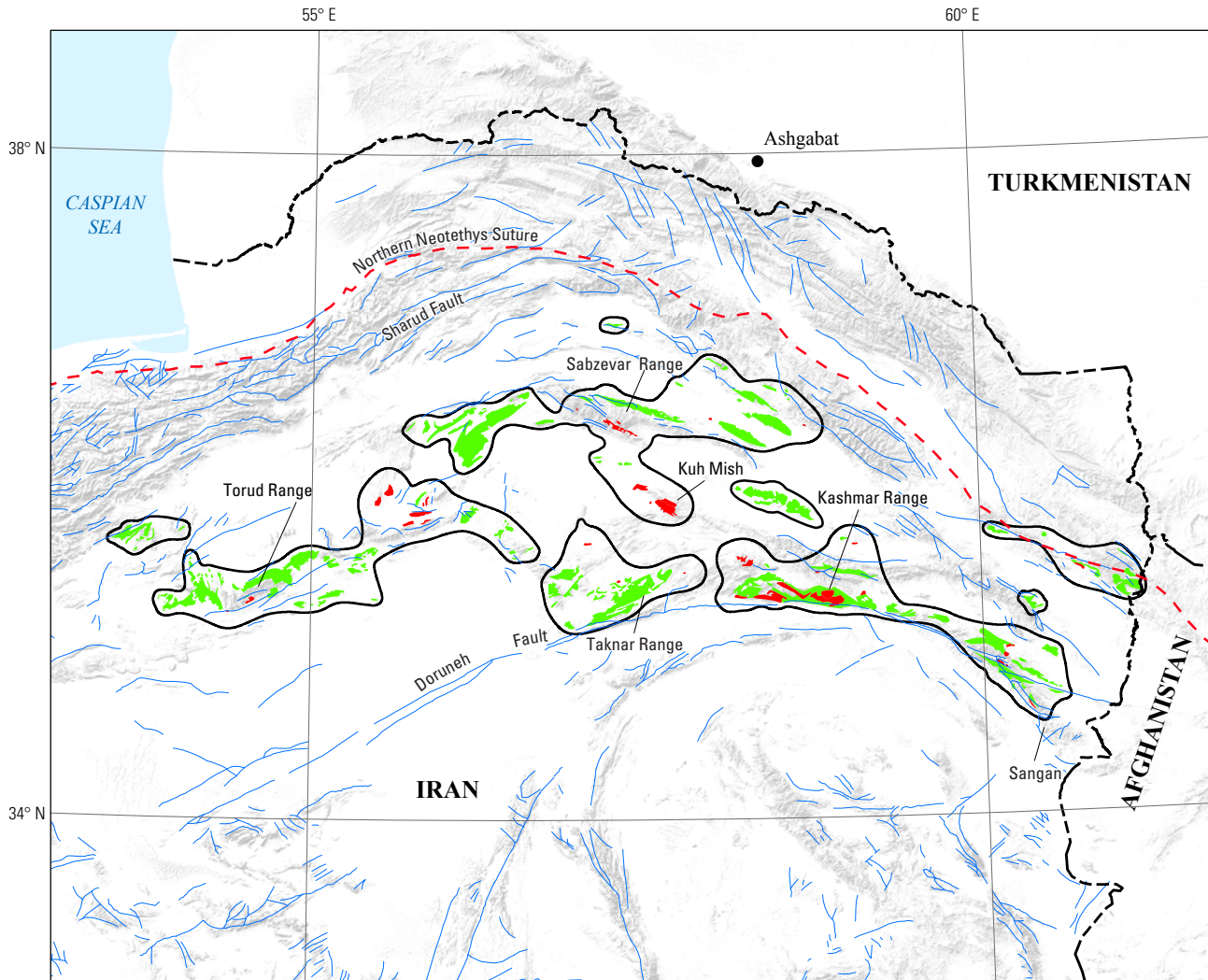


Figure 33. Map showing the location of known porphyry copper prospects for permissive tract 142pCu9009, Khorasan—Afghanistan and Iran. See appendix C for prospects and appendix D for accompanying spatial data.



Base from SRTM Global Digital Elevation Model, U.S. Geological Survey EROS Data Center, 2006. Political boundaries from U.S. Department of State (2009). Asia North Albers Equal-Area Conic Projection. Central meridian, 56.5° E., latitude of origin, 35° N.

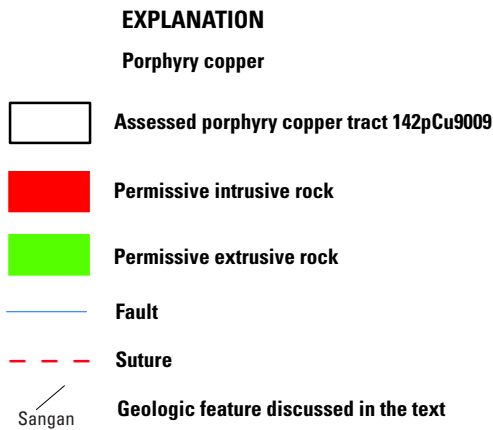
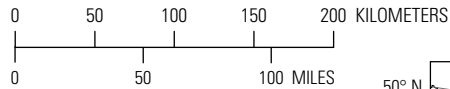


Figure 34. Map showing the distribution of permissive intrusive and extrusive rocks used to define tract 142pCu9009, Khorasan—Afghanistan and Iran. See appendix A for principal sources of information and appendix B for source map units.

and crystallization from juvenile magmas derived from partial melting of an oceanic source (Rossetti and others, 2013).

In the Torud Range (fig. 2) in the western part of the Khorasan tract, middle Eocene volcano-sedimentary rocks are overlain by Eocene-Oligocene calc-alkaline and local alkaline volcanic rocks, which are interlayered with shallow marine, lacustrine and subaerial sedimentary successions. These successions are intruded by basic tholeiitic dikes and calc-alkaline quartz monzodioritic to granodioritic stocks with typical arc compositions (Samani, 1998; Shamanian and others, 2004). The aluminum content of hornblendes indicate shallow emplacement depths based on pressures between 0.5 and 1 kb (Ghorbani and others, 2005).

Known Porphyry Prospects

Mineralization in the Khorasan tract includes Late Cretaceous ophiolite-related Cr and Mg and Late Cretaceous-Eocene copper manto occurrences, a number of Eocene and Oligocene-Miocene precious and base-metal acid sulfate and adularia-sericitic epithermal, as well as base-metal and iron skarn (IOCG), mines and prospects (Geological Survey of Iran, 2012e). Porphyry-style mineralization associated with several iron replacement and epithermal systems in the Taknar-Kashmar, Kuh Mish, and Torud ranges has only recently been recognized (Karimpour, 2007). In the Sabzevar Range, porphyry intrusions of uncertain origin and age are shown in the geologic map of Iran (Huber, 1978). A permissive porphyry copper setting has also been proposed (Geomatics Management, [n.d.]). However, no porphyry-style mineralization has positively been identified in this range.

Six Cu-Au porphyry (Argash, Halak Abad, Kalateh Now, Kalateh Timour, Tannurjeh, Uchplang-Baharieh), 1 Cu-Mo porphyry (Chah Shirin area [also known as Sar Kavir]), and 4 possible porphyry-related prospects (Chah Mussa, Kuh Zar Torbat-e-Heidarieh, Neyshabur, Sorkh Pey-Homeireh) are included in the porphyry occurrence database compiled for this assessment (fig. 33; appendix C). In the Sabzevar Range, the Divandar and Zarghan copper prospects of uncertain origin are also tentatively included here as possible porphyry-related occurrences.

Tannurjeh and Uchplang-Baharieh Porphyry Prospects

The Tannurjeh and Uchplang-Baharieh Cu-Au-bearing porphyry and associated iron skarn prospects are located in the Taknar-Kashmar Range (Karimpour and Malekzadeh, 2006; Karimpour, 2006; Karimpour and Stern, 2011). At Tannurjeh, Eocene rhyolite, dacite, rhyodacite, and minor andesite are intruded by Oligocene-Miocene meta-aluminous, I-type monzonite, quartz monzonite, and diorite, as well as quartz diorite-granodiorite, porphyry stocks. Gold and minor copper mineralization occurs with iron oxides and hydroxides in well-developed advanced argillic alteration, which is characterized by kaolinite, alunite, and vuggy silica. Hypogene mineralization consists of pyrite and chalcopyrite in hydrothermal breccias and quartz veins with anomalous gold, copper, and molybdenum. Quartz veins contain primary fluid inclusions with high homogenization temperatures in the range of

320–490 degrees Celsius (°C; Saadat and others, 2007). The acid sulfate environment is part of a porphyry system (Karimpour and Stern, 2011). At Uchplang-Baharieh about 12 km to the south of Tannurjeh, broad argillic alteration zones and anomalous gold and copper values for monzonite to quartz monzonite porphyry stocks also indicate the presence of a Cu-Au porphyry system (Karimpour, 2006; Karimpour and Stern, 2011).

Kalateh Timour Porphyry Prospect

The Kalateh Timour Cu-Au-bearing porphyry prospect in the Taknar-Kashmar Range is located in an old gold-silver base-metal mining district. Here, several quartz diorite and quartz monzodiorite porphyry stocks were emplaced along a west-northwest structural trend and intrude lower to middle Eocene basalts, andesites, latites, trachytes, dacites-rhyodacites, and associated pyroclastic rocks (Alaminia and others, 2011). Well-developed propylitic, sericitic, and argillic alteration are accompanied by quartz stockwork zones containing as much as 3 percent sulfides that are variably replaced by secondary iron oxides. Preliminary geochemical sampling indicates that the highest gold and copper values occur in the porphyry intrusions (Alaminia and others, 2011).

Halak Abad, Arghash, and Kalateh Now Porphyry Prospects

The Halak Abad, Argash, and Kalateh Now Cu-Au-bearing porphyry prospects occur in the Kuh Mish Range located between the Taknar-Kashmar Range to the south and the Sabzevar Range to the north. During the Eocene this area was characterized by extension-related calc-alkaline to alkaline magmatism associated with intra-arc rifting and caldera-forming events (Soltani, 2000).

In the Halak Abad porphyry and associated acid-sulfate epithermal prospect (Panahi Shahri and others, 2010), a monzonite porphyry stock hosts disseminated and quartz-pyrite-(chalcopyrite) stockworks associated with abundant kaolinite-pyrophyllite and alunite alteration. Hematite and jarosite after sulfide are widespread. Panahi Shahri and others (2010) report the presence of a Cu-Au porphyry system at depth.

At the Arghash porphyry and associated acid-sulfate epithermal prospect, a late Eocene-Oligocene quartz diorite to monzonite porphyry stock intrudes Eocene volcanic rocks that are intensively altered by argillic, sericitic, and propylitic mineral associations (Gholami and others, 2011). The presence of a porphyry stock, alteration types, and copper- and gold-bearing quartz stockworks are consistent with porphyry-style mineralization (Karimi Saeed Abadi and others, 2009; Alirezai and others, 2009).

In contrast to the Halak Abad and Arghash porphyry prospects that are associated with high-sulfidation systems, the Kalateh Now porphyry copper prospect is associated with a low-sulfidation epithermal system. At Kalateh Now, the kaolin-rich alteration zone occurs about subvolcanic monzonitic intrusions with associated porphyry-style mineralization (Kolahdani, 2009).

Chah Shirin Porphyry-Related Prospect

The Chah Shirin Cu-Mo-bearing porphyry prospect has a reported 3,500 Mt with copper grades in excess of 2 percent (Geological Survey of Iran, 2012a; Samani, 1998). It is located in the Torud Range, which besides epithermal systems also hosts proximal Fe-Cu-Au skarn and distal base-metal carbonate-replacement mineralization. Little is known about the Chah Shirin prospect. However, it occurs in the vicinity of the well-described Gandy and Abolhassani precious and base-metal epithermal district (Shamanian and others, 2004). About 15 km north of the Gandy and Abolhassani epithermal district, placer gold is the product of weathering of nearby quartz sulfide veins hosted by andesitic volcanic rocks. The presence of tourmaline in the wall rocks of these veins may indicate proximity to a porphyry system (Chah Shirin?).

Intrusions are also present in the late Eocene Gandy and Abolhassani intermediate-sulfidation Au-Ag-Pb-Zn-Cu epithermal deposits (Shamanian and others, 2004; Ziaii and others, 2009, 2010). These deposits are hosted by thin-bedded middle Eocene siltstones and sandstones, lapilli tuffs, volcanic breccias, and intermediate lava flows that exhibit typical arc signatures. These units are intruded by rhyolitic to rhyodacitic domes, hypabyssal monzodiorite and quartz monzonite stocks, and granitic dikes of Eocene or younger age.

Other Possible Porphyry-Related Deposits and Prospects

Other possible porphyry-related prospects may be present at (1) the Sorkh Pey-Homeireh copper district in the Kuh Mish Range (Geological Survey of Iran, 2012a; Bazin and Hübner, 1969a), (2) the Cha-Mussa polymetallic vein deposit in the Torud Range (Bastani and others, 2009; Geological Survey of Iran, 2012a; Bazin and Hübner, 1969a; Imamjomeh and others, 2009), (3) the iron skarn deposits at Kuh-e-Zar-Torbat-e-Heidarieh (Karimpour, 1998; Abedi and Ziaii, 2004; Mazloumi and others, 2008; Mazloumi Bajestani and Rasa, 2010) and Sangan (Ghavi and Karimpour, 2010; Malekzadeh Shafaroudi, Karimpour, and Golmohammadi, 2013; Boomeri and others, 2006; Boomeri, Ishiyama, and others, 2010; Karimpour and Malekzadeh, 2006) in the Taknar-Kashmar Range; and (4) perhaps also the Neyshabour Cu-U historic mining district east of the Sabzevar Range (Förster, 1978; Karimpour and others, 2012; Geological Survey of Iran, 2012a; Bazin and Hübner, 1969a). The relation to porphyry-style mineralization has not been established in these epithermal and iron skarn (IOCG?) mineral systems, but all contain calc-alkaline to alkaline porphyry intrusions and associated copper-gold mineralization.

At the Sorkh Pey-Homeireh copper district, a quartz porphyry stock is reported to intrude Late Cretaceous or younger andesite. Associated pyrite-chalcocopyrite mineralization occurs in quartz veins and disseminations (Bazin and Hübner, 1969a). An extensive 20- by 20-km ASTER-derived phyllic and argillic alteration zone occurs in this area (Mars, 2014).

At the Cha Mussa Cu-(Pb-Zn) vein deposit, located only about 35 km to the northeast of Cha Shirin, a calc-alkaline subvolcanic porphyry biotite-hornblende andesite-dacite stock

intrudes Eocene volcanic-pyroclastic sequences (Imamjomeh and others, 2009). Stockwork mineralization occurs in the western part of the area and polymetallic veins occupy the eastern part of the area. In the western part, disseminated and veinlet copper mineralization is associated with phyllic and propylitic alteration. Mineralization consists of hypogene pyrite, chalcocopyrite and bornite and secondary chalcocite, covellite, digenite, malachite, and neotocite (Imamjomeh and others, 2009). Drilling has identified a malachite-rich interval with greater than 3 percent copper at a depth of 20–80 m (Bastani and others, 2009; Ziaii and others, 2009; Imamjomeh and others, 2009).

In the Kuh-e-Zar Torbat-e-Heidarieh iron skarn deposit, Oligocene-Miocene porphyritic granite, granodiorite, syenogranite, and monzonite intrude late Eocene andesite-dacite-rhyolite. Geochemical data on these intrusions show I-type metaluminous, medium to high-K calc-alkaline compositions consistent with derivation from a subduction zone (Abedi and Ziaii, 2004). Fault-controlled specularite-quartz-gold-chlorite±chalcocopyrite±pyrite±galena±barite mineralization occurs in veins, stockworks, and hydrothermal breccias (Mazloumi Bajestani and Rasa, 2010).

In the easternmost part of the Taknar-Kashmar Range, the Sangan iron skarn deposit contains one of the largest resources in Iran with 600 Mt at greater than 45 percent iron (Ghavi and Karimpour, 2010). The deposit lies to the south of the Doruneh Fault, possibly on a southward-thrust nappe. At Sangan, upper Mesozoic sedimentary rocks are intruded by late Eocene biotite-hornblende quartz monzonite to syenogranite porphyry stocks and dikes that introduced local copper mineralization (Malekzadeh Shafaroudi and others, 2013; Boomeri and others, 2006; Boomeri and others, 2010a).

The Neyshabur mining district (Geological Survey of Iran, 2012a) is described as a Cu-U vein system hosted by Eocene andesitic and dacitic rocks. Turquoise has been mined for centuries in the area (Bazin and Hübner, 1969a). At Neyshabur, andesite-dacite and pyroclastic rocks are intruded by a subvolcanic magnetite-series diorite to syenite porphyry intrusion. Förster (1978) further indicates the presence of post-early Miocene latite-andesite, rhyolitic ignimbrite, and granodiorite porphyry intrusions. At Neyshabur, strong silicification and argillization and weak carbonate and propylitic alteration are recognized (Karimpour and others, 2012). Mineralization is present in stockworks, disseminations, and hydrothermal breccias. Hypogene minerals are pyrite, magnetite, specularite, chalcocopyrite, and bornite. Secondary minerals are turquoise, chalcocite, covellite, and iron oxides. Highly anomalous copper, gold, zinc, arsenic, molybdenum, cobalt, uranium, light rare earth, niobium, and thorium values occur in the broad 80-m-thick gossan zone (Karimpour and others, 2012).

No porphyry-style mineralization has positively been identified in the Sabzevar Range. However, possible porphyry-related mineralization may occur at the Divandar and Zarghan copper prospects (Geological Survey of Iran, 2012a), where porphyritic granite intrusions are reported by Huber (1978).

Preservation Level

The Khorasan tract delimits the extent of island-arc segments preserved in accretionary prisms that are exposed along ranges. It does not include any segments that may be buried under younger cover rocks that are likely more than 1 km thick across large parts of the broad intervening basins. Several acid-sulfate systems above known porphyry prospects in the tract indicate shallow levels of preservation. In general, this is also shown by the high ratio of permissive volcanic-to-plutonic units ($\{\text{volcanic}/[\text{volcanic}+\text{plutonic}]\} \times 100=89$) in the tract. As derived from the 1:1,000,000-scale map of Huber (1978), pre-Late Cretaceous basement rocks constitute about 12 percent of the tract area, about half of which consist of metamorphic units of Jurassic or older age, and Late Cretaceous to middle Miocene permissive plutonic and volcanic units occupy 2 and 15 percent, respectively, of the tract area. Broadly coeval nonpermissive mafic, sedimentary, and volcano-sedimentary units account for a further 21 percent of the tract (fig. 34), whereas younger rocks cover the large remaining fraction (50 percent) of the tract. Overall, preservation level data suggest that undiscovered porphyry copper systems are partly concealed under permissive volcanic units and (or) largely buried under younger cover rocks.

Magnetic Anomalies

The regional aeromagnetic map (Maus and others, 2009) was used to confirm the location and character of regional geologic features (for example, arcs, basins, faults, terrane boundaries). In this region, positive magnetic anomalies generally coincide with ophiolitic belts and tectonically juxtaposed island-arc rocks. Porphyry and porphyry-related occurrences identified in this tract lie along the margins of high-intensity magnetic anomalies.

A conspicuous magnetic high projects beyond the tract boundary to the southwest along the north side of the Great Kafir-Doruneh Fault (fig. 2), which marks the boundary between the Central Iranian and the Yazd Terranes (fig. 3). This suggests that the accretionary prism exposed in the Taknar and Kashmar Ranges (fig. 2) continues under cover to the southwest for about 450 km along this tectonic boundary. Beyond the tract boundary to the east, this anomaly also extends well into Afghanistan. Similarly, other more subdued parallel anomalies project from the Sabzevar and Torud Ranges (fig. 2) across central Iran to the southwest. They eventually abut the Urumieh-Dokhtar Magmatic Belt (fig. 2). These magnetic signatures are interpreted to be reflecting deeply buried southwestward extensions of the accretionary prisms that are exposed in the Sabzevar and Torud Ranges.

ASTER Alteration Data

Processed ASTER data (Mars, 2014) available for the Torud and Sabzevar Ranges in the western and northern parts (55 percent) of the Khorasan tract were used to evaluate potential hydrothermal alteration that could be associated with unidentified porphyry systems in this part of the tract. Out of the 21 ASTER-derived alteration zones identified, 2 are underlain by Jurassic or Paleozoic rocks, 15 are associated

with permissive Late Cretaceous-middle Miocene rocks, and 4 are related to younger Pliocene-Holocene rocks. Of the 17 ASTER alteration zones that occur in middle Miocene and older units, 11 are spatially associated with known precious and base-metal districts that are or may be porphyry-related (Neyshabur [2 zones], Sorkh Pey [4 zones], and Chah Shirin [5 zones]). The nature of the remaining 6 ASTER-derived alteration zones is not known. However, 2 are proximal to known barite and phosphate occurrences, and another 3 lie in an area dominated by Pliocene-Holocene igneous rocks. Hence, ASTER data in the western and northern part of the Khorasan tract suggest the existence of perhaps one site of potential hydrothermal alteration that could be associated with an unidentified porphyry system of Late Cretaceous to middle Miocene age. The most extensive ASTER-derived alteration zone (20- by 20-km) in the Khorasan tract occurs over the Sorkh Pey district.

Probabilistic Assessment

Grade and Tonnage Model Selection

There were no resource data on any of the prospects in the Khorasan tract. Hence, a pooled *t*-test assuming equal variances could not be run. However, the oceanic island-arc environment and dominant Cu-Au association reported from most porphyry-related prospects in this region suggest that these adhere to the Cu-Au descriptive and grade-tonnage models (Cox and others, 1986; Singer and others, 2008). Thus, the porphyry Cu-Au model of Singer and others (2008) was selected to estimate undiscovered copper, gold, molybdenum, and silver resources in this tract.

Estimates of Undiscovered Deposits and Rationale

Favorable geologic factors for the occurrence of undiscovered porphyry deposits in the Khorasan tract include (1) two or more intraoceanic island arcs, (2) protracted (albeit independent from arc to arc) alkaline and calc-alkaline magmatism, and (3) shallow levels of preservation hosting epithermal acid-sulfate and associated Cu-Au porphyry copper mineralization. Unfavorable geologic factors for the occurrence of undiscovered porphyry deposits include (1) smaller than average arc size(s) largely built on thin oceanic crust, (2) arc segments likely buried under cover, and (3) no known porphyry deposits with reported resources.

Overall, the lack of known porphyry deposits compared to tracts of equivalent aerial extent elsewhere suggests that undiscovered deposits are likely present. Furthermore, the moderate number of porphyry-related occurrences identified to date appears consistent with early-stage exploration efforts for porphyry systems in this shallowly preserved but otherwise relatively favorable tract.

The assessment team established that the Khorasan tract was geologically favorable but that estimates of numbers of undiscovered porphyry copper deposits could be only

carried out with high uncertainty. The tract would contribute significant copper resources from undiscovered deposits to the overall assessment. Therefore, quantitative assessment of undiscovered deposits in this tract was warranted. Table 9A shows the consensus estimates for undiscovered porphyry copper deposits in the Khorasan tract at the 90-, 50-, and 10-percent probability levels and the associated summary statistics. At the 90-percent probability level, all assessors estimated that there were no undiscovered deposits. At the 50-percent probability level, the numbers ranged between 1 and 2, and at the 10-percent probability level, the numbers increased to between 2 and 7. On the basis of these numbers, the team reached a consensus estimate of 0, 2, and 5 undiscovered deposits at the 90-, 50-, and 10-percent probability levels, respectively. This resulted in a mean of 2.53 undiscovered deposits with a standard deviation of 2.42 ($C_v=96$), reflecting the level of favorability and relatively high uncertainty assessed for this tract.

Probabilistic Assessment Simulation Results

Simulation results for estimates for copper, molybdenum, gold, silver, and the total volume of mineralized rock are summarized in table 9B. The mean estimate of undiscovered copper resources in the Khorasan porphyry tract is 8.1 Mt. Results of the Monte Carlo simulation are also presented as cumulative frequency plots (fig. 35). The cumulative frequency plots show the cumulative probabilities of occurrence-estimated resources and total mineralized rock, as well as the mean for each commodity and for total mineralized rock.

Makran Tract (142pCu9011)

Descriptive model: General porphyry copper (Cox, 1986a; Berger and others, 2008; John and others, 2010)

Geologic feature assessed: Late Cretaceous to late Eocene island arcs of the Tethyan Eurasian Metallogenic Belt

Location

The Makran tract (fig. 36) located in southeastern Iran delimits an arcuate, 420-km-long and as much as 110-km-wide east-west subduction-related island-arc volcano-plutonic belt of Late Cretaceous to late Eocene age. It covers an area of 24,100 km². The tract lies within the Makran Terrane, which is one of the largest accretionary prisms on Earth. The Makran tract is bounded on the east by the Sistan suture zone along the Nostratabad Fault. On the west, it is separated from the Sanandaj-Sirjan Terrane along the right-lateral Minab-Zendan Fault system, which marks the southern end of the Bitlis-Zagros Thrust. Its northern part is delimited by younger cover in the Jaz Murian Depression, which is in turn bordered on the north by the Lut Terrane.

Tectonic Setting and Magmatism

The evolution of magmatism in the Makran Terrane has progressed by northward subduction of the Arabian Platform under the Lut Terrane (Farhoudi and Karig, 1977) with temporal variations in slab dip (Shahabpour, 2010). From the Middle Jurassic to the early Paleocene, a steep-dip slab produced a continental arc in the Sanandaj-Sirjan Terrane. This arc continues into the Makran Terrane where it is preserved in the Bajgan-Durkan continental sliver that is wedged between the Jaz Murian Depression to the north and the Makran accretionary prism to the south (McCall, 1997; Shahabpour, 2010; Leturmy and Robin, 2010; Kazmin and others, 1986).

In the Late Cretaceous-early Paleocene, continued subduction initiated an extensional back-arc basin north of the Bajgan-Durkan continental sliver in the Jaz Murian Depression. Back-arc magmatism is represented by Late Cretaceous tholeiitic ocean floor and calc-alkaline island-arc rocks. This back-arc and intraoceanic island-arc setting was part of the inner sea that connected with the Sistan and Sabzevar Oceans to the east and north around the East-Central Iranian Terrane. The setting is characterized by basalts and volcano-sedimentary successions with minor andesite and dacite-rhyolite dikes and associated VMS deposits (Geological Survey of Iran, 2012e; Förster, 1978) preserved in deformed ophiolite mélanges. In the Jaz Murian Depression, these rocks are largely covered by younger sedimentary formations.

To the south of the Bajgan-Durkan continental sliver, late Paleocene and Eocene subduction of a moderate-dip slab in the Southern Neotethys Ocean Branch (fig. 4D) caused the active trench to progressively move seaward leading to the emplacement of ophiolite mélanges along the growing fore-arc region (Shahabpour, 2010). These fore-arc rocks are represented by Late Cretaceous marine sediments and tholeiitic ocean floor basalts and associated economic chromite deposits. Also present are Eocene mafic to intermediate plutons with island-arc signatures, which are preserved in imbricated south-vergent thrust sheets in the accretionary prism (McCall, 1997). Arc accretion continued during the late Eocene (fig. 4E) with uplift and unconformable deposition of thick synorogenic flysch successions (Berberian and Berberian, 1981; Berberian and King, 1981; Boulin, 1991).

The Makran accretionary prism continues to the east, where it underlies much of southern Pakistan and is dominated by sedimentary rocks (Golonka, 2004; Platt and others, 1985; Kazmi and Rana, 1982; Farhoudi and Karig, 1977).

The Makran tract delineates the Late Cretaceous-early Paleocene back-arc events that developed in the Jaz Murian Depression behind the Bajgan-Durkan continental sliver, as well as the late Paleocene-late Eocene island-arc and fore-arc events that occurred in front of the Bajgan-Durkan continental sliver. Permissive igneous units used to define the Makran tract (appendix B) are shown in figure 37, along with locations of igneous complexes and other geologic features mentioned in this section.

Table 9. Probabilistic assessment for tract 142pCu9009, Khorasan—Afghanistan and Iran.

A. Undiscovered deposit estimates, deposit numbers, tract area, and deposit density.

[N_{xx} , estimated number of deposits associated with the xxth percentile; N_{und} , expected number of undiscovered deposits; s , standard deviation; $C_v\%$, coefficient of variance; N_{known} , number of known deposits in the tract that are included in the grade and tonnage model; N_{total} , total of expected number of deposits plus known deposits; tract area, area of permissive tract in square kilometers (km^2); deposit density reported as the total number of deposits per 100,000 km^2 . N_{und} , s , and $C_v\%$ are calculated using a regression equation (Singer and Menzie, 2005)]

Consensus undiscovered deposit estimates					Summary statistics					Tract area (km^2)	Deposit density ($N_{total}/100,000 km^2$)
N_{90}	N_{50}	N_{10}	N_{05}	N_{01}	N_{und}	s	$C_v\%$	N_{known}	N_{total}		
0	2	5	8	8	2.5	2.4	96	0	2.5	38,300	7

B. Results of Monte Carlo simulations of undiscovered resources.

[Cu, copper; Mo, molybdenum; Au, gold; and Ag, silver; in metric tons; Rock, in million metric tons]

Material	Probability of at least the indicated amount						Probability of	
	0.95	0.9	0.5	0.1	0.05	Mean	Mean or greater	None
Cu	0	0	2,600,000	22,000,000	37,000,000	8,100,000	0.25	0.2
Mo	0	0	1,800	120,000	260,000	47,000	0.19	0.47
Au	0	0	230	1,600	2,500	580	0.29	0.2
Ag	0	0	360	5,600	12,000	2,600	0.19	0.4
Rock	0	0	590	4,500	7,800	1,600	0.26	0.2

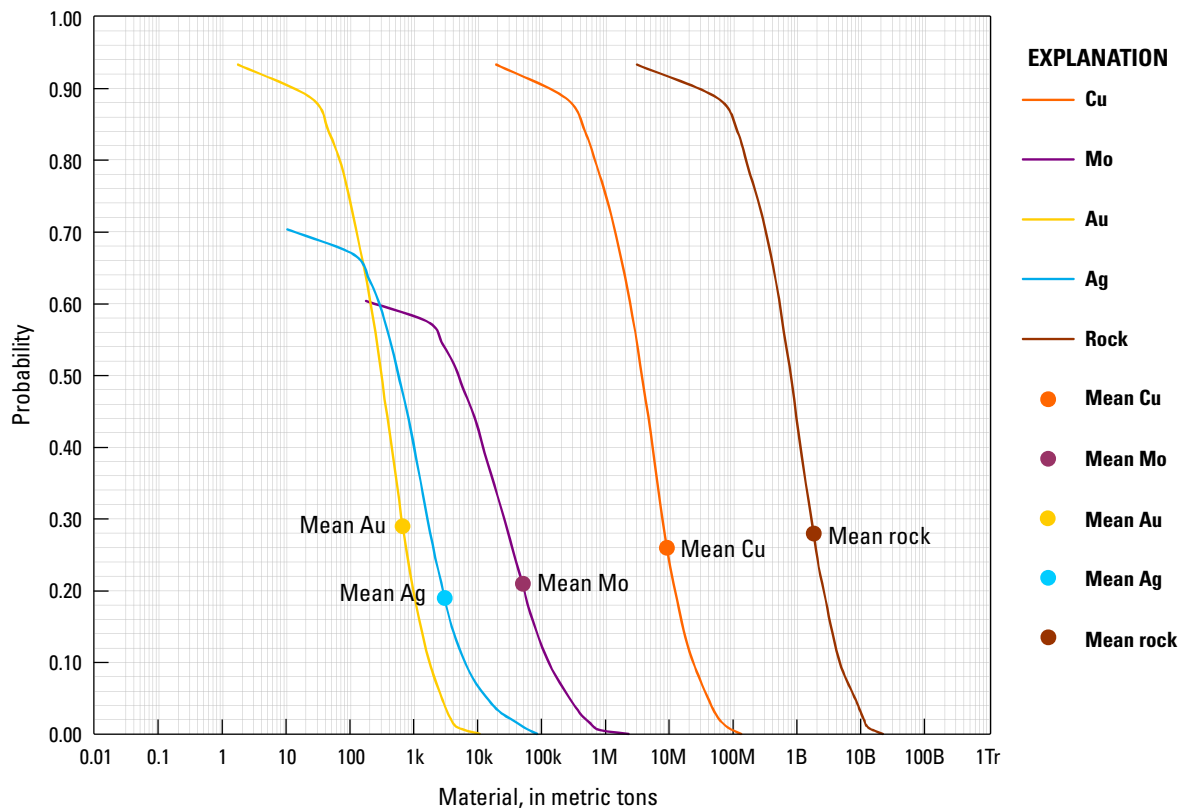


Figure 35. Cumulative frequency plot showing the results of Monte Carlo simulation of undiscovered resources in porphyry copper deposits in tract 142pCu9009, Khorasan—Afghanistan and Iran. k, thousand; M, million; B, billion; Tr, trillion.

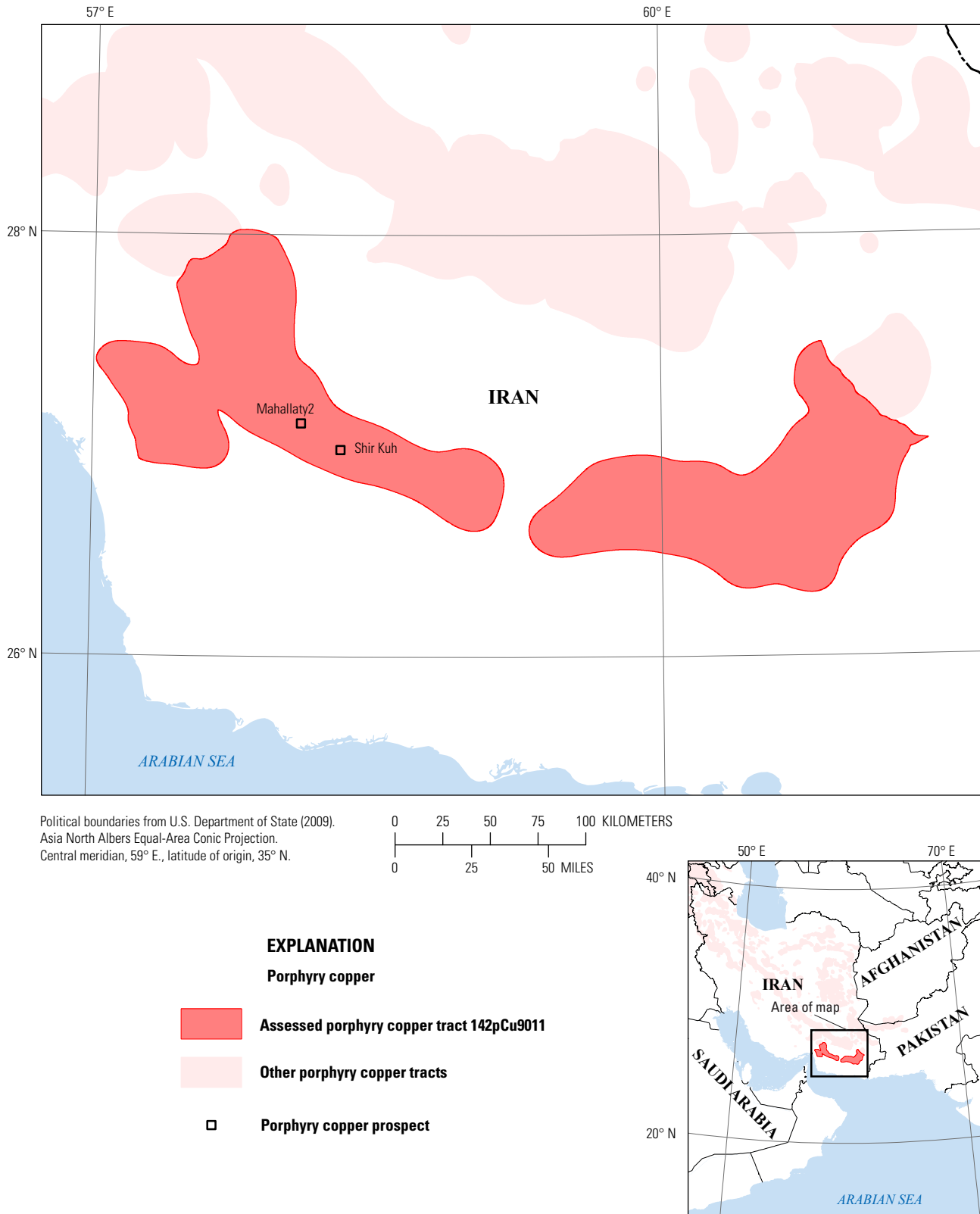


Figure 36. Map showing the location of known porphyry copper prospects for permissive tract 142pCu9011, Makran—Iran. See appendix C for prospects and appendix D for accompanying spatial data.

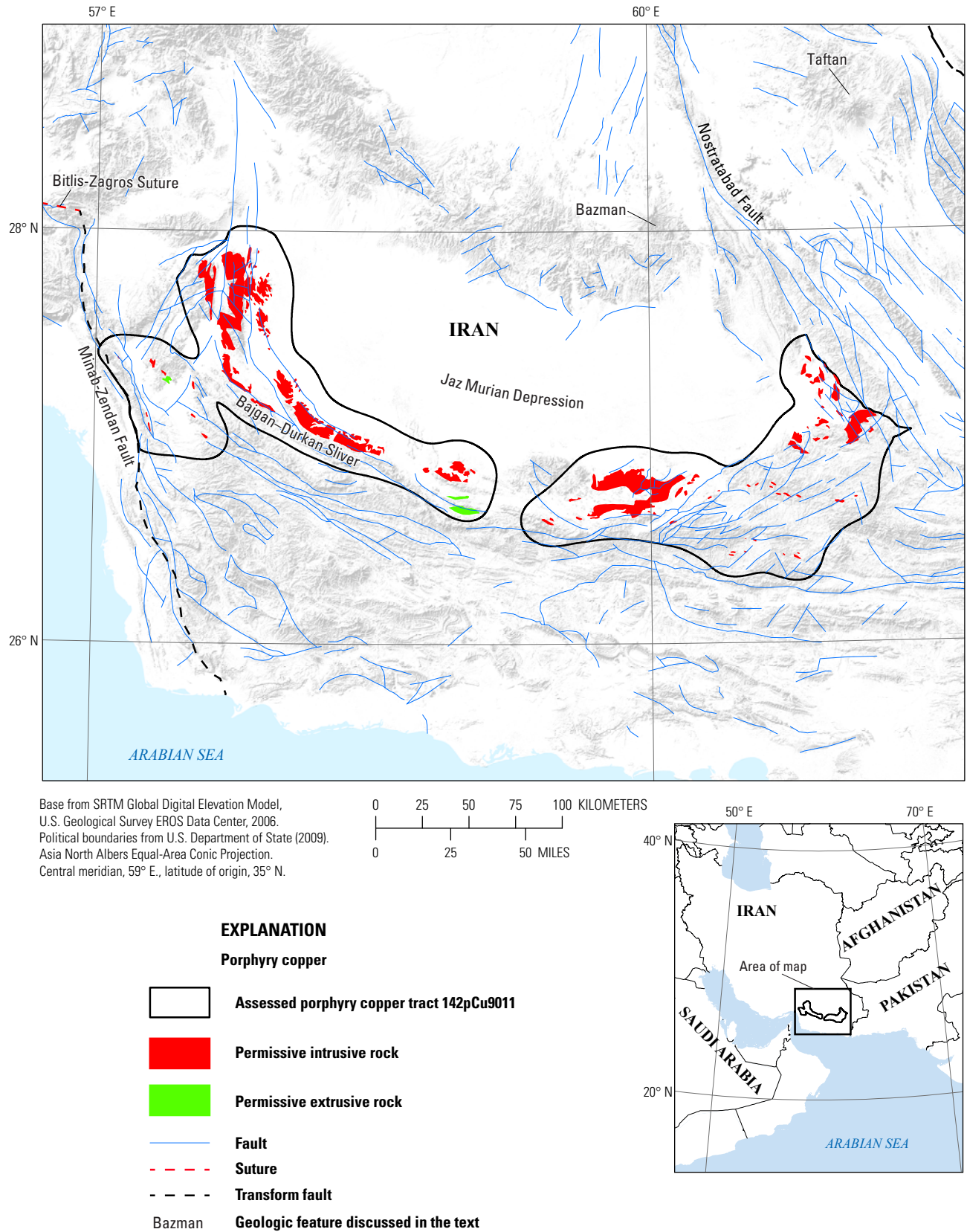


Figure 37. Map showing the distribution of permissive intrusive and extrusive rocks used to define tract142pCu9011, Makran—Iran. See appendix A for principal sources of information and appendix B for source map units.

In the Oligocene and Miocene, subduction-related magmatism was replaced by extension, subsidence, and deposition of shallow marine sedimentary rocks. In the Pliocene, renewed subduction with a very shallow slab dip (2.3–5.7°; Platt and others, 1985) developed to the south, forming a continental arc that is presently being built inland across the southern parts of the Lut, Chagai-Darirod, and Helmand Terranes. This continental arc includes the Pliocene to Holocene Bazman, Taftan, and Koh-i-Sultan volcanic edifices (see Pliocene-Quaternary–Bazman sub-tract below). In the fore-arc region of this young arc, thick successions of synorogenic molasses continue to be deposited concurrently with uplift, folding, thrusting, and erosion. A 4-km-thick sedimentary section overlies the present-day subduction trench located 150 km offshore in the Arabian Sea.

Porphyry-Related Prospects

The Makran region hosts placer gold, copper-bearing VMS, and ophiolite-related chromium deposits. However, no porphyry systems have positively been identified to date in this otherwise permissive island-arc setting (Walther, 1960; Samani, 1998; Förster, 1978; Shahabpour, 2010; Bazin and Hübner, 1969a). As in the Sanandaj-Sirjan Terrane to the west, Late Cretaceous-late Eocene igneous rocks in this fold-and-thrust belt appear deeply exhumed. As derived from the geologic map of Huber (1978), permissive units amount to 10 percent of the tract area and are composed of plutonic rocks only. Broadly coeval nonpermissive units constitute 44 percent, and younger rocks cover 41 percent of the tract area. Thus, relatively deep erosion coupled with thick intervening synorogenic and younger sedimentary cover may be responsible for limiting appropriate preservation and exposure levels for porphyry systems. Based on reports of copper occurrences that are spatially associated with subvolcanic porphyry intrusions (Geological Survey of Iran, 2012a; Huber, 1978; Walther, 1960; Shahabpour, 1999), two copper-bearing prospects that may be porphyry-related (Mahallaty2 and Shir Kuh (Makran) are tentatively included in this tract (see appendix C; fig. 36).

Qualitative Assessment

The occurrence of porphyry copper deposits is permissive in this relatively long-lived calc-alkaline to alkaline multiple island-arc setting. However, factors that considerably diminish favorability for occurrence of porphyry copper mineralization include deep levels of preservation and extensive cover. This is supported by the very low permissive unit {volcanic/[volcanic+plutonic]}×100 ratio of 3, a low permissive unit proportion (10 percent of the tract area; fig. 37), and relatively high percentage of younger cover rocks (41 percent). The absence of identified porphyry prospects not only argues in favor of inappropriate preservation and (or) exposure levels but also limited exploration for porphyry systems in this region (McCall, 1997). Despite the permissive geology, the assessment team felt that the favorability was too low to

add significant undiscovered copper resources to the overall assessment (less than a 10-percent chance of 1 undiscovered deposit). Therefore, quantitative assessment of the Makran tract was not warranted.

Eocene to Miocene Tracts

The six Eocene to Miocene permissive tracts are shown in figure 7. A probabilistic assessment of undiscovered resources was conducted for all six tracts (the Lut Tertiary, the Sistan, the Chagai, the Azerbaijan, the Yazd, and the Kerman tracts).

Lut Tertiary Tract (142pCu9010)

Descriptive model: Porphyry copper-gold (Cox, 1986b; Berger and others, 2008; John and others, 2010)

Grade and tonnage model: Porphyry copper, copper-gold subtype (Singer and others, 2008)

Geologic feature assessed: Middle Eocene to lower Miocene island to continental arc of the Tethyan Eurasian Metallogenic Belt

Location

The Lut Tertiary tract located in eastern Iran delimits a north-northeast–south-southwest 700-km-long and as much as 250-km-wide subduction-related magmatic arc of middle Eocene to early Miocene age. It covers an area of 56,300 km² within the Lut Terrane and small parts of the easternmost Tabas Terrane (fig. 38). The Lut Terrane is delimited by the right-lateral Nayband Fault system, which marks the boundary with the Tabas Terrane to the west. To the east, the Lut Terrane is bounded by the right-lateral Nehbandan Fault system, which separates it from the Sistan Terrane (fig. 3). The northern and southern limits of the Lut Terrane occur along the left-lateral Doruneh Fault on the north and the Jaz Murian Depression of the Makran Terrane on the south, respectively.

Tectonic Setting

Middle Eocene to early Oligocene convergence between India, Afghanistan, and the East-Central Iranian Terranes with Eurasia (fig. 4E) initiated closure of the Sistan Ocean (Golonka, 2004), as well as associated subduction and concurrent ±90-degree counterclockwise rotation of the East-Central Iranian Terrane (Dercourt and others, 1986). As a result of rotation, the present eastern border of the Lut Terrane represents the Lut Terrane's former southern margin. Structural relations present in deformed accretionary units of the Sistan Terrane suggest that convergence occurred along a two-sided east- and west-vergent subduction zone between the Lut and Afghanistan Terranes (Arjmandzadeh and others, 2011b), or alternatively, a single initially north-vergent subduction zone that is now folded and faulted on itself (Golonka, 2004). The latter scenario is supported by regional fold patterns observed in satellite imagery.

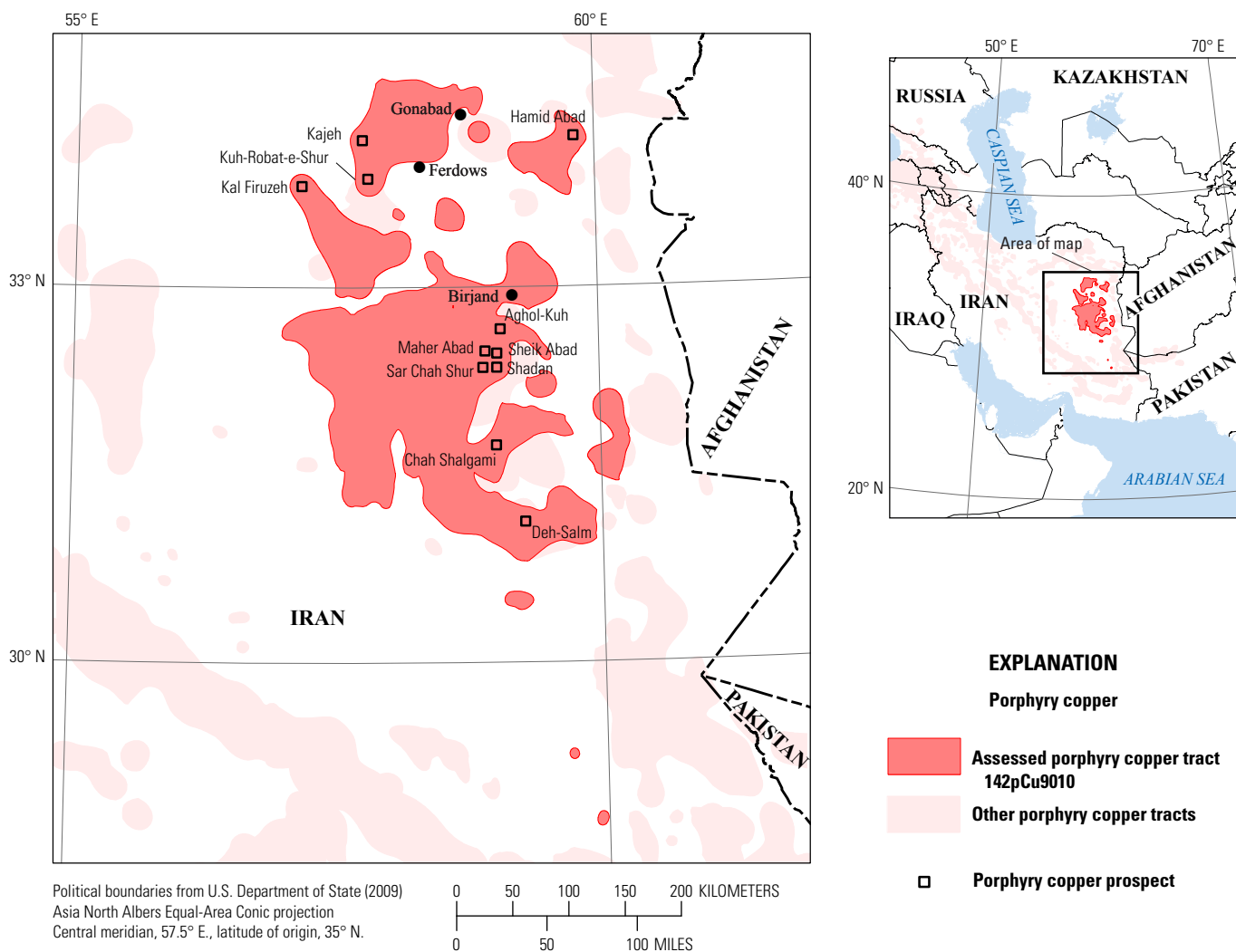


Figure 38. Map showing the location of known porphyry copper prospects for permissive tract 142pCu9010, Lut Tertiary—Iran. See appendix C for prospects and appendix D for accompanying spatial data.

Magmatism

Deposition of widespread Paleocene-early Eocene back-arc volcanism (Karimpour and others, 2011b) associated with the Border Folds and (or) the Lut Cretaceous arc-building events was followed by an evolving middle Eocene to early Miocene island to continental-arc setting emplaced along the eastern margin of the Lut Terrane. Middle Eocene to early Miocene subduction-related magmatism on the Lut Terrane (fig. 3) persisted until the collision between the East-Central Iranian and the Farah Terranes (fig. 4E, F) in the middle Miocene (Golonka, 2004). Volcanic rocks associated with this event are preserved to the west, whereas both volcanic and plutonic rocks are exposed in the arcuate thrust-bounded accretionary prism to the east. Permissive igneous units used to define the Lut Tertiary tract (appendix B) are shown in figure 39, along with locations of igneous complexes and other geologic features mentioned in this section.

The middle Eocene early stage of this volcano-plutonic event is represented by high-K calc-alkaline and alkaline basaltic and dacitic volcanic rocks and the 42-Ma Cu-(Au)-bearing syenite porphyry stock at Kuh-e-Robat-Shur (fig. 38). These rocks exhibit primitive island-arc affinities and are capped by ignimbritic deposits (Karimpour and others, 2011b).

The late Eocene intermediate stage is represented by subduction-related high-K calc-alkaline to shoshonitic mafic to intermediate volcanism and plutonism. Several intrusive stocks with associated porphyry Cu-Au mineralization form part of this event (Malekzadeh and others, 2010). These include the 40–37-Ma Maher Abad, Shadan, Sar Chah Shur, and Sheik Abad porphyry and related acid-sulfate prospects about 50 km southwest of the town of Birjand (fig. 38) and the Najmabad barren monzonite porphyry stock (fig. 39) southeast of the town of Gonabad (Karimpour and others, 2011b; Richards and others, 2012; Malekzadeh Shafaroudi and others, 2009b; Karimpour and Moradi Noghondar, 2010).

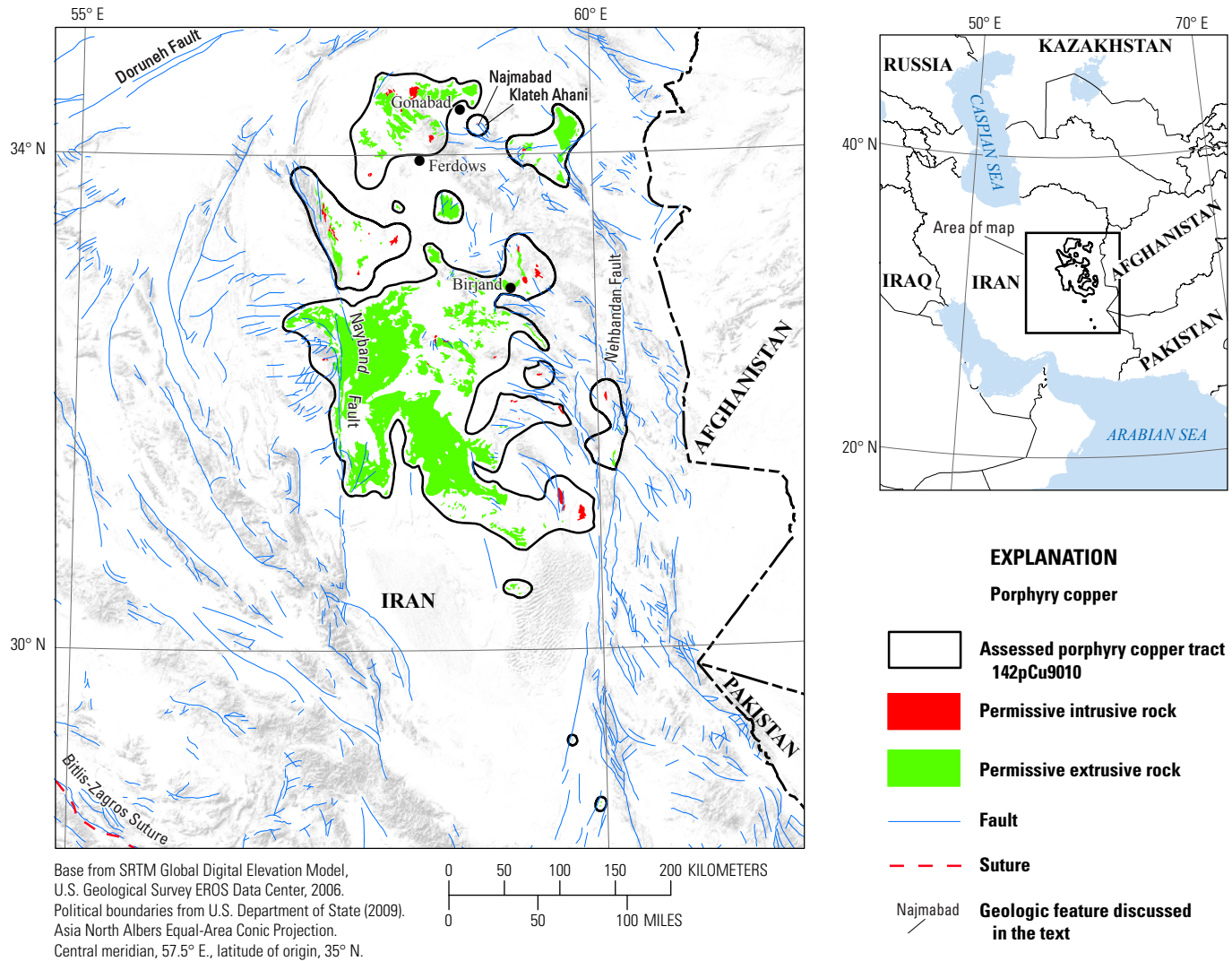


Figure 39. Map showing the distribution of permissive intrusive and extrusive rocks used to define tract 142pCu9010, Lut Tertiary—Iran. See appendix A for principal sources of information and appendix B for source map units.

The early Oligocene late stage consists of high-K calc-alkaline volcano-plutonic activity represented by the 34–33-Ma- Deh-Salm and Cha-Shaljami (fig. 38) Cu-Mo-Au diorite to quartz monzonite porphyry prospects (Karimpour and others, 2011b), and the Kajeh (fig. 38) diorite to monzonite porphyry Cu-Au-Mo prospect (Karimpour and others, 2008). Geochemical data indicate that these magmas originated above a subduction zone and that assimilation of crustal materials was not significant (Arjmandzadeh and others, 2011b). These intrusions were emplaced before the onset of uplift and erosion associated with the collision between the East-Central Iranian and Farah Terranes, given that igneous or sedimentary rocks of late Oligocene to middle Miocene age are generally not preserved on the Lut Terrane (Huber, 1978; Richards and others, 2012). These rocks were likely deposited, but largely eroded, during the pronounced and combined compressional events related to the middle to late Miocene final collision between the Lut and Farah, and Arabian Platform, and Sanandaj-Sirjan Terranes.

Known Porphyry Prospects

Porphyry copper and precious and base-metal epithermal systems are associated with middle Eocene to early Miocene magmatism in the Lut Terrane (Geological Survey of Iran, 2012e; Förster, 1978; Karimpour and Stern, 2011). However, known porphyry copper mineralization is of middle Eocene to early Oligocene age. Ziaii and others (2007) propose two north-northwest–south-southeast-trending metallogenetic zones in the Lut Terrane. The eastern zone is characterized by Cu-dominated systems, whereas the western zone is characterized by Pb-Zn-dominated mineralization. This metallogenetic pattern has been interpreted to represent a proximal Cu-bearing arc over a west-dipping subduction zone and a distal Pb-Zn-bearing back arc behind the arc. Within the Cu-dominated belt, a secular evolution from Cu-Au to Cu-Mo porphyry systems (Arjmandzadeh and others, 2011a) is supported by geochemical data that indicate progressive arc maturity from an island to a continental-arc

setting over time (Richards and others, 2012). No resource data are reported on the 10 positively identified porphyry prospects in the tract (appendix C; fig. 38), because exploration for porphyry copper deposits in the Lut Terrane is in its initial stages (Karimpour, 2007). Nevertheless, available information indicates that the late Eocene Maher Abad and Shadan porphyry prospects exhibit a Cu-Au metal association, whereas the early Oligocene Chah-Shaljami and Deh-Salm porphyry prospects display a Cu-Mo association.

Shadan, Maher Abad, Sar Cha Shur, and Sheik Abad Porphyry Prospect District

More than 15 late Eocene intrusive stocks with associated porphyry Cu-Au mineralization have been recognized in this district (Malekzadeh Shafaroudi, Karimpour, and Stern, 2009; Malekzadeh Shafaroudi and others, 2009; Malekzadeh and others, 2010; Karimpour and others, 2011b; Dorsa, 2011). At the Shadan (or Khopik of Karimpour and Stern, 2010) porphyry prospect, a (38.2 Ma, Karimpour and others, 2011b; or 37.3 Ma, Richards and others, 2012) diorite porphyry intrudes andesite and dacite units. The Shadan porphyry prospect consists of a 2-by 2-km partially covered phyllic alteration zone with a strong biotite-rich inner potassic core that is centered on a porphyry intrusion with unidirectional solidification textures (USTs). Surface gossans suggest the possibility of secondary enrichment. The Shadan prospect has not been systematically explored, but 0.44 g/t gold and 0.12 percent copper is indicated in surface rock samples from an area of 400 by 150 m (Dorsa PLC, 2011).

At the nearby 39-Ma Maher Abad Cu-Au prospect, a diorite porphyry intrudes Eocene dacitic rocks (Karimpour, Stern and others, 2011; Richards and others, 2012). Oxidation occurs around quartz stockworks in a 1- by 1-km partially covered outcrop of phyllic alteration overprinting potassic alteration (Malekzadeh Shafaroudi, Karimpour, and Stern, 2009; Malekzadeh Shafaroudi and others, 2009; Malekzadeh and others, 2010; Karimpour and Stern, 2010, 2011; Arjmandzadeh and others, 2011a). In the same area, porphyry prospects have also been identified at Sar Chah Shur and Sheik Abad. Copper mineralization at the Sar Chah Shur diorite to monzonite porphyry prospect is largely controlled by K-silicate alteration (Malekzadeh Shafaroudi and others, 2009), whereas the nearby 39.3-Ma Sheik Abad Au-(Cu) acid-sulfate epithermal prospect is believed to represent the shallow part of an underlying dioritic porphyry system (Malekzadeh Shafaroudi and others, 2009; Richards and others, 2012).

Cha-Shaljami Porphyry Prospect

The early Oligocene (33.3 Ma) Cha-Shaljami high-sulfidation gold and underlying Cu-Mo-Au-bearing porphyry prospect is 10–15 km south of the coeval (33.7 Ma) Qaleh Zari polymetallic vein (Richards and others, 2012) or IOCG (Karimpour and others, 2005; Karimpour and Stern, 2009) deposit. At the Cha Shaljami prospect, quartz monzonite to diorite stocks and dikes that intrude Eocene (40 Ma) andesite and andesitic basalt exhibit alteration characterized

by a 3- by 4-km outcrop of vuggy quartz and quartz-alunite associated with a porphyry system (Karimpour and Stern, 2011; Karimpour and others, 2011b; Malekzadeh Shafaroudi and others, 2009). The main sulfide minerals are pyrite, molybdenite, chalcopyrite, sphalerite, galena, and enargite (Arjmandzadeh and others, 2011a).

Deh-Salm Porphyry Prospect

At the early Oligocene (33.6 Ma) Deh-Salm (Mikh-Kh) Cu-Mo-Au-bearing prospect, porphyry stocks of intermediate to felsic composition intrude Eocene volcanic and sedimentary sequences (Karimpour and others, 2011b). Alteration zones include biotite, epidote-chlorite, quartz-sericite, and sericite-clay. Vein and disseminated mineralization include magnetite, pyrite, molybdenite, chalcopyrite, bornite, arsenopyrite, sphalerite, galena, covellite, digenite, and sulfosalts (Karimpour and others, 2011a; Ziaii and others, 2007; Karimpour and Stern, 2011).

Kajeh Porphyry Prospect

At the Kajeh Cu-Au-Mo-bearing porphyry prospect, an Oligocene-Miocene porphyry complex intrudes Cretaceous carbonates and Eocene volcanoclastic rocks (Karimpour and others, 2008). Sericitic and argillic alteration are associated with early diorite to monzonite phases, whereas quartz-sericite is better developed around the late felsic granite porphyry stock located to the north. Copper, gold, lead, and zinc occur in anomalous concentrations around the diorite-monzonite, whereas molybdenum, silver, lead, and zinc are anomalous around the granite porphyry stock (Pourkhosrow and others, 2007).

Other Porphyry-Related Mineral Occurrences

The 39.9 Ma Najmabad porphyry system about 100 km east of Kajeh appears to be barren (Karimpour and Moradi Noghondar, 2010). Spatially associated Sn-W-Cu mineralization may be related to the nearby Jurassic Klatah Ahani S-type granitoid (see Lut Jurassic tract above). Similarly, a porphyry-related origin for the Kal Firuzeh Mo-Zn-Cu skarn is uncertain (Geological Survey of Iran, 2012e). Kal Firuzeh is located about 70 km southwest of Kajeh, near the Lut-Tabas Terrane boundary (fig. 39). The Kal Firuzeh possible porphyry-related occurrence is included in the database (appendix C).

Preservation Level

As derived from the 1:1,000,000-scale map of Huber (1978), basement rocks underlie 14 percent of the Lut Tertiary tract area, whereas middle Eocene to early Miocene permissive volcanic and plutonic rocks occupy 29 and 1 percent of the tract area, respectively (fig. 39). Nonpermissive mafic, sedimentary, and volcano-sedimentary units constitute 17 percent of the tract, whereas younger rocks cover the remaining 38 percent of the tract.

Permissive units exhibit a very high {volcanic/[volcanic+plutonic]} $\times 100$ ratio of 97. However, these high volcanic-to-plutonic ratios occur principally in the larger western part of the Lut Tertiary tract, where Precambrian-Mesozoic basement is variably covered by as much as 2-km of volcanic and volcano-sedimentary successions. Most of the plutonic rocks and associated porphyry copper prospects in the Lut Tertiary tract are confined to a ± 100 -km-wide north-northwest–south-southeast corridor along the eastern side of the Lut Terrane. This corridor occupies the interface between Late Cretaceous to Eocene ophiolitic belts to the east and late Paleocene to early Oligocene volcanic- and volcano-sedimentary-dominated successions to the west. Levels of preservation of porphyry systems along this corridor are appropriate to shallow, as evidenced by the exposure of potassic and phyllic alteration associations, as well as related acid-sulfate alteration above several porphyry systems. Levels of preservation of porphyry systems in the western part of the Lut Tertiary tract are generally too shallow. However, possible porphyry-related occurrences in this region occur along tectonically disrupted areas (for example, the Kal Firuzeh Mo-Zn-Cu occurrence about the Nayband Fault).

Magnetic Anomalies

The regional aeromagnetic map (Maus and others, 2009) was used to confirm the location and character of regional geologic features (for example, arcs, basins, faults, terrane boundaries). The eastern boundary of the Lut Tertiary tract is marked by strong magnetic highs that coincide with northwest-southeast-trending ophiolite-bearing accretionary belts. A more subdued but continuous magnetic anomaly in the western part of the Lut Tertiary tract trends parallel to the Nayband Fault system. It does not convincingly image the location of the middle Eocene to lower Miocene volcanic-dominated units that define the tract or younger mafic cover rocks. Therefore, it may be reflecting deeper sources of unknown origin. Porphyry prospects identified in this tract are located in the intervening region between these two principal magnetic features. They generally lie along the margins of positive magnetic anomalies.

Probabilistic Assessment

Grade and Tonnage Model Selection

Resource data on the known porphyry prospects in the Lut Tertiary tract were not available to allow classification into Cu-Mo or Cu-Au porphyry deposit subtypes or to run pooled *t*-tests for model selection. Both Cu-Au and Cu-Mo metal associations are reported to be present and believed to be the result of progressive arc maturity from an island to a continental-arc setting over time (Richards and others, 2012). However, the Cu-Au association appears to dominate in the majority of known porphyry prospects. Therefore, the porphyry Cu-Au model of Singer and others (2008) was selected to estimate undiscovered copper, gold, molybdenum, and silver resources in this tract.

Estimates of Undiscovered Deposits and Rationale

Geologic factors favorable for the occurrence of undiscovered porphyry deposits in the Lut Tertiary tract include (1) a relatively large island to continental arc, (2) permissive alkaline and calc-alkaline compositions, and (3) shallow and intermediate levels of exposure for Cu-Au and Cu-Mo porphyry systems in the eastern part. Unfavorable factors for the occurrence of undiscovered porphyry deposits include (1) a relatively short-lived magmatic arc system, (2) unknown size of identified porphyry prospects, and (3) large parts of the tract that are overlain by permissive volcanic, as well as younger cover.

Overall, the lack of known porphyry deposits compared to that in other tracts of equivalent aerial extent elsewhere suggests that undiscovered deposits likely are present. However, this is not reflected by the relatively low numbers of known porphyry prospects in a region that is just beginning to see increased exploration for porphyry copper deposits (Karimpour, 2007; Richards and others, 2012). Vast areas in the western part (back arc?) of the tract that are shallowly to deeply covered by volcanic and sedimentary successions, under which undiscovered deposits may be present.

The assessment team established that the Lut Tertiary tract was geologically favorable and that estimates of numbers of undiscovered porphyry copper deposits could be carried out with moderate levels of uncertainty. The tract would contribute significant copper resources from undiscovered deposits to the overall assessment. Therefore, quantitative assessment of undiscovered deposits in this tract was warranted. Table 10A shows the consensus estimates for undiscovered porphyry copper deposits in the Lut Tertiary tract at the 90-, 50-, and 10-percent probability levels and the associated summary statistics. At the 90-percent probability level, assessors felt that there was no likelihood for undiscovered deposits. At the 50-percent probability, the numbers ranged between 1 and 2, and at the 10-percent probability level the numbers increased to between 4 and 5. On the basis of these numbers, the team reached a consensus estimate of 0, 2, and 5 undiscovered deposits for the 90-, 50-, and 10-percent probability levels, respectively, which resulted in a mean of 2.38 undiscovered deposits with a standard deviation of 2.03 ($C_v=85$). The estimate reflects the level of favorability and moderate uncertainty assessed for this tract.

Probabilistic Assessment Simulation Results

Simulation results for estimates for copper, molybdenum, gold, silver, and the total volume of mineralized rock are summarized in table 10B. The mean estimate of undiscovered copper resources in the Lut Tertiary porphyry tract is 7.5 Mt. Results of the Monte Carlo simulation are also presented as cumulative frequency plots (fig. 40). The cumulative frequency plots show the cumulative probabilities of occurrence-estimated resources and total mineralized rock, as well as the mean for each commodity and for total mineralized rock.

Table 10. Probabilistic assessment for tract 142pCu9010, Lut Tertiary—Iran.

A. Undiscovered deposit estimates, deposit numbers, tract area, and deposit density.

[N_{xx} , estimated number of deposits associated with the xxth percentile; N_{und} , expected number of undiscovered deposits; s , standard deviation; $C_v\%$, coefficient of variance; N_{known} , number of known deposits in the tract that are included in the grade and tonnage model; N_{total} , total of expected number of deposits plus known deposits; tract area, area of permissive tract in square kilometers (km^2); deposit density reported as the total number of deposits per 100,000 km^2 . N_{und} , s , and $C_v\%$ are calculated using a regression equation (Singer and Menzie, 2005)]

Consensus undiscovered deposit estimates					Summary statistics					Tract area (km^2)	Deposit density ($N_{total}/100,000 km^2$)
N_{90}	N_{50}	N_{10}	N_{05}	N_{01}	N_{und}	s	$C_v\%$	N_{known}	N_{total}		
0	2	5	5	5	2.4	2.0	85	0	2.4	56,300	4

B. Results of Monte Carlo simulations of undiscovered resources.

[Cu, copper; Mo, molybdenum; Au, gold; and Ag, silver; in metric tons; Rock, in million metric tons]

Material	Probability of at least the indicated amount						Probability of	
	0.95	0.9	0.5	0.1	0.05	Mean	Mean or greater	None
Cu	0	0	2,600,000	20,000,000	33,000,000	7,500,000	0.27	0.2
Mo	0	0	1,900	120,000	250,000	44,000	0.2	0.47
Au	0	0	220	1,500	2,300	540	0.29	0.2
Ag	0	0	330	5,200	10,000	2,400	0.19	0.4
Rock	0	0	580	4,200	7,200	1,500	0.28	0.2

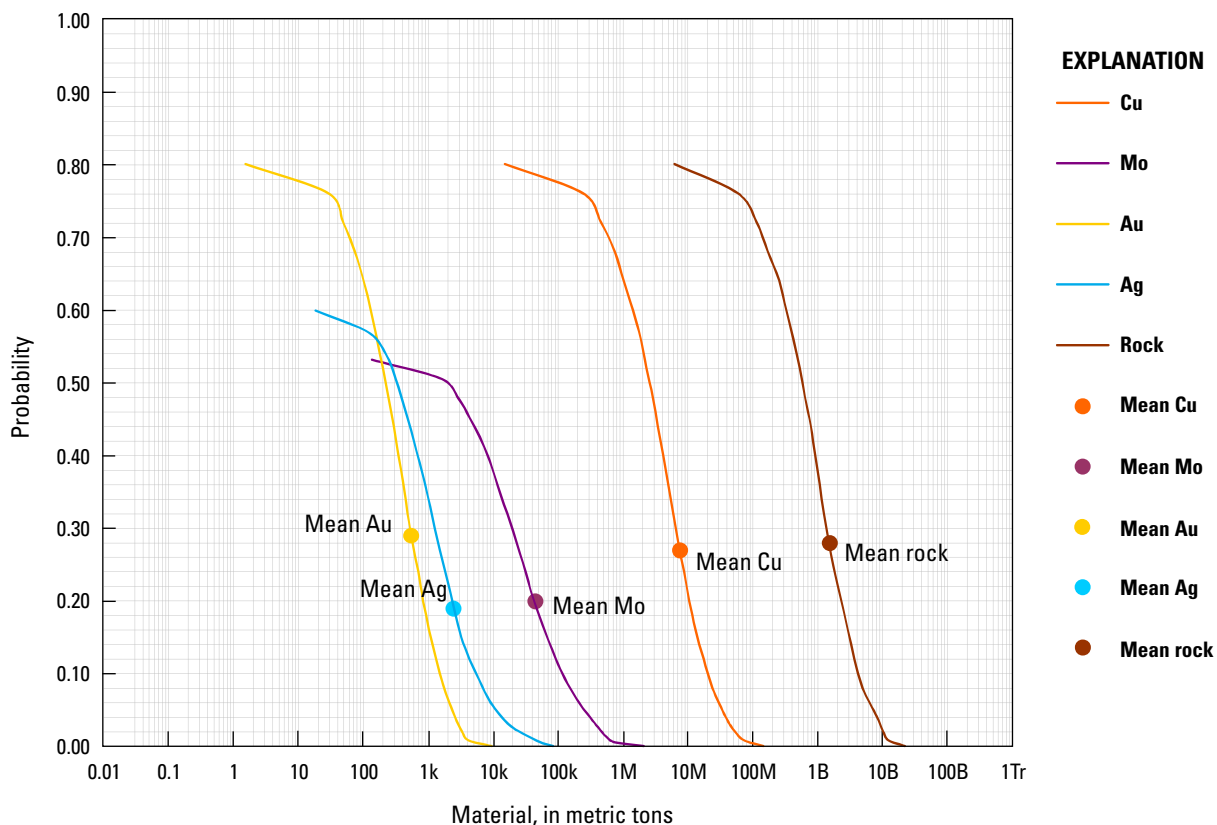


Figure 40. Cumulative frequency plot showing the results of Monte Carlo simulation of undiscovered resources in porphyry copper deposits in tract 142pCu9010, Lut Tertiary—Iran. k, thousand; M, million; B, billion; Tr, trillion.

Sistan Tract (142pCu9012)

Descriptive model: General porphyry copper (Cox, 1986a; Berger and others, 2008; John and others, 2010)

Grade and tonnage model: General Cu-Au-Mo porphyry copper model (Singer and others, 2008)

Geologic feature assessed: Late Cretaceous to early Miocene island arcs of the Tethyan Eurasian Metallogenic Belt

Location

The Sistan tract is located in easternmost Iran, where it covers an area of 32,800 km² (fig. 41). It delimits a Late Cretaceous to early Miocene island-arc volcano-plutonic belt within the Sistan suture zone (also known as Eastern Iranian Ranges). The Sistan suture zone consists of a north-south-trending deformed accretionary complex that separates the Lut Terrane of eastern Iran from the Farah Terrane in western Afghanistan. To the southeast, the Sistan suture zone continues into Baluchistan (Pakistan), where it rims the southern margin of the Chagai-Darirod Terrane.

In the south, the Sistan tract is juxtaposed against the Makran Terrane along the dextral Nehbandan-Nostratabad Fault system to the west and against the Chagai-Darirod Terrane along the dextral Neh-Zahedan Fault system to the east (fig. 2). In the north, the Sistan tract extends as far as the sinistral Great Kafir-Doruneh Fault system (fig. 2).

Tectonic Setting

The Sistan suture zone is divided into the Late Cretaceous Ratuk and Late Cretaceous-Eocene Neh (fig. 3) accretionary complexes (Tirrul and others, 1983). These complexes include island-arc rocks that were emplaced during the convergent tectonic setting that eventually closed the Sistan Ocean. They occupy the northeastern and southwestern parts of the suture zone, respectively. The Late Cretaceous Ratuk and Late Cretaceous to Eocene Neh complexes are composed of ophiolitic mélanges and marine sedimentary rocks, which are separated and unconformably overlain by thick early Eocene flysch sequences interbedded with subordinate calc-alkaline flows and volcanoclastic rocks of the Sefidabeh fore-arc basin (Fotoohi Rad and others, 2009; Camp and Griffis, 1982; Tirrul and others, 1983).

Between the middle Eocene and middle Miocene, convergence between the Farah Terrane in Afghanistan and Lut Terrane in Iran (fig. 4D, E, F) progressively closed the Sistan Ocean (Golonka, 2004). The polarity of subduction zones in the Sistan Ocean remains a subject of debate. Recent studies (Arjmandzadeh and others, 2011b) favor a two-sided subduction setting facing both the Lut and Farah Terranes. Given the coupled rotational and compressional history in the region, as well as regional structural patterns observed on satellite imagery, Golonka (2004) proposes that this two-sided subduction scenario may instead be a single initially north-vergent subduction zone that is now folded and faulted on itself (fig. 4G).

Magmatism

The Sistan tract delineates the Late Cretaceous to early Miocene island-arc rocks defined by permissive igneous units (appendix B) that are shown in figure 42, along with locations of igneous complexes and other geologic features mentioned in this section.

Late Cretaceous-early Eocene igneous rocks that define the Sistan tract are characterized by subaqueous tholeiitic to calc-alkaline intermediate to silicic volcanic flows and volcanoclastic units that are interbedded with marine sediments. Representative intrusions include the 42 Ma calc-alkaline north-trending Rud-e-Shur diorite-quartz diorite dikes (fig. 42). These dikes are as much as 10 m wide and traceable for distances of as much as 2 km. No mineralization is known to be associated with these folded dikes (Camp and Griffis, 1982). However, this event exemplifies immature island-arc magmatism in the region, which may be similar in character to the depositional environment of the Late Cretaceous-early Eocene volcano-sedimentary formations in the Chagai Hills (see Chagai tract below) of Pakistan (Perelló and others, 2008).

Convergence of the Sistan Ocean produced island-arc magmatism that was most widespread between middle Eocene to early Miocene times (Berberian and King, 1981). Middle Eocene to early Oligocene magmatism is characterized by calc-alkaline andesitic and minor basaltic flows and pyroclastics deposited in a subaqueous environment, which are comparable in age and composition to island-arc magmatism in both the Lut (see Lut Tertiary tract above) and Chagai-Darirod (see Chagai tract below) Terranes (Richards and others, 2012; Karimpour and others, 2011b). In the Sistan suture zone, early Eocene and older units were affected by a late Eocene folding event.

The early Oligocene (31–34 Ma) Zahedan-Saravan Batholith is the most prominent expression of plutonism in the Sistan suture zone. It consists of a 180-km-long and 25-km-wide batholith composed of metaluminous to weakly peraluminous I-type calc-alkaline granites, granodiorites, quartz monzonites, tonalites, minor two-mica pegmatites, and late cross-cutting andesitic to dacitic dikes (Camp and Griffis, 1982) that extends from the Nehbandan Fault on the northwest to the Shah-Kuh (Sistan) pluton on the southeast (fig. 42). Field relations and compositional data suggest that these calc-alkaline intrusions assimilated large amounts of sedimentary materials, were emplaced in a relatively passive manner, and crystallized at moderate depths.

The 1:1,000,000-scale geologic map of Iran (Huber, 1978) shows that the Zahedan-Saravan Batholith is in part flanked on its sides by Paleozoic basement units that are equivalent to the ones found in the Bajgan-Durkan continental sliver of the Makran Terrane. If correct, this may suggest that part of the Sanandaj-Sirjan Terrane is also present in the Sistan suture zone and could also explain why plutonic units in the Zahedan-Saravan Batholith reach peraluminous compositions.

In the late Oligocene, a shift from calc-alkaline to alkaline magmatism occurred in a subaerial setting, marking a change in tectonic regime and an increased rate of uplift related to

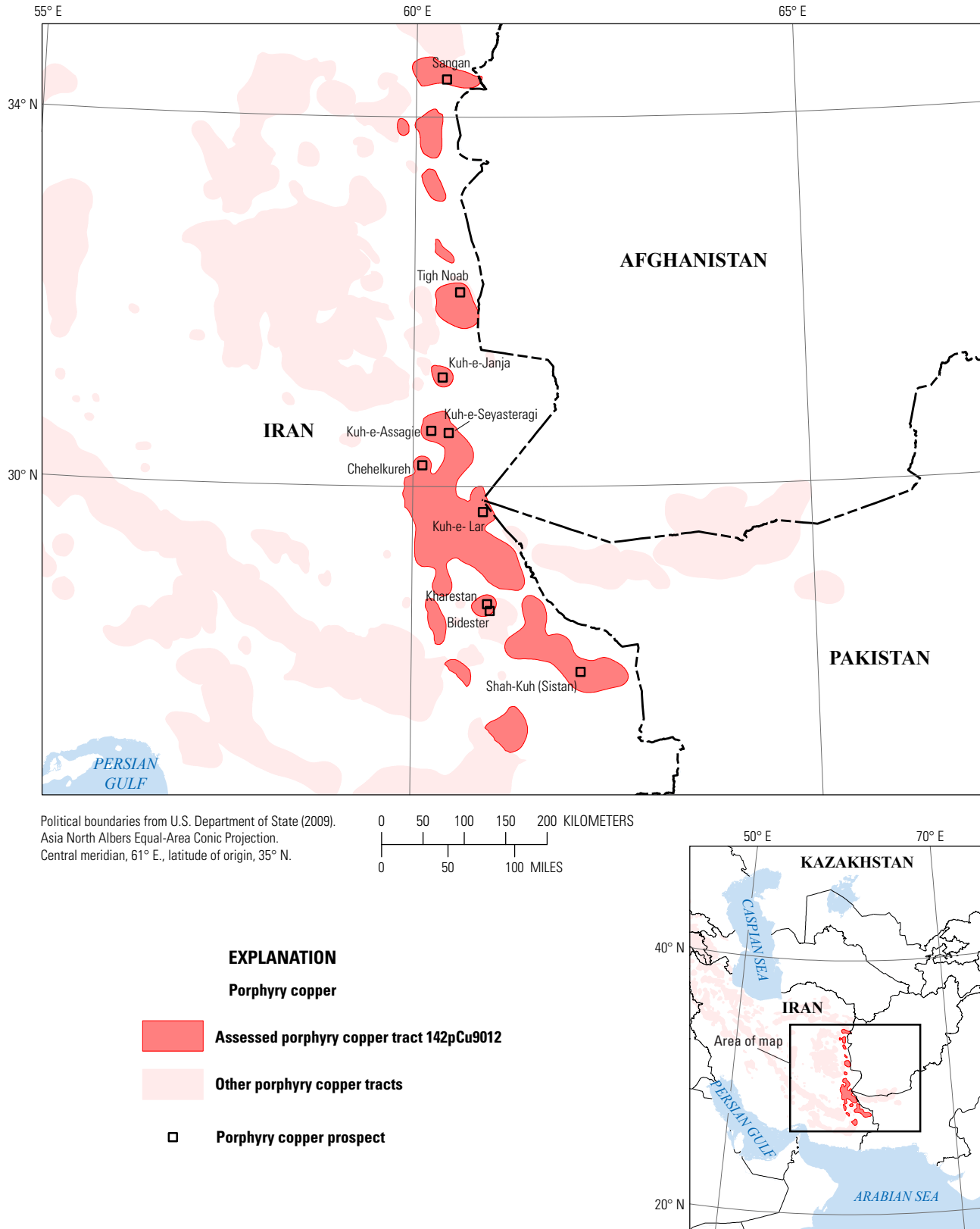
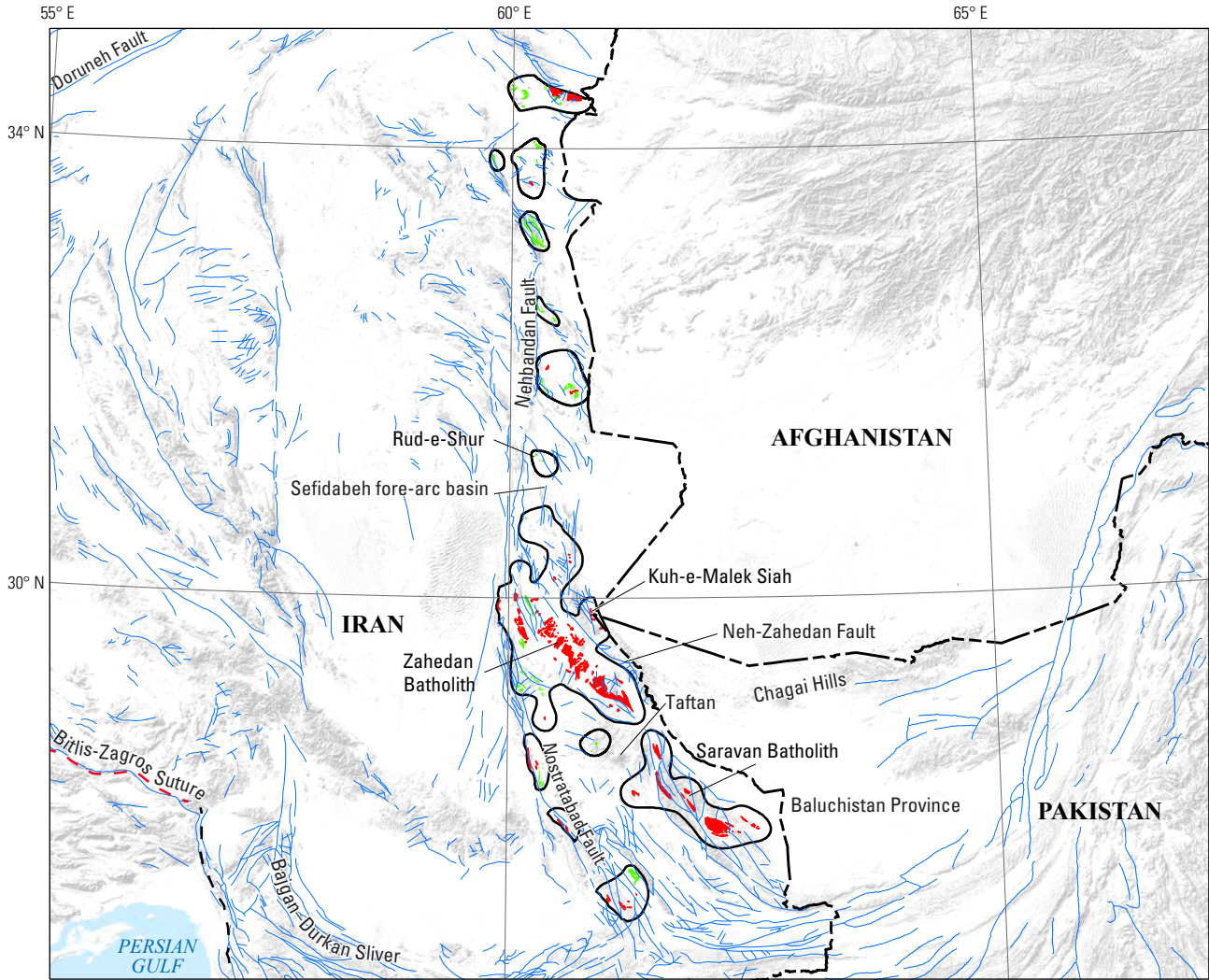
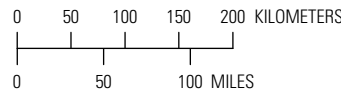


Figure 41. Map showing the location of known porphyry copper prospects for permissive tract 142pCu9012, Sistan—Afghanistan, Iran, and Pakistan. See appendix C for prospects and appendix D for accompanying spatial data.



Base from SRTM Global Digital Elevation Model, U.S. Geological Survey EROS Data Center, 2006. Political boundaries from U.S. Department of State (2009). Asia North Albers Equal-Area Conic Projection. Central meridian, 61° E., latitude of origin, 35° N.



- EXPLANATION**
- Porphyry copper**
 - Assessed porphyry copper tract142pCu9012**
 - Permissive intrusive rock**
 - Permissive extrusive rock**
 - Fault**
 - Suture**
 - Transform fault**
 - Rud-e-Shur **Geologic feature discussed in the text**

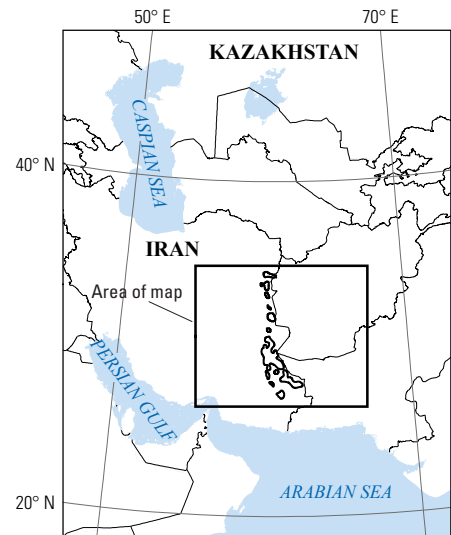


Figure 42. Map showing the distribution of permissive intrusive and extrusive rocks used to define tract 142pCu9012, Sistan—Afghanistan, Iran, and Pakistan. See appendix A for principal sources of information and appendix B for source map units.

the ongoing closure of the Sistan Ocean (McCall, 1997). This event is represented by the Kuh-e-Lar (27.8 Ma), Kuh-e-Malek Siah (27.2–28.8 Ma), and Kuh-e-Assagi (27.5 Ma) caldera complexes. With the exception of the K-rich Kuh-e-Lar complex, these dominantly mafic alkaline complexes are Na-rich. These volcano-plutonic complexes are preferentially located in extensional pull-apart basins along major strike-slip faults. They are believed to be derived from partial melting of either ocean crust or upper mantle.

In the early Miocene subaerial magmatism changed again from alkaline to calc-alkaline. Older moderately to strongly alkali, mafic to intermediate flows and minor volcanoclastic deposits were followed by thick successions of calc-alkaline basaltic to rhyodacitic flows, domes, and pyroclastic rocks. Intrusive complexes related to this time period include the Kuh-e-Seyasteragi (19.2 Ma) and Kuh-e-Janja (16.5 Ma) calc-alkaline intermediate to felsic porphyry prospects (McCall, 1997).

These and older units were folded along north-northwest-trending axes and cut by middle Miocene and younger conjugate left- and right-lateral strike-slip faults. In the middle Miocene, arc-related magmatism in the southern part of the Sistan suture zone was arrested by final collision between the Lut and Farah Terranes (Tirrul and others, 1983).

To the south, however, subduction along the southern margin of the Makran Terrane was reinitiated, generating continental arc magmatism (see Pliocene-Quaternary–Bazman sub-tract below) on the sutured Lut, Sistan, and Chagai-Darirod Terranes beginning in the latest Miocene (Camp and Griffis, 1982).

Known Porphyry Prospects

Intrusion-related mineralization styles in the Sistan tract evolved from vein and replacement Cu-Zn-Pb-Ag and greisen tin systems associated with Eocene-Oligocene locally porphyritic calc-alkaline plutons, to base-metal veins and Cu-Mo-Au porphyry systems related to late Oligocene alkaline complexes, and to porphyry-related Cu-Au-Zn-Pb skarn systems associated with early Miocene calc-alkaline intrusions (Förster, 1978). In addition, possible porphyry-related prospects are associated with iron skarn (IOCG) systems in the northern part of the tract. Ten porphyry and possible porphyry-related prospects were identified in the Sistan tract (see fig. 41; appendix C). Positively identified porphyry prospects are of late Oligocene and early Miocene ages and occur at Kuh Assagi, Kuh Lar, Kuh-e-Seyasteragi, Kuh-e-Janja, and Shah Kuh (Sistan).

Shah-Kuh (Sistan) Porphyry Prospect

The Oligocene calc-alkaline Shah-Kuh biotite granodiorite batholith is located in the southern part of the Neh Complex. The batholith intruded and contact-metamorphosed Eocene flysch units. A copper prospect is associated with a 3- by 1-km porphyry diorite stock that was emplaced into a middle Eocene sandstone-shale sequence on the eastern part of the batholith (McCall, 1997; Eftekhari-Nezad and McCall, 1993). Little is known about the character of mineralization

at this site, but it is included as a prospective area in the Cu porphyry potential map of Geomatics Management [n.d.].

Kuh-e-Lar and Kuh-e-Assagi Porphyry Prospects

The late Oligocene Kuh-e-Lar and Kuh-e-Assagi Cu-Mo-Au-bearing porphyry prospects occur in the Ratuk Complex (Camp and Griffis, 1982; Samani, 1998). Alkaline intrusive phases contained within the eroded core of the 8- by 5-km (27.8 Ma) Kuh-e-Lar collapsed caldera include mafic to late monzonite, syenite, and quartz syenite stocks that are in part porphyritic (Karimi, 2002). These stocks are crosscut by numerous north-northeast fractures that control Cu-Mo-Au mineralization (Zarcán International Resources, 2000; Camp and Griffis, 1982). The 27.5 Ma Kuh-e-Assagi intrusive-volcanic complex is similar to Kuh-e-Lar (Camp and Griffis, 1982). It consists of intermediate to felsic flows and shallow plutons, including a monzonite porphyry stock with breccia bodies that host copper, lead, zinc, and silver mineralization (Zarcán International Resources, 2000, 2003).

Kuh-e-Seyasteragi and Kuh-e-Janja Porphyry Prospects

The early Miocene Kuh-e-Seyasteragi and Kuh-e-Janja porphyry prospects also occur in the Ratuk Complex. The 19.2-Ma Kuh-e-Seyasteragi and 16.5-Ma Kuh-e-Janja calc-alkaline intermediate to felsic porphyry intrusions are small in outcrop, but they exhibit well-developed contact metamorphic halos. Cu-Au-(Zn-Pb)-bearing porphyry- and replacement-style mineralization is centered on these shallowly emplaced intrusions (Camp and Griffis, 1982).

Other Possible Porphyry-Related Deposits and Prospects

Middle Eocene to early Oligocene plutonic rocks of the Zahedan Batholith are emplaced in strongly folded low-grade metamorphic ophiolite and flysch formations of the Neh Complex (McCall, 1997; Tirrul and others, 1983). The foliated concordant and sill-like Zahedan Batholith is composed of early biotite granite, hornblende-biotite granodiorite, and late diorite stocks that partially developed hornfels and skarn halos. Abundant north-south to north-northeast–south-southwest andesite and porphyritic dacite dike swarms cut early Oligocene and older units (Sadeghian and others, 2005). No porphyry-style mineralization is reported from the Zahedan Batholith. However, the presence of base-metal vein, high-temperature replacement and skarn deposits, as well as the temporal and spatial association with porphyritic diorite intrusions (Maanijou and others, 2012; Boomeri and others, 2005) suggest that these deposits may be related to porphyry copper mineralization at depth. Possible porphyry-related mineralization occurs at the 33.6-Ma Chehelkureh Cu-Zn-Pb-(Ag-Au) vein and high-temperature replacement mine (resource of 14 Mt at 1.5 percent copper, 1.81 percent zinc, 0.88 percent lead, 22 ppm silver, and 0.14 ppm gold; Maanijou and others, 2012). Proven and probable reserves at the Chehelkureh deposit have been estimated at 5.6 Mt at

1.27 percent copper at a 0.2 percent cutoff (National Iranian Copper Industries Company, 2012). This deposit is spatially associated with an Oligocene I-type calc-alkaline porphyritic quartz monzodiorite-tonalite-granodiorite pluton that intruded an Eocene turbiditic sequence (Camp and Griffis, 1982). Fluid inclusion and stable isotope studies of the Chehelkureh deposit show that the mineralization formed around 450 °C from moderately saline solutions of magmatic origin (Maanijou and others, 2012). These high-temperature moderately saline magmatic fluids are consistent with formation in a porphyry environment.

The Zahedan Batholith also hosts contrasting tin-tourmaline mineralization that is centered on the more peraluminous phases of the batholith (Camp and Griffis, 1982; Tirrul and others, 1983). These peraluminous units are believed to have resulted from assimilation of significant fractions of basinal sediments despite having been emplaced in an island-arc environment (Berberian and Berberian, 1981).

The northern part of the Sistan tract hosts numerous copper occurrences, including the Sangan Fe-(Au±Cu) skarn deposit (see Khorasan tract above). The Sangan deposit contains one of the largest iron resources in Iran with 600 Mt at greater than 45 percent iron (Ghavi and Karimpour, 2010). The deposit lies on the eastern extension of the Doruneh Fault, possibly on a southward-thrust sheet of the Taknar-Kashmar Belt (see figs. 41 and 42). At Sangan, upper Mesozoic sedimentary rocks and iron replacement bodies are intruded by late Eocene biotite-hornblende quartz monzonite to syenogranite porphyry stocks and dikes (Malekzadeh Shafaroudi and others, 2013; Boomeri and others, 2006; Boomeri, Ishiyama, and others, 2010). Reported K₂O contents in these intrusive units are too high (8.5–13 percent; Karimpour and Malekzadeh, 2006) even for highly alkaline rocks, proposing the existence of potassic alteration instead. Copper and gold mineralization and spatially associated porphyry intrusions suggest the presence of porphyry-style mineralization. A similar possible porphyry-related system occurs at the Tigh Noab Cu-Fe bearing skarn prospect (Geological Survey of Iran; 2012a), about 250 km south of Sangan deposit. However, the age of mineralization here is not constrained.

In the southern part of the Sistan tract, the Kharestan and Bidseter Cu-Zn-Pb-Au-Ag epithermal vein prospects (Samani, 1998; National Iranian Copper Industries Company, 2012; Zanganeh and others, 2010) exhibit large 5- by 2-km and 6- by 3-km oxidation zones of intense hematite, goethite, and jarosite that also include alunite, kaolinite, white mica, chlorite, and opaline silica (HYPERION hyperspectral data; Zarcán International Resources, 2003). Oxidation and alteration minerals may indicate the presence of porphyry-style mineralization at depth, as suggested by Samani (1998). However, the age of mineralization here is not well-constrained. As shown on the geologic map (Huber, 1978), rocks in the area include Paleozoic extrusive, Cretaceous carbonate, Paleogene clastic, Oligocene-Miocene andesitic, and abundant Pliocene-Holocene volcanic rocks. Thus, these

epithermal prospects may be as young as Pliocene-Holocene and related to the adjacent Taftan volcanic edifice (see Pliocene-Quaternary–Bazman sub-tract below) rather than the older middle Eocene to early Miocene magmatic event delimited by the Sistan tract.

Preservation Level

As derived from the 1:1,000,000-scale map of Huber (1978), overall aerial proportions of older basement (9 percent), permissive plutonic and volcanic units (6 and 2 percent, respectively), broadly coeval nonpermissive units (41 percent), and younger cover rocks (41 percent) occupy the Sistan tract (fig. 42).

The overall permissive volcanic-to-plutonic ratio across the Sistan tract is low at $\{\text{volcanic}/[\text{volcanic}+\text{plutonic}]\} \times 100 = 28$. However, this ratio is influenced by the deeply exhumed Zahedan-Saravan Batholith, which occupies a large area of the Sistan tract. In the region of the Neh accretionary complex, strong folding and faulting juxtapose both deeper and shallower levels of the upper crust, exposing foliated granitoids with no known porphyry systems against relatively unmetamorphosed wallrocks that host vein-replacement deposits. Available information, such as at the Chehelkureh vein-replacement deposit, suggests that related porphyry-style mineralization may be present.

To the northeast in the Ratuk accretionary complex, in contrast, the permissive volcanic-to-plutonic ratio is much higher. This suggests that levels of crustal preservation are shallower and more appropriate for porphyry copper mineralization. This is consistent with known alkaline to calc-alkaline porphyry prospects that are emplaced in relatively well-preserved caldera complexes. The isolated spatial distribution of these caldera complexes further suggests that volcano-plutonic complexes and associated porphyry mineralization of this age range may be buried under younger cover.

Magnetic Anomalies

The regional aeromagnetic map (Maus and others, 2009) was used to confirm the location and character of regional geologic features (for example, arcs, basins, faults, terrane boundaries). In the Sistan suture zone, strong magnetic anomalies coincide with the location of several ophiolite-bearing accretionary belts. Magnetic anomalies across the rest of the Sistan suture zone are otherwise subdued. Thus, prominent batholithic masses, such as the relatively felsic Zahedan-Saravan, are not well-imaged at the regional scale.

With exception of the Kuh-e-Janga and Kuh-e-Seyasteragi porphyry prospects, other porphyry-related occurrences identified in this tract are located along the margins of positive magnetic anomalies.

ASTER Alteration Data

Processed ASTER data (Mars and Rowan, 2006; Mars, 2014) were used to evaluate potential hydrothermal alteration that could be associated with unidentified porphyry systems in the Sistan tract. ASTER coverage was available only across the

central-southern part (12 percent) of the Sistan tract, where 8 ASTER-derived argillic and phyllic alteration zones are spatially associated with the Zahedan Batholith, 3 with the Taftan volcano, and 1 with the Shah-Kuh (Sistan) pluton. ASTER-derived alteration zones associated with plutonic units are about 3 km in diameter in the Zahedan Batholith (where no porphyry prospects have positively been identified) and in the Shah-Kuh (Sistan) pluton (where a porphyry prospect is known). Larger, about 6 km long, more linear alteration zones characterize Pliocene-Holocene volcanic units with epithermal vein systems northwest of the Taftan volcano (Kharestan and Bidseter). Hence, across the central-southern part of the Sistan tract, ASTER-derived alteration data suggest the existence of several potential hydrothermal alteration zones that could be related to unidentified porphyry systems.

Probabilistic Assessment

Grade and Tonnage Model Selection

No available resource data on prospects in the Sistan tract precluded evaluation of dominant metal associations in porphyry systems, or the running of a pooled *t*-test for model selection. Identified porphyry copper prospects include late Oligocene Cu-Mo-Au(\pm Zn-Pb-Ag)-bearing alkaline to early Miocene Cu-Au(\pm Zn-Pb)-bearing calc-alkaline systems. These complex base-metal associations are consistent with geologic and geochemical data, which indicate primitive island-arc magmatism that was, however, significantly modified by assimilation of sedimentary materials. Given the variability in metal associations, the general Cu-Au-Mo model of Singer and others (2008) was selected to estimate undiscovered copper, gold, molybdenum, and silver resources in this tract.

Estimates of Undiscovered Deposits and Rationale

Geologic factors favorable for the occurrence of undiscovered porphyry deposits in the Sistan tract include (1) one or more island-arc systems, (2) permissive alkaline and calc-alkaline compositions, and (3) appropriate shallow and intermediate levels of exposure for porphyry deposits (particularly in the Ratuk accretionary prism). Other factors that may increase the likelihood of undiscovered deposits include the possibility that a displaced segment of the very productive Chagai Belt in Pakistan may be present in the Sistan tract and, to a lesser extent, that porphyry copper mineralization may be found below known vein and replacement deposits (particularly in the Neh accretionary prism). Unfavorable factors for the occurrence of undiscovered porphyry deposits include (1) relatively small and short-lived magmatic event(s), (2) complex deformation including partial anatexis in postmineral fold-and-thrust belt, (3) unknown resources in porphyry systems, (4) a relatively reduced outcrop area of permissive units (11 percent), and (5) younger cover (41 percent).

Overall, the density of known porphyry deposits (zero) compared to that in other tracts of equivalent aerial extent elsewhere suggests that undiscovered deposits are likely present. However, the possibility that the Sistan tract may contain a displaced segment of the productive Chagai Belt in Pakistan contrasts with the likelihood that undiscovered deposits may largely be concealed, exhumed, or buried across large parts of this complexly deformed and variably preserved region. This is suggested by the relatively low number of known porphyry occurrences, which is also consistent with the low level of exploration that the region has experienced (Richards and others, 2012). Thus, the assessment team established that the Sistan tract was geologically favorable but that estimates of numbers of undiscovered porphyry copper deposits could only be carried out with moderate to high levels of uncertainty. The tract would contribute significant copper resources from undiscovered deposits to the overall assessment. Therefore, quantitative assessment of undiscovered deposits in this tract was warranted. Table 11A shows the consensus estimates for undiscovered porphyry copper deposits in the Sistan tract at the 90-, 50-, and 10-percent probability levels and the associated summary statistics. Among assessors, the 90-percent probability estimates were equally divided at 0 and 1 undiscovered deposit. At the 50-percent probability, the numbers ranged from 1 to 3 undiscovered deposits, and at the 10-percent probability level, the numbers increased to between 3 and 7. On the basis of these numbers, the team reached a consensus estimate of 0, 2, and 5 undiscovered deposits at the 90-, 50-, and 10-percent probability levels, respectively. This resulted in an expected mean of 2.53 undiscovered deposits with a standard deviation of 2.42 ($C_v=96$), reflecting the level of favorability but relatively high uncertainty assessed for this tract.

Probabilistic Assessment Simulation Results

Simulation results for estimates for copper, molybdenum, gold, silver, and the total volume of mineralized rock are summarized in table 11B. The mean estimate of undiscovered copper resources in the Sistan porphyry tract is 9.8 Mt. Results are reported at selected quantile levels, along with the mean expected amount of metal, the probability of the mean, and the probability of no metal. The amount of metal reported at each quantile indicates the least amount of metal expected from the ranked data of 4,999 Monte Carlo simulations. The quantiles are linked to each tract simulation and are therefore not added. However, mean estimates can be added to obtain total amounts of metal and mineralized rock in undiscovered deposits. Results of the Monte Carlo simulation are also presented as cumulative frequency plots (fig. 43). The cumulative frequency plots show the cumulative probabilities of occurrence-estimated resources and total mineralized rock, as well as the mean for each commodity and for total mineralized rock.

Table 11. Probabilistic assessment for tract 142pCu9012, Sistan—Afghanistan, Iran, and Pakistan.

A. Undiscovered deposit estimates, deposit numbers, tract area, and deposit density.

[N_{xx} , estimated number of deposits associated with the xxth percentile; N_{und} , expected number of undiscovered deposits; s , standard deviation; $C_v\%$, coefficient of variance; N_{known} , number of known deposits in the tract that are included in the grade and tonnage model; N_{total} , total of expected number of deposits plus known deposits; tract area, area of permissive tract in square kilometers (km^2); deposit density reported as the total number of deposits per 100,000 km^2 . N_{und} , s , and $C_v\%$ are calculated using a regression equation (Singer and Menzie, 2005)]

Consensus undiscovered deposit estimates					Summary statistics					Tract area (km^2)	Deposit density ($N_{total}/100,000 km^2$)
N_{90}	N_{50}	N_{10}	N_{05}	N_{01}	N_{und}	s	$C_v\%$	N_{known}	N_{total}		
0	2	5	8	8	2.5	2.4	96	0	2.5	32,800	8

B. Results of Monte Carlo simulations of undiscovered resources.

[Cu, copper; Mo, molybdenum; Au, gold; and Ag, silver; in metric tons; Rock, in million metric tons]

Material	Probability of at least the indicated amount						Probability of	
	0.95	0.9	0.5	0.1	0.05	Mean	Mean or greater	None
Cu	0	0	3,200,000	24,000,000	41,000,000	9,800,000	0.27	0.2
Mo	0	0	35,000	630,000	1,200,000	270,000	0.22	0.34
Au	0	0	57	650	1,000	240	0.26	0.31
Ag	0	0	270	7,700	15,000	3,200	0.22	0.42
Rock	0	0	740	4,800	8,100	2,000	0.28	0.2

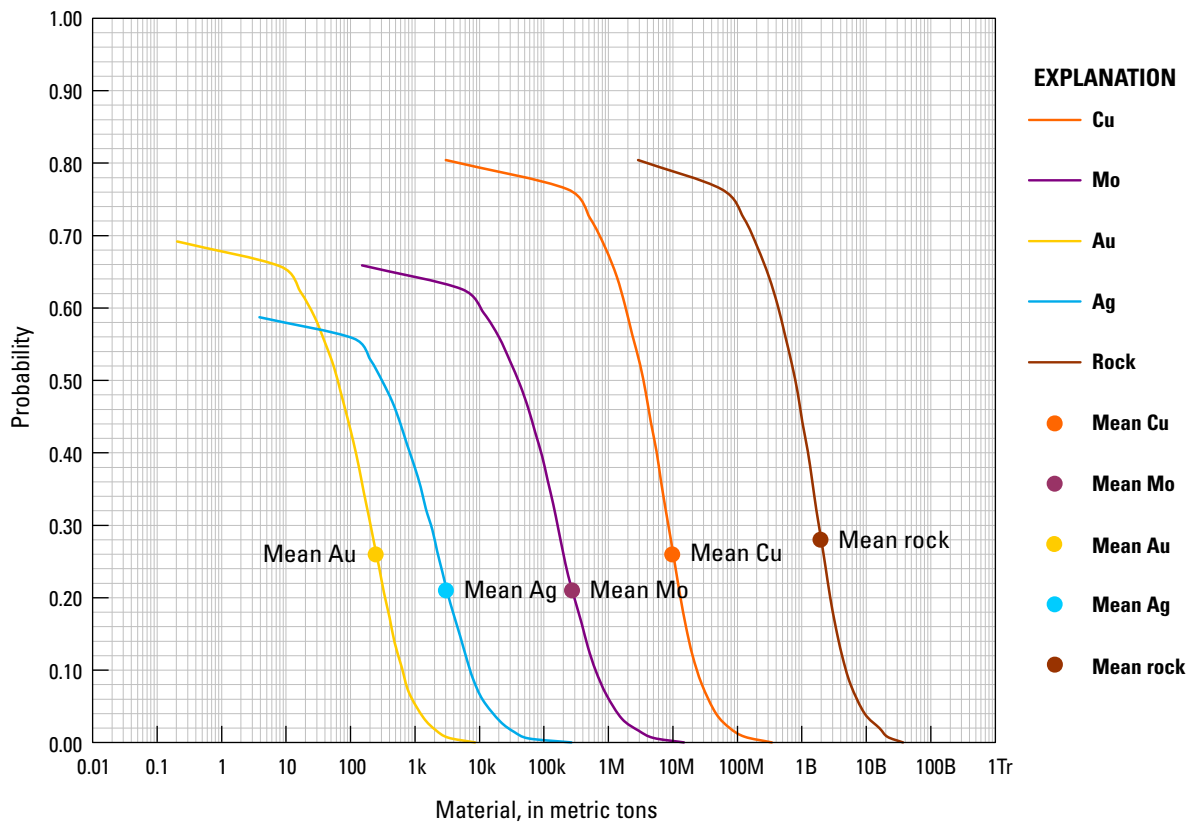


Figure 43. Cumulative frequency plot showing the results of Monte Carlo simulation of undiscovered resources in porphyry copper deposits in 142pCu9012, Sistan—Afghanistan, Iran, and Pakistan. k, thousand; M, million; B, billion; Tr, trillion.

Chagai Tract (142pCu9013)

Descriptive model: General porphyry copper (Cox, 1986a; Berger and others, 2008; John and others, 2010)

Grade and tonnage model: General Cu-Au-Mo porphyry copper model (Singer and others, 2008)

Geologic feature assessed: Late Cretaceous to late Miocene island to continental arc of the Tethyan Eurasian Metallogenic Belt

Location

The Chagai tract covers an area of 19,100 km² (fig. 44). It delimits a relatively well-preserved east-west 400-km-long by as much as 75-km-wide volcano-plutonic belt located in western Pakistan and southern Afghanistan, which is known as the Chagai Arc. The Late Cretaceous to late Miocene island to continental Chagai Arc is part of the accretionary prism that makes up the Chagai-Darirod Terrane, which formed as a result of northward subduction of the Arabian Platform under the amalgamated Farah and Helmand Terranes of Afghanistan (Nicholson and others, 2010; figs. 3, 4C). The Chagai Arc continues to the east as far as the sinistral Chaman transform zone. This segment of the Chagai Arc in Afghanistan is only briefly touched on here because it is treated in much more detail in another assessment study (see Ludington and others, 2007; Peters and others, 2011; and King and others, 2011).

The Chagai tract is bounded to the south by the 4.5-km-thick folded and thrust-faulted Oligocene-Miocene Dalbandin intra-arc basin (fig. 2) and Pleistocene and Holocene clastics. To the south, however, the Dalbandin basin abuts against the Ras-Koh Range, which is considered to be part of the fore arc of the Chagai Arc (Sillitoe, 1978; Richards and others, 2012; Dykstra and Birnie, 1979). Thus, the Ras-Koh Range is included here as part of Chagai tract (fig. 45). To the west, the Chagai tract terminates against the dextral Neh-Zahedan strike-slip fault system (Richards and others, 2012). To the north, the Chagai tract is delimited by relatively thick Pliocene-Holocene sedimentary rocks deposited along the Pakistan-Afghanistan border. These young sedimentary formations conceal the nature of the contact between the Chagai Arc and the Farah and Helmand Terranes on the Eurasian margin (Nicholson and others, 2010).

Tectonic Setting

The oldest rock formation in the Chagai volcano-plutonic belt is the Upper Cretaceous Sinjrani Group. The Sinjrani Group consists of a 2.5-km-thick volcanoclastic succession that includes tholeiitic to calc-alkaline pillow basalts and lesser andesitic and rhyolitic flows, as well as abundant tuffs and pyroclastic rocks that are interlayered with flysch-like sedimentary units (Hunting Survey Corp., Ltd., 1960). These have recently been found to be locally intruded by isolated calc-alkaline plutons (87 Ma; Richards and others, 2012). The Sinjrani Group is unconformably overlain by a 6-km-thick sequence of Upper Cretaceous to Oligocene shallow marine sedimentary units of the Humai, Juzzak, Saindak, and Amalaf Formations (Perelló and others, 2008).

Basalt and andesite flows are interbedded in the lower parts of the Juzzak and Saindak Formations and the upper part of the Amalaf Formation. These rock formations, as well as the Upper Cretaceous Sinjrani Group, indicate the presence of a Late Cretaceous to Oligocene volcano-sedimentary-dominated intraoceanic arc environment (see fig. 4D, E, F; Richards and others, 2012). Red-bed clastic strata and subaerial volcanic rocks of the Oligocene-Miocene Dalbandin and Reko Diq Formations rest unconformably on older deformed units. These formations mark the onset of uplift associated with accretion and transition from an island-arc to a continental-arc setting (fig. 4F). Deposition of the Dalbandin and Reko Diq Formations was followed by a pronounced late Miocene depositional hiatus that coincides with the final collision between the Arabian Platform and the Eurasian margin (Breitzman and others, 1983).

Three superimposed deformational events have been recognized in the Chagai Belt. They resulted from continued subduction of the Arabian Platform beneath the Eurasian margin (fig. 2). The first deformational event occurred in the Late Cretaceous, the second in the late Oligocene to late Miocene, and the third in the Pleistocene. The best-preserved structural feature is a large arcuate fold-and-thrust belt associated with the late Oligocene-late Miocene event, which is only weakly overprinted by the Pleistocene event. In the Chagai Hills, ages and dips of geologic formations in this south-vergent fold-and-thrust belt suggest a broad antiform. Folds are cut by perpendicular and thrust-parallel steeply dipping reverse and right-lateral strike-slip faults exhibiting separations of as much as 1,000 m in the western part of the belt (Ahmed and others, 1972) and range-parallel left-lateral faults in the eastern part of the belt (Perelló and others, 2008).

Late Miocene uplift and termination of Chagai Arc magmatism was followed by unconformable deposition of Pliocene-Pleistocene alluvial and volcanic units of the Kameron and Koh-i-Sultan formations (Ahmed and others, 1972). Across Pakistan and Afghanistan, these formations are obliquely superimposed on older rocks of the Chagai belt, and they form part of the continental arc that developed above the present-day Makran Trench (fig. 2). These rocks are in turn covered by Holocene unconsolidated alluvial and eolian deposits (Perelló and others, 2008).

Magmatism

Permissive igneous units used to define the Chagai tract (appendix B) are shown in figure 45, along with locations of igneous complexes and other geologic features mentioned in this section. Volcanic units in the sedimentary and volcano-sedimentary-dominated formations of the Chagai Belt are not differentiated in the regional-scale maps (Qureshi and others, 1993; Peters and others, 2007). Therefore, they are not represented in figure 45. These permissive volcanic units, however, are estimated to constitute about 25 percent of the igneous units that define the tract, based on a more detailed section of the Chagai Belt provided by Perelló and others (2008).

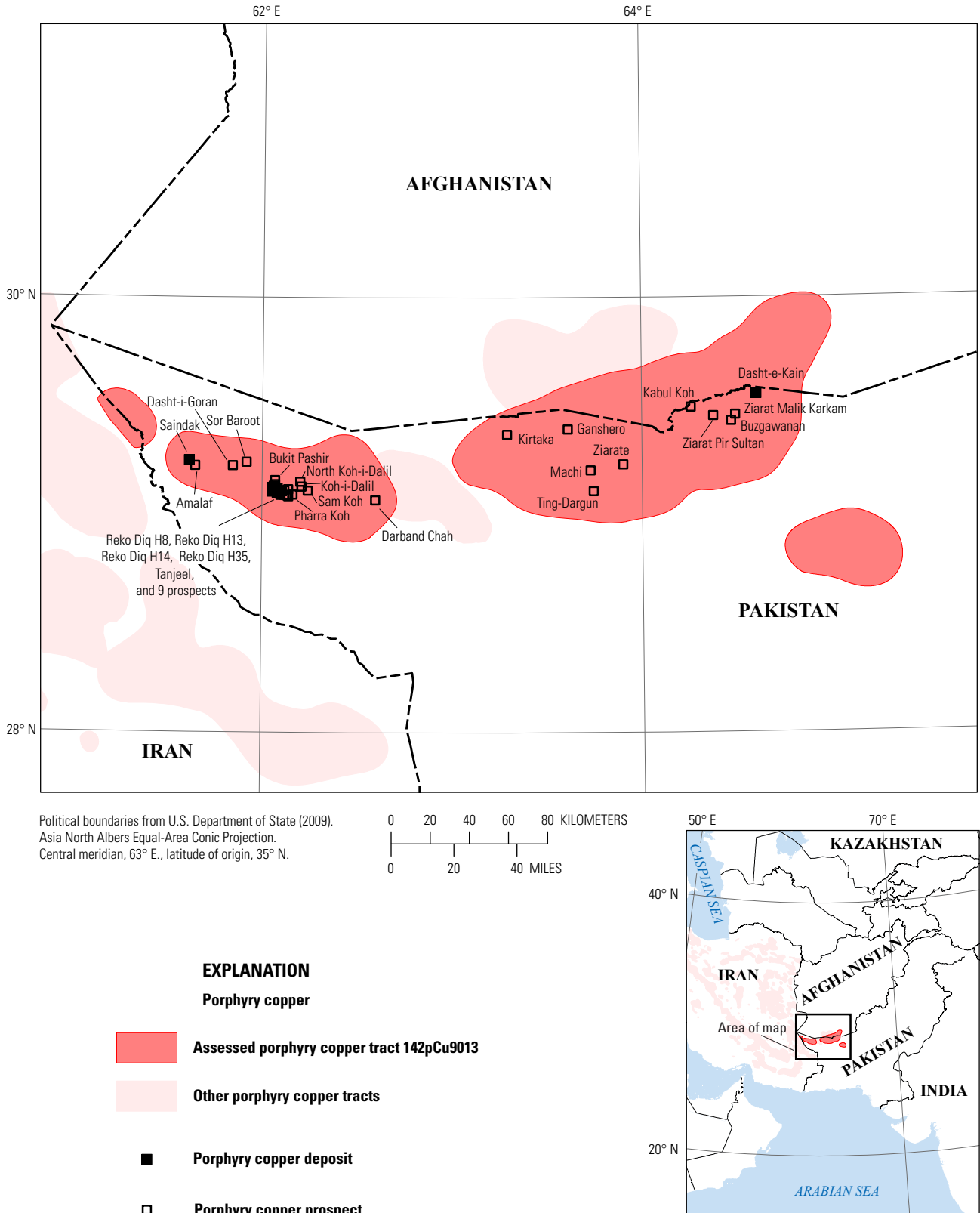
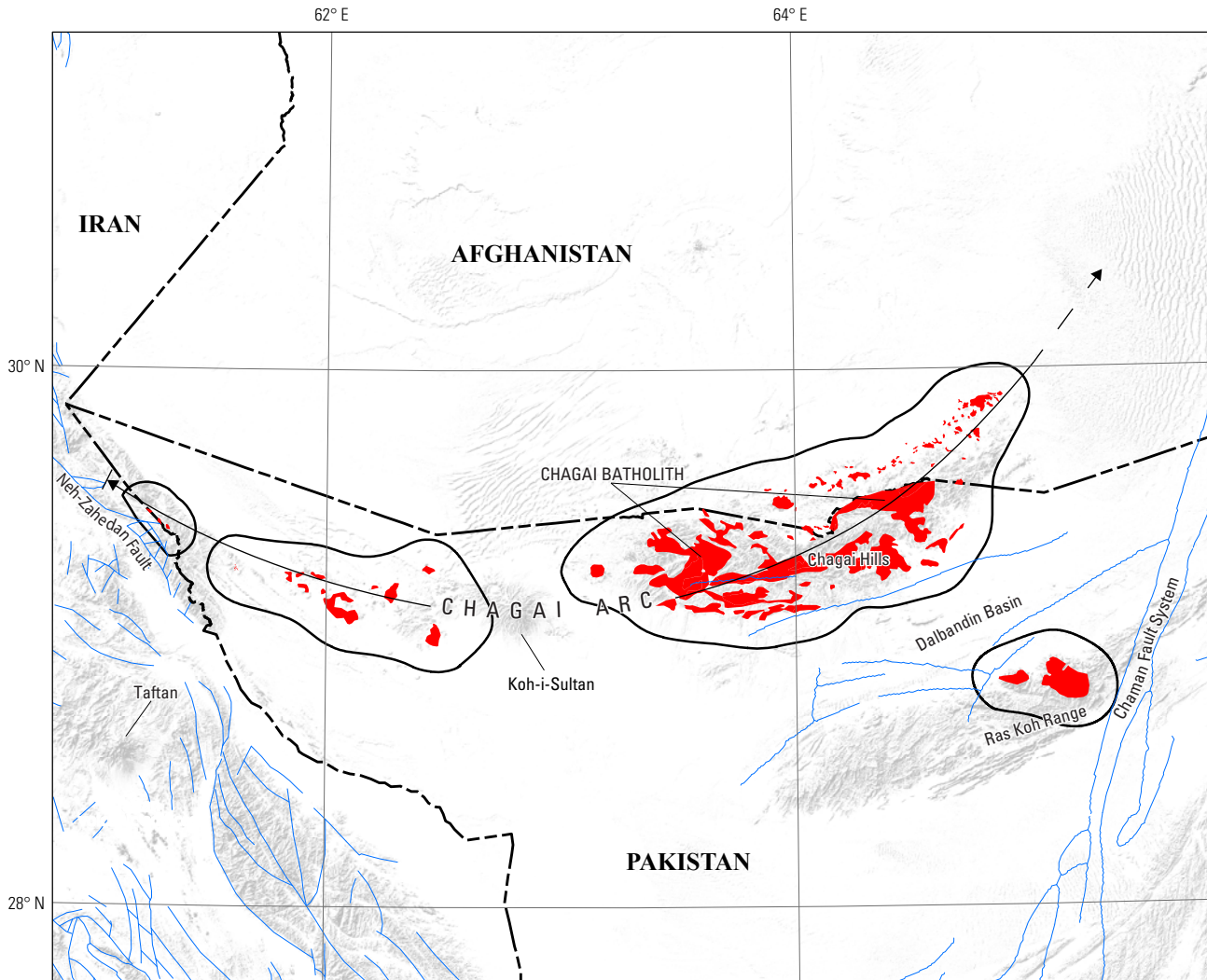
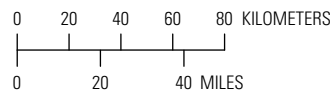


Figure 44. Map showing the location of known porphyry copper deposits and prospects for permissive tract 142pCu9013, Chagai—Afghanistan, Iran, and Pakistan. See table 2 for deposits, appendix C for prospects, and appendix D for accompanying spatial data.



Base from SRTM Global Digital Elevation Model, U.S. Geological Survey EROS Data Center, 2006. Political boundaries from U.S. Department of State (2009). Asia North Albers Equal-Area Conic Projection. Central meridian, 63° E., latitude of origin, 35° N.



- EXPLANATION**
- Porphyry copper
 - Assessed porphyry copper tract 142pCu9013
 - Permissive intrusive rock
 - Fault
 - Koh-i-Sultan **Geologic features discussed in text**



Figure 45. Map showing the distribution of permissive intrusive and extrusive rocks used to define tract 142pCu9013, Chagai—Afghanistan, Iran, and Pakistan. See appendix A for principal sources of information and appendix B for source map units.

The Chagai Arc includes several superimposed magmatic episodes. Intense intrusive activity in the middle to late Eocene (43–37 Ma; Perelló and others, 2008) produced magnetite series calc-alkaline quartz dioritic to granodioritic island-arc plutons, which formed the main Chagai Batholith (fig. 45). The middle to late Eocene magmatic episode culminated with emplacement of porphyry stocks and associated mineralization (Ziarate and Ganshero prospects).

In the Ras-Koh fore-arc region, approximately 75 km south of the Chagai Belt, post-middle Eocene syenodioritic plutons cut Late Cretaceous andesitic and basaltic volcanic and volcano-sedimentary rocks of island-arc affinity (Siddiqui and others, 2012). No porphyry-style mineralization is reported in this area, but Fe-(Cu) skarn mineralization such as at the Dilband deposit has been recognized (Sillitoe, 1978; Geological Survey of Pakistan, 2009; Hagen, 2009).

Late Oligocene-late Miocene island-arc accretion onto the cratonic margin in Afghanistan produced emergence accompanied by continental-arc magmatism. This event is characterized by distinct magmatic pulses and Cu-Mo±Au and Cu-Au±Mo porphyry copper mineralization (Perelló and others, 2008). These mineralizing events occurred in the Oligocene-Miocene (Saindak, Dasht-e-Kain, Machi, Ziarat Pir Sultan, and Tanjeel porphyry systems), early Miocene (Kirtaka, Sor Baroot, and Ting-Dargun prospects), and late Miocene (Reko Diq cluster, and Bukit Pashir, Darband Chah, and Pharra Koh porphyry systems). The main porphyry copper mineralizing event occurred in the late Miocene, and it coincides with the period of rapid uplift associated with the onset of collision between the Arabian Platform and the Indian Plate with Eurasia.

The geochemical characteristics of the Late Cretaceous-Paleocene, Eocene, and late Oligocene-late Miocene volcanic rocks are consistent with an evolving subduction-related island to continental-arc setting. Late Cretaceous-Paleocene volcanic units are dominated by low-K tholeiites typical of an intraoceanic island-arc environment (Siddiqui and others, 2010). Eocene units show tholeiitic to calc-alkaline compositions that indicate formation in a transitional island- to continental-arc setting, whereas late Oligocene to late Miocene units include calc-alkaline and lesser alkaline rocks (Siddiqui and others, 2007) characteristic of an Andean-type continental margin (Khan and others, 2010).

Known Porphyry Deposits and Prospects

About 40 late Eocene to late Miocene porphyry prospects and 4 Cu-Mo±Au and Cu-Au±Mo porphyry deposits—including the giant Reko Diq deposit and the Saindak mine—have been recognized within the Chagai tract in Pakistan (Perelló and others, 2008). The region also contains Late Cretaceous podiform chromite, manto copper, Pb-Zn-Ag-Cu VMS, Eocene iron-copper skarn, and Neogene epithermal gold-silver systems (Sillitoe, 1978; Perelló and others, 2008; Siddiqui and others, 2010). Across the border in Afghanistan, in contrast, Cretaceous-Paleogene tin and rare metal pegmatites and base-metal skarns and Neogene carbonatite and travertine (onyx) deposits are known, but porphyry copper mineralization remains to be identified (Afghanistan

Geological Survey, 2007; Abdullah and Chmyriov, 1977a; Orris and Bliss, 2002; Shroder, 1981; Doebrich and Wahl, 2006; Ludington and others, 2007; Stoesser, 2011). However, HyMap-derived alteration data suggest the presence of several potentially porphyry-related acid-sulfate alteration zones (King and others, 2011).

In the Chagai tract (fig. 44), the 4 porphyry copper deposits (Dasht-e-Khain, Reko Diq, Saindak, and Tanjeel) and 27 of the ~40 prospects were identified and are included in the database (table 2 and appendix C, respectively). The ~12 unidentified prospects probably cluster around other prospects and deposits, and thus they are not recorded in the available literature. Two of the identified prospects are adjacent to known deposits and are, therefore, considered in this study to be part of the same mineralization center. Furthermore, the Reko Diq resource base reported in table 2 is the weighted average of Reko Diq H8, Reko Diq H13, Reko Diq H14, and Reko Diq H35. These, as well as Reko Diq H15, are listed as independent sites in the accompanying GIS.

The majority of porphyry copper deposits and prospects in the western part of the Chagai Belt are hosted by Paleocene-Oligocene volcanoclastic rocks. Porphyry deposits and prospects in the eastern part of the belt, in contrast, generally occur at or near the contacts between the Late Cretaceous volcanoclastic rocks and the Eocene Chagai Batholith. Deposits and selected prospects are described below from oldest to youngest, as determined by geochronologic data (Perelló and others 2008).

Ziarate and Ganshero Porphyry Prospects

The late Eocene (37–36 Ma) Ziarate and Ganshero Cu-Mo-(Au)-bearing porphyry prospects intrude Late Cretaceous Sinjrani Group andesitic rocks and the Eocene Chagai Batholith (Perelló and others, 2008). The Ziarate granodiorite to monzonite porphyry stock exhibits alteration dominated by a 2-km² sericite zone and breccias controlled by east-west-trending faults. At Ganshero, the quartz diorite to granodiorite porphyry stock displays alteration dominated by a concentric 1-km² sericite zone. In this porphyry prospect, hydrothermal breccias are absent. In both systems, supergene mineralization is weak (Perelló and others, 2008).

Dasht-e-Kain Porphyry Deposit

The early Oligocene (32 Ma) Dasht-e-Kain Cu-Mo-Au deposit is located in the eastern part of the Chagai tract. The deposit has reported resources of 350 Mt at 0.3 percent copper and 0.001 percent molybdenum (Singer and others, 2008). Mineralization is associated with two quartz diorite-tonalite porphyry stocks known as the “eastern” and “western” stocks (Ahmad, 1986; Ahmad and others, 1986). These intrude the Late Cretaceous Sinjrani Group and the Eocene Chagai Batholith (Ahmad, 1992). The northern parts of both stocks are covered by alluvium. K-silicate and quartz-sericite alteration are dominant in the western stock, whereas K-silicate and propylitic alteration are more common in the eastern stock. Mineralization is mostly associated with K-silicate alteration and contained within the

western and eastern porphyry stocks. However, the eastern porphyry stock, which largely consists of an intrusive breccia, is comparatively better mineralized. Supergene enrichment is only slightly developed (Perelló and others, 2008).

Tanjeel Porphyry Deposit

The late Oligocene Tanjeel (also known as H4 [Schloderer, 2003]) Cu-Mo deposit is located in the Reko Diq District. The deposit contains reported resources of 214 Mt at 0.6 percent copper and 0.01 percent molybdenum (Perelló and others, 2008). At Tanjeel, east-west-striking (23.8 Ma; Perelló and others, 2008) feldspar and quartz-feldspar granodiorite porphyry dikes and associated quartz-sericite alteration with chalcopyrite mineralization are cut by pebble dikes and tourmaline breccias. The relatively pyrite-rich Tanjeel deposit is the only porphyry center with significant supergene enrichment in the Chagai tract. Supergene mineralization consists of a 10–100-m-thick chalcocite blanket (Perelló and others, 2008).

Saindak Porphyry Deposit

The early Miocene Saindak Cu-Au-(Mo) deposit in the western part of the Chagai Tract (Ahmed and others, 1972; Singer and others, 2008) contains an estimated 440 Mt at 0.41 percent copper, 0.002 percent molybdenum, and 0.5 g/t gold (Richards and others, 2012). The deposit is centered about three adjacent quartz diorite-tonalite porphyry stocks and dikes, dated at 22.4 Ma (Perelló and others, 2008) or 22.3 Ma (Richards and others, 2012). These are the North, East, and South ore bodies of Sillitoe and Khan (1977) and Sillitoe (1978), and they intrude siltstones, sandstones, and tuffs of the Eocene Saindak and Oligocene Amalaf formations. The 2-km² alteration is zoned outward from K-silicate, sericitic, to propylitic. Chalcopyrite-dominated mineralization was mostly contained within the early K-silicate alteration (Perelló and others, 2008). Supergene enrichment developed only poorly (Ahmad, 1992).

Ziarat Pir Sultan Porphyry Prospect

At the early Miocene Ziarat Pir Sultan Cu-Mo-bearing porphyry prospect (200 Mt resource; Everest Gold, Inc., 2012) is located in the eastern part of the Chagai tract. Here, a 21-Ma (Perelló and others, 2008) quartz diorite porphyry stock intrudes the Late Cretaceous Sinjrani Group and the Eocene Chagai Batholith. A hydrothermal breccia pipe is located within the 500-by-250-m stock. The associated alteration zone covers an area of 2 km², and the zone consists of K-silicate and sericite-chlorite with chalcopyrite mineralization. Supergene enrichment is minor (Perelló and others, 2008).

Kirtaka and Sor Baroot Porphyry Prospects

In the early to middle Miocene (18–17 Ma; Perelló and others, 2008) Kirtaka and Sor Baroot copper porphyry prospects (Everest Gold, Inc., 2012), exploration efforts have not constrained the dominant metal associations (Cu-Au or Cu-Mo). At Sor Baroot, a quartz diorite to granodiorite

porphyry stock and late west-northwest-trending dacite dikes intrude volcanic and sedimentary rocks of the Juzzak and Saindak Formations. Hydrothermal alteration covers an area of 2 km² and exhibits concentric zoning from K-silicate to strong sericite-chlorite. Chalcopyrite mineralization is hosted by both alteration associations. At Kirtaka, a quartz diorite porphyry stock is centered about K-silicate, sericite-chlorite, and sericite alteration zones that occupy an area of 0.6 km². Chalcopyrite mineralization occurs mainly with K-silicate alteration. Supergene enrichment is minor in both prospects (Perelló and others, 2008).

Reko Diq Porphyry Deposit

The giant Reko Diq Cu-Au-(Mo) porphyry deposit is located in the western part of the Chagai tract. It contains 5.9 Bt at 0.41 percent copper and 0.22 g/t gold, with an economically mineable part calculated at 2.2 Bt, with 0.53 percent copper and 0.30 g/t gold (Antofagasta PLC, 2010), or 2.42 Bt, with 0.51 percent copper and 0.27 g/t gold (Singer and others, 2008). The resource reported in table 2 is the weighted average of Reko Diq H8, Reko Diq H13, Reko Diq H14, and Reko Diq H35.

The late Miocene (12 Ma; Perelló and others, 2008) Reko Diq complex consists of several quartz diorite to granodiorite and dacite porphyry stocks, dikes, and breccias (Schloderer, 2003). These intrude volcanic, volcanoclastic, and sedimentary rocks of the early Miocene Reko Diq Formation. Mineralization episodes introduced by these porphyry intrusions occurred over a timespan of as much as 3 m.y. (Perelló and others, 2008). Hydrothermal alteration consists of early K-silicate, sericite-chlorite, and late sericite. Typically, the earliest porphyry phase in each suite coincides with the main stage of copper and gold mineralization, which is largely associated with K-silicate alteration. As much as 0.01 percent molybdenum was locally introduced during late mineralizing stages in several of the porphyry centers. Advanced argillic alteration is not common. Overall, supergene enrichment is not well-developed because of the relatively low sulfide contents and high neutralization potential of K-silicate alteration (Perelló and others, 2008).

Koh-i-Dalil Porphyry Prospect

At the late Miocene (10 Ma; Perelló and others, 2008) Koh-i-Dalil porphyry copper prospect in the vicinity of the large Koh-i-Dalil stratovolcano, several shallowly emplaced intrusions are exposed in a deeply eroded valley. These plutons intrude rocks of the Sinjrani Group and are composed of quartz diorite, granodiorite, and dacite porphyry intrusions that are in turn cut by mineralized tonalite porphyry and late andesitic and dacitic dikes (Bhutta, 2004; Singer and others, 2008). The alteration zone consists of a 400 by 300 m concentric K-silicate to sericite-chlorite to sericite alteration zone. Chalcopyrite mineralization is controlled by K-silicate alteration and breccias. Supergene enrichment is minor (Perelló and others, 2008).

Preservation Level

Rocks older than Late Cretaceous are not known in the Chagai-Darirod Terrane of Pakistan (Abdullah and Chmyriov, 1977b; Kazmi and Rana, 1982). As derived from geologic map bases (Peters and others, 2007; Qureshi and others, 1993), areas underlain by coeval permissive and nonpermissive units account for 14 and 42 percent of the Chagai tract, and younger rocks cover the remaining 44 percent of the tract (fig. 45).

Permissive igneous units are represented exclusively by plutonic rocks in the 1:850,000 and 1:1,000,000-scale geologic maps of Peters and others (2007) and Qureshi and others (1993). However, this is only apparent because permissive volcanic units are known to exist. Based on a more detailed stratigraphic section of the Chagai belt provided by Perelló and others (2008), volcanic units interbedded with Late Cretaceous to late Miocene volcano-sedimentary rocks constitute about 25 percent of the section. Nonetheless, a conspicuous absence of volcanic units that are coeval with the younger late Miocene intrusions has been noted (Perelló and others, 2008) and coincides with the pronounced uplift and erosional event that affected the region during that time.

Overall, the large number of exposed porphyry deposits and prospects in the Chagai tract suggests that concurrent and postmineral uplift, erosion, and burial events occurred mostly to the extent that favorably exposed porphyry systems of this age range. However, in the northeastern part of the Chagai tract in Afghanistan, permissive igneous units occur as smaller more isolated outcrops. This suggests that shallower levels of preservation and (or) more substantial cover may be present in this part of the tract, potentially limiting exposure of porphyry systems of this age range.

Magnetic Anomalies

The regional aeromagnetic map (Maus and others, 2009) was used to confirm the location and character of regional geologic features (for example, arcs, basins, faults, terrane boundaries). In the Afghan part of the tract, geophysical information was complemented with data from Sweeney and others (2006). Most prominent is a magnetic high that marks the southern boundary of the Chagai tract, which is likely imaging the fore-arc or intra-arc ophiolite-bearing accretionary prism that underlies the Dalbandin Basin. To the north in the Chagai Belt, magnetic highs in the western part of the tract give way to more subdued and isolated positive and negative anomalies in the eastern part of the tract. These eastern anomalies appear to reflect in part the location of Pliocene-Holocene ultramafic to felsic alkaline igneous and sedimentary cover rocks. A magnetic low also occurs in the Ras Koh segment of the Chagai tract. Furthermore, the magnetic low located between the western and eastern parts of the Chagai tract is consistent with the absence of permissive units in this area. The northern boundary of the Chagai tract generally coincides with an abrupt change in the texture of the magnetic response, which becomes smoother north of the boundary (Sweeney and others, 2006).

As seen in the regional-scale aeromagnetic map of Maus and others (2009), the Reko Diq and Saindak deposits, as well as many porphyry prospects in the western part of the Chagai tract, lie at the margins of magnetic highs. Conversely, the Dasht-e-Khain and most other known prospects in the eastern part of the tract occur around magnetic lows. This is an interesting contrast in magnetic signatures, given that outcrops of the Chagai Batholith are far more widespread in this area.

ASTER and Airborne Hyperspectral Alteration Data

Processed ASTER data (Mars, 2014) were used to evaluate potential hydrothermal alteration that could be associated with unidentified porphyry systems in the Chagai tract. With the exception of the eastern part of the Ras Koh tract segment (7 percent of the tract), ASTER coverage was complete. HyMap data were also available over the part of the Chagai tract in Afghanistan (King and others, 2011).

Of the 10 ASTER-derived alteration zones identified in the part of the Chagai tract in Pakistan, 9 occur in known porphyry deposits and prospects (Dasht-i-Goran, Ganshero, Kabul Koh, Machi, Reko Diq, Saindak, Ziarat Pir Sultan, Ziarate, and Koh i-Dalil). The most prominent ASTER-derived alteration zone occurs as an 8-km-wide phyllic envelope around the Reko Diq porphyry cluster (Rowan and others, 2006). The remaining ASTER-derived alteration zone occurs in Late Cretaceous Sinjrani Group volcano-sedimentary rocks, about 20 km southeast and northwest of the Ganshero and Ziarate porphyry prospects, respectively. It consists of a large but discontinuous 7- by 3-km west-northwest-south-southeast-trending phyllic and lesser argillic ASTER signature.

Of the 13 ASTER- and HyMap-derived alteration zones identified in the part of the Chagai tract in Afghanistan (King and others, 2011), 3 are associated with Pliocene-Holocene units. The other 10 are associated with permissive plutons and (or) Late Cretaceous Sinjrani Group rocks. Six ASTER- and HyMap-derived alteration zones are dominated by the presence of hematite, jarosite, and goethite, two of which also contain muscovite. The remaining four include pyrophyllite in addition to kaolinite, chlorite, and epidote, suggesting shallower level acid-sulfate epithermal environments. Advanced argillic alteration is uncommon in the porphyry systems in the Chagai Belt (Perelló and others, 2008), but it is abundantly present in Pliocene-Holocene volcanic edifices such as at Koh-i-Sultan. Thus, several of these alteration zones may be marking the location of younger Pliocene-Holocene mineralization.

Overall, ASTER- and HyMap-derived alteration data potentially indicate the location of 1 additional unidentified porphyry system in the well-explored Pakistan part of Chagai tract and perhaps 6 more possible porphyry systems in the underexplored Afghan part of the Chagai tract. However, the latter ASTER-derived alteration zones could be related to younger hydrothermal occurrences.

Probabilistic Assessment

Grade and Tonnage Model Selection

In the Chagai tract, available resource data from the Reko Diq and Saindak deposits indicates that these classify as Cu-Au porphyry systems. Data on Dasht-e-Kain and Tanjeel are insufficient to classify these deposits based on the relative gold and molybdenum contents. However, deposit descriptions imply that molybdenum contents are higher than gold, suggesting that these deposits adhere more to the Cu-Mo subtype category. Pooled *t*-test results assuming equal variances show that the four known deposits in the tract are not significantly different at the 1-percent level from the tonnages and copper and gold grades in the general porphyry Cu-Au-Mo model. Therefore, this model was selected to estimate undiscovered copper, gold, molybdenum, and silver resources in this tract. In comparison to the median tonnage in the general porphyry Cu-Au-Mo model of Singer and others (2008), the Tanjeel deposit exhibits comparable tonnage, whereas the Reko Diq, Saindak, and Dash-e-Khain deposits are larger. Furthermore, Reko Diq deposit contains higher copper and gold grades than the median deposit in model, whereas the Tanjeel deposit exhibits higher copper and molybdenum grades.

Estimates of Undiscovered Deposits and Rationale

Favorable geologic factors for the occurrence of undiscovered porphyry copper deposits in the Chagai tract include (1) a relatively long-lived extensional to compressional island to mature Andean-type continental arc, (2) permissive calc-alkaline magmatism, (3) exhumation events that resulted in appropriate exposure of Cu-Au and Cu-Mo-Au and porphyry systems, (4) known tonnages and copper grades in deposits that exceed those of the median porphyry deposit around the world, and (5) as many as a half-dozen ASTER-derived zones of potential hydrothermal alteration that could be associated with unidentified porphyry systems. Other possible favorable factors for the likelihood of undiscovered porphyry deposits include the fact that the Afghanistan part of the tract, where no porphyry deposits have been positively identified, appears to exhibit many of the same geological features that characterize the very productive Pakistan part (Ludington and others, 2007). This is supported by several possible porphyry-related HyMap-derived alteration areas in Afghanistan (King and others, 2011). Unfavorable geologic factors for the occurrence of undiscovered porphyry copper deposits in the Chagai tract include (1) the existence of only one ASTER alteration zone that does not identify a known porphyry occurrence in the part of the tract in Pakistan and (2) higher proportions of younger cover and less exposure of permissive rocks in the Afghanistan part of the tract, suggesting levels of exposure of porphyry systems that may be less favorable than those in Pakistan.

The lower density of known porphyry deposits relative to other tracts of equivalent aerial extent elsewhere in the world suggests that undiscovered deposits are likely present. The Chagai Hills of Pakistan are well endowed, adequately exposed, and have experienced a high level of exploration, resulting in a large number of identified porphyry occurrences. This level of exploration has not taken place in the smaller Afghan part of the tract. Thus, contrasting low and high levels of uncertainty in the estimation of undiscovered deposits would be expected in the Pakistan and Afghanistan parts of the tract, respectively. Overall, however, the favorability of the smaller Afghan part is believed to be comparable to that of the larger Chagai part in Pakistan, for which high favorability and low uncertainty in the estimation process is expected. Thus, the assessment team concluded that the Chagai tract was favorable, and that estimates of numbers of undiscovered porphyry copper deposits could be carried out with low levels of uncertainty. Therefore, quantitative assessment of undiscovered deposits in this tract was completed. Table 12A shows the consensus estimates for undiscovered porphyry copper deposits in the Chagai tract at the 90-, 50-, and 10-percent probability levels and the associated summary statistics. At the 90-percent probability level, all assessors estimated the presence of one undiscovered deposit. At the 50-percent probability level, numbers of undiscovered deposits ranged between 2 and 4, and at the 10-percent probability level, the numbers increased to between 4 and 6. On the basis of these numbers, the team reached a consensus estimate of 1, 3, and 6 undiscovered deposits at the 90-, 50-, and 10-percent probability levels, respectively, which resulted in a mean of 3.23 undiscovered deposits with a standard deviation of 1.88 ($C_v\%=58$). This result reflects the level of favorability and low uncertainty assessed for this tract. The resulting total deposit density per 100,000 km² obtained is comparable to the median porphyry deposit density expected in well-explored tracts of equivalent size elsewhere around the world (Singer and Menzie, 2010).

Probabilistic Assessment Simulation Results

Simulation results for estimates for copper, molybdenum, gold, silver, and the total volume of mineralized rock are summarized in table 12B. The mean estimate of undiscovered copper resources in the Chagai porphyry tract is 12 Mt, which represents about half of the resources presently known in this tract. In the Tethys region of western and southern Asia, the Chagai tract is the only one estimated to contain fewer undiscovered resources than those already identified. This result reflects the influence of the very large resource base contributed by the giant Reko Diq deposit. Results of the Monte Carlo simulation are also presented as cumulative frequency plots (fig. 46). The cumulative frequency plots show the cumulative probabilities of occurrence-estimated resources and total mineralized rock, as well as the mean for each commodity and for total mineralized rock.

Table 12. Probabilistic assessment for tract 142pCu9013, Chagai—Afghanistan, Iran, and Pakistan.

A. Undiscovered deposit estimates, deposit numbers, tract area, and deposit density.

[N_{xx} , estimated number of deposits associated with the xxth percentile; N_{und} , expected number of undiscovered deposits; s , standard deviation; $C_v\%$, coefficient of variance; N_{known} , number of known deposits in the tract that are included in the grade and tonnage model; N_{total} , total of expected number of deposits plus known deposits; tract area, area of permissive tract in square kilometers (km^2); deposit density reported as the total number of deposits per 100,000 km^2 . N_{und} , s , and $C_v\%$ are calculated using a regression equation (Singer and Menzie, 2005)]

Consensus undiscovered deposit estimates					Summary statistics					Tract area (km^2)	Deposit density ($N_{total}/100,000 km^2$)
N_{90}	N_{50}	N_{10}	N_{05}	N_{01}	N_{und}	s	$C_v\%$	N_{known}	N_{total}		
1	3	6	6	6	3.2	1.9	58	4	7.2	19,100	38

B. Results of Monte Carlo simulations of undiscovered resources.

[Cu, copper; Mo, molybdenum; Au, gold; and Ag, silver; in metric tons; Rock, in million metric tons]

Material	Probability of at least the indicated amount						Probability of	
	0.95	0.9	0.5	0.1	0.05	Mean	Mean or greater	None
Cu	0	250,000	5,600,000	29,000,000	48,000,000	12,000,000	0.27	0.07
Mo	0	0	79,000	770,000	1,500,000	340,000	0.22	0.2
Au	0	0	120	750	1,200	310	0.28	0.17
Ag	0	0	800	9,000	17,000	3,800	0.22	0.29
Rock	0	60	1,200	6,000	9,700	2,500	0.29	0.07

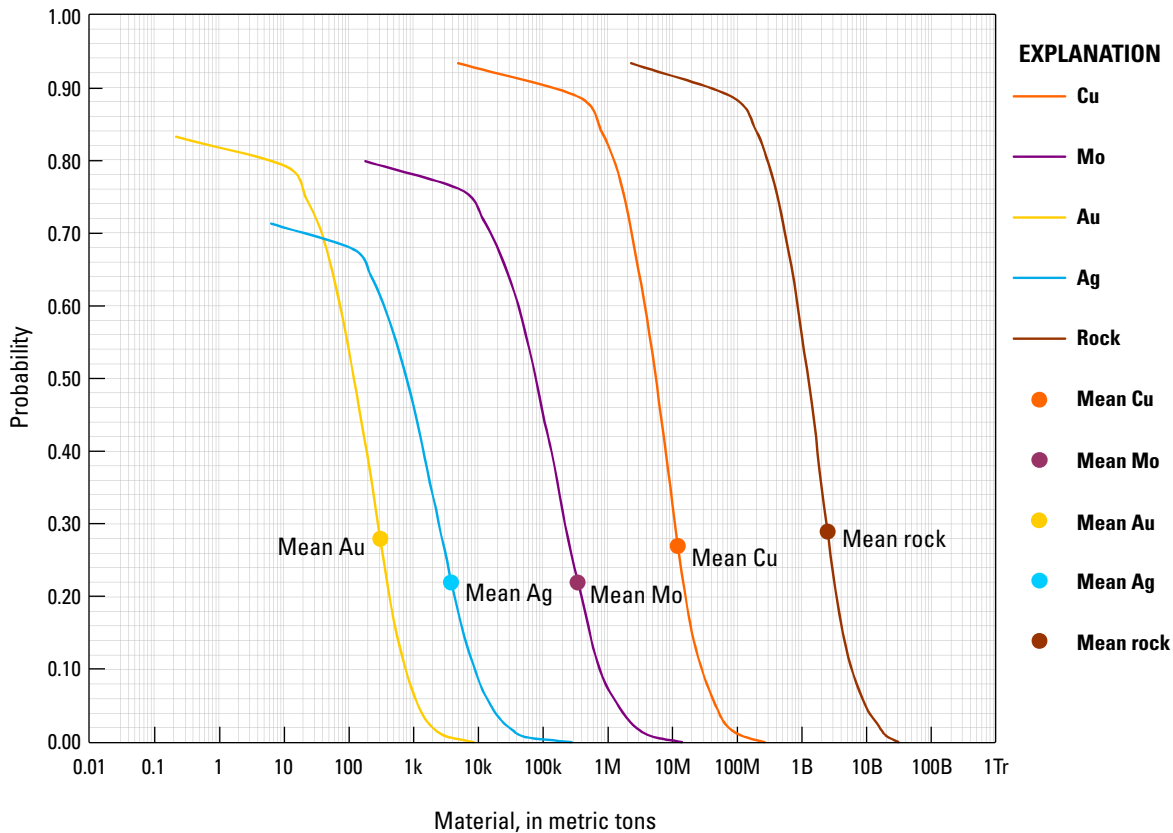


Figure 46. Cumulative frequency plot showing the results of Monte Carlo simulation of undiscovered resources in porphyry copper deposits in tract 142pCu9013, Chagai—Afghanistan, Iran, and Pakistan. k, thousand; M, million; B, billion; Tr, trillion.

Azerbaijan Tract (142pCu9014)

Location

The Azerbaijan tract (fig. 47) covers an area of 131,000 km² across Turkey, Armenia, Azerbaijan (including Nakhchivan), and northern Iran. It delimits a 2,500 km long and 50–300 km wide late Eocene to early Miocene extension-related back arc and postcollisional volcano-plutonic belt, which is well preserved in western Turkey and northern Iran but less so in eastern Turkey. In Iran, igneous units of this volcano-plutonic event are widespread across the western Alborz and northern Central Iranian Terranes. In the Lesser Caucasus and eastern Turkey, they largely occupy the eastern Anatolide-Tauride Terrane, and in western Turkey they overlie large parts of the Sakarya and western Anatolide-Tauride Terranes. The boundaries with the Sanandaj-Sirjan and Bitlis-Pötürge Terranes, in general, mark the extent of the Azerbaijan tract to the south. This late Eocene to early Miocene tract partially overlies older porphyry copper tracts.

Tectonic Setting

In the Pontide, Transcaucasus, and Alborz Terranes, Late Cretaceous to Eocene rock successions show a transition from a period of subsidence during the early Late Cretaceous to a period of compression and arc and back-arc magmatism in the Late Cretaceous-Paleocene (see Pontide (Asia) tract above) to a period of extension and back-arc magmatism in the late Paleocene and Eocene (Stöcklin, 1974; Berberian and King, 1981; Boulin, 1991). South of the suture, Late Cretaceous-Eocene magmatism (see Anatolide-Tauride and Esfahan tracts above) intermittently shifted from calc-alkaline arc-related to calc-alkaline and shoshonitic back-arc-related compositions (Adamia and others, 1977; Adamia and others, 2011).

Over the Transcaucasus and Alborz Terranes of the Lesser Caucasus and northern Iran, the Paleocene-Eocene extensional event was interrupted by the collision between the South Armenian Block and the Transcaucasus Terrane (Sosson and others, 2010a; Sosson and others, 2010b). South of the suture, renewed subsidence occurred in the early Oligocene-early Miocene (Morley and others, 2009; Adamia and others, 2010; Rezaeian, 2008), which was in turn followed by uplift associated with the final Arabian Platform-Eurasian collision, which in this region occurred in the early Miocene (Stöcklin, 1968; Berberian and King, 1981; Ballato and others, 2011; Adamia and others, 2011; Dilek, 2010).

The extensional regime bracketed between the Eocene-Oligocene and early Miocene compressional events was accompanied by prominent magmatism in the Lesser Caucasus and northern Iran. Early Oligocene and early Miocene igneous rock associations evolved from high-K calc-alkaline to alkaline compositions. This is consistent with termination of subduction-related arc magmatism and transition to postcollisional magmatism in relatively warm and attenuated crust (Jahangiri, 2007; Ballato and others, 2011; Gamkrelidze, 1986; Hou and others, 2011). This magmatic event is part of the Azerbaijan tract of the lesser Caucasus and northern Iran described in this section.

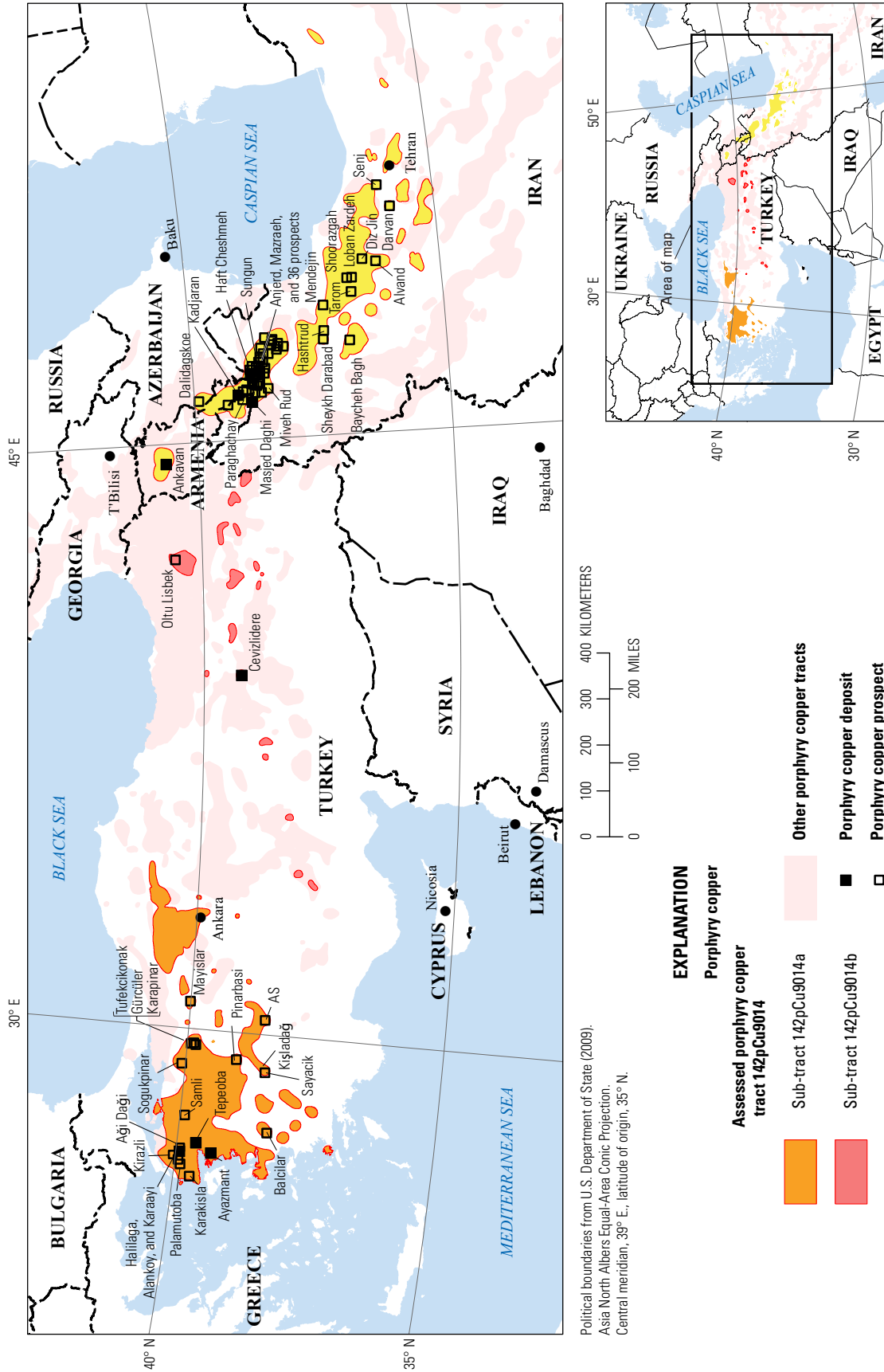
This extensional event was followed by late Miocene to Holocene mafic to felsic magmatism (see Pliocene-Quaternary tract below) with more typical within-plate geochemical signatures (Keskin, 2003; Kheirkhah and others, 2009). These igneous rocks were emplaced in the setting that followed collision between the Arabian Platform and the Eurasian margin (Şengör and Kidd, 1979; Guest and others, 2006, 2007).

In eastern Turkey, Late Cretaceous-Paleocene arc convergence along the southern branch of the Neotethys Ocean (see Border Folds tract above) produced late Paleocene-early Eocene back-arc extension (see Anatolide-Tauride tract above) across the eastern Anatolide-Tauride Terrane to the rear (Agard and others, 2011; Verdel and others, 2011). This back-arc event continued from the late Eocene to the early Miocene until the middle Miocene Arabia-Eurasia collision (fig. 4F) in this region (Şengör and Yilmaz, 1981; Hüsing and others, 2009; Dilek and others, 2010; Kaymakci and others, 2010). Thus, in contrast to postcollisional Oligocene-Miocene magmatism in northern Iran, available constraints indicate that Oligocene-Miocene magmatism in eastern Turkey occurred in the waning subduction setting that preceded final collision. This magmatic event is part of the Azerbaijan tract of eastern Turkey described in this section.

Middle-late Miocene north-directed compression in eastern Turkey initiated the westward tectonic escape of the Anatolian Block away from the Arabia-Eurasia collision zone along the North and East Anatolian Fault systems (Hubert-Ferrari and others, 2002; Chakrabarti and others, 2012). Postcollisional alkaline-dominated igneous rocks were emplaced during this time and are described below with Pliocene-Quaternary tract (Yilmaz, 1990; Keskin, 2003).

In western Turkey (see Anatolide-Tauride tract above), the compressional regime associated with convergence and collision between the Anatolide-Tauride and Sakarya Terranes along the Izmir-Ankara-Erzincan Suture ended by the middle Eocene (Şengör and Yilmaz, 1981; Yilmaz, 2003b). This compressional event (and associated burial of the western Anatolide-Tauride Terrane under the weight of southward-advancing ophiolite-bearing nappes) was followed by a late Eocene to middle Oligocene extensional episode. This episode is believed to have resulted from collapse of overthickened crust (Chakrabarti and others, 2012; Delaloye and Bingöl, 2000; Harris and others, 1994) in a period that post-dated collision to the north and predated the late Oligocene onset of subduction along the Hellenic-Cyprian Trench in the Mediterranean Sea to the south (fig. 4E).

The prevailing Eocene-Oligocene postcollisional extensional regime in western Turkey (fig. 4F) was overprinted by development of a back arc to the rear of the north-dipping Hellenic subduction zone, where the African Plate has been converging with the Eurasian margin since the late Oligocene, at about 26 Ma (Jackson and McKenzie, 1984). This subduction-related event is expressed by back-arc rifting, continued crustal attenuation, and exposure of metamorphic basement as a result of normal fault-related cordilleran core complex formation at about 23–19 Ma (Erkül and Erkül, 2010; Kuşçu, 2007). Therefore, late Eocene to middle Miocene magmatism in western Turkey consists of both postcollisional and back arc-related igneous products. These



Political boundaries from U.S. Department of State (2009). Asia North Albers Equal-Area Conic Projection. Central meridian, 39° E, latitude of origin, 35° N.

Figure 47. Map showing the location of known porphyry copper deposits and prospects for permissive tract 142pCu9014, Azerbaijan—Armenia, Azerbaijan, Iran, and Turkey. Sub-tracts: 142pCu9014a, Azerbaijan—Western Turkey, Turkey, 142pCu9014b, Azerbaijan—Eastern Turkey, Iran and Turkey; and 142pCu9014c, Azerbaijan—Caucasus-Iran, Armenia, Azerbaijan, and Iran. See table 2 for deposits, appendix C for prospects, and appendix D for accompanying spatial data.

magmatic events are part of the Azerbaijan tract of western Turkey described in this section.

These events were superseded by late Miocene to Holocene extension-related magmatism in western Turkey (fig. 4G), which is attributed to the combined effects of slab steepening (Delaloye and Bingöl, 2000) and subduction rollback at about 12 Ma (Meulenkamp and others, 1988), as well as westward escape of the Anatolian Block described with the Pliocene-Quaternary tract, below (Bozkurt and others, 2000; Keskin, 2003).

Hence, from west to east, variations in the overall tectonic setting occur along the Azerbaijan porphyry tract. In western Turkey, the tract delineates postcollisional and superimposed back-arc settings. In eastern Turkey, the tract delimits a back-arc environment, whereas in the Lesser Caucasus and northern Iran the tract outlines a postcollisional volcano-plutonic belt. Accordingly, the nature of late Eocene to early Miocene magmatism associated with these tectonic settings is separated here into the Azerbaijan–Western Turkey sub-tract (142pCu9014a), the Azerbaijan–Eastern Turkey sub-tract (142pCu9014b), and the Azerbaijan–Caucasus–Iran (142pCu9014c) sub-tract. These sub-tracts are described and are individually assessed below.

Azerbaijan–Western Turkey Sub-tract (142pCu9014a)

Descriptive model: General porphyry copper (Cox, 1986a; Berger and others, 2008; John and others, 2010)

Grade and tonnage model: General Cu–Au–Mo porphyry copper model (Singer and others, 2008)

Geologic feature assessed: Late Eocene to early Miocene postcollisional and back-arc magmatism of the Tethyan Eurasian Metallogenic Belt

Magmatism

The Azerbaijan–Western Turkey sub-tract covers an area of 65,200 km² (fig. 47). Permissive igneous units used to define this sub-tract (appendix B) are shown in figure 48, along with locations of igneous complexes and other geologic features mentioned in this section.

Extension-related magmatism in western Turkey is believed to have evolved from middle Eocene to early Oligocene crustal collapse, to relative uplift associated with asthenospheric upwelling, and to late Oligocene to early Miocene back arc initiation related to the onset of subduction along the Hellenic Trench to the south (Şengör and Yilmaz, 1981; Meulenkamp and others, 1988; Delaloye and Bingöl, 2000; Bozkurt and others, 2000; Yilmaz, 2003b; Chakrabarti and others, 2012). Changes in the tectonic regime are expressed by middle Eocene to early Oligocene subaqueous mafic to intermediate volcanic and volcanoclastic rocks and epizonal granitoids. These are followed by widespread Oligocene to early Miocene subaerial deposits and hypabyssal granodioritic-granitic to monzogranitic-syenogranitic suites, which developed metamorphic aureoles in adjacent andesitic to rhyolitic hosts (Okay, 2008). These magmatic suites progressively change from Oligocene more juvenile calc-alkaline

and high-K calc-alkaline volcano-plutonic to early Miocene more evolved mildly alkaline volcanic-dominated products (Altunkaynak and Genç, 2008). Delaloye and Bingöl (2000) postulate a general evolution in time and space for these volcano-plutonic units, consisting of north-to-south younging coupled with increasing K₂O contents. Oligocene-Miocene magmatism occurred during pronounced extension that culminated with formation of cordilleran metamorphic core complexes (Erkül and Erkül, 2010; Institute for Geo-Resources and Environment, 2005).

This late Eocene-early Miocene igneous event was followed by late Miocene magmatism (11–8 Ma), which is represented by transtensional fault-controlled strongly alkaline and isotopically primitive basalts, basanites, and trachybasalts (Akay, 2009). These rocks are associated with continued extension related to the combined effects of back-arc propagation (fig. 4G) and the westward escape of the Anatolian Block (Bozkurt and others, 2000; Keskin, 2003).

Known Porphyry Deposits and Prospects

Considerable exploration efforts are underway in western Turkey. Late Eocene to early Miocene mineralization is represented by numerous acid-sulfate and adularia-sericite epithermal precious metal occurrences, as well as iron, base-metal, W–Mo skarn, and porphyry occurrences (Yücel Öztürk and others, 2008). Three late Eocene to early Miocene porphyry deposits (Tepeoba, Halılağa, and Ayazmant, see fig. 47) and 16 porphyry and porphyry-related prospects are associated with epithermal and skarn systems (Yigit, 2006, 2009, 2012). The varied metal associations in these porphyry systems overlap but generally follow the calc-alkaline to alkaline magmatic trend that evolved over this time period in the region. Available information on deposits and prospects indicate late Eocene to early Miocene calc-alkalic to alkalic Au–(Cu) porphyry-related acid sulfate systems, early Oligocene to early Miocene calc-alkalic Cu–Mo porphyry-related skarn systems, and late Oligocene to early Miocene Au–(Mo) alkalic porphyry systems (Yigit, 2012). Descriptions of representative older to younger porphyry deposits and prospects are presented below.

Palamutoba Porphyry Prospect

The Palamutoba Au–(Cu–Mo)-bearing porphyry prospect is of probable late Eocene age (Yigit, 2009, 2012). Here, several synmineral granodioritic porphyry dikes, as well as postmineral porphyritic dikes, intrude schists of Paleozoic age. Two alteration zones, each approximately 2 km long and 0.8 km wide, host quartz-sericite-pyrite sheeted veins and stockworks with copper, molybdenum, lead, and gold mineralization. The oxidation cap is well-developed (Yigit, 2012).

Alankoy Porphyry Prospect

The early Oligocene 28.3 Ma Alankoy acid-sulfate Au and Au–Cu porphyry-skarn prospect was discovered in the early 1990s by a MTA and MMAJ joint venture in an area of ancient surface and underground workings (Yigit, 2012). Epithermal mineralization,

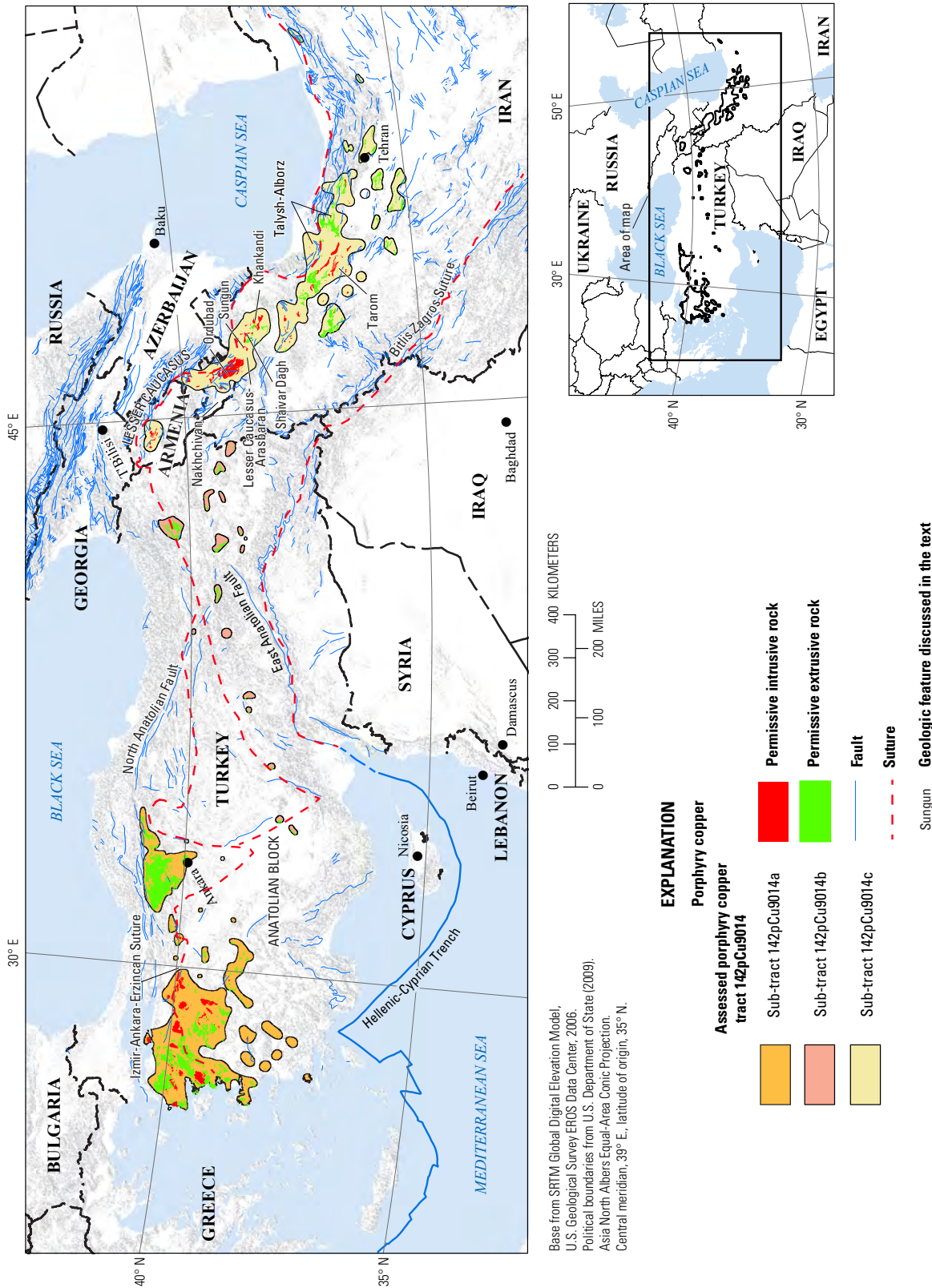


Figure 48. Map showing the distribution of permissive intrusive and extrusive rocks used to define tract 142pCu9014, Azerbaijan—Armenia, Azerbaijan, Iran, and Turkey. Sub-tracts: 142pCu9014a, Azerbaijan—Western Turkey, Turkey, 142pCu9014b, Azerbaijan—Eastern Turkey, Iran and Turkey; and 142pCu9014c, Azerbaijan—Caucasus-Iran, Armenia, Azerbaijan, and Iran. See appendix A for principal sources of information and appendix B for source map units.

which includes a steam-heated zone with chalcedonic quartz and native sulfur, as well as vuggy silica, occupies a 2- by 1.7-km area controlled by a northeast structural trend. Alteration and gold-bearing quartz-sulfide stockworks are associated with a granodioritic stock that intrudes Oligocene andesite lavas and pyroclastic units that overlie Triassic carbonate, metavolcanic, and sedimentary rocks. Zn-Pb-Cu-Sb-Au-Ag garnet-rich skarn zones developed at the contact between the intrusion and the limestone host (Yigit, 2012).

Halilağa Porphyry Deposit

The Halilağa porphyry Cu-Au-(Mo) and associated skarn and acid-sulfate deposit was discovered in 2007 and is presently undergoing feasibility studies (Pilot Gold, Inc., 2011, 2012a, b, c; Mining Journal, 2010). It has indicated resources of 168 Mt at 0.30 percent copper, 0.006 percent molybdenum, and 0.31 g/t gold and inferred resources of 199 Mt at 0.23 percent copper, 0.007 percent molybdenum, and 0.26 g/t gold, using a 0.2 percent copper equivalent and a 0.2 g/t gold cutoff (Scott and others, 2012). Table 2 lists the weighted average of 372 Mt at 0.26 percent copper, 0.0065 percent molybdenum, and 0.29 g/t gold. The alteration zone covers an area of 4 by 2 km and is centered about quartz-feldspar porphyry stocks of probable Oligocene age that intrude andesitic flows and tuffs. Porphyry-style mineralization occurs in both K-silicate and overprinting quartz-sericite alteration. It consists of pyrite, magnetite, and chalcocite with minor chalcopyrite and molybdenite. Secondary copper enrichment zones contain as much as 2.15 percent copper and 0.93 g/t gold (Yigit, 2009). In addition to porphyry-style mineralization, the deposit also includes Au-Ag-Cu-Mo-Zn-Pb skarn and gold-bearing acid-sulfate epithermal mineralization (Yigit, 2012). The skarn developed along the contact of the granodiorite with limestone, recrystallized marble, and schist. However, whether this spatially related skarn is genetically and temporally related to the main porphyry system is not known (Yigit, 2012).

Tepeoba Porphyry Deposit

The Tepeoba Cu-Mo-(Au) porphyry-skarn deposit was discovered by the MTA in 2002 (Institute for Geo-Resources and Environment, 2005; Singer and others, 2008; Yigit, 2009). It contains a reported resource of 24.1 Mt at 0.33 percent copper and 0.042 percent molybdenum (Yigit, 2012). Gold grades are not reported, but gold is known to be present. Mineralization is controlled by a 200-m-wide by 800-m long elliptical breccia that developed above an S-type granite stock that intruded the margin of a larger late Oligocene (25.6 Ma; Murakami and others, 2005) I-type granodioritic pluton. A hornfels halo and skarn developed along the contact of this pluton with Permian-Triassic metabasic and metasedimentary rocks. Alteration and mineralization consist of phlogopite-chalcocite with accessory molybdenite and surrounding quartz-sericite-tourmaline-pyrite with lesser sphalerite and electrum (Murakami and others, 2005). The Tepeoba deposit has been tilted by normal faults (Institute for Geo-Resources and Environment, 2005).

Ayazmant Porphyry Deposit

The small Ayazmant Fe-Cu-(Au) porphyry-related skarn deposit has a reported reserve of 5.75 Mt at 46 percent iron and 0.6 percent copper (Oyman, 2010). It occurs at the contact between early Triassic metapelites and metabasites and an early Miocene (20.1 Ma) calc-alkaline porphyry stock (Oyman, 2010; Yigit, 2006, 2009). The skarn is made up of early diopside-grossularite; scapolite and magnetite(±hematite); andradite-salite-actinolite-sulfide; and late actinolite, epidote, orthoclase, phlogopite, and chlorite. Mineralization consists of chalcocopyrite and subordinate molybdenite, pyrite, cubanite, bornite, pyrrhotite, galena, sphalerite, and idaite (Oyman, 2010).

Other Porphyry-Related Deposits and Prospects

The 25.8 Ma Aği Daği acid-sulfate and Au-Cu porphyry deposit is in development (Yigit, 2006, 2009, 2012; InfoMine, Inc., 2012c). At a 0.2 g/t gold cutoff grade, Yigit (2012) reports indicated resources of 26.6 Mt at 0.52 g/t gold and 0.60 g/t silver (Baba Zone) and 25.4 Mt at 0.67 g/t gold and 5.96 g/t silver (Deli Zone). The inferred resources are 9.9 Mt at 0.48 g/t gold and 0.50 g/t silver (Baba Zone) and 8.0 Mt at 1.17 g/t gold and 11.18 g/t silver (Deli Zone). Appendix C lists a weighted average of 66.32 Mt at 0.61 g/t gold and 3.59 g/t silver. The Aği Daği deposit is associated with a 5-km-long and 2-km-wide northeast-trending alteration zone that occurs around a middle Oligocene flow-dome complex (Yigit, 2009). Volcanic and subvolcanic rocks including rhyolite, dacite, and andesite are cut by synmineral breccia bodies and porphyry, as well as postmineral quartz-feldspar porphyry intrusions. Alteration is mainly controlled by stockworks and breccia bodies and consists of vuggy silica, alunite, dickite, and kaolinite at high levels and pyrophyllite, halloysite, illite and sericite at depth. Mineralization includes auriferous pyrite and minor to trace amounts of enargite, covellite, galena, and molybdenite (Yigit, 2012; Keane and others, 2010).

At the 28.3 Ma Kirazlı (Aladag) acid-sulfate and Au-Cu porphyry deposit, located some 25 km northwest of Aği Daği, development is also in progress (Yigit, 2006, 2009). Yigit (2012) reports indicated resources of 11.8 Mt at 0.83 g/t gold and 13.90 g/t silver at a 0.2 g/t gold cutoff grade. Inferred resources are 8.6 Mt at 0.65 g/t gold and 15.93 g/t silver. Appendix C lists the weighted average of 27.06 Mt at 0.76 g/t gold and 8.92 g/t silver. At the Kirazlı deposit, a 1.2-km-long and 0.4-km-wide alteration zone is controlled by a north and east-northeast structural intersection situated along the rim of a caldera (Yigit, 2012). Chalcedonic quartz, vuggy silica, alunite, dickite, and kaolinite are hosted by stockworks and breccias in middle Oligocene andesitic and dacitic lavas, intrusives, volcanoclastic, and tuffaceous lacustrine sedimentary rocks. These are, in turn, cut by postmineral diabase dikes. Higher grade gold mineralization in the oxide zone occurs with secondary hematite after pyrite in flat-lying chalcedonic quartz seams (aquitarde). In the sulfide zone, gold occurs in late arsenic-poor spheroidal pyrite. Early arsenic-rich euhedral pyrite is

commonly gold-poor (Keane and others, 2010). The Ađı Dađı and Kirazlı porphyry deposits are included in appendix C.

The Kişladađ Au-(Mo) porphyry deposit is the largest mining operation in Turkey (Yigit, 2009). It contains a NI 43–101-compliant measured and indicated resource of 412 Mt at 0.78 g/t gold and an additional inferred resource of 182 Mt at 0.5 g/t gold at a 0.3 g/t gold cutoff (Juras and others, 2010). At the Kişladađ deposit, two or three separate compositionally and texturally similar mineralized latite porphyry phases of early Miocene age intrude broadly coeval pyroclastic rocks, which are in turn cut by a late weakly mineralized to barren stock (Yigit, 2006, 2009, 2012). The 5- by 3-km alteration zone is composed by early feldspar-biotite, tourmaline-sericite, and kaolinite-secondary alunite. Gold stockwork- and breccia-controlled mineralization was introduced with quartz-tourmaline and quartz-pyrite-(molybdenum-sphalerite-galena-chalcopyrite-tetrahedrite) veins. Late vuggy silica is affected by intense acid leaching but is effectively barren of gold mineralization (Juras and others, 2010). Because it is the largest mine in Turkey, the Kişladađ Au-(Mo) porphyry deposit is included in appendix C.

Other possible porphyry-related systems of late Eocene to middle Miocene include the Taztepe, Tepekoy, Tongurlu, and Kocayayla North prospects in the Biga Peninsula (Yigit, 2012), as well as several other Mo-bearing skarn and vein prospects in western Turkey (Yigit, 2009).

Preservation Level

As derived from the 1:500,000-scale geologic map of Turkey (General Directorate of Mineral Research and Exploration, 2000), older basement rocks underlie 31 percent Azerbaijan–Western Turkey sub-tract, whereas late Eocene to early Miocene permissive volcanic and plutonic units occupy 21 and 4 percent of the sub-tract, respectively (fig. 48). Late Eocene to early Miocene nonpermissive mafic, sedimentary and volcano-sedimentary units constitute 23 percent of the sub-tract area, and younger rocks (and water bodies [1 percent]) cover the remaining 20 percent.

The comparatively high proportion of permissive units and low proportion of cover rocks indicate a relatively well-exposed volcano-plutonic belt. However, permissive units exhibit a high $\{\text{volcanic}/[\text{volcanic}+\text{plutonic}]\} \times 100$ ratio of 83, which suggests overall shallow levels of preservation of porphyry systems. This is supported by the dominance of epithermal mineralization above a number of known porphyry prospects in this sub-tract.

The eastern part of the Azerbaijan–Western Turkey sub-tract is underlain by extensive late Eocene to early Miocene volcanic rocks. No coeval plutonic rocks appear on the 1:500,000-scale geologic map of Turkey. This points to levels of preservation that are too shallow for porphyry systems, consistent with the absence of known porphyry systems and the presence instead of epithermal gold and kaolinite occurrences of this age bracket in this part of the sub-tract.

Magnetic Anomalies

The regional aeromagnetic maps of Ates and others (1999) and Maus and others (2009) were used to confirm the location and character of regional geologic features (for example, arcs, basins, faults, terrane boundaries). The aeromagnetic map generally shows subdued anomalies across the highly extended region of western Turkey. However, high-amplitude anomalies occur to the north across the Izmir-Ankara-Erzincan Suture in the Sakarya Terrane and image composite batholithic masses that are older but in part also late Eocene to early Miocene in age. Overall, late Eocene to early Miocene porphyry copper systems in western Turkey appear to be located along the margins of positive magnetic anomalies.

Probabilistic Assessment

Grade and Tonnage Model Selection

According to the criteria based on Au/Mo ratios and gold and molybdenum contents, the Halılađa and Tepeoba deposits belong to the Cu-Au and the Cu-Mo porphyry deposit subtypes, respectively. The Kişladađ Au-Mo porphyry deposit was not considered because it does not contain reported copper resources. The metal association in this deposit is also not represented in the available grade and tonnage models. Existing information on porphyry prospects in the Azerbaijan–Western Turkey sub-tract further indicate diverse metal associations that span the much of the Au-(Cu) to Au-(Mo) porphyry metal association spectrum. However, pooled *t*-test results assuming equal variances show that the three known deposits in the tract are not significantly different at the 1-percent level from tonnages or copper, molybdenum, and gold grades in the general porphyry Cu-Au-Mo model of Singer and others (2008). Therefore, this model was selected to estimate undiscovered copper, gold, molybdenum, and silver resources in this sub-tract. In comparison with the median tonnage and grade in the general porphyry Cu-Au-Mo model, the Halılađa deposit contains larger tonnage and higher gold grade but lower copper grades. Tepeoba is smaller and exhibits lower copper but higher molybdenum grades. The identified resource at Ayazmant is small but exhibits higher copper grades than the median deposit in the model.

Estimates of Undiscovered Deposits and Rationale

In the Azerbaijan–Western Turkey sub-tract, geologic factors favorable for the occurrence of undiscovered porphyry deposits include (1) relatively large postcollisional to back-arc extensional magmatic belt built on attenuated warm crust, (2) permissive calc-alkaline to alkaline magmatism, (3) shallow to intermediate levels of exposure for porphyry-skarn systems in several areas, (4) favorable conditions for supergene enrichment (enhanced by postmineral extensional tectonics), and (5) a porphyry deposit with larger than median tonnages and gold (but not copper) grades (for example, Halılađa). Unfavorable factors for the occurrence of undiscovered porphyry deposits include (1) relatively short-lived magmatic event(s) and (2) large areas with levels of preservation that may be too shallow or too deep for exposure porphyry systems.

The relatively low density of known porphyry deposits compared to that in other tracts of equivalent aerial extent elsewhere around the world suggests that undiscovered deposits are likely present. However, the relatively low number of porphyry occurrences of this age range identified to date does not yet reflect the high level of exploration that this region, which is dominated by shallow levels of exposure of porphyry systems, is experiencing (Yigit, 2012). These contrasting factors suggest overall moderate levels of uncertainty expected in the estimation of numbers of undiscovered deposits for this sub-tract.

No copper is reported as part of the resource base at the Kışladağ Au-(Mo), Aği Dağı, and Kirazlı Au-(Cu) porphyry deposits. Given the igneous composition and associated hydrothermal characteristics at Kışladağ, the assessment team concluded that no significant copper resources were likely to occur at depth. Conversely, igneous compositions and the character of alteration and mineralization at the Aği Dağı and Kirazlı acid sulfate-porphyry deposits (combined resources of 64 Mt at 0.64 g/t gold and 5.20g/t silver; Mining Journal, 2011b; Keane and others, 2010) suggest that copper resources can be expected to occur at depth.

The assessment team considered the Azerbaijan–Western Turkey sub-tract to be geologically favorable and that estimates of numbers of undiscovered porphyry copper deposits could be carried out with moderate levels of uncertainty. The tract would contribute significant copper resources from undiscovered deposits to the overall assessment. Therefore, quantitative assessment of undiscovered deposits in this tract was completed. Table 13a–A shows the consensus estimates for undiscovered porphyry copper deposits in the Azerbaijan–Western Turkey sub-tract at the 90-, 50-, and 10-percent probability levels and the associated summary statistics. The team estimated 1, 2, and 8 undiscovered deposits at the 90-, 50-, and 10-percent probability levels, respectively, which resulted in a mean of 3.43 undiscovered deposits with a standard deviation of 2.73 ($C_v\%=80$). The result reflects the level of favorability and moderate level of uncertainty. The estimated total deposit density per 100,000 km² obtained is comparable to the median porphyry deposit density expected in well-explored tracts of equivalent size elsewhere around the world (Singer and Menzie, 2010).

Probabilistic Assessment Simulation Results

Simulation results for estimates for copper, molybdenum, gold, silver, and the total volume of mineralized rock are summarized in table 13a–B. The mean estimate of undiscovered copper resources in the Azerbaijan–Western Turkey sub-tract is 14 Mt. Results of the Monte Carlo simulation are also presented as cumulative frequency plots (fig. 49A). The cumulative frequency plots show the cumulative probabilities of occurrence-estimated resources and total mineralized rock, as well as the mean for each commodity and for total mineralized rock.

Azerbaijan–Eastern Turkey Sub-tract (142pCu9014b)

Descriptive model: General porphyry copper (Cox, 1986a; Berger and others, 2008; John and others, 2010)

Grade and tonnage model: General Cu-Au-Mo porphyry copper model (Singer and others, 2008).

Geologic feature assessed: Late Eocene to early Miocene back-arc magmatism of the Tethyan Eurasian Metallogenic Belt

Magmatism

The Azerbaijan–Eastern Turkey sub-tract covers an area of 7,800 km² (fig. 47). Permissive igneous units used to define this sub-tract (appendix B) are shown in figure 48, along with locations of igneous complexes and other geologic features mentioned in this section.

In eastern Turkey, Oligocene-Miocene magmatism supersedes Late Cretaceous to late Eocene subduction-related igneous rocks of the Baskil Arc, described with the Border Folds tract, above, and the associated back arc, described above with the Anatolide-Tauride tract (Yiğitbaş and Yılmaz, 1996; Şengör and Yılmaz, 1981).

During the Oligocene to middle Miocene, shallowing of the subduction angle along the Bitlis-Zagros convergent margin (Pearce and others, 1990) led to reduction in volume of associated arc and back-arc volcanism and eventually to cessation of subduction. As shown on the 1:500,000 geologic map of Turkey (General Directorate of Mineral Research and Exploration, 2000), volcanic-dominated successions associated with this back-arc or intraoceanic-arc setting during the Oligocene-middle Miocene are preserved across central-eastern Turkey along a narrow and intermittently exposed east-west arcuate belt (Yılmaz, 1993; Kuşçu and others, 2010; Robertson and Mountrakis, 2006; Bozkurt and Mittweide, 2001). Thus, in contrast to the Oligocene-Miocene postsubduction extensional setting in northern Iran and the Lesser Caucasus, structural relations in the Oligocene-Miocene belt of eastern Turkey show that units were emplaced during a still active subduction-related setting (Kaymakci and others, 2010). Porphyry Cu-Mo deposits such as Cevizlidere (26 Ma; Marinov and others, 2011) and likely also the Mamlis, Silic, and Sin porphyry prospects (for which age dates are not available) are associated with this Oligocene-Miocene igneous event.

Known Porphyry Deposits and Prospects

Across eastern Turkey, known porphyry mineralization of Oligocene-Miocene age is scarce. One porphyry deposit (Cevizlidere) and one porphyry prospect (Oltu-Lisbek) were identified and are included in the Azerbaijan–Eastern Turkey sub-tract (fig. 47, table 2, and appendix C).

Cevizlidere Porphyry Deposit

The Cevizlidere porphyry Cu-Mo-Au deposit has a NI 43–101-compliant inferred resource of 446 Mt at 0.38 percent copper, 0.0048 percent molybdenum, and 0.11 g/t gold

Table 13. Probabilistic assessment for tract 142pCu9014, Azerbaijan—Armenia, Azerbaijan, Iran and Turkey.

[Coded_ID, a unique number assigned to each permissive tract in the spatial data (appendix D)]

Sub-tract name	Coded_ID	Countries
Azerbaijan—Western Turkey	142pCu9014a	Turkey
Azerbaijan—Eastern Turkey	142pCu9014b	Iran and Turkey
Azerbaijan—Caucasus-Iran	142pCu9014c	Armenia, Azerbaijan, and Iran

Table 13a. Probabilistic assessment for sub-tract 142pCu9014a, Azerbaijan—Western Turkey sub-tract, Turkey.

A. Undiscovered deposit estimates, deposit numbers, tract area, and deposit density.

[N_{xx} , estimated number of deposits associated with the xxth percentile; N_{und} , expected number of undiscovered deposits; s , standard deviation; $C_v\%$, coefficient of variance; N_{known} , number of known deposits in the tract that are included in the grade and tonnage model; N_{total} , total of expected number of deposits plus known deposits; tract area, area of permissive tract in square kilometers (km²); deposit density reported as the total number of deposits per 100,000 km². N_{und} , s , and $C_v\%$ are calculated using a regression equation (Singer and Menzie, 2005)]

Consensus undiscovered deposit estimates					Summary statistics					Tract area (km ²)	Deposit density ($N_{total}/100,000$ km ²)
N_{90}	N_{50}	N_{10}	N_{05}	N_{01}	N_{und}	s	$C_v\%$	N_{known}	N_{total}		
1	2	8	8	8	3.4	2.7	80	3	6.4	65,200	7

B. Results of Monte Carlo simulations of undiscovered resources.

[Cu, copper; Mo, molybdenum; Au, gold; and Ag, silver; in metric tons; Rock, in million metric tons]

Material	Probability of at least the indicated amount						Probability of	
	0.95	0.9	0.5	0.1	0.05	Mean	Mean or greater	None
Cu	0	190,000	5,500,000	34,000,000	54,000,000	14,000,000	0.27	0.07
Mo	0	0	80,000	910,000	1,800,000	390,000	0.22	0.23
Au	0	0	110	870	1,400	350	0.27	0.2
Ag	0	0	800	10,000	19,000	4,600	0.22	0.31
Rock	0	50	1,200	6,700	12,000	2,800	0.29	0.07

Table 13b. Probabilistic assessment for sub-tract 142pCu9014b, Azerbaijan—Eastern Turkey sub-tract, Iran and Turkey.

A. Undiscovered deposit estimates, deposit numbers, tract area, and deposit density.

[N_{xx} , estimated number of deposits associated with the xxth percentile; N_{und} , expected number of undiscovered deposits; s , standard deviation; $C_v\%$, coefficient of variance; N_{known} , number of known deposits in the tract that are included in the grade and tonnage model; N_{total} , total of expected number of deposits plus known deposits; tract area, area of permissive tract in square kilometers (km²); deposit density reported as the total number of deposits per 100,000 km². N_{und} , s , and $C_v\%$ are calculated using a regression equation (Singer and Menzie, 2005)]

Consensus undiscovered deposit estimates					Summary statistics					Tract area (km ²)	Deposit density ($N_{total}/100,000$ km ²)
N_{90}	N_{50}	N_{10}	N_{05}	N_{01}	N_{und}	s	$C_v\%$	N_{known}	N_{total}		
0	0	1	1	2	0.33	0.62	190	1	1.3	7,750	17

B. Results of Monte Carlo simulations of undiscovered resources.

[Cu, copper; Mo, molybdenum; Au, gold; and Ag, silver; in metric tons; Rock, in million metric tons]

Material	Probability of at least the indicated amount						Probability of	
	0.95	0.9	0.5	0.1	0.05	Mean	Mean or greater	None
Cu	0	0	0	2,500,000	5,600,000	1,500,000	0.14	0.69
Mo	0	0	0	34,000	140,000	40,000	0.09	0.83
Au	0	0	0	58	170	36	0.12	0.8
Ag	0	0	0	280	1,400	430	0.09	0.87
Rock	0	0	0	560	1,200	290	0.15	0.69

Table 13c. Probabilistic assessment for sub-tract 142pCu9014c, Azerbaijan—Caucasus-Iran sub-tract, Armenia, Azerbaijan, and Iran.

A. Undiscovered deposit estimates, deposit numbers, tract area, and deposit density.

[N_{xx} , estimated number of deposits associated with the xxth percentile; N_{und} , expected number of undiscovered deposits; s , standard deviation; $C_v\%$, coefficient of variance; N_{known} , number of known deposits in the tract that are included in the grade and tonnage model; N_{total} , total of expected number of deposits plus known deposits; tract area, area of permissive tract in square kilometers (km²); deposit density reported as the total number of deposits per 100,000 km². N_{und} , s , and $C_v\%$ are calculated using a regression equation (Singer and Menzie, 2005)]

Consensus undiscovered deposit estimates					Summary statistics					Tract area (km ²)	Deposit density ($N_{total}/100,000$ km ²)
N_{90}	N_{50}	N_{10}	N_{05}	N_{01}	N_{und}	s	$C_v\%$	N_{known}	N_{total}		
1	6	15	15	15	7.1	5.0	70	5	12	58,300	21

B. Results of Monte Carlo simulations of undiscovered resources.

[Cu, copper; Mo, molybdenum; Au, gold; and Ag, silver; in metric tons; Rock, in million metric tons]

Material	Probability of at least the indicated amount						Probability of	
	0.95	0.9	0.5	0.1	0.05	Mean	Mean or greater	None
Cu	0	560,000	16,000,000	65,000,000	97,000,000	27,000,000	0.34	0.07
Mo	0	0	310,000	1,900,000	3,100,000	760,000	0.27	0.13
Au	0	0	390	1,700	2,500	700	0.33	0.11
Ag	0	0	3,300	22,000	37,000	9,300	0.26	0.18
Rock	0	140	3,500	13,000	19,000	5,500	0.36	0.07

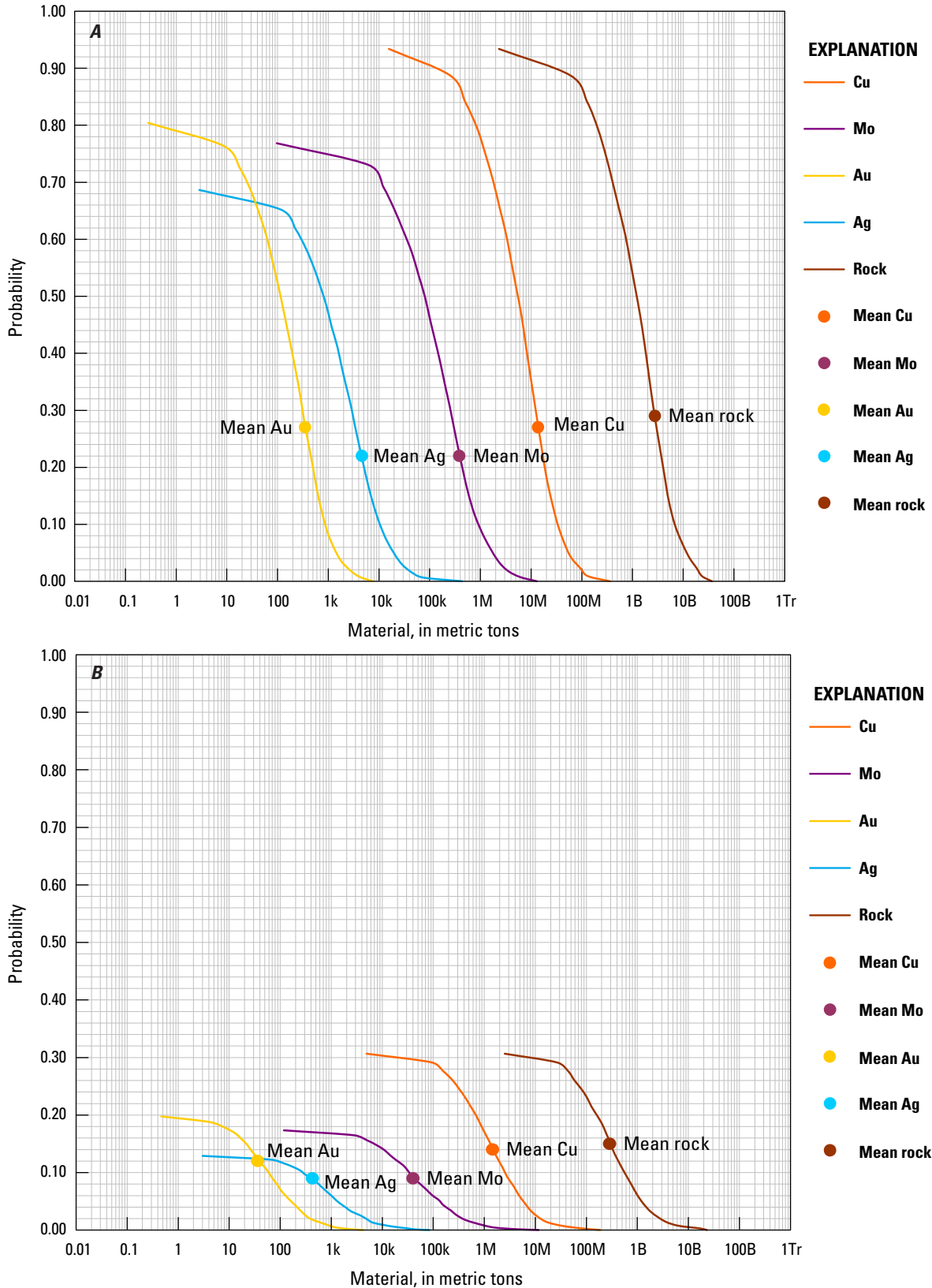


Figure 49. Cumulative frequency plot showing the results of Monte Carlo computer simulation of undiscovered resources in porphyry copper deposits in tract 142pCu9014, Azerbaijan—Armenia, Azerbaijan, Iran, and Turkey. *A*, Sub-tract 142pCu9014a, Azerbaijan—Western Turkey, Turkey. *B*, Sub-tract 142pCu9014b, Azerbaijan—Eastern Turkey, Iran and Turkey. *C*, Sub-tract 142pCu9014c, Azerbaijan—Caucasus-Iran, Armenia, Azerbaijan, and Iran. k, thousand; M, million; B, billion; Tr, trillion.

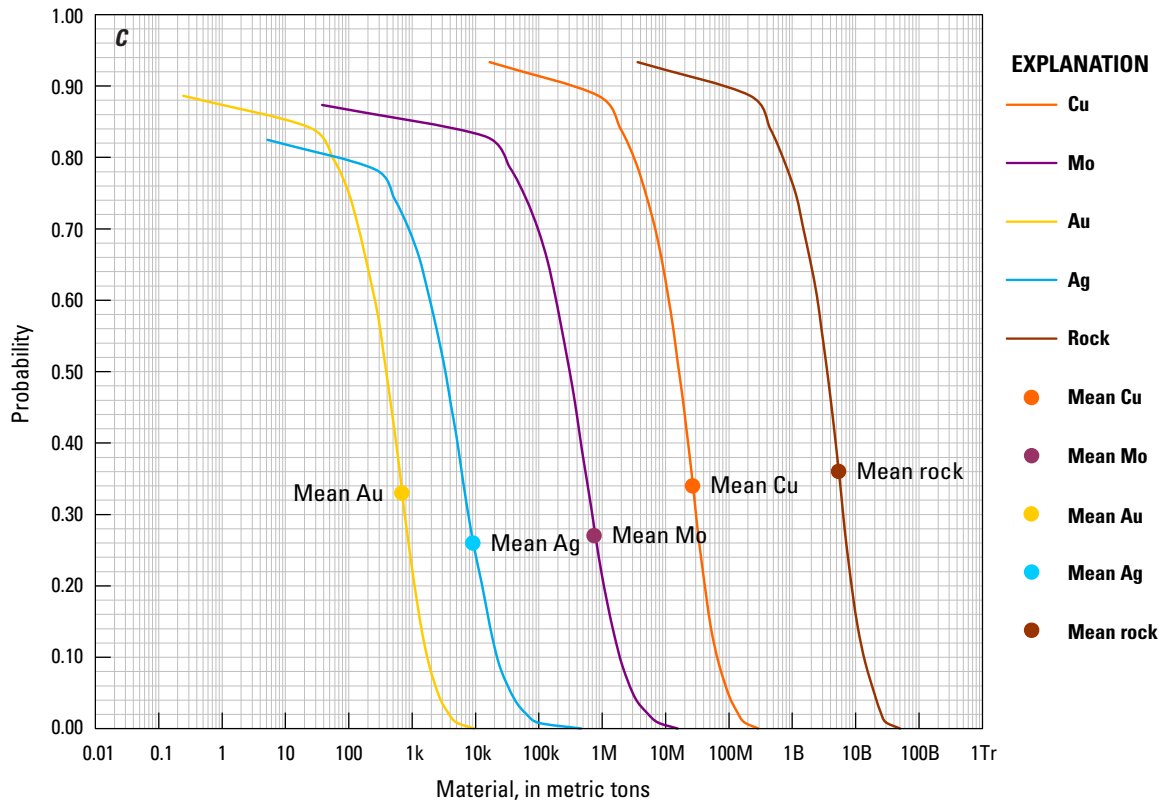


Figure 49.—Continued

(Kociumbas and Page, 2009). The deposit is located about 40 km southeast of the Au-Cu Çöpler-Karakartal porphyry district (see Anatolide-Tauride tract above) of eastern Turkey. However, unlike the early Eocene Çöpler and Karakartal systems, recent Re-Os age dating at Cevizlidere indicates a younger late Oligocene (26 Ma) mineralization age (Marinov and others, 2011). Furthermore, the Cu-Mo metal association of the calc-alkaline Cevizlidere Cu-Mo porphyry deposit contrasts with the Au-(Cu) association of the older more alkalic Çöpler and Karakartal porphyry systems. If this younger age date correctly constrains porphyry mineralization at the Cevizlidere deposit, Oligocene-Miocene magmatism in eastern Turkey is not only permissive, but also favorable for the occurrence of porphyry copper systems.

At the Cevizlidere porphyry deposit, early synmineral “crowded” dacitic porphyry intrusions, to late postmineral diorite stock and feldspar porphyry dikes intrude Mesozoic limestones overlain by Paleogene andesitic flows and pyroclastic rocks (Kociumbas and Page, 2009; Singer and others, 2008). Alteration and mineralization associations include deep early quartz-orthoclase-biotite-magnetite-chalcopryrite, which is overprinted by well-developed and mineralized “green” sericite-chlorite-quartz-chalcopryrite, lesser quartz-sericite-pyrite and argillization, and minor supergene enrichment. Gold shows a positive correlation with copper, and molybdenum appears to be independently distributed. The quality and quantity of Cu-Zn-Pb-Ag skarn mineralization at Cevizlidere remains to be tested.

Other Porphyry-Related Prospects

The Oltu-Lisbek Cu-Au porphyry prospect is located north of the Izmir-Ankara-Erzincan Suture in the eastern Sakarya Terrane, about 100 km north of the Oligocene-Miocene subduction-related belt defined by the Azerbaijan–Eastern Turkey sub-tract. Its setting and age are not well constrained. This prospect could be Eocene in age (Aslan and others, 2010). Thus, porphyry-style mineralization at Oltu-Lisbek could be Late Cretaceous-Eocene (see Pontide (Asia)–NE Turkey sub-tract above) or Oligocene-Miocene. If Oligocene-Miocene, mineralization could further be associated to either the subduction-related setting delimited by the Azerbaijan–Eastern Turkey sub-tract or the postcollisional setting defined by the Azerbaijan–Caucasus-Iran sub-tract (see below).

The Oltu-Lisbek (also known as Erzurum-Oltu-İnanmış or Oltu-Erzurum) Cu-Au porphyry prospect lies along a northeast-trending chaotically overthrust Late Cretaceous to late Paleocene ophiolitic belt that includes Jurassic-Cretaceous mafic volcanic rocks (Sezener Kuru and others, 2010; Özkümüş, 2009). The belt is bordered to the south by an Eocene marine clastic and volcanic succession overlain by Oligocene-Miocene continental evaporitic, clastic, and andesitic-basaltic units. Jurassic-Cretaceous mafic volcanic rocks are intruded by felsic, intermediate, and mafic porphyry dikes and typical porphyry-style alteration. Alteration is represented by quartz stockworks and breccias within clay, limonite, pyrite, chlorite, and epidote

zones (Sezerer Kuru and others, 2010). Mineralization consists of chalcopyrite and bornite, and anomalous gold values have been detected in soil and rock samples (Özkümüş, 2009).

In addition, a Late Cretaceous to middle Eocene age for the probably younger Mamlis, Silic, and Sin Cu-Mo porphyry prospects that occur in the vicinity of the Cevizlidere porphyry deposit has not been confirmed. These three prospects could be Oligocene-Miocene, and thus belong to the younger Azerbaijan–Eastern Turkey sub-tract, rather than the older Anatolide–Tauride–Eastern Turkey–Caucasus sub-tract (see above).

Preservation Level

As derived from the 1:500,000-scale geologic map of Turkey (General Directorate of Mineral Research and Exploration, 2000), older basement units underlie 26 percent of the Azerbaijan–Eastern Turkey sub-tract, whereas late Eocene to early Miocene permissive volcanic rocks occupy 18 percent of the sub-tract (fig. 48). The proportion of area underlain by permissive plutonic rocks is negligible. Broadly coeval nonpermissive mafic, sedimentary and volcano-sedimentary units constitute 10 percent of the sub-tract area, and younger rocks cover the remaining 46 percent of the sub-tract area.

Overall, the $\{\text{volcanic}/[\text{volcanic}+\text{plutonic}]\} \times 100$ ratio of nearly 100 suggests levels of preservation for porphyry systems that are too shallow. However, the existence of Cevizlidere implies that other porphyry deposits are likely present under younger cover rocks, which occupy almost half of the tract area.

Magnetic Anomalies

The regional aeromagnetic map (Maus and others, 2009) was used to confirm the location and character of regional geologic features (for example, arcs, basins, faults, terrane boundaries). The correlation between the aeromagnetic anomaly map and the narrow subduction-related belt of Oligocene-Miocene age that is exposed across eastern Turkey is unclear. Much of this region is covered by older and younger mafic-dominated units that mask the magnetic signature associated with late Eocene to early Miocene rocks. The Azerbaijan–Eastern Turkey sub-tract occurs within a broad negative Bouguer gravity anomaly that reflects the isostatically thickened continental crust of eastern Turkey and the Caucasus (Ates and others, 1999).

As seen on the regional-scale aeromagnetic map of Maus and others (2009), the Cevizlidere porphyry deposit and the Mamlis, Sin, and Silic prospects lie along a corridor of intermediate magnetic susceptibility that is located between a magnetic high to the north and a magnetic low to the south.

Probabilistic Assessment

Grade and Tonnage Model Selection

Resource data were insufficient to classify the Cevizlidere porphyry deposit into a Cu-Au or Cu-Mo porphyry subtype

according to the criteria based on Au/Mo ratios and gold and molybdenum contents. However, available information support a Cu-Mo-(Au) metal association for Cevizlidere. Pooled *t*-test results assuming equal variances show that this deposit is not significantly different at the 1-percent level from tonnages and copper and gold grades in the general porphyry Cu-Au-Mo model of Singer and others (2008). Therefore, this model was selected to estimate undiscovered copper, gold, molybdenum, and silver resources in the Azerbaijan–Eastern Turkey sub-tract. Compared with the median tonnage and grade in the general porphyry Cu-Au-Mo model, the Cevizlidere deposit contains larger tonnage, lower copper, and comparable gold grades.

Estimates of Undiscovered Deposits and Rationale

In the part of the Azerbaijan tract in eastern Turkey, geologic factors favorable for the occurrence of undiscovered porphyry deposits include (1) a subduction-related back-arc (and (or) intraoceanic arc?) setting, (2) dominant calc-alkaline compositions, (3) appropriate levels of exposure of porphyry-skarn systems along deformed and uplifted accretionary prisms, (4) one deposit (Cevizlidere) with larger tonnage but lower copper grade relative to the median porphyry deposit, and possibly (5) more porphyry prospects (including Mamlis, Sin, and Silic) of this age range, pending age confirmation. Unfavorable factors for the occurrence of undiscovered porphyry deposits include (1) a relatively small and waning magmatic event, (2) preservation levels that are in general too shallow for porphyry systems, and (3) large areas covered by younger rocks.

The low density of known porphyry deposits in this sub-tract relative to other tracts of equivalent size around the world suggests that the occurrence of undiscovered deposits is likely. However, the relatively low number of known porphyry occurrences suggests that these may be largely buried under coeval volcanic and younger cover and (or) that limited exploration for porphyry copper deposits of this age range has occurred in this region.

The assessment team established that the Azerbaijan–Eastern Turkey sub-tract exhibited low geological favorability and that estimates of numbers of undiscovered porphyry copper deposits could only be carried out with high uncertainty. However, the tract would contribute significant copper resources from undiscovered deposits to the overall assessment. Therefore, quantitative assessment of undiscovered deposits in this tract was warranted. Table 13b–A shows the team estimates for undiscovered porphyry copper deposits in the Azerbaijan–Eastern Turkey sub-tract. The team reached a consensus estimate of 0, 0, 1 undiscovered deposits for the 90-, 50-, and 10-percent probability levels, respectively, which resulted in a mean of 0.33 undiscovered deposits with a standard deviation of 0.62 ($C_v\%=189$). The result reflects the level of favorability and high uncertainty assessed for this sub-tract. The estimate was influenced by levels of exposure for porphyry systems that were deemed too shallow and a sub-tract that is furthermore largely covered by younger rocks.

Probabilistic Assessment Simulation Results

Simulation results for estimated for copper, molybdenum, gold, silver, and the total volume of mineralized rock are summarized in table 13b–B. The mean estimate of undiscovered copper resources in the Azerbaijan–Eastern Turkey porphyry sub-tract is 1.5 Mt. Results of the Monte Carlo simulation are also presented as cumulative frequency plots (fig. 49B). The cumulative frequency plots show the cumulative probabilities of occurrence-estimated resources and total mineralized rock, as well as the mean for each commodity and for total mineralized rock.

Azerbaijan–Caucasus-Iran Sub-tract (142pCu9014c)

Descriptive model: General porphyry copper (Cox, 1986a; Berger and others, 2008; John and others, 2010)

Grade and tonnage model: General Cu-Au-Mo porphyry copper model (Singer and others, 2008)

Geologic feature assessed: Late Eocene to early Miocene postcollisional magmatism of the Tethyan Eurasian Metallogenic Belt

Magmatism

The Azerbaijan–Caucasus-Iran sub-tract covers an area of 58,300 km² (fig. 47). Permissive igneous units used to define this sub-tract (appendix B) are shown in figure 48, along with locations of igneous complexes and other geologic features mentioned in this section.

The late Eocene to early Miocene volcano-plutonic belt of northern Iran and the Lesser Caucasus can be divided into eastern (Talysh-Alborz) and western (Lesser Caucasus-Arasbaran-Tarom) sectors. The eastern sector is underlain by Eocene-Oligocene shales, interlayered shoshonitic and alkaline mafic and felsic tuffs and lavas (Dilek and others, 2010), evaporites, and sedimentary rocks, but there are few intrusions (Jamali and others, 2010; Bazargani-Guilani and others, 2008; Adamia and others, 2010). In contrast, the western sector consists mainly of Eocene-Oligocene calc-alkaline and shoshonitic volcano-sedimentary and volcanic rocks intruded by numerous Oligocene-Miocene high-K calc-alkaline granodioritic, monzonitic, syenitic, and younger lamprophyric intrusions (Azizi and Jahangiri, 2008; Alavi, 1996; Aghazadeh and others, 2010, 2011; Jamali and others, 2012; Adamia and others, 2011; Lordkipanidze and others, 1989). U-Pb age dates show that the majority of high-K calc-alkaline plutons were emplaced about 31 Ma and that monzonitic and syenitic plutons were intruded between 29–27 and 26–24 Ma, respectively (Aghazadeh and others, 2012). In Armenia and Nakhchivan, the composite Eocene-Miocene Ordubad Batholith includes Oligocene-Miocene (32–17 Ma) gabbros, diorites, granodiorites, granites, monzonites, and quartz syenites (Adamia and others, 2011; Dilek and others, 2010; Khain, 1975).

This extension-related magmatic belt projects from the Lesser Caucasus into northeastern Turkey. However, in this region it consists mainly of volcano-sedimentary-dominated

successions. These nonpermissive units are not included in the sub-tract.

Oligocene-Miocene plutonic rocks of the Lesser Caucasus-Arasbaran-Tarom sector (fig. 48) are represented by the Khankandi, Shaivar Dagh and Sungun batholiths. The Oligocene (33.6–23.7 Ma) Khankandi Batholith intrudes a ~4-km-thick Eocene andesite, basaltic andesite, dacitic tuff, and trachyandesite back-arc succession. It consists of an early partly porphyritic calc-alkaline granodioritic suite that is intruded by a volumetrically more extensive shoshonitic gabbroic-monzogabbroic-monzonitic suite and late lamprophyric and dacitic dikes. Both suites exhibit similar metasomatized mantle-derived radiogenic isotope ratios. However, a subduction-related signature is preserved in the older granodioritic suite (Aghazadeh and others, 2010). Results from Al-in-Hornblende barometry indicate very shallow subvolcanic emplacement depths for the early granodiorite (with emplacement pressures around 0.2 kb).

The Oligocene Shaivar Dagh Batholith intrudes Late Cretaceous and Eocene marine volcano-sedimentary successions with intercalated calc-alkaline and shoshonitic volcanic flows. As the Khankandi Batholith, the Shaivar Dagh Batholith is composed of an early and a late intrusive suite. The early suite consists of 33–31 Ma calc-alkaline gabbro-dioritic, porphyritic hornblende-biotite granodioritic, and late peraluminous biotite-garnet granite dikes. The more voluminous late suite consists of 25.1–23.3-Ma nepheline-bearing monzodiorite and monzonite stocks and associated pegmatitic dikes (Aghazadeh and others, 2011). With the exception of evolved garnet-biotite granites, which appear to have been derived from assimilation of subducted sediments, older and younger suites of the Shaivar Dagh Batholith exhibit radiogenic isotope signatures that are similar to those of the Khankandi Batholith. Barometric estimates indicate a large range of emplacement depths based on emplacement pressures between 0.4 and 2.0 kb (Moazzen and Modjarrad, 2005; Aghazadeh and others, 2011). These estimates suggest variable levels of exposure likely produced by normal faulting.

The early Miocene (19–21 Ma; Aghazadeh and others, 2012) Sungun plutonic complex is younger than the Oligocene Khankandi and Shaivar Dagh batholiths. It consists of biotite-hornblende monzonite to quartz monzonite and high-K calc-alkaline hornblende-biotite diorite and granodiorite porphyry stocks. These intrude Late Cretaceous carbonate rocks, Eocene arenaceous-argillaceous rocks, and Oligocene dacitic breccias, tuffs, and trachyandesitic lavas. Porphyry stocks are in turn cut by four sets of trachyandesitic dikes (Hezarkhani, 2006; Asghari and Hezarkhani, 2010; Calagari, 2003). Stratigraphic reconstructions show that the maximum depth of porphyry intrusion was about 2 km (Hezarkhani and Williams-Jones, 1998).

In contrast to the older Khankandi and Shaivar Dagh batholiths, which do not host any known large porphyry-related systems, the Sungun plutonic suite exhibits a reverse order of intrusion. The alkaline monzonite/quartz-monzonite suite was intruded before the calc-alkaline diorite/granodiorite suite, which introduced the bulk of the mineralization that formed the world-class Sungun Cu-Mo porphyry-skarn deposit.

Known Porphyry Deposits and Prospects

Mineralization in the eastern (Talysh-Alborz) sector of the Azerbaijan–Caucasus–Iran sub-tract includes MVT and replacement lead-zinc occurrences that are hosted by Late Cretaceous and older sedimentary rocks. The eastern (Talysh-Alborz) sector of the sub-tract does not host major porphyry occurrences (Bazin and Hübner, 1969a; Azizi and Moinevaziri, 2009; Geological Survey of Iran, 2012e). Only two Mo–Cu-bearing porphyry-related prospects have been identified (Darvan and Senj). These appear as two individual localities in the Geological Survey of Iran (2012a, e) databases but may be the same (see fig. 47).

The southern segment (Tarom) of the western (Lesser Caucasus–Arasbaran–Tarom) sector of the Azerbaijan–Caucasus–Iran sub-tract has been divided into acid-sulfate alunitic, low-sulfidation kaolinitic, and base-metal vein and replacement metallogenic zones from north to south (Mirnejad and others, 2011; Barzagani-Guilani and others, 2008; Förster, 1978). In this segment, deeper porphyry and skarn mineralization are associated with precious metal acid-sulfate and precious and base-metal low-sulfidation epithermal occurrences (Samani, 1998). Identified Cu–Mo and Cu–Au porphyry and porphyry-related prospects included in the database (appendix D) are Alvand, Diz Jin, Hashtrud, Loban Zardeh, Mendejin, Sheykh Darabad, Shoorazgah, and Tarom (fig. 47).

The northern segment (Lesser Caucasus–Arasbaran) of the western (Lesser Caucasus–Arasbaran–Tarom) sector of the Azerbaijan–Caucasus–Iran sub-tract hosts 5 known porphyry deposits (including the world-class Sungun and Kadjaran mines, the Haft Chesmeh and Masjed Daghi deposits, currently in development, and the historic Ankavan porphyry-skarn mine), 35 porphyry prospects, and an additional 7 possible porphyry-related occurrences (fig. 47, table 2, appendix C). From north to south, the Lesser Caucasus–Arasbaran segment has been metallogenetically separated into (1) calc-alkaline granodiorite to more alkaline monzonite-related Cu–Mo porphyry and skarn systems, (2) gold-silver acid-sulfate and base-metal low-sulfidation epithermal systems, and (3) monzonite to diorite-related acid-sulfate and associated Cu–Au porphyry systems (Jamali and others, 2010; Somarin and others, 2005).

The northern sector of the Azerbaijan–Caucasus–Iran sub-tract contains the Ankavan porphyry deposit (Mining Journal, 2005), located in northern Armenia, and possibly also the Oltu Lisbek–Inanmis prospect (see Azerbaijan–Eastern Turkey sub-tract above) in northeastern Turkey (Özkümüş, 2009; Sezerer Kuru and others, 2010). The Ankavan and Oltu Lisbek–Inanmis porphyry systems are spatially associated with adularia-sericite (Wheatley and Acheson, 2011) and acid-sulfate epithermal systems (Barnett and others, 2011), respectively.

Kadjaran Porphyry Deposit

The world-class Kadjaran Cu–Mo–Au porphyry deposit is located in southern Armenia. It has reported resources of 1,700 Mt at 0.27 percent copper, 0.055 percent molybdenum, 0.65 g/t gold, and 2 g/t silver (Singer and others, 2008). This

deposit is characterized by high molybdenum and gold grades (Zvezdov and others, 1993; Mining Journal, 2005).

At the late Oligocene Kadjaran deposit (27 Ma; Moritz and others, 2012), early Eocene volcanic rocks are intruded by a late Oligocene alkalic to calc-alkalic monzonite–granodiorite–granite pluton, which is estimated to have been emplaced at a 1.5-km depth (Murakami and others, 2010). K-silicate and sericite alteration are overprinted by advanced argillic alteration (Gilmour and others, 1995). Mineralization consists of chalcopyrite, bornite, and molybdenite with minor sphalerite and tetrahedrite–tennantite (Tarkian and Stribny, 1999).

Ankavan Porphyry Deposit

The relatively small but molybdenum-rich Ankavan Cu–Mo–Au porphyry-skarn deposit is located in northern Armenia. It has a reported resource of 115 Mt at 0.57 percent copper, 0.054 percent molybdenum, and 1.42 g/t gold (Mining Journal, 2005). At this early Oligocene (33 Ma; Singer and others, 2008) deposit, granodiorite and syenite porphyry dikes intrude a gabbro–plagiogranite pluton emplaced into limestone and schist. Sulfide minerals include bornite, chalcopyrite, molybdenite, scheelite, galena sphalerite, tennantite, covellite, chalcocite, as well as tellurides (Singer and others, 2008; Zvezdov and others, 1993; Mining Journal, 2005).

Sungun Porphyry Deposit

The world-class Sungun Cu–Mo–(Au–Ag) porphyry deposit is located in northern Iran. It was discovered in 1977 (Etminan, 1977, 2003). Previous resources were 740 Mt at 0.661 percent copper and 0.024 percent molybdenum, and an inferred resource of 1,700 Mt (Singer and others, 2008). Recent data now estimate proven and probable reserves at 846 Mt at 0.6 percent copper at a 0.15 percent cutoff (National Iranian Copper Industries Company, 2012).

The Sungun deposit is an early Miocene (Aghazadeh and others, 2012) porphyry-skarn system related to shallowly emplaced (± 2 km) high-K calc-alkaline hornblende–biotite diorite and granodiorite porphyry stocks (Hezarkhani and Williams-Jones, 1998; Jamali and others, 2010). These stocks intrude Late Cretaceous carbonate rocks, Eocene arenaceous–argillaceous rocks, and Oligocene dacitic breccias, tuffs and trachyandesitic lavas. Four sets of largely postmineral subvolcanic dikes cut the porphyry stocks (Hezarkhani, 1997, 2006e; Asghari and Hezarkhani, 2010; Calagari, 2003). Alteration consists of a K-silicate core, deep albite, and overprinting quartz-sericite zones. Cu–Mo mineralization is contained in both the potassic and phyllic zones, with molybdenum introduced at an early stage (Hezarkhani and others, 1999; Calagari, 2004; Samani, 1998). Garnet–pyroxene and later epidote, actinolite, and chlorite skarn and associated pyrite and magnetite–hematite with chalcopyrite, galena, and sphalerite mineralization occurs along the eastern and northern margin of the intrusive complex (Hezarkhani, 1997; Calagari and Hosseinzadeh, 2006; Somarin and others, 2005). Supergene mineralization is restricted to a thin blanket of chalcocite, covellite, and minor bornite, native copper, and cuprite below the leached cap. Supergene processes do not appear to have raised overall copper grades (Calagari, 2003).

Haft Cheshmeh Porphyry Deposit

The Haft Cheshmeh porphyry Cu-Mo-Au deposit located in northern Iran is in development. Current proven and probable reserves are estimated at 184 Mt at 0.26 percent copper at a 0.15 percent cutoff (National Iranian Copper Industries Company, 2012). The plutonic complex consists of a gabbrodiorite-monzodiorite intruded by a granodiorite porphyry stock, which hosts an alteration zone with well-developed K-silicate, quartz-sericite, and argillic hydrothermal associations. Mineralization occurs mainly in A-type but also D-type quartz veins (Hassanpour and others, 2010; Hassanpour and Afzal, 2013).

Masjed Daghi Porphyry Deposit

The Masjed Daghi acid-sulfate and porphyry Cu-Au-(Mo) deposit is located in northern Iran. It has reported proven and probable reserves of 204 Mt at 0.34 percent copper at a 0.15 percent cutoff (National Iranian Copper Industries Company, 2012). Here, Eocene andesite, trachyandesite, dacite, tuffs, and agglomerates are intruded by a shallow diorite porphyry (Alirezai and others, 2008; Jamali and others, 2010). Auriferous veins cut the porphyry stock and are surrounded by more or less concentric alteration zones of kaolinite, vuggy quartz, alunite, and chlorite alteration. Base-metal mineralization occurs in brecciated quartz and quartz-barite veins with pyrite and lesser chalcopyrite, molybdenite, sphalerite, and galena. Gold in free form and in sulfides occurs in concentrations that range between 0.1 and 30 ppm (Ebrahimi, 2011; Geological Survey of Iran, 2010). With increasing depth, acid-sulfate alteration gives way to deeper phyllic and potassic alteration with copper (1,000 to greater than 10,000 ppm), molybdenum (50–400 ppm), and arsenic (100–3,000 ppm) (Alirezai and others, 2008).

Other Porphyry-Related Prospects and Possible Porphyry-Related Mineral Occurrences

In the eastern (Talysh-Alborz) sector of the sub-tract in northern Iran, the Senj Mo-(Cu-Au) porphyry prospect consists of a gabbro and monzogabbro to monzodiorite porphyry complex that intruded and contact-metamorphosed Eocene pyroclastic rocks. High potassium and anomalous copper, gold, and molybdenum contents suggest association with an alkalic pluton and (or) the presence of K-silicate alteration (Farahkhah and others, 2010).

In the western (Arasbaran) segment of the sub-tract in northern Iran, the 31-Ma Shaivar Dagh Batholith hosts several small deposits, including the Anjerd and Mazraeh porphyry-related Cu-(Fe-Au) endo- and exo-skarns that developed at the contact of an intrusion with Upper Cretaceous carbonate rocks (Samani, 1998; Somarin and others, 2005; Jamali and others, 2010; Aghazadeh and others, 2011). Hydrothermal alteration and related mineralization at the Anjerd skarn includes early garnet-pyroxene-wollastonite and associated magnetite and minor molybdenite (which is otherwise hosted by potassic alteration observed in the adjacent diorite-granodiorite stock) and later

tremolite-actinolite-epidote-quartz. Associated magnetite and lesser hematite are more prominent in the exoskarn, whereas copper sulfides occur mainly within the endoskarn (Hezarkhani, 2006c; Mollai and others, 2009). The Mazraeh skarn is also associated with a calc-alkaline granodiorite pluton. The skarn mineralogy consists of early pyroxene-garnet and late scapolite, actinolite-tremolite, epidote, chlorite, calcite, and quartz. Mineralization consists of chalcopyrite, pyrite, magnetite, hematite, bornite, covellite, and chalcocite (Somarin, 2004, 2006, 2010; Mollai and others, 2009).

Also in the western (Arasbaran) segment of the sub-tract in northernmost Iran, the Oligocene-Miocene or younger Miveh-Rud Cu-Mo-(W) porphyry-skarn and epithermal Au-Ag-Sb prospect is hosted by a thick sequence of Paleocene sandstone, shale, siltstone, marl, and marly limestone that were intruded by a granodiorite to quartz monzonite porphyritic intrusion and trachyandesitic to dacitic dikes (Einali and Alirezai, 2005; Jamali and others, 2010). The porphyry system exhibits potassic, propylitic, sericitic, and argillic alteration. Early porphyry and skarn copper, bismuth, tungsten, and molybdenum mineralization is located in the southern part of the intrusive complex, whereas late epithermal gold, silver, and antimony mineralization occurs in the northern part (Jamali and others, 2010).

In the western (Lesser Caucasus) segment of the sub-tract in Armenia and Nakhchivan, other possible porphyry-related prospects include Aramazd (Cu-Mo-Au-Ag-Pb-Zn), Bartsravan-Brnakot (Cu-Mo-Au-Pb), Balishen (Cu-Au-Ag-Mo-Pb), and Hankasar (Cu-Mo-Au-Ag) (Mining Journal, 2011a; Wikipedia, 2013a; Azerbaijan Ministry of Ecology and Natural Resources, [2006?]). However, the deposit type and age of these occurrences is uncertain. They are not included in appendix D.

Preservation Level

As derived from the geologic maps of Huber (1978) and Kekelia and others (2001), older basement units underlie 45 percent the Azerbaijan-Caucasus-Iran sub-tract, whereas late Eocene to early Miocene permissive volcanic and plutonic rocks occupy 7 and 6 percent of the sub-tract, respectively (fig. 48). Broadly coeval nonpermissive mafic, sedimentary and volcano-sedimentary units constitute only 4 percent of the sub-tract area, and younger rocks cover the remaining 38 percent of the sub-tract area.

The $\{\text{volcanic}/[\text{volcanic}+\text{plutonic}]\} \times 100$ ratio of 55 suggests levels of crustal preservation that are appropriate for porphyry copper systems, particularly in the Arasbaran segment of the sub-tract in northern Iran and the southern Lesser Caucasus. Deeper and shallower levels of porphyry system preservation exist in the Talysh-Alborz and the Tarom parts of the sub-tract. Overall, the large number of exposed porphyry deposits and prospects in the Arasbaran segment of the Azerbaijan-Caucasus-Iran sub-tract suggest that concurrent and postmineral uplift, erosion, and burial events occurred only to the extent that favorably exposed porphyry systems of this age range.

Magnetic Anomalies

The regional aeromagnetic map (Maus and others, 2009) was used to confirm the location and character of regional geologic features (for example, arcs, basins, faults, terrane boundaries). Prominent positive anomalies coincide well with Oligocene-Miocene batholiths in the western Lesser Caucasus-Arasbaran-Tarom sector of the Azerbaijan-Caucasus-Iran sub-tract. In this part of the tract, Oligocene-Miocene porphyry copper systems generally straddle the boundaries of magnetic highs. Another prominent anomaly occurs in the southernmost part of the sub-tract in the Central Iranian Terrane. This is an area dominated by Oligocene-Miocene andesite lava flows. No intrusions or porphyry occurrences are reported from this area. Conversely, only smaller and more isolated anomalies occur in the eastern (Talysh-Alborz) sector of the tract in northern Iran, where Mesozoic and older sedimentary formations are more common.

ASTER Alteration Data

Processed ASTER data (Mars, 2014), available for 65 percent of the Azerbaijan-Caucasus-Iran sub-tract segment of northern Iran, were used to evaluate potential hydrothermal alteration that could be associated with unidentified porphyry systems.

Of the 108 ASTER-derived alteration zones, 30 occur in the Arasbaran segment of the tract. Here, 12 are associated with younger Pliocene-Holocene rocks, and 4 are spatially related to the Sungun, Dustbeiglu, Shirin Daragh, and Miveh Rud porphyry sites, respectively. Prominent phyllic alteration ASTER-derived alteration zones occur at Sungun and Dustbeiglu. Of the remaining 14 ASTER alteration zones, two are spatially related to iron and base-metal occurrences, respectively. The origin of the other 12 ASTER-derived alteration zones is unknown. They could be related to older, Oligocene-Miocene, or younger hydrothermal systems. Two of them exhibit well-developed ASTER-derived phyllic and argillic alteration zones, and two additional alteration zones are dominated by phyllic and argillic alteration halos, respectively. Thus, ASTER-derived alteration data could indicate the presence of perhaps four additional unidentified porphyry systems of late Eocene to early Miocene age in the Arasbaran sector of the Azerbaijan-Caucasus-Iran sub-tract.

Of the 78 ASTER-derived alteration zones distributed across the epithermal-dominated Tarom segment of the tract to the south, 18 are associated with younger Pliocene-Holocene rocks, and 8 are spatially related to known mineral occurrences (including the Tarom, Sheykh Darabad, Mendejin, and Baycheh Bagh porphyry and porphyry-related prospects). The remaining 52 ASTER-derived alteration zones could be related to older, Oligocene-Miocene, or younger hydrothermal systems. However, well-developed ASTER-derived phyllic, phyllic-argillic, and argillic alteration zones are few. Hence, across the Tarom segment of the Azerbaijan-Caucasus-Iran sub-tract, ASTER-derived alteration data suggest the existence of a few sites of potential hydrothermal alteration that could be associated with unidentified porphyry-related systems of late Eocene to early Miocene age.

Probabilistic Assessment

Grade and Tonnage Model Selection

According to the criteria based on Au/Mo ratios and gold and molybdenum contents, the Masjed Daghi and Kadjaran deposits belong to the Cu-Au and Cu-Mo porphyry deposit subtype categories, respectively. Resource data are not sufficient to classify the Ankavan, Haft Cheshmeh, or Sungun deposits. However, available information support a Cu-Mo-(Au) association for these deposits, as well as a large number of other porphyry prospects in the Azerbaijan-Caucasus-Iran sub-tract. Pooled *t*-test results assuming equal variances show that the five known deposits in the tract are not significantly different at the 1-percent level from tonnages and grades in the general porphyry Cu-Au-Mo model of Singer and others (2008). Therefore, this model was selected to estimate undiscovered copper, gold, molybdenum, and silver resources. In comparison with the median tonnage and grade in the general porphyry Cu-Au-Mo model, the Sungun deposit is larger and contains higher copper and molybdenum grades; the Kadjaran deposit is also larger but exhibits lower copper grade. Furthermore, Kadjaran and Ankavan show higher molybdenum and gold grades than the median deposit in the model, whereas Haft Cheshmeh and Masjed Daghi are smaller and also exhibit lower copper grades. Masjed Daghi contains more gold than the median deposit in the model. However, this gold appears to be mostly associated with the overlying acid-sulfate system.

Estimates of Undiscovered Deposits and Rationale

In the Azerbaijan-Caucasus-Iran sub-tract, geologic factors favorable for the occurrence of undiscovered porphyry deposits include (1) relatively large postcollisional magmatic belt built on attenuated warm crust, (2) permissive calc-alkaline and alkaline magmatism, (3) shallow to intermediate levels of exposure of Cu-Au and Cu-Mo porphyry-skarn systems, (4) operating porphyry copper deposits with substantially larger than median tonnages and subequal copper but higher molybdenum and gold grades (for example, Kadjaran, Sungun), and (5) perhaps as many as 10 sites of ASTER-derived potential hydrothermal alteration associated with possible unidentified porphyry systems. Unfavorable factors for the occurrence of undiscovered porphyry deposits include (1) possible disparate levels of exposure related to relatively large displacements along synmineral and postmineral normal faults and (2) local volcanic-dominated preservation levels that appear too shallow for exposure of porphyry systems (for example, southernmost sector of the tract).

The lower density of known porphyry deposits in the sub-tract compared to other tracts of equivalent size around the world suggests that the occurrence of undiscovered deposits is likely. Extensive exploration in the well-endowed and adequately exposed Arasbaran region of the sub-tract is further supported by the high number of known porphyry occurrences (Jamali and others, 2010).

The assessment team established that the Azerbaijan-Caucasus-Iran sub-tract was exceptionally favorable and that estimates of numbers of undiscovered porphyry copper deposits

could be carried out with low uncertainty. Therefore, quantitative assessment of undiscovered deposits in this tract was completed. Table 13c–A shows the team estimates for undiscovered porphyry copper deposits in the Azerbaijan–Caucasus–Iran sub-tract. The team reached a consensus estimate of 1, 6, and 15 undiscovered deposits for the 90-, 50-, and 10-percent probability levels, respectively, which resulted in a mean of 7.13 undiscovered deposits with a standard deviation of 5.01 ($C_v\%=70$). The estimate reflects the level of favorability and low uncertainty assessed for this sub-tract. The resulting total deposit density per 100,000 km² obtained is comparable to the median porphyry deposit density expected in well-explored tracts of equivalent size elsewhere around the world (Singer and Menzie, 2010).

Probabilistic Assessment Simulation Results

Simulation results for estimates for copper, molybdenum, gold, silver, and the total volume of mineralized rock are summarized in table 13c–B. The mean estimate of undiscovered resources in the Azerbaijan–Caucasus–Iran sub-tract is 27 Mt of copper. Undiscovered copper resources in this sub-tract are estimated to amount to about 2.3 times the copper that has already been identified. However, these resources may be inaccessible or uneconomic at present. Furthermore, a substantial fraction of the inventory can be expected to be distributed among numerous already identified small prospects or known deposits with resource bases that are undefined or only partially defined at present.

Results of the Monte Carlo simulation are also presented as cumulative frequency plots (fig. 49C). The cumulative frequency plots show the cumulative probabilities of occurrence-estimated resources and total mineralized rock, as well as the mean for each commodity and for total mineralized rock.

Yazd Tract (142pCu9015)

Descriptive model: General porphyry copper (Cox, 1986a; Berger and others, 2008; John and others, 2010)

Grade and tonnage model: General Cu–Au–Mo porphyry copper model (Singer and others, 2008)

Geologic feature assessed: Middle Eocene to middle Miocene back arc and continental arc of the Tethyan Eurasian Metallogenic Belt

Location

The Yazd tract located in central Iran covers an area of 25,700 km² (fig. 50). It delimits a continuously exposed 550-km-long and 50–90-km-wide middle Eocene to middle Miocene continental arc along the central segment of the Urumieh–Dokhtar Magmatic Belt. To the southwest, the Yazd tract is bounded by the suture between the Sanandaj–Sirjan and Central Iranian Terranes (fig. 3), which is roughly marked by a southwest-vergent thrust fault system best recognized in the northern and central parts along the tract boundary. To the northeast, the Yazd tract is delimited by the Saveh–Rafsanjan Basin (fig. 51) and by a series of northeast-vergent en-echelon thrust faults (Alavi, 1994). To the southeast, the Yazd tract terminates against the

ophiolite-bearing right-lateral strike-slip Dehshir Fault, which separates it from the Kerman tract to the south (Moghadam and others, 2010). The northwestern boundary of the Yazd tract marks the extent of the exposed arc, which may terminate or continue to the northwest under thick Eocene volcano-sedimentary-dominated successions, coeval Oligocene–Miocene sedimentary rocks, and younger terrestrial deposits (Azizi and Moinevaziri, 2009).

Tectonic Setting

Several scenarios have been proposed for the origin and subsequent evolution of the Late Cretaceous to middle Eocene igneous rocks that occupy much of central Iran (Berberian and Berberian, 1981; Ghasemi and Talbot, 2006; Arfania and Shahriari, 2009; Agard and others, 2011). However, it is generally accepted that Late Cretaceous to middle Eocene oblique subduction along the Bitlis–Zagros zone produced an Andean-type continental arc in the Sanandaj–Sirjan Terrane (see Border Folds tract above) and an associated back arc (see Esfahan tract above) in the Central Iranian Terrane.

By middle Eocene times, the arc axis migrated from the Sanandaj–Sirjan Terrane onto the Central Iranian Terrane. Igneous rocks associated with this arc-building event are well preserved along the Urumieh–Dokhtar Magmatic Belt in this region (Kazmin and others, 1986).

Along the central (Yazd) segment of the Urumieh–Dokhtar Magmatic Belt, arc migration caused uplift and emplacement of middle-late Eocene calc-alkaline arc rocks overprinting earlier middle Eocene calc-alkaline to alkaline back-arc successions (fig. 4E). This was followed by significant extension, subsidence, and sedimentary basin formation during the Oligocene–Miocene, and renewed uplift and subduction-related calc-alkaline to alkaline magmatism intruding thinned crust in the early-middle Miocene (fig. 4F). In central Iran, subduction-related arc magmatism terminated by the middle Miocene with the oblique collision between the Arabian Platform and the Eurasian margin (Agard and others, 2005; Allen and Armstrong, 2008). This collision initiated southwest-vergent folds and thrusts (fig. 4G), as well as oblique cross-cutting dextral strike-slip faults along the Bitlis–Zagros Suture (Jackson and McKenzie, 1984). In the Urumieh–Dokhtar Magmatic Belt, deformation and uplift were accompanied by late Miocene–Holocene postcollisional alkalic magmatism (Omrani and others, 2008).

Magmatism

Permissive igneous rocks used to define the Yazd tract (appendix B) are shown in figure 51, along with geologic features described in this section. The Yazd tract delineates the middle-late Eocene back-arc and arc and early-middle Miocene arc magmatic events mentioned above. Magmatism along this segment of the Urumieh–Dokhtar Magmatic Belt can be summarized as (1) early Eocene deposition of back-arc volcanoclastic sequences interlayered with tholeiitic and calc-alkaline ignimbritic, as well as andesitic to rhyodacitic units (Torabi, 2009); (2) unconformable deposition of middle

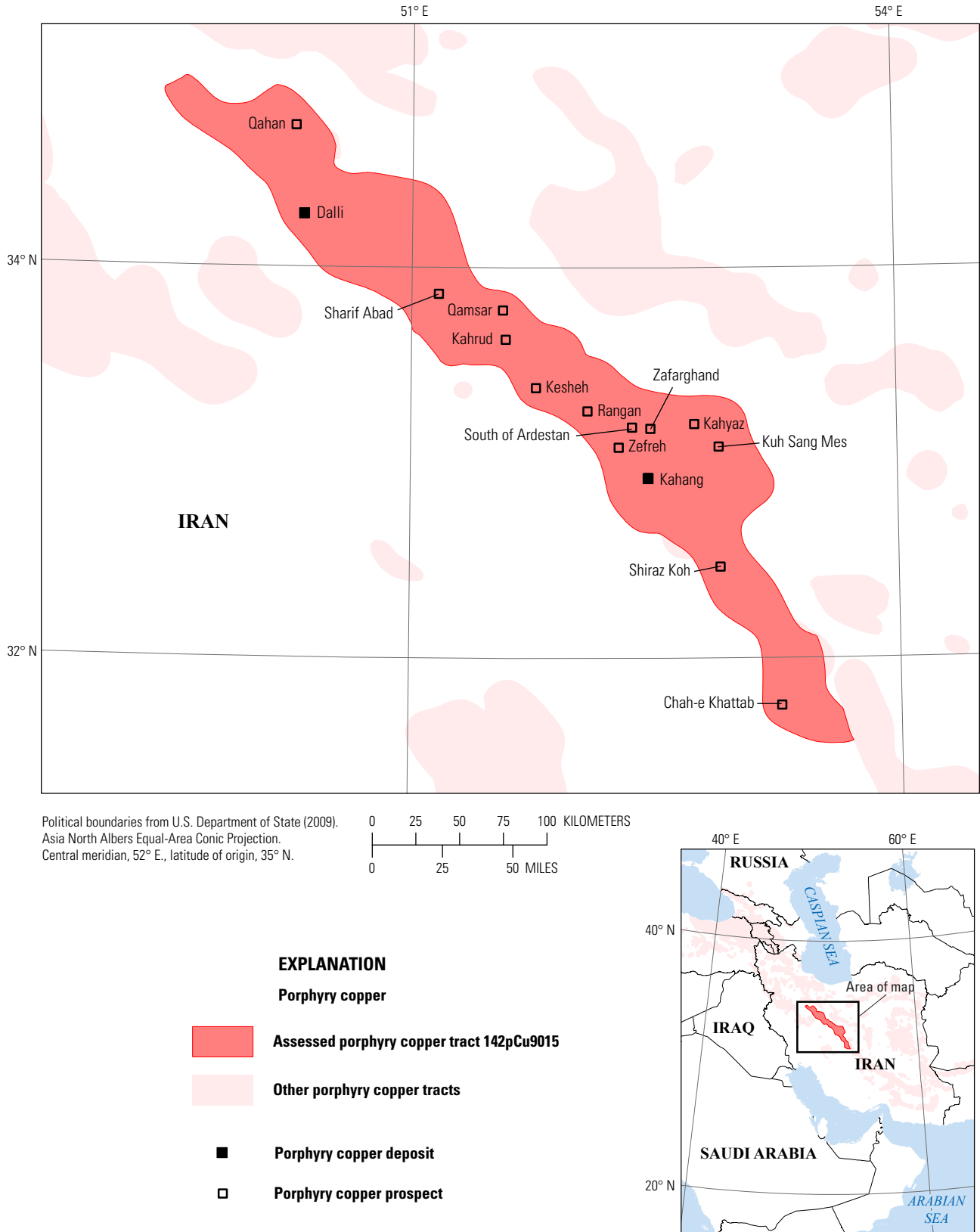
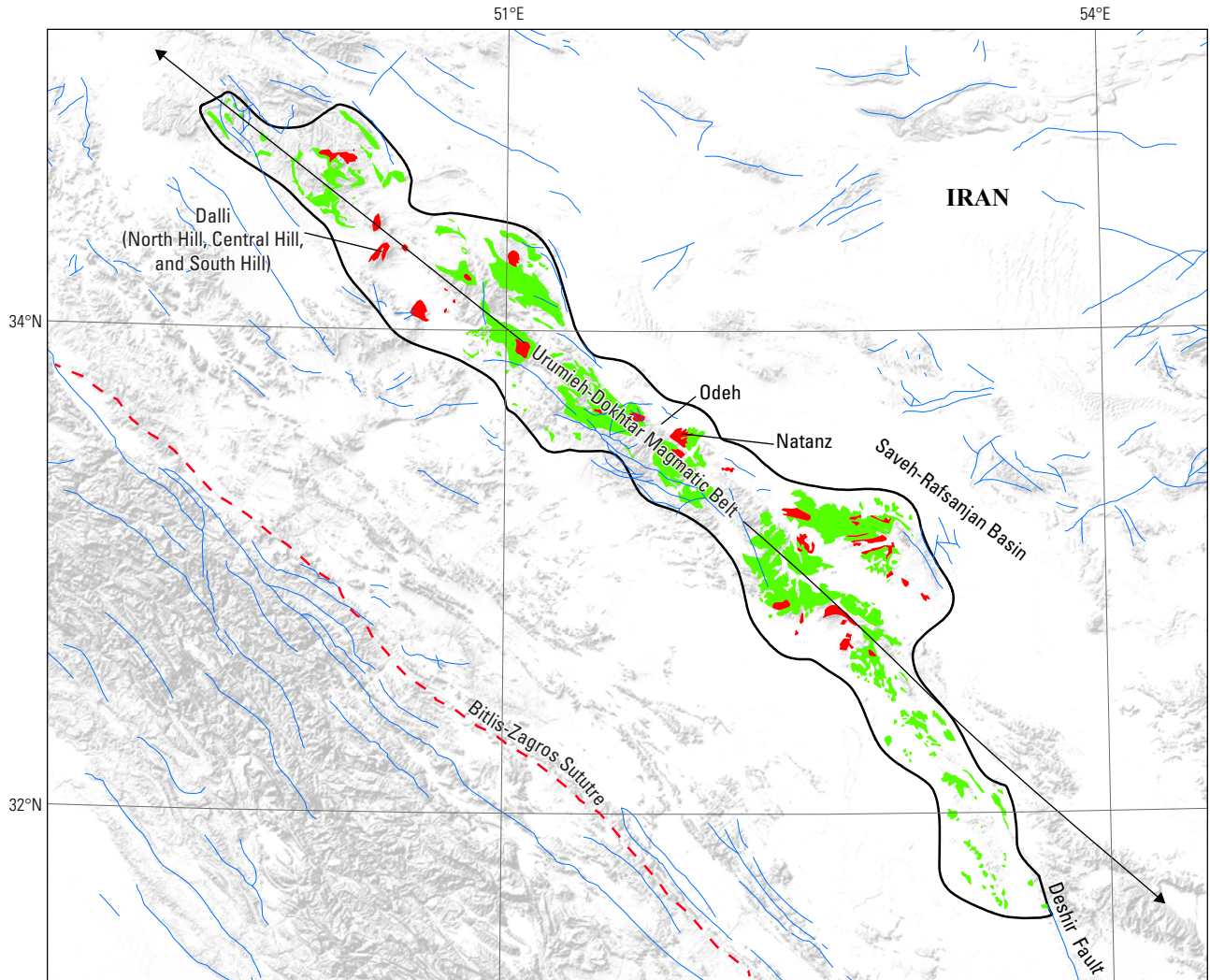
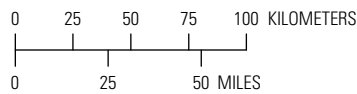


Figure 50. Map showing the location of known porphyry copper deposits and prospects for permissive tract 142pCu9015, Yazd—Iran. See table 2 for deposits, appendix C for prospects, and appendix D for accompanying spatial data.



Base from SRTM Global Digital Elevation Model, U.S. Geological Survey EROS Data Center, 2006. Political boundaries from U.S. Department of State (2009). Asia North Albers Equal-Area Conic Projection. Central meridian, 52° E., latitude of origin, 35° N.









- EXPLANATION**
- Porphyry copper**
 -  Assessed porphyry copper tract 142pCu9015
 -  Permissive intrusive rock
 -  Permissive extrusive rock
 -  Fault
 -  Suture
 -  Natanz **Geologic feature discussed in the text**



Figure 51. Map showing the distribution of permissive intrusive and extrusive rocks used to define tract 142pCu9015, Yazd—Iran. See appendix A for principal sources of information and appendix B for source map units.

Eocene back-arc volcanoclastic sequences with interbedded mafic to felsic alkalic rocks of continental arc affinity (Torabi, 2009; Sepahi and Malvandi, 2008) and middle to late Eocene intrusion of the Older Natanz Batholith suite of calc-alkaline mafic to felsic plutons (Berberian and others, 1982; Haschke and others, 2010); (3) early Oligocene uplift and deposition of continental red beds of the Lower Red Formation (Reuter and others, 2009); (4) Oligocene-Miocene subsidence and deposition of the extensive shallow marine Qom Formation (Reuter and others, 2009; Morley and others, 2009); (5) early to middle Miocene (24–21 Ma) emplacement of the Younger Natanz Batholith suite of calc-alkaline to alkaline gabbro, diorite, quartz diorite, tonalite, granodiorite, quartz monzonite, and lesser monzogranite and syenogranite plutons (Haschke and others, 2010, and references therein); (6) middle Miocene collision, uplift, and deposition of continental red beds of the Upper Red Formation (Morley and others, 2009); and (7) late Miocene-Holocene emplacement of postcollisional calc-alkaline and alkaline rocks (Jackson and McKenzie, 1984; Omrani and others, 2008; Khodami and others, 2010a, b).

Geochemical data of granitoids of the middle to late Eocene Older Natanz Batholith and early to middle Miocene Younger Natanz Batholith indicate a subduction-related arc affinity. However, geochemical signatures of granitoids from the Older Natanz Batholith indicate calc-alkaline Andean-type arc magmas derived from thick garnet-bearing asthenosphere, whereas geochemical signatures of granitoids from the Younger Natanz Batholith indicate calc-alkaline and alkaline magmas emplaced in thin or attenuated continental crust (Haschke and others, 2010).

In general, ages and geochemical characteristics of intrusive rocks in the Yazd tract are hard to distinguish from those associated with the Paleocene to middle Eocene and late Eocene-early Miocene extension-related tectono-magmatic events in central Iran (see Esfahan and Azerbaijan tracts above).

Known Porphyry Deposits and Prospects

Porphyry Cu-Mo-Au, skarn Cu-(Co-Fe), epithermal base and precious metal, and exhalative Mn-Fe occurrences characterize the mineralization styles present in the Yazd tract (Samani, 1998; Moghadam and others, 2010). Two porphyry deposits (Dalli and Kahang), 8 porphyry prospects, and 5 other possible porphyry-related occurrences are included in this tract (table 2, appendix C, fig. 50). Porphyry systems in the Yazd arc segment are dominated by Cu-Mo-bearing associations, with the exception of the Dalli Cu-Au porphyry deposit and the Qahan and Kesheh porphyry-related acid sulfate gold prospects.

Available information on the porphyry occurrences in the Yazd tract is sparse. However, existing age constraints suggest that most of these porphyry systems are associated with the early to middle Miocene Younger Natanz Batholith. Dated granitic and rhyolitic porphyry intrusions exhibit an age range between 21.3 and 18.6 Ma (Berberian and others,

1982; Berberian and Berberian, 1981; Haschke and others, 2010). In addition, available geobarometric data include 1.5–2-kb-emplacement pressures that support appropriate levels of preservation of porphyry-style mineralization (Shahrokhi and others, 2010; Honarmand and Ahmadian, 2008). Descriptions of porphyry deposits and selected prospects in the Yazd tract are presented below.

Dalli Porphyry Deposit

The Dalli Cu-Au porphyry deposit located in the northern part of the Yazd tract is under development. It has reported proven reserves of 8 Mt with 0.5 percent copper and 0.75 g/t gold (Ayati and others, 2013). Current probable reserves stand at 76 Mt of 0.35 percent copper and 0.66 g/t gold (weighted average of South Hill and North Hill; Dorsa, 2013).

At the Dalli porphyry deposit, several early Miocene (21 Ma; Ayati and others, 2013) porphyritic diorite, quartz diorite, tonalite, and granodiorite stocks and late andesite dikes intrude Oligocene red beds, roughly coeval and comagmatic calc-alkaline basaltic-andesitic volcanics and andesitic-rhyodacitic pyroclastic rocks (Haroni, 2005, 2008; Dorsa PLC, 2012a; Singer and others, 2008). Al-in-hornblende data indicate an emplacement depth ranging between 3 and 12 km, based on pressures of 2.6 ± 1.7 kb for the porphyry intrusions (Ayati and others, 2013). The Dalli deposit consists of three mineralized zones that lie along a 2.5-km-long NE trend—the North Hill, the Central Hill, and the South Hill. The larger mineralized zone occurs in the South Hill, which is underlain by porphyritic diorite and tonalite. Chalcopyrite, sparse bornite, and gold included in pyrite and chalcopyrite occur in a quartz stockwork within a 200- by 200-m alteration zone. Alteration minerals include secondary biotite, rare K-feldspar, magnetite, pyrite, chlorite, and specularite, which are overprinted by quartz-sericite-pyrite. Weak argillic alteration surrounds potassic and phyllic alteration. Calcic alteration with epidote-actinolite occurs locally. The oxidized hematite, goethite, and jarosite lithocap includes malachite, azurite, and cuprite. A limited chalcocite and covellite supergene zone developed below. Mineralization in the Central Hill is hosted by porphyritic tonalite only, but otherwise mineralization exhibits the same characteristics as that in the South Hill. The North Hill intrusions consist of more felsic porphyritic granodiorites that display phyllic and locally argillic alteration with better developed limonites. The alteration zone here covers an area of 400 by 200 m (Ayati and others, 2008). Geochemical data on volcanic and subvolcanic rocks from the Dalli porphyry Cu-Au deposit support a subduction-related arc setting that evolved on relatively thin (30–35 km) continental crust (Ayati and others, 2013).

Kahang (Gor Gor) Porphyry Deposit

The Kahang Cu-Mo porphyry deposit located in the central part of the Yazd tract is under development. The deposit has reported proven and probable reserves of 38.74 Mt at 0.59 percent copper at a 0.25 percent cutoff (National Iranian Copper Industries Company, 2012).

The Kahang porphyry deposit is centered on three Oligocene-Miocene quartz monzonite and diorite porphyry stocks that intrude Eocene dacite and andesite (Afzal and others, 2010). Copper and molybdenum mineralization is hosted by tourmaline breccias and strong K-silicate and quartz-sericite alteration. The alteration zone covers an approximate area of 2 by 5 km (10 km²). Malachite, Cu-Mn oxide, jarosite, hematite, and goethite overprint intense hypogene quartz stockwork- and breccia-controlled mineralization. Breccias show the highest copper and molybdenum grades (Dorsa PLC, 2012b; Afzal and others, 2010).

Qahan Porphyry Prospect

The Qahan Cu-Mo-bearing porphyry prospect (National Iranian Copper Industries Company, 2012) is located in the northernmost part of the Yazd tract about 50 km north of the Dalli Cu-Au porphyry deposit. At the Qahan prospect, an Eocene sequence of pyroclastic, tuff, and volcanic rocks is intruded by several stocks, including a dacitic quartz-eye porphyry intrusion (Dorsa PLC, 2012c). Associated quartz-sericite-pyrite stockworks and argillic alteration is present within a 300 m by 1,000 m area. The leached cap has malachite, goethite, jarosite, and local hematite. Preliminary sampling in the leached cap shows anomalous copper, gold and molybdenum values. An acid-sulfate gold system adjacent to this porphyry prospect has been mined in the past (Dorsa PLC, 2012c).

Qamsar Porphyry Prospect

In the Sharif Abad area, the Qamsar (Kashan) Mo-(Cu)-bearing porphyry prospect (Bazin and Hübner, 1969a; Geological Survey of Iran, 2012d) consists of Miocene calc-alkaline I-type quartz gabbro, quartz diorite, granodiorite, and aplitic dikes that intrude Eocene volcanic (basaltic andesite, andesite, trachyandesite, trachyte, dacite, and rhyolite), pyroclastic (felsic tuff and agglomerate), and sedimentary (sandstone, shale, and limestone) rocks (Sepahi and Malvandi, 2008).

South of Ardestan and Sharif Abad Porphyry Prospects

These two porphyry copper prospects (Bazin and Hübner, 1969a; Förster, 1978; Shahabpour and Kramers, 1987) are mentioned in the literature. However, little is known about their geology, alteration, mineralization, and resource base.

The South of Ardestan porphyry prospect is located about 30 km northwest of the Kahang deposit. In the area, Torabi (2009) reports the occurrence of late Eocene subaerial trachybasalt, tephriphonolite, trachyte, and trachydacite arc-related rocks, and Sepahi and Malvandi (2008) mention Miocene gabbro to diorite intrusions. Haschke and others (2010) further add that Eocene arc rocks are only moderately mineralized and that early Miocene granite porphyry intrusions are essentially barren.

The Sharif Abad porphyry-related skarn is located about 90 km southeast of the Dalli deposit. This old mining locality is described as a Cu-Fe-Mo-Pb-Zn-W skarn that developed along the contact between an Oligocene-Miocene porphyritic diorite and limestone (Geological Survey of Iran, 2012a). Molybdenum, lead, zinc, and tungsten occur in the ore mineral assemblage (chalcopyrite, bornite, and covellite, as well as malachite and azurite). These copper minerals are hosted by two subparallel specularite-magnetite-pyrite-bearing epidote-amphibole-garnet skarn zones. The skarn deposits are about 2 m wide and 400 m long. Before the mine was abandoned in 1962, 200 t of 10 percent copper was exported to the Soviet Union (Bazin and Hübner, 1969a).

Zafarghand Porphyry Prospect

The Zafarghand Cu-Mo-bearing porphyry prospect (National Iranian Copper Industries Company, 2012) is located about 30 km north of the Kahang deposit. It consists of largely covered 1.5- by 4.5-km K-silicate-magnetite-pyrite, quartz-sericite, and kaolinite stockworks that developed in dacite porphyry and microdiorite stocks (Dorsa PLC, 2012d). These stocks intrude andesite. Weak to moderate secondary goethite-jarosite-hematite and alunite are present in the lithocap. Samples from the potassic and phyllic alteration zones contain as much as 1,473 ppm copper and 158 ppm molybdenum. A lead-zinc prospect occurs in the vicinity of the porphyry system (Dorsa PLC, 2012d).

Zefreh Porphyry Prospect

The Zefreh porphyry Cu-Mo-bearing prospect (National Iranian Copper Industries Company, 2012) is located about 24 km northwest of the Kahang deposit. The prospect consists of a 2- by 5-km quartz-sericite and quartz-clay alteration zone around a dacite porphyry stock (Dorsa PLC, 2012e). Within the alteration zone and across the porphyry intrusion, an area of 600 by 1,500 m consists of strong quartz-sericite-pyrite stockworks and iron oxides (goethite+jarosite+hematite). Samples from the leached cap contain anomalous copper and molybdenum (Dorsa PLC, 2012e).

Other Porphyry-Related Prospects and Possible Porphyry-Related Mineral Occurrences

Porphyry units are reported in the copper occurrence database of Iran at both the Kesheh gold acid-sulfate and Kahrud copper skarn prospects (Geological Survey of Iran, 2012a). The Kesheh prospect lies about 80 km northwest of the Kahang porphyry deposit, and the Kahrud prospect is located near the Sharif Abad porphyry-related skarn. At Kahrud, magnetite and chalcopyrite occur in a pyroxene, garnet, and epidote skarn that developed along the contact of a porphyry intrusion (Bazin and Hübner, 1969a). At Kesheh, a kaolinite, alunite, and jarosite alteration zone is associated with Oligocene-Miocene stocks that intrude Eocene volcanic and pyroclastic rocks (Taghipour and others, 2007).

The Rangan acid-sulfate prospect consists of post-Oligocene diorite to monzodiorite stocks that intrude Eocene andesite to rhyolite flows and ignimbritic tuffs and a late Eocene rhyolite dome. The Mesozoic carbonate and clastic wallrocks exhibit the effects of thermal metamorphism and skarn alteration (Parsapoor and others, 2009). A quartz-sericite-pyrite alteration zone surrounded by advanced argillic alteration with pyrophyllite, diaspore, vuggy silica, alunite, and barite occurs on the northwest side of the rhyolite dome. Quartz-sericite-pyrite alteration overprinted by abundant clay and jarosite-(goethite) also occurs on the southeast side of the rhyolite dome, and active hot springs have precipitated travertine along the western margin of the rhyolitic dome. This suggests that the Rangan acid-sulfate system may be Pliocene to Holocene. A diorite to monzodiorite pluton crops out a few hundred meters south and east of the rhyolite dome. However, its relation to the skarn or the acid-sulfate system at Rangan is unclear.

The Shiraz Koh kaolin mine lies within a low-sulfidation alteration zone that covers an area of 1 by 5 km (Dorsa PLC, 2012f). On the western side of the alteration zone (West Shiraz Koh), intermediate tuffs and minor flows are intruded by a granodiorite intrusion. Hydrothermal alteration around the intrusion includes a central kaolinite, sericite, and quartz zone, which is surrounded by chalcedonic and brecciated quartz veins containing chalcopyrite and minor galena. Samples collected from the leached cap in the central zone exhibit values of as much as 0.2 percent copper and 0.25 g/t gold. Silver, lead, molybdenum, arsenic, and bismuth contents are also anomalous (Dorsa PLC, 2012f). An association of this low-sulfidation prospect with a porphyry system is uncertain.

Other possibly porphyry-related occurrences in the Yazd tract include the copper-iron skarn prospects at Chah-e Khattab, Kahyaz, and Kuh Sang Mes (Bazin and Hübner, 1969a; Somarin and others, 2005; Geological Survey of Iran, 2012a).

Preservation Level

As derived from the geologic map of Huber (1978), older basement rocks underlie 10 percent of the Yazd tract area, and middle Eocene to middle Miocene permissive volcanic and plutonic units occupy 18 and 3 percent, respectively, of the tract area (fig. 51). Broadly coeval nonpermissive rocks occur in 19 percent of the tract, and younger rocks cover the remaining 51 percent of the tract. The overall $\{\text{volcanic}/(\text{volcanic}+\text{plutonic})\} \times 100$ ratio of 87 further suggests that shallow levels of preservation of porphyry systems are dominant across the Yazd tract. This is supported by the presence of acid-sulfate systems associated with a number of the known porphyry prospects. Exposure of porphyry copper systems appears to be also limited by widespread younger cover.

However, Eocene back-arc and Oligocene-Miocene arc environments are superimposed in the Yazd tract. These

two settings cannot be differentiated effectively at the geologic map scales available (Huber, 1978; Haghipour and Aghanabati, 1985; Agard and others, 2011). As roughly estimated, Eocene permissive units underlie about 15 percent of the tract area and have high volcanic-to-plutonic rock ratios that suggest shallow levels of preservation for porphyry copper systems. Oligocene-Miocene permissive units occupy only about 5 percent of the tract area, but otherwise they exhibit subequal plutonic to volcanic rock ratios that support appropriate levels of preservation for porphyry copper systems.

Magnetic Anomalies

The regional aeromagnetic map (Maus and others, 2009) was used to confirm the location and character of regional geologic features (for example, arcs, basins, faults, terrane boundaries). A prominent magnetic high images this segment of the Urumieh-Dokhtar Magmatic Belt. In contrast to the more diffuse magnetic signatures in the back arc to the northeast and southwest, this continuous and high intensity magnetic anomaly appears to be imaging a well-preserved volcano-plutonic belt. Units with high magnetic susceptibilities such as ophiolite-bearing complexes are exposed in the southern part, but otherwise they are mostly absent. Furthermore, Pliocene-Holocene intermediate and mafic unit outcrops are comparatively limited across much of the area. Thus, the magnetic anomaly delimits the extent of the Yazd tract well. To the south, the tract boundary at the Dehshir Fault coincides with the magnetic anomaly. To the north, the tract boundary also corresponds with the extent the magnetic anomaly, suggesting that the arc may not continue under cover. With exception of the Dalli porphyry deposit, all other porphyry occurrences identified in the tract occur along the margins of magnetic highs.

ASTER Alteration Data

Processed ASTER data (Mars and Rowan, 2006; Mars, 2014) coverage for the entire Yazd tract was used to evaluate potential hydrothermal alteration that could be associated with unidentified porphyry systems in the tract. Of the 38 ASTER-derived alteration zones that were identified within the tract, 8 are spatially associated with the known Kahang, Zafarghand, South of Ardestan, Zefreh, Kahrud, Rangan, Kahyaz, and Kuh Sang Mes prospects; 4 are spatially associated with known copper skarn or vein occurrences; 3 are related to lead-zinc skarn or vein systems; and 1 is in the Miocene-Pliocene Odeh molybdenum-rich (porphyry?) occurrence. No ASTER-derived alteration zone was identified at the more mafic Dalli porphyry deposit.

Of the remaining 22 ASTER-derived alteration zones, 6 are associated with intrusions that otherwise have no reported mineral occurrences. The first exhibits a prominent 9-km-wide ASTER-derived phyllic-argillic alteration zone; the second is associated with a strong 8-km phyllic zone; the third consists of a conspicuous 4-km-wide phyllic zone,

and the fourth shows a poorly developed and discontinuous 6-km-wide phyllic zone. The fifth and sixth ASTER-derived alteration zones consist of large argillic areas. The remaining 16 ASTER-derived zones are relatively smaller and more poorly developed. They may not be related to hydrothermal alteration. Hence, perhaps six ASTER-derived alteration zones may be marking the location of unknown but potential porphyry-related hydrothermal alteration in the Yazd Tract.

Probabilistic Assessment

Grade and Tonnage Model Selection

With exception of the resource bases reported for the Kahang Cu-Mo and Dalli Cu-Au porphyry deposits, no tonnage or grade data are known for the porphyry prospects of the Yazd tract. The Dalli porphyry deposit is classified as a Cu-Au system based on the criteria for molybdenum and gold contents and ratios. However, the Cu-Mo-(Au) association appears to dominate in the tract, based on available data on the Qahan, Qamsar, Zafarghand, and Zefreh porphyry prospects. Furthermore, several porphyry and porphyry-related prospects in the Yazd tract are associated with acid-sulfate systems, suggesting that gold contents could be related to the overlying epithermal mineralization and not to the underlying porphyry mineralization. Pooled *t*-test results assuming equal variances show that the two known deposits in the tract are not significantly different at the 1-percent level from tonnages and copper and gold grades in the general porphyry Cu-Au-Mo model of Singer and others (2008). Therefore, this model was selected to estimate undiscovered copper, gold, molybdenum, and silver resources in this tract. In comparison to the median tonnage and grade in the general porphyry Cu-Au-Mo model, the two known deposits in the tract exhibit smaller tonnages but higher copper grades. Dalli also contains higher gold grade.

Estimates of Undiscovered Deposits and Rationale

Favorable geologic factors for the occurrence of undiscovered porphyry copper deposits in the Yazd tract include (1) extensional back-arc to compressional continental-arc setting, (2) permissive alkaline and calc-alkaline compositions, (3) acid-sulfate epithermal systems with known association to porphyry systems, (4) appropriate levels of preservation of porphyry systems associated with Oligocene-Miocene permissive rocks, (5) favorable conditions for supergene enrichment in Cu-Mo porphyry systems, (6) a half-dozen relatively large potentially porphyry-related ASTER-derived alteration zones, and also (7) northward continuation of highly favorable Kerman arc segment to the south. Unfavorable geologic factors for the occurrence of undiscovered porphyry copper deposits include (1) an arc segment built on relatively thin crust; (2) postmineral thrust faulting and possible concealment or

exhumation of porphyry systems; (3) inadequate levels of preservation of porphyry systems, particularly those that may be associated with the older Eocene permissive rocks; (4) known porphyry deposits with smaller than median size; (5) small exposure (5 percent of the tract area) of the more prospective Oligocene-Miocene permissive rocks; and (6) extensive cover (50 percent of the tract area).

A density of known porphyry deposits that is lower than that in other tracts of equivalent extent around the world suggests that undiscovered deposits are likely present. Despite the smaller numbers and sizes of known porphyry deposits, this tract is deemed to be favorable because it is the projection of the well-endowed and geologically similar Kerman tract to the southeast. The level of expected uncertainty to which the number of undiscovered deposits can be estimated is lowered by the relatively large number of known porphyry occurrences, but otherwise it is raised by the limited information on exploration projects in the region.

Hence, the assessment team established that the Yazd tract was geologically favorable, and that estimates of numbers of undiscovered porphyry copper deposits could be carried out with overall moderate levels of uncertainty. The tract would contribute significant copper resources from undiscovered deposits to the overall assessment. Therefore, quantitative assessment of undiscovered deposits in this tract was completed. Table 14A shows the consensus estimates for undiscovered porphyry copper deposits in the Yazd tract at the 90-, 50-, and 10-percent probability levels and the associated summary statistics. All assessors estimated that there was a 90-percent probability of 1 undiscovered deposit. At the 50-percent probability, the numbers ranged between 2 and 3 undiscovered deposits, and at the 10-percent probability level, the numbers increased to between 5 and 8. On the basis of these numbers, the team reached a consensus estimate of 1, 2, and 8 undiscovered deposits for the 90-, 50-, and 10-percent probability levels, respectively, which resulted in a mean of 3.43 undiscovered deposits with a standard deviation of 2.73 ($C_v=80$). This result reflects the level of favorability and moderate uncertainty assessed for this tract. The resulting total deposit density per 100,000 km² obtained is comparable to the median porphyry deposit density expected in well-explored tracts of equivalent size elsewhere around the world (Singer and Menzie, 2010).

Probabilistic Assessment Simulation Results

Simulation results for estimates for copper, molybdenum, gold, silver, and the total volume of mineralized rock are summarized in table 14B. The mean estimate of undiscovered resources in the Yazd tract is 13 Mt of copper. Results of the Monte Carlo simulation are also presented as cumulative frequency plots (fig. 52). The cumulative frequency plots show the cumulative probabilities of occurrence-estimated resources and total mineralized rock, as well as the mean for each commodity and for total mineralized rock.

Table 14. Probabilistic assessment for tract 142pCu9015, Yazd—Iran.

A. Undiscovered deposit estimates, deposit numbers, tract area, and deposit density.

[N_{xx} , estimated number of deposits associated with the xxth percentile; N_{und} , expected number of undiscovered deposits; s , standard deviation; $C_v\%$, coefficient of variance; N_{known} , number of known deposits in the tract that are included in the grade and tonnage model; N_{total} , total of expected number of deposits plus known deposits; tract area, area of permissive tract in square kilometers (km^2); deposit density reported as the total number of deposits per 100,000 km^2 . N_{und} , s , and $C_v\%$ are calculated using a regression equation (Singer and Menzie, 2005)]

Consensus undiscovered deposit estimates					Summary statistics					Tract area (km^2)	Deposit density ($N_{total}/100,000 km^2$)
N_{90}	N_{50}	N_{10}	N_{05}	N_{01}	N_{und}	s	$C_v\%$	N_{known}	N_{total}		
1	2	8	8	8	3.4	2.7	80	2	5.4	25,700	21

B. Results of Monte Carlo simulations of undiscovered resources.

[Cu, copper; Mo, molybdenum; Au, gold; and Ag, silver; in metric tons; Rock, in million metric tons]

Material	Probability of at least the indicated amount						Probability of	
	0.95	0.9	0.5	0.1	0.05	Mean	Mean or greater	None
Cu	0	230,000	5,500,000	32,000,000	53,000,000	13,000,000	0.29	0.06
Mo	0	0	79,000	880,000	1,600,000	360,000	0.23	0.23
Au	0	0	120	900	1,400	330	0.29	0.19
Ag	0	0	760	10,000	18,000	4,400	0.22	0.32
Rock	0	56	1,200	6,700	11,000	2,700	0.3	0.06

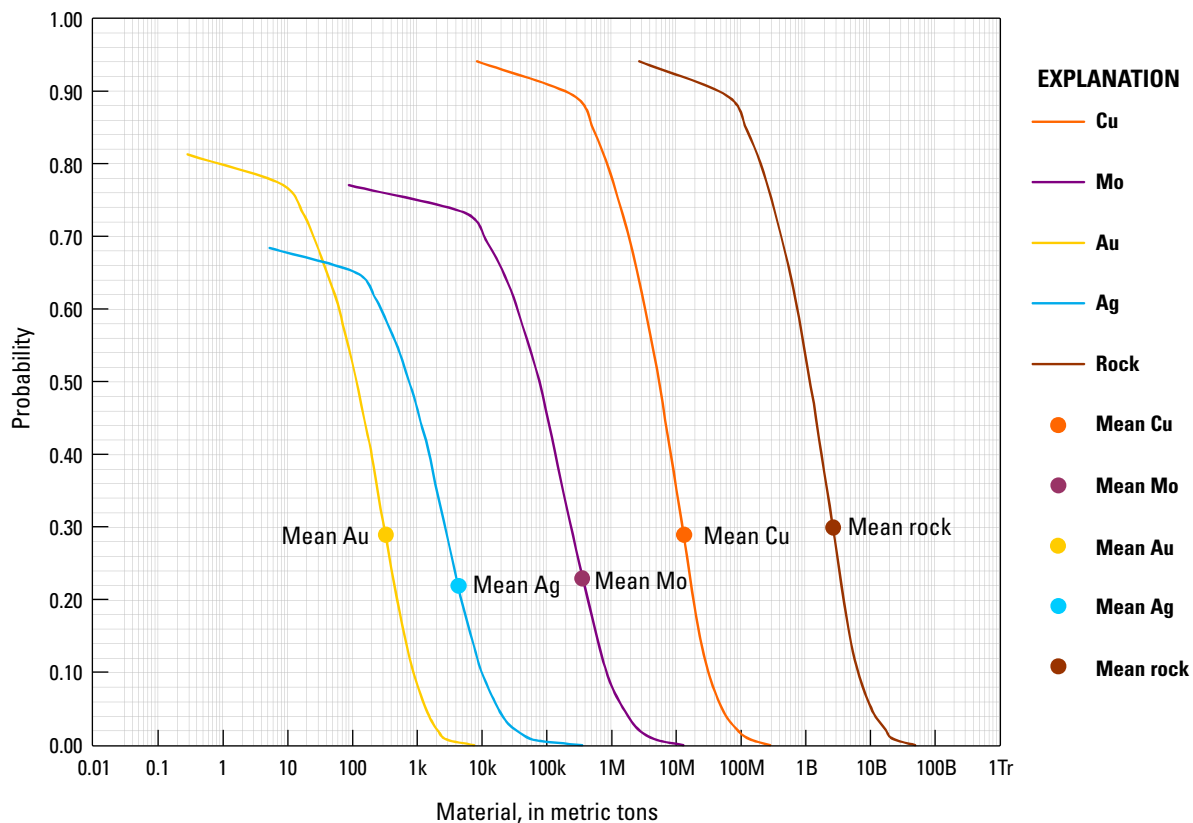


Figure 52. Cumulative frequency plot showing the results of Monte Carlo simulation of undiscovered resources in porphyry copper deposits in tract 142pCu9015, Yazd—Iran. k, thousand; M, million; B, billion; Tr, trillion.

Kerman Tract (142pCu9016)

Descriptive model: General porphyry copper (Cox, 1986a; Berger and others, 2008; John and others, 2010)

Grade and tonnage model: General Cu-Au-Mo porphyry copper model (Singer and others, 2008)

Geologic feature assessed: Late Eocene to late Miocene continental arc of the Tethyan Eurasian Metallogenic Belt

Location

The Kerman tract is located in south-central Iran where it covers an area of 32,800 km² (fig. 53). It delimits a continuously exposed 650-km-long and as much as 75-km-wide late Eocene-late Miocene continental arc segment that occupies the southeastern part of the Urumieh-Dokhtar Magmatic Belt.

The southwestern boundary of the Kerman tract lies along the northwest-southeast Nain-Baft ophiolite belt (fig. 3), which marks the suture between the Central Iranian and the Sanandaj-Sirjan Terranes (Shahabpour, 2005, 2007). To the northeast, the Kerman tract is delimited by dextral strike-slip faults that juxtapose the continental arc against the Saveh-Rafsanjan Basin (fig. 54). To the northwest, the tract terminates against the dextral Dehshir Fault (Moghadam and others, 2010), which separates the Kerman from the adjacent Yazd tract (see Yazd tract above). To the southeast, the Kerman tract continues in the southwestern margin of the Lut Terrane across the north-northeast-south-southwest dextral Sar Bisian-Nayband Fault system (fig. 3).

Tectonic Setting

Late Cretaceous to middle Eocene convergence between the Arabian Platform and the Sanandaj-Sirjan Terranes along the Bitlis-Zagros subduction zone resulted in continental arc, intraoceanic arc, and back-arc magmatism (Berberian and Berberian, 1981; Omrani and others, 2008). The continental arc was built on the Sanandaj-Sirjan Terrane in the Late Cretaceous (see Border Folds tract above). The associated extensive back arc developed behind the continental arc in the Central Iranian Terrane during the Late Cretaceous and Eocene (see Esfahan tract above). Late Cretaceous-middle Paleocene island-arc rocks are preserved in ophiolitic complexes along the suture between the Sanandaj-Sirjan and Central Iranian Terranes, which gradually amalgamated during this time (Ghazi and Hassanipak, 2000; Moghadam and others, 2009; Delaloye and Desmons, 1980; Desmons and Beccaluva, 1983).

Between the middle Paleocene and the late Eocene, the arc axis migrated from the Sanandaj-Sirjan Terrane onto the Central Iranian Terrane (Omrani and others, 2008), producing progressively more mature Andean-type continental arc magmatism. This arc is known as the Kerman Arc. This subduction-related arc event terminated in the late Miocene (fig. 4G) with oblique collision between the Arabian Platform and the Sanandaj-Sirjan Terrane (Agard and others, 2005; Allen and Armstrong, 2008; Shafiei and others, 2009). Available data indicate that collision in southeastern

Iran occurred 5–10 m.y. later than it did in central Iran, as described above with the Yazd tract (Agard and others, 2011; Aftabi and Atapour, 2009).

Magmatism

Permissive igneous rocks used to define the Kerman tract (appendix B) are shown in figure 54, along with geologic features described in this section. The tectono-magmatic evolution along the Kerman segment of the Urumieh-Dokhtar Magmatic Belt is characterized by:

1. Early Eocene deposition of back-arc volcanoclastic sequences interlayered with tholeiitic to calc-alkaline dominantly felsic rocks of the Bahr Aseman complex (Shafiei and others, 2008; Aliani and others, 2009).
2. Middle to late Eocene unconformable deposition of back-arc volcanoclastic sequences with interbedded bi-modal volcanic rocks of the Razak complex, followed by high-K calc-alkaline Jebal Barez gabbroic to granitic intrusions with primitive arc signatures (Shafiei, 2010). The Jebal Barez plutons occur throughout the Kerman arc segment, but they are most widespread in its southern parts (Shafiei and others, 2008).
3. Early Oligocene conformable deposition of the Hezar alkalic volcanic complex (Shahabpour, 2007) followed by uplift and deposition of Lower Red Formation red beds.
4. Middle Oligocene to early Miocene subsidence and deposition of the shallow marine Qom Formation (Reuter and others, 2009; Morley and others, 2009), which was followed by uplift, deformation, and deposition of Upper Red Formation red beds related to the collision between the Arabian Platform and the Central Iranian Terrane (Berberian and others, 1982; Ghasemi and Talbot, 2006; Agard and others, 2005; Allen and Armstrong, 2008).
5. Middle-late Miocene intrusion of progressively more felsic calc-alkaline mature arc Kuh Panj dioritic, quartzdioritic, and granodioritic stocks exposed mainly in the northwestern and central parts of the Kerman arc segment (Shafiei and others, 2008). Coeval middle-late Miocene volcanic rocks are not well preserved, suggesting concurrent uplift and magmatism (Shafiei, 2010). Porphyry copper mineralization is mostly related to this magmatic episode, which occurred during the final stages of subduction that preceded the ~10-Ma collision between the Arabian Platform and the Eurasian margin in this region (McQuarrie and others, 2003; Guest and others, 2006).
6. Latest Miocene-early Pliocene emplacement of syncollisional to postcollisional Dehaj subvolcanic dacite-rhyolite domes (Shafiei and others, 2009); and

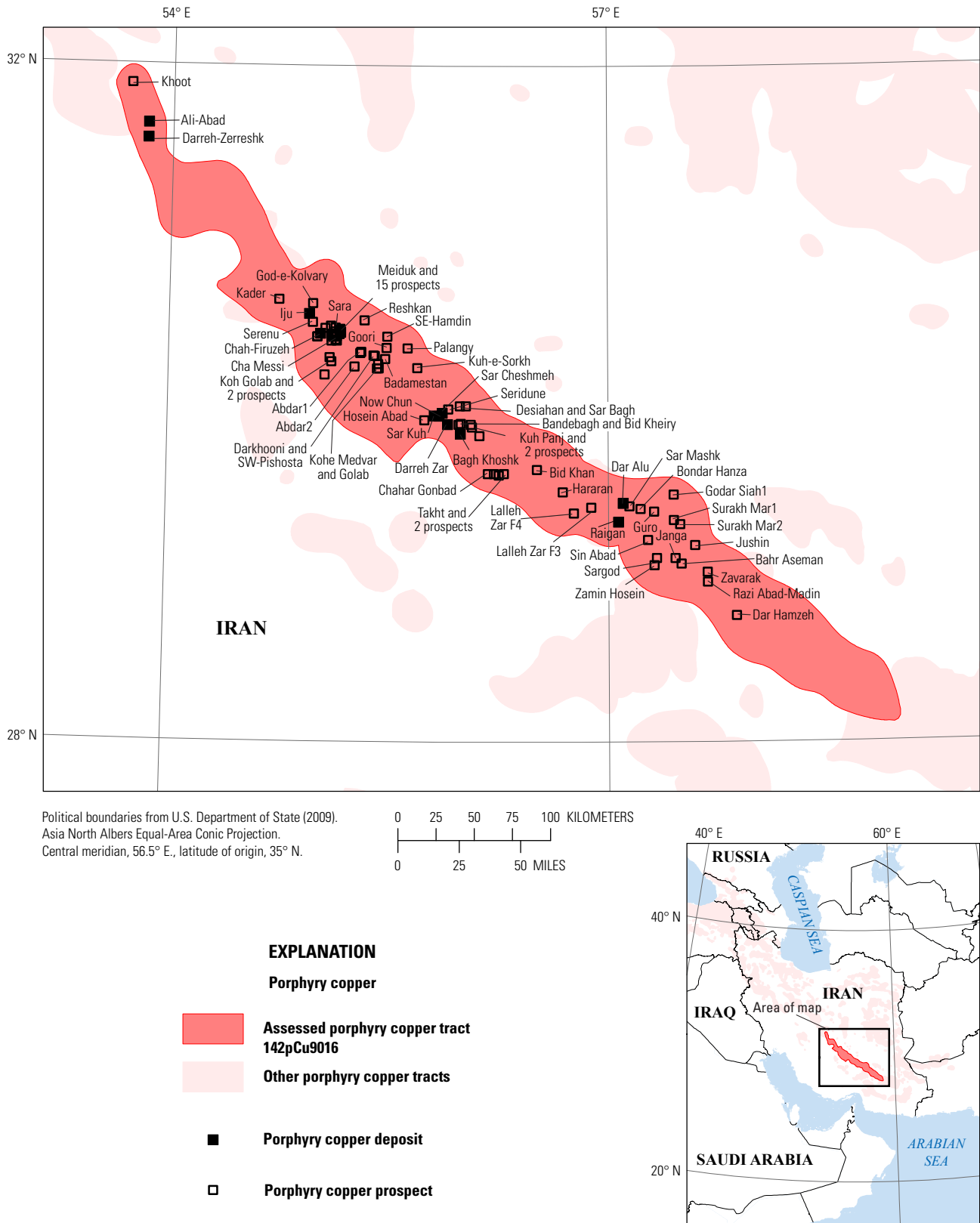
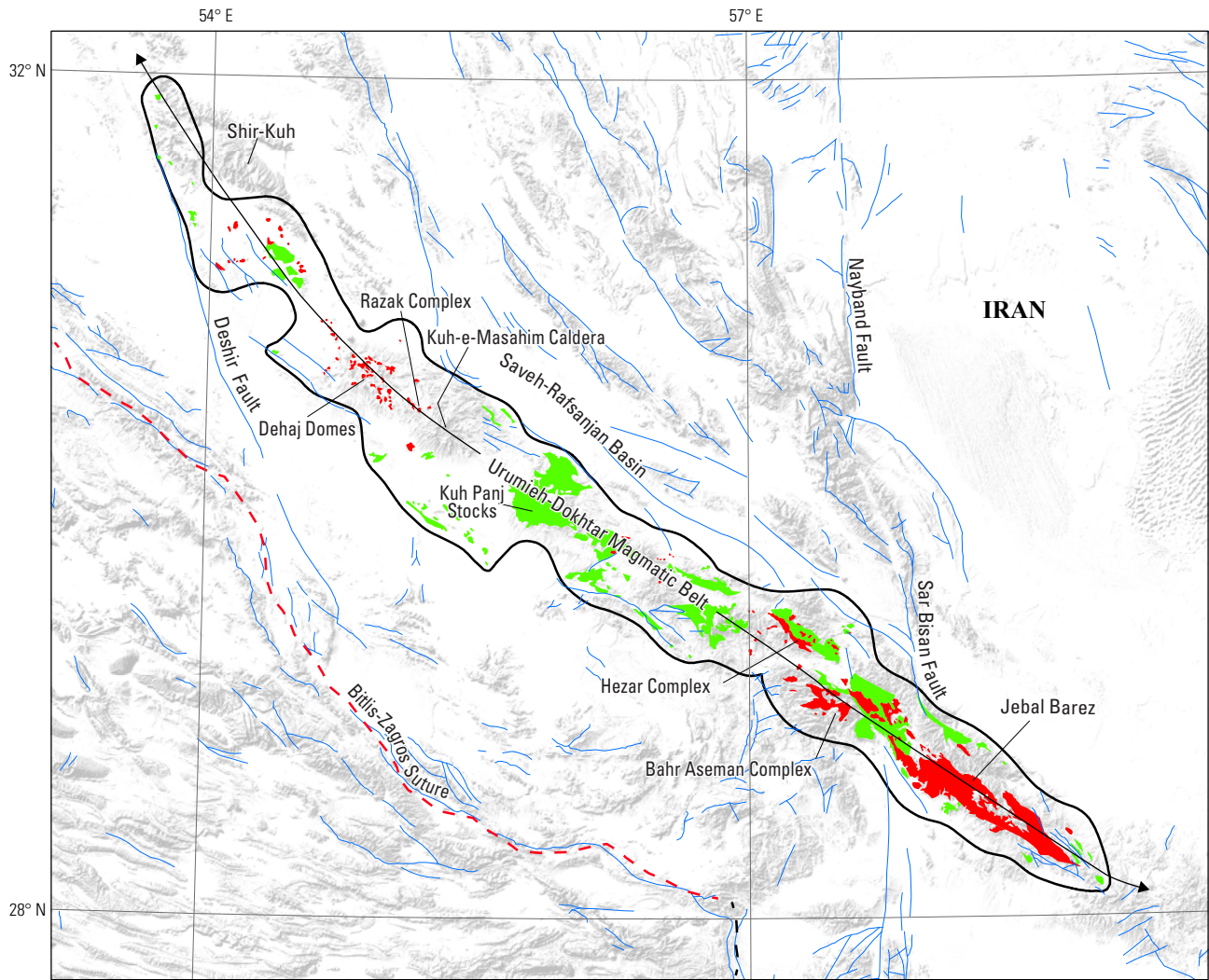
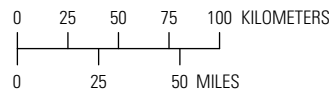


Figure 53. Map showing the location of known porphyry copper deposits and prospects for permissive tract 142pCu9016, Kerman—Iran. See table 2 for deposits, appendix C for prospects, and appendix D for accompanying spatial data.



Base from SRTM Global Digital Elevation Model, U.S. Geological Survey EROS Data Center, 2006. Political boundaries from U.S. Department of State (2009). Asia North Albers Equal-Area Conic Projection. Central meridian, 56.5° E.; latitude of origin, 35° N.



- EXPLANATION**
- Porphyry copper**
 - Assessed porphyry copper tract 142pCu9016**
 - Permissive intrusive rock**
 - Permissive extrusive rock**
 - Fault**
 - Suture**
 - Transform fault**
 - Jebal Barez Geologic feature discussed in the text**



Figure 54. Map showing the distribution of permissive intrusive and extrusive rocks used to define tract 142pCu9016, Kerman—Iran. See appendix A for principal sources of information and appendix B for source map units.

7. Pliocene-Holocene postcollisional alkaline magmatism controlled by dextral strike-slip faults (Ghadami and others, 2008; Shahrabaky, 1997).

Geochemical data for the weakly mineralized late Eocene-early Oligocene Jebal Barez and strongly mineralized middle to late Miocene Kuh Panj plutonic suites indicate emplacement in thicker crust and greater assimilation of crustal materials by the later suite (Shafiei and others, 2009; Shafiei, 2010).

Age and geochemical contrasts between the early Eocene to middle Miocene and early Eocene to late Miocene back-arc to continental-arc setting in the central and southeastern parts of the Urumieh-Dokhtar Magmatic Belt are recognizable. The secular evolution of oblique collision is consistent with the more protracted magmatism observed in the southeastern Kerman than in the central Yazd (see Yazd tract above) segments. Geochemical data further show that magmatism in the Yazd segment occurred in crust that was being attenuated during that time. In the Kerman segment, geochemical data support an opposite thin-to-thick crustal evolution. As a result, the otherwise continuous volcano-plutonic setting of the central and southeastern Urumieh-Dokhtar Magmatic Belt exhibits contrasting characteristics that are separated here into the Yazd (see above) and Kerman tracts, respectively.

Known Porphyry Deposits and Prospects

The Kerman tract contains numerous epithermal, skarn, and porphyry copper occurrences (Walther, 1960; Bazin and Hübner, 1969a, b; Geological Survey of Iran, 2012e). Twelve known porphyry deposits and 70 prospects were identified and are included in the Kerman tract (see table 2 and appendix C). Porphyry deposits in the Kerman tract (fig. 53) are represented by Cu-Mo±(Ag-Au) porphyry (that is, Sar Cheshmeh, Now Chun, Darreh Zar, Dar Alu, Meiduk, Chah-Firuzeh) and Cu-Mo(±Ag-Au) porphyry-skarns (that is, Darreh-Zerreshk). With exception of the early Oligocene Bagh Koshk, Bandedbagh, Desiahan, and Raigan (associated with the Jebal Barez-Hezar intrusive suites) and latest Miocene Iju and Abdar porphyry systems (related to the Dehaj intrusive suite), all known porphyry occurrences are related to the well-endowed middle to late Miocene Kuh Panj intrusive suite. The latest Miocene Abdar Cu-Au-Mo prospect is one of the only Au-rich porphyry systems recognized to date in the Kerman tract (Shafiei and others, 2009), but much of the reported gold may be contained in the acid-sulfate lithocap. Descriptions of porphyry deposits and selected prospects in the Kerman tract are presented below. Middle to late Miocene porphyry systems related to the Kuh Panj suite are described first, followed by older early Oligocene and younger Miocene-Pliocene systems.

Sar Cheshmeh Porphyry Deposit

The middle Miocene (13.6 Ma; McInnes and others, 2005) Sar Cheshmeh Cu-Mo-(Ag-Au) porphyry deposit located in the central part of the Kerman tract is the largest in the Urumieh-Dokhtar Magmatic Belt (Hassanzadeh, 1993).

Shafiei (2010) reports a mineral resource of 1,200 Mt at 0.7 percent copper, 0.03 percent molybdenum, 0.06 g/t gold, and 1.14g/t silver based on 1998 data. Singer and others (2008) report the same tonnage but higher grades of 1.2 percent copper, 0.03 percent molybdenum, 0.27 g/t gold, and 3.9 g/t silver at a cutoff of 0.25 percent copper. More recent proven and probable reserve estimates are 1,538 Mt at 0.58 percent copper at a 0.15 percent cutoff (National Iranian Copper Industries Company, 2012).

At Sar Cheshmeh, folded and thrust-faulted early Eocene volcanic and volcano-sedimentary rocks (Boomeri and others, 2010b) are cut by east-northeast–west-southwest faults (Atapour and Aftabi, 2007). This sequence is intruded by calc-alkaline Oligocene-Miocene quartz diorite to quartz monzonite and a middle Miocene granodiorite porphyry stock (Waterman and Hamilton, 1975). The complex is in turn cut by a series of late Miocene intramineral and postmineral porphyry dikes with a predominant north-northwest strike. Three main porphyry phases are recognized—(1) synmineral hornblende porphyry dikes, (2) synmineral feldspar porphyry dikes, and (3) postmineral biotite porphyry dikes. Igneous breccias were emplaced with the early porphyry dike phases. The late Miocene rocks are locally covered by Pliocene-Holocene trachytic to dacitic ignimbrites and volcanic breccias.

The Sar Cheshmeh deposit has a K-silicate alteration zone associated with the granodiorite and porphyry dike swarm. It is characterized by a central K-feldspar-quartz-pyrite-chalcocopyrite-molybdenite association that surrounds a strongly biotitized but poorly mineralized core. Biotite-pyrite-chalcocopyrite bearing zones extend beyond the intrusive complex into the andesitic wall rocks (Ghorashi-Zadeh, 1978; Aftabi and Atapour, 2011). Higher copper grades are associated with the K-silicate alteration zone, which is overprinted and surrounded by quartz-sericite-pyrite-chalcocopyrite. The quartz-sericite zone extends down to 400 m and outward into the host rocks, where it is the strongest and corresponds roughly with the 0.4 percent copper grade boundary. Propylitization surrounds the entire complex and grades outward into unaltered andesite (Shahabpour and Kramers, 1987).

Significant supergene enrichment occurs under the hematite-rich leached cap and is developed best in areas of higher grade primary mineralization. The chalcocite blanket averages 37 m in thickness and contains copper grades that are about twice as those of hypogene mineralization. Covellite occurs towards the bottom of the supergene blanket (Waterman and Hamilton, 1975; Shahabpour, 1991).

The Sar Cheshmeh porphyry system is estimated to have been emplaced at a paleodepth of 3.8–5.5 km (McInnes and others, 2005).

Now Chun and Sar Kuh Porphyry Deposits

The Now Chun and Sar Kuh porphyry deposits are located 3 and 6 km to the southeast of the Sar Cheshmeh operation, respectively.

The Now Chun Cu-Mo porphyry deposit has proven and probable reserve estimates of 527 Mt with 0.26 percent copper at a

0.15 percent cutoff (National Iranian Copper Industries Company, 2012). At the Nochon deposit, Oligocene-Miocene granodiorite, quartz diorite, diorite, and younger monzonite porphyry dikes intrude Eocene trachybasalts, andesites, dacites, rhyodacites, and pyroclastic rocks (Ranjbar and Honarmand, 2004; Abedi and Norouzi, 2012). The most intense alteration occurs in subvolcanic rhyodacite units, where it is controlled by northeast-southwest faults. It consists of K-silicate, sericite, and argillic alteration. Mineralization includes primary chalcopyrite, molybdenite, and lesser galena, sphalerite, and tetrahedrite, as well as secondary chalcocite, bornite, and covellite (Saein and others, 2012).

The small Sar Kuh Cu-Mo-Au deposit has reported resources of 16 Mt at 0.46 percent copper (Shafiei, 2010). Samples from this deposit average 0.003 percent molybdenum and 0.083 g/t gold (Shafiei and Shahabpour, 2008). Here, Eocene volcano-sedimentary rocks are intruded by an east-west trending Oligocene granodiorite pluton, which in turn is cut by quartz diorite porphyry dikes recently dated at 15.2 Ma (Mirnejad and others, 2013). K-feldspar-biotite and chlorite-epidote-actinolite alteration are overprinted by lesser sericite, and more widespread kaolinite, montmorillonite, illite, and pyrophyllite. Mineralization is mainly associated with K-silicate alteration (Mirnejad and others, 2013).

Seridune Porphyry Prospect

The Seridune Cu-Mo-(Au)-bearing porphyry copper prospect is located about 5 km northeast of the Sar Cheshmeh deposit. Samples from this prospect average 0.26 percent copper, 0.011 percent molybdenum, and 0.024 g/t gold (Shafiei and Shahabpour, 2008). Here, an Eocene andesite succession was intruded by a calc-alkaline middle to late Miocene granodiorite porphyry stock and granodiorite porphyry dikes. These copper-bearing intrusions were in turn cut by barren quartz monzonite dikes and partly overlain by Miocene-Pliocene dacite lavas (Barzegar, 2008). Hydrothermal alteration consists of early K-silicate and chlorite-epidote, transitional quartz-sericite, and late quartz-alunite-pyrophyllite. Chalcopyrite occurs mainly in quartz veins introduced during the early and transitional hydrothermal stages. The leached cap is well developed and is composed of hematite, jarosite, and goethite (Barzegar, 2007). Emplacement pressures of about 1 kb at the Seridune porphyry prospect indicate that the porphyry intrusion was emplaced about 4 km below the paleosurface (Barzegar, 2008).

Darrehzar Porphyry Deposit

The middle Miocene (14.9 Ma; Singer and others, 2008) Darrehzar (also known as Kangan) Cu-Mo-(Au) porphyry deposit is located 8 km southeast of Sar Cheshmeh. Previous resource estimates of 49 Mt at 0.64 percent copper and 0.004 percent molybdenum (Shafiei and others, 2009), or 49 Mt at 0.64 percent copper, 0.018 percent molybdenum, and 0.036 g/t gold (Shahabpour, 2008) have been superseded by a more recent proven and probable reserve base of 283 Mt at 0.38 percent copper with a 0.15 percent copper cutoff (National Iranian Copper Industries Company, 2012).

At the Darrehzar deposit, a diorite-quartz diorite-granodiorite porphyry stock, dikes, and associated igneous breccias intrude a folded and faulted Eocene succession comprised of volcanoclastic, andesite, trachyandesite, and sedimentary rocks (Ranjbar and Honarmand, 2004). The alteration zone occupies an area of about 1 by 2 km, and consists of pervasive phyllic and propylitic alteration, which largely overprint potassic alteration (Ranjbar and others, 2005). Argillic zones occupy small areas within the overall alteration zone. Chalcopyrite is the most abundant hypogene mineral. Copper grades average 0.3 percent but can be as much as 0.5 percent at deeper levels, where molybdenite is also more abundant. Oxidation has produced an extensive limonitic leached cap, with an underlying 34-m-thick supergene chalcocite blanket averaging about 0.8 percent copper (Mirnejad and others, 2010b; Derakhshani and Abdolzadeh, 2009).

Kuh Panj Porphyry Prospect

The middle to late Miocene Kuh Panj Cu-Mo-bearing porphyry prospect (National Iranian Copper Industries Company, 2012) is located 20 km southeast of the Sar Cheshmeh porphyry deposit. At the Kuh Panj prospect, a diorite-quartz diorite porphyry stock intrudes an andesite-dacite sequence (Shafiei and others, 2009; Roshani and others, 2013). This sequence is covered by andesitic agglomerate and tuff units that are in turn cut by andesite dikes. Breccias and quartz stockworks occur within a 400- by 600-m K-silicate-sericite-advanced argillic alteration zone. Mineralization consists of chalcopyrite and subsidiary galena (Roshani and others, 2013).

Dar Alu Porphyry Deposit

The Dar Alu Cu-Mo-(Au) porphyry deposit is located about 130 km southeast of Sar Cheshmeh. The deposit has reported proven and probable reserves of 186.1 Mt at 0.36 percent copper at a 0.15 percent cutoff (National Iranian Copper Industries Company, 2012). Shafiei and Shahabpour (2008) report average contents of 0.007 percent molybdenum and 0.031 g/t gold in samples from this deposit. The Dar Alu deposit is related to a northwest-southeast-trending 0.7-km² synmineral quartz diorite-granodiorite porphyry stock cut by postmineral diorite dikes. These stocks and dikes intrude Eocene volcano-sedimentary rocks. The emplacement of the intrusive complex is controlled by northwest-southeast strike-slip faults (Salehian and Ghaderi, 2010a). A central biotite-magnetite-anhydrite-K-feldspar-quartz alteration zone is overprinted and surrounded by a quartz-sericite zone. The outermost halo of alteration is characterized by a propylitic association of epidote, chlorite, and albite. Hypogene mineralization is associated with the K-silicate and quartz-sericite alteration and is respectively represented by quartz-magnetite±pyrite-chalcopyrite±bornite±molybdenite and quartz-pyrite±chalcopyrite(±molybdenite) veins. Supergene enrichment is limited and occurs in the northern part of the deposit, where the leached cap is better developed (Salehian and Ghaderi, 2010a, b).

Meiduk Porphyry Deposit

The middle-late Miocene (12.5 Ma; McInnes and others, 2005) Meiduk Cu-Mo-(Au-Ag) porphyry deposit is located about 90 km northwest of Sar Cheshmeh in the central-northern part of the Kerman tract (Singer and others, 2008; Hassanzadeh, 1993; Shafiei and others, 2009). The deposit is the largest of the numerous porphyry occurrences identified in this area (Derakhshani and Mehrabi, 2009; Tangestani and Moore, 2001, 2002a, b). The supergene and hypogene mineralization at the Meiduk deposit has reported proven and probable reserves of 176 Mt with 0.61 percent copper at a 0.15 percent cutoff (National Iranian Copper Industries Company, 2012). Taghipour and others (2008) report grades of 0.007 percent molybdenum, 82 ppb gold, and 1.8 ppm silver. Samples collected from this deposit also average 0.053 g/t gold (Shafiei and Shahabpour, 2008). Hypogene mineralization is known to continue at depths extending 1 km below the surface (Boomeri and others, 2009).

The Meiduk district is underlain by an early Eocene complex formed by rhyolite lavas, breccias, felsic tuffs, and pyroclastic rocks. These volcano-sedimentary rocks are in turn overlain by an Eocene to Oligocene complex of trachybasalt, andesite and trachyandesite, andesite-basalt, and felsic tuffs. These two volcanic complexes (37.5 ± 1.4 – 32.7 ± 6.3 Ma, based on $^{40}\text{Ar}/^{39}\text{Ar}$ dating of albite and analcime; Hassanzadeh, 1993) are intruded by the ~500-m-wide middle-late Miocene Meiduk granodiorite-diorite-quartz diorite porphyry stock. The porphyry stock is in turn cut by synmineralization and postmineralization north-south-trending latitic porphyry dikes and Miocene-Pliocene dacitic domes (Aliani and others, 2009). The Meiduk porphyry system is estimated to have been emplaced at a paleodepth of 2–3 km (McInnes and others, 2005).

The Meiduk deposit is about 700 by 1,000 m in plan-view. The deposit is hosted by porphyry intrusions and volcanic wallrocks (Taghipour and others, 2008). It consists of a central intense biotite and K-feldspar alteration core with associated hypogene chalcopyrite±molybdenite, which is surrounded by a quartz-sericite-chalcopyrite and minor bornite and enargite zone. Supergene chalcocite and covellite mineralization is moderately developed. The overlying lithocap contains iron hydroxides, copper oxides, copper carbonates, copper phosphates, copper sulfates, and copper silicates (Taghipour and others, 2008).

The small Lachah porphyry deposit (20 Mt at 0.1–1.5 percent copper; Geological Survey of Iran, 2012a) is located about 3 km northwest of Meiduk. Quartz-pyrite chalcopyrite veinlets in argillic alteration developed in a porphyritic diorite stock that is about 1.5 km in diameter (Bazin and Hübner, 1969a; Förster, 1978). Given its proximity to the Meiduk deposit, its resource base is considered here to be part of Meiduk.

Sara Porphyry Prospect

The middle-late Miocene (13.3 Ma; Hassanzadeh, 1993) Sara Cu-Mo-(Au)-bearing porphyry copper prospect (also known as Parkam; Mirnejad and others, 2010b; National Iranian Copper Industries Company, 2012; Honarmand and others, 2011) is located a few kilometers northwest of Meiduk. Shafiei and Shahabpour

(2008) report average contents of 0.37 percent copper, 0.005 percent molybdenum, and 0.034 g/t gold in samples collected from this prospect. At the Sara prospect, a quartz diorite porphyry stock is overprinted by quartz-sericite-pyrite alteration and chalcopyrite mineralization. No substantial supergene enrichment developed below (Tangestani and Moore, 2001, 2002a, b).

Cha Messi Porphyry-Related Deposit

The Chah Messi porphyry-related Cu-Zn-Pb-Ag-Au polymetallic vein deposit (Honarmand and others, 2011; Derakhshani and Mehrabi, 2009) is located about 4 km southwest of Meiduk. Reserves in this vein deposit are estimated at 0.89 Mt with 1.65 percent copper at a 0.15 percent cutoff (National Iranian Copper Industries Company, 2012). Grades of 1.27 percent copper, 1.01 percent lead, and 2.12 percent zinc, as well as variable amounts of silver (10–150 ppm) and gold (as much as 7 ppm) are also reported by Tangestani and Moore (2002b). Veins are emplaced in Eocene volcano-sedimentary rocks and subvolcanic intrusive bodies of intermediate composition. The richest mineralization occurs along a fault contact between Eocene volcanics and diorite porphyry intrusions.

Chah-Firuzeh Porphyry Deposit

The Chah-Firuzeh Cu-Mo porphyry deposit is located about 15 km west of Meiduk. It contains a reported proven and probable reserves of 149.1 Mt with 0.41 percent copper at 0.15 percent cutoff (National Iranian Copper Industries Company, 2012). The deposit is associated with a mid to late Miocene 1,500- by 400-m diorite-granodiorite to quartz monzonite stock and quartz monzonite to latite porphyry dikes that intrude Eocene calc-alkaline to alkaline volcanic flows, tuffs, and coeval sedimentary rocks. Eocene rocks unconformably overlie folded and eroded Late Cretaceous volcanic and sedimentary rocks (Hezarkhani, 2009). The intrusive complex is cut by diorite dikes that postdate mineralization. Alteration consists of a concentric early K-silicate to propylitic zone, which is surrounded by a late quartz-sericite-carbonate-pyrite zone. Early chalcopyrite and minor bornite appear to have been introduced during the transition from the potassic to phyllic alteration event. Late chalcopyrite and rare molybdenite occur within the quartz-sericite zone (Alirezai and Mohammadzadeh, 2009). Supergene enrichment is also present (Mirnejad and others, 2010b), and it is characterized by chalcocite and lesser digenite, chrysocolla, azurite and malachite (Afzal and others, 2011).

God-e-Kolvari (Gowde Kolvary) Porphyry Prospect

The God-e-Kolvari porphyry copper prospect is located about 25 km northwest of the Meiduk deposit. The prospect lies in a peneplain with well-developed copper-bearing ferricretes (Shahabpour, 1992). The prospect is related to a porphyritic diorite-granodiorite stock that intruded Eocene andesites (Honarmand and others, 2011). Alteration is characterized by K-silicate and lesser quartz-sericite. Eight holes drilled before

the early 1990s intercepted low hypogene copper concentrations of less than 0.1 percent. Despite the presence of ferricretes, a secondary enrichment blanket has not been identified (Shahabpour, 1992).

Ali-Abad and Darreh-Zerreshk (Taft Project) Porphyry Deposits

The early to middle Miocene (16.3–16.7 Ma) Darreh-Zerreshk porphyry-skarn and (15.8–16.1 Ma) Ali-Abad porphyry deposits are located about 180 km northwest of the Meiduk deposit in the northern part of the Kerman tract (Zarasvandi and others, 2007; Hassanzadeh, 1993). They were both identified in 1972 as a result of geophysical surveys and drilling by the French company COFIMINS. Resources were estimated at 40 Mt at 0.73 percent copper, 0.0059 percent molybdenum, and 19 g/t silver for the Ali-Abad, and 23 Mt at 0.80–0.90 percent copper, 0.0040 percent molybdenum, and 1 g/t silver for the Darreh-Zerreshk deposits (Singer and others, 2008). Current proven and probable reserves at the combined Darreh-Zerreshk and Ali-Abad deposits (Taft Project) are estimated at 167 Mt and 0.43 percent copper at a 0.15 percent cutoff (National Iranian Copper Industries Company, 2012).

The oldest rocks exposed in the area are Paleozoic and Triassic sedimentary formations and the Jurassic granitic Shir-Kuh batholith, which contact-metamorphosed these rock units. These Paleozoic and Triassic formations are overlain by Lower Cretaceous conglomerate, sandstone, and shale, and unconformable Upper Cretaceous limestones at Darreh-Zerreshk but not at Ali-Abad. The Mesozoic rocks are partly covered by Eocene rhyolitic tuff, andesitic lava, and pyroclastic units. These are in turn intruded by Eocene-Oligocene granodiorite-granite and more mafic early to middle Miocene quartz monzodiorite, quartz diorite, and diorite porphyry stocks (Zarasvandi and others, 2007). Miocene-Pliocene dacitic subvolcanic domes intrude the southwestern section of the Darreh-Zerreshk area, and they host travertine deposits (Zarasvandi and others, 2005).

At the Darreh-Zerreshk Cu-Mo-(Ag) porphyry-skarn deposit, magnetite-pyrite-chalcopyrite±bornite (±molybdenite) mineralization is associated with K-silicate alteration, and pyrite-chalcopyrite(±molybdenite) mineralization dominates in the overprinting quartz-sericite alteration zone (Zarasvandi and others, 2005). Lesser kaolinite and pyrophyllite are also present in the quartz diorite, quartz monzodiorite, tonalite, and granitic porphyry intrusions. A limited supergene chalcocite blanket developed below an oxidized lithocap. A small fraction of the mineralization occurs in skarns and consists of iron-copper-bearing exoskarn formed within the calcareous wall rock and of endoskarn formed within the associated granitoids (Hosseini and others, 2010).

At the Ali-Abad Cu-Mo-(Ag) porphyry deposit, pyrite-chalcopyrite(±molybdenite) are associated with breccia zones and quartz-sericite alteration in quartz monzodiorite, granodiorite, and alkali granite porphyry intrusions (Zarasvandi and others, 2005). Potassic alteration has not been recognized. Argillic zones in the intrusive and adjacent volcanic hosts overprint phyllic alteration. As at Darreh-Zerreshk, a small supergene chalcocite blanket developed below an oxidized lithocap.

Takht and Chahar Gonbad Porphyry Prospects

The Takht porphyry-skarn and Chahar Gonbad porphyry-related skarn prospects have not been dated. The Takht Cu-Mo-(Au)-bearing porphyry-skarn prospect is located about 55 km southeast of Sar Cheshmeh (Dorsa PLC, 2012g). In the 1970s, 6 short holes were drilled at the Takht porphyry prospect. Estimated resources included 3 Mt at 0.6 percent copper in the oxide zone, and 10 Mt at 0.5 percent copper and low gold contents in the underlying sulfide zone. Drilling results suggest that mineralization is open at depth. Here, a monzonitic porphyry stock about 200 m in diameter caused stockwork and calc-silicate mineralization in porphyry, sandstone, conglomerate, and hornfelsed tuff rock units. The porphyry stock occurs along the margin of a granodioritic-granitic batholith, which exhibits widespread clay alteration. Weak to moderate quartz-sericite alteration and local K-silicate alteration at depth are cut by abundant quartz-magnetite-pyrite-chalcopyrite veins. In the skarn, chlorite, epidote, and tremolite have been recognized (Dorsa PLC, 2012g).

The nearby Chahar Gonbad Cu-Zn-Pb-Ag-bearing porphyry-related skarn prospect (80,000 t at 1.5 percent copper and 20 g/t silver; U.S. Geological Survey, 2012) has been mined underground since the early 1960s. Here, a quartz diorite porphyry stock intrudes andesitic tuffs (Mehrabi and Derkshani, 2010; Geological Survey of Iran, 2012a).

Dar Hamzeh Porphyry Prospect

The Dar Hamzeh (also known as Kerver(?); National Iranian Copper Industries Company, 2012) Cu-Mo-bearing porphyry prospect is located in the southern part of the Kerman tract about 215 km southeast of the Sar Cheshmeh deposit. The porphyry prospect is centered on quartz monzonite, diorite, granodiorite, and andesite-dacite porphyry intrusions (Afzal and Rajoli, 2010). Alteration includes K-silicate, quartz-sericite, argillic, and propylitic associations. Mineralization is controlled by quartz-magnetite-pyrite stockwork zones containing hypogene bornite and chalcopyrite. Secondary mineralization includes chalcocite, covellite, and malachite below a jarosite-goethite lithocap (Afzal and Rajoli, 2010).

Raigan (Rigan Bam) Porphyry Deposit

In contrast to most porphyry systems in the Kerman tract, which are middle to late Miocene in age, the Raigan deposit is older by 10 m.y. Other porphyry systems of probable early Oligocene age include the Bande Bagh and Dehsiahhan porphyry prospects and the Bagh Khoshk porphyry deposit in the vicinity of Sar Cheshmeh (whole rock Rb-Sr date of 33 ± 1 Ma; Dargahi and others, 2010). These small porphyry systems differ from younger Kuh Panj porphyry deposits and prospects in that they are centered about the older Jebal Barez more alkaline diorite, monzogranite, monzonite, syenite, and alkali granite intrusions.

The early Oligocene (29.7 Ma; Shafiei and others, 2009) Raigan porphyry copper deposit is located in the central part of the Kerman tract (Karimi and Valadan Zoej, 2004). Known resources are estimated at 10 Mt at 0.63 percent copper (Singer

and others, 2008). The deposit is hosted by a 3-km² northwest-southeast monzonite-quartz monzonite pluton that is cut by a diorite-granodiorite porphyry stock (Hezarkhani, 2006a, b, d). The complex intruded into folded and deeply eroded Upper Cretaceous sedimentary rocks unconformably overlain by Eocene volcanic and volcanoclastic rocks. Potassic, phyllic, and propylitic alteration are zoned concentrically about the porphyry stock. Well-developed quartz-sericite alteration irregularly overprints the earlier potassic and propylitic alteration. Potassic and phyllic alteration and mineralization are characterized by early K-feldspar-biotite-quartz veins with patchy magnetite, pyrite, chalcopyrite, and pyrrhotite, as well as by late sericite-quartz veins with pyrite, pyrrhotite, chalcopyrite, and hematite. Early sodic albite-amphibole and late calcic epidote-chlorite alteration are also present. Supergene enrichment is restricted to a very thin blanket with subeconomic copper grades. Fluid inclusion data indicate that the hydrothermal system was emplaced at a depth of 1.5–1.9 km (Hezarkhani, 2006a, b, d).

Bagh Khoshk Porphyry Deposit

The early Oligocene Bagh Khoshk Cu-Mo porphyry deposit is located about 15 km southeast of Sar Cheshmeh. It contains reported resources of 24 Mt at 0.27 percent copper (Shafiei and others, 2009). The Bagh Khoshk deposit is centered on a metaluminous to slightly peraluminous diorite-monzonite-syenite-alkalic granite plutonic complex, which exhibits juvenile radiogenic signatures. The complex intruded Eocene volcano-sedimentary rocks, generating albite-epidote and hornblende facies hornfels. Hypogene mineralization occurs within equigranular and younger porphyritic intrusions. Both intrusive suites and their host rocks are affected by K-silicate and tourmaline (\pm quartz-chalcopyrite-pyrite-molybdenite veins), sericite (\pm barren quartz-pyrite veins), and chlorite (\pm carbonate vein) alteration associations (Einali and others, 2011). The igneous rocks associated with this porphyry system are similar in composition to those associated with the nearby early Oligocene Dehsiahan and Bande Bagh porphyry prospects (Dargahi and others, 2010).

Iju Porphyry Deposit and Abdar Porphyry Prospect

The Kerman segment of the Urumieh-Dokhtar Magmatic Belt also hosts Miocene-Pliocene porphyry systems, which are associated with the Dehaj subvolcanic dacite-rhyolite-dominated suite (Shafiei and others, 2009). The latest Miocene (9.3 Ma; Mirnejad and others, 2013) Iju Cu-Mo porphyry deposit and (7.5 Ma; McInnes and others, 2005) Abdar Cu-Au-Mo prospect are located 20 km to the northwest and southeast, respectively, of the Meiduk deposit. Compared to most other porphyry systems in the Kerman tract, the Iju and Abdar prospects are younger by 3 and 5 m.y., respectively. These younger systems are tentatively included here in the Kerman tract but are more likely associated with younger superimposed postcollisional magmatism in the region (see Pliocene-Quaternary tract below).

The Iju Cu-Mo porphyry deposit contains reported proven and probable reserves of 73.9 Mt at 0.31 percent copper; National

Iranian Copper Industries Company, 2012). It is underlain by Eocene volcanic and pyroclastic rocks. The Eocene rock sequence is intruded by a northwest-trending, 18- by 4-km late Miocene diorite-quartz diorite-tonalite porphyry stock that is in turn cut by porphyritic diorite and quartz-diorite dikes. Alteration consists of biotite and K-feldspar overprinted by more extensive quartz-sericite-pyrite, and minor argillic zones (Mirnejad and others, 2013; Honarmand and others, 2011). Hypogene chalcopyrite mineralization occurs mostly within potassic alteration in the tonalite porphyry. Supergene chalcocite mineralization also developed in the Iju porphyry deposit (Mirnejad and others, 2010b).

The Abdar (Abdar1 in appendix C) Cu-Au-Mo-bearing prospect is located within the collapsed and partially eroded caldera of the Kuh-e-Masahim stratovolcano (Boomeri and others, 2011a). Samples from this prospect average 0.3 percent copper, 0.013 percent molybdenum, and 0.072 g/t gold (Shafiei and Shahabpour, 2008). Mineralization occurs within a K-silicate, phyllic, and argillic alteration zone that developed in a diorite-quartz diorite to granodiorite-dacite porphyry intrusion (Shafiei, 2010; Honarmand and others, 2011) that is estimated to have been emplaced at a paleodepth of 2–3.2 km (McInnes and others, 2005).

Preservation Level

As derived from the geologic map of Huber (1978), older basement rocks underlie 24 percent and late Eocene to late Miocene permissive volcanic and plutonic units amount to 9 and 7 percent, respectively, of the Kerman tract area (fig. 54). Broadly coeval nonpermissive rocks occur in 14 percent, and younger rocks cover the remaining 46 percent of the tract. The $\{\text{volcanic}/[\text{volcanic}+\text{plutonic}]\} \times 100$ ratio of 58 across the tract suggests that levels of preservation of porphyry copper systems are appropriate. However, the exposure of porphyry copper systems is also affected by younger cover.

In more detail, levels of preservation vary from place to place in the folded and thrust-faulted late Eocene back-arc to relatively undeformed late Miocene arc environments that are superimposed in the Kerman tract. These settings cannot be effectively differentiated at the geologic map scales used (Agard and others, 2011; Huber, 1978; Haghypour and Aghanabati, 1985). However, as estimated from the larger scale map of Shafiei and others (2009), the late Eocene Jebal Barez igneous suite may underlie about 10 percent of the central part of the tract where variable but overall high volcanic-to-plutonic permissive unit ratios indicate levels of preservation that are too shallow for porphyry systems. Coeval Eocene volcano-sedimentary and sedimentary rocks may amount to an additional 25 percent, whereas younger Oligocene-Miocene sedimentary rocks of the Lower Red, Qom, and Upper Red formations constitute a further 5 percent of the tract area.

The middle to late Miocene Kuh Panj igneous suite appears to occupy only about 5 percent of the tract area. However, in contrast to the late Eocene Jebal Barez igneous suite, the Kuh Panj suite is dominated by plutonic units that

suggest more appropriate levels of preservation for porphyry copper systems. This is consistent with the large number of identified prospects of this age range. The Kuh Panj suite is also present in the large batholithic mass in the southern part of the tract. However, only a few porphyry occurrences are reported in this area, suggesting that the batholith there may be largely eroded below the level of preservation of porphyry systems. Overall, the large number of exposed middle to late Miocene porphyry deposits and prospects in the Kerman tract suggest that concurrent and postmineral uplift, erosion, and burial events were favorable for exposure of porphyry systems of this age range.

Magnetic Anomalies

The regional aeromagnetic map (Maus and others, 2009) was used to confirm the location and character of regional geologic features (for example, arcs, basins, faults, terrane boundaries). A prominent positive magnetic anomaly occurs in the central part of the magmatic belt delimited by the Kerman tract. This part hosts the Sar Cheshmeh and Meiduk porphyry deposit districts. However, this magnetic anomaly may be reflecting in part the Pliocene-Holocene intermediate and mafic units that also overlie the area. Another conspicuous magnetic high occurs in the south-central part of the magmatic belt where it closely images the early Eocene Bahr Aseman volcanic complex. In the southern part of the magmatic belt, the well-exposed batholith across the Sar Bisan-Nayband Fault system, in contrast, is not imaged well by a magnetic anomaly. The reason is unknown, but it suggests that the volume of the batholithic mass may be reduced and (or) confined to the surface. Other magnetic anomalies are associated with the exposed ophiolite-bearing complexes in the southern and northern parts of the magmatic belt. The anomaly in the northern part extends from the ophiolite-bearing Nain-Baft Zone to the east between the Meiduk and Darreh-Zerreshk/Ali-Abad districts, where it occupies an area largely underlain by Paleogene volcano-sedimentary units and younger cover rocks. Permissive units could be shallowly buried in this area. In general, the Paleogene Saveh-Rafsanjan basin that delimits the Kerman tract to the east is well-imaged by a marked magnetic low.

The Dar Alu and Raigan porphyry deposits are associated with magnetic lows, and the Abdar prospect corresponds to a high-intensity magnetic high. Otherwise, all other porphyry deposits and prospects in the tract generally lie at the margins of magnetic highs.

ASTER Alteration Data

Processed ASTER data (Mars and Rowan, 2006; Mars, 2014; Pour and Hashim, 2011; Pour and others, 2011; Khaleghi and Ranjbar, 2011) available for 100 percent of the Kerman tract were used to evaluate potential hydrothermal alteration that could be associated with unidentified porphyry systems. Of the 62 ASTER-derived alteration zones identified in the Kerman tract, 24 are centered about known porphyry prospects. Phyllic ASTER alteration zones 5 km in diameter or larger are evident in the Kader Abdar and Lalleh Zar F3 porphyry prospects, the Sar Cheshmeh

district, and the Chahar Gonbad-Takht trend. Well-developed argillic alteration is present at Kader, Sar Cheshmeh, and Lalleh Zar F4. Smaller, as much as 3-km-wide, phyllic ASTER alteration zones occur in the Iju, Serenu, Sara, Meiduk, Dehsiahan, Kuh Panj, Bid Khan, Sin Abad, and Raigan porphyry systems. Even smaller and lesser developed ASTER-derived phyllic alteration zones are associated with Darreh-Zerreshk, Darreh Zar, God-e-Kolvary, Janga, Bahr Aseman, Guro, Hararan, Dar Alu, and Surak Mar1. No ASTER-derived alteration zones were recognized over the Ali-Abad, Khooteh, and Hosein Abad porphyry-skarn systems.

Of the ASTER-derived alteration zones that are not spatially associated with known porphyry occurrences, 8 are centered about known copper, 3 about lead-zinc, and 2 about gold (epithermal or skarn?) prospects. An additional five occur in younger cover units. Of the remaining 20 ASTER-derived alteration zones, 10 are located in the batholith that occupies the southern part of the Kerman tract where few porphyry prospects have been identified. Five of these are large (more than 5 km across) phyllic ASTER alteration zones, one of which is spatially associated with 1 of 2 known pyrite (barren porphyry?) occurrences located in this part of the tract. Argillic alteration is only associated with 1 of the 5 phyllic alteration locations.

Overall, of the 20 ASTER-derived alteration zones of unknown origin in the Kerman porphyry tract, several could potentially indicate the location of unreported or unidentified porphyry systems. Based on ASTER data, the batholith in the southern part of the tract appears favorable for the occurrence of porphyry systems despite the fact that the batholith is otherwise too deeply eroded. It contains only three known porphyry occurrences in its northern sector.

Probabilistic Assessment

Grade and Tonnage Model Selection

Of the 12 porphyry deposits in the Kerman tract, Sar Cheshmeh is the only deposit for which both gold and molybdenum grades are reported. Based on Au/Mo ratios and molybdenum concentrations, Sar Cheshmeh classifies as a Cu-Mo subtype. Available information on most the porphyry deposits and prospects in the Kerman Tract further suggest that the Cu-Mo metal association is dominant. Pooled *t*-test results assuming equal variances further show that the 12 known deposits in the tract are not significantly different at the 1-percent level from tonnages and grades in the general porphyry Cu-Au-Mo model of Singer and others (2008). Therefore, the general porphyry Cu-Au-Mo model was used to estimate undiscovered copper, gold, molybdenum, and silver resources in the Kerman tract. In comparison to the median tonnage and grade in the general porphyry Cu-Au-Mo model, the Darreh Zar, Now Chun, and Sar Cheshmeh deposits are larger, with Sar Cheshmeh also exhibiting higher copper and molybdenum grades. The Ali Abad, Darreh-Zerreshk, Meiduk, Raigan, and Sar Kuh deposits are smaller but contain higher copper grades, whereas the Bagh Khoshk, Chah-Firuzeh, Dar Alu, and Iju deposits are smaller and have lower copper grades than the median deposit in the model.

Estimates of Undiscovered Deposits and Rationale

Favorable geologic factors for the occurrence of undiscovered porphyry copper deposits in the Kerman tract include (1) relatively long-lived juvenile to mature Andean-type arc built on thick crust, (2) dominant calc-alkaline and lesser alkaline igneous compositions, (3) appropriate levels of exposure of porphyry systems associated with Miocene permissive rocks, (4) several larger than median (including the world-class Sar Cheshmeh) porphyry deposits with copper and molybdenum grades that are comparable or higher to those in other porphyry deposits worldwide, (5) favorable conditions for supergene enrichment, and (6) as many as 20 potentially porphyry-related ASTER-derived alteration zones that are not associated with known porphyry prospects. Unfavorable geologic factors for the occurrence of undiscovered porphyry copper deposits include (1) postmineral faulting and possible concealment or exhumation of porphyry systems, (2) only partially adequate levels of exposure of porphyry systems associated with older Eocene-Oligocene permissive rocks, and (3) small exposure (5 percent of the tract area) of the more prospective Miocene permissive rocks.

The well-endowed Kerman tract exhibits a high density of known porphyry deposits relative to other tracts of equivalent aerial extent around the world (Singer and Menzie, 2010). It is the only tract in the study region that is situated well above the expected median deposit density, suggesting that the likelihood of occurrence of undiscovered deposits is, therefore, low. Appropriate levels of exposure of porphyry systems and extensive exploration in the region are further supported by the high number of well-described porphyry prospects.

The assessment team established that the Kerman tract was exceptionally favorable and that estimates of numbers of undiscovered porphyry copper deposits could be carried out with low uncertainty. Therefore, quantitative assessment of undiscovered deposits in this tract was completed. The consensus estimates for undiscovered porphyry copper deposits in the Kerman tract at the 90-, 50-, and 10-percent probability levels and associated summary statistics are shown in table 15A. At the 90-percent probability, estimates ranged from 2 to 4 undiscovered deposits. At the 50-percent probability level, the numbers increased to between 3 and 10 undiscovered deposits, and at the 10-percent probability level, the numbers increased to between 6 and 30. On the basis of these numbers, the team reached a consensus estimate of 3, 5, and 10 undiscovered deposits for the 90-, 50-, and 10-percent probability levels, respectively, which resulted in a mean of 5.70 undiscovered deposits with a standard deviation of 2.74 ($C_v=48$). The estimate reflects the level of favorability and low uncertainty for undiscovered porphyry copper deposits deemed to be present in a tract that already exhibits a high known porphyry deposit density. However, the estimated total deposit density per 100,000 km² obtained remains within the 50th- and 10th-percentile interval of the deposit density model of Singer and Menzie (2010).

Probabilistic Assessment Simulation Results

Simulation results for estimates for copper, molybdenum, gold, silver, and the total volume of mineralized rock are summarized in table 15B. The mean estimate of undiscovered resources in the Kerman porphyry tract is 22 Mt of copper, 1.5 times that of the resources presently known in this well-explored tract. However, these resources may be inaccessible or uneconomic at present. Furthermore, a substantial fraction of the inventory can be expected to be distributed among numerous already identified prospects or known deposits with resource bases that are undefined or only partially defined at present. Results of the Monte Carlo simulation are also presented as cumulative frequency plots (fig. 55). The cumulative frequency plots show the cumulative probabilities of occurrence-estimated resources and total mineralized rock, as well as the mean for each commodity and for total mineralized rock.

Late Miocene to Holocene Tracts

The late Miocene to Holocene permissive tracts are shown in figure 8. The tract consists of three sub-tracts, all of which were assessed qualitatively.

Pliocene-Quaternary Tract (142pCu9017)

Tectonic Setting

The latest Miocene to Holocene neotectonic settings in the assessment region were described above (see Neotectonic Setting of the Tethys region of western and southern Asia). Latest Miocene to Holocene magmatism has occurred along subduction-related, as well as postcollisional extensional regimes (fig. 56). The subduction-related Konya Arc spans south-central to southwestern Turkey, and the Bazman-Taftan-Koh-i-Sultan Arc occupies southeastern Iran, western Pakistan, and southern Afghanistan. These subduction-related settings occur on the western and eastern extremities of the Tethys region of western and southern Asia, respectively, where the last remnants of the Southern Neotethys Ocean Branch are still closing along subduction zones. The large intervening region between these two subduction-related settings is occupied by irregularly distributed outcrops of igneous rocks emplaced in a postcollisional setting. Magmatism in this setting occurs in pull-apart basins along transpressional and transtensional strike-slip faults and in grabens that are parallel and orthogonal to the north-northeast-directed principal compressional stress component. These postcollisional igneous rocks reach their maximum extent and volume in eastern Turkey and the Lesser Caucasus. In general, about half of the aerial extent of these postcollisional igneous units consists of mafic compositions. These nonpermissive mafic igneous rocks were not used to define tracts. Therefore, they extend well beyond tract boundaries in several areas.

Table 15. Probabilistic assessment for tract 142pCu9016, Kerman—Iran.

A. Undiscovered deposit estimates, deposit numbers, tract area, and deposit density.

[N_{xx} , estimated number of deposits associated with the xxth percentile; N_{und} , expected number of undiscovered deposits; s , standard deviation; $C_v\%$, coefficient of variance; N_{known} , number of known deposits in the tract that are included in the grade and tonnage model; N_{total} , total of expected number of deposits plus known deposits; tract area, area of permissive tract in square kilometers (km^2); deposit density reported as the total number of deposits per 100,000 km^2 . N_{und} , s , and $C_v\%$ are calculated using a regression equation (Singer and Menzie, 2005)]

Consensus undiscovered deposit estimates					Summary statistics					Tract area (km^2)	Deposit density ($N_{total}/100,000 km^2$)
N_{90}	N_{50}	N_{10}	N_{05}	N_{01}	N_{und}	s	$C_v\%$	N_{known}	N_{total}		
3	5	10	10	10	5.7	2.7	48	12	18	32,800	54

B. Results of Monte Carlo simulations of undiscovered resources.

[Cu, copper; Mo, molybdenum; Au, gold; and Ag, silver; in metric tons; Rock, in million metric tons]

Material	Probability of at least the indicated amount						Probability of	
	0.95	0.9	0.5	0.1	0.05	Mean	Mean or greater	None
Cu	950,000	2,400,000	13,000,000	49,000,000	78,000,000	22,000,000	0.3	0.03
Mo	0	8,100	230,000	1,400,000	2,300,000	570,000	0.27	0.07
Au	0	22	300	1,300	1,900	540	0.31	0.05
Ag	0	0	2,700	17,000	28,000	7,100	0.25	0.12
Rock	230	550	2,800	10,000	16,000	4,400	0.32	0.03

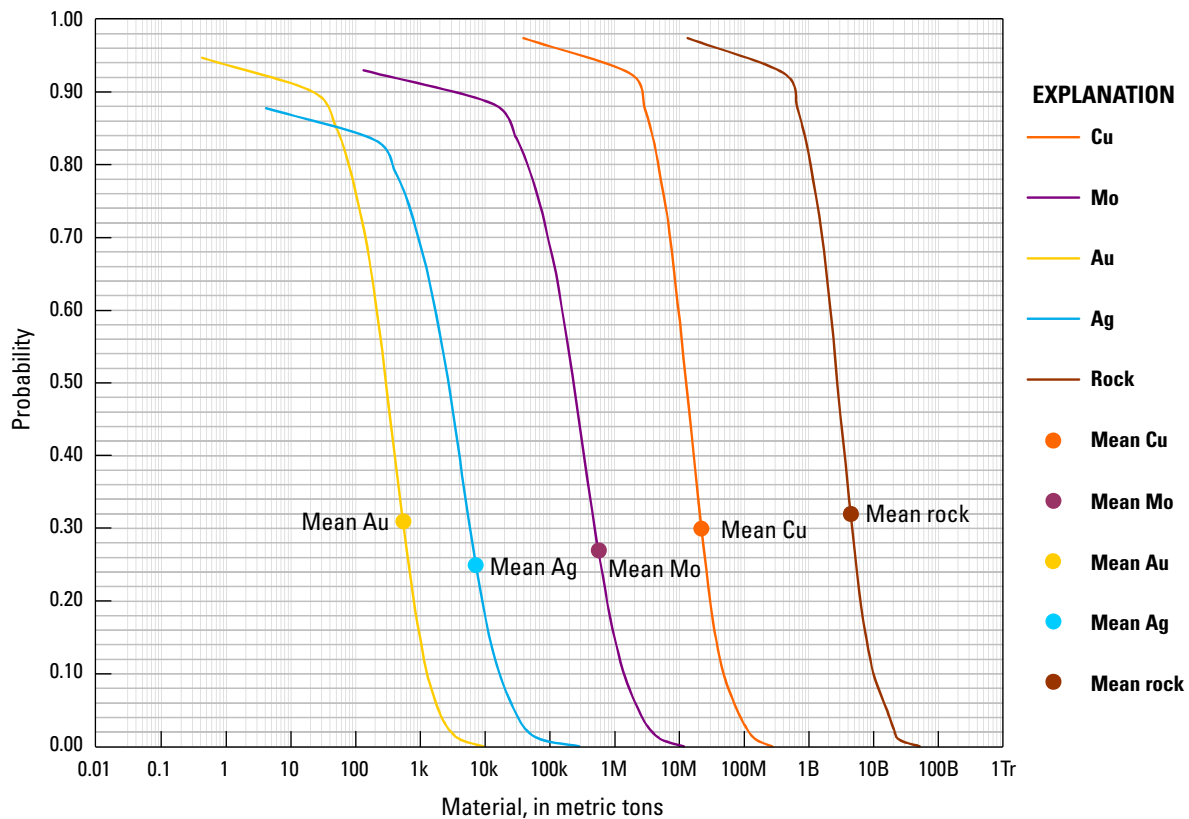
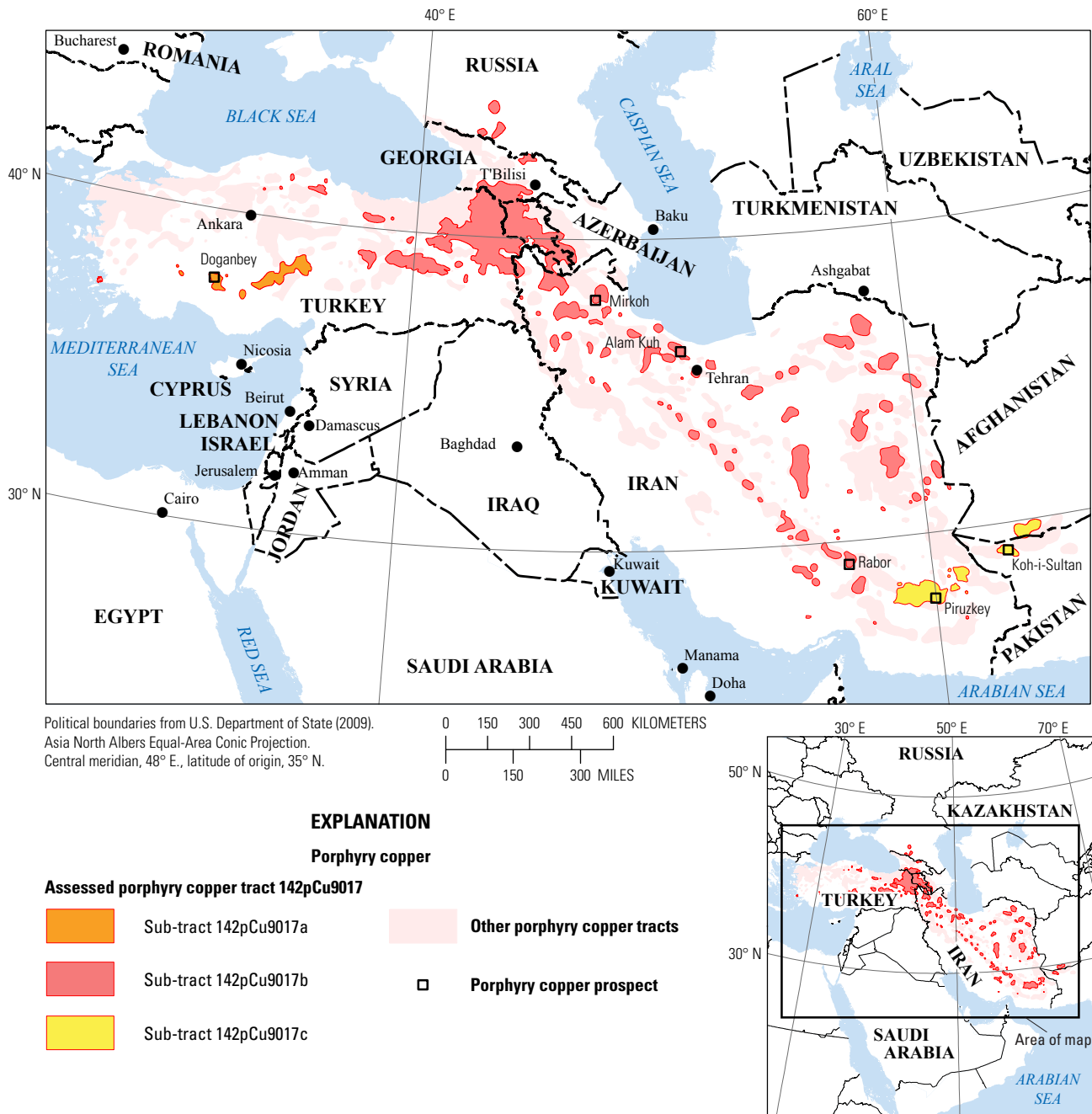


Figure 55. Cumulative frequency plot showing the results of Monte Carlo simulation of undiscovered resources in porphyry copper deposits in tract 142pCu9016, Kerman—Iran. k, thousand; M, million; B, billion; Tr, trillion.



Given the contrasting tectonic settings, the Pliocene-Quaternary tract is subdivided here into three sub-tracts—the Pliocene-Quaternary–Bazman and the Pliocene-Quaternary–Konya subduction-related sub-tracts and the Pliocene-Quaternary–Post-collisional sub-tract.

Pliocene-Quaternary–Konya Sub-tract (142pCu9017a)

Descriptive model: General porphyry copper (Cox, 1986a; Berger and others, 2008; John and others, 2010)

Geologic feature assessed: Late Miocene to Holocene continental arc and back arc of the Tethyan Eurasian Metallogenic Belt

Location

The Pliocene-Quaternary–Konya sub-tract covers an area of 11,800 km² across southwestern and south-central Turkey (fig. 56). It delimits a 300-km-long and as much as 75-km-wide late Miocene to Holocene continental-arc and back-arc volcano-plutonic belt related to the active Hellenic-Cyprian subduction zone. The Pliocene-Quaternary–Konya tract is partially superimposed on parts of the older Anatolide-Tauride–Central Turkey and Azerbaijan–Eastern Turkey sub-tracts (see above).

Tectonic Setting and Magmatism

Late Miocene to Holocene subduction-related arc and back-arc magmatism in southwestern and south-central Turkey, known as the Konya Arc, is related to the Hellenic-Cyprian subduction system located to the south in the Mediterranean Sea (fig. 57). Permissive igneous units of intermediate to felsic composition used to define this sub-tract (appendix B) are shown in figure 57, along with locations of igneous complexes and other geologic features mentioned in the text. The Hellenic subduction zone is characterized by a shallow-dipping slab, an uncommonly voluminous accretionary fore-arc prism, and a trench that is filled with thick sedimentary successions (Hatzfeld and others, 1989).

In the arc environment of south-central Turkey, the structural framework is expressed by east-west normal faults that have been active at least since 26 Ma (Meulenkamp and others, 1988). These faults are in turn cut by a set of conjugate northwest and northeast normal faults with significant oblique-slip components. These faults are the product of north-south-directed compression and have resulted in the westward tectonic escape of the Anatolian Block. The tectonic escape of the Anatolian Block has been active since 6 Ma but may have commenced as early as 12 Ma (Boztuğ and others, 2004). Late Miocene to Holocene arc magmatism forms a belt of well-preserved volcanic edifices. These are emplaced in pull-apart basins along these conjugate dextral and sinistral oblique-slip faults (Toprak, 1998). The volcanism can be divided into three periods that are separated by deformational and erosional events. The first period (11–8.5 Ma) is represented by andesitic flows and the

second period (8.5–2.7 Ma) is characterized by thick ignimbritic sequences, whereas the third period (3.6 Ma to recent) is embodied by large andesitic-basaltic stratovolcanoes and a number of felsic monogenic cones (Pasquarè and others, 1988). These volcanic suites exhibit high-K calc-alkaline compositions and relatively evolved isotopic signatures that are consistent with a continental-arc setting (Keller and others, 1977).

Behind the arc in the back-arc region of western Turkey, Oligocene-early Miocene calc-alkaline magmatism was followed by late Miocene-Pliocene alkaline volcanism (Yılmaz, 1990; Delaloye and Bingöl, 2000; Yılmaz, Genç, and others, 2001). The 14–10 Ma transition from a back arc to a combined back-arc and tectonic-escape extensional regime is represented by major east-west oblique-slip normal faults. Eruption of large volumes of anatectic alkaline rhyolites along these structures started at 12.5 Ma (Lordkipanidze and others, 1989). North-south extension was interrupted at the end of the late Miocene by an uplift event but resumed in the early Pliocene with steep normal faults that crosscut earlier structures and produced east-west and northeast-trending grabens. Widespread late Miocene-Pliocene (9–6 Ma) rift-related isotopically primitive alkaline basaltic lavas were emplaced along these graben-bounding structures (Akay, 2009; Bozkurt and others, 2000). During the more advanced stage of rifting in the Pliocene to Holocene, alkalic magmatism propagated from north to south across western Turkey. It evolved from older trachyandesitic and trachytic extrusives derived from a lamprophyric parental magma, to tephriphonolitic dikes, and to trachytic lava domes derived from a basanitic parent. The geochemical signatures indicate that crustal contamination was more significant in Pliocene than in younger volcanic rocks. These data are also consistent with preservation of a subduction-related component during the transition from the calc-alkaline to the alkaline regime (Temel and others, 1998a, b; Şen and others, 2004). The gradual reduction in silica and changes in trace element contents with decreasing eruption age further show that an enriched oceanic island basalt (OIB)-like mantle component increased over time (Aldanmaz and others, 2000; Elitok and others, 2010).

Based on the geologic map of the General Directorate of Mineral Research and Exploration (2000), nonpermissive late Miocene-Holocene mafic units are more widespread than permissive intermediate to felsic units in the back-arc region of southwestern Turkey. In contrast, permissive intermediate to felsic units in the arc region of south-central Turkey delimit a fairly well-defined magmatic belt.

Known Porphyry Prospects

The Konya Arc of southwestern and south-central Turkey hosts numerous epithermal prospects, some of which are associated with porphyry systems (Stratex International PLC, 2012a). However, most porphyry systems are not well exposed in this volcanic-dominated belt delimited by the Pliocene-Quaternary–Konya sub-tract. To date, the only positively identified porphyry prospect is Doğanbey, which is located in the western part of the sub-tract (fig. 56; appendix C).

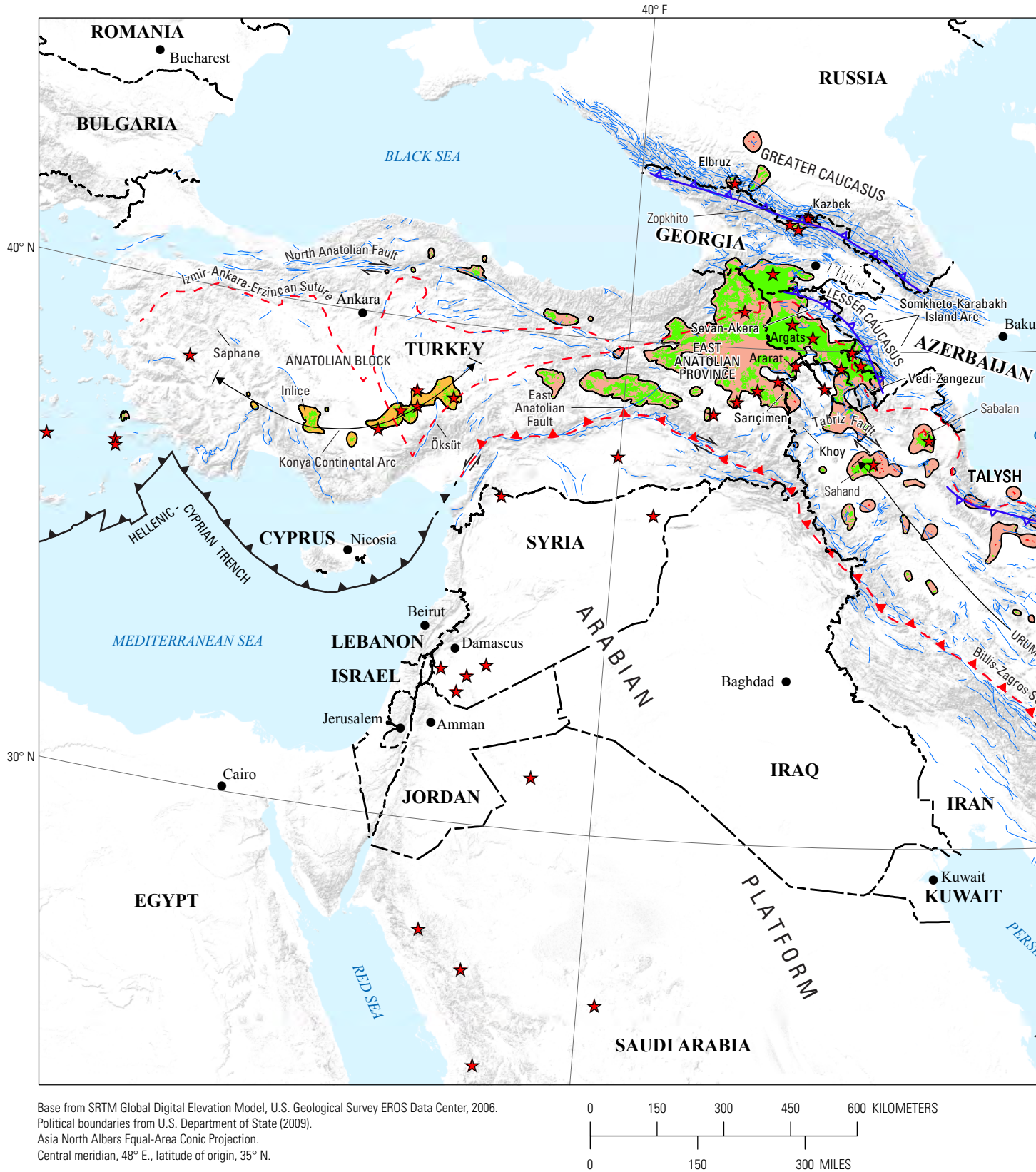
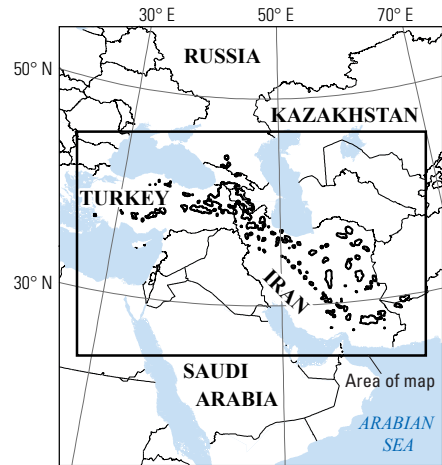
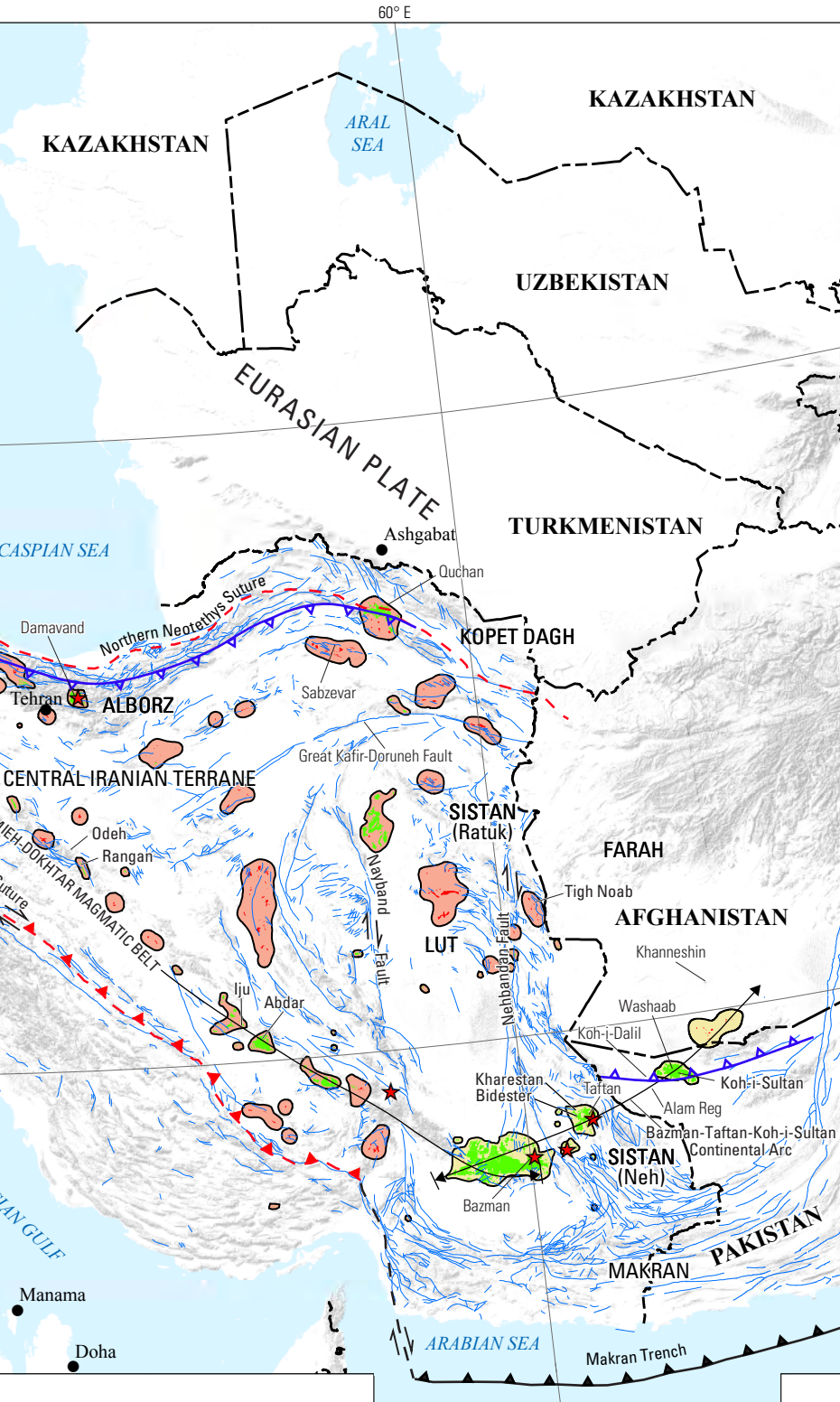


Figure 57. Map showing the distribution of permissive intrusive and extrusive rocks used to define tract 142pCu9017, Plio-Quaternary—Afghanistan, Armenia, Azerbaijan, Georgia, Iran, Pakistan, Russian Federation, and Turkey. Sub-tracts: 142pCu9017a, Plio-Quaternary—Konya, Turkey; 142pCu9017b, Plio-Quaternary—Postcollisional, Armenia, Azerbaijan, Georgia, Iran, Russian Federation, and Turkey; and 142pCu9017c, Plio-Quaternary—Bazman, Afghanistan, Iran, Pakistan. See appendix A for principal sources of information and appendix B for source map units.



EXPLANATION

Porphyry copper

- Assessed porphyry copper tract 142pCu9017a
- Sub-tract 142pCu9017b
- Sub-tract 142pCu9017c
- Permissive intrusive rock
- Permissive extrusive rock
- Terrane suture
- ▲
▲
 Thrust along suture, triangles on upper plate
- ▲
▲
 Thrust fault, triangles on upper plate
- ←
→
 Transform fault, arrows indicate relative motion
- ▲
▲
 Oceanic trench, triangles on upper plate
- ←
→
 Strike-slip fault, arrows indicate relative movement
- Fault, undifferentiated
- Recent volcano
- Geologic feature discussed in the text

Doğanbey Porphyry Prospect

The Miocene-Pliocene Doğanbey acid-sulfate and associated porphyry prospect is located in the epithermal Inlice district of southwestern Turkey (Yigit, 2009). At Doğanbey, drill holes have intercepted porphyry-style Cu-Au-Mo mineralization at depth. Other epithermal prospects in the district are also associated with underlying porphyry stocks (that is, Karacaören and Gölcük [Stratex International PLC, 2012a] and Oğlakçı [Yigit, 2009]).

The Doğanbey prospect is centered on a 1-km-diameter andesite porphyry dome. The 2.5- by 2.0-km kaolin, silica, hematite, alunite, and native-sulfur alteration zone hosts hydrothermal breccias, as well as numerous sulfide-bearing vuggy silica ledges. The northwest- to north-south-striking vuggy silica ledges range from 1 to 50 m in width. Lower temperature hydrothermal alteration minerals such as opal and chalcedony are also present (Stratex International PLC, 2012a).

Other Possible Porphyry-Related Prospects

Other possible Pliocene-Holocene porphyry-related prospects include Öksüt (Stratex International PLC, 2010) in the northern part of the sub-tract and the largest acid-sulfate alunite deposit in Turkey at Şaphane (Mutlu and others, 2005) in the western part of the sub-tract (fig. 56).

Qualitative Assessment

This subduction-related setting is permissive for porphyry copper deposits; however, factors that greatly diminish the favorability include a predominantly volcanic sub-tract with levels of preservation that are, for the most part, too shallow for porphyry systems. This is consistent with the permissive $\{\text{volcanic}/[\text{volcanic}+\text{plutonic}]\} \times 100$ ratio of 100 derived from the 1:500,000-scale geologic map of Turkey (General Directorate of Mineral Research and Exploration, 2000). Middle Miocene and older rocks underlie 6 percent of the sub-tract area. Permissive late Miocene to recent volcanic units account for 20 percent of the tract area, whereas widespread nonpermissive rocks occupy 74 percent (fig. 57). With exception of the Doğanbey acid-sulfate epithermal and associated Cu-Au-Mo porphyry prospect, exploration for porphyry copper deposits in this region is in its early stages (Yigit, 2009). This is reflected in part by the very few identified porphyry occurrences of this age range. Despite the permissive geology, geologic favorability was deemed unlikely to add significant copper resources to the overall assessment (less than a 10-percent chance of 1 undiscovered deposit). Therefore, quantitative assessment of undiscovered porphyry copper deposits in the Pliocene-Quaternary–Konya sub-tract was not warranted.

Pliocene-Quaternary–Postcollisional Sub-tract (142pCu9017b)

Descriptive model: General porphyry copper (Cox, 1986a; Berger and others, 2008; John and others, 2010)

Geologic feature assessed: Late Miocene to Holocene postcollisional magmatism of the Tethyan Eurasian Metallogenic Belt

Location

The Pliocene-Quaternary–Postcollisional sub-tract extends across much of the Tethys region of western and southern Asia (fig. 56). It covers an area of 193,800 km² in Turkey, the Greater and Lesser Caucasus, and Iran. The tract is defined by isolated and irregular but widespread outcrops of latest Miocene to Holocene intermediate to felsic permissive igneous units that are distributed throughout a 3,500-km-long and as much as 750-km-wide region. As a result, this tract is superimposed on large parts of older porphyry copper tracts.

Tectonic Setting and Magmatism

Compared to subduction-related magmatism, which is commonly distributed along distinct arcuate belts, postcollisional magmatism in the Tethys region of western and southern Asia is preserved in isolated and irregularly distributed outcrops. Igneous centers generally occur in pull-apart basins along transtensional and transpressional strike-slip faults. Pliocene to Holocene shallow volcanic-dominated magmatism is most widespread in the Lesser Caucasus and eastern Turkey. In this region, collision between the Arabian Platform and the Eurasian margin has generated the most intense deformation (Kazmin and others, 1986). The postcollisional igneous suites exhibit variable chemical compositions, ranging from tholeiitic to calc-alkaline metaluminous and local peraluminous, as well as mafic to felsic alkaline to ultra-alkaline. Permissive igneous units of intermediate to felsic composition used to define this sub-tract (appendix B) are shown in figure 57, along with locations of igneous complexes and other geologic features mentioned in the text.

Northern Turkey

Postcollisional latest Miocene to Holocene magmatism in north-central and northeastern Turkey is a far-field result of transpression associated with north-south collision of the Arabian Platform and resulting westward escape of the Anatolian Block along the dextral west-northwest North Anatolian Fault system since 12 Ma (Hubert-Ferrari and others, 2002; Chakrabarti and others, 2012). Across north-central and northeastern Turkey, pressure release associated with this tectonic event triggered postcollisional volcanism along pull-apart basins in east-west fault systems (Boztuğ and others, 2004). This magmatic event is represented by three suites—(1) an older basanite-tephrite, (2) a 5–3-Ma feldspathoid-bearing tephrite-tephriphonolite, and (3) a younger bimodal alkaline basalt-rhyolite association. Magmas equilibrated at shallow crustal depths (less than approximately 9 to 15 km) under a pressure of about 3–4.5 kb. Latest magmatism is dominated by mildly to strongly alkaline trachyandesitic and trachytic compositions with geochemical signatures that retain a subduction component but appear otherwise largely derived from partial melting of asthenospheric mantle (Aydin and others, 2008; Keskin, 2003; Yilmaz, 1990).

Eastern Turkey, Lesser Caucasus, and Northwestern Iran

In eastern Turkey and the Lesser Caucasus, collision-related tectonics and extensive volcanic activity began in the middle-late Miocene and continued into historical times (Şengör and Kidd, 1979; Dilek, 2010). An east-west belt that extends from northwestern Iran across the Lesser Caucasus and eastern Turkey is formed by three distinct volcanic assemblages. The first assemblage consists of a middle-late Miocene-earliest Pliocene minor eruptive phase of basic and intermediate alkaline to silica-saturated felsic members. The second assemblage is characterized by widespread eruptions of late Miocene-early Pliocene andesitic to dacitic calc-alkaline lavas, domes, and late northeast-striking dacitic-rhyolitic dikes that are emplaced along northeast-trending graben-bounding structures. Calc-alkaline basaltic andesites and subordinate ignimbrites occur mainly in the northern part of the belt where they form relatively flat volcanic plateaus, whereas high-K calc-alkaline andesites and dacites are more common in the south where they consist of stratovolcanoes with marked relief. The third late Pliocene-Holocene volcanic assemblage is represented by volcanoes composed of lavas with transitional tholeiitic to alkaline mafic to felsic compositions that are mainly emplaced along north-northeast-south-southwest-trending transensional left-lateral structures parallel to the main compression direction (Philip and others, 1989; Adamia and others, 2010; Yilmaz, 1990; Kürüm and others, 2008; Dilek and others, 2010; Veliev and others, 2010). This chain of volcanoes extends from southeastern Turkey across the Caucasus and into Russia (fig. 57). Notable stratovolcanoes with recent activity include Ararat in Turkey, Aragats in Armenia, Kasbek in Georgia, and Elbrus in Russia (Smithsonian Institution, 2013).

Geochemical data from middle-late Miocene-early Pliocene calc-alkaline to late Pliocene-Holocene alkaline igneous units across eastern Turkey, the Lesser Caucasus, and northwestern Iran indicate an increasing role of partial melting of subduction-metasomatized subcontinental mantle and a degree of magma-crust interaction that is larger in the south than in the north (Dilek and others, 2010; Kheirkhah and others, 2009; Kürüm and others, 2008; Keskin, 2003). In the southernmost part across the Bitlis-Zagros Suture in the Arabian Platform, volcanism consists dominantly of mafic lavas erupted along normal faults. Basalts show geochemical signatures that are consistent with deep partial melting of an enriched source similar to oceanic island basalt (OIB) (Kheirkhah and others, 2009).

In northwestern Iran, initiation of postcollisional magmatism in the northern part of the Urumieh-Dokhtar Magmatic Belt is represented by late Miocene to Pliocene calc-alkaline andesitic to rhyodacitic volcanoes and high K calc-alkaline to mildly alkaline subvolcanic domes. At the Sabalan (4,811 m) and Sahand (3,707 m) stratovolcanoes (fig. 57), these domes exhibit subduction-related geochemical signatures (Azizi and Moinevaziri, 2009; Jahangiri, 2007; Omrani and others, 2008; Jamali and others, 2012; Smithsonian Institution, 2002b, c). This calc-alkaline to mildly alkaline event is followed by extensive Pliocene to Holocene alkaline sodic to high-potassic and ultrapotassic mafic-dominated rocks. These occur in calderas and pull-apart basins

along the Tabriz dextral strike-slip fault system (Berberian and King, 1981; Berberian and Berberian, 1981; Ahmadzadeh and others, 2010). Isotopic data indicate that these alkali rocks were generated from enriched mantle sources (Shahrbabaky, 1997). However, crustal contamination accompanied by fractional crystallization appears to have played a role in the petrogenesis of the relatively more felsic trachyandesitic suites (Dabiri and others, 2011). Widespread Pliocene-Holocene mafic to felsic volcanic cones continue to the northeast into the Talysh and western and central Alborz Terranes (fig. 3), where they are also spatially associated with strike-slip and oblique normal faults.

Greater Caucasus and Northern Iran

In the western Greater Caucasus and central Alborz regions, latest Miocene to recent magmatism is represented by isolated volcanic flows, stratovolcanoes, and hypabyssal intrusions that have been unroofed by rapid erosion. In the Greater Caucasus, late Miocene-early Pliocene subvolcanic alkaline successions exhibit K_2O contents that increase from south to north. In the central most uplifted segment of the Greater Caucasus, these volcanic rocks are intruded by late Miocene (9.6–8.8 Ma) subvolcanic granites and granosyenites, which are strongly enriched in upper crustal elements (tin, tungsten, molybdenum, lead). These felsic peraluminous plutons are considered to be the product of anatexis of upper crustal melts formed at depths of 18–20 km (Lordkipanidze and others, 1989). Deeply exhumed intrusions with similar geochemical characteristics occur in the Alborz Terrane of northern Iran, as exemplified by the 6.8-Ma Alam Kuh alkali granite (Axen and others, 2001; Berberian and Berberian, 1981). The limited aerial extent of these deeply exhumed peraluminous intrusions is not well-represented at the 1:1,000,000 scale of the geologic map of Huber (1978). Therefore, these otherwise nonpermissive peraluminous units could not be effectively excluded.

In the Greater Caucasus, late Miocene-early Pliocene magmatism is superseded by a change from a compressional to a transpressional regime and late Pliocene-Holocene calc-alkaline andesite, dacite, and rhyolite (locally alkali) sequences that originated from the mixing of mantle-derived melts with felsic upper crust (Dilek and others, 2010). Associated stratovolcanoes along the north-northeast volcanic chain that projects from eastern Turkey exhibit northward increase in silica content (Pearce and others, 1990). Plutonism is represented by felsic subalkaline 4.5–1.5-Ma granitoids (Mosar and others, 2010), which are believed to have resulted from partial melting of overthickened continental crust (Mitchell and Westaway, 1999).

In the central Alborz and Kopet Dag regions (fig. 57) of northern and northeastern Iran, Miocene-Pliocene to recent igneous rocks are represented by the Pliocene-Holocene Damavand stratovolcano (Brousse and Vaziri, 1982; Dilek and others, 2010) and the Miocene-Pleistocene Quchan volcanic field (Ghasemi and others, 2010; Shabanian and others, 2012).

In the central Alborz region, the 5,670-m above sea level Damavand alkali olivine basalt, trachybasalt to trachyandesite, and trachyte stratovolcano is the highest in the Middle East

(Smithsonian Institution, 2002a). Alkaline volcanic units at Damavand exhibit primitive isotopic compositions that are consistent with derivation from an OIB-like mantle source (Mirnejad and others, 2010a). No historical eruptions are known, but hot springs are located on the volcano's flanks, and fumaroles are found at the summit crater (Berberian and King, 1981).

In the Kopet Dagh region, the Quchan volcanic field (fig. 57) consists of Miocene-Pliocene augite-diopside olivine basalts and alkaline mafic lavas followed by Pleistocene (2.5 Ma) calc-alkaline dacitic plugs, domes, and dikes emplaced along tensional gaps in northwest-southeast right-lateral faults (Ghasemi and others, 2010; Shabanian and others, 2012). As at Damavand, Quchan Miocene-Pliocene volcanic rocks display primitive isotopic signatures that indicate mantle derivation and nonsignificant crustal contamination (Spies and others, 1984; Berberian and King, 1981). However, younger Pleistocene dacitic domes display contrasting arc-related geochemical signatures that suggest an origin related to the break off of the Sabzevar oceanic crust beneath the Kopet Dagh Terrane (Ghasemi and others, 2010; Shabanian and others, 2012). Miocene-Pliocene and younger alkali basalt, tephrite, and trachyandesite volcanic fields also occur along the Great Kafir-Doruneh strike-slip fault system (fig. 2; Förster, 1978).

Eastern Iran

In easternmost Iran, middle Miocene to recent east-northeast-directed compression is expressed by north-northeast-trending en-echelon right-slip faults that are parallel to the Nehbandan Fault system (fig. 57; Tirrul and others, 1983). Relatively isolated outcrops of latest Miocene-Pleistocene (7.3–3.8 Ma) mafic and lesser intermediate volcanic rocks occur in pull-apart basins along these transpressional faults; more commonly, these are the better developed dextral sets. Mafic rocks have alkaline compositions that range from olivine basalt to mugearite, with hawaiite being the most common. These compositions, as well as primitive isotopic signatures, support partial melting of upper mantle peridotite or Cretaceous oceanic crust (Camp and Griffis, 1982).

Central-Eastern Iran

In central-eastern Iran, Neogene-Quaternary alkaline to ultra-alkaline mafic lavas, dikes, and vents occur mainly along the dextral Nayband and Nehbandan strike-slip faults (fig. 3). Along the Nayband Fault, 15–2-Ma volcanic suites exhibit compositions that evolved in time from the north to the south. Both the older and younger suites exhibit geochemical compositions that support a within-plate OIB-derived origin (Pang and others, 2012; Karimpour and others, 2011b). However, more significant crustal contamination was involved in the genesis of the older suite to the north (Saadat and others, 2010). Geochemical data also suggest that partial melting occurred at depths of about 80 km (Walker and others, 2009).

Central and Southeastern Iran

Diachronous middle to late Miocene south-to-north oblique collision along the Bitlis-Zagros Suture from central to

southeastern Iran (fig. 57) initiated postcollisional magmatism along the Urumieh-Dokhtar Magmatic Belt (Berberian and others, 1982; Alavi, 1994). Latest Miocene-Holocene calc-alkalic and alkalic magmatism in the central and southeastern parts Urumieh-Dokhtar Magmatic Belt appears to be largely controlled by tensional gaps along thrust-parallel right-lateral strike-slip faults (Shahrbabaky, 1997).

In the central segment of the Urumieh-Dokhtar Magmatic Belt, late Miocene-Pliocene to Holocene volcanic rocks consist of tholeiitic to calc-alkaline basalts, basaltic andesites, and andesites exhibiting relatively evolved radiogenic signatures (Omrani and others, 2008). These signatures support derivation from a depleted mantle source and assimilation of marine sediments. Dacitic domes with contrasting medium- to high-K calc-alkaline compositions intrude these units. Geochemical data from these dacitic domes indicate preservation of a subduction-related signature, derivation from an enriched lithospheric mantle source, and assimilation of heterogeneous lower crustal materials (Omrani and others, 2008).

In the southeastern segment of the Urumieh-Dokhtar Magmatic Belt, late Miocene-Pliocene volcanic rocks are represented by two suites. The older suite is dominated by tholeiitic to calc-alkaline compositions, whereas the younger suite consists of calc-alkaline andesite, dacite, and rhyodacitic flows and domes (Ghadami and others, 2008; Shahrbabaky, 1997). The younger Miocene-Pliocene intrusions show typical subduction-related geochemical signatures, which also support derivation from a garnet-bearing mantle source (Omrani and others, 2008). Pliocene postcollisional mafic and lesser felsic calc-alkaline and alkaline volcanic rocks are exemplified by ~6-Ma-trachyandesitic and ~3-Ma-dacitic stratovolcanoes emplaced along local fault-controlled extensional zones. Isotopic data from these Pliocene units indicate more primitive island-arc affinities than the Miocene-Pliocene dacitic domes. However, these geochemical data otherwise support similar derivation from the supra-subduction mantle wedge (Shahrbabaky, 1997; Shafiei and others, 2008, 2009). Holocene volcanic units are represented by mafic-dominated alkaline flows with more distinct asthenospheric mantle signatures (Agard and others, 2011).

From the central to the southeastern segment of the Urumieh-Dokhtar Magmatic Belt, geochemical data indicate that Miocene-Pliocene dacitic domes were emplaced during the transition from a subduction-related to a postcollisional setting, with preservation of a strong subduction-related signature in both regions, and the presence of much thicker crust in southeastern segment of the Urumieh-Dokhtar Magmatic Belt (Khodami and others, 2010b; Sherafat and others, 2010).

Known Porphyry Deposits or Prospects, and other Possible Porphyry-Related Occurrences

The volcanic-dominated Pliocene-Quaternary–Postcollisional sub-tract hosts numerous epithermal and several active geothermal systems. Under some of these, porphyry-style alteration has been recognized. Known porphyry complexes associated with this late Miocene to recent postcollisional setting exhibit varied igneous compositions and, where mineralized, equally diverse

Au-Cu to Mo-(Cu) metal associations. About a dozen porphyry and possible porphyry-related occurrences were identified during this study. With exception of one (Iju), these prospects display resource quantities or qualities that appear of limited economic interest at present. They are exemplified by the Mirkoh epithermal and Cu-Mo porphyry prospect in northwestern Iran (Maghsoudi and others, 2009), the Rabor Cu-Au porphyry prospect in the southern Urumieh-Dokhtar Magmatic Belt (Geological Survey of Iran, 2012d; Shahabpour, 2007; Biabangard and others, 2011), and the Alam Kuh Mo-(Cu) porphyry occurrence in northern Iran (Axen and others, 2001; Berberian and Berberian, 1981). Additional porphyry prospects associated with syncollisional to postcollisional magmatism occur also at the Abdar Cu-Au-Mo prospect and Iju Cu-Mo porphyry deposit in the southern Urumieh-Dokhtar Magmatic Belt (see Kerman tract above).

Other possible porphyry-related systems of latest Miocene to recent age occur at Quchan in northeastern Iran (Ghasemi and others, 2010; Shabani and others, 2012), at Tyrnyauz and Zopkhito in Georgia (Kekelia and others, 2008), in the Sarıçimen-Khoy area of easternmost Turkey and northwesternmost Iran (Çolakoğlu and Arehart, 2010; Khalatbari-Jafari and others, 2004), and at Odeh Mo-(Cu) in the central Urumieh-Dokhtar Magmatic Belt.

Porphyry-Related Mineral Occurrences in Northern Turkey

No porphyry copper mineralization of latest Miocene to recent age is reported from this alkaline igneous province. However, several epithermal systems that are associated with intrusions of intermediate alkaline composition are reported to transition into porphyry-style mineralization at depth (Yigit, 2009).

Porphyry-Related Prospects and other Possible Porphyry-Related Mineral Occurrences in Eastern Turkey and Northwestern Iran

On the western flanks of the Sabalan stratovolcano in northwestern Iran, the Mirkoh porphyry Cu-Au-bearing prospect (fig. 56; appendix C) is associated with Miocene-Pliocene calc-alkaline to mildly alkaline dacitic dome intrusions (Maghsoudi and others, 2009). Copper and gold mineralization occurs in quartz veins within propylitic, argillic, and sericitic alteration zones. Concentric metal zonation changes from proximal Cu-(Mo) to Au-Ag to distal antimony, lead, zinc, barium, and manganese. Mineralization developed best along faults and fault intersections. A prominent ASTER-derived alteration zone coincides with the location of this porphyry prospect (Mars, 2014).

An active geothermal field is also under development on the northwestern flanks of the Sabalan stratovolcano. This geothermal field is associated with a porphyry system at depth (Bogie and others, 2005). Results from drilling indicate that hydrothermally altered Pliocene trachyandesite, Eocene andesite, and Paleozoic meta-arenite are intruded by a Miocene monzonite pluton and Pliocene-Holocene diorite porphyry dikes. Alteration appears to be associated with both intrusive events and is represented by quartz-pyrite veins with K-feldspar and sericite envelopes at depth, and illite-clay envelopes at shallow levels. Copper or gold

grades associated with this porphyry system are not reported. About 140 km to the southwest of the Sabalan volcano (fig. 57), similar porphyry settings may be associated with several of the numerous dacitic domes around the Sahand volcano (Geomatix Management, [n.d.]).

Postcollisional magmatism has also been identified in the Khoy area of easternmost Turkey and northwesternmost Iran (fig. 57). In northwesternmost Iran, 11.5–10.5-Ma hydrothermally altered monzodioritic-monzonitic porphyry dikes intrude the Khoy ophiolite complex and overlying Paleogene volcano-sedimentary rocks (Khalatbari-Jafari and others, 2004). These subvolcanic dikes exhibit weak contact metamorphic halos and are preferentially emplaced along northwest-southeast structures. These structures are approximately parallel to the paleosubduction zone along the Bitlis-Zagros Suture. Several late Miocene subvolcanic plutons also occur across the border in easternmost Turkey (Çolakoğlu and Arehart, 2010). They are exemplified by the 12-Ma Sarıçimen hornblende-biotite-(pyroxene) quartz monzodiorite porphyry stock, which also intrudes the Khoy ophiolitic complex. Trace element data in samples from this intrusion show anomalous copper (as much as 230 ppm), zinc (as much as 225 ppm), and lead (as much as 134 ppm). This calc-alkaline pluton exhibits geochemical characteristics that indicate mantle derivation followed by crustal contamination and fractionation in a subduction-related setting (Çolakoğlu and Arehart, 2010). The age of these intrusions indicates emplacement after the final closure of the Southern Neotethys Ocean Branch.

Porphyry-Related Prospects and Other Possible Porphyry-Related Mineral Occurrences in the Greater Caucasus and Northern Iran

No porphyry copper prospects of latest Miocene to Holocene age are known in the Greater Caucasus and across northern Iran. However, molybdenum, tungsten, and associated antimony, mercury, gold, and silver hydrothermal systems are related to latest Miocene to Pleistocene felsic metaluminous to peraluminous porphyry intrusions. These include the Tyrnyauz W-Mo skarn and Zopkhito Sb-Mo-Au vein deposits in the Greater Caucasus (Kekelia and others, 2008; Gugushvili and others, 2010) and the possible porphyry-related Alam Kuh molybdenum occurrence (fig. 56; appendix C) in the western Alborz Mountains (Axen and others, 2001; Berberian and Berberian, 1981). The 6.8-Ma Alam Kuh leucocratic alkali granite is a relatively exhumed (5–7 km) pluton hosted by Paleozoic rocks. The pluton is cut by aplitic and east-west two-mica porphyritic dikes with K-feldspar-quartz-fluorite and sericite-chlorite veins and abundant radial acicular tourmaline.

In northeastern Iran, the Pleistocene dacitic plugs around Quchan (Ghasemi and others, 2010; Shabani and others, 2012) may also be related to a porphyry system at depth. Förster (1978) and Huber (1978) report granodiorite porphyry units in the area (fig. 57). In addition, this area is considered favorable for copper and molybdenum based on the mineral potential maps (Geomatix Management, [n.d.]).

Possible Porphyry-Related Mineral Occurrences in Eastern and Central-Eastern Iran

In the Sistan Zone of Iran, Huber (1978) shows a number of Quaternary porphyry granites in the Tigh Noab area (fig. 57). If confirmed, porphyry-style mineralization could potentially be associated with these intrusions. In the Lut and Kashmar-Kerman (as well as in the southern Sanandaj-Sirjan) Terranes, clusters of felsic porphyritic subvolcanic intrusions attributed with Neogene and Quaternary ages are also shown in the geologic map of Iran (Huber, 1978). Again, the nature of these felsic Neogene and younger units is unknown, but they could conceivably be permissive for porphyry mineralization.

Porphyry-Related Prospects and Other Possible Porphyry-Related Mineral Occurrences in Central and Southeastern Iran

The central and southeastern segments of the Urumieh-Dokhtar Magmatic Belt also host Miocene-Pliocene porphyry systems that are associated with dacitic domes. In the southeastern segment of the Urumieh-Dokhtar Magmatic Belt, the latest Miocene ages of the Iju (9.2 Ma) Cu-Mo porphyry deposit and Abdar (7.5 Ma) Cu-Au-Mo porphyry prospect contrast with the middle Miocene ages of most other porphyry systems in the late Eocene to late Miocene Kerman tract (fig. 57). The younger Iju and Abdar porphyry systems are more closely associated with the late Miocene-early Pliocene Dehaj subvolcanic dacitic syncollisional to postcollisional suite than the older middle-late Miocene subduction-related Kuh Panj suite (Shafiei and others, 2009). Another porphyry copper prospect occurs at Rabor (fig. 56; appendix C), where as much as 4 m-wide, north-south trending calc-alkaline quartz-diorite and dacite porphyry dikes of Pliocene age intrude Eocene pyroclastic and Miocene sedimentary hosts (Biabangard and others, 2011; Shahabpour, 2007). In the central segment of the Urumieh-Dokhtar Magmatic Belt (fig. 57), possible porphyry-related mineralization occurs at the Miocene-Pliocene Odeh molybdenum-rich prospect (Geological Survey of Iran, 2012d) and the Miocene or younger Rangan acid-sulfate Au-Cu prospect, described above with the Yazd tract (Parsapoor and others, 2009).

Qualitative Assessment

Although porphyry copper deposits may have formed in this postcollisional setting, factors that greatly diminish favorability for porphyry copper mineralization include a volcanic-dominated sub-tract with levels of preservation that are for the most part too shallow for porphyry systems (fig. 57). This is reflected by the very high permissive $\{\text{volcanic}/[\text{volcanic}+\text{plutonic}]\} \times 100$ ratio of 97. With exception of the Iju porphyry deposit located in the well-known Kerman porphyry belt, exploration for porphyry copper deposits of this age range appears to have been limited elsewhere in this sub-tract. These two factors are in part reflected by the very few porphyry occurrences identified to date in this otherwise very large sub-tract. Despite the permissive geology, geologic favorability was deemed too low to add significant copper

resources to the overall assessment (less than a 10-percent chance of 1 undiscovered deposit). Therefore, quantitative assessment of undiscovered porphyry copper deposits in the Pliocene-Quaternary–Postcollisional sub-tract was not warranted.

Pliocene-Quaternary–Bazman Sub-tract (142pCu9017c)

Descriptive model: General porphyry copper (Cox, 1986a; Berger and others, 2008; John and others, 2010)

Geologic feature assessed: Early Pliocene to Holocene continental arc of the Tethyan Eurasian Metallogenic Belt

Location

The Pliocene-Quaternary–Bazman sub-tract covers an area of 21,300 km² that extends from southern Iran across southern Pakistan and into Afghanistan. It delimits a 600-km-long and as much as 100-km-wide latest Miocene to Holocene continental arc related to the active Makran subduction zone (fig. 56). Not considered in this study is the extension of this arc to the north and northeast across eastern Afghanistan, where a broad rift is also present (Krumstiek, 1980). The Pliocene-Quaternary–Bazman continental arc is partially superimposed on parts of the older Lut Cretaceous, Sistan, Chagai, and Kerman tracts (see above).

Tectonic Setting and Magmatism

Early Pliocene to Holocene subduction-related arc magmatism in southern Iran, Pakistan, and Afghanistan is related to the Makran subduction zone located in the Arabian Sea. Permissive igneous units of intermediate to felsic composition used to define this sub-tract (appendix B) are shown in figure 57, along with locations of igneous complexes and other geologic features mentioned in the text. Similar to the Hellenic-Cyprian subduction zone that produced the Konya Arc in Turkey (see Pliocene-Quaternary–Konya sub-tract above), the Makran subduction zone is characterized by a shallow-dipping slab, an uncommonly voluminous accretionary fore-arc prism, and a trench that is filled with thick sedimentary successions (Platt and others, 1985).

Late Miocene uplift and associated Chagai Arc (see Chagai tract above) magmatism (Breitzman and others, 1983) were followed by Pliocene-Pleistocene alluvial and volcanic rock units of the Kameron and Koh-i-Sultan formations (Ahmed and others, 1972), which were deposited unconformably on variably deformed older rocks. These rocks are in turn covered by Holocene unconsolidated alluvial and eolian units (Perelló and others, 2008). The Kameron and Koh-i-Sultan formations are part of the Bazman-Taftan-Koh-i-Sultan continental arc (fig. 57), which was initiated in the Miocene-Pliocene as a result of southward migration and flattening of the subducted slab along the Makran Trench (Shahabpour, 2010; Richards and others, 2012). Shallow subduction between 2.3 to 5.7 degrees is supported by fault

plane solutions and epicentral depths (Platt and others, 1985; Gealy, 1988). As a consequence, the continental arc is being constructed some 500 km north of the subduction zone, across several terranes, including the Lut, Sistan, and Chagai-Darirod Terranes (fig. 3).

This east-northeast trending continental arc is represented by volcanic rocks of the about 8-Ma to recent Bazman and Taftan (Jafarian, 2011; Biabangard and Moradian, 2008) in Iran, and about 6-Ma to recent Koh-i-Sultan (Nicholson and others, 2010) calc-alkaline andesitic to dacitic stratovolcanoes in Pakistan (fig. 57). In addition to composite stratovolcanoes, the arc includes a number of lava domes, isolated vents, and volcanic plugs. The trend of Pliocene to Holocene edifices continues along strike into eastern Afghanistan, where more alkalic compositions occur (Peters and others, 2011). This continental-arc setting has been experiencing uplift and exhumation since about 4 Ma (Siddiqui and others, 2007).

Development of an incipient but extensive continental rift basin is evident north of the Bazman-Taftan-Koh-i-Sultan Arc. The cratonic Helmand Terrane of southern Afghanistan is presently undergoing southwestward translation and internal dilation in response to continued northward thrusting of the Indian Plate (Krumnsiek, 1980). Pliocene-Holocene magmatism in this region is controlled by extensional faults. It is dominated by strongly alkaline volcanoes, exemplified by the Pleistocene U-Th-REE carbonatite deposit at Khanneshin (fig. 57), as well as widespread telethermal aragonite-onyx occurrences (Orris and Bliss, 2002; Peters and others, 2011; King and others, 2011). The latter are also likely associated with alkalic magmatism (Abdullah and Chmyriov, 1977a). To the south in the fore-arc region that makes up the Makran Terrane (fig. 57), thick successions of synorogenic flysch deposits are being deposited concurrently with uplift, folding, thrusting, and erosion along narrow basins that separate accretionary ridges. A 4-km-thick sedimentary section overlies the present-day Makran Trench (fig. 57), located 150 km offshore in the Arabian Sea (Berberian and King, 1981).

Known Porphyry Prospects

The Pliocene-Quaternary–Bazman sub-tract delimits the Bazman-Taftan-Koh-i-Sultan Arc of southeastern Iran and western Pakistan. The Bazman-Taftan-Koh-i-Sultan Arc host numerous epithermal systems, some of which are porphyry-related. However, documentation of porphyry mineralization remains scanty in this volcanic-dominated belt (fig. 56).

Koh-i-Sultan Porphyry Prospect

In the Bazman-Taftan-Koh-i-Sultan Arc segment of southern Pakistan, acid-sulfate epithermal systems around the Koh-i-Sultan stratovolcano include Koh-i-Sultan (6–4 Ma), Koh-i-Dalil Vent (2.0 ± 0.8 Ma), Washaab (possibly also known as Missy; Bhutta, 2004), and Alam Reg (Perelló and others, 2008). At Koh-i-Sultan, extensive zones of advanced argillic alteration contain gypsum, native sulfur, barite, and silica stockworks. A drilling program completed in 2008 confirmed the presence of porphyry copper-gold mineralization hosted in

a K-silicate altered intrusive at depth (128 m at 0.14 percent copper and 0.19 ppm gold; Lake Resources N.L., 2012; InfoMine, Inc., 2012j).

Other Possible Porphyry-Related Prospects

In the Bazman-Taftan-Koh-i-Sultan Arc segment of southeastern Iran, the foot of the Bazman stratovolcano hosts the low-sulfidation gold and silver system near Piruzkey (Geological Survey of Iran, 2012a, e; Bazin and Hübner, 1969a; Boomeri and others, 2011b). Here, crustiform, banded, and brecciated quartz-adularia northeast-trending ($25\text{--}35^\circ$) veins, as much as 1 km long and 0.5–2 m wide, occur in basaltic and andesitic flows and pyroclastic units. The veins have sericite and clay alteration envelopes. Mineralization consists of chalcopyrite, covellite, silver-rich covellite, galena, sphalerite, tetrahedrite, and an unknown Ag-rich phase. Gold (less than 1 micron to as much as 2–3 microns) occurs in late hydrothermal breccias (Boomeri and others, 2011b). A possible association with a porphyry system at depth has not been established but has been proposed (Shahabpour, 1999). Three additional ASTER-derived alteration zones that could potentially be related to porphyry-style mineralization occur about 50 km west of the Piruzkey prospect (Mars, 2014).

Northwest of the Taftan stratovolcano, the Kharestan and Bidseter Cu-Zn-Pb-Au-Ag epithermal vein prospects occur within large 2- by 5-km and 3- by 6-km alteration zones of intense hematite, goethite, and jarosite that may be related to porphyry mineralization (Samani, 1998; National Iranian Copper Industries Company, 2012; Zanganeh and others, 2010). HYPERION hyperspectral data indicates the presence of alunite, kaolinite, white mica, chlorite, and opaline silica (Zarcán International Resources, 2003). These prospects are listed in this study as part of the Late Cretaceous to early Miocene Sistan porphyry tract. However, their age is not well constrained. They may be as young as Quaternary and associated with the Taftan stratovolcano, which exhibits active sulfur-rich fumaroles at its summit. Thus, these prospects are also discussed in this section.

Qualitative Assessment

The occurrence of porphyry copper deposits is permissive in this subduction-related setting. However, factors that greatly diminish the favorability for occurrence of porphyry copper mineralization include a volcanic-dominated tract with levels of preservation that are too shallow for porphyry systems ($\{\text{volcanic}/[\text{volcanic}+\text{plutonic}]\}=99$), and perhaps also a fledgling arc-building event that has been only active for the past 8 m.y. This may be reflected in part by the very few identified porphyry occurrences of this age range. Despite the permissive geology, geologic favorability was deemed unlikely to add significant copper resources to the overall assessment (less than a 10-percent chance of 1 undiscovered deposit). Therefore, quantitative assessment of undiscovered porphyry copper deposits in the Pliocene-Quaternary–Bazman sub-tract was not warranted.

Discussion

Compilation of geodynamic, geochemical, geochronologic, and ore-deposit data provided an opportunity to review the continental margin, intraoceanic, and postcollisional tectonic settings in the Tethys region of western and southern Asia. Assessment of favorabilities and associated uncertainties in the estimation of undiscovered porphyry copper deposits not only relied on available knowledge of the intrinsic environment of porphyry copper formation but also on the interrelation among the geologic endowment, levels of preservation and exposure, and the extent of exploration. Much of the magmatism can be explained in terms of fundamental plate-tectonic principles. However, mantle-involved post-subduction processes also played an important role, and uplift, erosion, subsidence, and burial of porphyry copper deposits contributed to the observed metallogenic patterns. The following sections summarize several of the salient findings.

Tectonic Settings and Distribution of Porphyry Copper Deposits and Prospects

Of the 367 porphyry, porphyry-related, and possible porphyry-related copper deposits and prospects identified in the Tethys region of western and southern Asia:

1. Sixty-five percent of all porphyry sites occur in only 5 belts.
2. Fifty-eight percent are associated with relatively mature compressional calc-alkaline continental-arc settings (6 percent also exhibit more evolved metaluminous to peraluminous affinities).
3. Nineteen percent are related to juvenile compressional to extensional island-arc and more diverse intermediate to felsic calc-alkaline to alkaline back-arc environments.
4. Twenty-four percent are linked to the even more varied compressional anatectic syncollisional and extensional calc-alkaline to strongly alkaline postcollisional tectonic regimes.

Furthermore, of the 42 known porphyry copper deposits in the assessment region, roughly comparable fractions are distributed among these tectonic settings. However, the most important porphyry copper deposits occur in continental arc (Reko Diq and Sar Cheshmeh) and postcollisional settings (Sungun and Kadjaran).

Postcollisional Magmatism and Porphyry Copper Mineralization

Based on the known record of collisional events and the present-day distribution of nonsubduction-related igneous rocks, postcollisional magmatism occurred at several times during the tectonic evolution of the Tethys region of western and southern

Asia. However, postcollisional magmatism can be effectively distinguished from available data only in the better preserved and understood Oligocene and younger magmatic belts. In the comparatively lesser preserved and understood older magmatic belts, it is challenging to recognize and differentiate postcollisional from other magmatic events, particularly those that occurred in extensional back-arc settings (for example, parts of Pontide and Anatolide-Tauride tracts).

Given that important porphyry copper mineralization has been recognized in this tectonic environment (Richards, 2009; Richards and Kerrich, 2007), more detailed documentation on the timing of collisional events and associated postcollisional magmatism through time is warranted. Several observations regarding the nature of postcollisional (or postsubduction) magmatism in the Tethys region of western and southern Asia include:

1. *Pliocene-Holocene postcollisional magmatism*—Postcollisional igneous rocks are irregularly distributed but are most widespread and transgress tectonic boundaries in the more protracted collisional setting of the Lesser Caucasus region. Magmatic activity is commonly controlled by normal fault-bounded grabens or pull-apart basins along transtensional or transpressional strike-slip structures. Magmatism consists of intermediate to felsic but also subequal to dominant volumes of (nonpermissive) mafic calc-alkaline to alkaline units. Permissive intermediate to felsic rocks are overwhelmingly represented by volcanic units. These shallow levels of preservation are consistent with regional or local subsidence and burial under an extensional regime. Plutonic units are exposed only in more deeply exhumed regions that are currently under compression (that is, Greater Caucasus and Urumieh-Dokhtar). Postcollisional porphyry systems (that is, Mirkoh, Rabor, Iju and Abdar) are associated with well-preserved volcanic edifices. They underlie shallow acid-sulfate, as well as adularia-sericite epithermal and active geothermal systems.
2. *Older postcollisional magmatism*—Unlike known Pliocene-Holocene porphyry systems, Oligocene-Miocene postcollisional porphyry systems in the region delimited by the Azerbaijan-Caucasus-Iran sub-tract include large known deposits (that is, Sungun, Kadjaran). These may be only exposed at present because of an adequate balance in the extent of synmineral and postmineral subsidence and uplift events in this region. A postcollisional setting for some of the Late Cretaceous-middle Eocene porphyry systems is difficult to discern because of insufficient geologic constraints on these older magmatic belts (arcs migrated and back arcs propagated, and some back arcs evolved into postsubduction environments where they were interrupted by a collisional event). Furthermore, subsequent compressional and extensional deformation structurally juxtaposed different tectonic environments.

Thus, distinction between back-arc and postcollisional environments is problematic. Constraining the timing of a collisional event also presents challenges. In the Tethys region of western and southern Asia, insufficient field evidence has generated confusion between:

- i. The onset versus termination of a collisional event, and
- ii. The “soft” (island arc-continent accretion) versus “hard” (continent-continent) collision.

The first process is less consequential for mantle-involved postcollisional processes.

Preservation-Erosion Record and Porphyry Copper Deposits and Prospects

Results from this study indicate that there is a general correspondence between the number of known porphyry occurrences and the level of crustal preservation (estimated from relative permissive volcanic-to-plutonic ratios) and exposure (the extent of younger cover rocks) in each tract. Magmatic belts with numerous porphyry occurrences exhibit comparable areas of coeval plutonic and volcanic rocks and lesser cover. Magmatic belts with fewer porphyries display high or low volcanic-to-plutonic ratios and (or) greater cover. This suggests that levels of preservation and exposure are variables that make an important contribution to the observed distribution of porphyry copper systems.

At the regional scales analyzed in this study, the correlation is remarkable because uplift, erosional, subsidence, and burial processes commonly happen at time and space scales an order of magnitude smaller, and what is observed today is the sum product of several partially juxtaposed exhumation and burial events. These relations across the 26 tracts identified in the Tethys region of western and southern Asia are shown in figure 58.

The central part of figure 58 shows that tracts or sub-tracts with the highest number of known porphyry copper occurrences (Kerman, Azerbaijan–Caucasus–Iran, Pontide–NE Turkey, and Chagai) are also tracts that are underlain by subequal areas of coeval permissive volcanic and plutonic rocks ($\{\text{volcanic}/[\text{volcanic}+\text{plutonic}]\}$ proportions between 33 and 67), and lesser cover. This reflects appropriate levels of preservation (the coeval volcanic/plutonic interface where hypabyssal intrusions commonly occur) and exposure (where larger fractions of permissive rock relative to younger cover occur) of porphyry systems.

The left part of figure 58 includes tracts where fewer known porphyry systems occur. In these tracts, the proportion of coeval permissive volcanic-to-plutonic rocks is high, as is the fraction of younger cover. This reflects shallow levels of preservation (where volcanic rocks are more common than coeval plutonic rocks) and inadequate exposure (where smaller fractions of permissive rock to younger cover occur) of porphyry systems.

The right part of figure 58 also consists of tracts where fewer porphyry systems are known to occur. Here, the proportion of

coeval permissive volcanic-to-plutonic rocks is variable but in general low, and the fraction of younger cover is high. This reflects deep levels of preservation (where volcanic rocks are less common than coeval plutonic rocks) and lack of exposure (where smaller fractions of permissive rock to younger cover occur) of porphyry systems. Deep levels of preservation are also indicated by the high proportions of metamorphic rocks in these more exhumed tracts. As derived from available geologic map bases, the proportion of metamorphic rocks is 35 percent in the Sanandaj–Sirjan tract, 25 percent in the Border Folds tract, and 23 percent in the Anatolide–Tauride–Western Turkey sub-tract. These metamorphic rocks are not only associated with older events but also with younger deformation and uplift events that occurred during or after the volcano-plutonic event delimited by the tract. This is particularly evident in the Sanandaj–Sirjan and western Anatolide–Tauride Terranes.

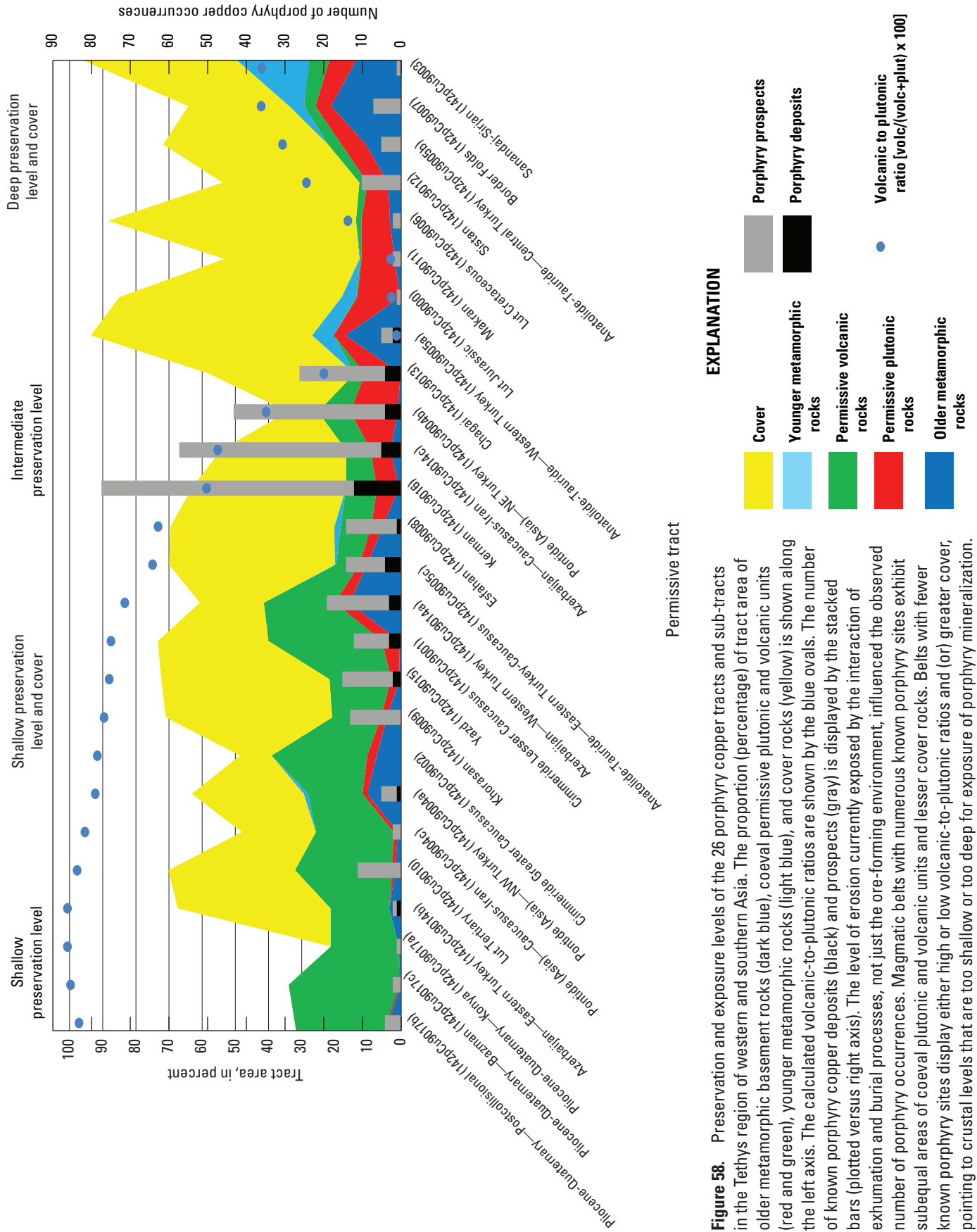
Changes in Tectonic Regime and Porphyry Copper Deposits

The highest rates of uplift, erosion, and removal of volcanic rocks that are coeval with porphyry intrusions coincide with pronounced tectonic changes. This is particularly evident in the Chagai and Kerman tracts and Azerbaijan–Caucasus–Iran sub-tract. These tracts also host most of the known porphyry copper resources in the Tethys region of western and southern Asia. The formation of world-class porphyry deposits in the magmatic belts delimited by these tracts suggests that these deposits were emplaced during a time that closely preceded or followed the final and “hard” continent-continent collision between the Arabian Platform and the Eurasian margin. Collision occurred in the early Miocene in the Arasbaran part of the Azerbaijan tract and the late Miocene in the Kerman tract. The southward migration or rollback and flattening of the subducted slab along the Makran Trench occurred in the Miocene–Pliocene in the Chagai tract.

Concluding Remarks

Ore-Forming Environment, Level of Preservation and Exposure, Number of Porphyry Occurrences, Extent of Exploration, and Copper Endowment

Results from this study indicate that the largest known porphyry copper deposits in the assessment region occur in subduction-related compressional arcs and postsubduction or postcollisional extensional magmatic belts that at present exhibit appropriate preservation and exposure levels. Available geochronologic age constraints indicate that emplacement of these porphyry systems closely corresponds with episodes of pronounced tectonic change (that is, collision, greatest extension). Preservation and exposure level analysis showed that uplift, erosion, subsidence, and burial processes made an important contribution to the observed distribution of



porphyry copper systems in the assessment region. The tracts with appropriate degrees of preservation and exposure levels and numerous porphyry occurrences contain the largest deposits and also have experienced the most exploration.

In summary, the assessment team recognized that there is a general correlation between the relative endowment of the porphyry setting, the level of preservation and exposure, the number of porphyry deposits and prospects, and the extent of exploration in a permissive tract.

Utility of Data

Available tectonic (including ophiolite-bearing accretionary belts), lithologic, and geochemical data were sufficient to establish the setting, nature, and extent of exposed magmatic belts and associated porphyry mineralization in time and space at the regional scale. Compilation of existing and new data on porphyry, porphyry-related, and possible porphyry-related porphyry copper occurrences in the assessment region provided an expanded and better documented database of geologic relations at the local scale. This compilation effort augmented the number of porphyry deposits and associated resource information known in the assessment region by 40 percent. It also doubled the number of known porphyry prospects. Deposits and prospects served as effective geochemical probes, because they provided information on the locations, the geochemical signatures of porphyry intrusions, the abundance and aerial extent of hydrothermal alteration minerals, the dominant metal associations, and the levels of preservation and exposure of individual mineral systems. Integration of these data with regional-scale geologic information allowed definition and delimitation of tracts permissive for porphyry copper mineralization and comparison of characteristics and resources in porphyry copper deposits in the assessment region with descriptive and grade-tonnage models constructed from data around the world.

The extent of exploration in the assessment region could not be derived satisfactorily from information in the available literature. However, the assessment team recognized that there is broad correlation between the level of preservation and exposure of a tract, the number of porphyry occurrences contained within it, and the extent of exploration.

The regional-scale magnetic anomaly map base served to confirm the location and extent of magmatic belts, basins, and other regional-scale structural features. Largely because of masking by younger units with high magnetic susceptibilities, these data were deemed to have insufficient resolution to allow interpretation of whether shallowly buried (for example, less than 1 km from the surface) extensions of permissive units of a given age range projected beyond permissive tract boundaries. Thus, these data could not be relied on to adjust these boundaries.

Processed ASTER-derived alteration data were used to identify the location and aerial extent of possible hydrothermal phyllic and argillic alteration zones that could be associated

with potential porphyry copper mineralization. In more thoroughly explored tracts with numerous known porphyry copper occurrences, these data confirmed the location of many but not all known porphyry occurrences, as well as alteration associated with other types of mineral occurrences. In less-explored tracts with few known porphyry copper occurrences, and after filtering out ASTER-derived alteration zones associated with other known types of mineral occurrences, ASTER-derived alteration data were considered along with other information to deduce potential unidentified porphyry-related occurrences. Given that ASTER data were not available for large parts of several tracts, these data were only of partial use during the estimation process.

Utility of Available Models

Existing descriptive models appropriately incorporated the characteristics of both subduction- and nonsubduction-related porphyry deposits (John and others, 2010), porphyry-related deposits (Sillitoe, 2010), and igneous compositions and associated metal concentrations (Seedorff and others, 2005). Resources and metal associations of several deposits in the assessment region were not well represented in the grade and tonnage model of Singer and others (2008). This is because tonnage and grade estimates reported for many porphyry copper deposits in the assessment region and the model only partially reflect the contained metal resources. Current efforts are underway to update the grade and tonnage model with new and revised resource data obtained during the global assessment effort. Similarly, the available Singer and Menzie (2005) regression algorithm used to derive expected numbers of deposits relied on data that are almost 10 years old. The grade and tonnage model (as well as the density model of Singer and Menzie, 2010) needs to be updated. However, the Singer and Menzie (2005) relation was used to allow more meaningful comparisons with previous assessments that relied on it. The code of the probabilistic Monte Carlo simulation software (EMINERS) is also being updated.

Summary of Probabilistic Assessment Results

The assessment team estimated that there are 47 undiscovered deposits in the region that are within 1 km of the surface. Based on the mean estimates from Monte Carlo simulations, undiscovered deposits may contain at least 180 Mt of copper distributed among the 18 tracts for which probabilistic estimates were conducted. These undiscovered copper resources are 2.8 times the 62 Mt of copper already identified in the known 42 porphyry deposits in the assessment area. The eight permissive tracts for which probabilistic estimates were not done are unlikely to contribute significant resources to the copper endowment of the study area.

The estimated numbers of undiscovered deposits at selected quantile levels for each tract, the resulting mean undiscovered deposits with associated uncertainty reported as standard deviation and coefficient of variation, the numbers of known and total numbers of porphyry deposits, the tract area, and the deposit density calculated from the sum of known and undiscovered deposits per 100,000 km², are summarized in table 16. The estimated total deposit densities are comparable to median porphyry deposit densities expected in well-explored tracts of equivalent size elsewhere around the world (Singer and Menzie, 2010) in 10 of the 18 tracts and sub-tracts for which probabilistic estimates were conducted. These include the Cimmeride–Lesser Caucasus, Pontide–NE Turkey, Anatolide–Tauride–Western Turkey, Anatolide–Tauride–Eastern Turkey–Caucasus, Esfahan, Chagai, Azerbaijan–Western Turkey, Azerbaijan–Caucasus–Iran, Yazd, and Kerman. The other eight tracts have lower estimated deposit densities because of their limited favorability, insufficient available grade and tonnage data for known porphyry copper deposits, and (or) deposit characteristics that differ from those in the available descriptive and grade-tonnage models.

For each tract, table 17 shows the identified resources in known porphyry deposits, the mean and median²¹ estimates of contained copper and gold and the mean estimates of molybdenum, silver, and total mineralized rock in undiscovered resources. Identified resources are based on total production, if any, published data for measured and indicated reserves, and inferred resources at the lowest cutoff grade reported. Identified resources may include substantial amounts of metal that already have been produced. Note that byproduct metals in deposits with reliable tonnages and copper grades frequently are not reported (table 3). Table 17 shows that about half of the undiscovered copper resources are estimated to be contained in only 5 of the 26 tracts and sub-tracts. Two-thirds of the undiscovered copper resources are estimated to be contained in only 7 of the 26 tracts and sub-tracts.

Identified resources are compared with mean and with median estimates of undiscovered copper and gold resources by tract in figures 59A and B, respectively. With the exception of the Chagai tract, which includes the exceptionally large copper resource contributed by the giant Reko Diq deposit, the mean estimated undiscovered copper resources in all the other tracts exceed the identified copper resources. The largest undiscovered copper and molybdenum resources are estimated to be contained in the Kerman tract and the Azerbaijan–Caucasus–Iran sub-tract. Compared to the identified resources, however, these tracts contribute lower proportions of undiscovered copper resources than the other tracts (fig. 59A). This is because in these two relatively well-explored tracts, most porphyry copper deposits are estimated

to have already been identified. With exception of the relatively well-explored Azerbaijan–Caucasus–Iran sub-tract and Chagai tract, the largest undiscovered gold resources are estimated to be contained in the Kerman Cu–Mo–Au porphyry tract and the Lut Tertiary and Khorasan Cu–Au porphyry tracts (fig. 59B).

The probabilistic assessment of the metal resources associated with undiscovered porphyry copper deposits in the Tethys region of western and central Asia indicates that significant amounts of additional resources may be present. However, these undiscovered copper resources, if present, may be inaccessible or uneconomic. Results should be interpreted with caution pending application of economic filters to evaluate what part of the estimated undiscovered resources might be economic under various conditions, such as metal prices and capital development costs.

The 260 Mt of copper resources identified in known porphyry deposits in the well-explored Western United States is substantially larger than the 62 Mt of copper resources known at present in the less explored Tethys region of western and southern Asia. However, the estimated 180 Mt of copper in 47 undiscovered porphyry deposits in the Tethys region of western and southern Asia is considerably more than the 46 Mt of copper estimated in 14 undiscovered porphyry deposits in the Tethys region of Europe to the west (Sutphin and others, 2013) and the 28.5 Mt of copper in the 9 undiscovered porphyry deposits estimated in the Tethys region of Afghanistan to the east (Ludington and others, 2007). It (the estimated 180 Mt of copper in the Tethys region of western and southern Asia) is comparable to the 200 Mt of copper estimated in undiscovered porphyry deposits in the world-class province of the Western United States (U.S. Geological Survey National Mineral Resource Assessment Team, 2000) and to the 144 Mt of copper in 39 undiscovered deposits in Mexico (Hammarstrom and others, 2010) but substantially less than the 750 Mt of copper in the 145 undiscovered porphyry deposits of the Andes (Cunningham and others, 2008).

Acknowledgments

The authors thank members of the USGS Assessment Oversight Committee—Dave John, Rob Robinson, Barney Berger, Kate Johnson, Jeff Doebrich, and technical reviewers Jeff Doebrich, Don Singer, Greg Fernette, and Pam Cossette for their helpful insight, comments, and suggestions. We also thank our international colleagues Richard Herrington, Mario Billa, Ilkay Kuşcu, Charles Moon, and Jeremy Richards and their institutions for their contributions, as well as USGS Mineral Resources Program Coordinators Jeff Doebrich and Larry Meinert for their support.

²¹Amount of metal at the 0.5 quantile or 50-percent chance of occurrence of that amount of metal or more based on simulation for the estimated numbers of undiscovered deposits.

Table 16. Summary of estimates of undiscovered deposits, numbers of known deposits, tract areas, and deposit densities for the porphyry copper assessment of the Tethys region of western and southern Asia.

[N_{xx} estimated number of deposits associated with the xxth percentile; N_{und} expected number of undiscovered deposits; s , standard deviation; C_v %, coefficient of variance; N_{known} , number of known deposits in the tract that are included in the grade and tonnage model; N_{total} , total of expected number of deposits plus known deposits; tract area (km^2), area of permissive tract in square kilometers, rounded to three significant figures; deposit density reported as the total number of deposits per 100,000 km^2 . N_{und} , s , and C_v % are calculated using a regression equation (Singer and Menzie, 2005)]

Tract name	Coded_ID	Consensus estimates of numbers of undiscovered deposits										Summary statistics					Tract area (km^2)	Deposit density ($N_{total}/100k km^2$)
		N_{90}	N_{50}	N_{10}	N_{05}	N_{01}	N_{und}	s	C_v %	N_{known}	N_{total}							
Anatolide-Tauride—Central Turkey sub-tract	142pCu9005b	0	0	1	1	2	0.33	0.62	190	0	0.33	36,200	1					
Anatolide-Tauride—Eastern Turkey-Caucasus sub-tract	142pCu9005c	0	2	4	7	7	2.2	2.0	92	4	6.2	21,700	29					
Anatolide-Tauride—Western Turkey sub-tract	142pCu9005a	0	1	1	2	3	0.78	0.60	78	2	2.8	5,940	47					
Azerbaijan—Caucasus-Iran sub-tract	142pCu9014c	1	6	15	15	15	7.1	5.0	70	5	12	58,300	21					
Azerbaijan—Eastern Turkey sub-tract	142pCu9014b	0	0	1	1	2	0.33	0.62	190	1	1.3	7,750	17					
Azerbaijan—Western Turkey sub-tract	142pCu9014a	1	2	8	8	8	3.4	2.7	80	3	6.4	65,200	10					
Border Folds	142pCu9007	0	1	2	4	4	1.2	1.2	100	0	1.2	45,300	3					
Chagai	142pCu9013	1	3	6	6	6	3.2	1.9	58	4	7.2	19,100	38					
Cimmeride Lesser Caucasus	142pCu9001	0	2	3	5	5	1.9	1.5	79	3	4.9	17,400	28					
Esfahan	142pCu9008	0	2	8	18	18	4.0	4.9	120	1	5.0	56,900	9					
Kerman	142pCu9016	3	5	10	10	10	5.7	2.7	48	12	18	32,800	54					
Khorasan	142pCu9009	0	2	5	8	8	2.5	2.4	96	0	2.5	38,300	7					
Lut Tertiary	142pCu9010	0	2	5	5	5	2.4	2.0	85	0	2.4	56,300	4					
Pontide (Asia)—Caucasus-Iran sub-tract	142pCu9004c	0	1	1	3	3	0.85	0.80	94	0	0.85	24,300	3					
Pontide (Asia)—NE Turkey sub-tract	142pCu9004b	1	3	9	9	9	4.1	3.0	73	4	8.1	45,500	18					
Pontide (Asia)—NW Turkey sub-tract	142pCu9004a	0	1	2	4	4	1.2	1.2	100	1	2.2	32,700	7					
Sistan	142pCu9012	0	2	5	8	8	2.5	2.4	96	0	2.5	32,800	8					
Yazd	142pCu9015	1	2	8	8	8	3.4	2.7	80	2	5.4	25,700	21					

Table 17. Summary of simulations of undiscovered resources in porphyry copper deposits and comparison with identified copper and gold resources in porphyry copper deposits within each permissive tract, Tethys region of western and southern Asia.

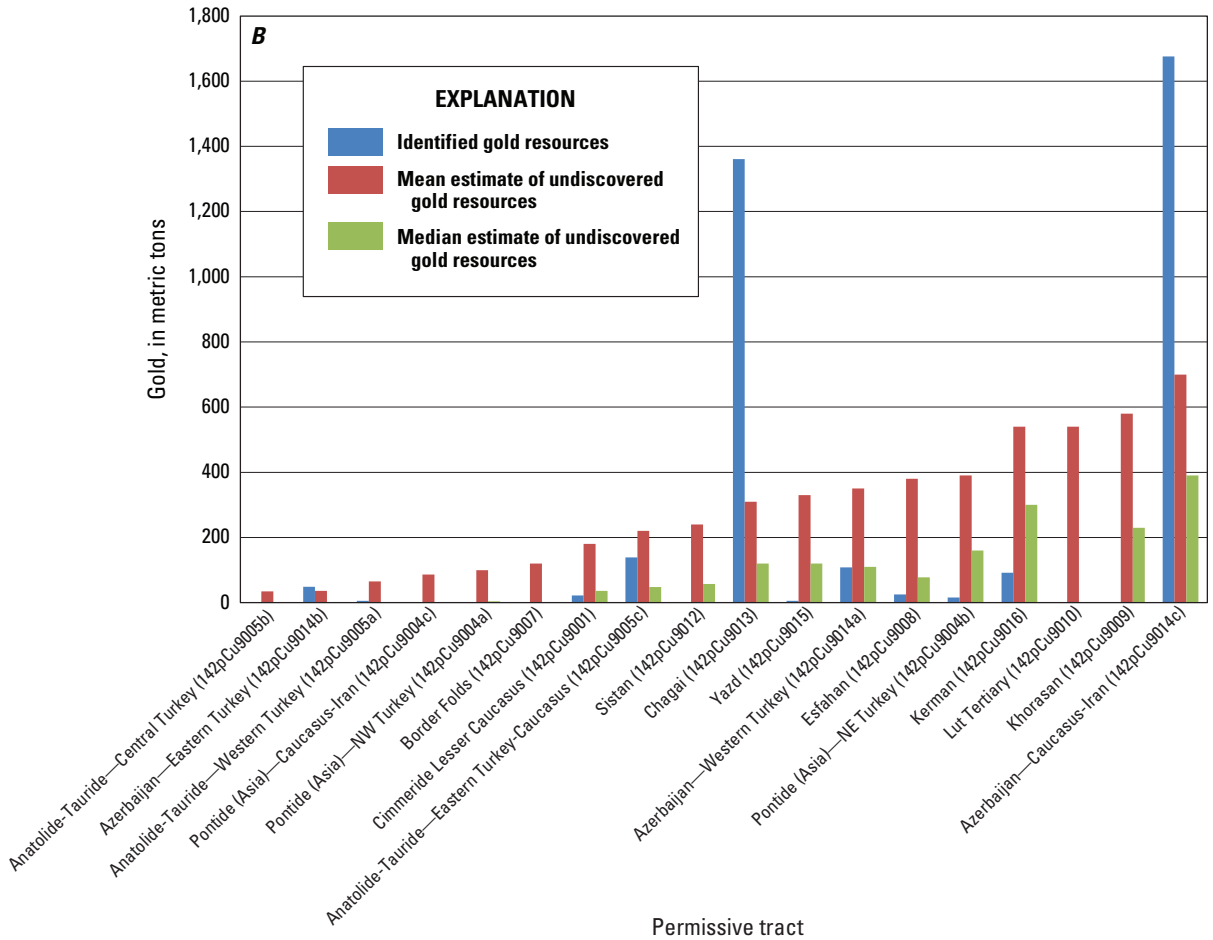
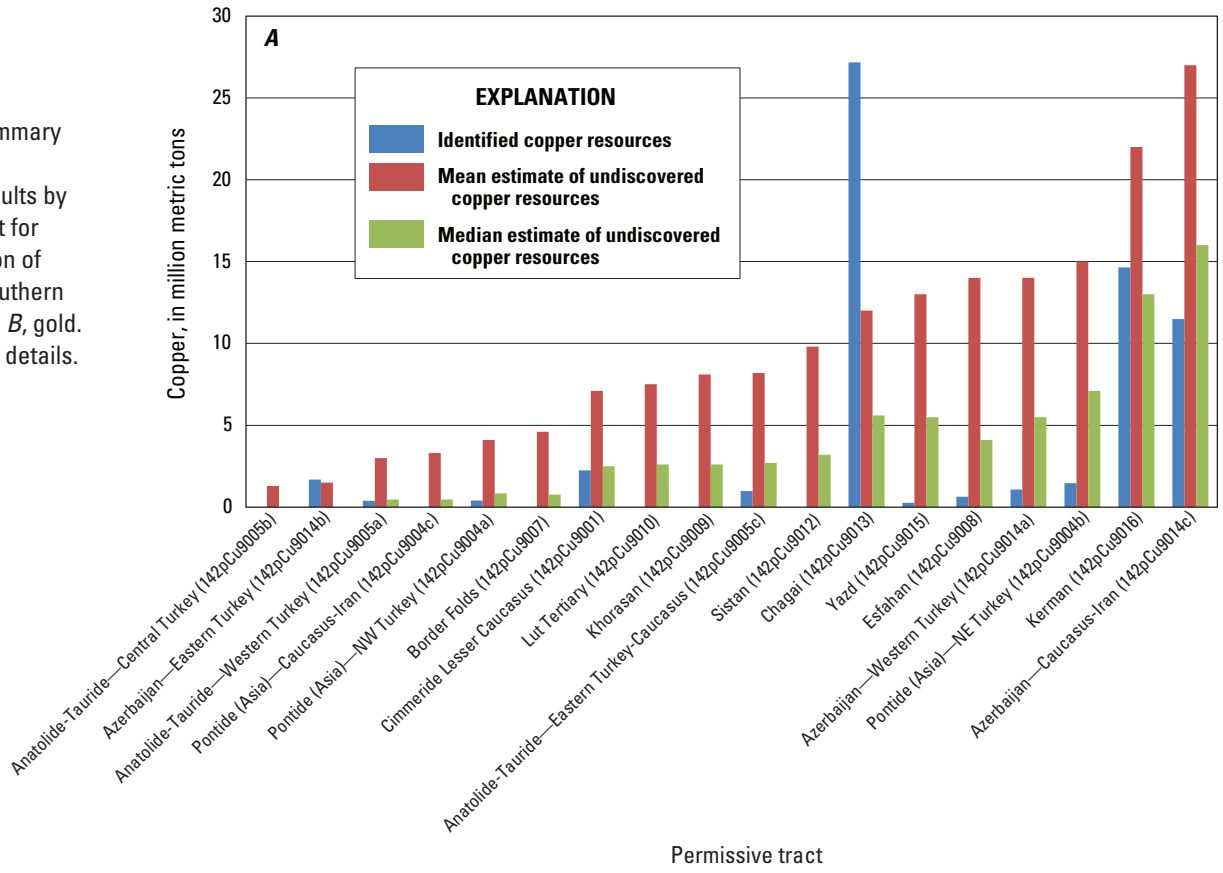
[Model, grade and tonnage model used for simulations: General porphyry copper or Cu-Au subtype models of Singer and others (2008). t, metric tons; Mt, million metric tons; NA, not applicable (for totals, only the means are additive). Totals rounded to two significant figures]

Tract name	Coded_ID	Model	Identified copper resources (t)	Mean estimate of undiscovered copper resources (t)	Ratio of mean estimate to identified copper resources	Median estimate of undiscovered copper resources (t)	Identified gold resources (t)	Mean estimate of undiscovered gold resources (t)	Ratio of mean estimate to identified gold resources	Median estimate of undiscovered gold resources (t)	Mean estimate of undiscovered molybdenum resources (t)	Mean estimate of undiscovered silver resources (t)	Mean estimate of rock of rock (Mt)
Anatolide-Tauride—Central Turkey sub-tract	142pCu9005b	General porphyry copper	0	1,300,000	NA	0	0	35	NA	0	41,000	460	270
Anatolide-Tauride—Eastern Turkey-Caucasus sub-tract	142pCu9005c	General porphyry copper	1,177,000	8,200,000	7	2,700,000	219	220	1	48	230,000	2,700	1,700
Anatolide-Tauride—Western Turkey sub-tract	142pCu9005a	General porphyry copper	380,000	3,000,000	8	460,000	6	65	11	0	79,000	900	610
Azerbaijan—Caucasus-Iran sub-tract	142pCu9014c	General porphyry copper	11,430,000	27,000,000	2	16,000,000	1,663	700	0	390	760,000	9,300	5,500
Azerbaijan—Eastern Turkey sub-tract	142pCu9014b	General porphyry copper	1,700,000	1,500,000	1	0	49	36	1	0	40,000	430	290
Azerbaijan—Western Turkey sub-tract	142pCu9014a	General porphyry copper	1,080,000	14,000,000	13	5,500,000	110	350	3	110	390,000	4,600	2,800
Border Folds	142pCu9007	General porphyry copper	0	4,600,000	NA	760,000	0	120	NA	0	120,000	1,400	930
Chagai	142pCu9013	General porphyry copper	26,100,000	12,000,000	0	5,600,000	1,570	310	0	120	340,000	3,800	2,500
Cimmeride Lesser Caucasus	142pCu9001	General porphyry copper	2,238,000	7,100,000	3	2,500,000	22	180	8	36	200,000	2,400	1,400
Esfahan	142pCu9008	General porphyry copper	640,000	14,000,000	22	4,100,000	20	380	19	78	390,000	4,800	2,900
Kerman	142pCu9016	General porphyry copper	14,710,000	22,000,000	1	13,000,000	90	540	6	300	570,000	7,100	4,400
Khorasan	142pCu9009	Cu-Au subtype	0	8,100,000	NA	2,600,000	0	580	NA	230	47,000	2,600	1,600
Lut Tertiary	142pCu9010	Cu-Au subtype	0	7,500,000	NA	2,600,000	0	540	NA	0	44,000	2,400	1,500
Makran	142pCu9011	NA	0	NA	NA	NA	0	NA	NA	NA	NA	NA	NA

Table 17.—Continued

Tract name	Coded_ID	Model	Identified copper resources (t)	Mean estimate of undiscovered copper resources (t)	Ratio of mean estimate to identified copper resources	Median estimate of undiscovered copper resources (t)	Identified gold resources (t)	Mean estimate of undiscovered gold resources (t)	Ratio of mean estimate to identified gold resources	Median estimate of undiscovered gold resources (t)	Mean estimate of undiscovered molybdenum resources (t)	Mean estimate of undiscovered silver resources (t)	Mean estimate of rock of rock (Mt)
Pontide (Asia)—Caucasus-Iran sub-tract	142pCu9004c	General porphyry copper	0	3,300,000	NA	470,000	0	86	NA	0	91,000	1,200	670
Pontide (Asia)—NE Turkey sub-tract	142pCu9004b	General porphyry copper	1,530,000	15,000,000	10	7,100,000	20	390	20	160	420,000	5,100	3,100
Pontide (Asia)—NW Turkey sub-tract	142pCu9004a	General porphyry copper	400,000	4,100,000	10	840,000	0	100	NA	4	110,000	1,400	830
Sistan	142pCu9012	General porphyry copper	0	9,800,000	NA	3,200,000	0	240	NA	57	270,000	3,200	2,000
Yazd	142pCu9015	General porphyry copper	270,000	13,000,000	48	5,500,000	6	330	55	120	360,000	4,400	2,700
Total			62,000,000	180,000,000	NA	NA	3,800	5,200	NA	NA	4,500,000	58,000	36,000

Figure 59. Summary of probabilistic assessment results by permissive tract for the Tethys region of western and southern Asia. *A*, copper. *B*, gold. See table 17 for details.



References Cited

- Abdullah, S., and Chmyriov, V.M., eds., 1977a, Geology and mineral resources of Afghanistan: Afghanistan Geological Survey Mineral Resources of Afghanistan, v. 2, scale 1:4,000,000.
- Abdullah, S., and Chmyriov, V.M., 1977b, Tectonic map of Afghanistan, *in* Abdullah, S., and Chmyriov, V.M., eds., Geology and mineral resources of Afghanistan: Afghanistan Geological Survey Mineral Resources of Afghanistan, v. 1, scale 1:2,500,000.
- Abedi, M., and Norouzi, G-H., 2012, Integration of various geophysical data with geological and geochemical data to determine additional drilling for copper exploration: *Journal of Applied Geophysics*, v. 83, p. 35–45.
- Abedi, M., and Ziari, M., 2004, Cu (Au) mineralization in the Kuhe-Zar area, NE of Iran: *Romanian Journal of Mineral Deposits*, v. 81, p. 61–62.
- Abedpour, Z., and Tarrah, J., 2010, Petrography and mineralogical reactions relating skarn zones at the Kuh-e-Gabbri, northwestern Kerman: *International Applied Geological Congress, 1st, Mashad, Iran, April 26–28, 2010 [Proceedings]*, p. 1321–1325.
- Adamia, S.A., Lordkipanidze, M.B., and Zakariadze, G.S., 1977, Evolution of an active continental margin as exemplified by the Alpine history of the Caucasus: *Tectonophysics*, v. 40, p. 183–199.
- Adamia, S.A., Chkhotua, T., Kekelia, M., Lordkipanidze, M.B., Shavishvili, I., and Zakariadze, G., 1981, Tectonics of the Caucasus and adjoining regions—Implications for the evolution of the Tethys Ocean: *Journal of Structural Geology*, v. 3, p. 437–447.
- Adamia, S., Alania, V., Chabukiani, A., Chichua, G., Enukidze, O., and Sadradze, N., 2010, Evolution of the Late Cenozoic basins of Georgia (SW Caucasus)—A review, *in* Sosson, M., Kaymakci, N., Stephenson, R.A., Bergerat, F., and Starostenko, V., eds., *Sedimentary basin tectonics from the Black Sea and Caucasus to the Arabian Platform*: London, Geological Society Special Publication 340, p. 239–259.
- Adamia, S., Zakariadze, G., Chkhotua, T., Sadradze, N., Tsereteli, N., Chabukiani, A., and Gventsadze, A., 2011, Geology of the Caucasus—A review: *Turkish Journal of Earth Sciences*, v. 20, p. 489–544.
- Afghanistan Geological Survey, 2007, Minerals in Afghanistan—The Hajigak iron deposit: Afghanistan Geological Survey brochure, accessed September 27, 2012, at http://www.bgs.ac.uk/AfghanMinerals/docs/Hajigak_A4.pdf.
- Aftabi, A., and Atapour, H., 2009, Comments on “Arc magmatism and subduction history beneath the Zagros Mountains, Iran—A new report of adakites and geodynamic consequences” by J. Omrani, P. Agard, H. Whitechurch, M. Bennoit, G. Prouteau, and L. Jolivet: *Lithos*, v. 113, p. 884–846.
- Aftabi, A., and Atapour, H., 2011, Alteration geochemistry of volcanic rocks around Sarcheshmeh porphyry copper deposit, Rafsanjan, Kerman, Iran—Implications for regional exploration: *Resource Geology*, v. 61, p. 76–90.
- Afzal, P., and Rajoli, M.E., 2010, Separating geochemical anomalies by applying fractal concentration-area method—Case study, Kerver porphyry system, SE Iran: *International Applied Geological Congress, 1st, Mashad, Iran, April 26–28, 2010 [Proceedings]*, p. 190–195.
- Afzal, P., Alghalandis, Y.F., Khakzad, A., Moarefvand, P., and Omran, N.R., 2011, Delineation of mineralization zones in porphyry Cu deposits by fractal concentration-volume modeling: *Journal of Geochemical Exploration*, v. 108, p. 220–232.
- Afzal, P., Khakzad, A., Moarefvand, P., Omran, N.R., Esfandiari, B., and Alghalandis, Y.F., 2010, Geochemical anomaly separation by multifractal modeling in Kahang (Gor Gor) porphyry system, central Iran: *Journal of Geochemical Exploration*, v. 104, p. 34–46.
- Agard, P., Omrani, J., Jolivet, L., and Mouthereau, F., 2005, Convergence history across Zagros (Iran)—Constraints from collisional and earlier deformation: *International Journal of Earth Sciences*, v. 94, p. 401–419.
- Agard, P., Omrani, J., Jolivet, L., Whitechurch, H., Vrielynck, B., Spakman, W., Monié, P., Meyer, B., and Wortel, R., 2011, Zagros orogeny—A subduction-dominated process: *Geological Magazine*, v. 148, p. 692–725.
- Aghazadeh, M., Castro, A., Badrzadeh, Z., and Vogt, K., 2011, Post-collisional polycyclic plutonism from the Zagros hinterland—The Shaivar Dagh plutonic complex, Alborz Belt, Iran: *Geological Magazine*, v. 148, p. 980–1008.
- Aghazadeh, M., Castro, A., Omran, N.R., Emami, M.H., Moinvaziri, H., and Badrzadeh, Z., 2010, The gabbro (shoshonitic)-monzonite-granodiorite association of Khankandi pluton, Alborz Mountains, NW Iran: *Journal of Asian Earth Sciences*, v. 38, p. 199–219.
- Aghazadeh, M., Hou, Z., and Badrzadeh, Z., 2012, Porphyry copper mineralization in Iran—Main metallogenic belts and ore-forming episodes [abs.]: *International Geological Congress, 34th, Brisbane, Australia, August 5–10, 2012 [Proceedings]*, abstract 247.

- Ahmad, M.U., 1986, Dasht-e-Kain porphyry copper prospect in context of the metallogeny of Chagai calc-alkaline volcano-intrusive complex, Chagai district (Baluchistan) Pakistan: Belgrad University, Yugoslavia, Ph.D. dissertation, 115 p.
- Ahmad, M.U., 1992, Porphyry copper in Pakistan: Geological Survey of Pakistan Mineral Information Series 9, 21 p.
- Ahmad, M.U., Siddiqui, R.H., and Chaudhary, M.A., 1986, Geological and geochemical exploration and preliminary evaluation of Dasht-e-Kain porphyry copper-molybdenum prospect, Chāgai District, Baluchistan, Pakistan: Geological Survey of Pakistan Economic Geology Record, v. 72, 44 p.
- Ahmadi Khalaji, A., Tahmasbi, Z., and Zarei Sahemieh, R. 2009, Petrography and mineral chemistry of the Boroujerd pluton (Sanandaj-Sirjan Zone, western Iran): *Journal of Applied Sciences*, v. 9, p. 843–853.
- Ahmadian, J., Haschke, M., McDonald, I., Regelous, M., RezaGhorbani, M., Emami, M.H., and Murata, M., 2009, High magmatic flux during Alpine-Himalayan collision—Constraints from the Kal-e-Kafi complex, central Iran: *Geological Society of America Bulletin*, v. 121, p. 857–868.
- Ahmadzadeh, G., Jahangiri, A., Lentz, D., and Mojtahedi, M., 2010, Petrogenesis of Pliocene-Quaternary post-collisional ultrapotassic volcanism in NW of Marand, NW Iran: *Journal of Asian Earth Sciences*, v. 39, p. 37–50.
- Ahmed, W., Khan, S.N., and Schmidt, R.G., 1972, Geology and copper mineralization of the Saindak quadrangle, Chagai district, West Pakistan: U.S. Geological Survey Professional Paper 716–A, 21 p., scale 1:50,000, available at <http://pubs.er.usgs.gov/publication/pp716A>.
- Akay, E., 2009, Geology and petrology of the Simav magmatic complex (NW Anatolia) and its comparison with the Oligo-Miocene granitoids in NW Anatolia—Implications on Tertiary tectonic evolution of the region: *International Journal of Earth Sciences*, v. 98, p. 1655–1675.
- Akçay, M., and Gündüz, Ö., 2004, Porphyry Cu-Au mineralisation associated with a multi-phase intrusion, and related replacement fronts in limestones in an island-arc setting near the Gümüşhane village (Artvin) in the eastern Black Sea Province (Turkey): *Chemie der Erde—Geochemistry*, v. 64, p. 359–383.
- Akçay, M., and Moon, C.J., 2004, The environmental impact of mining in the Pontides, Turkey—Reconnaissance sampling and GIS-based analysis: *Geochemistry—Exploration, Environment, Analysis*, v. 4, p. 1–12.
- Akiman, O., Erler, A., Göncüoğlu, M.C., Güleç, N., Geven, A., Türel, T.K., and Kadioğlu, Y.K., 1993, Geochemical characteristics of granitoids along the western margin of the Central Anatolian Crystalline Complex and their tectonic implications: *Geological Journal*, v. 28, p. 371–382.
- Akın, Hikmet, 1978, Geologie, Magmatismus und Lagerstättenbildung im ostpontischen Gebirge-Türkei aus der Sicht der Plattentektonik: *Geologische Rundschau*, v. 68, p. 253–283. [In German.]
- Akıncı, Ö.T., 1984, The Eastern Pontide volcano-sedimentary belt and associated massive sulphide deposits, *in* Dixon, J.E., and Robertson, A.H.F., eds., *The geological evolution of the eastern Mediterranean*: London, Geological Society Special Publication 17, p. 415–428.
- Akıncı, Ö.T., 2004, The porphyry copper deposits of Turkey: International Symposium on Eastern Mediterranean Geology, 5th, Thessaloniki, Greece, April 14–20, 2004 [Proceedings], p. 1375–1378.
- Aktaş, G., and Robertson, A.H.F., 1984, The Maden complex, SE Turkey—Evolution of a Neotethyan active margin, *in* Dixon, J.E., and Robertson, A.H.F., eds., *The Geological evolution of the eastern Mediterranean*: London, Geological Society Special Publication 17, p. 375–402.
- Aktimur, T., Tekirli, M.E., and Yurdakul, M.E., 1990, Geology of the Sivas-Erzincan Tertiary basin: *Maden Tetkik ve Arama Dergisi*, v. 111, p. 25–36. [In Turkish, English abstract.]
- Alacer Gold, 2012, Karakartal: Alacer Gold Web page, accessed July 11, 2012, at <http://alacergold.com/en/projects/karakartal>.
- Alaminia, Z., Karimpour, M.H., and Haidarian Shahri, M.R., 2011, Geology, alteration, mineralization and geochemical study in Kalateh Taimour area, NE Iran: Mashhad, Iran, Ferdowsi University of Mashhad, *Journal of Economic Geology*, v. 2, p. 217–234. [In Persian, English abstract.]
- Alamos Gold, Inc., 2010, Alamos Gold Inc. completes acquisition of Agi Dagi and Kirazli gold projects in northwestern Turkey and announces 2010 budget for Turkish operations: Toronto, Alamos Gold, Inc., press release, January 6, 2012, 1 p., accessed January 4, 2012, at <http://www.alamosgold.com/node/148>.
- Alamos Gold, Inc., 2012, December 2012 corporate presentation: Alamos Gold, Inc., corporate presentation, 35 p.
- Alavi, M., 1994, Tectonics of the Zagros orogenic belt of Iran—New data and interpretations: *Tectonophysics*, v. 229, p. 211–238.
- Alavi, M., 1996, Tectonostratigraphic synthesis and structural style of the Alborz mountain system in northern Iran: *Journal of Geodynamics*, v. 21, p. 1–33.
- Al-Bassam, K.S., 2008, Mineral Resources of Kurdistan Region, Iraq: GEOSURV report, Baghdad, 26 p.
- Al-Bassam, K.S., and Hak, J., 2006, Metallic and industrial rocks and minerals, *in* Jassim, S.Z., and Goff, J.C., eds., *Geology of Iraq*: Dolin, Prague (and Moravian Museum, Czech Republic), p. 288–302.

- Aldanmaz, E., Pearce, J.A., Thirlwall, M.F., and Mitchell, J.G., 2000, Petrogenetic evolution of late Cenozoic, post-collision volcanism in western Anatolia, Turkey: *Journal of Volcanology and Geothermal Research*, v. 102, p. 67–95.
- Aliani, F., Alirezaei, A., Moradian, A., and Abbasloo, Z., 2009, Geochemistry and petrography of the Meiduk porphyry copper deposit, Kerman, Iran: *Australian Journal of Basic and Applied Sciences*, v. 3, p. 3786–3800.
- Alirezaei, S., and Mohammadzadeh, Z., 2009, Hydrothermal alteration-mineralization at Chahfiroozeh porphyry copper deposit, Kerman Province, southern Iran [abs.]: Geological Association of Canada 2009 Joint Assembly, Toronto, 2009 [Proceedings].
- Alirezaei, S., Ebrahimi, S., and Pan, Y., 2008, Fluid inclusion characteristics of epithermal precious metal deposits in the Arasbaran metallogenic zone, northwestern Iran: *Asian Current Research on Fluid Inclusions Meeting*, 2d, Kharagpur, India, November 12–14, 2008 [Proceedings].
- Alirezaei, S., Ashrafpour, E., and Ansdell, K.M., 2009, Hydrothermal fluid evolution during vein formation in Arghash gold prospect, northeast of Iran [abs.]: American Geophysical Union, Spring meeting, 2009 [Proceedings], abstract V23A-03.
- Aliyari, F., Rastad, E., and Mohajjel, M., 2012, Gold deposits in the Sanandaj-Sirjan zone—Orogenic gold deposits or intrusion-related gold systems?: *Resource Geology*, v. 62, p. 296–315.
- Allen, M.B., and Armstrong, H.A., 2008, Arabia-Eurasia collision and the forcing of mid-Cenozoic global cooling: *Palaeogeography, Palaeoclimatology, Palaeoecology*, v. 265, p. 52–58.
- Allen, M.B., Blanc, E.J-P., Walker, R., Jackson, J., Talebian, M., and Ghassemi, M.R., 2006, Contrasting styles of convergence in the Arabia-Eurasia collision—Why escape tectonics does not occur in Iran, *in* Dilek, Yildirim, and Pavlides, Spyros, eds., *Postcollisional tectonics and magmatism in the Mediterranean region and Asia*: Geological Society of America Special Paper 409, p. 579–589.
- Altunkaynak, Ş., 2007, Collision-driven slab breakoff magmatism in northwestern Anatolia, Turkey: *Journal of Geology*, v. 115, p. 63–82.
- Altunkaynak, Ş., and Genç, Ş.C., 2008, Petrogenesis and time-progressive evolution of the Cenozoic continental volcanism in the Biga Peninsula, NW Anatolia (Turkey): *Lithos*, v. 102, p. 316–340.
- Amidi, S.M., and Michel, R., 1985, Cenozoic magmatism of the Surk area (central Iran)—Stratigraphy, petrography, geochemistry and their geodynamic implications: *Géologie Alpine*, v. 61, p. 1–16.
- Amidi, S.M., Emami, M.H., and Michel, R., 1984, Alkaline character of Eocene volcanism in the middle part of central Iran and its geodynamic situation: *Geologische Rundschau*, v. 73, p. 917–932.
- Anglo Asian Mining PLC, 2007, Annual report and accounts 2006: Anglo Asian Mining PLC, 32 p.
- Anglo Asian Mining PLC, 2009, Annual report and accounts 2008: Anglo Asian Mining PLC, 40 p.
- Anglo Asian Mining PLC, 2011, Annual report and accounts 2010: Anglo Asian Mining PLC, 48 p.
- Antofagasta PLC, 2010, Mining exploration and projects: Antofagasta PLC Web page, accessed August 27, 2012, at http://www.antofagasta.co.uk/interior/operations/f_explora.html.
- Arculus, R.J., 2003, Use and abuse of the terms calcalkaline and alkalic: *Journal of Petrology*, v. 44, p. 929–935.
- Arfania, R., and Shahriari, S., 2009, Role of southeastern Sanandaj-Sirjan Zone in the tectonic evolution of Zagros Orogenic Belt: *Island Arc*, v. 18, p. 555–576.
- Arian, M., Alizadeh, H., and Noroozpour, H., 2011, Satellite geometry of faults and fractures and its relationship with porphyry deposits in northern parts of Dahaj-Sardoieyh belt, south of Iran: *Indian Journal of Science and Technology*, v. 4, no. 10, p. 1303–1306.
- Ariana Resources PLC, 2013, Maiden JORC resource at Sanlinbas and Ardala, north-east Turkey: Ariana Resources Web page, accessed August 6, 2013, at <http://www.arianaresources.com/investors/news-releases/2013/316-maiden-jorc-resource-at-salinbas-and-ardala-north-east-turkey>.
- Arikan, Y., 1975, The geology and petroleum prospects of the Tuz Gölü basin: *Turkey Mineral Research and Exploration Institute Bulletin, foreign edition*, v. 85, p. 17–37.
- Arjmandzadeh, R., Karimpour, M.H., Mazaheri, S.A., Santos, J.F., Medina, J.M., and Homam, S.M., 2011a, Sr-Nd isotope geochemistry and petrogenesis of the Chah-Shaljami granitoids (Lut block, eastern Iran): *Journal of Asian Earth Sciences*, v. 41, p. 283–296.
- Arjmandzadeh, R., Karimpour, M.H., Mazaheri, S.A., Santos, J.F., Medina, J.M., and Homan, S.M., 2011b, Two-sided asymmetric subduction—Implications for tectonomagmatic and metallogenic evolution of the Lut block, eastern Iran: Mashhad, Iran, Ferdowsi University of Mashhad, *Journal of Economic Geology*, v. 3, p. 93.
- Arribas, A., Jr., Hedenquist, J.W., Tetsumaru, I., Toshinori, O., Concepción, R.A., and Garica, J.S., 1995, Contemporaneous formation of adjacent porphyry and epithermal Cu-Au deposits over 300 ka in northern Luzon, Philippines: *Geology*, v. 23, no. 4, p. 337–340.

- Arslan, M., and Aliyazicioglu, I., 2001, Geochemical and petrological characteristics of the Kale (Gümüşhane) volcanic rocks—Implications for the Eocene evolution of Eastern Pontide arc volcanism, northeast Turkey: *International Geology Review*, v. 43, p. 595–610.
- Arslan, M., and Arslan, Z., 2006, Mineralogy, petrography and whole-rock geochemistry of the Tertiary granitic intrusions in the Eastern Pontides, Turkey: *Journal of Asian Earth Sciences*, v. 27, p. 177–193.
- Arvin, M., Pan, Y., Dargahi, S., Malekizadeh, A., and Babaei, A., 2007, Petrochemistry of the Siah-Kuh granitoid stock southwest of Kerman, Iran—Implications for initiation of Neotethys subduction: *Journal of Asian Earth Sciences*, v. 30, p. 474–489.
- Asghari, O., and Hezarkhani, A., 2010, Investigations of alteration zones based on fluid inclusion microthermometry at Sungun porphyry copper deposit, Iran: *Bulletin of the Mineral Research and Exploration Institute of Turkey*, v. 140, p. 19–34.
- Aslan, M., Cengiz, İ., Özküçük, S., Yiğmatepe, M., Kesgin, Ö., Tuvar, O., Deniz, N., Çakir, C., and Konak, N., 2010, The geological features of Dutlu (Oltu-Erzurum-NE Turkey) porphyry Cu mineralisation [abs.]: Ankara, Turkey, Chamber of Geological Engineers, Proceedings of the 63rd Geological Congress of Turkey, April 5–9, 2010, 1 p.
- Atapour, H., and Aftabi, A., 2007, The geochemistry of gossans associated with Sarcheshmeh porphyry copper deposit, Rafsanjan, Kerman, Iran—Implications for exploration and the environment: *Journal of Geochemical Exploration*, v. 93, p. 47–65.
- Ates, A., Kearey, P., and Tufan, S., 1999, New gravity and magnetic anomaly maps of Turkey: *Geophysical Journal International*, v. 136, p. 499–502.
- Axen, G.J., Lam, P.S., Grove, M., Stockli, D.F., and Hassanzadeh, J., 2001, Exhumation of the west-central Alborz Mountains, Iran—Caspian subsidence, and collision-related tectonics: *Geology*, v. 29, p. 559–562.
- Ayati, F., Yavuz, F., Noghreyan, M., Haroni, H.A., and Yavuz, R., 2008, Chemical characteristics and composition of hydrothermal biotite from the Dalli porphyry copper prospect, Arak, Central Province of Iran: *Mineralogy and Petrology*, v. 94, p. 107–122.
- Ayati, F., Yavuz, F., Asadi, H.H., Richards, J.P., and Jourdan, Fred, 2013, Petrology and geochemistry of calc-alkaline volcanic and subvolcanic rocks, Dalli porphyry copper-gold deposit, Markazi Province, Iran: *International Geology Review*, v. 55, p. 158–184.
- Aydin, N.S., Göncüoğlu, M.C., and Erler, A., 1998, Latest Cretaceous magmatism in the Central Anatolian Crystalline Complex—Review of field, petrographic and geochemical features: *Turkish Journal of Earth Sciences*, v. 7, p. 259–268.
- Aydin, F., Karsli, O., and Chen, B., 2008, Petrogenesis of the Neogene alkaline volcanics with implications for post-collisional lithospheric thinning of the Eastern Pontides, NE Turkey: *Lithos*, v. 104, p. 249–266.
- Azerbaijan Ministry of Ecology and Natural Resources, [2006?], Minerals of Azerbaijan: Azerbaijan Ministry of Ecology and Natural Resources Web page accessed March 11, 2013, at <http://eco.gov.az/en/faydaliqazintilar.php>.
- Azizi, H., Asahara, Y., Mehrabi, B., and Chung, S.L., 2011, Geochronological and geochemical constraints on the petrogenesis of high-K granite from the Suffi Abad area, Sanandaj-Sirjan Zone, NW Iran: *Chemie der Erde*, v. 71, p. 363–376.
- Azizi, H., and Jahangiri, A., 2008, Cretaceous subduction-related volcanism in the northern Sanandaj-Sirjan Zone, Iran: *Journal of Geodynamics*, v. 45, p. 178–190.
- Azizi, H., and Moinevaziri, H., 2009, Review of the tectonic setting of Cretaceous to Quaternary volcanism in northwestern Iran: *Journal of Geodynamics*, v. 47, p. 167–179.
- Azizi, H., Rsaouli, A.A., and Babaei, K., 2007, Using SWIR bands from ASTER for discrimination of hydrothermal altered minerals in the northwest of Iran (Se-Sanandaj City)—A key for exploration of copper and gold mineralization: *Research Journal of Applied Sciences*, v. 2, p. 763–768.
- Babaie, H.A., Ghazi, A.M., Babaei, A., La Tour, T.E., and Hassanipak, A.A., 2001, Geochemistry of arc volcanic rocks of the Zagros Crush Zone, Neyriz, Iran: *Journal of Asian Earth Sciences*, v. 19, p. 61–76.
- Baba-Zade, V.M., Makhmudov, A.I., and Ramazanov, V.G., 1990, Copper and molybdenum porphyry deposits: Baku, Azerbaijan State Publishing House, 353 p. [In Russian.]
- Baharifar, A., Moinevaziri, H., Bellon, H., and Piqué, A., 2004, The crystalline complexes of Hamadan (Sanandaj-Sirjan Zone, western Iran)—Metasedimentary Mesozoic sequences affected by Late Cretaceous tectono-metamorphic and plutonic events: *Comptes Rendus Geoscience*, v. 336, p. 1443–1452.
- Ballato, P., Uba, C.E., Landgraf, A., Strecker, M.R., Sudo, M., Stockli, D.F., Friedrich, A., and Tabatabaei, S.H., 2011, Arabia-Eurasia continental collision—Insights from late Tertiary foreland-basin evolution in the Alborz Mountains, northern Iran: *Geological Society of America Bulletin*, v. 123, p. 106–131.
- Barnett, W., Doerksen, G., Murphy, B., Nowak, M., Pilotto, D., Rykaart, M., and Bonson, C., 2011, Preliminary economic assessment on the Taç and Çorak deposits, Yusufeli property, Artvin Province, Turkey: SRK Consulting technical report prepared for Mediterranean Resources, Ltd., 199 p., addenda and appendix.

- Barzegar, H., 2007, Geology, petrology and geochemical characteristics of alteration zones within the Seridune prospect, Kerman, Iran: Aachen, Germany, Rheinisch Westfälischen Technische Hochschule (RWTH) Aachen University, Ph.D. dissertation, 180 p.
- Barzegar, H., 2008, Relationship between biotite composition and tectonomagmatic affinity of the granodiorite intrusion at the Seridune prospect, Iran [abs.]: International Geological Congress, 33d, Oslo, August 6–14, 2008.
- Bascombe, L., Shoemaker, S.J., Mach, L., Benbow, R., and Altman, K.A., 2012, Technical report on the Çöpler mineral resource update, Erzincan Province, Turkey: Alacer Gold, Inc., Canadian National Instrument 43–101 Technical Report, 154 p.
- Bastani, M., Malehmir, A., Ismail, N., Pedersen, L.B., and Hedjazi, F., 2009, Delineating hydrothermal stockwork copper deposits using controlled-source and radio-magnetotelluric methods—A case study from northeast Iran: *Geophysics*, v. 74, no. 5, p. B167–B181.
- Bates, R.L., and Jackson, J.A., eds., 1987, *Glossary of geology* (3rd ed.): Alexandria, Va., American Geological Institute, 788 p.
- Bawiec, W.J., and Spanski, G.T., 2012, Quick-start guide for version 3.0 of EMINERS—Economic mineral resource simulator: U.S. Geological Survey Open-File Report 2009–1057, 26 p., available at <http://pubs.usgs.gov/of/2009/1057/>. (This report supplements USGS OFR 2004–1344.)
- Bazargani-Guilani, K., Parchekani, M., and Nekouvaght Tak, M.A., 2008, Mineralization in the Taroum Mountains with special reference to the Barik-Ab Pb-Zn (Cu) deposit, west central Alborz, Iran: IASME/WSEAS International Conference on Geology and Seismology, 2nd, (GES '08), Cambridge, United Kingdom, February 23–25, 2008, p. 55–62.
- Bazin, D., and Hübner, H., 1969a, Copper deposits in Iran: Geological Survey of Iran Report 13, 232 p.
- Bazin, D., and Hübner, H., 1969b, La région cuprifère à gisements porphyriques de Kerman (Iran): *Mineralium Deposita*, v. 4, p. 200–212.
- Bektaş, O., Yılmaz, C., Taşlı, K., Akdağ, K., and Özgür, S., 1995, Cretaceous rifting of the Eastern Pontide carbonate platform (NE Turkey)—The formation of carbonate breccias and turbidites as evidence of a drowned platform: *Giornali di Geologia*, v. 57, p. 233–244.
- Berberian, F., and Berberian, M., 1981, Tectonoplutonic episodes in Iran, *in* Gupta, H.K., and Delany, F.M., eds., *Zagros, Hindu Kush, Himalaya—Geodynamic evolution*: American Geophysical Union, *Geodynamics Series*, v. 3, p. 5–32.
- Berberian, F., Muir, I.D., Pankhurst, R.J., and Berberian, M., 1982, Late Cretaceous and early Miocene Andean-type plutonic activity in northern Makran and central Iran: *Journal of the Geological Society*, v. 139, p. 605–614.
- Berberian, M., and King, G.C.P., 1981, Towards a paleogeography and tectonic evolution of Iran: *Canadian Journal of Earth Science*, v. 18, p. 210–265.
- Berger, B.R., Ayuso, R.A., Wynn, J.C., and Seal, R.R., 2008, Preliminary model of porphyry copper deposits: U.S. Geological Survey Open-File Report 2008–1321, 55 p., available at <http://pubs.usgs.gov/of/2008/1321/>.
- Bhutta, A.M., 2004, Porphyry type systems—Configuration and distribution in the Chagai Metallogenic Belt with a reference to Koh-i-Dalil copper deposit, Balochistan, Pakistan: *Geological Bulletin of University of Peshawar*, v. 37, p. 179–189.
- Biabangard, H., and Moradian, A., 2008, Geology and geochemical evaluation of Taftan Volcano, Sistan and Baluchestan Province, southeast of Iran: *Chinese Journal of Geochemistry*, v. 27, p. 356–369.
- Biabangard, H., Boomeri, M., and Salare, M.A., 2011, Geochemical, petrological and environmental tectonomagmatic dykes in north of Rabor (Southeast of Iran) [abs.]: Japan Geoscience Union, Makuhari, Chiba, Japan, May 22–27, 2011 [Proceedings].
- Bogie, I., Khosrawi, K., and Talebi, B., 2005, Geological results from the drilling of the Northwest Sabalan Geothermal Project, Iran: World Geothermal Congress, Antalya, Turkey, April 24–29, 2005 [Proceedings], p. 1–5.
- Boomeri, M., Lashkaripour, G.R., and Gorgij, M.N., 2005, F and Cl in biotites from Zahedan granitic rocks: *Iranian Journal of Crystallography and Mineralogy*, v. 13, [16] p. [In Persian, English abstract.]
- Boomeri, M., Mizuta, T., Ishiyama, D., and Nakashima, K., 2006, Fluorine and chlorine in biotite from the Samwosar granitic rocks, northeastern Iran: *Iranian Journal of Science and Technology, Transaction A*, v. 30, p. 111–125.
- Boomeri, M., Nakashima, K., and Lentz, D.R., 2009, The Miduk porphyry Cu deposit, Kerman, Iran—A geochemical analysis of the potassic zone including halogen element systematics related to Cu mineralization processes: *Journal of Geochemical Exploration*, v. 103, p. 17–29.
- Boomeri, M., Ishiyama, D., Mizuta, T., Matsubaya, O., and Lentz, D.R., 2010a, Carbon and oxygen isotopic systematics in calcite and dolomite from the Sangan iron skarn deposit, northeastern Iran: *Iran, Journal of Sciences*, v. 21, p. 213–224.
- Boomeri, M., Nakashima, K., and Lentz, D.R., 2010b, The Sarcheshmeh porphyry copper deposit, Kerman, Iran—A mineralogical analysis of the igneous rocks and alteration zones including halogen element systematics related to Cu mineralization processes: *Ore Geology Reviews*, v. 38, p. 367–381.

- Boomeri, M., Nakashima, K., and Abasszadeh, Gh., 2011a, Hydrothermal alteration and mineralization [sic] in Abdar Caldera, Kerman Province, Iran [abs.]: Japan Geoscience Union, Makuhari, Chiba, Japan, May 22–27, 2011 [Proceedings].
- Boomeri, M., Nakashima, K., and Gholami, M.J., 2011b, Bazman epithermal gold-silver mineralization, Sistan and Baluchestan Province, Iran [abs.]: Japan Geoscience Union, Makuhari, Chiba, Japan, May 22–27, 2011 [Proceedings].
- Bortnikov, N.S., Genkin, A.D., and Troneva, N.V., 1993, Tennantite decomposition—Evidence from the Kedabek copper deposit, Azerbaijan: *Mineralogy and Petrology*, v. 47, p. 171–181.
- Bortolotti, V., and Principi, G., 2005, Tethyan ophiolites and Pangea break-up: *The Island Arc*, v. 14, p. 442–470.
- Boulin, J., 1991, Structures in southwest Asia and evolution of the eastern Tethys: *Tectonophysics*, v. 196, p. 211–268.
- Bozkurt, E., and Mittweide, S.K., 2001, Introduction to the geology of Turkey—A synthesis: *International Geology Review*, v. 43, p. 578–594.
- Bozkurt, E., Winchester, J.A., and Piper, J.D.A., 2000, Introduction, *in* Bozkurt, E., Winchester, J.A., and Piper, J.D.A., eds., *Tectonics and magmatism in Turkey and the surrounding area*: London, Geological Society Special Publication 173, p. i–xvii.
- Boztuğ, D., and Arehart, G.B., 2007, Oxygen and sulfur isotope geochemistry revealing a significant crustal signature in the genesis of the post-collisional granitoids in central Anatolia, Turkey: *Journal of Asian Earth Sciences*, v. 30, p. 403–416.
- Boztuğ, D., Kuşcu, İ., Erçin, A.İ., Avcı, N., and Şahin, S.Y., 2003, Mineral deposits associated with the pre-, syn- and post-collisional granitoids of the Neo-Tethyan convergence system between the Eurasian and Anatolian Plates in NE and central Turkey, *in* Eliopoulos, D., and others, eds., *Mineral exploration and sustainable development*: Rotterdam, Millpress, p. 1141–1144.
- Boztuğ, D., Jonckheere, R., Wagner, G.A., and Yeğingil, Z., 2004, Slow Senonian and fast Paleocene-Early Eocene uplift of the granitoids in the central Eastern Pontides, Turkey—Apatite fission-track results: *Tectonophysics*, v. 382, p. 213–228.
- Boztuğ, D., Erçin, A.İ., Kuruçelik, M.K., Göç, D., Kömür, İ., and İskenderoğlu, A., 2006, Geochemical characteristics of the composite Kaçkar batholith generated in a Neo-Tethyan convergence system, Eastern Pontides, Turkey: *Journal of Asian Earth Sciences*, v. 27, p. 286–302.
- Boztuğ, D., Harlavan, Y., Arehart, G.B., Satir, M., and Necmettin, A., 2007, K-Ar age, whole-rock and isotope geochemistry of A-type granitoids in the Divriği-Sivas region, eastern-central Anatolia, Turkey: *Lithos*, v. 97, p. 193–218.
- Boztuğ, D., Jonckheere, R.C., Heizler, M., Ratschbacher, L., Harlavan, Y., and Tichomirova, M., 2009, Timing of post-obduction granitoids from intrusion through cooling to exhumation in central Anatolia, Turkey: *Tectonophysics*, v. 473, p. 223–233.
- Breitzman, L.L., Birnie, R.W., and Johnson, G.D., 1983, Fission-track ages of the Chagai intrusives, Baluchistan, Pakistan: *Geological Society of America Bulletin*, v. 94, p. 253–258.
- British Geological Survey, 2006a, Minerals in Afghanistan—The Aynak copper deposit: Afghanistan Geological Survey brochure, [6] p., accessed September 27, 2012, at http://www.bgs.ac.uk/afghanminerals/docs/Aynak_A4.pdf.
- British Geological Survey, 2006b, Minerals in Afghanistan—The potential for copper: Afghanistan Geological Survey brochure, [6] p., accessed November 26, 2013, at http://www.bgs.ac.uk/AfghanMinerals/docs/copper_A4.pdf.
- Brousse, R., and Vaziri, H.M., 1982, L'association shoshonitique du Damavand (Iran): *Geologische Rundschau* v. 71, p. 687–702. [In French, English abstract.]
- Brown, T.J., Shaw, R.A., Bide, T., Petavrazi, E., Raycraft, E.R., and Walters, A.S., 2013, World Mineral Production 2007–2011: British Geological Survey Natural Environment Research Council, 85 p.
- Bureau of Land Management, 2015, BLM Manual MS2800 Glossary of Terms: BLM Web page, accessed April 15, 2015, at http://www.blm.gov/wo/st/en/info/regulations/Instruction_Memos_and_Bulletins/blm_manual.html.
- CAE Mining, 2012, Updated mineral resources, Gedabek mineral deposit, Republic of Azerbaijan: Technical report prepared for Azerbaijan International Mining Company, Ltd., 50 p.
- Calagari, A.A., 2003, Stable isotope (S, O, H and C) studies of the phyllic and potassic-phyllic alteration zones of the porphyry copper deposit at Sungun, East Azarbaijan, Iran: *Journal of Asian Earth Sciences*, v. 21, p. 767–780.
- Calagari, A.A., 2004, Fluid inclusion studies in quartz veinlets in the porphyry copper deposit at Sungun, East-Azarbaijan, Iran: *Journal of Asian Earth Sciences*, v. 23, p. 179–189.
- Calagari, A.A., and Hosseinzadeh, G., 2006, The mineralogy of copper-bearing skarn to the east of the Sungun-Chay River, East Azarbaijan, Iran: *Journal of Asian Earth Sciences*, v. 28, p. 423–438.
- Camp, V.E., and Griffis, R.J., 1982, Character, genesis and tectonic setting of igneous rocks in the Sistan suture zone, eastern Iran: *Lithos*, v. 15, p. 221–239.
- Çamur, M.Z., Güven, İ.H., and Er, M., 1996, Geochemical characteristics of the eastern Pontide volcanics, Turkey—An example of multiple volcanic cycles in the arc evolution: *Turkish Journal of Earth Sciences*, v. 5, p. 123–144.

- Canby, V.M., 2007, A brief review of metal discoveries in the Tethyan belt since 1992, *in* Andrew, C.J., ed., *Digging deeper: Dublin, Irish Association for Economic Geology, Society for Geology Applied to Mineral Deposits Biennial Meeting, 9th, Dublin, August 20–23, 2007* [Proceedings], p. 97–99.
- Centerra Gold, Inc., 2012, Corporate: Centerra Gold, Inc., Web page accessed October 24, 2012, at <http://www.centerragold.com/corporate/corporate>.
- Chakrabarti, R., Basu, A.R., and Ghatak, A., 2012, Chemical geodynamics of western Anatolia: *International Geology Review*, v. 54, p. 1–22.
- Chatroodi, A.Y., Karizaki, H.S., and Ghorbani, M.R., 2010, Petrology and geochemistry of volcanic rocks in Hoz-e-Soltan area: *World Academy of Science, Engineering and Technology*, v. 71, p. 44–48.
- Chesser Resources, Ltd., 2011a, Karaayi, Turkey: Chesser Resources, Ltd., Web page accessed January 4, 2012, at http://www.chesserresources.com.au/karaayi_turkey.
- Chesser Resources, Ltd., 2011b, Sisorta, Turkey: Chesser Resources, Ltd., Web page accessed January 4, 2012, at http://www.chesserresources.com.au/sisorta_turkey.
- Cliff, D.C., 2007, The Bursa East area, Bursa and Kutahya Provinces, western Anatolia, Turkey: DC Minerals Consultants technical report prepared for Empire Mining Corp., 53 p.
- Çolakoğlu, A.R., and Arehart, G.B., 2010, The petrogenesis of Sariçimen (Çaldıran-Van) quartz monzodiorite—Implication for initiation of magmatism (Late Medial Miocene) in the east Anatolian collision zone, Turkey: *Lithos*, v. 119, p. 607–620.
- Committee for Mineral Reserves International Reporting Standards, 2006, International reporting template for the public reporting of exploration results, mineral resources, and mineral reserves: Committee for Mineral Reserves International Reporting Standards (CRIRSCO), 33 p.
- Cooke, D.R., Hollings, P., and Walshe, J.L., 2005, Giant porphyry deposits—Characteristics, distribution, and tectonic controls: *Economic Geology*, v. 100, no. 5, p. 801–818.
- Cox, D.P., 1986a, Descriptive model of porphyry Cu, *in* Cox, D.P., and Singer, D.A., eds., *Mineral deposit models: U.S. Geological Survey Bulletin 1693*, p. 76., available at <http://pubs.usgs.gov/bul/b1693/>.
- Cox, D.P., 1986b, Descriptive model of porphyry Cu-Au, *in* Cox, D.P., and Singer, D.A., eds., *Mineral deposit models: U.S. Geological Survey Bulletin 1693*, p. 110., available at <http://pubs.usgs.gov/bul/b1693/>.
- Cox, D.P., and Singer, D.A., 1986, *Mineral deposit models: U.S. Geological Survey Bulletin 1693*, 379 p., available at <http://pubs.usgs.gov/bul/b1693/>.
- Cunningham, C.G., Zappettini, E.O., Vivallo S., W., Celada, C.M., Quispe, Jorge, Singer, D.A., Briskey, J.A., Sutphin, D.M., Gajardo M., M., Diaz, A., Portigliati, C., Berger, V.I., Carrasco, R., and Schulz, K.J., 2008, Quantitative mineral resource assessment of copper, molybdenum, gold, and silver in undiscovered porphyry copper deposits in the Andes Mountains of South America: U.S. Geological Survey Open-File Report 2008–1253, 282 p., available at <http://pubs.usgs.gov/of/2008/1253/>.
- Dabiri, R., Emami, M.H., Mollaei, H., Chen, B., Vosogi Abedini, M., Omran, N.R., and Ghaffari, M., 2011, Quaternary post-collision alkaline volcanism NW of Ahar (NW Iran)—Geochemical constraints of fractional crystallization process: *Geologica Carpathica*, v. 62, p. 547–562.
- Darbani, M.H., Karimpour, M.H., Malekzadeh Shafaroudi, A.M., and Mazlumi Bajestani, A., 2005, Geology, alteration, mineralization and geochemistry of Gazu prospect area, southeast of Tabas [abs.]: Ferdowsi University of Mashhad, accessed November 20, 2012, at http://profdoc.um.ac.ir/pubs_files/p11025154.pdf.
- Dargahi, S., Arvin, M., Pan, Y., and Babaei, A., 2010, Petrogenesis of post-collisional A-type granitoids from the Urumieh-Dokhtar magmatic assemblage, southwestern Kerman, Iran—Constraints on the Arabian-Eurasian continental collision: *Lithos*, v. 115, p. 190–204.
- Delaloye, M., and Desmons, J., 1980, Ophiolites and melange terranes in Iran—A geochronological study and its paleotectonic implications: *Tectonophysics*, v. 68, p. 83–111.
- Delaloye, M., and Bingöl, E., 2000, Granitoids from western and northwestern Anatolia—Geochemistry and modeling of geodynamic evolution: *International Geology Review*, v. 42, p. 241–268.
- Delibaş, O., and Genç, Y., 2012, Re-Os molybdenite ages of granitoid-hosted Mo-Cu occurrences from central Anatolia (Turkey): *Ore Geology Reviews*, v. 44, p. 39–48.
- Demir Export A.S., 2013, Sivas-Bakırtepe Gold Project: Demir Export A.S. Web page, accessed December 4, 2013, at <http://www.demirexport.com/en/operational-fields/new-projects/balikesir-samli-copper-project/>.
- Derakhshani, R., and Abdolzadeh, M., 2009, Geochemistry, mineralization and alteration zones of Darrehzar porphyry copper deposit, Kerman, Iran: *Journal of Applied Sciences*, v. 9, p. 1628–1646.
- Derakhshani, R., and Mehrabi, A., 2009, Geologically constrained fuzzy mapping of porphyry copper mineralization potential, Meiduk district, Iran: *Trends in Applied Sciences Research*, v. 4, p. 229–240.

- Dercourt, J., Zonenshain, L.P., Ricou, L.-E., Kazmin, V.G., Le Pichon, X., Knipper, A.L., Grandjacquet, C., Sbertshikov, I.M., Geysant, J., Lepvrier, C., Pechersky, D.H., Boulin, J., Sibuet, J.-C., Savostin, L.A., Sorokhtin, O., Westphal, M., Bazhenov, M.L., Lauer, J.P., and Biju-Duval, B., 1986, Geological evolution of the Tethys Belt from the Atlantic to the Pamirs since the Lias: *Tectonophysics*, v. 123, p. 241–315.
- Desmons, J., and Beccaluva, L., 1983, Mid-ocean ridge and island-arc affinities in ophiolites from Iran—Palaeographic implications: *Chemical Geology*, v. 39, p. 39–63.
- Dewey, J.F., Pitman, W.C., III, Ryan, W.B.F., and Bonnin, J., 1973, Plate tectonics and the evolution of the Alpine system: *Geological Society of America Bulletin*, v. 84, p. 3137–3180.
- Dilek, Y., 2010, Introduction—Eastern Mediterranean geodynamics: *International Geology Review*, v. 52, p. 111–116.
- Dilek, Y., Thy, P., Hacker, B., and Grundvig, S., 1999, Structure and petrology of Tauride ophiolites and mafic dike intrusions (Turkey)—Implications for the Neotethyan Ocean: *Geological Society of America Bulletin*, v. 156, p. 929–941.
- Dilek, Y., Imamverdiyev, N., and Altunkaynak, Ş., 2010, Geochemistry and tectonics of Cenozoic volcanism in the Lesser Caucasus (Azerbaijan) and the peri-Arabian region—Collision-induced mantle dynamics and its magmatic fingerprint: *International Geology Review*, v. 52, p. 536–578.
- Doeblich, J.L., and Wahl, R.R., 2006, Geologic and mineral resource map of Afghanistan: U.S. Geological Survey Open-File Report 2006–1038, scale 1:850,000, available at <http://pubs.usgs.gov/of/2006/1038/>.
- Dorsa PLC, 2011, Shadan: Dorsa PLC Web page, accessed December 20, 2011, at <http://www.dorsapl.com/en/7-exploration-projects/62-shadan.html>.
- Dorsa PLC, 2012a, Rio Tinto report of Dalli: Dorsa PLC Web page, accessed July 25, 2012, at <http://www.dorsapl.com/en/dalli-cu-au/reports.html>, 24 p.
- Dorsa PLC, 2012b, Kahang Cu-Mo porphyry: Dorsa PLC Web page, accessed September 20, 2012, at <http://www.dorsapl.com/en/component/content/article/7-exploration-projects/60-kahang-cu-mo-porphyry.html>.
- Dorsa PLC, 2012c, Qahan: Dorsa PLC Web page, accessed September 20, 2012, at <http://www.dorsapl.com/en/7-exploration-projects/70-qahan.html>.
- Dorsa PLC, 2012d, Zafarghand: Dorsa PLC Web page, accessed September 20, 2012, at <http://www.dorsapl.com/en/7-exploration-projects/64-zafarghand.html>.
- Dorsa PLC, 2012e, Zefreh: Dorsa PLC Web page, accessed September 20, 2012, at <http://www.dorsapl.com/en/7-exploration-projects/65-zefreh.html>.
- Dorsa PLC, 2012f, West Shirazkoh: Dorsa PLC Web page, accessed September 20, 2012, at <http://www.dorsapl.com/en/7-exploration-projects/68-west-shirazkoh.html>.
- Dorsa PLC, 2012g, Takht: Dorsa PLC Web page, accessed September 20, 2012, at <http://www.dorsapl.com/en/7-c>.
- Dorsa PLC, 2013, Dalli Cu-Au Mine: Dorsa PLC Web page, 17 p., accessed July 25, 2013 at <http://www.dorsapl.com/en/dalli-cu-au/reports.html>.
- Drew, L.J., Sutphin, D.M., Berger, Byron, Mars, J.C., Herrington, R.J., Billa, M., Kuşcu, I., Moon, C.J., and Richards, J.P., 2009, Preliminary porphyry Cu assessment for the Central Tethys region: *Geological Society of America Abstracts with Programs*, v. 42, no. 7, p. 611.
- Dumanlilar, H., Aydal, D., and Dumanlilar, Ö., 1999, Geology, mineralogy and geochemistry of sulphite mineralization in the Ispendere region (Malatya): *Mineral Resources Exploration Bulletin*, v. 121, p. 57–82.
- Duval, J.S., 2012, Version 3.0 of EMINERS—Economic mineral resource simulator: U.S. Geological Survey Open-File Report 2004–1344, available at <http://pubs.usgs.gov/of/2004/1344/>.
- Düzgören-Aydin, N.S., Malpas, J., Göncüoğlu, M.C., and Erler, A., 2001, A review of the nature of magmatism in central Anatolia during the Mesozoic post-collisional period: *International Geology Review*, v. 43, p. 695–710.
- Dykstra, J.D., and Birnie, R.W., 1979, Reconnaissance geologic mapping in Chagai Hills, Baluchistan, Pakistan, by computer processing of Landsat data: *American Association of Petroleum Geologists Bulletin*, v. 63, p. 1490–1503.
- Ebrahimi, S., 2011, Geology, mineralogy and fluid characteristics of the Masjed Daghi epithermal gold deposit, NW Iran [abs.]: *Geophysical Research Abstracts*, v. 13, abstract EGU2011-236.
- Eftekhari-Nezad, J., and McCall, G.J.H., 1993, Saravan quadrangle map: Tehran, Geological Survey of Iran, Sheet M13, scale 1:250,000.
- Einali, M., and Alirezai, S., 2005, Source of sulfur in Miveh Rood mineralized dykes and skarns, East Azerbaijan, NW Iran [abs.]: *Geological Survey of Iran Symposium on Geosciences, Exploration and Economic Geology*, 24th, Iran, 2005 [Proceedings].
- Einali, M., Bakker, R.J., Alirezai, S., and Mohammedzadeh, Z., 2011, Fluid inclusions and evolution of ore fluids in the Baghkhoshk porphyry copper system, Urumieh-Dokhtar Magmatic Belt, Iran: *European Current Research on Fluid Inclusions (ECROFI)*, 21st, Leoben, Austria, August 9–11, 2011 [Proceedings], *Berichte der Geologische Bundesanstalt, Abstracts*, v. 87, p. 80–81.

- Einaudi, M.T., 1982, Descriptions of skarns associated with porphyry copper plutons, southwestern North America, in Tittley, S.R., ed., *Advances in the geology of the porphyry copper deposits, southwestern North America*: Tucson, University of Arizona Press, p. 139–184.
- Eldorado Gold Corp., 2001, Sayacik reconnaissance drilling intersects 5.0 m of 8.2% Cu: Eldorado Gold Corp. press release August 8, 2001, accessed March 13, 2013, at <http://www.eldoradogold.com/s/NewsReleases.asp?ReportID=355146>.
- Eldorado Gold Corp., 2005, AS project grows—New extensive Cu/Au anomaly identified: Eldorado Gold Corp. press release, November 7, 2005, accessed October 23, 2012, at <http://www.eldoradogold.com/s/NewsReleases.asp?ReportID=355235>.
- Eldorado Gold Corp., 2009, Eldorado Gold 2009 exploration program: Eldorado Gold Corp. press release, March 27, 2009, accessed October 24, 2012, at <http://www.eldoradogold.com/s/NewsReleases.asp?ReportID=355351>.
- Elitok, Ö., Özgür, N., Drüppel, K., Dilek, Y., Platevoet, B., Guillou, H., Poisson, A., Scaillet, S., Satir, M., Siebel, W., Bardintzeff, J.-M., Deniel, C., and Yılmaz, K., 2010, Origin and geodynamic evolution of late Cenozoic potassium-rich volcanism in the Isparta area, southwestern Turkey: *International Geology Review*, v. 52, p. 454–504.
- Ellis, R., 1991, Sar Cheshmeh: *Mining Magazine*, v. 165, no. 4, p. 192–196.
- Empire Mining Corp., 2012, Drilling commences at Empire's Karapinar copper porphyry project, Turkey—New mapping shows porphyry to extend to at least 1,500 meters by 450 meters at surface: Empire Mining Corp. press release, October 30, 2012, 8 p., accessed November 5, 2012, at <http://www.infomine.com/index/pr/PB247215.PDF>.
- Empire Mining Corp., 2013a, Bursa-Demirtepe: Empire Mining Corp. Web page, accessed November 5, 2013, at http://www.empireminingcorp.com/s/Bursa_Demirtepe.asp.
- Empire Mining Corp., 2013b, Bursa-Karapinar: Empire Mining Corp. Web page, accessed November 5, 2013, at http://www.empireminingcorp.com/s/Bursa_Karapinar.asp.
- Engin, T., Özkan, Y.Z., Şener, F., and Toprak, B., 2000, Metallogenic map of Turkey: Ankara, Turkey, General Directorate of Mineral Research and Exploration, 3 sheets, scale 1:1,000,000.
- Erkül, F., and Erkül, S.T., 2010, Geology of the early Miocene Alaçamdağ (Dursunbey-Balikesir) magmatic complex and implications for the western Anatolian extensional tectonics: *Turkey Mineral Research and Exploration Institute Bulletin*, v. 141, p. 1–25.
- Esmaeily, D., Nédélec, A., Valizadeh, M.V., Moore, F., and Cotten, J., 2005, Petrology of the Jurassic Shah-Kuh granite (eastern Iran), with reference to tin mineralization: *Journal of Earth Sciences*, v. 25, p. 961–980.
- Esna-Ashari, A., Tiepolo, M., Valizadeh, M.-V., Hassanzadeh, J., and Sepahi, A.-A., 2012, Geochemistry and zircon U-Pb geochronology of Aligoodarz granitoid complex, Sanandaj-Sirjan Zone, Iran: *Journal of Asian Earth Sciences*, v. 43, p. 11–22.
- Espanhod, M.R., 1992, Metallogenic consequences due to compressional stress of Cu-Mo-Au systems regarding to low-grade uranium mineralization in marginal part of ophiolite zone of central Iran: *International Geological Congress, 29th, Tokyo, 1992 [Proceedings], Mineral Resources Symposia, v. A, Resource Geology Special Issue 15*, p. 191–198.
- Etminan, H., 1977, The discovery of porphyry copper-molybdenum mineralization adjacent to Sungun village in the northwest of Ahar and a proposed program for its detailed exploration: Dr. Hashem Etminan report submitted to Geological Survey of Iran, 26 p.
- Etminan, H., 2003, History of discovery of Sungun porphyry copper deposit, NW of Ahar, Azarbaijan, Iran: Deakin, Australian Capital Territory, Australia, Dr. Hashem Etminan Web page accessed June 25, 2012, at <http://www.sunguncopperdeposit.com/about.html>.
- Eurasian Minerals, Inc., 2012, Sisorta: Eurasian Minerals, Inc., Web page, accessed January 4, 2012, at <http://www.eurasianminerals.com/s/Sisorta.asp>.
- Everest Gold, Inc., 2012, Exploring the Tethyan copper gold belt—The world's next major copper belt (2012 draft ed.): Everest Gold, Inc., Corporate Presentation, 24 slides, accessed August 27, 2012, at <http://www.everestgoldinc.com/Default.aspx>.
- Farahkhah, N., Razavi, M.H., Masoudi, F., and Eskandary, A., 2010, Potassic nature of Karaj Dam sill and its association with Cu, Au, Mo mineralization of Senj deposit: *International Applied Geological Congress, 1st, Mashad, Iran, April 26–28, 2010 [Proceedings]*, p. 168–173.
- Farhoudi, G., and Karig, D.E., 1977, Makran of Iran and Pakistan as an active arc system: *Geology*, v. 5, p. 664–668.
- Fazlnia, A., Moradian, A., Rezaei, K., Moazzen, M., and Alipour, S., 2007, Synchronous activity of anorthositic and S-type granitic magmas in Chah-Dozdan batholith, Neyriz, Iran—Evidence of zircon SHRIMP and monazite CHIME dating: *Iran, Journal of Sciences*, v. 18, p. 221–237.
- Förster, H., 1978, Mesozoic-Cenozoic metallogenesis in Iran: London, *Journal of the Geological Society*, v. 135, p. 443–455.

- Fotoohi Rad, G.R., Droop, G.T.R., and Burgess, R., 2009, Early Cretaceous exhumation of high-pressure metamorphic rocks of the Sistan suture zone, eastern Iran: *Geological Journal*, v. 44, p. 104–116.
- Gamkrelidze, I.P., 1986, Geodynamic evolution of the Caucasus and adjacent areas in Alpine time: *Tectonophysics*, v. 127, p. 261–277.
- Gansser, A., and Huber, H., 1962, Geological observations in the central Elburz, Iran: *Zürich, Schweizerische Mineralogische und Petrographische Mitteilungen*, v. 42, p. 583–630.
- Garwin, S., Hall, R., and Watanbe, Y., 2005, Tectonic setting, geology, and gold and copper mineralization in Cenozoic magmatic arcs of southeast Asia and the west Pacific, in Hedenquist, J.W., Thompson, J.F.H., Goldfarb, R.J., and Richards, J.P., eds., *Economic Geology one hundredth anniversary volume, 1905–2005: Society of Economic Geologists*, p. 891–930.
- Gealy, W.K., 1988, Plate tectonic evolution of the Mediterranean-Middle East region: *Tectonophysics*, v. 155, p. 285–306.
- Gençaloğlu-Kuşçu, G., Göncüoğlu, M.C., and Kuşçu, İ., 2001, Post-collisional magmatism on the northern margin of the Taurides and its geological implications—Geology and petrology of the Yahyalı-Karamadazi granitoid: *Turkish Journal of Earth Sciences*, v. 10, p. 103–119.
- General Directorate of Mineral Research and Exploration (MTA), 2000, Geological map of Turkey: Ankara, General Directorate of Mineral Research and Exploration (MTA), 18 sheets, scale 1:500,000. [Digital version in vector format.]
- Geological Survey of Iran, 2010, 3-Copper, Masjed Daqi: Geological Survey of Iran Web page, accessed October 3, 2012, at <http://intl.mim.gov.ir/index.php?module=content&func=viewpage&pageid=9201>.
- Geological Survey of Iran, 2012a, Distribution of mineral deposits and occurrences of copper: Iran Geological and Mineral Exploration Survey database, accessed June 25, 2012, at http://www.gsi.ir/Images/WEBMINE/cu/prj_cu.htm.
- Geological Survey of Iran, 2012b, Distribution of mineral deposits and occurrences of gold: Iran Geological and Mineral Exploration Survey database, accessed June 25, 2012, at http://www.gsi.ir/Images/WEBMINE/au/au-vein/prj_au_v.htm.
- Geological Survey of Iran, 2012c, Distribution of mineral deposits and occurrences of lead and zinc: Iran Geological and Mineral Exploration Survey database, accessed June 25, 2012, at http://www.gsi.ir/Images/WEBMINE/pb,zn/PRJ_pb,zn.htm.
- Geological Survey of Iran, 2012d, Distribution of mineral deposits and occurrences of molybdenum: Iran Geological and Mineral Exploration Survey database, accessed June 25, 2012, at http://www.gsi.ir/Images/WEBMINE/mo/prj_mo.htm.
- Geological Survey of Iran, 2012e, Minerals information of Iran: Iran Geological and Mineral Exploration Survey Web page accessed June 25, 2012, at http://www.gsi.ir/General/Lang_en/Page_43/WebsiteId_17/Minerals.Distribution.html.
- Geological Survey of Pakistan, 2009, Mineral profile of Balochistan: Geological Survey of Pakistan, [24] p.
- Geomatics Management, [n.d.], Potential map for Cu (Mo): Geological Survey of Iran, scale 1:5,000,000.
- GeoProMining, 2012, Agarak Copper-Molybdenum Mine Complex: GeoProMining Web page, accessed September 13, 2013 at <http://www.geopromining.com/en/our-business/operations/agarak/>.
- Ghadami, G., Shahre Babaki, A.M., and Mortazavi, M., 2008, Post-collisional Pliocene-Pleistocene adakitic volcanism in Central Iranian Volcanic Belt—Geochemical and geodynamic implications: Iran, *Journal of Sciences*, v. 19, p. 223–235.
- Ghalamghash, J., Bouchez, J.L., Vosoughi-Abedini, M., and Nédélec, A., 2009, The Urumieh plutonic complex (NW Iran)—Record of the geodynamic evolution of the Sanandaj-Sirjan Zone during Cretaceous times, part II—Magnetic fabrics and plate tectonic reconstruction: *Journal of Asian Earth Sciences*, v. 36, p. 303–317.
- Ghalamghash, J., Nédélec, A., Bellon, H., Vosoughi-Abedini, M., and Bouchez, J.L., 2009, The Urumieh plutonic complex (NW Iran)—A record of the geodynamic evolution of the Sanandaj-Sirjan Zone during Cretaceous times, part I—Petrogenesis and K/Ar dating: *Journal of Asian Earth Sciences*, v. 35, p. 401–415.
- Ghanbari, E., 2000, Tectonics of copper deposits of Sungun (Karadagh region) in Azerbaijan-Iran [abs.]: International Geological Congress, 31st, Rio de Janeiro, 2000 [Proceedings], Section 11–8, CD-ROM.
- Ghasemi, A., and Talbot, C.J., 2006, A new tectonic scenario for the Sanandaj-Sirjan Zone (Iran): *Journal of Asian Earth Sciences*, v. 26, p. 683–693.
- Ghasemi, H.E., Sadeghian, M., Khan Alizadeh, A.R., Tanha, Ali, 2010, Petrology, geochemistry and radiometric ages of high silica adakitic domes of Neogene continental arc, south of Quchan: *Iranian Journal of Crystallography and Mineralogy*, v. 18, p. 347–370. [In Persian, English abstract.]
- Ghavi, J., and Karimpour, M.H., 2010, Geological investigation and mineralization of the Dardway iron deposit, Sangan ore field, northeast Iran: International Applied Geological Congress, 1st, Mashad, Iran, April 26–28, 2010 [Proceedings], p. 296–302.

- Ghazban, F., McNutt, R.H., Schwarcz, H.P., 1994, Genesis of sediment-hosted Zn-Pb-Ba deposits in the Irankuh district, Esfahan area, west-central Iran: *Economic Geology*, v. 89, p. 1262–1278.
- Ghazi, A.M., and Hassanipak, A.A., 2000, Petrology and geochemistry of the Shahr-Babak ophiolite, central Iran, *in* Dilek, Y., Moores, E.M., Elthon, D., and Nicolas, A. eds., *Ophiolites and oceanic crust—New insights from field studies and the ocean drilling program*: Boulder, Colo., Geological Society of America Special Paper 349, p. 485–497.
- Gholami, N., Karimpour, M.H., and Mazaheri, S.A., 2011, Geology, alteration, mineralization and geochemistry of eastern Arghash (southwest of Neyshabour), with respect to Cu-porphyry system: *Iranian Journal of Crystallography and Mineralogy*, v. 19, no. 1, p. 15–28. [In Persian, English abstract.]
- Ghorashi-Zadeh, M., 1978, Development of hypogene and supergene alteration and copper mineralization patterns Sar Cheshmeh porphyry copper deposits, Iran: St. Catharines, Ontario, Brock University, Master of Science thesis, 223 p.
- Ghorbani, G., Vosoughi Abedini, M., and Ghasemi, H.A., 2005, Geothermobarometry of granitoids from Torud-Chah Shirin area (south Damghan): *Iranian Journal of Crystallography and Mineralogy*, v. 13, p. 95–106. [In Persian, English abstract.]
- Ghorbani, M.R., 2006, Lead enrichment in Neotethyan volcanic rocks from Iran—The implications of a descending slab: *Geochemical Journal*, v. 40, p. 557–568.
- Gilmour, P., Andrew, R.L., Bernstein, M., Maxwell, I., and Morrissey, C.J., 1995, Porphyry copper deposits—History, recent developments, exploration, economics, *in* Pierce, F.W., and Bolm, J.G., eds., *Porphyry copper deposits of the American Cordillera*: Arizona Geological Society Digest 20, p. 128–155.
- Global Business Reports, 2012, Mining in Turkey—A country thirsty for its own mineral reserves: *Engineering and Mining Journal*, v. 213, p. 40–67.
- Global Metals, Ltd., 2013, Molibdeny Ashkharh LLC, Dastakert copper-molybdenum deposit: Global Metals, Ltd., Web page, accessed July 5, 2013, at http://www.globalmetals.am/en/projects/molibdeny_ashkharh/.
- Gökten, E., 1993, Geology of the southern boundary of the Sivas basin east of Ulaş (Sivas, central Anatolia)—Tectonic development related to the closure of the Inner Tauride Ocean: *Türkiye Petrol Jeologları Derneği Bülteni*, v. 5, p. 35–55. [In Turkish.]
- Golonka, J., 2004, Plate tectonic evolution of the southern margin of Eurasia in the Mesozoic and Cenozoic: *Tectonophysics*, v. 381, p. 235–273.
- Görür, N., 1988, Timing of opening of the Black Sea Basin: *Tectonophysics*, v. 147, p. 247–262.
- Görür, N., Oktay, F.Y., Seymen, İ., and Şengör, A.M.C., 1984, Palaeotectonic evolution of the Tuzgölü basin complex, central Turkey—Sedimentary record of a Neo-Tethyan closure, *in* Dixon, J.E., and Robertson, A.H.F., eds., *The geological evolution of the eastern Mediterranean*: London, Geological Society Special Publication 17, p. 467–482.
- Grima, V., 2008, Good prospects for Turkey: *Mining Journal*, April 25, 2008, p. 17–25.
- Groves, D.I., Vielreicher, R.M., Goldfarb, R.J., and Condie, K.C., 2005, Controls on the heterogeneous distribution of mineral deposits through time: *Geological Society of London, Special Publications*, v. 248, p. 71–101.
- Guest, B., Stockli, D.F., Grove, M., Axen, G.J., Lam, P.S., and Hassanzadeh, J., 2006, Thermal histories from the central Alborz Mountains, northern Iran—Implications for the spatial and temporal distribution of deformation in northern Iran: *Geological Society of America Bulletin*, v. 118, p. 1507–1521.
- Guest, B., Guest, A., and Axen, G., 2007, Late Tertiary tectonic evolution of northern Iran—A case for simple crustal folding: *Global and Planetary Change*, v. 58, p. 435–453.
- Gugushvili, V., Popkhadze, N., Beridze, T., and Khutsishvili, S., 2010, Sources of base, precious and rare metals during the Tethyan Phanerozoic evolution of the Caucasus and Pontides: *Aristotle University of Thessaloniki, School of Geology Scientific Annals, Carpathian Balkan Geological Association Congress, 19th, Thessaloniki, Greece, September 23–26, 2010*, [Proceedings], v. 100, p. 333–341.
- Gulyan, E.K., Karamyan, K.A., Bartikyan, P.M., and Tayan, R.N., 1986, Phases of copper-molybdenum mineralization of the Lesser Caucasus: *Proceedings of the Academy of Sciences of Armenia Socialist Republic, Earth Sciences*, v. 29, no. 4, p. 17–23. [In Russian.]
- Gürer, Ö.F., and Aldanmaz, E., 2002, Origin of the Upper Cretaceous-Tertiary sedimentary basins within the Tauride-Anatolide Platform in Turkey: *Geological Magazine*, v. 139, p. 191–197.
- Hagen, H., 2009, Pakistan—Emerging markets in cement and minerals industries: ABB Switzerland, Ltd., *Emerging Markets Report*, p. 95–98, accessed August 27, 2012, at [http://www05.abb.com/global/scot/scot244.nsf/veritydisplay/e7af7737478c69ecc12575e60026c013/\\$File/CH_EMR_2009.pdf](http://www05.abb.com/global/scot/scot244.nsf/veritydisplay/e7af7737478c69ecc12575e60026c013/$File/CH_EMR_2009.pdf).
- Haghipour, A., and Aghanabati, A., 1985 [1989], Geological map of Iran (2nd ed. 1989): Geological Survey of Iran, scale 1:2,500,000.

- Hammarstrom, J.M., Robinson, G.R., Jr., Ludington, Steve, Gray, Floyd, Drenth, B.J., Cendejas-Cruz, F., Espinosa, E., Pérez-Segura, E., Valencia-Moreno, M., Rodríguez-Castañeda, J.L., Vásquez-Mendoza, R., and Zürcher, L., 2010, Porphyry copper assessment of Mexico: U.S. Geological Survey Scientific Investigations Report 2010-5090-A, 176 p., available at <http://pubs.usgs.gov/sir/2010/5090/a/>.
- Haroni, H.A., 2005, Preliminary exploration at Dalli porphyry Cu-Au prospect, Central Province of Iran: Dorsa PLC, [21] p.
- Haroni, H.A., 2008, First stage drilling report on Dalli porphyry Cu-Au prospect, Central [Markazi] Province of Iran: Dorsa PLC Technical Report, [29] p.
- Harris, N.B.W., Kelley, S., and Okay, A.I., 1994, Post-collision magmatism and tectonics in northwest Anatolia: Contributions to Mineralogy and Petrology, v. 117, p. 241–252.
- Haschke, M., Ahmadian, J., Murata, M., and McDonald, I., 2010, Copper mineralization prevented by arc-root delamination during Alpine-Himalayan collision in central Iran: Economic Geology, v. 105, p. 855–865.
- Hassanipak, A.A., and Ghazi, A.M., 2000, Petrology, geochemistry and tectonic setting of the Khoy ophiolite, northwest Iran—Implications for Tethyan tectonics: Journal of Asian Earth Sciences, v. 18, p. 109–121.
- Hassanpour, S., and Afzal, P., 2013, Application of concentration-number (C-N) multifractal modeling for geochemical anomaly separation in Haftcheshmeh porphyry system, NW Iran: Arabian Journal of Geosciences, v. 6, p. 957–970.
- Hassanpour, S., Rasa, I., Heydari, M., Matkan, A.A., and Moayyed, M., 2010, Geology, alteration and mineralization of the Haftcheshmeh Cu-Mo porphyry deposit: Iranian Journal of Geology, v. 4, no. 15, p. 15–28.
- Hassanzadeh, J., 1993, Metallogenic and tectono-magmatic events in the SE sector of the Cenozoic active continental margin of Iran (Shahr e Babak area, Kerman Province): Los Angeles, University of California, Ph.D. dissertation, 204 p.
- Hatzfeld, D., Pedotti, G., Hatzidimitriou, P., Panagiotopoulos, D., Scordilis, M., Drakopoulos, I., Makropoulos, K., Delibasis, N., Latousakis, I., Baskoutas, J., and Frogneux, M., 1989, The Hellenic subduction beneath the Peloponnese—First results of a microearthquake study: Earth and Planetary Science Letters, v. 93, p. 283–291.
- HB Corporate, [2005], Placing of 37,400,000 new ordinary shares of 1p each at 5p per share and admission to trading on AIM: Stratex International PLC, 101 p.
- Hess, J.C., Aretz, J., Gurbanov, A.G., Emmerman, R., and Lippolt, H.J., 1995, Subduction-related Jurassic andesites in the northern Great Caucasus: Geologische Rundschau, v. 84, p. 319–333.
- Hezarkhani, A., 1997, Physicochemical controls on alteration and copper mineralization in the Sungun porphyry copper deposit, Iran: Montreal, McGill University, Ph.D. dissertation, 281 p. and figs.
- Hezarkhani, A., 2006a, Alteration/mineralization and controls of chalcopyrite dissolution/deposition in the Raigan porphyry system, Bam-Kerman, Iran: International Geology Review, v. 48, p. 561–572.
- Hezarkhani, A., 2006b, Fluid inclusion investigations of the Raigan porphyry copper system, Kerman-Bam, Iran: International Geology Review, v. 48, p. 255–270.
- Hezarkhani, A., 2006c, Geochemistry of the Enjerd skarn and its association with copper mineralization, northwestern Iran: International Geology Review, v. 48, p. 892–909.
- Hezarkhani, A., 2006d, Mineralogy and fluid inclusion investigations in the Reagan porphyry system, Iran—The path to an uneconomic porphyry copper deposit: Journal of Asian Earth Sciences, v. 27, p. 598–612.
- Hezarkhani, A., 2006e, Petrology of the intrusive rocks within the Sungun porphyry copper deposit, Azerbaijan, Iran: Journal of Asian Earth Sciences, v. 27, p. 326–340.
- Hezarkhani, A., 2008, Hydrothermal evolution of the Sonajil porphyry copper system, East Azarbaijan Province, Iran—The history of an uneconomic deposit: International Geology Review, v. 50, p. 483–501.
- Hezarkhani, A., 2009, Hydrothermal fluid geochemistry at the Chah-Firuzeh porphyry copper deposit, Iran—Evidence from fluid inclusions: Journal of Geochemical Exploration, v. 101, p. 254–264.
- Hezarkhani, A., and Williams-Jones, A.E., 1998, Controls of alteration and mineralization in the Sungun porphyry copper deposit, Iran—Evidence from fluid inclusions and stable isotopes: Economic Geology, v. 93, p. 651–670.
- Hezarkhani, A., Williams-Jones, A.E., and Gammons, C.H., 1999, Factors controlling copper solubility and chalcopyrite deposition in the Sungun porphyry copper deposit, Iran: Mineralium Deposita, v. 34, p. 770–783.
- Hijmans, R., 2011, Global administrative areas—GADM database, version 2.0: accessed January 23, 2013, at <http://www.gadm.org>.
- Hollingsworth, J., Fattahi, M., Walker, R., Talebian, M., Bahroudi, A., Bolourchi, M.J., Jackson, J., and Copley, A., 2010, Oroclinal bending, distributed thrust and strike-slip faulting, and the accommodation of Arabia-Eurasia convergence in NE Iran since the Oligocene: Geophysical Journal International, v. 181, p. 1214–1246.

- Honarmand, M., and Ahmadian, J., 2008, Mineral chemistry, geothermobarometry and oxygen fugacity of igneous rocks—Natanz complex, central Iran: Saint Petersburg, Russia, Russian Mineralogical Society, Fodorov Session 2008, Saint Petersburg, October 8–10, 2008 [Proceedings], p. 81–82.
- Honarmand, M., Ranjbar, H., and Shahabpour, J., 2011, Application of spectral analysis in mapping hydrothermal alteration of the northwestern part of the Kerman Cenozoic magmatic arc, Iran: *Iran, Journal of Sciences*, v. 22, p. 221–238.
- Horton, B.K., Hassanzadeh, J., Stockli, D.F., Axen, G.J., Gillis, R.J., Guest, B., Amini, A., Fakhari, M.D., Zamanzadeh, S.M., and Grove, M., 2008, Detrital zircon provenance of Neoproterozoic to Cenozoic deposits in Iran—Implications for chronostratigraphy and collisional tectonics: *Tectonophysics*, v. 451, p. 97–122.
- Hosseini, M., Zarasvandi, A., and Liaghat, S., 2010, Tectonic setting and petrogenesis of Darreh-Zereshk granitoids (SW Yazd, Iran) and comparison with some world skarn granitoids: International Applied Geological Congress, 1st, Mashad, Iran, April 26–28, 2010 [Proceedings], p. 78–83.
- Hosseinzadeh, Gh., Calagari, A.A., Moayyed, M., Hadj-Alilu, B., and Moazzen, M., 2010, Study of hypogene alteration and copper mineralization in Sonajil area (east of Herris, East Azerbaijan): *Geological Survey of Iran Geosciences*, no. 74. [In Persian, English abstract.]
- Hou, Z., Zhang, H., Pan, X., and Yang, Z., 2011, Porphyry Cu (-Mo-Au) deposits related to melting of thickened mafic lower crust—Examples from the eastern Tethyan metallogenic domain: *Ore Geology Reviews*, v. 39, p. 21–45.
- Huber, H., 1978, Geological map of Iran: Tehran, National Iranian Oil Company, 6 sheets, scale 1:1,000,000, digital version in vector format.
- Hubert-Ferrari, A., Armijo, R., King, G., Meyer, B., and Barka, A., 2002, Morphology, displacement, and slip rates along the North Anatolian Fault, Turkey: *Journal of Geophysical Research*, v. 107, no. B10, 33 p.
- Hunting Survey Corp., Ltd., 1960, Reconnaissance geology of part of West Pakistan: Toronto, Government of Canada, a Colombo Plan Co-operative project report prepared for the Government of Pakistan, 550 p.
- Hüsing, S.K., Zachariasse, W.-J., van Hisbergen, D.J.J., Krijgsman, W., Inceöz, M., Harzhauser, M., Mandic, O., and Kroh, A., 2009, Oligocene-Miocene basin evolution in SE Anatolia, Turkey—Constraints on the closure of the eastern Tethys gateway, *in* van Hisbergen, D.J.J., Edwards, M.A., and Govers, R., eds., *Collision and collapse at the Africa-Arabia-Eurasia subduction zone*: London, Geological Society Special Publication 311, p. 107–132.
- İlbelyli, N., 2005, Mineralogical-geochemical constraints on intrusives in central Anatolia, Turkey—Tectono-magmatic evolution and characteristics of mantle source: *Geological Magazine*, v. 142, p. 187–207.
- İlbelyli, N., Pearce, J.A., Meighan, I.G., and Fallick, A.E., 2009, Contemporaneous Late Cretaceous calc-alkaline and alkaline magmatism in central Anatolia, Turkey—Oxygen isotope constraints on petrogenesis: *Turkish Journal of Earth Sciences*, v. 18, p. 529–547.
- Imamjomeh, A., Rastad, E., Bouzari, F., and Omran, N. R., 2009, An introduction to individual disseminated-veinlet and vein mineralization system of Cu (Pb-Zn) in the Chahmoosa-Gholekaftaran mining district, eastern part of Toroud-Chahshirin magmatic arc: *Geological Survey of Iran Geosciences*, v. 18, no. 70. [In Persian, English abstract.]
- İmer, A., Richards, J.P., and Creaser, R.A., 2013, Age and tectonomagmatic setting of the Eocene Çöpler-Kabataş magmatic complex and porphyry-epithermal Au deposit, east central Anatolia, Turkey: *Mineralium Deposita*, v. 48, no. 5, p. 557–583.
- InfoMine, Inc., 2012a, Mining company and property/mine database: InfoMine, Inc., Web page, accessed November 5, 2012, at <http://www.infomine.com/index/properties/ARDALA.html>.
- InfoMine, Inc., 2012b, Mining company and property/mine database: InfoMine, Inc., Web page, accessed November 5, 2012, at <http://www.infomine.com/index/properties/MURATDERE.html>.
- InfoMine, Inc., 2012c, Mining company and property/mine database: InfoMine, Inc., Web page, accessed November 5, 2012, at http://www.infomine.com/index/properties/AGI_DAGI.html.
- InfoMine, Inc., 2012d, Mining company and property/mine database: InfoMine, Inc., Web page, accessed November 5, 2012, at <http://www.infomine.com/index/properties/AMALAF.html>.
- InfoMine, Inc., 2012e, Mining company and property/mine database: InfoMine, Inc., Web page, accessed November 5, 2012, at <http://www.infomine.com/index/properties/AS.html>.
- InfoMine, Inc., 2012f, Mining company and property/mine database: InfoMine, Inc., Web page, accessed November 5, 2012, at http://www.infomine.com/index/properties/BERTA_NUINSCO.html.
- InfoMine, Inc., 2012g, Mining company and property/mine database: InfoMine, Inc., Web page, accessed November 5, 2012, at <http://www.infomine.com/index/properties/DASHT-I-GAURAN.html>.

- InfoMine, Inc., 2012h, Mining company and property/mine database: InfoMine, Inc., Web page, accessed November 5, 2012, at <http://www.infomine.com/index/properties/DERINKOY.html>.
- InfoMine, Inc., 2012i, Mining company and property/mine database: InfoMine, Inc., Web page, accessed November 5, 2012, at http://www.infomine.com/index/properties/BURSA_KARAPINAR.html.
- InfoMine, Inc., 2012j, Mining company and property/mine database: InfoMine, Inc., Web page, accessed November 5, 2012, at <http://www.infomine.com/index/properties/KOH-I-SULTAN.html>.
- InfoMine, Inc., 2013a, Mining company and property/mine database: InfoMine, Inc., Web page, accessed March 11, 2013, at <http://www.infomine.com/index/properties/Agarak.html>.
- InfoMine, Inc., 2013b, Mining company and property/mine database: InfoMine, Inc., Web page, accessed March 11, 2013, at http://www.infomine.com/index/properties/ALIABAD_DAREH_ZERESHK.html.
- InfoMine, Inc., 2013c, Mining company and property/mine database: InfoMine, Inc., Web page, accessed March 11, 2013, at <http://www.infomine.com/index/properties/HANKAVAN.html>.
- InfoMine, Inc., 2013d, Mining company and property/mine database: InfoMine, Inc., Web page, accessed March 11, 2013, at http://www.infomine.com/index/properties/CELTIK_YUSUFELI.html.
- InfoMine, Inc., 2013e, Mining company and property/mine database: InfoMine, Inc., Web page, accessed March 11, 2013, at <http://www.infomine.com/index/properties/Cevizlidere.html>.
- InfoMine, Inc., 2013f, Mining company and property/mine database: InfoMine, Inc., Web page, accessed March 11, 2013, at http://www.infomine.com/index/properties/CEVRELI_YUSUFELI.html.
- InfoMine, Inc., 2013g, Mining company and property/mine database: InfoMine, Inc., Web page, accessed March 11, 2013, at <http://www.infomine.com/index/properties/Copler.html>.
- InfoMine, Inc., 2013h, Mining company and property/mine database: InfoMine, Inc., Web page, accessed March 11, 2013, at <http://www.infomine.com/index/properties/DALLI.html>.
- InfoMine, Inc., 2013i, Mining company and property/mine database: InfoMine, Inc., Web page, accessed March 11, 2013, at http://www.infomine.com/index/properties/Darreh_Zar.html.
- InfoMine, Inc., 2013j, Mining company and property/mine database: InfoMine, Inc., Web page, accessed March 11, 2013, at http://www.infomine.com/index/properties/ALIABAD_DAREH_ZERESHK.html.
- InfoMine, Inc., 2013k, Mining company and property/mine database: InfoMine, Inc., Web page, accessed March 11, 2013, at <http://www.infomine.com/index/properties/Demirtepe.html>.
- InfoMine, Inc., 2013l, Mining company and property/mine database: InfoMine, Inc., Web page, accessed March 11, 2013, at <http://www.infomine.com/index/properties/DIKMEN.html>.
- InfoMine, Inc., 2013m, Mining company and property/mine database: InfoMine, Inc., Web page, accessed March 11, 2013, at http://www.infomine.com/index/properties/INLICE_KONYA.html.
- InfoMine, Inc., 2013n, Mining company and property/mine database: InfoMine, Inc., Web page, accessed March 11, 2013, at <http://www.infomine.com/index/properties/ESENDAL.html>.
- InfoMine, Inc., 2013o, Mining company and property/mine database: InfoMine, Inc., Web page, accessed March 11, 2013, at <http://www.infomine.com/index/properties/GELEMIC.html>.
- InfoMine, Inc., 2013p, Mining company and property/mine database: InfoMine, Inc., Web page, accessed March 11, 2013, at http://www.infomine.com/index/properties/GUMUSHANE_DURUSU.html.
- InfoMine, Inc., 2013q, Mining company and property/mine database: InfoMine, Inc., Web page, accessed March 11, 2013, at <http://www.infomine.com/index/properties/HALILAGA.html>.
- InfoMine, Inc., 2013r, Mining company and property/mine database: InfoMine, Inc., Web page, accessed March 11, 2013, at <http://www.infomine.com/index/properties/Ispir.html>.
- InfoMine, Inc., 2013s, Mining company and property/mine database: InfoMine, Inc., Web page, accessed March 11, 2013, at http://www.infomine.com/index/properties/Karaayi_Project.html.
- InfoMine, Inc., 2013t, Mining company and property/mine database: InfoMine, Inc., Web page, accessed March 11, 2013, at <http://www.infomine.com/index/properties/Karakartal.html>.
- InfoMine, Inc., 2013u, Mining company and property/mine database: InfoMine, Inc., Web page, accessed March 11, 2013, at <http://www.infomine.com/index/properties/KEBAN.html>.
- InfoMine, Inc., 2013v, Mining company and property/mine database: InfoMine, Inc., Web page, accessed March 11, 2013, at http://www.infomine.com/index/properties/KHARESTAN_BALUCHESTAN.html.

- InfoMine, Inc., 2013w, Mining company and property/mine database: InfoMine, Inc., Web page, accessed March 11, 2013, at <http://www.infomine.com/index/properties/KIRAZLI.html>.
- InfoMine, Inc., 2013x, Mining company and property/mine database: InfoMine, Inc., Web page, accessed March 11, 2013, at <http://www.infomine.com/index/properties/KISLADAG.html>.
- InfoMine, Inc., 2013y, Mining company and property/mine database: InfoMine, Inc., Web page, accessed March 11, 2013, at [http://www.infomine.com/index/properties/LICHKVADZ___TERTERASAN_\(SIPAN.html](http://www.infomine.com/index/properties/LICHKVADZ___TERTERASAN_(SIPAN.html).
- InfoMine, Inc., 2013z, Mining company and property/mine database: InfoMine, Inc., Web page, accessed March 11, 2013, at <http://www.infomine.com/index/properties/MIDUK.html>.
- InfoMine, Inc., 2013aa, Mining company and property/mine database: InfoMine, Inc., accessed March 11, 2013, at <http://www.infomine.com/index/properties/BASKIL.html>.
- InfoMine, Inc., 2013ab, Mining company and property/mine database: InfoMine, Inc., Web page, accessed March 11, 2013, at http://www.infomine.com/index/properties/Reko_Diq_Complex.html.
- InfoMine, Inc., 2013ac, Mining company and property/mine database: InfoMine, Inc., Web page, accessed March 11, 2013, at <http://www.infomine.com/index/properties/SAMLI.html>.
- InfoMine, Inc., 2013ad, Mining company and property/mine database: InfoMine, Inc., Web page, accessed March 11, 2013, at <http://www.infomine.com/index/properties/SARCHESHMEH.html>.
- InfoMine, Inc., 2013ae, Mining company and property/mine database: InfoMine, Inc., Web page, accessed March 11, 2013, at <http://www.infomine.com/index/properties/SONGUN.html>.
- InfoMine, Inc., 2013af, Mining company and property/mine database: InfoMine, Inc., Web page, accessed March 11, 2013, at [http://www.infomine.com/index/properties/TANJEEL_\(H4.html](http://www.infomine.com/index/properties/TANJEEL_(H4.html).
- InfoMine, Inc., 2013ag, Mining company and property/mine database: InfoMine, Inc., Web page, accessed March 11, 2013, at http://www.infomine.com/index/properties/SISORTA_PROPERTY.html.
- Institute for Geo-Resources and Environment, 2005, Japan-Turkey Project—Study on hydrothermal deposits and metallogeny of western Turkey: National Institute of Advanced Industrial Science and Technology (AIST), accessed November 3, 2012, at <http://staff.aist.go.jp/y-watanabe/Turkeyreport.pdf>.
- Jackson, J., and McKenzie, D., 1984, Active tectonics of the Alpine-Himalayan Belt between western Turkey and Pakistan: *Geophysical Journal of the Royal Astronomical Society*, v. 77, p. 185–264.
- Jafarian, A., 2011, Geochemical signatures of Bazman volcano—Evidence from Makran subduction zone, southeast Iran [abs.]: *Geophysical Research Abstracts*, v. 13, abstract EGU2011-470-1, European Geosciences Union General Assembly, Vienna, April 3–8, 2011[Proceedings].
- Jahangiri, A., 2007, Post-collisional Miocene adakitic volcanism in NW Iran—Geochemical and geodynamic implications: *Journal of Asian Earth Sciences*, v. 30, p. 433–447.
- Jamali, H., Dilek, Y., Daliran, F., Yaghubpur, A., and Mehrabi, B., 2010, Metallogeny and tectonic evolution of the Cenozoic Ahar-Arasbaran volcanic belt, northern Iran: *International Geology Review*, v. 52, p. 608–630.
- Jamali, H., Yaghubpur, A., Mehrabi, B., Dilek, Y., Daliran, F., and Meshkani, A., 2012, Petrogenesis and tectono-magmatic setting of Meso-Cenozoic magmatism in Azerbaijan Province, northwestern Iran, in Al-Juboury, A.I., ed., *Petrology—New perspectives and applications*: Rijeka, Croatia, InTech, p. 51–68.
- Janković, S., 1977, The copper deposits and geotectonic setting of the Thethyan Eurasian Metallogenic Belt: *Mineralium Deposita*, v. 12, p. 37–47.
- Janković, S., and Petrascheck, W.E., 1987, Tectonics and metallogeny of the Alpine-Himalayan Belt in the Mediterranean area and western Asia: *Episodes*, v. 10, p. 169–175.
- Jensen, E.P., and Barton, M.D., 2000, Gold deposits related to alkaline magmatism, in Hagemann, S.G., and Brown, P.E., eds., *Gold in 2000: Reviews in Economic Geology*, v. 13, p. 279–314.
- John, D.A., Ayuso, R.A., Barton, M.D., Blakely, R.J., Bodnar, R.J., Dilles, J.H., Gray, F., Graybeal, F.T., Mars, J.C., McPhee, D.K., Seal, R.R., Taylor, R.D., and Vikre, P.G., 2010, Porphyry copper deposit model, chap. B of *Mineral deposit models for resource assessment*: U.S. Geological Survey Scientific Investigations Report 2010–5070-B, 186 p, available at <http://pubs.usgs.gov/sir/2010/5070/b/>.
- Juras, S., Miller, R., and Skayman, P., 2010, Technical report for the Kışladağ gold mine, Turkey: National Instrument 43–101 report prepared for Eldorado Gold Corp., [120] p.
- Kadioglu, Y.K., and Dilek, Y., 2010, Structure and geochemistry of the adakitic Horoz granitoid, Bolkar Mountains, south-central Turkey, and its tectonomagmatic evolution: *International Geology Review*, v. 52, p. 505–535.
- Kalender, L., 2011, Oxygen, carbon and sulphur isotope studies in the Keban Pb-Zn deposits, eastern Turkey—An approach on the origin of hydrothermal fluids: *Journal of African Earth Sciences*, v. 59, p. 341–348.

- Karakaya, M.Ç., Karakaya, N., Küpeli, Ş., and Yavuz, F., 2012, Mineralogy and geochemical behavior of trace elements of hydrothermal alteration types in the volcanogenic massive sulfide deposits, NE Turkey: *Ore Geology Reviews*, p. 197–224.
- Karim, K.H., Al-Barzinjy, S.T., and Bakhtiar, M.A., 2008, History and geological setting of Intermontane Basin in the Zagros Fold-Thrust Belt, Kurdistan, Region, NE Iraq: *Iraqi Bulletin of Geology and Mining*, v. 4, no. 1, p. 21–33.
- Karimi, A., 2002, Geochemical behaviors and geological studies of copper and paragenesis elements in Lar prospect (north Zahedan): *Geological Survey of Iran Geosciences*, v. 11, no. 43–44, p. 56–67. [In Persian, English abstract.]
- Karimi, M., and Valadan Zoej, M.J., 2004, Mineral potential mapping of copper minerals with GIS: *International Society for Photogrammetry and Remote Sensing*, v. 35, part B4, p. 1103–1108.
- Karimi Saeed Abadi, Z., Karimpour, M.H., and Mazaheri, S.A., 2009, Petrography, alteration and magnetic susceptibility of Cu-Au mineralization in south west of Argash Neyshabour: Ferdowsi University of Mashhad [Iran] Web page, accessed on August 29, 2012, at <http://profdoc.um.ac.ir/articles/a/1011975.pdf>. [In Persian, English abstract and figures.]
- Karimpour, M.H., 1998, Geochemistry, genesis, and gold potential in Kuh-e-zar prospecting area, Torbate Heydariyeh: *Geological Survey of Iran Geosciences*, no. 27–28. [In Persian, English abstract.]
- Karimpour, M.H., 2006, Petrology, mineralization and geochemistry of the Sarsfidal prospecting area (Kashmar, Khorasan Razavi): *Ahwaz, Iran, Shahid Chamran University Journal of Science, new series*, v. 14, p. 30–52.
- Karimpour, M.H., 2007, Exploration opportunities for gold and copper in eastern Iran—A new mineral deposits database [abs.]: Denver, Colo., Denver Region Exploration Geologists' Society, accessed November 18, 2013, at <http://www.dregs.org/abs2007.html>.
- Karimpour, M.H., and Malekzadeh, A., 2006, Comparison of the geochemistry of source rocks at Tannurjeh Au-bearing magnetite and Sangan Au-free magnetite deposits, Khorasan Razavi, Iran: *Iranian Journal of Crystallography and Mineralogy*, v. 13, no. 1, [25] p. [In Persian, English abstract.]
- Karimpour, M.H., and Moradi Noghondar, M., 2010, Alteration, mineralization, and geochemical exploration (stream sediment and rock) of eastern Najmabad, Ghonabad: Iran, *Journal of Geology*, v.4, no. 13, p. 61–74. [In Persian, English abstract.]
- Karimpour, M.H., and Stern, C.R., 2009, Advanced spaceborne thermal emission and reflection radiometer mineral mapping to discriminate high sulfidation, reduced intrusion related and iron oxide gold deposits, eastern Iran: *Journal of Applied Sciences*, v. 9, p. 815–828.
- Karimpour, M.H., and Stern, C.R., 2010, Mineralogical and chemical composition of tourmaline from Najmabad, Gheshlagh, Hired, and Maherabad-Khopik and their relationship with types of mineralization, eastern Iran: *Iranian Journal Crystallography and Mineralogy*, v. 18, no. 2, p. 43–54. [In Persian, English abstract.]
- Karimpour, M.H., and Stern, C.R., 2011, Mineral deposits of the Lut block, eastern Iran, *in* Barra, Fernando, Reich, M., Campos, E., and Tornos, F., eds, *Let's talk ore deposits: Society for Geology Applied to Mineral Deposits Biennial Meeting*, 11th, Antofagasta, Chile, September 26–29, 2011, 3 p.
- Karimpour, M.H., Zaw, Khin, and Huston, D.L., 2005, S-C-O isotopes, fluid inclusion microthermometry, and the genesis of ore bearing fluids at Qaleh-Zari Fe-oxide Cu-Au-Ag mine, Iran: *Iran, Journal of Sciences*, v. 16, p. 153–168.
- Karimpour, M.H., Khosravi, M., Pourkhosro, M., Heydarian Shahri, M.R., and Saadat, S., 2008, Geology, mineralization, alteration and geochemical exploration in Kajeh area, Ferdows: *Iranian Journal of Crystallography and Mineralogy*, v. 16, no. 2. [In Persian, English abstract.]
- Karimpour, M.H., Santos, J.F., Mazaheri, S.A., Medina, J.M., Arjmanzadeh, R., and Homan, S.M., 2011a, Hydrothermal fluids evolution from various alteration-mineralization zones of Dehsalm porphyry type system, Lut block, eastern Iran [abs.], *in* Iranian Society of Economic Geology Proceedings of the 2d National Symposium: Geological Survey of Iran Web page accessed October 25, 2012, at <http://www.gsinet.ir/en/articles/article/economic2-dehsalam.html>.
- Karimpour, M.H., Stern, C.R., Farmer, G.L., Saadat, S., and Malekezadeh Shafaroudi, A., 2011b, Review of age, Rb-Sr geochemistry and petrogenesis of Jurassic to Quaternary igneous rocks in Lut block, eastern Iran: *Geopersia*, v. 1, p. 19–36.
- Karimpour, M.H., Malekzadeh Shafaroudi, A., Esphandiarpour, A., and Mohammad Nejad, H., 2012, Neyshabour turquoise mine—The first iron oxide Cu-Au-U-LREE (IOCG) mineralized system in Iran: Mashhad, Iran, Ferdowsi University of Mashhad, *Journal of Economic Geology*, v. 3, no. 2, p. 193–216. [In Persian, English abstract.]
- Kay, S.M., Mpodozis, C., and Coira, B., 1999, Neogene magmatism, tectonism, and mineral deposits of the central Andes (22 degrees to 33 degrees S latitude), *in* Skinner, B.J., ed., *Geology and ore deposits of the central Andes: Economic Geology Special Publication 7*, p. 27–59.

- Kaymakci, N., Inceöz, M., Ertepinar, P., and Koç, A., 2010, Late Cretaceous to recent kinematics of SE Anatolia (Turkey), *in* Sosson, M., Kaymakci, N., Stephenson, R.A., Bergerat, F., and Starostenko, V., eds, *Sedimentary basin tectonics from the Black Sea and Caucasus to the Arabian Platform*: London, Geological Society Special Publication 340, p. 409–435.
- Kazmi, A.H., and Qasim Jan, M., 1997, *Geology and tectonics of Pakistan*: Karachi, Graphic Publishers, 554 p.
- Kazmi, A.H., and Rana, R.A., 1982, *Tectonic map of Pakistan*: Geological Survey of Pakistan, scale 1:2,000,000.
- Kazmin, V.G., 1991, Collision and rifting in the Tethys Ocean—Geodynamic implications: *Tectonophysics*, v. 196, p. 371–384.
- Kazmin, V.G., Sbertshikov, I.M., Ricou, L-E., Zonenshain, L.P., Boulin, J., and Knipper, A.L., 1986, Volcanic belts as markers of the Mesozoic-Cenozoic active margin of Eurasia: *Tectonophysics*, v. 123, p. 123–152.
- Keane, J., Jutras, M., Welhener, H., and Browne, R., 2010, An independent technical report on the Ağı Dağı-Kirazlı gold project, Çanakkale Province, Republic of Turkey: KD Engineering, prepared for Alamos Gold, Inc., 451 p. (Available for download at www.sedar.com.)
- KEFI Minerals, 2012, Turkey: KEFI Minerals Web page, accessed January 4, 2012, at <http://www.kefi-minerals.com/turkey.html>.
- Kekelia, S., Kekelia, M., and Moon, C.J., 2001, *ArcView metallogenic map of the Caucasus*: Leicester, England, University of Leicester, CD-ROM, scale 1:1,000,000.
- Kekelia, S., Kekelia, M., Otkhmezuri, Z., Özgür, N., and Moon, C., 2004, Ore-forming systems in volcanogenic-sedimentary sequences by the example of base metal deposits of the Caucasus and East Pontic Metalotect: *Mineral Resources Exploration Bulletin*, v. 129, p. 1–16.
- Kekelia, S.A., Kekelia, M.A., Kuloshvili, S.I., Sadradze, N.G., Gagnidze, N.E., Yaroshevich, V.Z., Asatiani, G.G., Doeblich, J.L., Goldfarb, R.J., and Marsh, E.E., 2008, Gold deposits and occurrences of the Greater Caucasus, Georgia Republic—Their genesis and prospecting criteria: *Ore Geology Reviews*, v. 34, p. 369–386.
- Keller, J., Jung, D., Burgath, K., and Wolf, F., 1977, *Geologie und Petrologie des neogenen Kalkalkali-Vulkanismus von Konya (Erenler Dag-Alaca Dag-Massiv, Zentral Anatolien)*: *Geologisches Jahrbuch*, series B, v. 25, p. 37–117. [In German.]
- Keskin, M., 2003, Magma generation by slab steepening and breakoff beneath a subduction-accretion complex—An alternative model for collision-related volcanism in eastern Anatolia, Turkey: *Geophysical Research Letters*, v. 30, 4 p.
- Keskin, M., Genç Ş.C., and Tüysüz, O., 2008, Petrology and geochemistry of post-collisional middle Eocene volcanic units in north-central Turkey—Evidence for magma generation by slab breakoff following the closure of the northern Neotethys Ocean: *Lithos*, v. 104, p. 267–305.
- Kesler, S.E., and Wilkinson, B.H., 2008, Earth's copper resources estimated from tectonic diffusion of porphyry copper deposits: *Geology*, v. 36, p. 255–258.
- Kesler, S.E., Jones, L.M., and Walker, R.L., 1975, Intrusive rocks associated with porphyry copper mineralization in island arc areas: *Economic Geology*, v. 70, p. 515–526.
- Ketn, İ., 1966, Tectonic units of Anatolia (Asia Minor): *Turkey Mineral Research and Exploration Institute Bulletin*, v. 66, p. 23–34 and figures and plates, scale 1:2,500,000.
- Khain, V.E., 1975, Structure and main stages in the tectono-magmatic development of the Caucasus—An attempt at geodynamic interpretation: *American Journal of Science*, v. 275–A, p. 131–156.
- Khalaji, A.A., Esmaeily, D., Valizadeh, M.V., and Rahimpour-Bonab, H., 2007, Petrology and geochemistry of the granitoid complex of Boroujerd, Sanandaj-Sirjan Zone, western Iran: *Journal of Asian Earth Sciences*, v. 29, p. 859–877.
- Khalatbari-Jafari, M., Juteau, T., Bellon, H., Whitechurch, H., Cotton, J., and Emami, H., 2004, New geological, geochronological and geochemical investigations on the Khoy ophiolites and related formations, NW Iran: *Journal of Asian Earth Sciences*, v. 23, p. 507–535.
- Khaleghi, M., and Ranjbar, H., 2011, Alteration mapping for exploration of porphyry copper mineralization in the Sarduiyeh area, Kerman Province, Iran, using ASTER SWIR data: *Australian Journal of Basic and Applied Sciences*, v. 5, no. 8, p. 61–69.
- Khan, M.A., Siddiqui, R.H., and Jan, M.Q., 2010, Temporal evolution of Cretaceous to Pleistocene magmatism in the Chagai Arc, Balochistan, Pakistan, *in* Leech, M.L., Klemperer, S.L., and Mooney, W.D., eds., *Proceedings for the 25th Himalaya-Karakoram-Tibet Workshop*: U.S. Geological Survey Open-File Report 2010–1099, 240 p., available at <http://pubs.usgs.gov/of/2010/1099/>.
- Kheirkhah, M., Allen, M.B., and Emami, M., 2009, Quaternary syn-collision magmatism from the Iran/Turkey borderlands: *Journal of Volcanology and Geothermal Research*, v. 182, p. 1–12.
- Khodami, M., Noghrean, M., and Davoudian, A.R., 2010a, Geochemical constraints on the genesis of the volcanic rocks in the southeast of Isfahan area, Iran: *Arabian Journal of Geosciences*, v. 3, p. 257–266.

- Khodami, M., Noghreyan, M., and Davoudian, A.R., 2010b, Pliocene-Quaternary adakite volcanism in the Isfahan area, Central Iranian Magmatic Belt: *Neues Jahrbuch für Mineralogie—Abhandlungen*, v. 186, p. 235–248.
- Kines, M.T., 1969, The geology and the ore mineralization in the Keban area, east Turkey: Durham, U.K., Durham University, Ph.D. dissertation, 213 p., and figures, plates, and appendixes.
- King, T.V.V., Johnson, M.R., Hubbard, B.E., and Drenth, B.J., eds., 2011, Identification of mineral resources in Afghanistan—Detecting and mapping resource anomalies in prioritized areas using geophysical and remote sensing (ASTER and HyMap) data: U.S. Geological Survey Open-File Report 2011–1229, 327 p., available at <http://pubs.usgs.gov/of/2011/1229/>.
- Kirkham, R.V., and Dunne, K.P.E., 2000, World distribution of porphyry, porphyry-associated skarn, and bulk-tonnage epithermal deposits and occurrences: Canada Geological Survey, Open File 3792a, 26 p.
- Kociumbas, M., and Page, R.H., 2009, Technical report on the Cevizlidere porphyry deposit, Tunceli Province, Turkey: Toronto, Watts, Griffis and McOuatt, Ltd., National Instrument 43–101 technical report prepared for Anatolia Minerals Development, Ltd., 93 p. and appendixes.
- Koçyiğit, A., Özkan, S., and Rojay, B.F., 1988, Examples from the forearc basin remnants at the active margin of northern Neo-Tethys—Development and emplacement ages of the Anatolian nappe, Turkey: Ankara, Middle East Technical University, *Journal of Pure and Applied Sciences*, v. 21, p. 183–210.
- Köksal, S., and Göncüoğlu, M.C., 2008, Sr and Nd isotopic characteristics of some S-, I- and A-type granitoids from central Anatolia: *Turkish Journal of Earth Sciences*, v. 17, p. 111–127.
- Köksal, S., Göncüoğlu, M.C., and Floyd, P.A., 2001, Extrusive members of postcollisional A-type magmatism in central Anatolia—Karahidir Volcanics, Idis Dagi-Avanos Area, Turkey: *International Geology Review*, v. 43, p. 683–694.
- Kolahdani, S., 2009, Tectono-magmatism of the Kalateh No copper porphyry prospect—Episodic modeling for arc magmatism in Gonabad fault horsetail [abs.]: Geological Survey of Iran Symposium on Geosciences, 27th, and Geological Society of Iran Symposium, 13th, Tehran, 2009. [Proceedings.]
- Krumsiek, K., 1980, Zur plattentectonischen Entwicklung des Indo-Iranischen Raumes (Resultate palaomagnetischer Untersuchungen in Afghanistan): Stuttgart, Geotektonische Forschungen Band 60, 223 p. [In German.]
- Kuo, C.S., 2011a, The mineral industry of Afghanistan [advance release], in *Area reports—International—Asia and the Pacific*: U.S. Geological Survey Minerals Yearbook 2010, v. III, p. 2.1–2.3, accessed October 26, 2012, at <http://minerals.usgs.gov/minerals/pubs/country/2010/myb3-2010-af.pdf>.
- Kuo, C.S., 2011b, The mineral industry of Pakistan [advance release], in *Area reports—International—Asia and the Pacific*: U.S. Geological Survey Minerals Yearbook 2010, v. III, p. 21.1–21.6, accessed October 26, 2012, at <http://minerals.usgs.gov/minerals/pubs/country/2010/myb3-2010-pk.pdf>.
- Kürüm, S., Önal, A., Boztuğ, D., Spell, T., and Arslan, M., 2008, ⁴⁰Ar/³⁹Ar age and geochemistry of the post-collisional Miocene Yamadağ volcanics in the Arapkir area (Malatya Province), eastern Anatolia, Turkey: *Journal of Asian Earth Sciences*, v. 33, p. 229–251.
- Kuşçu, I., 2005, World skarn deposits—Skarns of Turkey, in Meinert, L.D., Dipple, G.M., and Nicolescu, S., World skarn deposits, in Hedenquist, J.W., Thompson, J.F.H., Goldfarb, R.J., and Richards, J.P., eds., *Economic Geology one hundredth anniversary volume, 1905–2005*: Society of Economic Geologists, CD-ROM, 2 p. and data (table 11.1) in appendix.
- Kuşçu, I., 2007, Discussion on “Gold in Turkey—A missing link in Tethyan metallogeny”: *Ore Geology Reviews*, v. 30, p. 135–140.
- Kuşçu, I., and Erler, A., 1998, Mineralization events in a collision-related setting—The central Anatolian crystalline complex, Turkey: *International Geology Review*, v. 40, p. 552–565.
- Kuşçu, I., Kusu, G.G., Tosdal, R.M., Ulrich, T.D., and Friedman, R., 2010, Magmatism in the southeastern Anatolian orogenic belt—Transition from arc to post-collisional setting in an evolving orogen, in Sosson, M., Kaymakci, N., Stephenson, R.A., Bergerat, F., and Starostenko, V., eds., *Sedimentary basin tectonics from the Black Sea and Caucasus to the Arabian Platform*: London, Geological Society Special Publication 340, p. 437–460.
- Kuşçu, I., Tosdal, R.M., Gencaloğlu-Kuşçu, Friedman, R., and Ullrich, T.D., 2013, Late Cretaceous to middle Eocene magmatism and metallogeny of a portion of the southeastern Anatolian orogenic belt, east central Turkey: *Economic Geology*, v. 108, p. 641–666.
- Lake Resources N.L., 2012, Exploration projects: Lake Resources N.L. Web page, accessed August 27, 2012, at <http://www.lakeresources.com.au/exploration.htm>.
- Le Maitre, R.W., ed., Streckeisen, A., Zanettin, B., Le Bas, M.J., Bonin, B., Bateman, P., Bellieni, G., Dudel, A., Efremova, S., Keller, A.J., Lameyre, J., Sabine, P.A., Schmid, R., Sørensen, H., and Woolley, A.R., 2002, *Igneous rocks—A classification and glossary of terms* (2nd ed.): Cambridge University Press, 236 p.
- Le Pichon, X., and Angelier, J., 1979, The Hellenic arc and trench system—A key to the neotectonic evolution of the eastern Mediterranean area: *Tectonophysics*, v. 60, p. 1–42.

- Leaman, P., and Staude, J.-M., 2002, Metallogenic evolution of the western Tethys of Turkey and Iran, *in* Sugiuchi, N., ed., *Mineral potential of Asia—A forum on Asian metallogeny and ore deposits, exploration and development potential, regulatory and investment climate, and management practicalities*, Vancouver, Canada, January 21, 2002, [Proceedings]: Metal Mining Agency of Japan, p. 15–16.
- Lefebvre, C., Meijers, M.J.M., Kaymakci, N., Peynircioğlu, A., Langereis, C.G., and van Hinsbergen, D.J.J., 2013, Reconstructing the geometry of central Anatolia during the Late Cretaceous—Large-scale Cenozoic rotations and deformation between the Pontides and Taurides: *Earth and Planetary Science Letters*, v. 366, p. 83–98.
- Leterrier, J., 1985, Mineralogical, geochemical and isotopic evolution of two Miocene mafic intrusions from the Zagros (Iran): *Lithos*, v. 18, p. 311–329.
- Leturmy, P., and Robin, C., 2010, Tectonic and stratigraphic evolution of Zagros and Makran during the Mesozoic-Cenozoic—Introduction, *in* Leturmy, P., and Robin, C., *Tectonic and stratigraphic evolution of Zagros and Makran during the Mesozoic-Cenozoic*: London, Geological Society Special Publication 330, p. 1–4.
- Levine, R., 2011a, The mineral industry of Armenia [advance release], *in* *Area reports—International—Europe*: U.S. Geological Survey Minerals Yearbook 2009, v. III, p. 3.1–3.6, accessed October 26, 2012, at <http://minerals.usgs.gov/minerals/pubs/country/2009/myb3-2009-am.pdf>.
- Levine, R., 2011b, The mineral industry of Azerbaijan [advance release], *in* *Area reports—International—Europe*: U.S. Geological Survey Minerals Yearbook 2009, v. III, p. 5.1–5.5, accessed October 26, 2012, at <http://minerals.usgs.gov/minerals/pubs/country/2009/myb3-2009-aj.pdf>.
- Levine, R., 2011c, The mineral industry of Georgia [advance release], *in* *Area reports—International—Europe*: U.S. Geological Survey Minerals Yearbook 2009, v. III, p. 17.1–17.6, accessed October 26, 2012, at <http://minerals.usgs.gov/minerals/pubs/country/2009/myb3-2009-gg.pdf>.
- Levine, R.M., and Wallace, G.J., 2010, The mineral industry of Azerbaijan, *in* *Area reports—International—Europe*: U.S. Geological Survey Minerals Yearbook 2007, v. III, p. 5.1–5.5, accessed December 11, 2013, at <http://minerals.usgs.gov/minerals/pubs/country/2007/myb3-2007-aj.pdf>.
- Lidya Madencilik, 2013a, Sariçayiryayla: Lidya Madencilik Web page, accessed March 11, 2013, at <http://www.lidyamadencilik.com.tr/en/OperationsProjects/Polimetal/2012/06/15/saricayiryayla>.
- Lidya Madencilik, 2013b, Balışeyh: Lidya Madencilik Web page, accessed March 11, 2013, at <http://www.lidyamadencilik.com.tr/en/OperationsProjects/Polimetal/2012/06/15/baliseyh>.
- Lidya Madencilik, 2013c, Bayramdere: Lidya Madencilik Web page, accessed March 11, 2013, at <http://www.lidyamadencilik.com.tr/en/OperationsProjects/Kartaltepe/2012/06/18/bayramdere>.
- Lidya Madencilik, 2013d, Mamlis: Lidya Madencilik Web page, accessed March 11, 2013, at <http://www.lidyamadencilik.com.tr/en/OperationsProjects/Tuncpinar/2012/06/19/mamlis>.
- Lidya Madencilik, 2013e, Sin: Lidya Madencilik Web page, accessed March 11, 2013, at <http://www.lidyamadencilik.com.tr/en/OperationsProjects/Tuncpinar/2012/06/18/sin>.
- Lidya Madencilik, 2013f, Karakartal: Lidya Madencilik Web page, accessed March 11, 2013, at <http://www.lidyamadencilik.com.tr/en/OperationsProjects/Kartaltepe/2012/06/19/karakartal-503856080651>.
- Lidya Madencilik, 2013g, Cevizlidere: Lidya Madencilik Web page, accessed March 11, 2013, at <http://www.lidyamadencilik.com.tr/en/OperationsProjects/Tuncpinar/2012/06/18/cevizlidere>.
- Lordkipanidze, M.B., Meliksetian, B., and Djarbashian, R., 1989, Mesozoic-Cenozoic magmatic evolution of the Pontian-Crimean-Caucasian region, *in* Miloš, R., Dercourt, J., and Nairn, A.E.M., eds., *Evolution of the northern margin of Tethys—The results of IGCP Project 198*: Columbia, University of South Carolina, Earth Sciences and Resources Institute, v. 1, p. 103–124.
- Ludington, S., Orris, G.J., Bolm, K.S., and Peters, S.G., 2007, Preliminary mineral resource assessment of selected mineral deposit types in Afghanistan: U.S. Geological Survey Open-File Report 2007–1005, 47 p., available at <http://pubs.usgs.gov/of/2007/1005/>.
- Maanijou, M., Rasa, I., and Lentz, D.R., 2012, Petrology, geochemistry, and stable isotope studies of the Chehelkureh Cu-Zn-Pb deposit, Zahedan, Iran: *Economic Geology*, v. 107, p. 683–712.
- Mackizadeh, M.A., and Taghipour, B., 2010, Skarn mineralization in Damak Cu-porphyry deposit (Shir-kuh), central Iran [abs.]: *Geochimica et Cosmochimica Acta*, v. 74, no. 11, Goldschmidt Conference, 20th, Knoxville, Tenn., June 13–18, 2010 [Proceedings], p. A653.
- Maghsoudi, A., Yazdi, M., Mehrparto, M., and Vosoghi Abideni, M., 2009, Geochemical zonation in Mirkoh Ali Mirza area, Arasbaran Zone, NW Iran [abs.]: *Geochimica et Cosmochimica Acta*, v. 73, no. 13, Goldschmidt Conference, 19th, Davos, Switzerland, June 21–26, 2009 [Proceedings], p. A815.
- Malekzadeh Shafaroudi, A., Karimpour, M.H., and Stern, C.R., 2009a, Petrology of ore-related intrusive rocks in Mahabad porphyry Cu-Au prospect area, east of Iran [abs.]: *Geological Society of America Abstracts with Programs*, v. 41, no. 7, p. 112.

- Malekzadeh Shafaroudi, A., Karimpour, M.H., Stern, C.R., and Mazaheri, S.A., 2009b, Hydrothermal alteration mapping in SW Birjand, Iran, using the Advanced Spaceborne Thermal Emission and Reflection Radiometer (ASTER) image processing: *Journal of Applied Sciences*, v. 9, p. 829–842.
- Malekzadeh Shafaroudi, A., Karimpour, M.H., and Mazaheri, S.A., 2010, Geology, alteration, mineralization and geochemistry of MA-II region, Mahebad porphyry copper-gold prospect area, South Khorasan Province: *Iranian Journal of Crystallography and Mineralogy*, v. 17, no. 4, p. 639–654. [In Persian, English abstract.]
- Malekzadeh Shafaroudi, A., Karimpour, M.H., and Golmohammadi, A., 2013, Zircon U-Pb geochronology and petrology of intrusive rocks in the C-North and Baghak districts, Sangan iron mine, NE Iran: *Journal of Asian Earth Sciences*, v. 64, p. 256–271.
- Marek, J.M., Benbow, P.E., and Penstrom, W., 2008, Çöpler gold project, east central Turkey: *Anatolia Minerals Development, Ltd., Technical Report* accessed December 22, 2008, at <http://alacergold.com/en/technical>, 132 p.
- Marinov, D., Barra, F., and Alizade, F., 2011, Re-Os dating of molybdenite mineralisation from Turkish porphyry copper prospects, *in* Barra, F., Reich, M., Campos, E., and Tornos, F., eds, *Let's talk ore deposits: Society for Geology Applied to Mineral Deposits (SGA) Biennial Meeting, 11th, Antofagasta, Chile, September 26–29, 2011 [Proceedings]*, p. 111–112.
- Mars, J.C., 2014, Regional mapping of hydrothermally altered igneous rocks along the Urumieh-Dokhtar, Chagai, and Alborz Belts of western Asia using Advanced Spaceborne Thermal Emission and Reflection Radiometer (ASTER) data and Interactive Data Language (IDL) logical operators—A tool for porphyry copper exploration and assessment: *U.S. Geological Survey Scientific Investigations Report 2010–5090–O*, 36 p., 10 plates, and spatial data, available at <http://dx.doi.org/10.3133/sir20105090O>.
- Mars, J.C., and Rowan, L.C., 2006, Regional mapping of phyllic- and argillic-altered rocks in the Zagros magmatic arc, Iran, using advanced spaceborne thermal emission and reflection radiometer (ASTER) data and logical operator algorithms: *Geosphere*, v. 2, no. 3, p. 161–186.
- Masoudi, F., Yardley, B.W.D., and Cliff, R.A., 2002, Rb-Sr geochronology of pegmatites, plutonic rocks and a hornfels in the region south-west of Arak, Iran: *Iranian Journal of Sciences*, v. 13, p. 249–254.
- Maus, S., Barchhausen, U., Berkenbosch, H., Boumas, N., and 19 others, 2009, EMAG2—A 2-arc min resolution Earth magnetic anomaly grid compiled from satellite, airborne, and marine magnetic measurements: *Geochemistry Geophysics Geosystems*, v. 10, Q08005, 12 p.
- Mazaheri, S.A., Amini, S., Galamghash, J., and Bea, F., 2011, Petrogenesis of granitic unit of Naqadeh complex, Sanandaj-Sirjan Zone, NW Iran: *Arabian Journal of Geosciences*, v. 4, p. 59–67.
- Mazloumi Bajestani, A.R., and Rasa, Iraj, 2010, Alteration and petrology of intrusive rocks associated with gold mineralization at Kuh-e-Zar gold deposit, Torbat-e-Heidaryeh: *Mashhad, Iran, Ferdowsi University of Mashhad, Journal of Economic Geology*, v. 1, p. 57–69. [In Persian, English abstract.]
- Mazloumi Bajestani, A.R., Karimpour, M.H., Rasa, Iraj, Rahimi, B., Vosoughi Abedini, M., 2008, Kuh-E-Zar gold deposit in Torbat-e-Heidaryeh—New model of gold mineralization: *Iranian Journal of Crystallography and Mineralogy*, v. 16, no. 3, 14 p. [In Persian, English abstract.]
- McCall, G.J.H., 1997, The geotectonic history of the Makran and adjacent areas of southern Iran: *Journal of Asian Earth Sciences*, v. 15, p. 517–531.
- McCann, T., Chalot-Prat, F., and Saintot, A., 2010, The early Mesozoic evolution of the western Greater Caucasus (Russia)—Triassic-Jurassic sedimentary and magmatic history, *in* Sosson, M., Kaymakci, N., Stephenson, R.A., Bergerat, F., and Starostenko, V., eds., *Sedimentary basin tectonics from the Black Sea and Caucasus to the Arabian Platform: London, Geological Society Special Publication 340*, p. 181–238.
- McInnes, B.I.A., Evans, N.J., Fu, F.Q., and Garwin, S., 2005, Application of thermochronology to hydrothermal ore deposits: *Reviews in Mineralogy and Geochemistry*, v. 58, p. 467–498.
- McQuarrie, N., Stock, J.M., Verdel, C., and Wernicke, B.P., 2003, Cenozoic evolution of Neotethys and implications for the causes of plate motions: *Geophysical Research Letters*, v. 30, no. 20, 4 p.
- Mehrabi, A., and Derkshani, R., 2010, Generation of integrated geochemical-geological predictive model of porphyry-Cu potential, Chahargonbad District, Iran [abs.]: *Geochimica et Cosmochimica Acta*, v. 74, no. 11, Goldschmidt Conference, 20th, Knoxville, Tenn., June 13–18, 2010 [Proceedings], p. A694.
- Meshkani, S.A., Mehrabi, B., Yaghubpur, A., and Alghalandis, Y.F., 2011, The application of geochemical pattern recognition to regional prospecting—A case study of the Sanandaj-Sirjan metallogenic zone, Iran: *Journal of Geochemical Exploration*, v. 108, p. 183–195.
- Metz, H.C., 1987, ed., *Iran—A country study: U.S. Library of Congress, Federal Research Division*, accessed June 25, 2012, at <http://countrystudies.us/iran/71.htm>.
- Meulenkamp, J.E., Wortel, M.J.R., van Wamel, W.A., Spakman, W., and Hoogerduyn Strating, E., 1988, On the Hellenic subduction zone and the geodynamic evolution of Crete since the late middle Miocene: *Tectonophysics*, v. 146, p. 203–215.

- Mincor Resources NL, 2003, Annual report 2002/03: West Perth, Western Australia, Mincor Resources NL, 76 p.
- Mining Journal, 2005, Armenia: Mining Journal special publication—Armenia, 12 p.
- Mining Journal, 2010, Turkey: Mining Journal special publication—Turkey, 32 p.
- Mining Journal, 2011a, Armenia: Mining Journal special publication—Armenia, 15 p.
- Mining Journal, 2011b, Turkey: Mining Journal special publication—Turkey, 15 p.
- Mirnejad, H., Hassanzadeh, J., Cousens, B.L., and Taylor, B.E., 2010, Geochemical evidence for deep mantle melting and lithospheric delamination as the origin of the inland Damavand volcanic rocks of northern Iran: *Journal of Volcanology and Geothermal Research*, v. 198, p. 288–296.
- Mirnejad, H., Mathur, R., Einali, M., Dendas, M., and Alirezaei, S., 2010, A comparative copper isotope study of porphyry copper deposits in Iran: *Geochemistry—Exploration, Environment, Analysis*, v. 10, p. 413–418.
- Mirnejad, H., Simonetti, A., and Molasalehi, F., 2011, Pb isotopic compositions of some Zn-Pb deposits and occurrences from Urumieh-Dokhtar and Sanandaj-Sirjan Zones in Iran: *Ore Geology Reviews*, v. 39, p. 181–187.
- Mirnejad, H., Mathur, R., Hassanzadeh, J., Shafie, B., and Nourali, S., 2013, Linking Cu mineralization to host porphyry emplacement—Re-Os ages of molybdenites versus U-Pb ages of zircons and sulfur isotope compositions of pyrite and chalcopyrite from the Iju and Sarkuh porphyry deposits in southeast Iran: *Economic Geology*, June–July, v. 108, p. 861–870.
- Mitchell, J., and Westaway, R., 1999, Chronology of Neogene and Quaternary uplift and magmatism in the Caucasus—Constraints from K-Ar dating of volcanism in Armenia: *Tectonophysics*, v. 304, p. 157–186.
- Moazzen, M., and Modjarrad, M., 2005, Contact metamorphism and crystal size distribution studies in the Shivar aureole, NW Iran: *Geological Journal*, v. 40, p. 499–517.
- Mobbs, P.M., 2012, The mineral industry of Turkey [advance release], in *Area reports—International—Africa and the Middle East*: U.S. Geological Survey Minerals Yearbook 2010, p. 56.1–56.13, accessed October 26, 2012, at <http://minerals.usgs.gov/minerals/pubs/country/2010/myb3-2010-tu.pdf>.
- Mobin Co., 2012, Sungun copper mine: Mobin Co, accessed November 3, 2012, at <http://www.mobinco.com/en/projects/sungun/index.php>.
- Moghadam, H.S., Whitechurch, H., Rahgoshay, M., and Monsef, I., 2009, Significance of Nain-Baft ophiolitic belt (Iran)—Short-lived, transtensional Cretaceous back-arc oceanic basins over the Tethyan subduction zone: *Comptes Rendus Geoscience*, v. 341, p. 1016–1028.
- Moghadam, H.S., Stern, R.J., and Rahgoshay, M., 2010, The Dehshir ophiolite (central Iran)—Geochemical constraints on the origin and evolution of the Inner Zagros ophiolite belt: *Geological Society of America Bulletin*, v. 122, p. 1516–1547.
- Moghaddasi, S.J., and Mohammadi, T.N., 2010, Geology of Kalkafi granitoid intrusive body—A possible porphyry copper-molybdenum deposit [abs.]: *International Symposium on Eastern Mediterranean Geology*, 7th, Adana, Turkey, October 18–22, 2010 [Proceedings].
- Mohajjel, M., Fergusson, C.L., and Sahandi, M.R., 2003, Cretaceous-Tertiary convergence and continental collision, Sanandaj-Sirjan Zone, western Iran: *Journal of Asian Earth Sciences*, v. 21, p. 397–412.
- Moix, P., Beccalotto, L., Kozur, H.W., Hochard, C., Rosselet, F., and Stampfli, G.M., 2008, A new classification of the Turkish terranes and sutures and its implication for the paleotectonic history of the region: *Tectonophysics*, v. 451, p. 7–39.
- Molinaro, M., Zeyen, H., and Laurencin, X., 2005, Lithospheric structure beneath the south-eastern Zagros Mountains, Iran—Recent slab break-off?: *Terra Nova*, v. 17, p. 1–6.
- Mollai, H., Sharma, R., and Pe-Piper, G., 2009, Copper mineralization around the Ahar batholith, north of Ahar (NW Iran)—Evidence for fluid evolution and the origin of the skarn ore deposit: *Ore Geology Reviews*, v. 35, p. 401–414.
- Momenzadeh, M., 2005, Metallic mineral resources of Iran mined in ancient times—A brief review, in Stöllner, T., Slotta, R., and Vatandoust, A., eds., *Persia's ancient splendour—Mining, handicraft and archaeology*: Bochum, Germany, German Mining Museum, p. 8–21.
- Moon, C.J., Gotsiridze, G., Gugushvili, V., Kekelia, M., Kekelia, S., Migineishvili, R., Otkhmezuri, Z., and Özgür, N., 2001, Comparison of mineral deposits between Georgian and Turkish sectors of the Tethyan Metallogenic Belt, in Piestrzynski, A., ed., *Mineral deposits at the beginning of the 21st century*: Society for Geology Applied to Mineral Deposits (SAG) Biennial Meeting, 6th, Krakow, Poland, August 2001 [Proceedings], p. 309–312.
- Moritz, R., Ghazban, F., and Singer, B.S., 2006, Eocene gold ore formation at Muteh, Sanandaj-Sirjan tectonic zone, western Iran—A result of late-stage extension and exhumation of metamorphic basement rocks within the Zagros orogen: *Economic Geology*, v. 101, p. 1497–1524.

- Moritz, R., Selby, D., Ovtcharova, M., Mederer, J., Melkonyan, R., Hovakimyan, S., Tayan, R., Popkhadze, N., Gugushvili, V., and Ramazanov, V., 2012, Diversity of geodynamic settings during Cu, Au and Mo ore formation in the Lesser Caucasus—New age constraints [abs.]: European Mineralogical Conference, 1st, Frankfurt, Germany, September 2–6, 2012, Proceedings, v. 1, abstract EMC2012-745, 1 p.
- Morley, C.K., Kongwung, B., Julapour, A.A., Abdoilghfourian, M., Haijan, M., Waples, D., Warren, J., Otterdoom, H., Srisuriyon, K., and Kazemi, H., 2009, Structural development of a major late Cenozoic basin and transpressional belt in central Iran—The Central Basin in the Qom-Saveh area: *Geosphere*, v. 5, p. 325–362.
- Mosar, J., Kangarli, T., Bochud, M., Glasmacher, U.A., Rast, A., Brunet, M-F., and Sosson, M., 2010, Cenozoic-Recent tectonics and uplift in the Greater Caucasus—A perspective from Azerbaijan, *in* Sosson, M., Kaymakci, N., Stephenson, R.A., Bergerat, F., and Starostenko, V., eds., *Sedimentary basin tectonics from the Black Sea and Caucasus to the Arabian Platform*: London, Geological Society Special Publication 340, p. 261–280.
- Murakami, H., Watanabe, Y., and Stein, H., 2005, Re-Os ages for molybdenite from the Tepeoba breccia-centered Cu-Mo-Au deposit, western Turkey—Brecciation-triggered mineralization, *in* Mao, J., and Bierlein, F.P., eds., *Mineral deposit research—Meeting the global challenge: Proceedings of the Eighth Biennial SGA (Society for Geology Applied to Mineral Deposits) Meeting*, Beijing, August 18–21, 2005, p. 805–808.
- Murakami, H., Seo, J.H., and Heinrich, C.A., 2010, The relation between Cu/Au ratio and formation depth of porphyry-style Cu-Au ± Mo deposits: *Mineralium Deposita*, v. 45, p. 11–21.
- Mutlu, H., Sariiz, K., and Kadir, S., 2005, Geochemistry and origin of the Şaphane alunite deposit, western Anatolia, Turkey: *Ore Geology Reviews*, v. 26, p. 39–50.
- National Iranian Copper Industries Company, 2012, National Iranian Copper Industries Company: International Copper Study Group Meeting, 39th, Lisbon, Portugal, April 25–27, 2012, 16 p., accessed February 28, 2013, at <http://www.icsg.org/index.php/meetings-and-presentations-2/finish/157-2012-04-icsg-39th-regular-meeting-and-joint-study-groups-seminar-lisbon-portugal/848-iran-copper-industry-nicico>.
- Nezafati, N., 2006, Au-Sn-W-Cu-mineralization in the Astaneh-Sarband area, west central Iran, including a comparison of the ores with ancient bronze artifacts from western Asia: Tübingen, Germany, Eberhard-Karls-Universität, Ph.D. dissertation, 128 p.
- Nezafati, N., Herzig, P.M., Pernicka, E., and Momenzadeh, M., 2005, Intrusion-related gold occurrences in the Astaneh-Sarband area, west central Iran, *in* Mao, J., and Bierlein, F.P., eds., *Mineral deposit research—Meeting the global challenge: Proceedings of the Eighth Biennial SGA (Society for Geology Applied to Mineral Deposits) Meeting*, Beijing, August 18–21, 2005, p. 445–448.
- Nezampour, M.H., and Rasa, I., 2005, Using remote sensing technology for the determination of mineralization in the Kal-e-Kafi porphyritic deposit, Anarak, Iran, *in* Mao, J., and Bierlein, F.P., eds., *Mineral deposit research—Meeting the global challenge: Proceedings of the Eighth Biennial SGA (Society for Geology Applied to Mineral Deposits) Meeting*, Beijing, August 18–21, 2005, p. 565–567.
- Nicholson, K.N., Khan, M., and Mahmood, K., 2010, Geochemistry of the Chagai-Raskoh arc, Pakistan—Complex arc dynamics spanning the Cretaceous to the Quaternary: *Lithos*, v. 118, p. 338–348.
- Niroomand, S., Goldfarb, R.J., Moore, F., Mohajjel, M., and Marsh, E.E., 2011, The Kharapeh orogenic gold deposit—Geological, structural, and geochemical controls on epizonal ore formation in West Azerbaijan Province, northwestern Iran: *Mineralium Deposita*, v. 46, p. 409–428.
- Noori, R., Jafari, M.R., and Feizi, F., 2010, Studies of remote sensing for exploring copper and associated elements in the Khatoonabad (west of Mianeh region): *International Applied Geological Congress*, 1st, Mashad, Iran, April 26–28, 2010 [Proceedings], p. 870–875.
- Noori, R., Feizi, F., and Jafari, M.R., 2011, Determination of Cu and Mo potential targets in the Khatunabad based on analytical hierarchy process, west of Mianeh, Iran: *World Academy of Science, Engineering and Technology*, v. 54, p. 662–665.
- Norman, T.N., 1984, The role of the Ankara Melange in the development of Anatolia (Turkey): London, Geological Society Special Publication 17, p. 441–447.
- Northern Miner, 2009, Anatolia builds oxide mine at Copley—Sulphide mineralization also showing strength: *Northern Miner*, Daily News, November 17, 2009.
- Norwest Mineral Sector Investment Focus, 2003, Armenia—Positive outlook for mineral sector growth: Norwest Corporation, Ltd., 8 p.
- Nuinsco Resources, Ltd., 2013, Berta (Turkey): Nuinsco Resources, Ltd., Web page accessed December 4, 2013, at <http://www.nuinsco.ca/projects/berta/>.
- Oberhänsli, R., Candan, O., Bousquet, R., Rimmelé, G., Okay, A., and Goff, J., 2010, Alpine high pressure evolution of the eastern Bitlis complex, SE Turkey, *in* Sosson, M., Kaymakci, N., Stephenson, R.A., Bergerat, F., and Starostenko, V., eds., *Sedimentary basin tectonics from the Black Sea and Caucasus to the Arabian Platform*: London, Geological Society Special Publication 340, p. 461–483.
- Okay, A.I., 1989, Tectonic units and sutures in the Pontides, northern Turkey, *in* Şengör, A.M.C., ed., *Tectonic evolution of the Tethyan region*: Boston, Mass., Kluwer Academic, p. 109–116.

- Okay, A.I., 2008, Geology of Turkey—A synopsis, *in* Yalçın, Ü., ed., *Anatolian metal IV: Bochum, Germany, Der Anschnitt*, v. 21, p. 19–42.
- Okay, A.I., and Şahintürk, Ö., 1997, Geology of the Eastern Pontides, *in* Robinson, A.G., ed., *Regional and petroleum geology of the Black Sea and surrounding region: American Association of Petroleum Geologists Memoir 68*, p. 291–311.
- Okay, A.I., and Satir, M., 2006, Geochronology of Eocene plutonism and metamorphism in northeast Turkey—Evidence for a possible magmatic arc: *Geodinamica Acta*, v. 19, p. 251–266.
- Okay, A.I., Şengör, A.M.C., and Görür, N., 1994, Kinematic history of the opening of the Black Sea and its effect on the surrounding regions: *Geology*, v. 22, p. 267–270.
- Okay, A.I., Satir, M., Maluski, H., Siyako, M., Monie, P., Metzger, R., and Akyüz, S., 1996, Paleo- and Neotethyan events in northwestern Turkey—Geologic and geochronologic constraints, *in* Yin, A., and Harrison, T.M., eds., *The tectonic evolution of Asia: Cambridge, U.K., Cambridge University Press*, p. 420–441.
- Okay, A.I., Tansel, İ., and Tüyzüz, O., 2001, Obduction, subduction and collision as reflected in the Upper Cretaceous-Lower Eocene sedimentary record of western Turkey: *Geological Magazine*, v. 138, p. 117–142.
- Omrani, J., Agard, P., Whitechurch, H., Benoit, M., Prouteau, G., and Jolivet, L., 2008, Arc-magmatism and subduction history beneath the Zagros Mountains, Iran—A new report of adakites and geodynamic consequences: *Lithos*, v. 106, p. 380–398.
- Önder, Ş., 2006, Turkey's mining regime: *Mining Journal Special Turkey Publication*, p. 7–8.
- Orris, G.J., and Bliss, J.D., 2002, Mines and mineral occurrences of Afghanistan: U.S. Geological Survey Open-File Report 02–110, 95 p., available at <http://pubs.usgs.gov/of/2002/0110/>.
- Oyman, T., 2010, Geochemistry, mineralogy and genesis of the Ayazmant Fe-Cu skarn deposit in Ayvalik (Balıkesir), Turkey: *Ore Geology Reviews*, v. 37, p. 175–201.
- Özkümüş, S., 2009, Geochemical investigation of Kurtyuvasi (Oltu-Erzurum) copper-gold mineralization: Turkey, University of Çukurova, Master of Science thesis, 64 p. [In Turkish, English abstract.]
- Geological Survey of Pakistan, 2009, Mineral profile of Balochistan: Geological Survey of Pakistan, [24] p.
- Pakistan Ministry of Petroleum and Natural Resources, 1995, National mineral policy, 1995: Pakistan Ministry of Petroleum and Natural Resources, [22] p.
- Panahi Shahri, M., Karimpour, M.H., and Shabani, F., 2010, Mineralization and geochemical exploration in volcanic-plutonic area of Halakabad village (Sabzevar), regarding to Cu-porphyry deposits: Mashhad, Iran, Ferdowsi University of Mashhad, *Journal of Economic Geology*, v. 2, p. 21–37. [In Persian, English abstract.]
- Pang, K-N., Chung, Sun-Lin, Zarrinkoub, M.H., Mohammadi, S.S., Yang, H-M., Chu, C-H., Lee, H-Y., and Lo, C-H., 2012, Age, geochemical characteristics and petrogenesis of Late Cenozoic intraplate alkali basalts in the Lut-Sistan region, eastern Iran: *Chemical Geology*, v. 306–307, p. 40–53.
- Parsapoor, A., Khalili, M., and Mackizadeh, M.A., 2009, The behaviour of trace and rare earth elements (REE) during hydrothermal alteration in the Rangan area (central Iran): *Journal of Asian Earth Sciences*, v. 34, p. 123–134.
- Pasquarè, G., Poli, S., Vezzoli, L., and Zanchi, A., 1988, Continental arc volcanism and tectonic setting in central Anatolia, Turkey: *Tectonophysics*, v. 146, p. 217–230.
- Pazand, K., Hezarkhani, A., and Ataei, M., 2011, The application of litho-geochemical and alteration index for copper mineralization in the Sonajil area, NW Iran: *Arabian Journal of Geosciences*, v. 6, p. 1447–1456.
- Pazand, K., Hezarkhani, A., Ataei, M., and Ghanbari, Y., 2011, Combining AHP with GIS for predictive Cu porphyry potential mapping—A case study in Ahar area (NW Iran): *Natural Resources Research*, v. 20, p. 251–262.
- Pazand, K., Hezarkhani, A., and Ataei, M., 2012, Using TOPSIS approaches for predictive porphyry Cu potential mapping—A case study in Ahar-Arasbaran area (NW, Iran): *Computers and Geosciences*, v. 49, p. 62–71.
- Pearce, J.A., Bender, J.F., De Long, S.E., Kidd, W.S.F., Low, P.J., Güner, Y., Saroglu, F., Yilmaz, Y., Moorbath, S., and Mitchell, J.G., 1990, Genesis of collision volcanism in eastern Anatolia, Turkey: *Journal of Volcanology and Geothermal Research*, v. 44, p. 189–229.
- Perelló, J., Raziq, A., Schloderer, J., and Ur-Rehman, A., 2008, The Chagai porphyry copper belt, Baluchistan Province, Pakistan: *Economic Geology*, v. 103, p. 1583–1612.
- Pessagno, E.A., Ghazi, A.M., Kariminia, Mohsen, Duncan, R.A., and Hassani, A.A., 2005, Tectonostratigraphy of the Khoy complex, northwestern Iran: *Stratigraphy*, v. 2, p. 49–63.
- Peters, S.G., Ludington, S.D., Orris, G.J., Sutphin, D.M., Bliss, J.D., and Rytuba, J.J., 2007, Preliminary nonfuel mineral resource assessment of Afghanistan 2007: U.S. Geological Survey Open-File Report 2007–1214, DVD-ROM, version 1.0, scale 1:850,000. (Also available at <http://pubs.usgs.gov/of/2007/1214/>.)

- Peters, S.G., King, T.V.V., Mack, T.J., and Chornack, M.P., eds., and the U.S. Geological Survey Afghanistan Mineral Assessment Team, 2011, Summaries of important areas for mineral investment and production opportunities of nonfuel minerals in Afghanistan: U.S. Geological Survey Open-File Report 2011–1204, v. 1, 810 p. plus appendixes on DVD. (Also available at <http://pubs.usgs.gov/of/2007/1204/>.)
- Philip, H., Cisternas, A., Gvishiani, A., and Gorshkov, A., 1989, The Caucasus—An actual example of the initial stages of continental collision: *Tectonophysics*, v. 161, p. 1–21.
- Pilot Gold, Inc., 2011, Turkey: Pilot Gold, Inc., Web page, accessed January 4, 2012, at <http://pilotgold.com/our-projects/turkey>.
- Pilot Gold, Inc., 2012a, Pilot Gold announces preliminary economic assessment results for Halilaga copper-gold porphyry project: Pilot Gold, Inc., press release, October 10, 2012, 6 p., accessed November 5, 2012, at <http://www.infomine.com/index/pr/PB239981.PDF>.
- Pilot Gold, Inc., 2012b, Pilot Gold launches 2012 work program at Halilaga: Pilot Gold, Inc., press release, May 30, 2012, 3 p. accessed November 5, 2012, at <http://www.infomine.com/index/pr/PB198556.PDF>.
- Pilot Gold, Inc., 2012c, Pilot Gold reports 0.64 g/t gold and 0.52% copper over 134.90 metres at Halilaga: Pilot Gold, Inc., press release, August 1, 2012, 3 p., accessed November 5, 2012, at <http://www.infomine.com/index/pr/PB218605.PDF>.
- Platt, J.P., Leggett, J.K., Young, J., Raza, H., and Alam, S., 1985, Large-scale sediment underplating in the Makran accretionary prism, southwest Pakistan: *Geology*, v. 13, p. 507–511.
- Pollastro, R.M., Karshbaum, A.S., and Viger, R.J., 1998, Maps showing geology, oil and gas fields and geologic provinces of the Arabian Peninsula (version 2.0): U.S. Geological Survey Open-File Report 97–470, digital map, scale 1:2,000,000, CD-ROM.
- Popovic, R., 1975, Some of the structural and genetic characteristics and the zonal distribution of nonferrous metals deposits in Eastern Pontides: *Turkey Mineral Research and Exploration Institute Bulletin*, no. 85, foreign edition, p. 1–16 and illustrations and map, scale 1:400,000.
- Pour, A.B., and Hashim, M., 2011, Identification of hydrothermal alteration minerals for exploring of porphyry copper deposit using ASTER data, SE Iran: *Journal of Asian Earth Sciences*, v. 42, p. 1309–1323.
- Pour, A.B., Hashim, M., and Marghany, M., 2011, Using spectral mapping techniques on short wave infrared bands of ASTER remote sensing data for alteration mineral mapping in SE Iran: *International Journal of the Physical Sciences*, v. 6, p. 917–939.
- Pourkhosrow, M., Karimpour, M.H., and Khosravi, M., 2007, Petrology, alteration, and geochemistry of Kajeh porphyry Cu-Au prospecting area, western Lut Zone (eastern Iran) [abs.]: *Iran Geological Society Symposium*, 11th, Mashhad [Proceedings], 1 p.
- PressTV, 2009, Kazakh to invest in Iran mining sector: PressTV press release, October 28, 2009, 1 p., accessed June 25, 2012, at <http://edition.presstv.ir/detail/109835.html>.
- Qureshi, M.J., Tariq, M.A., and Abid, Q.Z., 1993, Geological map of Pakistan: Geological Survey of Pakistan, 4 sheets, scale 1:1,000,000.
- Rajabi, A., Rastad, E., and Canet, C., 2012, Metallogeny of Cretaceous carbonate-hosted Zn-Pb deposits of Iran—Geotectonic setting and data integration for future mineral exploration: *International Geology Review*, v. 54, p. 1649–1672.
- Ramezani, J., and Tucker, R.D., 2003, The Saghand region, central Iran—U-Pb geochronology, petrogenesis and implications for Gondwana tectonics: *American Journal of Science*, v. 303, p. 622–665.
- Ranjbar, H., and Honarmand, M., 2004, Integration and analysis of airborne geophysical and ETM+ data for exploration of porphyry type deposits in the Central Iranian Volcanic Belt using fuzzy classification: *International Journal of Remote Sensing*, v. 25, p. 4729–4741.
- Ranjbar, H., Shahriari, H., and Honarmand, M., 2005, Integration of ASTER and airborne geophysical data for exploration of copper mineralization—A case study of Sar Cheshmeh area: *International Society for Photogrammetry and Remote Sensing Congress*, 20th, Istanbul, July 12–23, 2004, [Proceedings], v. 35, pt. B4, 6 p.
- Reuter, M., Piller, W.E., Harzhauser, M., Mandic, O., Berning B., Rögl, F., Kroh, A., Aubry, M-P., Wielandt-Schuster, U., and Hamedani A., 2009, The Oligo-Miocene Qom Formation (Iran)—Evidence for an early Burdigalian restriction of the Tethyan Seaway and closure of its Iranian gateways: *International Journal of Earth Sciences*, v. 98, p. 627–650.
- Rezaeian, M., 2008, Coupled tectonics, erosion and climate in the Alborz Mountains, Iran: Cambridge, U.K., University of Cambridge, Ph.D. dissertation, 219 p.
- Rice, S.P., Robertson, A.H.F., and Ustaömer, T., 2006, Late Cretaceous-early Cenozoic tectonic evolution of the Eurasian active margin in the Central and Eastern Pontides, northern Turkey, in Robertson, A.H.F., and Mountrakis, D., eds., *Tectonic development of the eastern Mediterranean region*: London, Geological Society Special Publication 260, p. 413–445.
- Richards, J.P., 2003, Tectono-magmatic precursors for porphyry Cu-(Mo-Au) deposit formation: *Economic Geology*, v. 96, p. 1515–1533.

- Richards, J.P., 2009, Postsubduction porphyry Cu-Au and epithermal Au deposits—Products of remelting of subduction-modified lithosphere: *Geology*, v. 37, p. 247–250.
- Richards, J.P., 2011, Magmatic to hydrothermal metal fluxes in convergent and collided margins: *Ore Geology Reviews*, v. 40, p. 1–26.
- Richards, J.P., and Kerrich, R., 2007, Special paper—Adakite-like rocks—Their diverse origins and questionable role in metallogenesis: *Economic Geology*, v. 102, p. 537–576.
- Richards, J.P., Wilkinson, D., and Ullrich, T., 2006, Geology of the Sari Gunay epithermal gold deposit, northwest Iran: *Economic Geology*, v. 101, p. 1455–1496.
- Richards, J.P., Spell, T., Rameh, E., Razique, A., and Fletcher, T., 2012, High Sr/Y magmas reflect arc maturity, high magmatic water content, and porphyry Cu ± Mo ± Au potential—Examples from the Tethyan arcs of central and eastern Iran and western Pakistan: *Economic Geology*, v. 107, p. 295–332.
- Ritz, J-F., Nazari, H., Ghassemi, A., Salamati, R., Shafei, A., Solaymani, S., and Vernant, P., 2006, Active transtension inside central Alborz—A new insight into northern Iran-southern Caspian geodynamics: *Geology*, v. 34, p. 477–480.
- Robertson, A.H.F., and Mountrakis, D., 2006, Tectonic development of the eastern Mediterranean region—An introduction, *in* Robertson, A.H.F., and Mountrakis, D., eds., *Tectonic development of the eastern Mediterranean region*: London, Geological Society Special Publication 260, p. 1–9.
- Robertson, A.H.F., Ustaömer, T., Parlak, O., Ünlügenç, U.C., Taşlı, K., and İnan, N., 2006, The Berit transect of the Tauride thrust belt, S Turkey—Late Cretaceous-early Cenozoic accretionary/collisional processes related to closure of the southern Neotethys: *Journal of Asian Earth Sciences*, v. 27, p. 108–145.
- Robinson, A.G., Banks, C.J., Rutherford, M.M., and Hirst, J.P.P., 1995, Stratigraphic and structural development of the Eastern Pontides, Turkey: *Journal of the Geological Society*, v. 152, p. 861–872.
- Rolland, Y., Billo, S., Corsini, M., Sosson, M., and Galoyan, G., 2009, Blueschists of the Amassia-Stepanavan suture zone (Armenia)—Linking Tethys subduction history from E-Turkey to W-Iran: *International Journal of Earth Sciences*, v. 98, p. 533–550.
- Rolland, Y., Galoyan, Gh., and Sosson, M., 2010, The Armenian ophiolite—Insights for Jurassic back-arc formation, Lower Cretaceous hot spot magmatism and Upper Cretaceous obduction over the South Armenian block, *in* Sosson, M., Kaymakci, N., Stephenson, R.A., Bergerat, F., and Starostenko, V., eds., *Sedimentary basin tectonics from the Black Sea and Caucasus to the Arabian Platform*: London, Geological Society Special Publication 340, p. 353–382.
- Rolland, Y., Perincek, D., Kaymakci, N., Sosson, M., Barrier, E., and Avagyan, A., 2012, Evidence for ~80–75 Ma subduction jump during Anatolide-Tauride-Armenian block accretion and ~48 Ma Arabia-Eurasia collision in Lesser Caucasus-East Anatolia: *Journal of Geodynamics*, v. 56–57, p. 76–85.
- Root, D.H., Menzie, W.D., and Scott, W.A., 1992, Computer Monte Carlo simulation in quantitative resource estimation: *Natural Resources Research*, v. 1, p. 125–138.
- Roshani, P., Mokhtari, A.R., and Tabatabaei, S.H., 2013, Objective based geochemical anomaly detection—Application of discriminant function analysis in anomaly delineation in the Kuh Panj porphyry Cu mineralization (Iran): *Journal of Geochemical Exploration*, v. 130, p. 65–73.
- Rossetti, F., Nasrabad, M., Theye, T., Gerdes, A., Monié, P., Lucci, F., and Vignaroli, G., 2013, Slab melting, adakite differentiation and emplacement—Evidence from the Late Paleocene Sabzevar subduction channel (NE central Iran): *Geological Society of America Abstracts with Programs*, v. 45, no. 7, p. 515.
- Rowan, L.C., Schmidt, R.G., and Mars, J.C., 2006, Distribution of hydrothermally altered rocks in the Reko Diq, Pakistan mineralized area based on spectral analysis of ASTER data: *Remote Sensing of Environment*, v. 104, p. 74–87.
- Rundkvist, D.V., ed., 2001 [2002], *Mineragenic map of Russian Federation and adjacent states (with the boundaries of former USSR)*: Ministry of Natural Resources of the Russian Federation, State Research and Development Enterprise (Aerogeologica), 49 p., Excel workbook, and 1 map on 18 sheets, scale 1:2,500,000, CD-ROM.
- Saadat, S., Karimpour, M.H., Ajayebi, Kimiya, and Stern, Charles, 2007, Petrology, fluid inclusion thermometry, and geochemistry of Tannurjeh porphyry Cu-Au, northeastern Iran [abs.]: *Geological Society of America Abstracts with Programs*, v. 39, no. 6, p. 412.
- Saadat, S., Karimpour, M.H., and Stern, C., 2010, Petrochemical characteristics of Neogene and Quaternary alkali olivine basalts from the western margin of the Lut block, eastern Iran: *Iranian Journal of Earth Sciences*, v. 2, p. 87–106.
- Sadeghian, M., Bouchez, J.L., Nédélec, A., Siqueira, R., and Valizadeh, M.V., 2005, The granite pluton of Zahedan (SE Iran)—A petrological and magnetic fabric study of a syntectonic sill emplaced in a transtensional setting: *Journal of Asian Earth Sciences*, v. 25, p. 301–327.
- Saein, L.D, Rasa, Iraj, Omran, N.R., Moarefvand, P., and Afzal, P., 2012, Application of concentration-volume fractal method in induced polarization and resistivity data interpretation for Cu-Mo porphyry deposits exploration, case study—Nowchun Cu-Mo deposit, SE Iran: *Nonlinear Processes in Geophysics*, v. 19, no. 4, p. 431–438.

- Safirova, E., 2013a, The mineral industry of Azerbaijan [advance release], *in* Area reports—International—Europe: U.S. Geological Survey Minerals Yearbook 2011, v. III, p. 5.1–5.5, accessed September 2013 at <http://minerals.usgs.gov/minerals/pubs/country/2011/myb3-2011-aj.pdf>.
- Safirova, E., 2013b, The mineral industry of Georgia [advance release], *in* Area reports—International—Europe: U.S. Geological Survey Minerals Yearbook 2011, v. III, p. 5.1–5.5, accessed September 2013 at <http://minerals.usgs.gov/minerals/pubs/country/2011/myb3-2011-gg.pdf>.
- Saintot, A., Brunet, M-F., Yakovlev, Fedor, Sébrier, Michel, Stephenson, Randell, Ershov, Andrei, Chalot-Prat, Françoise, and McCann, Tommy, 2006, The Mesozoic–Cenozoic tectonic evolution of the Greater Caucasus: London, Geological Society Memoir 32, p. 277–289.
- Salavati, M., 2008, Petrology, geochemistry and mineral chemistry of extrusive alkalic rocks of the southern Caspian Sea ophiolite, northern Alborz, Iran—Evidence of alkaline magmatism in southern Eurasia: *Journal of Applied Sciences*, v. 8, p. 2202–2216.
- Salehi, M.H., Doosti, E.A., and Ahadnejad, V., 2009, Mineralization related to Alvand pluton in the Hamadan, western Iran [abs.]: *Geophysical Research Abstracts*, v. 11, abstract EGU2009-315-2.
- Salehian, M., and Ghaderi, M., 2010a, Alteration and mineralization at Daralu porphyry copper deposit, south of Kerman, southeast Iran: *International Applied Geological Congress, 1st, Mashad, Iran, April 26–28, 2010 [Proceedings]*, p. 155–161.
- Salehian, M., and Ghaderi, M., 2010b, Fluid inclusion evolution at Daralu porphyry copper deposit, southeast Iran [abs.]: *Tectonic crossroads—Evolving orogens of Eurasia-Africa-Arabia Conference, Ankara, October 4–8, 2010 [Proceedings]*, p. 47, accessed July 15, 2014, at http://www.geosociety.org/meetings/2010turkey/TectonicCrossroads2010_AWP.pdf.
- Samani, B., 1998, Distribution, setting and metallogenesis of copper deposits in Iran, *in* Porter, T.M., ed., *Porphyry and hydrothermal copper and gold deposits—A global perspective*, Australian Mineral Foundation Conference, Perth, November 30–December 1, 1998 [Proceedings]: Adelaide, PGC Publishing, p. 151–174.
- Schloderer, J., 2003, Reko Diq exploration and discovery: Prospectors and Developers Association of Canada Annual Convention, 2003 [Proceedings], accessed July 15, 2014, at <http://www.pdac.ca/pdac/publications/papers/2003/Schloderer.pdf>.
- Scott, K., Gray, J., and Kirkham, G., 2012, Preliminary economic assessment technical report for the Halilağa project, Turkey: Vancouver, Canada, SRK Consulting, Inc., report prepared for Truva Bakir Maden İşletmeleri A.Ş. and Pilot Gold, Inc., 208 p. and appendixes.
- Seedorff, E., Dilles, J.H., Proffett, J.M., Einaudi, M.T., Zürcher, L., Stavast, W.J.A., Johnson, D. A., and Barton, M.D., 2005, Porphyry deposits: characteristics and origin of hypogene features, *in* Hedenquist, J.W., Thompson, J.F.H., Goldfarb, R.J., and Richards, J.P., eds., *Economic Geology one hundredth anniversary volume, 1905–2005: Society of Economic Geologists*, p. 251–298.
- Şen, C., Arslan, M., and Van, Ali, 1998, Geochemical and petrological characteristics of the Eastern Pontide Eocene (?) alkaline volcanic province, NE Turkey: *Turkish Journal of Earth Sciences*, v. 7, p. 231–239.
- Şen, P.A., Temel, A., and Gourgaud, A., 2004, Petrogenetic modelling of Quaternary post-collisional volcanism—A case study of central and eastern Anatolia: *Geological Magazine*, v. 141, p. 81–98.
- Şengör, A.M.C., 1979, Mid-Mesozoic closure of Permo-Triassic Tethys and its implications: *Nature*, v. 279, p. 590–593.
- Şengör, A.M.C., 1987, Tectonics of the Tethysides—Orogenic collage development in a collisional setting: *Annual Review of Earth and Planetary Sciences*, v. 15, p. 213–244.
- Şengör, A.M.C., and Kidd, W.S.F., 1979, Post-collisional tectonics of the Turkish-Iranian plateau and a comparison with Tibet: *Tectonophysics*, v. 55, p. 361–376.
- Şengör, A.M.C., and Yilmaz, Y., 1981, Tethyan evolution of Turkey—A plate tectonic approach: *Tectonophysics*, v. 75, p. 181–241.
- Şengör, A.M.C., Cin, ., Rowley, D.B., and Nie, S.Y., 1991, Magmatic evolution of the Tethysides—A guide to reconstruction of collage history: *Palaeogeography, Palaeoclimatology, Palaeoecology*, v. 87, p. 411–440.
- Şengör, A.M.C., Cin, A., Rowley, D.B., and Nie, S.Y., 1993, Space-time patterns of magmatism along the Tethysides—A preliminary study: *Journal of Geology*, v. 101, p. 51–84.
- Sepahi, A.A., and Malvandi, F., 2008, Petrology of the Bouein Zahra-Naein plutonic complexes, Urumieh-Dokhtar belt, Iran, with special reference to granitoids of the Saveh plutonic complex: *Neues Jahrbuch für Mineralogie*, v. 185, p. 99–115.
- Sezerer Kuru, G., Cengiz, I., Aslan, M., and Sakitas, A., 2010, Determination of fluid inclusion characteristics and mineral exploration using them in the zones of porphyry-type alteration in the locality of Erzurum-Oltu-İnanmış by means of fluid inclusion petrography [abs.]: *Geochimica et Cosmochimica Acta, Goldschmidt Conference, 20th, Knoxville, Tenn., June 13–18, 2010 [Proceedings]*, v. 74, no. 11, p. A938.
- Shabanian, E., Acocella, V., Gioncada, A., Ghasemi, H., and Bellier, O., 2012, Structural control on volcanism in intraplate post collisional settings—Late Cenozoic to Quaternary examples of Iran and eastern Turkey: *Tectonics*, v. 31, TC3013, 25 p.

- Shafiei, B., 2010, Lead isotope signatures of the igneous rocks and porphyry copper deposits from the Kerman Cenozoic magmatic arc (SE Iran), and their magmatic-metallogenic implications: *Ore Geology Reviews*, v. 38, p. 27–36.
- Shafiei, B., and Shahabpour, J., 2008, Gold distribution in porphyry copper deposits of Kerman region, southeastern Iran: *Iran, Journal of Sciences*, v. 19, p. 247–260.
- Shafiei, B., Shahabpour, J., and Haschke, M., 2008, Transition from Paleogene normal calc-alkaline to Neogene adakitic-like plutonism and Cu-metallogeny in the Kerman porphyry copper belt—Response to Neogene crustal thickening: *Iran, Journal of Sciences*, v. 19, p. 67–84.
- Shafiei, B., Haschke, M., and Shahabpour, J., 2009, Recycling of orogenic arc crust triggers porphyry Cu mineralization in Kerman Cenozoic arc rocks, southeastern Iran: *Mineralium Deposita*, v. 44, p. 265–283.
- Shahabpour, J., 1991, Some secondary ore formation features of the Sar-Cheshmeh porphyry copper-molybdenum deposit, Kerman, Iran: *Mineralium Deposita*, v. 26, p. 275–280.
- Shahabpour, J., 1992, Unroofing “fragmentites” as a reconnaissance exploration tool in the central Iranian porphyry copper belt: *Economic Geology*, v. 87, p. 1599–1606.
- Shahabpour, J., 1999, The role of deep structures in the distribution of some major ore deposits in Iran, NE of the Zagros Thrust Zone: *Geodynamics*, v. 28, p. 237–250.
- Shahabpour, J., 2005, Tectonic evolution of the orogenic belt in the region located between Kerman and Neyriz: *Journal of Asian Earth Sciences*, v. 24, p. 405–417.
- Shahabpour, J., 2007, Island-arc affinity of the central Iranian volcanic belt: *Journal of Asian Earth Sciences*, v. 30, p. 652–665.
- Shahabpour, J., 2010, Tectonic implications of the geochemical data from the Makran igneous rocks in Iran: *Island Arc*, v. 19, p. 676–689.
- Shahabpour, J., and Kramers, J.D., 1987, Lead isotope data from the Sar-Cheshmeh porphyry copper deposit, Iran: *Mineralium Deposita*, v. 22, p. 278–281.
- Shahbazi, H., Siebel, W., Pourmoafae, M., Ghorbani, M., Sephai, A.A., Shang, C.K., and Vousoughi Abedini, M., 2010, Geochemistry and U-Pb zircon geochronology of the Alvand plutonic complex in Sanandaj-Sirjan Zone (Iran)—New evidence for Jurassic magmatism: *Journal of Asian Earth Sciences*, v. 39, p. 668–683.
- Shahidi, A., Barrier, E., Brunet, M-F., Saidi, A., and Muller, C., 2007, Tectonic evolution of Alborz since Mesozoic (Iran) [abs.]: *Geophysical Research Abstracts*, v. 9, [2] p.
- Shahrbabaky, A.M., 1997, Geochemistry, geochronology and petrography of feldspathoid-bearing rocks in the Urumiyeh-Dokhtar volcanic belt, Iran: Wollongong, Australia, University of Wollongong, Ph.D. dissertation, 412 p.
- Shahrokhi, S.V., Rezaei, P., and Sahamieh, R.Z., 2010, Mineralogical and geochemical characteristics of metamorphic halo of Yazd magmatic rocks (central Iran): *International Applied Geological Congress, 1st, Mashad, Iran, April 26–28, 2010 [Proceedings]*, p. 260–266.
- Shamanian, G.H., Hedenquist, J.W., Hattori, K.H., and Hassanzadeh, Jamshid, 2004, The Gandy and Abolhassani epithermal prospects in the Alborz magmatic arc, Semnan Province, northern Iran: *Economic Geology*, v. 99, p. 691–712.
- Sheibi, M., Esmaeily, D., Nédélec, A., Bouchez, J-L., and Kananian, Ali, 2010, Geochemistry and petrology of garnet-bearing S-type Shir-Kuh Granite, southwest Yazd, central Iran: *Island Arc*, v. 19, p. 292–312.
- Sherafat, S., Khodami, M., and Mohammadi, F., 2010, Geochemistry of adakitic volcanism in central Iran: *International Applied Geological Congress, 1st, Mashad, Iran, April 26–28, 2010 [Proceedings]*, p. 229–232.
- Shojaat, B., Hassanipak, A.A., Mobasher, K., and Ghazi, A.M., 2003, Petrology, geochemistry and tectonics of the Sabzevar ophiolite, north central Iran: *Journal of Asian Earth Sciences*, v. 21, p. 1053–1067.
- Shroder, J.F., 1981, Physical resources and the development of Afghanistan: *Studies in Comparative International Development, Fall-Winter 1981*, v. 16, no. 3–4, p. 36–63.
- Siddiqui, R.H., Khan, M.A., and Jan, M.Q., 2007, Geochemistry and petrogenesis of the Miocene alkaline and sub-alkaline volcanic rocks from the Chagai arc, Baluchistan, Pakistan—Implications for porphyry Cu-Mo-Au deposits: *Journal of Himalayan Earth Sciences*, v. 40, p. 1–23.
- Siddiqui, R.H., Khan, M.A., Jan, M.Q., and Brohi, I.A., 2010, Paleocene tholeiitic volcanism and oceanic island arc affinities of the Chagai arc, Baluchistan, Pakistan: *Jamshoro, Pakistan, Sindh University Research Journal*, v. 42, p. 83–98.
- Siddiqui, R.H., Jan, M.Q., and Khan, M.A., 2012, Petrogenesis of Late Cretaceous lava flows from a Ceno-Tethyan island arc—The Raskoh arc, Baluchistan, Pakistan: *Journal of Asian Earth Sciences*, v. 59, p. 24–38.
- Sillitoe, R.H., 1978, Metallogenic evolution of a collisional mountain belt in Pakistan—A preliminary analysis: *London, Journal of the Geological Society*, v. 135, p. 377–387.
- Sillitoe, R.H., 2010, Porphyry copper systems: *Economic Geology*, v. 105, p. 3–41.
- Sillitoe, R.H., and Khan, S.N., 1977, Geology of Saindak porphyry copper deposit, Pakistan: *Transactions of the Institute of Mining and Metallurgy*, v. 86, p. B27–B42.

- Simmonds, V., Calagari, A.A., Moayyed, M., and Jahangiri, A., 2010, Petrologic and petrogenetic study of Kighal porphyry stock (north of Varzeghan, East Azarbaijan Province, NW Iran): Tectonic crossroads—Evolving orogens of Eurasia-Africa-Arabia Conference, Ankara, October 4–8, 2010, p. 47, accessed July 15, 2014 [Proceedings], at http://www.geosociety.org/meetings/2010turkey/TectonicCrossroads2010_AWP.pdf.
- Singer, D.A., 1993, Basic concepts in three-part quantitative assessments of undiscovered mineral resources: *Nonrenewable Resources*, v. 2, p. 69–81.
- Singer, D.A., 1995, World class base and precious metal deposits—A quantitative analysis: *Economic Geology*, v. 90, p. 88–104.
- Singer, D.A., 2007a, Estimating amounts of undiscovered resources, in Briskey, J.A., and Schulz, K.J., eds., Proceedings for a workshop on deposit modeling, mineral resource assessment, and their role in sustainable development, International Geological Congress, 31st, Rio de Janeiro, Brazil, August 18–19, 2000: U.S. Geological Survey Circular 1294, p. 79–84, available at <http://pubs.usgs.gov/circ/2007/1294/>.
- Singer, D.A., 2007b, Short course introduction to quantitative mineral resource assessments: U.S. Geological Survey Open-File Report 2007–1434, 13 p., available at <http://pubs.usgs.gov/of/2007/1434/>.
- Singer, D.A., 2008, Mineral deposit densities for estimating mineral resources: *Mathematical Geosciences*, v. 40, p. 33–46.
- Singer, D.A., and Menzie, W.D., 2005, Statistical guides to estimating the number of undiscovered mineral deposits—An example with porphyry copper deposits, in Cheng, Q., and Bonham-Carter, G., eds., Proceedings of IAMG—The annual conference of the International Association for Mathematical Geology: Toronto, Canada, York University, Geomatics Research Laboratory, p. 1028–1033.
- Singer, D.A., and Menzie, W.D., 2010, Quantitative mineral resource assessments—An integrated approach: New York, Oxford University Press, 232 p.
- Singer, D.A., Berger, V.I., Menzie, W.D., and Berger, B., 2005, Porphyry copper deposit density: *Economic Geology*, v. 100, p. 491–514.
- Singer, D.A., Berger, V.I., and Moring, B.C., 2008, Porphyry copper deposits of the world—Database and grade and tonnage models, 2008: U.S. Geological Survey Open-File Report 2008–1155, 45 p., available at <http://pubs.usgs.gov/of/2008/1155/>.
- Sissakian, V.K., 2000, Geological map of Iraq: Baghdad, Iraq, State Establishment of Geological Survey and Mining GEOSURV, scale 1:1,000,000, 1 sheet.
- Smithsonian Institution, 2002a, Damavand: Smithsonian Institution, National Museum of Natural History, Global Volcanism Program Web page, accessed February 8, 2013, at <http://www.volcano.si.edu/world/volcano.cfm?vnum=0302-01->.
- Smithsonian Institution, 2002b, Sabalan: Smithsonian Institution, National Museum of Natural History, Global Volcanism Program Web page, accessed February 8, 2013, at <http://www.volcano.si.edu/world/volcano.cfm?vnum=0302-002>.
- Smithsonian Institution, 2002c, Sahand: Smithsonian Institution, National Museum of Natural History, Global Volcanism Program Web page, accessed February 8, 2013, at <http://www.volcano.si.edu/world/volcano.cfm?vnum=0302-001>.
- Smithsonian Institution, 2013, Volcanoes by name: Smithsonian Institution, National Museum of Natural History, Global Volcanism Program Web page, accessed November 20, 2013, at http://www.volcano.si.edu/list_volcano.cfm.
- Soltani, A., 2000, Geochemistry and geochronology of I-type granitoid rocks in the northeastern central Iran Plate: Wollongong, Australia, University of Wollongong, Ph.D. dissertation, 321 p.
- Somarin, A.K., 2004, Garnet composition as an indicator of Cu mineralization—Evidence from skarn deposits of NW Iran: *Journal of Geochemical Exploration*, v. 81, p. 47–57.
- Somarin, A.K., 2006, Geology and geochemistry of the Mendejin plutonic rocks, Mianeh, Iran: *Journal of Asian Earth Sciences*, v. 27, p. 819–834.
- Somarin, A.K., 2010, Garnetization as a ground preparation process for copper mineralization—Evidence from the Mazraeh skarn deposit, Iran: *International Journal of Earth Sciences*, v. 99, p. 343–356.
- Somarin, A.K., and Lentz, D.R., 2008, Mineralogy, geochemistry and fluid evolution of a fossil hydrothermal system in the Paleogene Mendejin volcanic sequence, East Azarbaijan, Iran: *Mineralogy and Petrology*, v. 94, p. 123–143.
- Somarin, A.K., and Moayyed, M., 2002, Granite- and gabbrodiorite-associated skarn deposits of NW Iran: *Ore Geology Reviews*, v. 20, p. 127–138.
- Somarin, A.K., Liaghat, S., Hosseini, A., and Zarasvandi, M., 2005, World skarn deposits—Skarns of Iran, in Meinert, L.D., Dipple, G.M., and Nicolescu, Stefan, World skarn deposits, in Hedenquist, J.W., Thompson, J.F.H., Goldfarb, R.J., and Richards, J.P., eds., *Economic Geology one hundredth anniversary volume, 1905–2005*: Society of Economic Geologists, CD-ROM, 2 p. and data (table 10.1) in appendix.

- Sosson, M., Kaymakci, N., Stephenson, R., Bergerat, F., and Starostenko, V., 2010a, Sedimentary basin tectonics from the Black Sea and Caucasus to the Arabian Platform—Introduction, *in* Sosson, M., Kaymakci, N., Stephenson, R.A., Bergerat, F., and Starostenko, V., eds., *Sedimentary basin tectonics from the Black Sea and Caucasus to the Arabian Platform*: London, Geological Society Special Publication 340, p. 1–10.
- Sosson, M., Rolland, Y., Müller, C., Danelian, T., Melkonyan, R., Kekelia, S., Adamia, S., Babazadeh, V., Kangarli, T., Avagyan, A., Galoyan, G., and Mosar, J., 2010b, Subductions, obduction and collision in the Lesser Caucasus (Armenia, Azerbaijan, Georgia)—New insights, *in* Sosson, M., Kaymakci, N., Stephenson, R.A., Bergerat, F., and Starostenko, V. eds., *Sedimentary basin tectonics from the Black Sea and Caucasus to the Arabian Platform*: London, Geological Society Special Publication 340, p. 329–352.
- Soylu, M., 1999, Modeling of porphyry copper mineralization of the Eastern Pontides: Ankara, Turkey, Middle East Technical University, Ph.D. dissertation, 127 p.
- Spies, O., Lensch, G., and Mihm, A., 1984, Petrology and geochemistry of the post-ophiolitic Tertiary volcanics between Sabzevar and Quchan, NE Iran: *Neues Jahrbuch für Geologie und Paläontologie—Abhandlungen*, v. 168, p. 389–408.
- Stalder, Pierre, 1971, Magmatismes tertiaire et subrécent entre Taleghan et Alamout, Elbourz Central (Iran) [abs.]: Zurich, Switzerland, École Polytechnique Fédérale, Ph.D. thèse no. 4405, 3 p. [In French, English abstract.]
- Stampfli, G.M., and Borel, G.D., 2002, A plate tectonic model for the Paleozoic and Mesozoic constrained by dynamic plate boundaries and restored synthetic oceanic isochrons: *Earth and Planetary Science Letters*, v. 196, p. 17–33.
- Stöcklin, J., 1968, Structural history and tectonics of Iran—A review: *American Association of Petroleum Geologists Bulletin*, v. 52, p. 1229–1258.
- Stöcklin, J., 1974, Northern Iran—Alborz Mountains, *in* Spencer, A.M., *Mesozoic-Cenozoic orogenic belts—Data for orogenic studies*: London, Geological Society Special Publication 4, p. 213–234.
- Stoeser, D.B., 2011, Summary of the South Helmand travertine area of interest and geology and mineral resource potential of the Chagai Hills region, *in* Peters, S.G., King, T.V.V., Mack, T.J., and Chornack, M.P., eds., and the U.S. Geological Survey Afghanistan Mineral Assessment Team, 2011, Summaries of important areas for mineral investment and production opportunities of nonfuel minerals in Afghanistan: U.S. Geological Survey Open-File Report 2011–1204, p. 1673–1724, available at <http://pubs.usgs.gov/of/2011/1204/>.
- Stratex International PLC, 2010, Annual Report 2010: Stratex International, accessed July 11, 2012, at <http://www.stratexinternational.com/public/site/uploads/reportsFile-11.pdf>.
- Stratex International PLC, 2012a, Konya: Stratex International Web page, accessed July 11, 2012, at <http://www.stratexinternational.com/operations/exploration/turkey/konya.aspx>.
- Stratex International PLC, 2012b, Muratdere: Stratex International Webpage, accessed July 11, 2012, at <http://www.stratexinternational.com/operations/exploration/turkey/muratdere.aspx>.
- Sutphin, D.M., 2009, A geographic information system to support the mineral-resource assessment of the Central Tethys region: *Geological Society of America Abstracts with Programs*, v. 42, no. 7, p. 611.
- Sutphin, D.M., Hammarstrom, J.M., Drew, L., Large, D.E., Berger, B.R., Dicken, C.L., and DeMarr, M.W., with contributions from Billa, M., Briskey, J.A., Cassard, D., Lips, A., Pertold, Z., and Roşu, E., 2013, Porphyry copper assessment of Europe, exclusive of the Fennoscandian Shield: U.S. Geological Survey Scientific Investigations Report 2010–5090–K, 197 p. and GIS data, available at <http://pubs.usgs.gov/sir/2010/5090/k/>.
- Sweeney, R.E., Kucks, R.P., Hill, P.L., and Finn, C.A., 2006, Aeromagnetic and gravity surveys in Afghanistan—A Web site for distribution of data: U.S. Geological Survey Open-File Report 2006–1204, available at <http://pubs.usgs.gov/of/2006/1204/>.
- Taghipour, B., Noorbehesht, I., Mackizadeh, M.A., and Taghipour, O., 2007, Geological and mineralogical studies of hydrothermal alterations (alunitization and kaolinitization) in north of Isfahan (Kesheh area) [abs.]: *Geochimica et Cosmochimica Acta*, v. 71, no. 15, Goldschmidt Conference, 17th, Cologne, August 19–24, 2007 [Proceedings], p. A992.
- Taghipour, N., Aftabi, A., and Mathur, R., 2008, Geology and Re-Os geochronology of mineralization of the Miduk porphyry copper deposit, Iran: *Resource Geology*, v. 58, p. 143–160.
- Tahmasbi, Z., Khalili, M., and Ahmadi-Khalaji, A., 2009, Thermobarometry of the Astaneh pluton and its related subvolcanic rocks (Sanandaj-Sirjan Zone, western Iran): *Journal of Applied Sciences*, p. 874–882.
- Tahmasebi, P., Hezarkhani, A., and Mortazavi, M., 2010, Application of discriminant analysis for alteration separation—Sungun copper deposit, East Azerbaijan, Iran: *Australian Journal of Basic and Applied Sciences*, v. 6, p. 564–576.
- Talebian, M., and Jackson, J., 2002, Offset on the main recent fault of NW Iran and implications for the late Cenozoic tectonics of the Arabia-Eurasia collision zone: *Geophysical Journal International*, v. 150, p. 422–439.
- Tangestani, M.H., and Moore, F., 2001, Porphyry copper potential mapping using the weights of evidence model in a GIS, northern Shahr e Babak, Iran: *Australian Journal of Earth Sciences*, v. 48, p. 695–701.

- Tangestani, M.H., and Moore, Farid, 2002a, Porphyry copper alteration mapping at the Meiduk area, Iran: *International Journal of Remote Sensing*, v. 23, p. 4815–4825.
- Tangestani, M.H., and Moore, F., 2002b, The use of Dempster-Shafer model and GIS in integration of geoscientific data for porphyry copper potential mapping, north of Shahr-e-Babak, Iran: *International Journal of Applied Earth Observation and Geoinformation*, v. 4, p. 65–74.
- Tarkian, M., and Stribny, B., 1999, Platinum-group elements in porphyry copper deposits—A reconnaissance study: *Mineralogy and Petrology*, v. 65, p. 161–183.
- Taylor, R.P., 1978, The geology of the Bakırçay and Ulutaş porphyry copper prospects, northern Turkey [abs.], in Evans, A.M., ed., *Conference report—Mineralization associated with acid magmatism and other aspects of ore geology*: London, *Journal of the Geological Society*, v. 135, p. 257.
- Taylor, R.P., 1981, Isotope geology of the Bakırçay porphyry copper prospect, northern Turkey: *Mineralium Deposita*, v. 16, p. 375–390.
- Taylor, R.P., and Fryer, B.J., 1980, Multiple-stage hydrothermal alteration in porphyry copper systems in northern Turkey—The temporal interplay of potassic, propylitic, and phyllic fluids: *Canadian Journal of Earth Sciences*, v. 17, p. 901–926.
- Temel, A., Gündoğdu, M.N., and Gourgau, A., 1998, Petrological and geochemical characteristics of Cenozoic high-K calc-alkaline volcanism in Konya, central Anatolia, Turkey: *Journal of Volcanology and Geothermal Research*, v. 85, p. 327–354.
- Temel, A., Gündoğdu, M.N., Gourgau, A., and Le Pennec, J-L., 1998, Ignimbrites of Cappadocia (central Anatolia, Turkey)—Petrology and geochemistry: *Journal of Volcanology and Geothermal Research*, v. 85, p. 447–471.
- Tethyan Copper Company, [n.d.], Mining Project: Tethyan Copper Company Web page, accessed January 10, 2013, at <http://www.tethyan.com/TheRekoDiqProject/MiningProject.aspx>.
- Thalenhurst, H., 2005, Report on the Teghout copper-molybdenum project: Strathcona Mineral Services, Ltd., technical report prepared for Armenian Copper Programme, 11 p. and appendixes.
- Thalenhurst, H., 2007, Update report on the Teghout copper-molybdenum project, Lori, Armenia: Strathcona Mineral Services, Ltd., technical report prepared for Armenian Copper Programme, 32 p. and appendixes.
- Tirrul, R., Bell, I.R., Griffis, R.J., and Camp, V.E., 1983, The Sistan suture zone of eastern Iran: *Geological Society of America Bulletin*, v. 94, p. 134–150.
- Toprak, V., 1998, Vent distribution and its relation to regional tectonics, Cappadocian volcanics, Turkey: *Journal of Volcanology and Geothermal Research*, v. 85, p. 55–67.
- Torabi, G., 2009, Subduction-related Eocene shoshonites from the Cenozoic Urumieh-Dokhtar magmatic arc (Qaleh-Khargooshi area, western Yazd Province, Iran): *Turkish Journal of Earth Sciences*, v. 18, p. 583–613.
- Tüysüz, O., Dellaloğlu, A.A., and Terzioğlu, N., 1995, A magmatic belt within the Neo-Tethyan suture zone and its role in the tectonic evolution of northern Turkey: *Tectonophysics*, v. 243, p. 173–191.
- United Nations Economic and Social Commission for Asia and the Pacific, 2000, *Geology and mineral resources of Azerbaijan*: New York, United Nations, Atlas of mineral resources of the ESCAP Region, v. 15, 216 p.
- U.S. Bureau of Mines and U.S. Geological Survey, 1980, *Principles of a resource/reserve classification of minerals*: U.S. Geological Survey Circular 831, 5 p.
- U.S. Department of State, 2009, Small-scale digital international land boundaries (SSIB)—Polygons, beta edition 1, in *Boundaries and sovereignty encyclopedia (B.A.S.E.)*: U.S. Department of State, Office of the Geographer and Global Issues.
- U.S. Geological Survey, 2012, Mineral Resource Data System (MRDS): U.S. Geological Survey, accessed October 19, 2012, at <http://mrdata.usgs.gov/mrds/>.
- U.S. Geological Survey National Mineral Resource Assessment Team, 2000, 1998 Assessment of undiscovered deposits of gold, silver, copper, lead, and zinc in the United States: U.S. Geological Survey Circular 1178, 29 p., available at <http://pubs.usgs.gov/circ/c1178/>.
- Ustaömer, T., and Robertson, A.H.F., 2010, Late Palaeozoic–Early Cenozoic tectonic development of the Eastern Pontides (Artvin area), Turkey—Stages of closure of Tethys along the southern margin of Eurasia, in Sosson, M., Kaymakci, N., Stephenson, R.A., Bergerat, F., and Starostenko, V., eds., *Sedimentary basin tectonics from the Black Sea and Caucasus to the Arabian Platform*: London, Geological Society Special Publication 340, p. 281–327.
- Vallex Group, 2013, Teghout—News: Vallex Group Web page, accessed on November 20, 2013 at <http://www.teghout.am/en/news.htm>.
- Vasigh, Y., and Zamani, R., 2010, Mejdard deposit petrogenesis—A case study of copper mineralization belt in north west of Iran: *International Applied Geological Congress, 1st, Mashad, Iran, April 26–28, 2010 [Proceedings]*, p. 1315–1320.
- Veliev, A.A., Gasankuliyeva, M.Y., Imamverdiyev, N.A., and Babayeva, G.J., 2010, Petrogenetic evolution Late Cenozoic volcanism of the Lesser Caucasus: *International Applied Geological Congress, 1st, Mashad, Iran, April 26–28, 2010 [Proceedings]*, p. 2159–2167.

- Verdel, C., 2009, I. Cenozoic geology of Iran—An integrated study of extensional tectonics and related volcanism; II—Eadiacaran stratigraphy of the North American Cordillera—New observations from eastern California and northern Utah: Pasadena, California Institute of Technology, Ph.D. dissertation, chapters separately paged.
- Verdel, C., Wernicke, B.P., Ramezani, Jahandar, Hassanzadeh, Jamshid, Renne, P.R., and Spell, T.L., 2007, Geology and thermochronology of Tertiary Cordilleran-style metamorphic core complexes in the Saghand region of central Iran: *Geological Society of America Bulletin*, v. 119, p. 961–977.
- Verdel, C., Wernicke, B.P., Hassanzadeh, J., and Guest, Bernard, 2011, A Paleogene extensional arc flare-up in Iran: *Tectonics*, v. 30, 20 p.
- Vigar, A.J., Meldrum, S., Giroux, G., and Soyulu, M., 2009, Technical report on the exploration results and resource estimates for the Sisorta property Sivas Province, Turkey: Mining Associates Pty Limited, prepared for Chesser Resources Limited and Eurasian Minerals, Inc., 134 p.
- Vincent, S.J., Allen, M.B., Ismail-Zadeh, A.D., Flecker, R., Foland, K.A., and Simmons, M.D., 2005, Insights from the Talysh of Azerbaijan into the Paleogene evolution of the south Caspian region: *Geological Society of America Bulletin*, v. 117, p. 1513–1533.
- Walker, R.T., Gans, P., Allen, M.B., Jackson, J., Khatib, M., Marsh, N., and Zarrinkoub, M., 2009, Late Cenozoic volcanism and rates of active faulting in eastern Iran: *Geophysical Journal International*, v. 177, p. 783–805.
- Walker, R., and Jackson, J., 2004, Active tectonics and late Cenozoic strain distribution in central and eastern Iran: *Tectonics*, v. 23, TC5010, 24 p.
- Walther, H.W., 1960, Orogen-Struktur und Metallverteilung Im östlichen Zagros (Südost-Iran): *Geologische Rundschau*, v. 50, p. 353–374. [In German.]
- Waterman, G.C., and Hamilton, R.L., 1975, The Sar Cheshmeh porphyry copper deposit: *Economic Geology*, v. 70, p. 568–576.
- Wellman, H.W., 1966, Active wrench faults of Iran, Afghanistan and Pakistan: *Geologische Rundschau*, v. 55, p. 716–735.
- Westphal, M., Bazhenov, M.L., Lauer, J.P., Pechersky, D.M., and Sibuet, J.-C., 1986, Paleomagnetic implications on the evolution of the Tethys belt from the Atlantic Ocean to the Pamirs since the Triassic: *Tectonophysics*, v. 123, p. 37–82.
- Wheatley, C.J.V., and Acheson, Denis, 2011, Independent technical report on Toukhanuk mine project and Getik prospect, Armenia, in conformance with NI 43–101 guidelines: Ashford, U.K., Behre Dolbear Group, Inc., technical report, 83 p.
- Whitney, D.L., Teyssier, C., Fayon, A.K., Hamilton, M.A., and Heizler, M., 2003, Tectonic controls on metamorphism, partial melting, and intrusion: timing and duration of regional metamorphism and magmatism in the Niğde Massif, Turkey: *Tectonophysics*, v. 376, no. 1–2, p. 37–60.
- Wikipedia, 2013a, Mineral Industry of Armenia: Wikipedia Web page accessed July 19, 2013, at http://en.wikipedia.org/wiki/Mineral_industry_of_Armenia.
- Wikipedia, 2013b, Mining in Georgia: Wikipedia Web page accessed November 26, 2013, at [http://en.wikipedia.org/wiki/Mining_in_Georgia_\(country\)](http://en.wikipedia.org/wiki/Mining_in_Georgia_(country)).
- Wikipedia, 2013c, Saindak copper gold project: Wikipedia Web page accessed March 11, 2013, at http://en.wikipedia.org/wiki/Saindak_Copper_Gold_Project.
- Wolfe, B., and Gossage, B., 2009, Technical report for the Kapan project, Kapan, Armenia: West Perth, Western Australia, Coffey Mining Pty., Ltd., report prepared for Deno Gold Mining Company CJSC, 19 p.
- Yavuz, F., İskenderoğlu, A., and Jiang, S.-Y., 1999, Tourmaline compositions from the Salikvan porphyry Cu-Mo deposit and vicinity, northeastern Turkey: *The Canadian Mineralogist*, v. 37, p. 1007–1023.
- Yazami, N., Ebrahimi, M., and Motlag, S.H.M., 2010, Role of Oligocene intrusion in copper mineralization at Shoorazgah copper deposit, Zanjan, Iran: *International Applied Geological Congress, 1st, Mashad, Iran, April 26–28, 2010 [Proceedings]*, p. 162–167.
- Yigit, O., 2006, Gold in Turkey—A missing link in Tethyan metallogeny: *Ore Geology Reviews*, v. 28, p. 147–179.
- Yigit, O., 2009, Mineral deposits of Turkey in relation to Tethyan metallogeny—Implications for future mineral exploration: *Economic Geology*, v. 104, p. 19–51.
- Yigit, O., 2012, A prospective sector in the Tethyan Metallogenic Belt—Geology and geochronology of mineral deposits in the Biga Peninsula, NW Turkey: *Ore Geology Reviews*, v. 46, p. 118–148.
- Yiğitbaş, E., and Yılmaz, Y., 1996, New evidence and solution to the Maden complex controversy of the Southeast Anatolian orogenic belt (Turkey): *Geologische Rundschau*, v. 85, p. 250–263.
- Yılmaz, C., and Korkmaz, S., 1999, Basin development in the Eastern Pontides, Jurassic to Cretaceous, NE Turkey: *Zentralblatt für Geologie und Paläontologie*, v. 1, p. 1485–1494.
- Yılmaz, C., Şen, C., and Özgür, S., 2001, Timing of earliest andesitic volcanic activity in the Eastern Pontide volcanic arc: *International Earth Sciences Congress on Aegean Regions, Izmir, Turkey, October 1–6, 1990 [Proceedings]*, p. 47–55.

- Yilmaz, H., 2003a, Exploration at the Kusçayiri Au (Cu) prospect and its implications for porphyry-related mineralization in western Turkey: *Journal of Geochemical Exploration*, v. 77, p. 133–150.
- Yilmaz, H., 2003b, Geochemical exploration for gold in western Turkey—Success and failure: *Journal of Geochemical Exploration*, v. 80, p. 117–135.
- Yılmaz, O., and Boztuğ, D., 1986, Kastamonu granitoid belt of northern Turkey—First arc plutonism product related to the subduction of paleo-Tethys: *Geology*, v. 14, p. 179–183.
- Yilmaz, Y., 1990, Comparison of young volcanic associations of western and eastern Anatolia formed under a compressional regime—A review: *Journal of Volcanology and Geothermal Research*, v. 44, p. 69–87.
- Yılmaz, Y., 1993, New evidence and model on the evolution of the southeast Anatolian orogen: *Geological Society of America Bulletin*, v. 105, p. 251–271.
- Yılmaz, Y., Serdar, H.S., Genç, C., Yiğitbaş, E., Gürer, Ö.F., Elmas, A., Yıldırım, M., Bozcu, M., and Gürpınar, O., 1997, The geology and evolution of the Tokat Massif, south-central Pontides, Turkey: *International Geology Review*, v. 39, p. 365–382.
- Yılmaz, Y., Tüysüz, O., Yiğitbaş, E., Genç, Ş.C., and Şengör, A.M.C., 1997, Geology and tectonic evolution of the Pontides, in Robinson, A.G., ed., *Regional and petroleum geology of the Black Sea and surrounding region*: *American Association of Petroleum Geologists Memoir* 68, p. 183–226.
- Yilmaz, Y., Genç, Ş.C., Karacık, Z., Altunkaynak, Ş., 2001, Two contrasting magmatic associations of NW Anatolia and their tectonic significance: *Journal of Geodynamics*, v. 31, p. 243–271.
- Yılmaz-Şahin, S., 2005, Transition from arc- to post-collision extensional setting revealed by K-Ar dating and petrology—An example from the granitoids of the Eastern Pontide igneous terrane, Araklı-Trabzon, NE Turkey: *Geological Journal*, v. 40, p. 425–440.
- Yılmaz-Şahin, S., Güngör, Y., and Boztuğ, D., 2004, Comparative petrogenetic investigation of composite Kaçkar Batholith granitoids in Eastern Pontide magmatic arc, Northern Turkey: *Earth Planets Space*, v. 56, p. 429–446.
- Yücel Öztürk, Y., Helvacı, C., and Satır, M., 2008, The influence of meteoric water on skarn formation and late-stage hydrothermal alteration at the Evciler skarn occurrences, Kazdağ, NW Turkey: *Ore Geology Reviews*, v. 34, p. 271–284.
- Zanchi, A., Berra, F., Mattei, M., Ghassemi, M.R., and Sabouri, J., 2006, Inversion tectonics in central Alborz, Iran: *Journal of Structural Geology*, v. 28, p. 2023–2037.
- Zanchi, A., Zanchetta, S., Berra, F., Mattei, M., Garzanti, E., Molyneux, S., Nawab, A., and Sabouri, J., 2009, The Eo-Cimmerian (Late? Triassic) orogeny in north Iran, in Brunet, M-F., Wilmsen, M., and Granath, J.W., eds., *South Caspian to Central Iran Basins*: London, Geological Society Special Publication 312, p. 31–55.
- Zanganeh, G.S., Momenzadeh, M., and Rasa, I., 2010, Determining the position of erosion surface in the deposit of Bidester area: *International Applied Geological Congress*, 1st, Mashad, Iran, April 26–28, 2010 [Proceedings], p. 54–61.
- Zarasvandi, A., Liaghat, S., and Zentilli, M., 2005, Geology of the Darreh-Zerreshk and Ali-Abad porphyry copper deposits, central Iran: *International Geology Review*, v. 47, p. 620–646.
- Zarasvandi, A., Liaghat, S., Zentilli, M., and Reynolds, P.H., 2007, $^{40}\text{Ar}/^{39}\text{Ar}$ geochronology of alteration and petrogenesis of porphyry copper-related granitoids in the Darreh-Zerreshk and Ali-Abad area, central Iran: *Exploration and Mining Geology*, v. 16, p. 11–24.
- Zarcan International Resources, 2000, Zarcan claims 15 mineral concessions in Iran: Zarcan International Resources press release, September 6, 2000, accessed September 19, 2012, at <http://www.thefreelibrary.com/Zarcan+claims+15+mineral+concessions+in+Iran.-a065027685>.
- Zarcan International Resources, 2003, Zarcan receives extension for exploration licenses in Iran and updates on Shurchah, Bidester and Kharestan mineral concessions and Zarcan amends loan of \$300,000 to \$450,000: Zarcan International Resources press release, May 16, 2003, 3 p., accessed September 19, 2012, at <http://www.infomine.com/index/pr/pa128553.pdf>.
- Ziaii, M., Abedi, A., and Ziaei, M., 2007, Prediction of hidden ore bodies by new integrated computational model in marginal Lut region in east of Iran, in Milkereit, B., ed., *Proceedings of Exploration 07: International Conference on Mineral Exploration, 5th Decennial*, Toronto, September 9–12, 2007, p. 957–961.
- Ziaii, Mansour, Pouyan, Ali, and Ziaei, M., 2009, A computational optimized extended model for mineral potential mapping based on WofE method: *American Journal of Applied Sciences*, v. 6, p. 200–203.
- Ziaii, M., Abedi, A., Ziaei, M., Rouhani, A.K., and Zendahdel, A., 2010, GIS modeling for Au-Pb-Zn potential mapping in Torud-Chah Shirin area, Iran: *International Journal of Mining and Environmental Issues*, v. 1, p. 17–27.
- Zvezdov, V.S., Migachev, I.F., and Girfanov, M.M., 1993, Porphyry copper deposits of the CIS and the models of their formation: *Ore Geology Reviews*, v. 7, p. 511–549.

Appendixes A–D

Appendix A. Principal Sources of Information Used for the Porphyry Copper Assessment, Tethys Region of Western and Southern Asia

[Tables in this appendix are available online only as .xlsx tables at <http://dx.doi.org/10.3133/sir20105090V>]

Table A1. Principal sources of information used for delineation of tract 142pCu9000, Lut Jurassic—Iran.

Table A2. Principal sources of information used for delineation of tract 142pCu9001, Cimmeride Lesser Caucasus—Armenia, Azerbaijan, Georgia, and Iran.

Table A3. Principal sources of information used for delineation of tract 142pCu9002, Cimmeride Greater Caucasus—Armenia, Georgia, and Russian Federation.

Table A4. Principal sources of information used for delineation of tract 142pCu9003, Sanandaj-Sirjan—Iran, Iraq, and Turkey.

Table A5. Principal sources of information used for delineation of tract 142pCu9004, Pontide (Asia)—Armenia, Azerbaijan, Georgia, Iran, and Turkey.

Table A6. Principal sources of information used for delineation of tract 142pCu9005, Anatolide-Tauride—Armenia, Azerbaijan, Iran, and Turkey.

Table A7. Principal sources of information used for delineation of tract 142pCu9006, Lut Cretaceous—Iran.

Table A8. Principal sources of information used for delineation of tract 142pCu9007, Border Folds—Iran, Iraq, and Turkey.

Table A9. Principal sources of information used for delineation of tract 142pCu9008, Esfahan—Iran, Iraq, Turkey.

Table A10. Principal sources of information used for delineation of tract 142pCu9009, Khorasan—Afghanistan and Iran.

Table A11. Principal sources of information used for delineation of tract 142pCu9010, Lut Tertiary—Iran.

Table A12. Principal sources of information used for delineation of tract 142pCu9011, Makran—Iran.

Table A13. Principal sources of information used for delineation of tract 142pCu9012, Sistan—Afghanistan, Iran, and Pakistan.

Table A14. Principal sources of information used for delineation of tract 142pCu9013, Chagai—Afghanistan, Iran, and Pakistan.

Table A15. Principal sources of information used for delineation of tract 142pCu9014, Azerbaijan—Armenia, Azerbaijan, Iran, and Turkey.

Table A16. Principal sources of information used for delineation of tract 142pCu9015, Yazd—Iran.

Table A17. Principal sources of information used for delineation of tract 142pCu9016, Kerman—Iran.

Table A18. Principal sources of information used for delineation of tract 142pCu9017, Pliocene-Quaternary—Afghanistan, Armenia, Azerbaijan, Georgia, Iran, Pakistan, Russian Federation, and Turkey.

Appendix B. Geologic Map Units Used to Delineate Permissive Tracts (With References to Source Maps), Tethys Region of Western and Southern Asia

[Tables in this appendix are available online only as .xlsx tables at <http://dx.doi.org/10.3133/sir20105090V>]

Table B1. Permissive units for tract 142pCu9000, Lut Jurassic—Iran.

Table B2. Permissive units for tract 142pCu9001, Cimmeride Lesser Caucasus—Armenia, Azerbaijan, Georgia, and Iran.

Table B3. Permissive units for tract 142pCu9002, Cimmeride Greater Caucasus—Azerbaijan, Georgia, and Russian Federation.

Table B4. Permissive units for tract 142pCu9003, Sanandaj-Sirjan—Iran, Iraq, and Turkey.

Table B5. Permissive units for tract 142pCu9004, Pontide (Asia)—Armenia, Azerbaijan, Georgia, Iran, and Turkey.

Table B6. Permissive units for tract 142pCu9005, Anatolide-Tauride—Armenia, Azerbaijan, Iran, and Turkey.

Table B7. Permissive units for tract 142pCu9006, Lut Cretaceous—Iran.

Table B8. Permissive units for tract 142pCu9007, Border Folds—Iran, Iraq, and Turkey.

Table B9. Permissive units for tract 142pCu9008, Esfahan—Iran, Iraq, Turkey.

Table B10. Permissive units for tract 142pCu9008, Esfahan—Iran, Iraq, Turkey.

Table B11. Permissive units for tract 142pCu9010, Lut Tertiary—Iran.

Table B12. Permissive units for tract 142pCu9011, Makran—Iran.

Table B13. Permissive units for tract 142pCu9012, Sistan—Afghanistan, Iran, and Pakistan.

Table B14. Permissive units for tract 142pCu9013, Chagai—Afghanistan, Iran, and Pakistan.

Table B15. Permissive units for tract 142pCu9014, Azerbaijan—Armenia, Azerbaijan, Iran, and Turkey.

Table B16. Permissive units for tract 142pCu9015, Yazd—Iran.

Table B17. Permissive units for tract 142pCu9016, Kerman—Iran.

Table B18. Permissive units for tract 142pCu901a, Pliocene-Quaternary—Afghanistan, Armenia, Azerbaijan, Georgia, Iran, Pakistan, Russian Federation, and Turkey.

Appendix C. Significant Porphyry Copper Prospects and Occurrences, Tethys Region of Western and Southern Asia

[Tables in this appendix are available online only as .xlsx tables at <http://dx.doi.org/10.3133/sir20105090V>]

Table C1. Significant porphyry copper prospects and occurrences of the Tethys region of western and southern Asia.

Appendix D. Spatial Data

By Pamela Dunlap²²

Spatial and descriptive data were developed for use in Esri's ArcGIS software package (version 10), a geographic information system (GIS). An Esri file geodatabase (**Tethys_porphyry_copper.gdb**) contains two feature classes for permissive tracts (**Tethys_pCu_tracts**) and deposits and prospects (**Tethys_pCu_deposits_prospects**) and two tables of references (**Deposit_Refs**, **Tract_refs**). An Esri map document (**Tethys_porphyryCu.mxd**) and an Esri file geodatabase of political boundaries for countries in the study area (**Tethys_basemap.gdb**) are also provided for viewing the data. The spatial data are stored in geographic coordinates (WGS 1984). The spatial data and associated files may be downloaded from the USGS Web site (<http://dx.doi.org/10.3133/sir20105090V>) as the compressed archive file **sir20105090v_gis.zip**.

The feature class **Tethys_pCu_tracts** contains vector data (polygon) for 26 permissive tracts. Attributes include tract identifiers, tract name, a brief description of the basis for tract delineation, and assessment results. Attributes are defined in the metadata, which are both embedded in the feature class and provided in an Adobe Acrobat Portable Document Format file (**Tethys_pCu_tracts_metadata.pdf**).

The feature class **Tethys_pCu_deposits_prospects** contains vector data (point) for 365 sites with porphyry copper or porphyry-related mineralization. Attributes include the assigned tract, site and alternate site names, site and development status, location coordinates, country and state or province (derived from U.S. Department of State, 2009, and Hijmans, 2011, respectively), age, grades and tonnages, commodities, mineralogy, associated rocks, and abbreviated source references. Attributes are defined in the metadata which are both embedded in the feature class and provided in an Adobe Acrobat Portable Document Format file (**Tethys_pCu_deposits_prospects_metadata.pdf**).

The geodatabase table **Deposit_Refs** provides full reference citations and Web sites (if available) for the abbreviated source references listed for each site in the feature class **Tethys_pCu_deposits_prospects**. The geodatabase table **Tract_refs** provides full reference citations and Web sites (if available) for the abbreviated source references listed for each tract in the feature class **Tethys_pCu_tracts**.

The file geodatabase **Tethys_basemap.gdb** contains the feature class **Tethys_political_boundaries** for vector data (polygons) for political boundaries in the study area. The data were extracted from a GIS of country boundaries and shorelines maintained by the U.S. Department of State (2009).

References Cited

Hijmans, R., 2011, Global administrative areas—GADM database, version 2.0: Global Administrative Areas database, accessed January 23, 2013, at <http://www.gadm.org>.

U.S. Department of State, 2009, Small-scale digital international land boundaries (SSIB)—Lines, edition 10, and polygons, beta edition 1, *in* Boundaries and sovereignty encyclopedia (B.A.S.E.): U.S. Department of State, Office of the Geographer and Global Issues.

Appendix E. Assessment Team

Lukas Zürcher is a research geologist with the USGS in Tucson, Arizona. He received a B.S. degree in Geological Engineering from the Colorado School of Mines (1985) and M.S. and Ph.D. degrees in Geosciences from the University of Arizona in (1994 and 2002, respectively). He worked as an exploration and consulting geologist for the mining industry in Mexico, Cote d'Ivoire, Bolivia, Argentina, and the United States (1985–2010), as a postdoctoral fellow in the Department of Lunar and Planetary Sciences (2002–05), and as Manager of the Lowell Program in Economic Geology (2002–11) at the University of Arizona before joining the USGS in 2011. He has 26 years of combined industry and academic experience in geologic, alteration, and mineralization mapping, structural geology, igneous and hydrothermal geochemistry, statistical methods, mineral economics, and GIS-based favorability mapping. His research has included local- to regional-scale geologic, geochemical, and metallogenic studies of porphyry, skarn, impact-generated, and IOCG hydrothermal systems, as well as comparative analyses of favorability mapping methods. With the USGS, he has contributed to the porphyry copper resource

²²U.S. Geological Survey, Tucson, Arizona, United States.

assessments of Mexico, Central America, the Caribbean, and the Tethys region of western and southern Asia. Zürcher was a member of the assessment team for this study, and he is the lead author of this report.

Arthur A. Bookstrom is a research geologist with the USGS in Spokane, Washington. He received a B.A. degree in geology from Dartmouth College (1961), an M.S. in geology from the University of Colorado (1964), and a Ph.D. in geology from Stanford University (1975). He worked as a mine geologist at the Climax molybdenum mine in Colorado, El Romeral magnetite mine in Chile, and the Rochester silver mine in Nevada. He has done site-specific exploration in Colorado, Nevada, and Montana, as well as regional exploration for molybdenum in Colorado and for gold in Nevada, Montana, and Saudi Arabia. Bookstrom's work with the USGS has included regional geologic studies, metallogenic studies, mineral-environmental studies, and mineral-resource assessments. He was a member of the assessment team for this study.

Jane M. Hammarstrom is a research geologist with the USGS in Reston, Virginia. She received a B.S. in geology from George Washington University in 1972 and an M.S. in geology from Virginia Polytechnic Institute and State University in 1981. She is co-chief of the USGS Global Mineral Resource Assessment project and the task leader for the porphyry copper assessment. She has more than 30 years of research experience in igneous petrology, mineralogy, geochemistry, economic geology, and mineral resource assessment. Hammarstrom is a member of the assessment team, and she conducted the probabilistic simulations for this study.

John (Lyle) C. Mars is a research geologist with the USGS in Reston, Virginia. He is an expert in remote sensing. He developed algorithms for processing ASTER data to map hydrothermal alteration as an assessment tool, analyzed the ASTER data for the study area, and participated in assessment meetings. Mars was a member of the assessment team for this study.

Steve Ludington is a research geologist with the USGS in Menlo Park, California. He received a B.A. in geology from Stanford University (1967) and a Ph.D. in geology from the University of Colorado (1974). He worked as an exploration geologist in Colorado, New Mexico, and Arizona before joining the USGS in 1974. His work with the USGS has included regional geologic studies, metallogenic and geochemical studies, wilderness studies, and mineral-resource assessments. Ludington has done mineral-resource assessment work in the United States, Costa Rica, Bolivia, Mongolia, Afghanistan, and Mexico and was a coordinator for the 1998 USGS National Mineral Resource Assessment. He was a member of the assessment team for this study.

Michael L. Zientek is a research geologist with the USGS in Spokane, Washington. He is co-chief of the USGS Global Mineral Resource Assessment Project. He obtained a B.S. degree in geology from the University of the Texas in 1976 and a Ph.D. at Stanford University (1984). Zientek worked in industry before joining the USGS. He participated in the project workshops and provided reviews of drafts of the preliminary assessment of the Tethys region of western and southern Asia. He was a member of the assessment team for this study.

Pamela Dunlap is a geologist with the USGS in Tucson, Arizona. She received a B.A. in geology from the University of Rochester (1975) and an M.S. in geology from the College of Mines and Earth Resources at the University of Idaho (1977). She worked as an exploration geologist in Nevada, Montana, Idaho, and Washington and as a research geologist for various State geological surveys before joining the USGS in 1992. She completed mineral-resource assessments of phosphate in southeastern Idaho and oil shale in central Montana, in addition to countywide mine and mineral occurrence databases for Silver Bow and Madison Counties, Montana. Pamela has prepared numerous geologic map and mineral-resource assessment products in a geographic information system (GIS) while with the USGS. Dunlap built the GIS for deposits and prospects for this study, and she compiled the reference lists for the report and the GIS.

John C. Wallis is an illustrator/graphics and geographic information systems specialist with the USGS in Spokane, Washington. He received a B.S. in Geology (1997) and a BS in Biology (1998) from Eastern Washington University. Wallis provided GIS assistance and compiled illustrations for this report.

Lawrence J. Drew is a senior mineral economist, expert on mineral-resource assessment, and author of several studies (assessments) on the structural setting of porphyry copper and associated deposits of central Europe. He earned a Ph.D. at Penn State and has 40 years of experience with the USGS in Reston, Virginia. Drew led the preliminary assessment workshop in London.

David M. Sutphin is a geologist at the USGS in Reston, Virginia. He joined the USGS in 1981 after earning his B.S. in geology and attending graduate school at Arizona State University. He has been involved in several quantitative mineral-resource assessments, including the Roswell and Mimbres Bureau of Land Management (BLM) areas in New Mexico, sand and gravel resources of parts of New Hampshire, Global Mineral Resources Assessment Project assessments of Europe and South America, and assessments of various mineral commodities in Afghanistan. He contributed a draft report based on the preliminary assessment workshop in London. Sutphin coauthored (Sutphin and others, 2013) another report in this series—Porphyry Copper Assessment of Europe, Exclusive of the Fennoscandian Shield (U.S. Geological Survey Scientific Investigations Report 2010–5090–K).

Byron R. Berger was a research geologist with the USGS in Denver, Colorado. He had broad expertise on porphyry copper deposits, mineral-resource assessment, and porphyry- and porphyry-related mineral deposits. Berger participated in the London preliminary assessment workshop and prepared a draft report on the Caucasus region. He was senior author (Berger

and others, 2008) of Preliminary Model of Porphyry Copper Deposits (U.S. Geological Survey Open-File Report 2008–1321) and (Berger and others, 2014) Porphyry Copper Assessment of Western Central Asia (U.S. Geological Survey Scientific Investigations Report 2010–5090–N). He passed away December 10, 2013.

Richard J. Herrington is a Merit Researcher and head of mineral deposit research in the Department of Mineralogy at the Natural History Museum, London, United Kingdom. He provided data and expertise on the geology and mineral deposits of the Tethys region, and participated in the London workshop and follow-up discussions of preliminary assessment results.

Mario Billa is an economic geologist with the Bureau de Recherches Géologiques et Minières, Orléans, Cedex 2, France. He participated in the London preliminary assessment workshop.

Ilkay Kuşcu is a professor in the Department of Geology at the University of Muğla, Turkey. Kuşcu has published widely on the mineral deposits of Turkey and participated in the London workshop. Kuşcu is senior author of at least five reports cited in this text (and coauthor of several more).

Charles J. Moon is a teaching fellow at the Camborne School of Mines, Cornwall, United Kingdom, and an independent consulting geologist for the mining industry. His research interests include the geology and mineral deposits of Turkey and Georgia. Moon authored one and coauthored four reports cited in this paper. He participated in the London preliminary assessment workshop.

Jeremy P. Richards is a professor in the Department of Earth and Atmospheric Sciences at the University of Alberta, Canada. His research interests include regional controls on porphyry copper mineralization in Iran, Pakistan, and Turkey. Richards has authored or coauthored 11 reports cited in this paper. He participated in the London preliminary workshop.

Menlo Park Publishing Service Center, California
Manuscript approved for publication November 20, 2014
Edited by Larry Slack and James W. Hendley II
Layout and design by Cory Hurd

